Peptide-Based Probes To Monitor Cysteine-Mediated Protein Activities

Author: Nicholas Pace

Boston College

The Graduate School of Arts and Sciences

Department of Chemistry

PEPTIDE-BASED PROBES TO MONITOR CYSTEINE-MEDIATED PROTEIN ACTIVITIES

Dissertation

by

NICHOLAS J. PACE

submitted in partial fulfillment of the requirements

for the degree of

Doctor of Philosophy

May 2015

Peptide-Based Probes to Monitor Cysteine-Mediated Protein Activities

by

Nicholas J. Pace

Thesis Advisor: Eranthie Weerapana

Abstract

Cysteine residues are known to perform an array of functional roles in proteins, including nucleophilic and redox catalysis, regulation, metal binding, and structural stabilization, on proteins across diverse functional classes. These functional cysteine residues often display hyperreactivity, and electrophilic chemical probes can be utilized to modify reactive cysteines and modulate their protein functions. A particular focus was placed on three peptide-based cysteine-reactive chemical probes (NJP2, NJP14. and NJP15) and their particular biological applications. NJP2 was discovered to be an apoptotic cell-selective inhibitor of glutathione *S*-transferase omega 1 and shows additional utility as an imaging agent of apoptosis. NJP14 aided in the development of a chemical-proteomic platform to detect Zn^{2+}-cysteine complexes. This platform identified both known and unknown Zn^{2+}-cysteine complexes across diverse protein classes and should serve as a valuable complement to existing methods to characterize functional Zn^{2+}-cysteine complexes. Finally, NJP15 was part of a panel of site-selective cysteine-reactive inhibitors of protein disulfide isomerase A1 (PDIA1). These inhibitors show promise in clarifying the unique and redundant properties of PDIA1's dual active-sites, as well as interrogating the protein's role in cancer. Together, these case studies illustrate the potential of cysteine-reactive chemical probes to modulate protein activities, interrogate biological systems, and aid in the development of powerful therapeutic drugs.

Acknowledgements

I would like to begin by thanking my advisor, Professor Eranthie Weerapana. I cannot thank you enough for guidance over these years. From a scientific stand-point, you taught me how to solve problems and think critically and independently. Your patience and leadership was exemplary, and led to both a productive and pleasurable work environment for all of us. I truly enjoyed the opportunity to work in your lab. I would also like to extend a sincere thanks to all of my thesis committee, Mary Roberts, Jianmin Gao, and Abhishek Chatterjee for all your help and advice of the years.

Thank you to all of my collaborators. A special thanks goes to Sharon Louie, Dr. Mela Mulvihill, and Dr. Daniel Nomura from University of California Berkeley. Thank you for hosting me, teaching me countless techniques, and even letting me join in on a group camping trip! Additional thanks to Kimberly Miller from the Biology Department at Boston College for helping me with the RT-PCR experiments over the past six months.

Thank you to all the members of the Weerapana lab past and present: Tyler, Kyle, Lisa, Shalise, Dan, Ranjan, Masahiro, Haley, Julie, Yani, and Alex. You have all been such a pleasure to work with and learn from, and I truly enjoyed coming to lab each day. More than lab-mates you are all great friends. I will miss our "Saturday Only Playlists," Roggie's and Joey's nights, and constant sports conversations (and arguments). When I joined the newly found Weerapana lab almost five years ago, a small group of us assisted Eranthie in setting up the new lab, optimizing protocols, and learning countless techniques. A special thanks needs to be extended to Julie, Yani, and Alex. You three have been instrumental to my success in graduate school and there is no way I could have

succeeded without all your help. I could not think of three better people to have worked with these past years.

Thank you to all the lab technicians I have encountered over the years: John, TJ, Marek, and Bret. Thank you to all the support staff at Boston College. Steve, Ginny, Dale, Lynne P., Lynne O., Ian, Jen, Lori, Howard, Richard, and Bill "Success" Fogerty. I truly appreciate your tireless efforts and patience that allowed me to maintain focus on my studies. Your constant optimism and support was truly appreciated.

Thank you to all the friends at BC I have made over the years. There are way too many of you to name, but you all have been great and I truly appreciate our friendship. Special thanks to the "Chemistry Bro's," keep drinking chocolate milk.

Finally, I'd like to thank my family and friends outside of Boston College. My friends from SJP and Stonehill College are truly amazing. I am extremely close with my family (and future in-laws), and I cannot thank them enough for their support over these years. I special thanks has to be extended to my brother and sister for their support over these years. It is nice having siblings to discuss science with, and makes for interesting holiday conversation. I also need to thank my parents. They are two of the most self-less people I have ever encountered. Every decision they have ever made is always with me, my brother, or my sister in mind, and I truly cannot describe how much I have appreciated your love and support these years.

Lastly, I would like to thank my fiancée and future wife, Amanda. You have taught me so much over these years, have been so patient with me, and always keep me grounded. This is just as much your accomplishment as it is mine. I cannot thank you enough.

Table of Contents

List of Figures

Chapter 3

Appendix.

List of Tables

List of Abbreviations

Standard 3-letter and 1-letter codes are used for the 20 natural amino acids.

ABPP	activity-based protein profiling
ADH	alcohol dehydrogenase
AGEs	advanced glycation end products
AKT	protein kinase B
AOMK	acyloxymethyl ketone
Apaf-1	Apoptotic protease activating factor 1
ATF6	activating transcription factor 6
Azo-H	azobenzene heavy mass spectrometry tag
Azo-L	azobenzene light mass spectrometry tag
BHMT	betaine-homocysteine methyltransferase
BLMH	bleomycin hydrolase
CAD	caspase-activated DNase
CA-Rh	chloroacetamide rhodamine
Caspase	Cysteine-dependent aspartate directed proteases
cCMP	Cytidine 2′:3′-cyclic monophosphate
CCR5	C-C chemokine receptor type 5
CPT	camptothecin
CXCR4	chemokine C-X-C receptor 4
DCM	dichloromethane
DDAH-1	dimethylarginine dimethylaminohydrolase
DEPC	diethylpyrocarbonate
DHA	docosahexaenoic acid
DHFR	dihydrofolate reductase
DIPEA	*N,N*-diisopropylehtylamide

DISC	Death-inducing signaling complex
DMEM	Dulbecco's modified eagle media
DMF	dimethylformamide
DMSO	dimethylsulfoxide
dox	doxycycline
DTNB	5′5-dithio-bis(2-nitrobenzoic acid
DTT	dithiothreitol
EDTA	ethylenediaminetetraacetic acid
EGFR	epidermal growth factor receptor
eIF2	E74-like factor 2
ER	endoplasmic reticulum
ERK1/2	extracellular-signal-related kinase 1 or 2
Ero1	endoplasmic reticulum oxidoreductin 1
ESI	electrospray ionization
EtOH	ethanol
FADD	Fas-associated protein with death domain
FasL	Fas ligand
FasR	Fas receptor
FCS	fetal calf serum
Fmoc	fluoren-9-ylmethoxycarbonyl
Fmoc-Pra-OH	Fmoc-propargyl glycine
FTase	protein farnesyltransferase
GSH	glutathione (reduced)
GSSG	glutathione (oxidized)
GSR	glutathione reductase
GST	glutathione *S*-transferase
GSTO1	glutathione *S*-transferase omega 1

GSTO1 H-site	hydrophobic substrate-binding domain
GSTO1 G-site	GSH-binding site
HEDS	hydroxyethyl disulfide
HNE	4-hydroxynonenal
HPLC	high-performance liquid chromatography
HRMS	high resolution mass spectrometry
HRP	horseradish peroxidase
IA	iodoacetamide
IA-alkyne	iodoacetamide alkyne probe (N-(hex-5-yn-1-yl)-2-iodoacetamide)
ICAD	inhibitor of CAD
ICAM3	intercellular adhesion molecule 3
IRE1	inositol-requiring protein 1
IPTG	isopropyl β-D-1-thiogalactopyranoside
JNK1	mitogen-activated protein kinase 8
LC	liquid chromatography
MALDI	matrix-assisted laser desorption/ionization
MeOH	methanol
MHC	major histocompatibility complex
mRNA	messenger RNA
MS	mass spectrometry
NEt_3	triethylamine
NOS	nitric oxide synthase
NOS3	endothelial nitric oxide synthase
OAB	oxidative assay buffer
PAO	phenylarsine oxide
PBS	phosphate buffered saline (137 mM NaCl, 2.7 mM KCl, pH7.4)

PDI	protein disulfide isomerase protein family
PDIA1	protein disulfide isomerase isoform A1
PERK kinase	protein kinase RNA-like endoplasmic reticulum
Pen/Strep	Penicillin streptomycin
Pra	propargylglycine
Prdx4	peroxiredoxin 4
PS	phosphatidylserine
PS-alkyne	phenylsulfonate-ester alkyne probe
PS-Rh	phenylsulfonate-ester rhodamine probe
PyBOP	benzotriazole-1-yl-oxy-tris-pyrrolidino-phosphonium hexafluorophosphate
RAB	reductive assay buffer
ROS	reactive oxygen species
RT-PCR	real time polymerase chain reaction
SAR	structure-activity relationship
SCX	strong cation exchange resin
Sec	selenocysteine
SEM	standard error of the mean
SORD	sorbitol dehydrogenase
STS	staurosporine
Rh-N_3	Rhodamine-azide
RPMI	Roswell Park Memorial Institute media
RNase	ribonuclease
aRNase	active RNase A
rRNase	reduced RNase A
RSK	ribosomal s6 kinase
SAGA	Spt-Ada-Gcn5-acetyl transferase

SDS	sodium dodecyl sulfate
SDS-PAGE electrophoresis	sodium dodecyl sulfate polyacrylamide gel
shGFP protein	small hairpin RNA targeting green fluorescent
shPDIA1	small hairpin RNA targeting PDIA1
SPPS	solid-phase peptide synthesis
TBTA	tris[(1-benzyl-1*H*-1,2,3-triazol-4-yl)methyl]amine
TBS	tris-buffer saline
TBS-T	tris-buffer saline with 1% Tween-20
TCEP	tris(2-carboxyethyl)phosphine hydrochloride
tet	tetracycline
TFA	trifluoroacetic acid
TIS	triisopropylsilane
TLC	thin-layer chromatography
TMP	trimethoprim
TNF-R	tumor necrosis factor receptor
TOF	time-of-flight mass analyzer
TRADD	tumor necrosis factor type 1-associated death domain protein
TRAIL	TNF-related apoptosis-inducing ligand
TRAIL-R1	TNF-related apoptosis-inducing ligand receptor 1
Tris	tris(hydroxymethyl)aminomethane
Trityl	triphenylmethyl
Trx	thioredoxin
TrxR	thioredoxin reductase
UPR	unfolded protein response
USP22	ubiquitin carboxyl-terminal hydrolase 22

VEGF	vascular endothelial growth factor
XBP1	X-box binding protein 1

Chapter 1

Introduction

A significant portion of the work described in this chapter has been published in:

Pace, N. J.; Weerapana, E. Diverse Functional Roles of Reactive Cysteines. *ACS Chem. Biol.* **2013**, *8*, 283-296.

This thesis focuses on the continued annotation and characterization of functionally important cysteine residues. Cysteine residues are known to contribute to protein structure, catalysis, redox activity, regulation, and metal binding. Increased cysteine reactivity has been found to correlate with functionality; consequently, experimental approaches have been designed to detect these hyperreactive cysteines.[1] These methods typically rely on chemical probes possessing a cysteine-reactive electrophile to covalently bind nucleophilic (reactive) cysteines within the proteome for enrichment and subsequent identification by mass spectrometry. Cysteine-reactive probes have been designed to target diverse cysteine-mediated protein activities including proteases, kinases and oxidoreductases.[2] We sought to exploit the inherent diversity of peptide-based scaffolds to expand the protein classes amenable to covalent modification using cysteine-reactive probes. Herein, we provide a detailed account of three cysteine-reactive peptide-based probes (NJP2, NJP14 and NJP15) as tools to study different biological applications.

This thesis is divided into four chapters. Chapter 1 introduces the relevant roles of functional cysteines within proteins and provides classical examples of each. The remaining three chapters concentrate on individual probes that modulate a particular cysteine function and their biological consequences. Chapter 2 focuses on NJP2 and its application as an apoptotic cell-selective inhibitor of a catalytic cysteine within glutathione *S*-transferase omega 1 (GSTO1). Chapter 3 centers on NJP14 and the development of a chemical proteomic technology to identify cysteines with high affinity for Zn^{2+} within a complex proteome. Finally, Chapter 4 details a panel of cysteine-reactive inhibitors, including NJP15, selective for the redox-catalytic cysteines within

protein disulfide isomerase (PDIA1) to interrogate the role of this protein in cancer progression.

Cellular roles of reactive cysteines

Although cysteine is one of the least abundant amino acids incorporated into proteins (1.9% abundance), it concentrates at functionally important locations within protein scaffolds.[3, 4] Cysteine was a late evolutionary addition to the genetic code but has since accrued at a high frequency, hinting at the preferential incorporation of cysteines at functional loci.[5] Additionally, mutations of cysteine residues contribute to genetic diseases significantly more than mutations to any other amino acid.[6]

Cysteine residues possess unique physiochemical properties that allow them to facilitate diverse protein functions. Importantly, cysteine is the only amino acid that contains a thiol functional group. The large atomic radius of sulfur and the low dissociation energy of the S-H bond allow cysteine to perform both nucleophilic and redox-active functions that are unfeasible for other natural amino acids. The pK_a of the thiol group of cysteine (~8.0) is typically close to physiological pH (7.4) for a solvent exposed residue (Figure 1-1).[7] However, the ionization state is highly sensitive to slight changes within the local protein microenvironment, and in extreme cases, the pK_a of a specific cysteine thiol can drop as low as 2.0.[8]

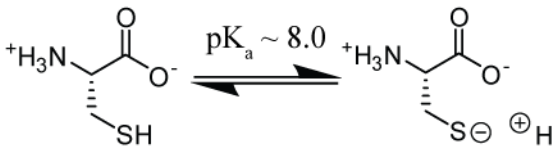

Figure 1-1. The thiol group of cysteine is readily ionized to a thiolate anion.

As a result, the thiol ionization state governs cysteine nucleophilicity and redox susceptibility, thereby facilitating the unique functions of cysteine: nucleophilic and redox catalysis, regulation, metal binding, and structural stabilization, on proteins across diverse functional classes (Figure 1-2).[9, 10] The proteins that are discussed in Chapters 2 - 4 contain cysteines that act in several of these functional roles. As an introduction to these diverse functions of cysteine, here we provide prototypical examples of proteins that utilize cysteines for redox catalysis, nucleophilic catalysis, metal binding and regulation. Furthermore, we highlight covalent inhibitors that have been developed to target these functional cysteines to demonstrate the potential of cysteine-reactive small molecules to modulate diverse protein activities.

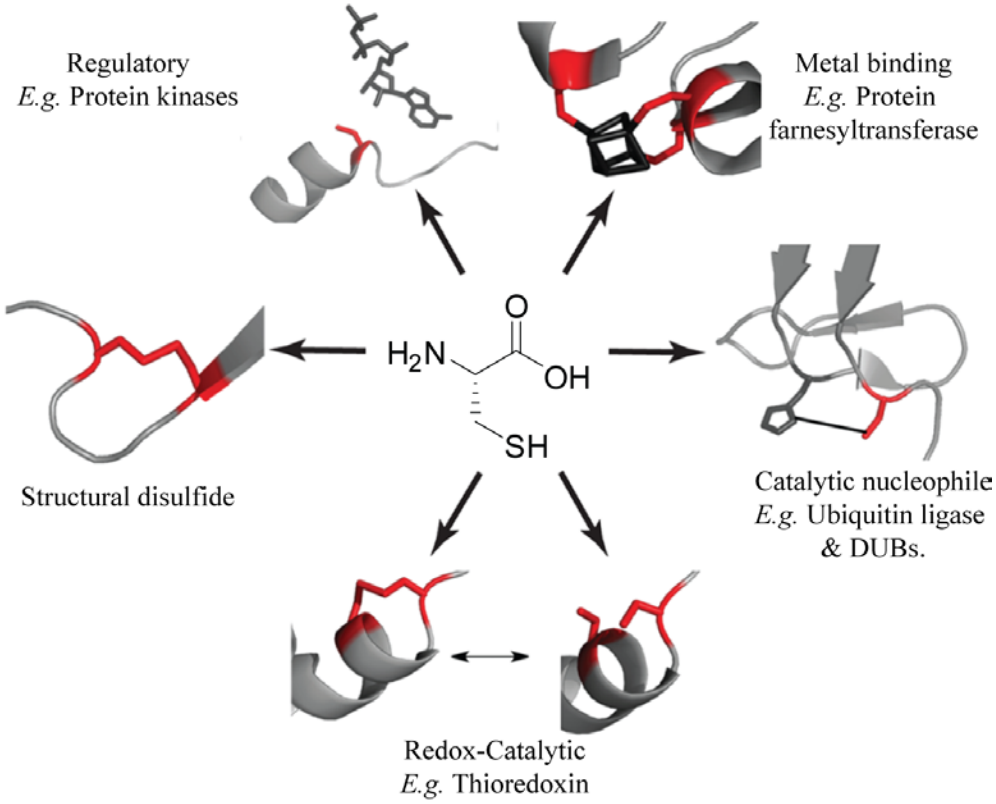

Figure 1-2. Functional roles performed by cysteine residues.

Redox catalytic cysteine residues

One of the most common functions of cysteines is their ability to catalyze redox-reactions, including substrate oxidation/reduction, disulfide bond formation/isomerization, and detoxification of reactive oxygen species.[11] The majority of these proteins belongs to the thiol oxidoreductase family and includes isoforms of thioredoxin, glutaredoxin, peroxiredoxin, and protein disulfide isomerase. Notably, many of these proteins contain a conserved CXXC motif,[12] and approximately half contain thioredoxin folds.[13] Herein, we will focus on thioredoxin, a prototypical member of the thiol oxidoreductase family.

The thioredoxin system is composed of the proteins thioredoxin (Trx) and thioredoxin reductase (TrxR), and together with NADPH[14] constitutes one of the major cellular redox-control systems. Trx1 and TrxR1 comprise the cytoplasmic system, whereas Trx2 and TrxR2 are localized to the mitochondria. The active site of human Trx contains a pair of highly conserved cysteine residues (Cys32 and Cys35), which serve as the center for redox catalysis. The active, dithiol version of Trx reduces a disulfide bond within the protein substrate and is concomitantly oxidized, forming an intramolecular disulfide bond. TrxR shuttles reducing equivalents from NADPH to Trx to recycle the enzyme back to its reduced, active form (Figure 1-3). Interestingly, TrxR is a selenoprotein, which utilizes a Cys/Sec sequence within its active-site to shuttle reducing equivalents from NAPDH to Trx.[15] The thioredoxin system was originally discovered as the essential reducing mechanism for the regeneration of ribonucleotide reductase activity, but since then the functions of Trx have expanded to numerous other cellular pathways. Among the multitude of functions attributed to the Trx/TrxR system are the

defense against oxidative stress, scavenging of reactive oxygen species, and regulation of redox signaling by messengers such as hydrogen peroxide and nitric oxide.[16, 17]

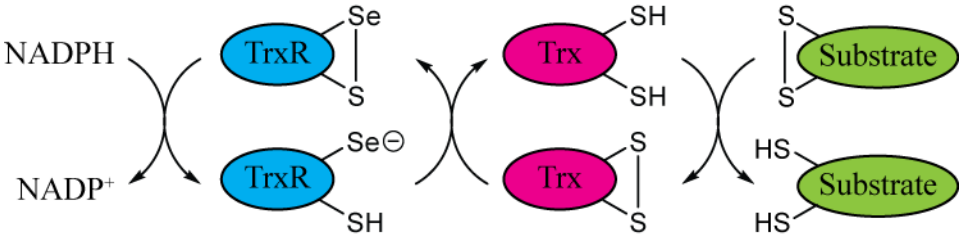

Figure 1-3. The thioredoxin system catalyzes disulfide bond reduction within its protein substrates.

The thioredoxin system is known to play a crucial role in both promoting cellular growth and inhibiting apoptosis, both of which are hallmarks of cancer progression. Toward this end, many inhibitors of Trx have been developed in recent years as a potential therapeutic pathway. One promising candidate, PX-12, is a covalent inhibitor that acts by binding to a cysteine proximal to the active-site (Cys73) of Trx1 through its disulfide moiety (Figure 1-4).[18] PX-12-modified Trx is no longer able to be recycled back to its reduced, active state by TrxR, leading to suppression of the entire thioredoxin system and the induction of apoptosis. This compound underwent phase II clinical trials for cancer treatment but is awaiting further development beyond this stage.[19, 20] PX-12 was shown to be a potent inducer of apoptosis in HL-60 cells, and patients treated with PX-12 demonstrated decreased expression of vascular endothelial growth factor (VEGF), an essential mediator of angiogenesis and cancer metastasis.[21] The continued development and clinical evaluation of PX-12 holds promise for inhibitors directed at Trx and supports the future exploration of covalent inhibitors targeting the redox catalytic cysteines of other thiol oxidoreductases for cancer therapy. Chapter 4 of this thesis

focuses on a panel of chemical probes that targets redox-catalytic cysteine residues within protein disulfide isomerase.

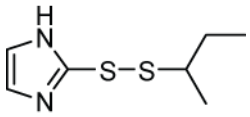

PX-12

Figure 1-4. Structure of the thioredoxin inhibitor PX-12, with its reactive group highlighted in red.

Cysteine residues as catalytic nucleophiles

Unlike redox-catalytic cysteines, cysteine residues that serve as catalytic nucleophiles do not undergo a change of oxidation state during their catalytic cycle. These enzymatic reactions often rely on a catalytic dyad, consisting of a cysteine residue and an adjacent basic residue to stabilize the thiolate anion within the active-site. Most of these cysteines are highly conserved and are found on proteins across diverse enzyme classes. Common examples include the active-site cysteine residue of cysteine proteases (*e.g.* caspases),[22] ubiquitin ligases and hydrolases,[23] phosphatases,[24] metabolic enzymes (*e.g* glyceraldehyde phosphate dehydrogenase),[25] and protein arginine deiminases.[26] Herein, we will highlight the roles of catalytic cysteines within the ubiquitin degradation system.

The ubiquitin degradation system employs cysteine residues acting as catalytic nucleophiles. Proteins are post-translationally tagged with ubiquitin as a cellular mechanism to signal for their degradation. The ubiquitin-mediated degradation system consists of the conserved 76-amino-acid protein ubiquitin, a series of ubiquitin ligases (E1, E2, and E3), deubiquitinases (DUBs), and the 26S-proteosome (Figure 1-5). The

ubiquitin ligases conjugate the C-terminus of ubiquitin to the ε-amino group of a lysine residue within the substrate protein, and those substrates tagged with a polyubiquitin chain are subsequently directed to the proteasome for degradation. DUBs modulate this process by removing ubiquitin from tagged proteins. Both ubiquitin ligases (E1, E2 and HECT E3) and DUBs act through cysteine residues acting as catalytic nucleophiles.

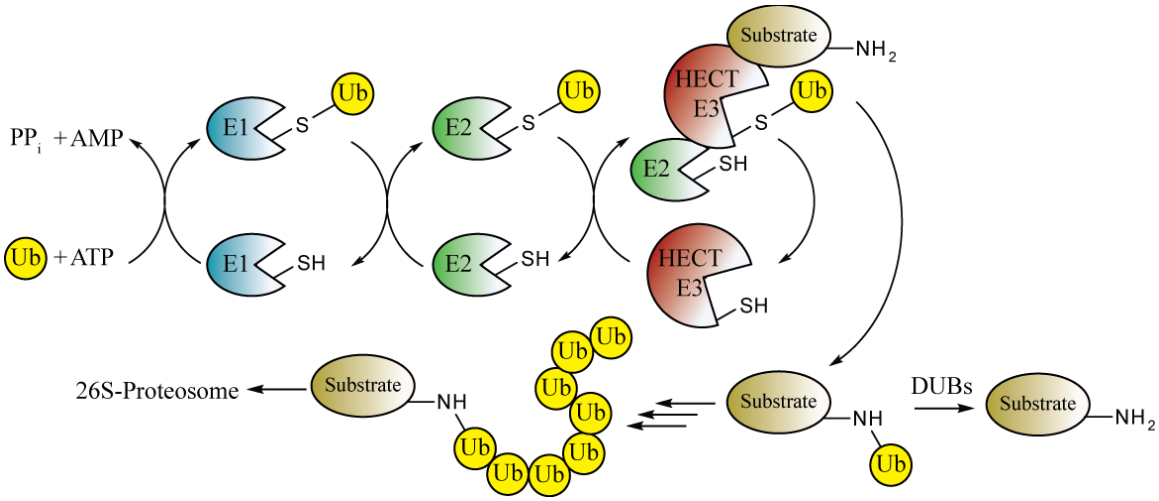

Figure 1-5. Ubiquitin-mediated protein degradation is comprised of a series of ubiquitin ligases (E1s, E2s, and HECT E3s) and deubiquitinating enzymes (DUBs) that possess catalytic cysteine residues.

A series of three ubiquitin ligases (E1, E2, an E3) act sequentially to conjugate ubiquitin to its substrate protein. First, a single ubiquitin is coupled to the ubiquitin-activating enzyme E1 through an ATP-dependent reaction. ATP binds first, followed by ubiquitin, resulting in an ubiquitin adenylate intermediate that is susceptible to nucleophilic attack by the proximal catalytic cysteine to generate a thioester.[27, 28] After activation, the ubiquitin is transferred to the cysteine nucleophile of an ubiquitin-conjugating enzyme E2 to produce another thioester intermediate.[27] Notably, unlike other

cysteine nucleophiles, the catalytic cysteine in the E2 active site does not contain a nearby basic residue (within 6 Å) to stabilize the nucleophilic thiolate anion.[29] One theory is the binding of E1 or E3 assembles a complex that provides the correct positioning of the necessary charged residues to facilitate ubiquitin transfer.[27] The organization of the ubiquitin ligation system is hierarchical: a single E1 couples with a limited number of E2s that interact with a larger subset of E3s specific for a diverse panel of substrate proteins. The E3s are grouped into 4 classes based on common structural and biological features, but only the Homologue of E6-AP C Terminus (HECT) E3s utilize a catalytic cysteine for its function. The HECT E3s form a complex with both an E2 and a substrate, after which the ubiquitin is sequentially transferred to the cysteine in the HECT E3 and finally to the lysine side chain on the substrate protein. Ubiquitination is a tightly regulated process mediated primarily by an intricate network of protein-protein interactions between the E1, E2, and E3 proteins and their substrate proteins.

Deubiquitinases (DUBs) further modulate ubiquitin-mediated protein degradation. Of the 5 known classes of DUBs, 4 are papain-like cysteine proteases and contain a canonical catalytic triad consisting of a nucleophilic cysteine residue adjacent to two histidines.[23] These proteases facilitate a variety of functions, including the activation of ubiquitin proproteins, the rescue of ubiquitin trapped by endogenous electrophiles, and the removal of ubiquitin from modified proteins. Because ubiquitin-mediated protein degradation governs many essential cellular functions, the activity of DUBs must be tightly regulated to ensure these processes are carried out definitively. Known mechanisms to regulate DUB activity include posttranslational modifications, transcriptional regulation, conformational changes, and cellular sequestration.[30]

Ubiquitin-mediated protein degradation is critical for maintaining protein homeostasis and thereby governs numerous cellular processes, including cell growth and apoptosis.[31, 32] As a result, a tremendous focus has been placed on the development of chemical regulators of ubiquitin-mediated protein degradation as therapeutics for disease pathways such as cancer.[33] Toward this end, the design of cysteine-reactive inhibitors for E1, E2, HECT E3s, and DUBs represents one promising approach.[34] A pyrozone derivative, PYR41, represents a successful example of a cysteine-reactive covalent inhibitor of E1 (Figure 1-6).[35] PYR41 has been shown to be cysteine-reactive, but unfortunately the structure of the resulting covalent adduct is poorly defined. This compound was shown to stabilize p53 in cells, and a related compound demonstrated anti-leukemic activity in a mouse cancer model.[36] Although these data are still preliminary, it provides promising support for the application of cysteine-reactive small molecules to target other proteins within the ubiquitin-mediated degradation pathway. Within this thesis, a chemical probe that targets the catalytic cysteine within GSTO1 will be detailed within Chapter 2.

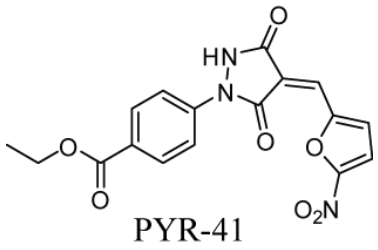

PYR-41

Figure 1-6. Structure of the cysteine-reactive E1 ubiquitin ligase inhibitor, PYR-41.

Metal-binding cysteine residues

A significant number of proteins bind metal ions to serve diverse functional roles including structural stabilization, catalysis, and regulation of protein activity. Cysteine is

one of the most common metal-binding residues within protein scaffolds, along with histidine, aspartate, and glutamate. Due to the multiple oxidation states available to the sulfur atom, cysteine is able to accommodate a large number of bonds and geometries resulting in a myriad of possible metal complexes. Because the cysteine thiolate is a "soft" ligand, it preferentially binds strongly to "soft" metals including $Fe^{2+/3+}$, Zn^{2+}, Cd^{2+}, and Cu^{+}.[9, 37] Because of the large diversity of putative metal-cysteine complexes, they facilitate a wide-range of protein functions, including structure, catalysis, and regulation. Herein, we will highlight the metal binding cysteine residue within protein farnesyltransferases (FTase) and its contribution to catalysis.

FTase is part of the prenyltransferase protein family and catalyzes the post-translational addition of the 15-carbon farnesyl isoprenoid to cysteine residues on proteins such as Ras, Rho, and Rab.[38, 39] The isoprenoid is attached through a thioether linkage to a cysteine residue within a C-terminal CaaX peptide and is required for proper protein function by mediating membrane association and protein-protein interactions.[40] A Zn^{2+} is coordinated to Asp297, Cys299, and His362 within the active-sit of the β-subunit of FTase (Figure 1-7a).[41] The cysteine residue of the protein substrate coordinates to the Zn^{2+}, displacing either a water or Asp ligand. The adjacently bound farnesyl diphosphate is now vulnerable to nucleophilic attack by the Zn^{2+}-activated thiol, resulting in the release of inorganic phosphate and the farnesylated protein (Figure 1-7b).[42, 43]

As discussed in Chapter 3, global methods to identify metal-binding cysteines, especially those with transient binding and low affinity, are lacking., Chapter 3 of this thesis illustrates a novel chemical proteomic platform utilizing cysteine-reactive probes to identify metal-binding cysteine residues, in particular, those that chelate Zn^{2+}.

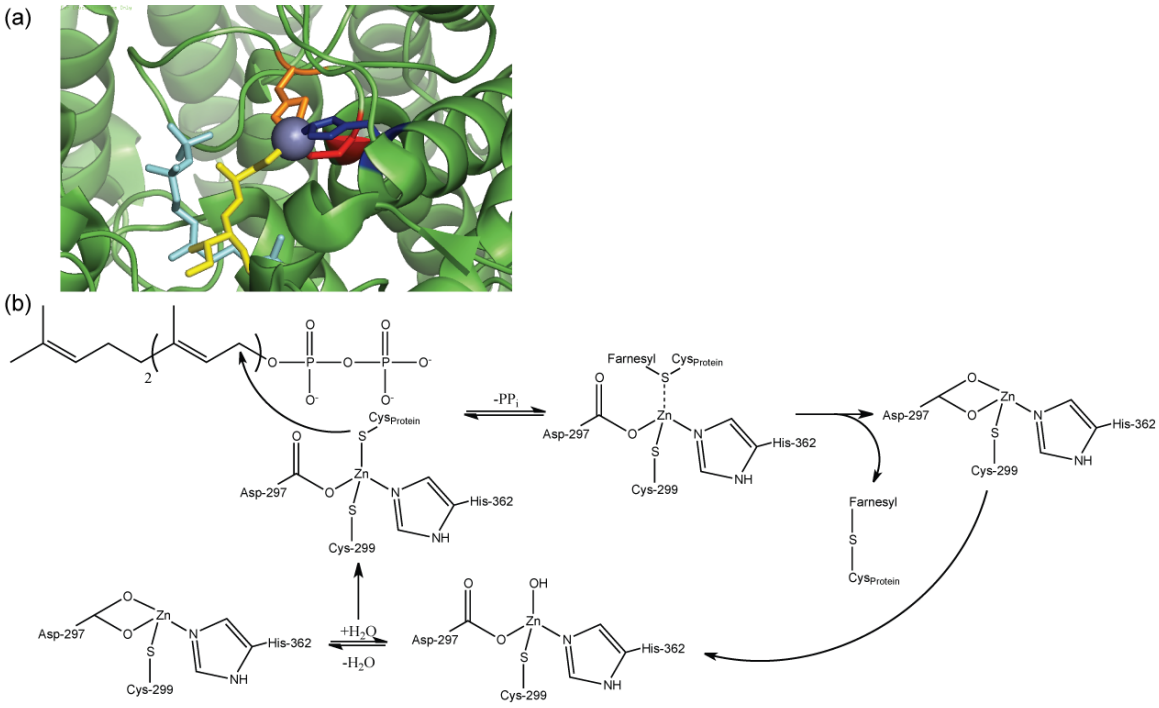

Figure 1-7. (a) The active-site of FTase contains a Zn2+ (purple) coordinated to Asp297 (orange), Cys299 (red), His362 (blue), and the thiol-containing target peptide (yellow) adjacent to the farnesyl diphosphate (cyan) (PDB ID: 1JCQ). (b) The cysteine of the target peptide is able to displace either an Asp297 or water ligand. The now-activated thiol forms a thioether linkage to the farnesyl diphosphate and is released by ligand exchange with Asp297 or water. Figure adapted from Pace *et al*.[44] and Ramos *et al*.[43]

Cysteine residues as regulators of protein functions

Regulatory cysteines do not directly act in catalysis; however, due to their proximity to either the active-site or surfaces involved in essential protein-protein interactions, these cysteines are key modulators of protein activities. Modification of these cysteine residues by reactive oxygen species or endogenous or exogenous

electrophiles regulates protein activity. A key example of proteins utilizing regulatory cysteines is the kinase family.

Protein kinase activity is regulated by cysteine residues

Sequencing the human genome, coupled with detailed structural information, has provided significant insight into structural and functional homology between the 518 human protein kinases. Numerous bioinformatics and inhibitor screening efforts revealed the presence of cysteine residues within the ATP-binding pocket of a large number of protein kinases (~200 out of the 518). These cysteines have recently been reviewed and were classified into five groups based upon the structural location of the each cysteine.[45] Group 1 kinases contain a cysteine within the glycine-rich or P-loop (*e.g.*, FGFR); group 2 kinases are those with cysteines positioned at the roof of the ATP-binding pocket (*e.g.*, RSK); group 3 kinases present a cysteine in the hinge region and front pocket (*e.g.*, EGFR); group 4 kinases are the most common and contain a cysteine adjacent to the DFG-motif (*e.g.*, ERK2); and group 6 cysteines have a cysteine located in the activation loop (*e.g.*, IKKα) (Figure 1-8).[46-49] Several of these cysteines were identified by isoTOP-ABPP,[1] hinting at their reactive nature.

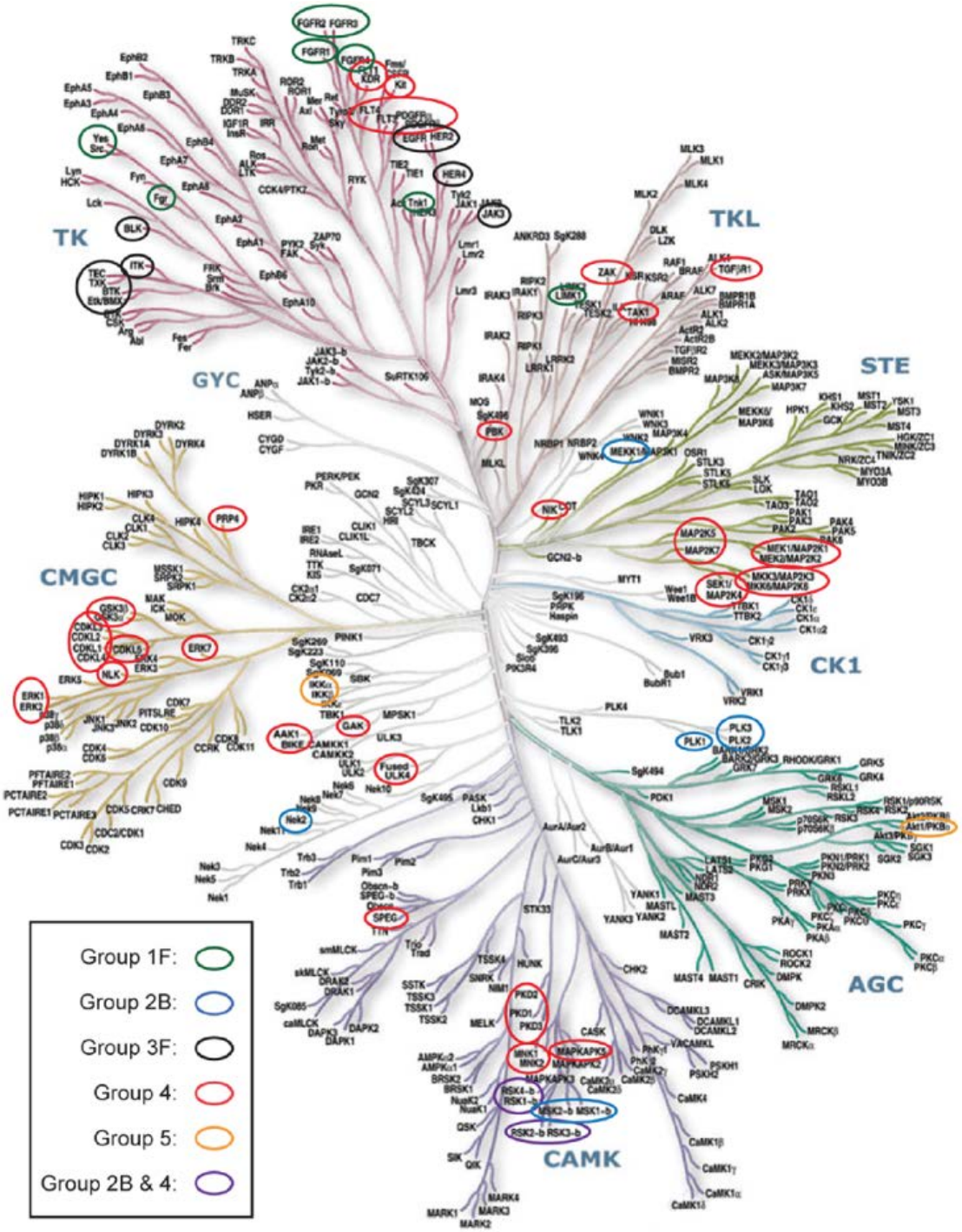

Figure 1-8. Human protein kinases with reactive cysteine residues were divided into five groups based on structural location: Group 1B (green), Group 2B (blue), Group 3F (black), Group 4 (red), and Group 5 (orange).

Protein kinases, many of which possess regulatory cysteine residues, play an important role in the progression of cancer.[46] In particular, epidermal growth factor receptor (EGFR), a receptor tyrosine kinase, is overexpressed in several cancer types, including breast, lung, esophageal, and head and neck.[50] Through phosphorylation-mediated signaling cascades, EGFR and its family members modulate growth, signaling, differentiation, adhesion, migration, and survival of cancer cells.[50, 51] Notably, Cys797 of EGFR is found close to the hinge region and was found to be sulfenylated in EGF-stimulated cells. Oxidation of Cys797 enhances tyrosine kinase activity, exemplifying its role as a regulatory residue: one that is not involved in catalysis but modulates protein activity.[52] Furthermore, the identification of this regulatory residue sparked the development of cysteine-reactive covalent inhibitors of EGFR. Four of these (HKI-272, CI-1033, EKB-569, and PF-00299804) are currently undergoing clinical trial, and one (Afatinib) has been approved in the United states as a first-line treatment for metastatic non-small cell lung carcinoma (Figure 1-9).[53, 54] An acrylamide electrophile was incorporated into all these inhibitors and undergoes a Michael addition with the reactive cysteine to form a covalent adduct.[55]

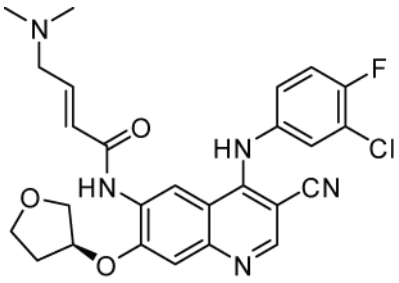

Affitinib

Figure 1-9. Structure of the EGFR inhibitor, Afatinib.

In addition to EGFR, cysteine-reactive small molecule inhibitors have been developed for both ribosomal s6 kinase (RSK) and extracellular signal-related kinase (ERK), although these have not yet advanced to clinical trials. Selective RSK inhibitors have been developed through incorporation of a cysteine-reactive fluoromethyl ketone electrophile into a scaffold of a pan-kinase inhibitor.[48] These compounds have been recently altered to produce slow dissociating, covalent inhibitors that may help circumvent toxicity issues typically encountered through irreversible inhibition.[56] Natural products of the resorcylic acid lactone family contain a *cis*-enone that forms a Michael adduct with the reactive cysteine within the ERK family.[47] Together, these studies demonstrate that reactive cysteines located at diverse positions within the ATP-binding pocket of kinases may be exploited in the development of covalent inhibitors. Traditional kinase inhibitors typically encounter high chemical resistance due to mutations within the ATP-binding site. This new approach displays potential to overcome any evolved resistance, as evidenced by the covalent EGFR inhibitors ability to still inhibit the protein with a mutation of the gatekeeper threonine (T790M).[57]

Conclusion

Cysteine residues are able to facilitate diverse protein functions that contribute to essential cellular processes. Electrophilic small molecules can be utilized to characterize and modulate cysteine-mediated protein activities across diverse protein classes. The expansion of new cysteine-reactive probes for other protein classes is essential to the continued annotation of functional cysteines. This thesis will focus on a cysteine-reactive inhibitor of the catalytic cysteine of GSTO1 that selectively targets apoptotic cell

populations (Chapter 2), a chemical-proteomic platform to identify Zn^{2+}-binding cysteine residues (Chapter 3), and use of a panel of cysteine-reactive inhibitors of the redox-catalytic cysteines in protein disulfide isomerase to interrogate the role of this protein in cancer progression (Chapter 4).

References

1. Weerapana, E.; Wang, C.; Simon, G. M.; Richter, F.; Khare, S.; Dillon, M. B. D.; Bachovchin, D. A.; Mowen, K.; Baker, D.; Cravatt, B. F., Quantitative Reactivity Profiling Predicts Functional Cysteines in Proteomes. *Nature* 2010, 468, 790-795.

2. Evans, M. J.; Cravatt, B. F., Mechanism-Based Profiling of Enzyme Families. *Chem. Rev.* 2006, 106, 3279-3301.

3. Pe'er, I.; Felder, C. E.; Man, O.; Silman, I.; Sussman, J.; Beckmann, J. S., Proteomic Signatures: Amino Acid and Oligopeptide Compositions Differentiate Among Phyla. *Proteins* 2004, 54, 20-40.

4. Marino, S. M.; Gladyshev, V. N., Cysteine Function Governs its Conservation and Degeneration and Restricts its Utilization on Protein Surfaces. *J. Mol. Biol.* 2010, 404, 902-916.

5. Jordan, I. K.; Kondrashov, F. A.; Adzhubel, I. A.; Wolf, Y. I.; Koonin, E. V.; Kondrashov, A. S.; Sunyaev, S., A Universal Trend of Amino Acid Gain and Loss in Protein Evolution. *Nature* 2005, 433, 633-638.

6. Wu, H.; Ma, B.-G.; Zhao, J.-T.; Zhang, H.-Y., How Similar are Amino Acid Mutations in Human Genetic Diseases and Evolution. *Biochem. Biophys. Res. Commun.* 2007, 362, 233-237.

7. Bulaj, G.; Kortemme, T.; Goldenberg, D. P., Ionization-Reactivity Relationships for Cysteine Thiols in Polypeptides. *Biochemistry* 1998, 37, 8965-8972.

8. Harris, T. K.; Turner, G. J., Structural Basis of Perturbed pKa values of catalytic groups in enzyme active sites. *IUBMB Life* 2002, 53, 85-98.

9. Giles, N. M.; Watts, A. B.; Giles, G. I.; Fry, F. H.; Littlechild, J. A.; Jacob, C., Metal and Redox Modulation of Cysteine Protein Function. *Chem. Biol.* 2003, 10, 677-693.

10. Pace, N. J.; Weerapana, E., Diverse Functional Roles of Reactive Cysteines. *ACS Chem. Biol.* 2013, 8, 283-296.

11. Fomenko, D. E.; Marino, S. M.; Gladyshev, V. N., Functional Diversity of Cysteine Residues in Proteins and Unique Features of Catalytic Redox-Active Cysteines in Thiol Oxidoreductases. *Mol. Cells* 2008, 26, 228-235.

12. Chivers, P. T.; Prehoda, K. E.; Raines, R. T., The CXXC Motif: A Rheostat in the Active Site. *Biochemistry* 1997, 36, 4061-4066.

13. Martin, J. L., Thioredoxin-A Fold for All Reasons. *Structure* 1995, 3, 245-250.

14. Luthman, M.; Holmgren, A., Rat Liver Thioredoxin and Thioredoxin Reductase: Purification and Characterization. *Biochemistry* 1982, 21, 6628-6633.

15. Arner, E. S., Focus on Mammalian Thioredoxin Reductases-Important Selenoproteins with Versatile Functions. *Biochim. Biophys. Acta* 2009, 1790, 495-526.

16. Nordberg, J.; Arner, E. S., Reactive Oxygen Species, Antioxidants, and the Mammalian Thioredoxin System. *Free Radicals Biol. Med.* 2001, 31, 1287-1312.

17. Holmgren, A.; Lu, J., Thioredoxin and Thioredoxin Reductase: Current Research with Special References to Human Disease. *Biochem. Biophys. Res. Commun.* 2010, 396, 120-124.

18. Kirkpatrick, D. L.; Kuperus, M.; Dowdeswell, M.; Potier, N.; Donald, L. J.; Kunkel, M.; Berggren, M.; Angulo, M.; Powis, G., Mechanisms of Inhibition of the Thioredoxin Growth Factor System by Antitumor 2-Imidazolyl Disulfides. *Biochem. Pharmacol.* 1998, 55, 987-994.

19. Baker, A. F.; Dragovich, T.; Tate, W. R.; Ramanathan, R. K.; Roe, D.; Hsu, C. H.; Kirkpatrick, D. L.; Powis, G., The Antitumor Thioredoxin-1 Inhibitor PX-12 (1-Methylpropyl 2-Imidazolyl Disulfide) Decreases Thioredoxin-1 and VEGF Levels in Cancer Patient Plasma. *J. Lab. Clin. Med.* 2006, 147, 83-90.

20. Ramanathan, R. K.; Kirkpatrick, D. L.; Belani, C. P.; Friedland, D.; Green, S. B.; Chow, H. H.; Cordova, C. A.; Stratton, S. P.; Sharlow, E. R.; Baker, A.; Dragovich, T., A Phase I Pharocokinetic and Pharmacodynamic Study of PX-12, a Novel Inhibitor of Thioredoxin-1, in Patients with Advanced Solid Tumors. *Clin. Cancer Res.* 2007, 13, 2109-2114.

21. Welsh, S. J.; Williams, R. R.; Birmingham, A.; Newman, D. J.; Kirkpatrick, D. L.; Powis, G., the Thioredoxin Redox Inhibitors 1-Methylpropyl 2-Imidazolyl Disulfide and Pleurotin Inhibit Hypoxia-Induced Factor 1Alpha and Vascular Endothelial Growth Factor Formation. *Mol. Cancer Ther.* 2003, 2, 235-243.

22. Chapman, H. A.; Riese, R. J.; Shi, G. P., Emerging Roles of Cysteine Proteases in Human Biology. *Annu. Rev. Physiol.* 1997, 59, 63-88.

23. Amerik, A. Y.; Hochstrasser, M., Mechanism and Function of Deubiquitinating Enzymes. *Biochim. Biophys. Acta* 2004, 1695, 189-207.

24. Tonks, N. K., Protein Tyrosine Phosphatases: From Genes, to Function, to Disease. *Nat. Rev. Mol. Cell. Biol.* 2006, 7, 833-846.

25. Sirover, M. A., Role of the Glycolytic Protein, Glyceraldehyde-3-Phosphate Dehydrogenase, in Normal Cell Function and in Cell Pathology. *J. Cell. Biochem.* 1997, 66, 133-140.

26. Jones, J. E.; Causey, C. P.; Knuckley, B.; Slack-Noyes, J. L.; Thompson, P. R., Protein Arginine Deiminase 4 (PAD4): Current Understanding and Future Therapeutic Potential. *Curr. Opin. Drug Discovery Dev.* 2009, 12, 616-627.

27. Pickart, C. M., Mechanism Underlying Ubiquitination. *Annu. Rev. Biochem.* 2001, 70, 503-533.

28. Haas, A. L.; Rose, I. A., The Mechanism of Ubiquitination Activating Enzyme. *J. Biol. Chem.* 1982, 257, 10329-10337.

29. Tong, H.; Hateboer, G.; Perrakis, A.; Bernards, R.; Sixma, T. K., Crystal Structure of Murine/Human Ubc9 Provides Insight into the Variability of the Ubiquitin-Conjugating System. *J. Biol. Chem.* 1997, 272, 21381-21387.

30. Reyes-Turcu, F. E.; Ventii, K. H.; Wilkinson, K. D., Regulation and Cellular Roles of Ubiquitin-Specific Deubiquitinating Enzmes. *Annu. Rev. Biochem.* 2009, 78, 363-397.

31. Nalepa, G.; Rolfe, M.; Harper, J. W., Drug Discovery in the Ubiquitin-Proteasome System. *Nat. Rev. Drug Discovery* 2006, 5, 596-613.

32. Vucic, D.; Dixit, V. M.; Wertz, I. E., Ubiquitylation in Apoptosis: A Post-Translational Modification at the Edge of Life and Death. *Nat. Rev. Mol. Cell. Biol.* 2011, 12, 439-452.

33. Bedford, L.; Lowe, J.; Dick, L. R.; Mayer, R. J.; Brownell, J. E., Ubiquitin-Like Protein Conjugation and the Ubiquitin-Proteasome System as Drug Targets. *Nat. Rev. Drug Discovery* 2011, 10, 29-46.

34. Edelmann, M. J.; Nicholson, B.; Kessler, B. M., Pharmacological Targets in the Ubiquitin System Offer New Ways of Treating Cancer, Neurodegenerative Disorders and Infectious Diseases. *Expert. Rev. Mol. Med.* 2011, 13, e35.

35. Yang, Y.; Kitagaki, J.; Dai, R. M.; Tsai, Y. C.; Lorick, K. L.; Ludwig, R. L.; Pierre, S. A.; Jensen, J. P.; Davydov, I. V.; Oberoi, P.; Li, C. C.; Kenten, J. H.; Beutler, J. A.; Vousden, K. H.; Weissman, A. M., Inhibitors of Ubiquitin-Activating Enzyme (E1), a New Class of Potential Cancer Therapeutics. *Cancer Res.* 2007, 67, 9472-9481.

36. Xu, G. W.; Ali, M.; Wood, T. E.; Wong, D.; Maclean, N.; Wang, X.; Gronda, M.; Skrtic, M.; Li, X.; Hurren, R.; Mao, X.; Venkatesan, M.; Beheshti Zavareh, R.; Ketela, T.; Reed, J. C.; Rose, D.; Moffat, J.; Batey, R. A.; Dhe-Paganon, S.; Schimmer, A. D., The Ubiquitin-Activation Enzyme E1 as a Therapeutic Target for the Treatment of Leukemia and Multiple Myeloma. *Blood* 2010, 115, 2251-2259.

37. Dudev, T.; Lim, C., Principles Governing Mg, Ca, and Zn Binding and Selectivity in Proteins. *Chem. Rev.* 2003, 103, 773-787.

38. Zhang, F. L.; Casey, P. J., Protein Prenylation: Molecular Mechanisms and Functional Consequences. *Annu. Rev. Biochem.* 1996, 65, 241-269.

39. Ashar, H. R.; James, L.; Gray, K.; Carr, D.; Black, S.; Armstrong, L.; Bishop, W. R.; Kirschmeier, P., Farnesyl transferase inhibitors block the farnesylation of CENP-E and CENP-F and alter the association of the CENP-E with microtubules. *J. Biol. Chem.* 2000, 275, 30451-30457.

40. Zverina, E. A.; Lamphear, C. L.; Wright, E. N.; Fierke, C. A., Recent advances in protein prenyltransferases: substrate identification, regulation, and disease interventions. *Curr. Opin. Chem. Biol.* 2012, 16, 544-552.

41. Long, S. B.; Hancock, P. J.; Kral, A. M.; Hellinga, H. W.; Beese, L. S., The Crystal Structure of Human Protein Farnesyltransferase Reveals the Basis for Inhibition by CaaX Tetrapeptides and Their Mimetics. *Proc. Nat. Acad. Sci. USA* 2001, 98, 12948-12953.

42. Long, S. B.; Casey, P. J.; Beese, L. S., Reaction Path of Protein Farnesyltransferase at Atomic Resolution. *Nature* 2002, 419, 645-650.

43. Sousa, S. F.; Fernandes, P. A.; Ramos, M. J., Unraveling the Mechanism of the Farnesyltransferase Enzyme. *J. Biol. Inorg. Chem.* 2004, 10, 3-10.

44. Pace, N. J.; Weerapana, E., Zinc-Binding Cysteines: Diverse Functions and Structural Motifs. *Biomolecules* 2014, 4, 419-434.

45. Barf, T.; Kaptein, A., Irreversible Protein Kinase Inhibitors: Balancing the Benefits and Risks. *J. Med. Chem.* 2012, 55, 6243-6262.

46. Zhang, J.; Yang, P. L.; Gray, N. S., Targeting Cancer with Small Molecule Kinase Inhibitors. *Nat. Rev. Cancer* 2009, 9, 28-39.

47. Schirmer, A.; Kennedy, J.; Murli, S.; Reid, R.; Santi, D. V., Targeted Covalent Inactivation of Protein Kinases by Resorcylic Acid Lactone Polyketides. *Proc. Natl. Acad. Sci. U.S.A.* 2006, 103, 4234-4239.

48. Cohen, M. S.; Zhang, C.; Shokat, K. M.; Taunton, J., Structural Bioinformatics-Based Design of Selective, Irreversible, Kinase Inhibitors. *Science* 2005, 308, 1318-1321.

49. Leproult, E.; Barleunga, S.; Moras, D.; Wurtz, J. M.; Winssinger, N., Cysteine Mapping in Conformationally Distinct Kinase Nucleotide Binding Sites: Application to the Design of Selective Covalent Inhibitors. *J. Med. Chem.* 2011, 54, 1347-1355.

50. Seshacharyulu, P.; Ponnusamy, M. P.; Haridas, D.; Jain, M.; Ganti, A. K.; Batra, S. K., Targeting the EGFR Signaling Pathway in Cancer Therapy. *Expert Opin. Ther. Targets* 2012, 16, 15-31.

51. Han, W.; Lo, H. W., Landscape of EGFR Signaling Network in Human Cancers: Biology and Therapeutic Reponse in Relation to Receptor Subcellular Locations. *Cancer Lett.* 2012, 318, 124-134.

52. Paulsen, C. E.; Truong, T. H.; Garcia, F. J.; Homann, A.; Gupta, V.; Leonard, S. E.; Carroll, K. S., Peroxide-Dependent Sulfenylation of the EGFR Catalytic Site Enhances Kinase Activity. *Nat. Chem. Biol.* 2012, 8, 57-64.

53. Singh, J.; Petter, R. C.; Kluge, A. F., Targeted Covalent Drugs of the Kinase Family. *Curr. Opin. Chem. Biol.* 2010, 14, 475-480.

54. Minkovsky, N.; Berezov, A., BIBW-2992, A Dual Receptor Tyrosine Kinase Inhibitor for the Treatment of Solid Tumors. *Curr. Opin. Investig. Drugs* 2008, 9, 1336-1346.

55. Carmi, C.; Lodola, A.; Rivara, S.; Vacondio, F.; Cavazzoni, A.; Alfieri, R. R.; Ardizzoni, A.; Petronini, P. G.; Mor, M., Epidermal Growth Factor Receptor Irreversible Inhibitors: Chemical Exploration of the Cysteine-Trap Portion. *Mini-Rev. Med. Chem.* 2011, 11, 1019-1030.

56. Serafimova, I. M.; Pufall, M. A.; Krishnan, S.; Duda, K.; Cohen, M. S.; Maglathlin, R. L.; McFarland, J. M.; Miller, R. M.; Frodin, M.; Taunton, J., Reversible Targeting of Noncatalytic Cysteines with Chemically Tuned Electrophiles. *Nat. Chem. Biol.* 2012, 8, 471-476.

57. Kwak, E. L.; Sordella, R.; Bell, D. W.; Godin-Heymann, N.; Okimoto, R. A.; Brannigan, B. W.; Harris, P. L.; Driscoll, D. R.; Fidias, P.; Lynch, T. J.; Rabindran, S. K.; McGinnis, J. P.; Wissner, A.; Sharma, S. V.; Isselbacher, K. J.; Settleman, J.; Haber, D. A., Irreversible Inhibitors of the EGF Receptor May Circumvent Acquired Resistance to Gefitinib. *Proc. Natl. Acad. Sci. U.S.A.* 2005, 96, 6161-6165.

Chapter 2

A peptide-based inhibitor of GSTO1 that selectively targets apoptotic cells

A significant portion of the work described in this chapter has been published in:

Pace, N. J.; Pimental, D. R.; Weerapana, E. An Inhibitor of Glutathione *S*-Transferase Omega 1 that Selectively Targets Apoptotic Cells. *Angew. Chem. Int. Ed.* **2012**, *51*, 8365-8368.

Daniel Pimental synthesized a portion of the peptide probe library.

Introduction

Since the mid-1800s, many observations have indicated that cell death plays a considerable role within physiological processes and the development of multicellular organisms. In 1964 the term *programmed cell death* was introduced, proposing that cell death during development is not accidental, but rather follows a sequence of controlled steps leading to locally and temporally defined self-destruction.[1] Kerr, Wyllie, and Currie first coined the term *apoptosis* in 1972 to describe the morphological processes leading to controlled cellular self-destruction.[2] Since this time, apoptosis has been distinguished as an active and defined process that plays an essential role in the development of multicellular organisms and in the regulation and maintenance of cell populations in tissues upon physiological and pathological conditions.[3] While apoptosis is possibly the most frequent form of programmed cell death, it should be noted that other non-apoptotic forms of controlled cell death, such as autophagy and programmed necrosis do exist.[4]

Because apoptosis is such an important biological process, tightly regulated intrinsic and extrinsic signaling cascades have evolved to facilitate its induction. Regardless of the initiating death stimulus or cell type, apoptosis always culminates in the fragmentation of several hundred proteins and DNA. Caspases (Cysteine-dependent aspartate-directed proteases) largely mediate this proteolysis and also activate CAD (caspase-activated DNase) by cleaving its chaperone/inhibitor ICAD (inhibitor of CAD) and allow CAD to fragment chromatin.[5] These caspases have been categorized into two groups based on their function: initiator caspases (caspase-2, 8, 9, 10) and executioner caspases (caspase-3, 6, 7).[6] The executioner caspases perform nearly all the proteolysis, including activation of CAD. To regulate their activity, executioner caspases are

synthesized as inactive zymogens and rely on proteolytic cleavage into a large and small subunit by the initiator caspases to assemble the constitutively active hetero-tetramer. The initiator caspases have long prodomains that, following an apoptotic signal, target them to specific scaffold proteins (Fas-associated protein with death domain (FADD) for caspase-8 & Apoptotic protease activity factor 1 (Apaf-1) for caspase-9) where conformational changes provoke their activation.[5]

While both ultimately converge upon executioner caspase activation, vertebrates possess two distinct apoptosis signaling cascades: an extrinsic death receptor pathway and an intrinsic mitochondrial pathway (Figure 2-1). The death receptor (extrinsic) pathway is triggered by ligand binding to the tumor necrosis factor receptor (TNF-R) superfamily, which contain intracellular "death domains" such as Fas, TNF-related apoptosis-inducing ligand receptor 1 (TRAIL-R1), and TNF-R1. Upon ligand binding, these receptors assemble the DISC (death-inducing signaling complex), within which the FADD adapter protein recruits and activates caspase-8.[7] In certain death receptors, FADD/caspase-8 binding is assisted by the adaptor protein Tumor necrosis factor type 1-associated Death Domain protein (TRADD). Once activated, caspase-8 cleaves the executioner caspases to initiate apoptosis. In the case of the mitochondrial (intrinsic) pathway, internal apoptotic stimuli (growth factor deprivation, exposure to DNA damage, or cancer therapeutics) trigger release of apoptogenic factors, such as cytochrome c, from the mitochondrial intermembrane space to the cytosol. This release induces the binding of Apaf-1 and caspase-9 and assembly of the apoptosome; after which, the now activated caspase-9 cleaves the executioner caspases to initiate apoptosis.[5]

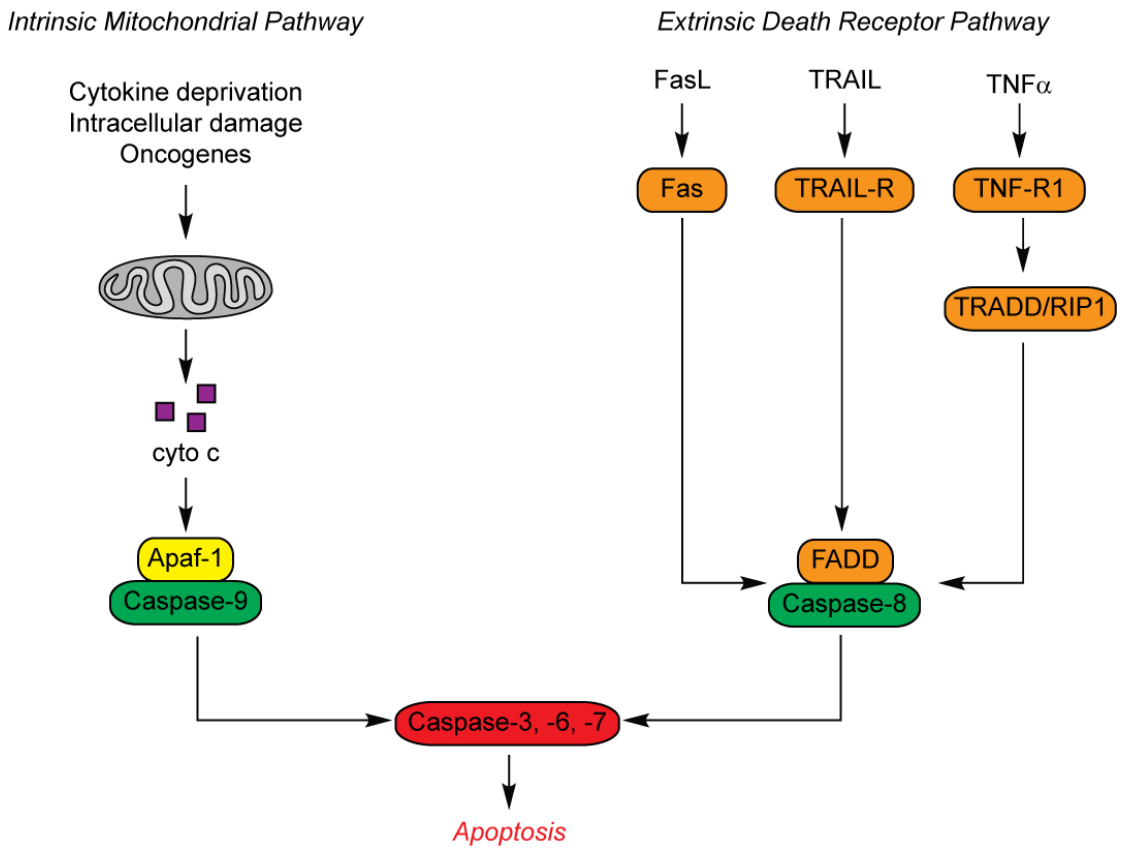

Figure 2-1. The two major apoptotic signaling pathways: the intrinsic or mitochondrial pathway (left) and the extrinsic or death receptor pathway (right). Figure adapted from Strasser et al.[5]

Upon triggering apoptosis, cells experience a variety of characteristic morphological changes, many of which can serve as biomarkers. First, the cell shrinks and becomes deformed, losing contact to its neighboring cells. The cell's chromatin condenses and marginates at the nuclear membrane, the plasma membrane undergoes blebbing or budding, and finally the cell is fragmented into compact membrane-enclosed structures termed *apoptotic bodies*, which contain cytosol, condensed chromatin, and organelles (Figure 2-2). These apoptotic bodies are engulfed by macrophages and removed from the tissue without eliciting an immune response. These morphological

changes are a consequence of characteristic molecular and biochemical events occurring within the apoptotic cell, including proteolysis and degradation of DNA as well as a change in lipid composition of the plasma membrane.[3] Anionic phosphatidylserines (PS), which are typically found within the inner leaflet of the plasma membrane,[8] are exposed to the outer surface of the cell and ultimately signal for the cell's clearance by macrophages.[9, 10] PS exposure is a near-universal event during apoptosis and occurs within a few hours of the apoptotic stimulus.[11] Importantly, apoptosis differs from the necrotic mode of cell-death, where the cells suffer a major insult resulting in loss of membrane integrity, swelling, and rupture of the cells. (Figure 2-2) The cellular contents are released uncontrollably into its surround environment and results in a strong inflammatory response in the corresponding tissue.[12]

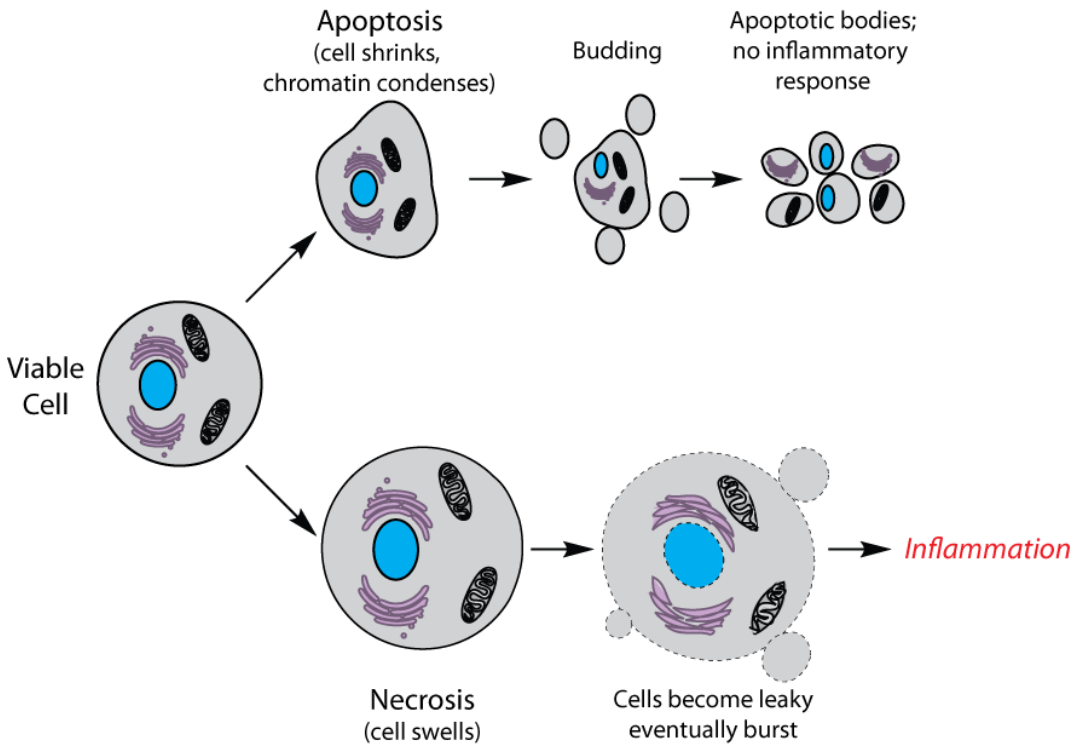

Figure 2-2. Hallmarks of apoptotic and necrotic cell death. Figure modified from Van Cruchten et al.[13]

Dysregulation of apoptotic signaling cascades plays a critical role in disease pathways, especially cancer progression.[14] Thus, cytotoxic cancer agents function by inducing apoptosis, and chemotherapeutic resistance is tightly coupled to defective progression of apoptotic signaling.[15] To identify proteins implicated in maintaining or accelerating apoptosis, it would be advantageous to develop apoptotic cell-selective inhibitors with no effect on healthy cells. Additionally, the use of a covalent inhibitor would allow for subsequent biochemical analysis due to their ability to stably tag a specific protein. Such context-dependent covalent inhibitors would serve as valuable tools to deconvolute protein activities implicated in chemotherapeutic resistance and accelerate apoptosis within a specific cell population.

Furthermore, apoptotic cell-selective covalent modifiers could also be employed as valuable imaging agents of cell death. Because the progression of many diseases functions through an imbalance of apoptosis, the ability to image and assess the degree of apoptosis allows for spatial recognition of a disease, evaluation of the efficacy of treatments, and correlates directly to patient prognosis. For these reasons, protein, peptide, and small molecule-derived imaging agents of apoptosis have been developed. These imaging agents typically function through detection of PS and caspase activity (Table 2-1). Annexin V, a 36 kD protein with strong affinity for PS, conjugated to either fluorophores or radionucleotides is the most highly studied imaging agent for apoptosis within both animal[16] and human models.[17] In addition to its high specificity for apoptotic cells, Annexin V also lacks immunogenicity and *in vivo* toxicity; however, several issues still limit its clinical use. Annexin V suffers from high cost, large size, slow clearance,

moderate stability, and requires micromolar concentrations of Ca^{2+} for optimal binding.[18, 19] In addition to Annexin V, peptide-based PS sensing agents have been developed in the form of cLac peptides[20]. These agents help circumvent some of the limitations of Annexin V but still require further optimization of their PS-affinity and fluorescence. As a whole, these current PS-targeting imaging agents are less than ideal because the binding interactions are non-covalent. Due to their lack of stability, these non-covalent adducts are limited by the types of systems chosen and analytical techniques. Additionally, necrotic cells also expose PS at the cell-surface and distinguishing between necrotic and apoptotic cells can therefore be problematic.

Name	Type	Interaction	Mechanism
Annexin-V	Protein	Non-covalent	PS exposure
cLac peptide	Peptide	Non-covalent	PS exposure
AB50-Cy5	Peptide	Covalent	Caspase activity
LE22-Cy5	Peptide	Covalent	Caspase activity
ApoSense	Small molecule	Non-covalent	Membrane Integrity
YO-PRO1	Small molecule	Non-covalent	Membrane Integrity
GSAO	Peptide	Non-covalent	Membrane Integrity

Table 2-1. Apoptotic cell-selective imaging agents.

Another common strategy to image apoptosis is through detection of caspase activity. Assessing caspase activity provides several inherent advantages over PS-exposure as a biomarker. Since caspase activity is unique to apoptotic cells, off-target signals by healthy or necrotic cells are of no concern. In addition, active caspases possess a hyperreactive cysteine residue that can be exploited as a handle for covalent modification. This covalent modification would allow for subsequent target detection through biochemical assays, which is not available for those agents that bind through non-covalent interactions. Cysteine-reactive acyloxymethyl ketone (AOMK)

electrophiles have been conjugated to caspase-directed peptide sequences to afford selective probes for caspase activity.[21] These initial covalent inhibitors have been further optimized to produce AB50-Cy5 and LE22-Cy5 (Figure 2-3), both of which are effective imaging agents of apoptosis *in vivo*.[19, 22] AB50-Cy5 was utilized to evaluate the degree of apoptosis within a tumor treated with the apoptosis-inducing monoclonal antibody, Apomab.[19] Through use of LE22-Cy5, the signaling pathway that triggers caspase-6 activity was further deconvoluted.[22] Together, these peptide-based inhibitors show the capacity to evaluate apoptosis *in vitro* and *in vivo* and show promise as imaging agents, evaluators of potential drugs, and as tools to deconvolute apoptotic signaling pathways. While these peptides represent a major achievement, their off-target reactivity with other potent cysteine proteases, such as legumain, must still be addressed.

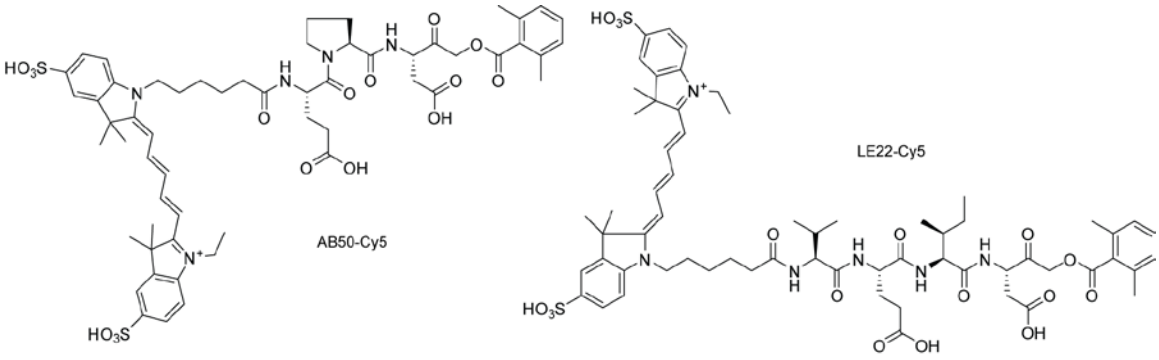

Figure 2-3. Structures of AB50-Cy5 and LE22-Cy5, probes from caspase activity.

We sought to expand the available apoptotic-cell selective covalent inhibitors for proteins beyond caspases to serve as tools to interrogate a protein's role within apoptosis. We also hoped to improve upon the properties of these covalent inhibitors in hopes of applying them as imaging agents. In order to achieve apoptotic-cell selectivity, we sought to exploit the characteristic changes in plasma membranes composition during apoptosis.

In a healthy cell, phosphatidylcholine and sphingomyelin are mainly present in the outer leaflet of the plasma membrane, whereas PS is restricted to the inner leaflet.[8] Cell membranes also contain phosphatidylinositol and phosphatidylethanolamine, which can be found distributed within both the inner and outer leaflet.[8] Upon induction of apoptosis, a calcium-dependent lipid scramblase, Xk-Related Protein 8 (Xkr8), is activated and randomly re-distributes lipids throughout the inner and outer leaflets, resulting in the traditionally observed PS exposure.[9, 11, 23] Proteins such as careticulin, annexin I, and intercellular adhesion molecule 3 (ICAM3) also translocate to the surface of the cell and are thought to serve as receptors.[24] Many membrane proteins also experience altered glycosylation patterns that are thought to play in role in extracellular signaling of macrophages to clear apoptotic debris.[25] Additionally, specific triggers during apoptosis disrupt the ion gradient and results in a depolarization of the plasma membrane potential.[26] Together, these changes result in a loss of membrane integrity and permits distinct small molecules to now be internalized.[27] This phenomenon has been exploited in the development of dyes to selectively detect apoptotic cells, such ApoSense,[28] YO-PRO1,[29] and GSAO.[30] The green fluorescent YO-PRO1 dye was found to preferentially accumulate in apoptotic cells (Figure 2-4).[29, 31] Similarly, an organoarsenic peptide-based agent, GSAO, was shown to be internalized into apoptotic cells at the stage at which plasma membrane integrity is compromised (Figure 2-4).[30] The mechanism of internalization of these molecules has yet to be determined, but future studies should aim to determine whether selectively permeable molecules enter by passive diffusion or active transport and which specific changes to the plasma membrane permit their internalization.

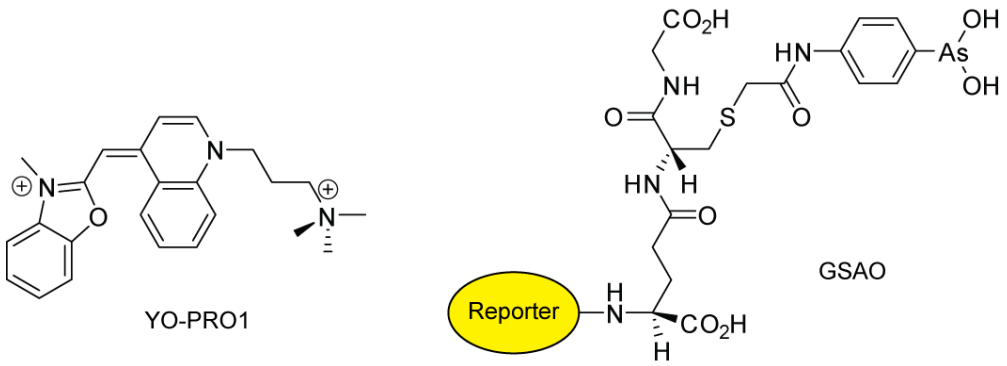

Figure 2-4. Structures of selectively permeable YO-PRO-1 and GSAO.

Although a correlation between molecular structure and apoptotic cell-permeability has yet to be achieved, the tri-peptide backbone of the organoarsenic agent suggested that small peptides could serve as a vehicle for internalization. Since many cysteine-mediated protein activities are known to be hyperactivated in apoptotic cells (*e. g.* caspases), we hypothesized that combining tri/tetrapeptide-based motifs with cysteine-reactive electrophiles will afford us chemical probes that covalently target proteins in apoptotic cell populations. In an effort to test this hypothesis, we aimed to synthesize a library of tri/tetrapeptides conjugated to cysteine-reactive electrophiles and screen the library to identify apoptotic cell-selective inhibitors of cysteine-mediated protein activities (Figure 2-5). Previously, a peptide-based library of chloroacetamides was shown to demonstrate intriguing proteome-labeling patterns, although these peptides were not evaluated in whole cells.[32] This work would expand upon this previous study by exploring protein labeling by cysteine-reactive peptides within both healthy and apoptotic cells, with the aim of developing an apoptotic-cell selective inhibitor.

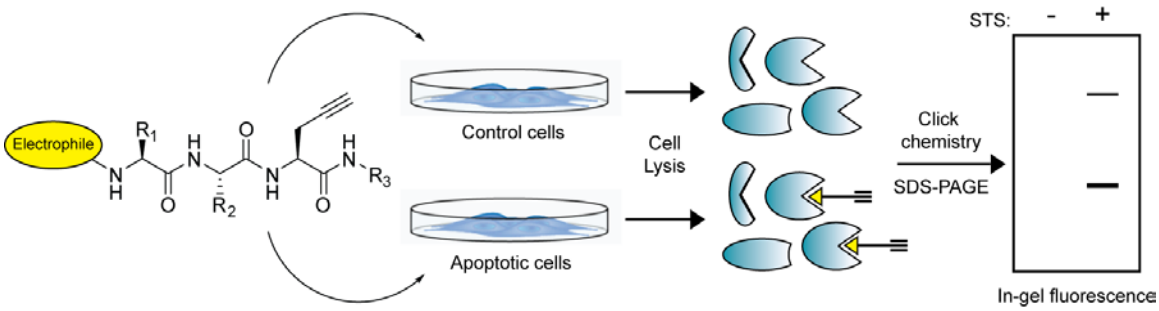

Figure 2-5. Proposed strategy for an apoptotic cell-selective inhibitor based on a peptide scaffold.

Results and Discussion

Synthesis of cysteine-reactive peptide library

The peptides were synthesized on solid-support using standard Fmoc-based solid-phase peptide synthesis (SPPS), and the acrylamide and sulfonate ester electrophiles were subsequently installed on resin (Figure 2-6).

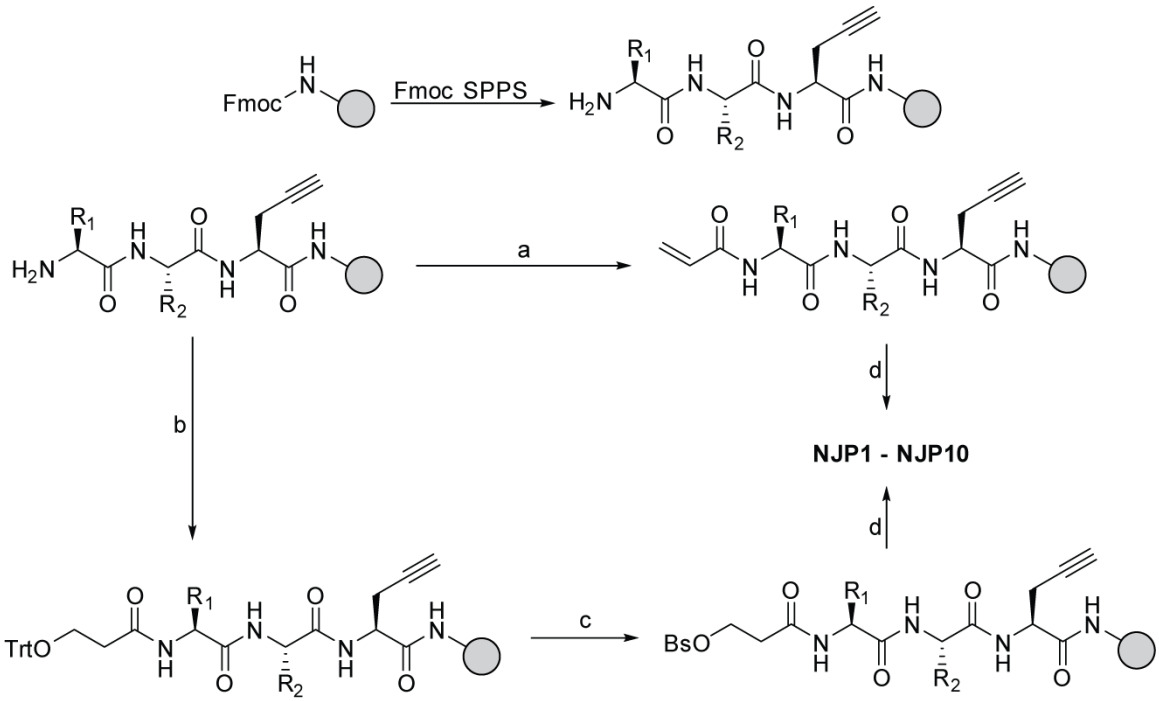

Figure 2-6. Synthetic route to cysteine-reactive peptide probes NJP1 – NJP10.[a]

[a]Reagents and conditions: (a) acrylic acid, PyBOP, DIPEA, DMF, rt; (b) 3-(trityloxy)propanoic acid, PyBOP, DIPEA, DMF, rt; (c) 1% TFA, 2% TIS, DCM, rt; benzene sulfonyl chloride, NEt_3, DCM, rt; (d) 90% TFA, 5% water, 2.5% DCM, 2.5% TIS.

A synthesized 3-(trityloxy)propanoic acid linker, upon deprotection, provided an alcohol for the addition of the sulfonate ester. This route generated the peptide-based chemical probes NJP1 – NJP10, each containing a variable peptide sequence to exploit the inherent structural diversity of commercially amino acids. An alkyne handle was incorporated in the form of a propargylglycine residue within the peptide for subsequent enrichment and visualization through click chemistry. The peptide scaffolds were conjugated to either an acrylamide or sulfonate-ester electrophile (Figure 2-7), both of which have been shown to be highly reactive towards cysteine residues.[33] Yields of peptides range from 6 – 40%.

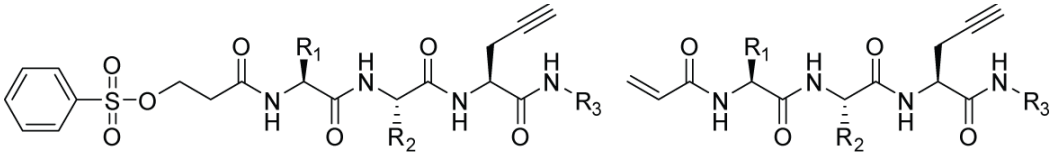

NJP1 - NJP5

Compound:	R_1:	R_2:	R_3:
NJP1	Phe	Phe	Lys
NJP2	Ile	Gly	H
NJP3	Val	Phe	H
NJP4	Leu	Asn	H
NJP5	Ala	Trp	H

NJP6 - NJP10

Compound:	R_1:	R_2:	R_3:
NJP6	Phe	Phe	Lys
NJP7	Ile	Gly	H
NJP8	Val	Phe	H
NJP9	Leu	Asn	H
NJP10	Ala	Trp	H

Figure 2-7. Library of sulfuonate ester (NJP1-5) and acrylamide (NJP6-10) electrophile-bearing peptides utilized in a screen for apoptotic-cell selective inhibitors.

Evaluation of the peptide inhibitor library

NJP1 – NJP10 were evaluated for apoptosis-specific labeling events in HeLa cells. Cells were first incubated with DMSO as a control or staurosporine (STS), a broad-spectrum kinase inhibitor[34] that is thought to induce apoptosis through caspase-3 activation,[35] and were subsequently treated with the peptides by adding each directly to the media. The cells were lysed, subjected to click chemistry to conjugate a fluorophore in the form of rhodamine azide (Rh-N_3), and analyzed by in-gel fluorescence (Figure 2-8).[36]

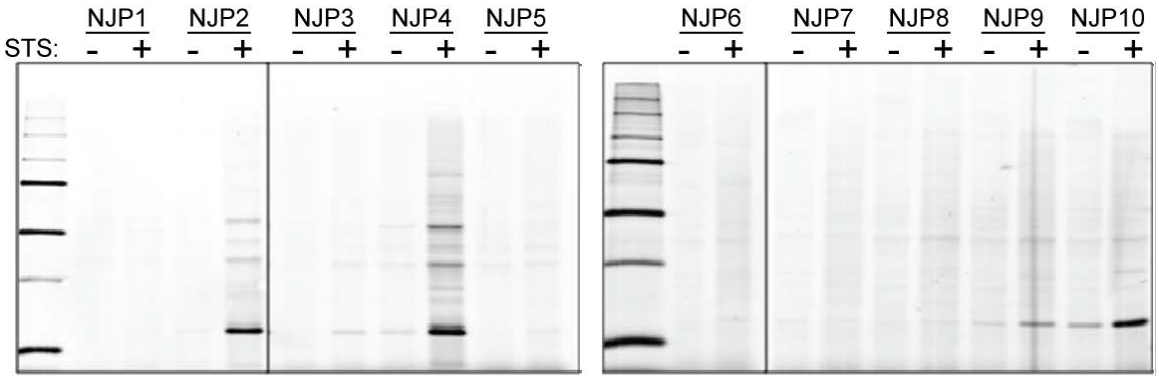

Figure 2-8. In-gel fluorescence analysis of control and apoptotic HeLa lysates treated with peptide-based probes NJP1 - 10.

Our aim was to identify a peptide from the initial 10-member library that demonstrated labeling of a single protein exclusively within apoptotic cells. Initially, three of our peptides (NJP2, NJP4, and NJP10) appeared to be of interest. In the case of NJP4, significant labeling of multiple proteins within the apoptotic cells was less than desirable, as we wanted our inhibitor to be selective for a specific protein. On the other hand, NJP10 did display labeling of a single protein within the STS-treated cells, but

unfortunately a significant signal was also observed within the untreated cells. Fortunately, NJP2 (Figure 2-9a) satisfied both of these criteria, displaying significant labeling of a single 28 kD protein in apoptotic cells with no significant signal within healthy cells (Figure 2-9b). To further characterize this unique labeling profile, we performed a time-course analysis of STS treatment while monitoring the extent of apoptosis by DNA fragmentation (Figure 2-9c). The intensity of protein labeling by NJP2 increased proportionally with the progression of apoptosis.

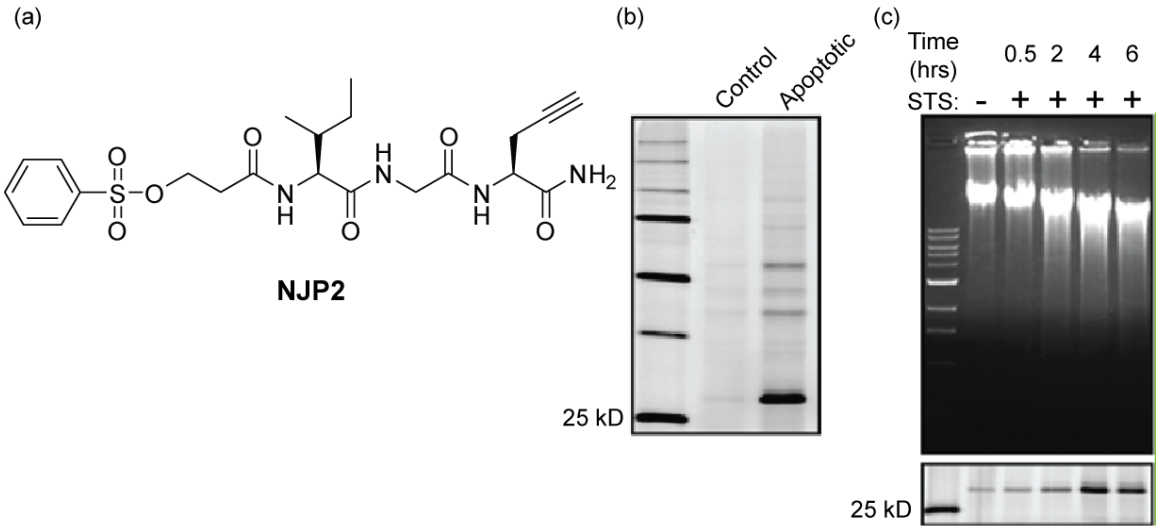

Figure 2-9. (a) The structure of NJP2. (b) In-gel fluorescence analysis of control and apoptotic HeLa cells treated with NJP2. (c) Time-course treatment of HeLa cells with STS. Cells were subjected to DNA fragmentation and in-gel fluorescence from NJP2 labeling at each time point.

To further substantiate this apoptotic cell-selective labeling, we extended this platform across different cell lines and apoptosis-inducing drugs. Control and STS-treated Jurkat cells were subjected to in-gel fluorescence after NJP2-treatment, and displayed the same differential labeling pattern (Figure 2-10a). Moreover, STS was

replaced with camptothecin (CPT), a DNA-topoisomerase inhibitor that triggers apoptosis through the resulting DNA damage,[37] and confirmed that the labeling event still occurs under other chemically induced models of apoptosis (Figure 2-10b).

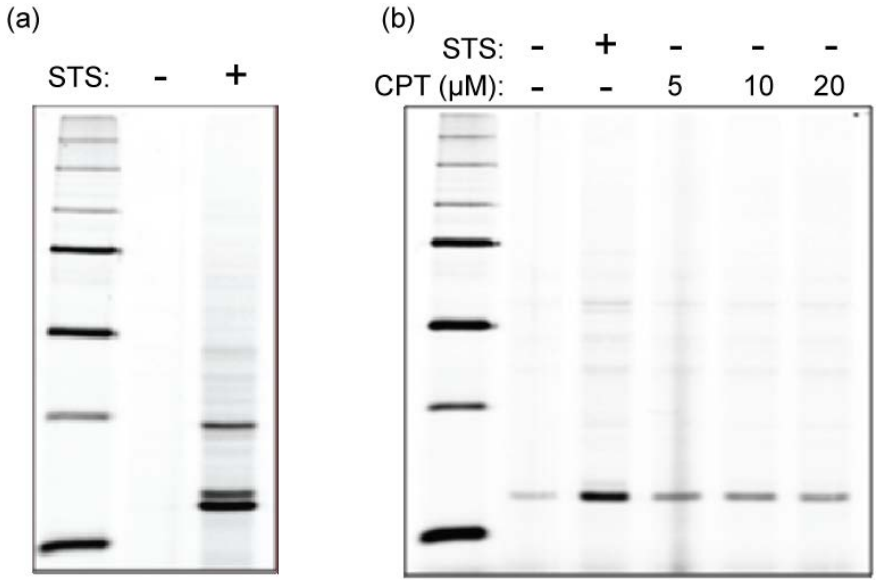

Figure 2-10. (a) In-gel fluorescence analysis of probe labeling by NJP2 in Jurkat cells. (b) Probe labeling by NJP2 within HeLa cells incubated at various concentrations of CPT.

Identification of the protein target of NJP2

Next, we sought to identify the major 28 kD target of NJP2. NJP2-labeled lysates underwent click chemistry to conjugate biotin-azide, followed by purification on streptavidin beads, on-bead trypsin digestion, and LC/LC-MS/MS analysis.[38] The proteins identified in NJP2-treated lysates were compared to a DMSO-treated control. This analysis revealed glutathione *S*-transferase omega 1 (GSTO1) as the major protein target of NJP2, since high spectral counts (142 and 155) were observed in duplicate NJP2-labeled samples, with no spectral counts in the DMSO-treated samples (Table 2-2).

The molecular weight of GSTO1 (27,566 Da) also coincides with the observed band migration during in-gel fluorescence analysis (Figure 2-9b).

		Spectral Counts				
Protein	Molecular Weight	No probe			NJP-2 treated	
IPI00019755 - Gene_Symbol=GSTO1 Glutathione transferase omega-1	27566	0	0	0	142	125
IPI00086909 - Gene_Symbol=LOC440917 similar to 14-3-3 protein epsilon	29603	0	0	0	7	4
IPI00013679 - Gene_Symbol=DUT Isoform DUT-M of Deoxyuridine 5'-triphosphate nucleotidohydrolase	26706	0	3	0	5	5
IPI00220301 - Gene_Symbol=PRDX6 Peroxiredoxin-6	25035	0	0	6	10	4
IPI00024919 - Gene_Symbol=PRDX3 Thioredoxin-dependent peroxide reductase, mitochondrial precur	27693	0	0	14	12	13
IPI00010896 - Gene_Symbol=DDAH2;CLIC1 Chloride intracellular channel protein 1	26923	6	5	4	18	7
IPI00549725 - Gene_Symbol=PGAM1;hCG_2015138 Phosphoglycerate mutase 1	28804	6	0	20	16	20
IPI00453476 - Gene_Symbol=- Uncharacterized protein	28850	3	0	10	8	10
IPI00017726 - Gene_Symbol=HSD17B10 Isoform 1 of 3-hydroxyacyl-CoA dehydrogenase type-2	26923	5	4	8	8	9
IPI00792352 - Gene_Symbol=RAN 26 kDa protein	26409	0	11	27	9	18
IPI00246975 - Gene_Symbol=GSTM3 Glutathione S-transferase Mu 3	26560	15	15	5	10	7
IPI00220642 - Gene_Symbol=YWHAG 14-3-3 protein gamma	28303	0	31	8	7	5
IPI00018146 - Gene_Symbol=YWHAQ 14-3-3 protein theta	27764	11	33	4	9	5
IPI00216318 - Gene_Symbol=YWHAB Isoform Long of 14-3-3 protein beta/alpha	28082	11	44	5	9	3
IPI00021263 - Gene_Symbol=YWHAZ 14-3-3 protein zeta/delta	27745	13	48	5	5	8

Table 2-2. All proteins in the 25 – 30 kD molecular weight range with spectral counts >5 in the NJP2-treated runs. The data are sorted by greatest-fold change in spectral counts in the NJP2 samples vs the DMSO samples.

Glutathione *S*-transferases (GSTs) catalyze nucleophilic attack by reduced glutathione (GSH) on nonpolar compounds that contain an electrophilic carbon, nitrogen, or sulfur atom. Their substrates include halogenated nitrobenzenes, arene oxides, quinones, and α,β-unsaturated carbonyls.[39] The conjugation of GSH to endogenous and exogenous electrophiles functions as a mechanism of cellular defense against carcinogens, therapeutic drugs, and oxidative stress.[40] GSTs encompass 3 major families of proteins: 1) cytosolic, 2) mitochondrial, and 3) microsomal, with the cytosolic GSTs accounting for the largest of the families. On the basis of amino acid sequence similarities, substrate specificity, and immunological cross-reactivity, seven classes of cytosolic GSTs have been identified in mammals. Most GST classes show a high degree of polymorphism and include several subunits (Table 2-3).[41] Each subunit (22 – 29 kD)

contains an amino-terminal GSH-binding site (G-site) and a carboxy-terminal hydrophobic substrate-binding domain (H-site).[42] The exact catalytic mechanisms for each class of GST are still largely unknown; however, they all encompass binding of GSH and stabilization of the thiolate anion within the G-site, followed by conjugation to a substrate bound within the H-site. This results in GST's ability to facilitate conjugation, isomerization, reduction, and thiolysis activities among others.

Class	Enzyme Designation	Subunits
Alpha	GSTA	1,2,3,4,5
Mu	GSTM	1,2,3,4,5
Omega	GSTO	1,2
Pi	GSTP	1,2
Sigma	GSTS	1
Theta	GSTT	1,2
Zeta	GSTZ	1

Table 2-3. Classes of cytosolic GSTs.

The omega class of GSTs was recently discovered through a sequence database.[43] Structurally, GSTO1 is very similar except that it contains a 19-20 residue N-terminal extension, and, while it contains high sequence and structural similarities to the other GST classes, GSTO1 behaves rather uniquely.[44] It possesses glutathione-dependent thiol transferase activity along with glutathione-dependent dehydroascorbate reductase activity, both of which are not observed within the other classes of GSTs and are more similar to that of glutaredoxins.[43, 45] GSTO1 displays only minimal activity with chloronitrobenzenes, which are generally good substrates for other classes of GSTs. Mechanistically, GSTO1 is also thought to be unique from other GSTs. GSH binding is analogous to what has been observed in other GSTs, except that GSTO1 possesses a catalytic cysteine residue (Cys32) in place of the canonical tyrosine or serine residue.[43]

Traditionally within GSTs, the catalytic tyrosine/serine residue stabilizes the thiolate anion within GSH; however, Cys32 of GSTO1 acts as a nucleophile to form a mixed disulfide with GSH. The H-site of GSTO1 also contains a larger pocket and Trp222 points its indole nitrogen into the pocket.[43, 44] This would allow GSTO1 to accommodate larger substrates that are not entirely hydrophobic, such as the peptides we employ here.

GSTO1 overexpression has been observed in highly aggressive human cancers,[46] and other studies have implicated GSTO1 in chemotherapeutic resistance.[47] Further interrogation revealed that GSTO1 overexpression averts cisplatin-induced toxicity and RNAi knockdown of GSTO1 sensitizes cancer cells to cytotoxic effects of cisplatin.[48] The mechanism of resistance is thought to be through GSTO1-modulation of apoptotic signaling cascades; in particular, GSTO1 overexpression appears to be associated with activation of proteins essential to survival pathways (Protein kinase B (AKT) and Extracellular-signal-related kinases (ERK1/2)) and inhibition of proteins contributing to apoptotic pathways (Mitogen-activated protein kinase 8 (JNK1)).[48] Despite its potential role in cancer, only a few inhibitors have been developed for GSTO1. A commercially available fluorescent protein tag from Invitrogen, CellTracker Green (5-chloromethylfluorescein diacetate, Figure 2-11), inhibits GSTO1 with good potency (IC_{50} = 51 nM) and selectivity.[49] Unfortunately, while this inhibitor may be useful in certain applications, it readily undergoes hydrolysis by endogenous esterases, rendering the active compound membrane-impermeable. More recently, a chloroacetamide-containing inhibitor, KT53 (Figure 2-11), was identified through a high-throughput screen as a GSTO1 inhibitor with improved potency (IC_{50} ~30-40 nM), selectivity, and cellular activity.[50] KT53 was shown to sensitize cancer cells to the cytotoxic effects of cisplatin,

providing the first pharmacologic evidence that GSTO1 contributes to chemotherapeutic resistance in cancer.[50] Notably, KT53 functions by covalently modifying the GSH-binding catalytic Cys32 through its cysteine-reactive chloroacetamide electrophile, which led us to believe our apoptotic-cell selective inhibitor of GSTO1 functioned in the same manner.

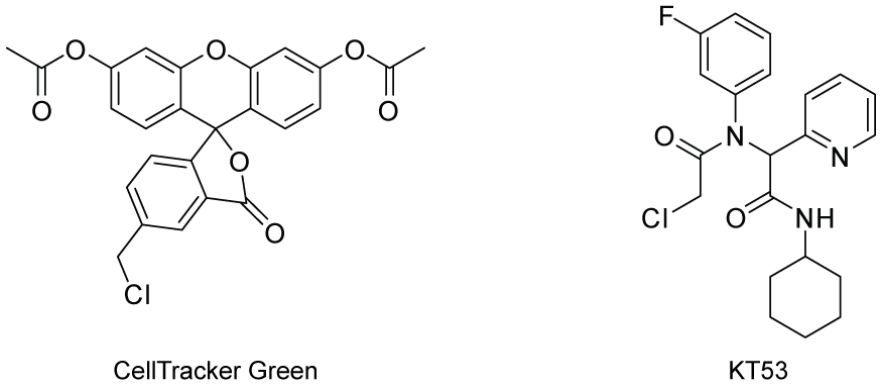

Figure 2-11. Structures of GSTO1 inhibitors CellTracker Green and KT53.

In order to confirm GSTO1 as the target protein and evaluate the mechanism of action of NJP2, we overexpressed the WT and C32A mutant of GSTO1 in HEK293T cells by transient transfection. These cells were then treated with NJP2 and subjected to in-gel fluorescence analysis revealing an extensive fluorescent signal of the WT overexpressed GSTO1 (Figure 2-12). This signal was absent for the C32A mutant, indicating that covalent modification of GSTO1 by NJP2 occurs at the catalytic Cys32 residue.

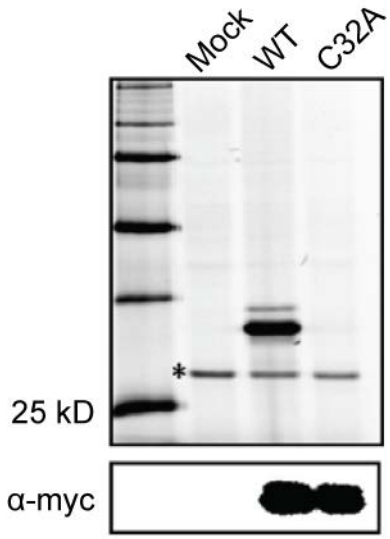

Figure 2-12. Mock-transfected, GSTO1 WT, and GSTO1 C32A mutant overexpressing cells labeled with NJP2 and analyzed by in-gel fluorescence (top panel). Western blots of an anti-myc antibody confirmed overexpression (bottom panel). The overexpressed GSTO runs higher on the gel than the endogenous GSTO1 (*) due to the additional mass of the linker sequence and C-terminal myc/His tag.

Application of NJP2 as an apoptotic cell-selective inhibitor and imaging agent

Once GSTO1 was identified as the target of NJP2, we investigated the mechanism of apoptotic-cell selectivity. To confirm our initial hypothesis that the peptide scaffold would be selectively internalized by compromised cell membranes, we had to eliminate any possibility of an increase in GSTO1 abundance or activity occurring during apoptosis. A previous proteomic study into proteolysis events during apoptosis revealed no change in GSTO1 abundance;[51] however, the possibility of post-translational activation of GSTO1 still existed. In order to refute this notion, we employed a non-specific sulfonate ester ABP, PS-alkyne (undec-10-yn-1-yl benzenesulfonate, Figure 2-13a). This more promiscuous cysteine-reactive inhibitor is known to be membrane

permeable in both healthy and apoptotic cells and labels GSTO1, amongst other targets.[52] Because its labeling can easily be competed with GSH, PS-alkyne is believed to bind within the G-site of GSTO1 and modifies Cys32 in the same manner as NJP2.[53, 54] Due to its binding mode, PS-alkyne binding should be indicative of GSTO1 activity since Cys32 is required for catalysis. *In vitro* (lysates) treatment of control and apoptotic HeLa lysates with PS-alkyne and subsequent in-gel fluorescence analysis indicated no change in GSTO1 activity during apoptosis (Figure 2-13b). Additionally, in-gel fluorescence analysis of *in situ* (whole-cell) PS-alkyne treated samples also detected no change in GSTO1 activity when employing an equally membrane permeable inhibitor. These data suggest that NJP2 is selectively internalized by apoptotic cells due to the compromised integrity of their cell membranes (Figure 2-13b).

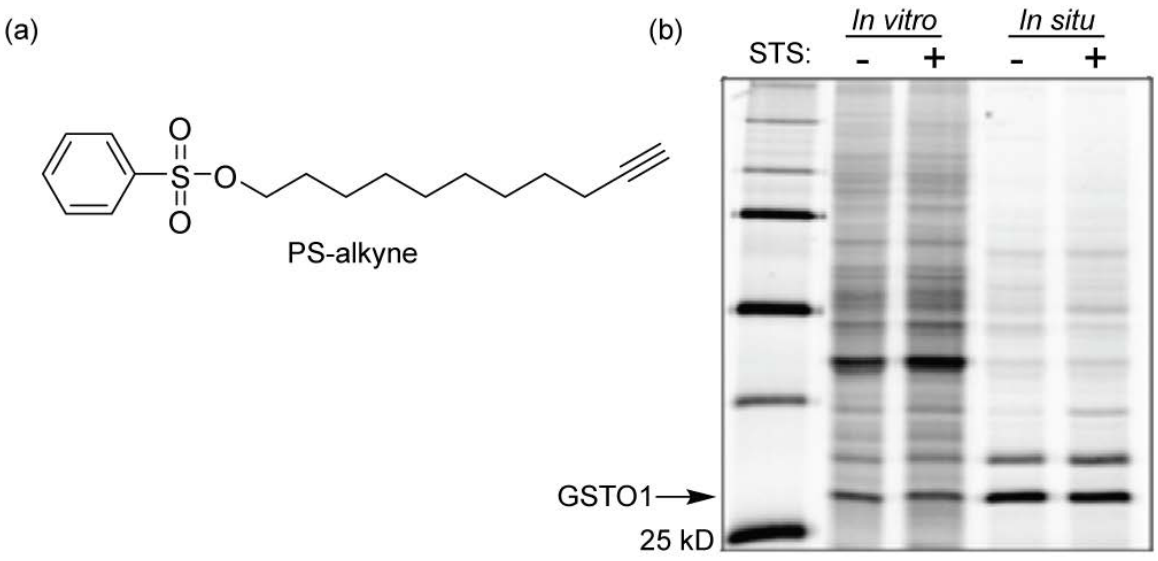

Figure 2-13. (a) Structure of cell permeable PS-alkyne. (b) PS-alkyne was administered to control and apoptotic HeLa cells *in vitro* and *in situ* and analyzed by in-gel fluorescence analysis.

To further interrogate the selective internalization of NJP2 by apoptotic cells and to demonstrate its utility as an imaging agent, a fluorescent analog, NJP13, was synthesized by appending a rhodamine fluorophore through click chemistry (Figure 2-14a). Both control and apoptotic HeLa cells were administered NJP13 and visualized by fluorescence microscopy. Apoptotic cells, upon exposure to NJP13, exhibited a significant fluorescent signal over background levels, and this increase in fluorescent intensity coincided with the characteristic morphological changes in cellular structure observed during apoptosis (Figure 2-14b). No fluorescence was detected in NJP13-treated control cells. This dramatic increase in cellular uptake upon inducing apoptosis confirms our hypothesis that the increased cell permeability during apoptosis can be exploited to selectively deliver peptide-based probes to apoptotic cells. Moreover, since only low concentrations of STS (1 μM) and short incubation times (30 mins) yielded a considerable fluorescent signal, these peptides may represent a valuable class of covalent imaging agents for early-stage apoptotic cells.

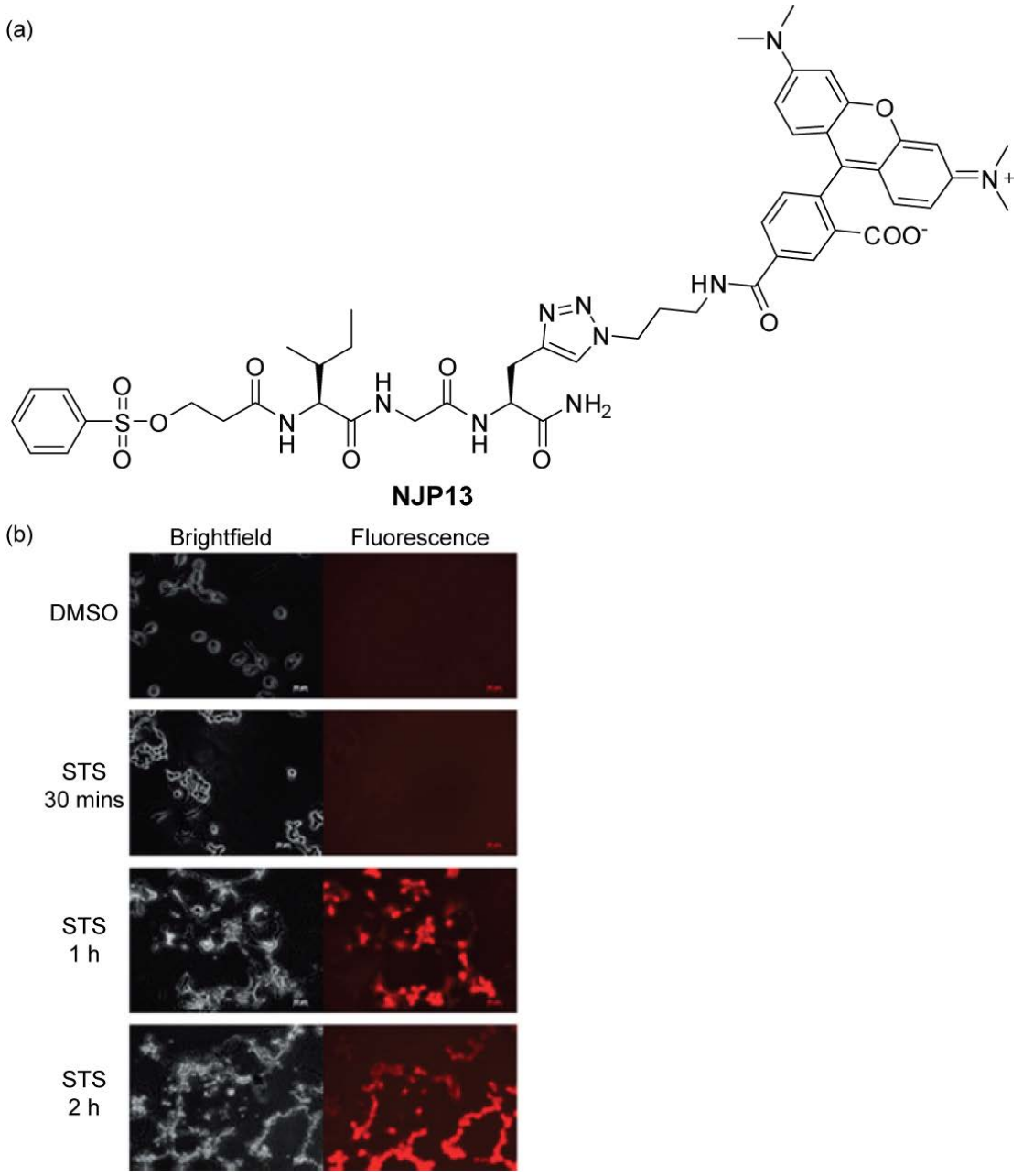

Figure 2-14. (a) Structure of fluorescent-functionalized apoptotic cell-selective probe, NJP13. (b) Fluorescence microscopy images of HeLa cells incubated with DMSO (control) or STS (1 μM) for 30 mins, 1 h, or 2 h, followed by NJP13-treatment.

In order to quantitatively evaluate the potency and cell-selectivity of GSTO1 inhibition by NJP2, we performed a dose-dependent labeling experiment in conjunction

with a competitive activity-based protein profiling (ABPP) experiment. The competitive ABPP experiment measured residual GSTO1 activity through use of a fluorescently-tagged phenyl sulfonate inhibitor (PS-Rh) after treatment with NJP2.[50] Previous research has determined that the degree of PS-Rh labeling of Cys32 correlates to GSTO1 activity, and thereby a loss of PS-Rh labeling signifies inhibition of GSTO1 activity.[50] Both control and apoptotic HeLa cells were treated with increasing concentrations of NJP2 (1 – 60 μM), and the resulting lysates were either subjected to click chemistry with Rh-N_3 or administered PS-Rh. Both sets of lysates were then analyzed by in-gel fluorescence. The Rh-N_3 gels illustrate the increase in labeling of GSTO1 by NJP2 in apoptotic cells, with only a minimal increase observed in the control (Figure 2-15a). As for the PS-Rh gel, a decrease in PS-Rh labeling, and thus GSTO1 activity, was only observed in apoptotic cells upon increasing concentrations of NJP2 (Figure 2-15b). These gel bands were integrated at each concentration to quantify the residual GSTO1 activity, and a plot of these demonstrates the remarkable selectivity of NJP2 towards GSTO1-inhibition solely within apoptotic cells (Figure 2-15c). In combination, the labeling of GSTO1 by NJP2 determined after click chemistry correlated with the loss of residual GSTO1 activity observed through the competitive ABPP assay as quantified by gel-band integration (Figure 2-15d). The quantified bands were plotted using Prism software and the IC_{50} value for NJP2 within apoptotic cells was calculated as 13 μM. Together, these data illustrate the specificity and potency of NJP2 as an inhibitor of GSTO1 solely within apoptotic cells.

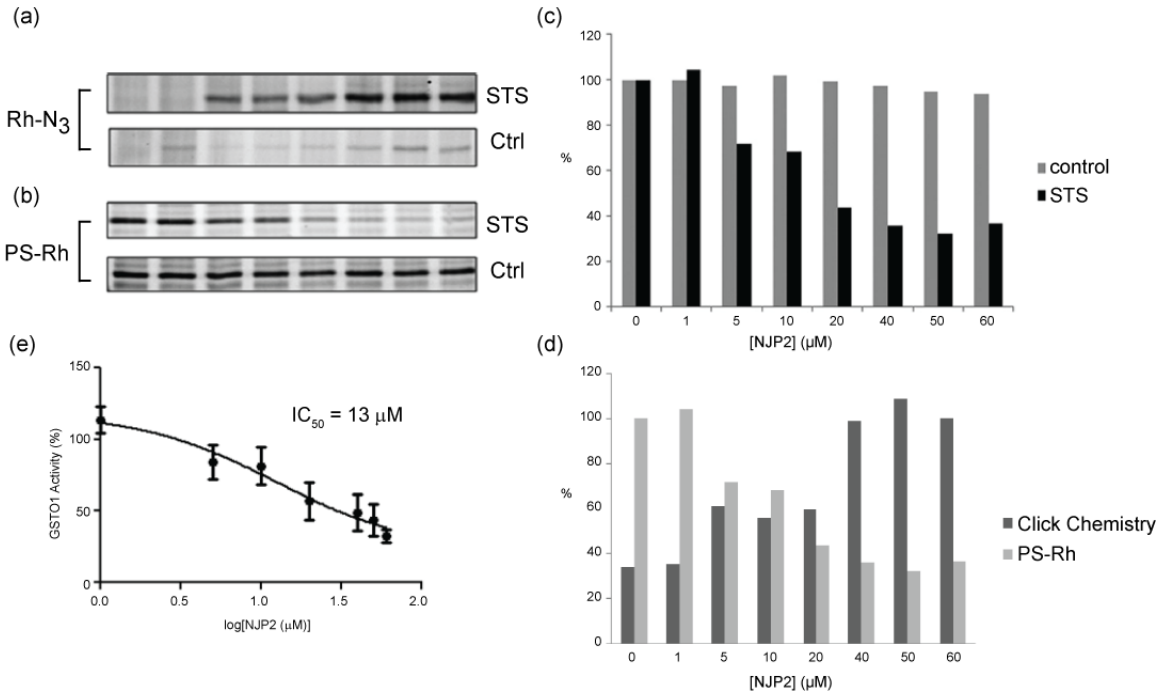

Figure 2-15. Control and apoptotic cells administered increasing concentrations of NJP2 were (a) subjected to click chemistry with Rh-N_3 or (b) treated with PS-Rh and analyzed by in-gel fluorescence. (c) Residual GSTO1 activity within control and apoptotic cells was quantified through gel-band integration. (d) Within apoptotic cells, quantification through gel-band integration demonstrated that the labeling of GSTO1 by NJP2 correlated with a loss of residual GSTO1 activity. (e) The quantified bands were plotted on Prism to determine the IC_{50} value for NJP2 within apoptotic cell populations.

Conclusions

Through the use of a library of cysteine-reactive peptides, we developed an apoptotic-cell selective inhibitor of GSTO1 that functions through covalent modification of its catalytic cysteine residue. Because of its importance in cancer progression and chemotherapeutic resistance, the discovery of selective inhibitors of GSTO1 is paramount. Other more potent GSTO1 inhibitors (IC_{50} of NJP2 for GSTO1 ≈ 13 μM)

have been described previously,[50, 55] but these existing inhibitors are equipotent for GSTO1 in both healthy and apoptotic cells. NJP2 should serve as a valuable complement to existing inhibitors because of its high specificity for GSTO1 over other protein targets along with its unique ability to solely target cells undergoing apoptosis. This context-dependent inhibitor could help elucidate the role of GSTO1 in apoptosis or be used to accelerate apoptosis within a distinct population of cells. We demonstrated that the characteristic loss of plasma membrane integrity in apoptotic cells can be exploited in the development of cell-selective inhibitors. Towards this end, other members of our peptide library, particularly NJP4, displayed labeling of other protein targets through in-gel fluorescence. This suggests that the peptide-based scaffold can be expanded upon to develop context-dependent inhibitors of diverse protein classes other than GSTO1. The visualization of NJP13 internalization using fluorescence microscopy also implies that these peptides can be added to the repertoire of selective imaging agents for apoptotic cells.[56] These covalent inhibitors targeting compromised membranes appear to provide an inherent advantage over PS-targeting agents (non-covalent, cannot distinguish from necrotic cells) and current caspase-targeting agents (off-target binding); however, the precise chemical changes occurring to plasma membranes during apoptosis must be better understood.

Acknowledgements

A significant portion of the peptide-probe library was synthesized and purified by Daniel Pimental. I would also like to acknowledge Yani Zhou for helping to teach me

subcloning and transfections and Dr. Fang Wang for her help with the fluorescence microscopy.

Experimental procedures

General procedures and materials

All materials were purchased from Sigma Aldrich or Fisher Scientific unless otherwise noted. Fmoc-propargyl glycine (Fmoc-Pra-OH) was purchased from BaCHEM. All other Fmoc-protected amino acids, PyBOP, and resin were purchased from Novabiochem. PBS buffer, DMEM/High glucose media, RPMI 1640 media, and penicillin streptomycin (Pen/Strep) were purchased from Thermal Scientific. Trypsin-EDTA and RPMI 1640 media (no phenol red) were purchased from Invitrogen. STS was purchased from Cell Signaling. CPT was purchased from MP Biomedicals LLC. The α-myc tag antibody and the α-rabbit IgG HRP-linker antibody were purchased from Cell Signaling. X-tremeGENE 9 DNA transfection reagent was purchased from Roche. Analytical TLC was performed on Sorbent Technologies Silica G TLC Plates w/UV354 (0.25 mm). All compounds were visualized on TLC by cerium sulfate-ammonium molybdate staining. Column chromatography was carried out using forced flow of indicated solvent on Sorbent Technology Standard grade silica gel (40 – 63 μm particle size, 60 Å pore size). Proton and Carbon NMR spectra were recorded on a Varian INOVA 500 NMR Spectrometer (500 MHz). Chemical shifts (δ) are reported in ppm with chemical shifts referenced to internal standards: $CDCl_3$ (7.26 ppm for ^{1}H, 77.0 ppm for ^{13}C). Coupling constants (*J*) are reported in Hz and multiplicities are abbreviated as

singlet (s), doublet (d), triplet (t), multiplet (m), doublet of doublets (dd), and doublet of triplets (dt). High resolution Mass Spectra (HRMS) were obtained at the Mass Spectrometry Facility at Boston College unless otherwise noted.

General procedures for solid-phase peptide synthesis

All peptides were synthesized by manual solid-phase methods on Rink Amide MBHA Resin using Fmoc as the protecting group for α-amino functionalities. Amino acids were coupled using PyBOP as the activating reagent. The following side-chain protecting groups were used: Asp(t-Bu), Lys(Boc), and Trp(Boc). The success of each Fmoc-deprotection and coupling reaction was qualitatively tested using the standard procedure for the Kaiser test. After the addition of the electrophile, cleavage from the resin was performed in TFA: DCM: TIS: water (90: 5: 2.5: 2.5) solution for 2 hrs. All peptides were purified by preparative HPLC with a gradient of increasing acetonitrile-0.1% TFA (solvent B) in water-0.1% TFA (solvent A). All peptides were analyzed by a Micromass LCT TOF mass spectrometer coupled to a Waters 2975 HPLC and a Waters 2996 photodiode array UV-vis detector.

Synthesis of BsO-(propanamide)-Phe-Phe-Pra-Lys-NH_2 (NJP1)

Rink Amide MBHA resin was used and Fmoc-Lys(Boc)-OH, Fmoc-Pra-OH, Fmoc-Phe-OH, and Fmoc-Phe-OH residues were added under standard conditions. After Fmoc-deprotection, 3-(trityloxy)propanoic acid (NJP12) (2 eq) and PyBOP (2 eq) were dissolved in DMF and this solution was added to the resin. DIPEA (4 eq) was added to the resin, and the reaction was shaken at room temperature for 2 hrs. The solvent was

removed by vacuum and the resin was washed with DMF (5 x 3 mL) and DCM (3 x 3 mL). The resin was shaken in a 1% TFA, 2% TIS in DCM solution to remove the trityl group (3 x 5 mins). Dry DCM was added to the resin and N_2 gas was bubbled through the reaction vessel. NEt_3 in large excess (~100 eq) followed by benzene sulfonylchloride in large excess (~100 eq) were added to the resin. N_2 gas was bubbled through the reaction mixture for 1 hr, and any solvent lost was replaced. The reaction vessel was capped, sealed with parafilm, and shaken for 15 hrs. The solvent was removed and the resin was washed with DCM (5 x 3 mL). The peptide was cleaved using the conditions described above and purified by HPLC to give the pure peptide NJP1 (8.6%). HPLC t_R = 20.00 min (C_{18}, 5-95% B in 30 mins); HRMS for NJP1 ($C_{38}H_{46}N_6O_8S + Na^+$): *m/z* calcd 769.2996; obsd [$M + Na^+$] 769.4025 (MALDI+).

Synthesis of BsO-(propanamide)-Ile-Gly-Pra-NH_2 (NJP2)

The standard procedure outlined above for NJP1 was used, except the lysine was not added and the Fmoc-Phe-OH and Fmoc-Phe-OH were replaced with Fmoc-Gly-OH and Fmoc-Ile-OH respectively. The peptide was cleaved and purified by HPLC as described above to give the pure peptide NJP2 (8.3%). HPLC t_R = 18.67 min (C_{18}, 5-95% B in 30 mins); HRMS for NJP2 ($C_{22}H_{30}N_4O_7S + Na^+$): *m/z* calcd 517.1733; obsd [$M + Na^+$] 517.1737 (MALDI+).

Synthesis of BsO-(propanamide)-Val-Phe-Pra-NH_2 (NJP3)

The standard procedure outlined for NJP2 was used except the Fmoc-Gly-OH and Fmoc-Ile-OH were replaced with Fmoc-Phe-OH and Fmoc-Val-OH respectively. The

peptide was cleaved and purified by HPLC using the conditions described above to give the pure peptide NJP3 (7.1%). HPLC t_R = 19.90 min (C_{18}, 5-95% B in 30 mins); HRMS for NJP3 ($C_{28}H_{34}N_4O_7S + Na^+$): *m/z* calcd 593.2046; obsd [M + Na^+] 593.2056 (ESI+).

Synthesis of BsO-(propanamide)-Leu-Asn-Pra-NH_2 (NJP4)

The standard procedure outlined for NJP2 was used except the Fmoc-Gly-OH and Fmoc-Ile-OH were replaced with Fmoc-Asn(t-Bu)-OH and Fmoc-Leu-OH respectively. The peptide was cleaved and purified by HPLC using the conditions described above to give the pure peptide NJP4 (12%). HPLC t_R = 18.05 min (C_{18}, 5-95% B in 30 mins); HRMS for NJP4 ($C_{24}H_{33}N_5O_8S + Na^+$): *m/z* calcd 574.1948; obsd [M + Na^+] 574.1931 (ESI+).

Synthesis of BsO-(propanamide)-Ala-Trp-Pra-NH_2 (NJP5)

The standard procedure outlined for NJP2 was used except the Fmoc-Gly-OH and Fmoc-Ile-OH were replaced with Fmoc-Trp(Boc)-OH and Fmoc-Ala-OH respectively. The peptide was cleaved and purified by HPLC using the conditions described above to give the pure peptide NJP5 (12%). HPLC t_R = 19.14 min (C_{18}, 5-95% B in 30 mins); HRMS for NJP5 ($C_{28}H_{31}N_5O_7S + Na^+$): *m/z* calcd 604.1842; obsd [M + Na^+] 604.1887 (ESI+).

Synthesis of Acrylamide-Phe-Phe-Pra-Lys-NH_2 (NJP6)

The Rink Amide MBHA resin was used and Fmoc-Lys(Boc)-OH, Fmoc-Pra-OH, Fmoc-Phe-OH, and Fmoc-Phe-OH residues were added under standard conditions. After

Fmoc-deprotection, acrylic acid (2 eq) and PyBOP (2 eq) were dissolved in DMF and were added to the resin. DIPEA (4 eq) was added to the resin and the reaction was shaken at room temperature for 2 hrs. The solvent was removed by vacuum and the resin was washed with DMF (5 x 3 mL) and DCM (3 x 3 mL). The peptide was cleaved and purified by HPLC as described above to give the pure peptide NJP6 (5.9%). HPLC t_R = 17.53 min (C_{18}, 5-95% B in 30 mins); HRMS for NJP6 ($C_{32}H_{40}N_6O_5$ + Na^+): *m/z* calcd 611.2958; obsd [M + Na^+] 611.2975 (ESI+).

Synthesis of Acrylamide-Ile-Gly-Pra-NH_2 (NJP7)

The standard procedure outlined above for NJP6 was used, except the lysine was not added and the Fmoc-Phe-OH and Fmoc-Phe-OH were replaced with Fmoc-Gly-OH and Fmoc-Ile-OH respectively. The peptide was cleaved and purified by HPLC as described above to give the pure peptide NJP7 (13%). HPLC t_R = 14.27 min (C_{18}, 5-95% B in 30 mins); HRMS for NJP7 ($C_{16}H_{24}N_4O_4$ + Na^+): *m/z* calcd 359.1696; obsd [M + Na^+] 359.1678 (ESI+).

Synthesis of Acrylamide-Val-Phe-Pra-NH_2 (NJP8)

The standard procedure outlined above for NJP7 was used except the Fmoc-Gly-OH and Fmoc-Ile-OH were replaced with Fmoc-Phe-OH and Fmoc-Val-OH respectively. The peptide was cleaved and purified by HPLC as described above to give the pure peptide NJP8 (7.7%). HPLC t_R = 16.39 min (C_{18}, 5-95% B in 30 mins); HRMS for NJP8 ($C_{22}H_{28}N_4O_4$ + Na^+): *m/z* calcd 435.2009; obsd [M + Na^+] 435.2010 (ESI+).

Synthesis of Acrylamide-Leu-Asn-Pra-NH_2 (NJP9)

The standard procedure outlined above for NJP7 was used except the Fmoc-Gly-OH and Fmoc-Ile-OH were replaced with Fmoc-Asn(t-Bu)-OH and Fmoc-Leu-OH respectively. The peptide was cleaved and purified by HPLC as described above to give the pure peptide NJP9 (40%). HPLC t_R = 15.07 min (C_{18}, 5-95% B in 30 mins); HRMS for NJP9 ($C_{18}H_{27}N_5O_5$ + Na^+): *m/z* calcd 416.1910; obsd [M + Na^+] 416.1901 (ESI+).

Synthesis of Acrylamide-Ala-Trp-Pra-NH_2 (NJP10)

The standard procedure outlined above for NJP7 was used except the Fmoc-Gly-OH and Fmoc-Ile-OH were replaced with Fmoc-Trp(Boc)-OH and Fmoc-Ala-OH respectively. The peptide was cleaved and purified by HPLC as described above to give the pure peptide NJP10 (21%). HPLC t_R = 16.53 min (C_{18}, 5-95% B in 30 mins); HRMS for NJP10 ($C_{22}H_{25}N_5O_4$ + Na^+): *m/z* calcd 446.1805; obsd [M + Na^+] 446.1801 (ESI+).

Synthesis of 3-(trityloxy)propan-1-ol (NJP11)

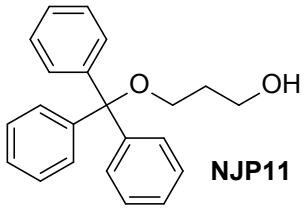

NJP11

A round bottom flask was flushed with N_2 gas. 1,3-propanediol (6.0 mL, 83.0 mmol) and pyridine (30 mL) were added to the flask. The solution was stirred and cooled on ice to 0 °C. Trityl chloride (23.3 g, 83.8 mmol) and pyridine (20 mL) were combined in a flask. This solution was added to the diol solution on ice. The reaction was left on ice and slowly warmed to room temperature overnight (15 hrs). The reaction mixture was

evaporated to dryness. The residue was dissolved in ethyl acetate (150 mL) and water (200 mL). The organic layer was separated from the aqueous layer. The organic layer was washed with 1 M HCl (3 x 100 mL), saturated sodium bicarbonate (3 x 100 mL), and brine (6 x 100 mL). The organic layer was dried with sodium sulfate, filtered, and evaporated to dryness to give the crude product. The crude product was dissolved in a small amount of DCM and purified by silica column chromatography using 5:1 hexane: ethyl acetate and 3:1 hexane: ethyl acetate. The fractions were analyzed by TLC in 1:1 hexane: ethyl acetate. This process resulted in the monotritylated product, NJP11 (10.1 g, 36.4%), a white powder. R_f 0.65 (1:1 hexane: ethyl acetate); ^{1}H NMR (500 MHz, CDC_{l3}): δ 7.18 – 7.37 (m, 15H), 3.70 (dt, *J* = 5.5Hz, 2H), 3.21 (t, *J* = 6.0 Hz, 2H), 1.79 (tt, *J* = 6.0 Hz, 2H); ^{13}C NMR (125 MHz, CDC_{l3}): 143.9, 128.4, 127.9, 127.1, 87.1, 62.2, 61.8, 32.3.

Synthesis of 3-(trityloxy)propanoic acid (NJP12)

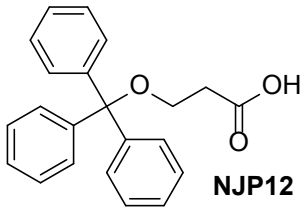

NJP12

A round bottom flask was flushed with N_2 gas. Oxalyl chloride (485 µL, 5.6 mmol) was added to the reaction vessel and was dissolved in dry DCM (10 mL). The solution was stirred in a dry ice/acetone bath under N_2. DMSO (935 µL, 13.2 mmol) and dry DCM (10 mL) were mixed in a N_2 flushed round bottom flask. This solution was added dropwise to the reaction vessel over 10 mins. The monotrityl-protected alcohol NJP11 (1.2 g, 3.8 mmol) was dissolved in dry DCM (7 mL) in a N_2 flushed round bottom flask. This solution was added to the reaction vessel dropwise. The reaction was stirred in

the dry ice/acetone bath for 10 mins under N_2 gas. NEt_3 (2 mL, 14.3 mmol) was added to the reaction dropwise. The reaction was stirred for 20 mins, then removed from the dry ice/acetone bath and stirred for 1 hour. The reaction was monitored by TLC in 1:1 hexane/ethyl acetate. The reaction mixture was washed with water (3 x 50 mL), and the organic and aqueous layers were collected and combined. The aqueous layer was extracted with DCM (3 x 50 mL). The organic layers were combined, dried with sodium sulfate, filtered, and evaporated to dryness. The crude product (766.8 mg) was recrystallized in warm hexane. The crude product underwent subsequent oxidation. A round bottom flask containing the crude product (766.8 mg) was flushed with N_2 gas. The crystals were dissolved in an acetone/water mixture (20 mL / 8 mL). $KMnO_4$ (385.8 mg, 2.4 mmol) was added to the stirring solution. The reaction was stirred under N_2 for 2 hrs 15 mins. The pH of the reaction mixture was adjusted to ~5 by the addition of 3 M HCl. A 40% sodium bisulfate solution was added until the reaction mixture turned colorless. The mixture was stirred for 45 mins. The mixture was acidified to a pH of 2 using 3 M HCl. The mixture was extracted with ethyl acetate (3 x 40 mL). The organic layers were collected, combined, and washed with water (3 x 70 mL). The organic layers were dried with sodium sulfate, filtered, and evaporated to dryness to form the crude product. The crude product was dissolved in a small amount of ethyl acetate and was purified by silica column chromatography using 3:2 hexane: ethyl acetate. The fraction was analyzed by TLC in 1:1 hexane: ethyl acetate. This process resulted in the pure monotritylprotected acid, NJP12 (314.4 mg, 25.1% over 2 steps), a white powder. R_f 0.25 (1:1 hexane: ethyl acetate); ^1H NMR (500 MHz, CDC_{l3}, TMS = 0.00 ppm): δ 11.1 (s, 1H, COO<u>H</u>), 7.23 –

7.47 (m, 15H), 3.41 (t, J = 6.5 Hz, 2H), 2.62 (t, J = 6.0 Hz, 2H); ^{13}C NMR (125 MHz, CDC_{l3}): 175.8, 142.8, 128.4, 127.9, 127.1, 87.1, 58.9, 35.0.

Probe labeling and preparation of cell lysates

STS and DMSO-treated cells were treated with NJP1 – 10 by adding directly to the media from a 10 mM probe stock in DMSO to give a final probe concentration of 50 μM. The plates were placed in the cell incubator at 37 °C under 5% CO_2 for 1 hr. The cells were washed 3 times with PBS, harvested by scraping, and resuspended in an appropriate amount of PBS. Cells were sonicated to lyse, and these lysates were separated by centrifugation (45 mins, 45,000 rpm) at 4 °C under high vacuum to yield the soluble and membrane proteomes. The supernatant was collected as the soluble protein fraction and the pellet was discarded. Protein concentrations of these soluble lysates were determined using the Bio-Rad DC Protein Assay (Bio-Rad).

In-gel fluorescent analysis

Protein samples (50 μL, 2 mg/mL) were subjected to click chemistry. Synthesized Rh-N_3[57] (20 μM), TCEP (1 mM, from 50x fresh stock in water), TBTA ligand (100 μM, from 17x stock in DMSO : t-butanol 1:4), and copper(II) sulfate (1 mM, from 50x stock in water) were added in this order to the protein. The samples were vortexed after every addition, except TCEP, and allowed to react at room temperature for 1 hr, while being vortexed periodically. SDS-PAGE loading buffer 2x (reducing, 50 μL) was added to the samples and 25 μL of each protein solution was separated by SDS-PAGE for 217 V hrs on a 10% polyacrylamide gel. Gels were visualized for fluorescence on a Hitachi FMBIO

II multiview flatbed laser-induced fluorescent scanner. After analysis, gels underwent a typical procedure for coomassie staining. Stained gels were visualized on a Stratagene Eagle Eye apparatus by a COHU High performance CCD camera.

HeLa cell culture and DNA fragmentation assay to monitor apoptosis

HeLa cells were grown at 37 °C under 5% CO_2 in DMEM media supplemented with 10% FCS, 2 mM glutamine, and 1% Pen/Strep. HeLa cells grown to 100% confluency were treated with STS (4 μM from 1 mM stock) or the corresponding amount of DMSO. These cells were incubated for various time points at 37 °C under 5% CO_2. The cells were washed 3 times with PBS, harvested by scraping, and lysed in 400 μL of lysis buffer (100 mM Tris pH 8.0, 5 mM EDTA, 0.2% SDS, 200 mM NaCl). Cells were incubated with RNase A (0.1 mg/mL) for 0.5 hr at 37 °C. Proteinase K was added to a concentration of 0.3 mg/mL and samples were incubated overnight at 55 °C. Genomic DNA was precipitated with isopropanol (1 volume) and resuspended in dH_2O (100 μL). The DNA (10 μL) and bromophenol blue were combined and visualized on a 1% agarose gel with ethidium bromide.

Jurkat cell culture, induction of apoptosis, probe labeling

Jurkat cells were grown at 37 °C under 5% CO_2 in RPMI 1640 media supplemented with 10% FCS, 2 mM glutamine, and 1% Pen/Strep. STS (4 μM from 1 mM stock) or the corresponding amount of DMSO was added to the media, and the cells were incubated at various time points at 37 °C under 5% CO_2. NJP1-10 (50 μM from 10 mM stocks) were added and the cells were incubated at 37 °C under 5% CO_2 for 1 hr.

Induction of apoptosis was monitored by DNA fragmentation in the same manner as described above. Fluorescent gel analysis was also performed in the same manner as described above.

Induction of apoptosis with CPT and fluorescent gel analysis

HeLa cells were grown at 37 °C under 5% CO_2 in DMEM media supplemented with 10% FCS, 2 mM glutamine, and 1% Pen/Strep and allowed to reach 100% confluency. CPT (5, 10, 20 μM from 50x stock in DMSO) or DMSO was added to the cells and they were incubated for 4 hrs at 37 °C under 5% CO_2. NJP2 (50 μM from 10 mM stock in DMSO) was added and the cells were incubated at 37 °C under 5% CO_2 for another hour. These CPT-treated cells were harvested and underwent fluorescent gel analysis as described above. STS-treated lysates were used as a control.

Click chemistry and streptavidin enrichment of probe-labeled proteins for mass spectrometry

HeLa soluble protein lysates treated with STS and subsequently administered NJP2 or DMSO were prepared as described above. These protein samples (500 μL, 2 mg/mL) were aliquoted to undergo click chemistry. Biotin azide[38] (200 μM from 5 mM DMSO stock), TCEP (1 mM, from fresh 50x stock in water), ligand (100 μM, from 17x stock of DMSO : t-butanol 1:4), and copper(II) sulfate (1 mM, from 50x stock in water) were added to the protein samples. The samples were allowed to react at room temperature for 1 hr and were vortexed periodically. Tubes were centrifuged (10 mins, 4 °C) to pellet the precipitated proteins. The pellets were resuspended in cold MeOH (500

μL) by sonication, centrifuged (10 mins, 4 °C), and the supernatants were removed. Following a second MeOH wash, the pelleted protein was solubilized in a 1.2% SDS in PBS solution (1 mL) by sonication and heating (5 mins, 80 °C). These solubilized samples were diluted with PBS (5 mL) to give a final SDS concentration of 0.2%. The solutions were incubated with streptavidin-agarose beads (100 μL, Thermo Scientific) at 4 °C for 16 hrs and then at room temperature for 2.5 hrs. The beads were washed with 0.2% SDS in PBS (5 mL), PBS (3 x 5 mL), and water (3 x 5 mL). The beads were pelleted by centrifugation (3 mins, 1400 x g) between washes.

On-bead trypsin digestion

The washed beads were suspended in a 6 M urea in PBS solution (500 μL). DTT (10 mM, from 20x stock in water) was added to the samples and they were reduced by heating to 65 °C for 15 mins. Iodoacetamide (20 mM, from 50x stock in water) was added and the samples were placed in the dark so alkylation could proceed at room temperature for 30 mins. Following reduction and alkylation, the beads were pelleted by centrifugation (2 mins, 1400 x g) and resuspended in 2 mM of urea (200 μL), $CaCl_2$ (1 mM, from 100x stock in water), and trypsin (2 μg, from a 20 μg in 40 μL of trypsin buffer) in PBS. The digestion was then allowed to proceed overnight at 37 °C. The digestion was separated from the beads using a Micro Bio-Spin column (Bio-Rad). The beads were washed with water (2 x 50 μL) and the washes were combined with the eluted peptides. Formic acid (15 μL) was added to the samples, and they were stored at -20 °C until analyzed by mass spectrometry.

Liquid chromatography/mass spectrometry (LC/MS) analysis

LC/MS analysis was performed on an LTQ Orbitrap Discovery mass spectrometer (ThermoFisher) coupled to an Agilent 1200 series HPLC. Digests were pressure loaded onto a 250 μm fused silica desalting column packed with 4 cm of Aqua C18 reverse phase resin (Phenomenex). The peptides were eluted onto a biphasic column (100 μm fused silica with a 5 μm tip, packed with 10 cm C18 and 3 cm Partisphere SCX (Whatman) using a gradient of 5-100% Buffer B in Buffer A (Buffer A: 95% water, 5 % acetonitrile, 0.1% formic acid; Buffer B: 20% water, 80% acetonitrile, 0.1% formic acid). The peptides were eluted from the SCX onto the C18 resin and into the mass spectrometer following the four salt steps outlined previously.[38] The flow rate through the column was set to ~0.25 μL/min and the spray voltage was set to 2.75 kV. One full MS scan (400-1800 MW) was followed by 8 data dependent scans of the n^{th} most intense ions with dynamic exclusion enabled.

MS Data Analysis

The generated tandem MS data were searched using the SEQUEST algorithm[58] against the human IPI database. A static modification of +57 on cysteine was specified to account for iodoacetamide alkylation. The SEQUEST output files generated from the digests were filtered using DTASelect 2.0.[59] The data were then sorted by protein molecular weight to yield those between 25-30 kD, and all proteins in this range with detected average-spectral counts >5 in the NJP2-treated samples are disclosed. The data are ordered by fold-change, which is the ratio of average spectral counts in the NJP2-treated sample, relative to those treated with DMSO. GSTO1 is the top hit in this table.

HEK 293T cell culture, recombinant expression of GSTO1-WT and GSTO1-C32A, and probe labeling

The cDNA for GSTO1-WT was subcloned into pcDNA3.1-myc-His mammalian expression vector. Site-directed mutagenesis was performed to obtain the C32A mutant (Quick-change, Stratagene), and all constructs were verified by sequencing (Genewiz, Cambridge, MA). HEK 293T cells were grown at 37 °C under 5% CO_2 in DMEM media supplemented with 10% FCS, 2 mM glutamine, and 1% Pen/Strep. Transfections were performed on 10 cm cell plates of ~50% confluency. DMEM serum free media (600 μL) and X-tremeGENE DNA transfection reagent (20 μL) were combined in an Eppendorf tube. Plasmids of GSTO1 WT or C32A (6 μg) were added and the sample was vortexed and remained at room temperature for 15 mins. This plasmid solution was added dropwise to HEK 293T cells. The plate was incubated at 37 °C under 5% CO_2 for 48 hrs. NJP2 (50 μM from 10 mM stock in DMSO) was added and the cells were incubated for another hour. HEK 293T cells transfected with the pcDNA3.1-myc/His plasmid were used as a mock negative control. The lysates were prepared as described above and underwent fluorescent gel analysis.

Western blot analysis

The SDS-PAGE gels from above were transferred by electroblotting into nitrocellulose membranes for 150 volt hours. The membranes were blocked with TBS-T and 5% (w/v) non-fat dry milk at room temperature for 2 hrs. The blot was washed with TBS-T three times (5 mins/wash), then treated with α-myc tag rabbit antibody (1:1000)

overnight at 4 °C. The blots were washed with TBS-T three times (5 mins/wash). The blots were treated with α-rabbit-HRP conjugated secondary antibody (1:10,000) for 2 hrs at room temperature. The blots were washed three times with TBS-T (5 mins/wash), treated with HRP super signal chemiluminescence reagents (Thermo) and exposed to film for 1 min before development. Development took place using a Kodak X-OMAT 2000A processor.

***In vitro* and *in situ* labeling with non-specific PS-alkyne**

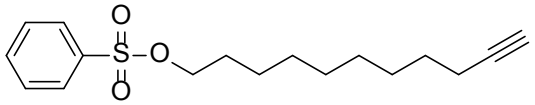

PS-alkyne

The PS-alkyne probe was synthesized according to a previous protocol.[33] HeLa cells were cultured as described above. Once the plates were grown to 100% confluency, STS (4 μM, from 1 mM stock in DMSO) or DMSO were added to the media and the cells were incubated for 4 hrs at 37 °C under 5% CO_2. The PS-alkyne probe (50 μM from 10 mM DMSO stock) was added and the cells were incubated for another hour. The lysates were prepared as described above. For the *in vitro* samples, unlabeled STS or DMSO-control HeLa cell lysates were aliquoted (50 μL, 2 mg/mL). The samples were vortexed and allowed to sit at room temperature for 1 hr. Click chemistry and fluorescent gel analysis was performed on the *in vitro* and *in situ* labeled samples as described above.

Synthesis of NJP13, a fluorescent version of NJP2

NJP2 (1.1 mg, 0.0022 mmol) and Rh-N_3 (0.8 mg, 0.002 mmol) were dissolved in a mixture of MeOH (300 μL) and water (70 μL). A fresh solution of sodium ascorbate in

water (10 μL, 200 mg/mL) and copper(II) sulfate in water (3 μL, 85 mg/mL) were added to the solution. The sample was vortexed for 1.5 hrs. The solvent was evaporated off to leave a crude pink solid. The fluorescent peptide was purified by HPLC to yield NJP13 (11.3%). HPLC t_R = 20.07 min (C_{18}, 5-95% B in 30 mins); HRMS for NJP13 ($C_{50}H_{59}N_{10}O_{11}S^+$): *m/z* calcd 1007.4080; obsd $[M]^+$ 1007.4087 (ESI+). The HRMS was performed on an LTQ Orbitrap Discovery mass spectrometer.

Fluorescence microscopy

HeLa cells were plated on each well of a Lab-Tek Chamber Slide System 4-well Permanox slide and the cells were incubated overnight at 37 °C under 5% CO_2. The cells were allowed to achieve ~50% confluency. All washes/media were removed gently with a pipet. The DMEM media was removed from each well and the wells washed with PBS (500 μL). RPMI 1640 media no phenol red supplemented with 10% FCS, 2 mM glutamine, and 1% Pen/Strep containing either DMSO (1 well per slide) or STS (1 μM from 1 mM stock in DMSO) was added to each well and the slides were incubated under the same conditions for the appropriate time course (30 mins, 1 hr, 2 hr – 1 well of each timepoint per slide). The media was removed from each well and the wells were washed with PBS (500 μL). RPMI 1640 media no phenol red containing NJP13 (1 μM) was added to each well. The slides were incubated for 1 hr. The media was removed from each well and the cells were washed with fresh RPMI 1640 clear media for 30 mins. The media was removed and each well was washed with PBS (3 x 500 μL) and cold MeOH (2 x 500 μL). The dividers were removed and the slide was fixed with a couple of drops of MeOH and 3 coverslips (Fisherfinest premium, 18 mm x 18 mm) were added. Images

were taken on a Zeiss Axioplan 2 microscope equipped with a filter that allowed detection of rhodamine (546 excitation, 580-640 emission). A dry 40x objective (Plan-NeoFluar, Zeiss) was used. Phase contrast images were taken by using the channel with polarized halogen light. All images were captured (time of exposure 527 msec), colored, and processed in OpenLab 5.5.2 following the same protocol.

***In situ* labeling with NJP2 and evaluation of inhibitor potency using PS-Rh**

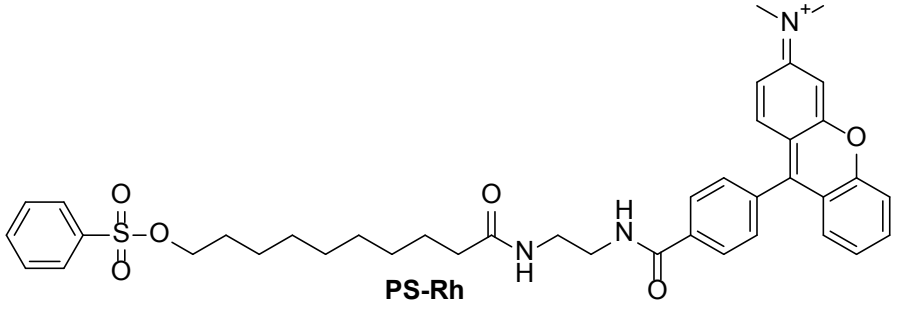

PS-Rh

STS and DMSO control-treated HeLa cells were administered NJP2 (from 10 mM stock in DMSO) to give final NJP2 concentrations of 1, 5, 10, 20, 40, 50, and 60 μM. Cells were harvested and lysates prepared as described above. PS-Rh (10 μM, from 500 μM stock in DMSO), as synthesized according to previous method,[54] was added to each protein aliquot (50 μL, 2 mg/mL). The samples were vortexed and allowed to sit at room temperature for 1 hr. The samples underwent fluorescent gel analysis as described above. Another set of these NJP2-treated protein samples (50 μL, 2 mg/mL) underwent click chemistry and fluorescent gel analysis as described above. The intensity of the bands from the PS-Rh-treated gel was quantified by ImageJ and the IC_{50} value for NJP2 inhibition of GSTO1 in apoptotic cells was calculated from two trials at each inhibitor

concentration (1 – 60 μM). An example of each gel for the apoptotic samples is presented in Appendix III (Figure 2A-1).

References

1. Lockshin, R. A.; Williams, C. M., Programmed Cell Death--II. Endocrine Potentiation of the Breakdown of the Intersegmental Muscles of Silkmoths. *J. Ins. Physiol.* **1964,** *10*, 643-649.

2. Kerr, J. F.; Wyllie, A. H.; Currie, A. R., Apoptosis: A Basic Biological Phenomenon with Wide-Ranging Implications in Tissue Kinetics. *Br. J. Cancer* **1972,** *26*, 239-257.

3. Gewies, A., Introduction to Apoptosis. *ApoReview* **2003**, 1-26.

4. Ouyang, L.; Shi, Z.; Zhao, S.; Wang, F.-T.; Zhou, T.-T.; Liu, B.; Bao, J.-K., Programmed Cell Death Pathways in Cancer: A Review of Apoptosis and Programmed Necrosis. *Cell Prolif.* **2012,** *45*, 487-498.

5. Strasser, A.; Cory, S.; Adams, J. M., Deciphering the Rules of Programmed Cell Death to Improve Therapy of Cancer and Other Diseases. *EMBO J.* **2011,** *30*, 3667-3683.

6. Denault, J.-B.; Salvesen, G. S., Caspases: Keys in the Ignition of Cell Death. *Chem. Rev.* **2002,** *102*, 4489-4499.

7. Kischkel, F. C.; Hellbardt, S.; Behrmann, I.; Germer, M.; Pawlita, M.; Krammer, P. H.; Peter, M. E., Cytotoxicity-Dependent APO-1 (Fas/CD95)-Associated Proteins Form a Death-Inducing Signaling Complex (DISC) with the Receptor. *EMBO J* **1995,** *14*, 5579-5588.

8. van Meer, G.; Voelker, D. R.; Feigenson, G. W., Membrane Lipids: Where They Are and How They Behave. *Nat. Rev. Mol. Cell. Biol.* **2008,** *9*, 112-124.

9. Fadok, V. A.; Voelker, D. R.; Campbell, P. A.; Cohen, J. J.; Bratton, D. L.; Henson, P. M., Exposure of Phosphatidylserine on the Surface of Apoptotic Lymphocytes Triggers Specific Recognition and Removal by Macrophages. *J. of Immunol.* **1992,** *148*, 2207-2216.

10. Fadok, V. A.; Bratton, D. L.; Frasch, S. C.; Warner, M. L.; Henson, P. M., The Role of Phosphatidylserine in Recognition of Apoptotic Cells by Phagocytes. *Cell Death and Differentiation* **1998,** *5*, 551-562.

11. Martin, S.; Reutelingsperger, C. P. M.; McGahon, A. J.; Rader, J. A.; van Schie, R. C. A. A.; LaFace, D. M.; Green, D. R., Early Redistribution of Plasma Membrane Phosphatidylserine is a General Feature of Apoptosis Regardless of the Initiation Stimulus: Inhibition by Overexpression of Bcl-2 and Abl. *J. Exp. Med.* **1995,** *182*, 1545-1556.

12. Leist, M.; Jaattela, M., Four Deaths and a Funeral: From Caspases to Alternative Mechanisms. *Nat. Rev. Mol. Cell Biol.* **2002,** *2*, 589-698.

13. Van Cruchten, S.; Van Den Broeck, W., Morphological and Biochemical Aspects of Apoptosis, Oncosis, and Necrosis. *Anat. Histol. Embryol.* **2002,** *31*, 214-223.

14. Johnstone, R. W.; Ruefli, A. A.; Lowe, S. W., Apoptosis: A Link Between Cancer Genetics and Chemotherapy. *Cell* **2002,** *108*, 153-164.

15. O'Connor, R., A Review of Mechanisms of Circumvention and Modulation of Chemotherapeutic Resistance. *Curr. Cancer Drug Targets* **2009,** *9*, 273-280.

16. Ntziachristos, V.; Schellenberger, E. A.; Ripoll, J.; Yessayan, D.; Graves, E.; Bogdanov Jr., A.; Josephson, L.; Weissleder, R., Visualization of Antitumor Treatment By Means of Fluorescence Molecular Tomography with an Annexin V-Cy5.5 Conjugate. *Proc. Natl. Acad. Sci. U.S.A.* **2004,** *101*, 12294-12299.

17. Belhocine, T.; Steinmetz, N.; Hustinx, R.; Bartsch, P.; Jerusalem, G.; Seidel, L.; Rigo, P.; Green, A., Increased Uptake of Apoptosis-Imaging Agent 99mTc Recombinant Human Annexin V in Human Tumors After One Course of Chemotherapy as a Predictor of Tumor Response and Patient Prognosis. *Clin. Cancer Res.* **2002,** *8*, 2766-2774.

18. Vermeersch, H.; Loose, D.; Lahorte, C.; Mervillie, K.; Dierckx, R.; Steinmetz, N.; Vanderheyden, J. L.; Cuvelier, C.; Slegers, G.; Van de Wiele, C., 99mTc-HYNIC Annexin-V Imaging of Primary Head and Neck Carcinoma. *Nucl. Med. Commun.* **2004,** *25*, 259-263.

19. Edgington, L. E.; Berger, A. B.; Blum, G.; Albrow, V. E.; Paulick, M. G.; Lineberry, N.; Bogyo, M., Noninvasive Optical Imaging of Apoptosis by Caspase-Targeted Activity-Based Probes. *Nat. Med.* **2009,** *15*, 967-973.

20. Zheng, H.; Wang, F.; Wang, Q.; Gao, J., Cofactor-Free Detection of Phosphatidylserine with Cyclic Peptides Mimicking Lactadherin. *J. Am. Chem. Soc.* **2011,** *133*, 15280-15283.

21. Berger, A. B.; Witte, M. D.; Denault, J. B.; Sadaghiani, A. M.; Sexton, K. M.; Salvesen, G. S.; Bogyo, M., Identification of Early Intermediates of Caspase Activition Using Selective Inhibitors and Activity-Based Probes. *Mol. Cell* **2006,** *23*, 509-521.

22. Edgington, L. E.; van Raam, B. J.; Verdoes, M.; Wierschem, C.; Salvesen, G. S.; Bogyo, M., An Optimized Activity-Based Probe for the Study of Caspase-6 Activation. *Chem Biol.* **2012,** *19*, 340-352.

23. Suzuki, J.; Umeda, M.; Sims, P. J.; Nagata, S., Calcium-Dependent Phospholipid Scrambling by TMEM16F. *Nature* **2010,** *468*, 834-838.

24. Taylor, R. C.; Cullen, S. P.; Martin, S. J., Apoptosis: Controlled Demolition at the Cellular Level. *Nat. Rev. Mol. Cell Biol.* **2008,** *9*, 231-241.

25. Bilyy, R. O.; Shkandina, T.; Tomin, A.; Munoz, L. E.; Franz, S.; Antonyuk, V.; Kit, Y. Y.; Zirngibl, M.; Furnrohr, B. G.; Janko, C.; Lauber, K.; Schiller, M.; Schett, G.; Stoika, R. S.; Herrmann, M., Macrophages Discriminate Glycosylation Patterns of Apoptotic Cell-Derived Microparticles. *J. Biol. Chem.* **2011,** *287*, 496-503.

26. Franco, R.; Bortner, C. D.; Cidlowski, J. A., Potential Roles of Electrogenic Ion Transport and Plasma Membrane Depolarization in Apoptosis. *J. Membrane Biol.* **2006,** *409*, 43-58.

27. Darzynkiewicz, Z.; Juan, G.; Li, X.; Gorczyca, W.; Murakami, T.; Traganos, F., Cytometry in Cell NecroBiology: Analysis of Apoptosis and Accidental Cell Death (Necrosis). *Cytometry* **1997,** *27*, 1-20.

28. Damianovich, M.; Ziv, I.; Heyman, S. N.; Rosen, S.; Shina, A.; Kidron, D.; Aloya, T.; Grimberg, H.; Levin, G.; Reshef, A.; Bentolila, A.; Cohen, A.; Shirvan, A., ApoSense: A Novel Technology for Functional Molecular Imaging of Cell Death in Models of Acute Renal Tubular necrosis. *Eur. J. Nucl. Med. Mol. Imaging* **2005,** *33*, 281-291.

29. Plantin-Carrenard, E.; Bringuier, A.; Derappe, C.; Pichon, J.; Guillot, R.; Bernard, M.; Foglietti, M. J.; Feldmann, G.; Aubery, M.; Braut-Boucher, F., A Fluorescence Microplate Assay Using Yo-pro1 to Measure Apoptosis: Application to HL60 Cells Subjected to Oxidative Stress. *Cell Biol. Toxicol.* **2003,** *19*, 121-133.

30. Park, D.; Don, A. S.; Massamiri, T.; Karwa, A.; Warner, B.; MacDonald, J.; Hemenway, C.; Naik, A.; Kuan, K. T.; Dilda, P. J.; Wong, J. W.; Camphausen, K.; Chinen, L.; Dyszlewski, M.; Hogg, P. J., Noninvasive Imaging of Cell Death Using an HSP90 Ligand. *J. Am. Chem. Soc.* **2011,** *133*, 2832-2835.

31. Idziorek, T.; Estaquier, J.; De Bels, F.; Ameisen, J. C., YO-PRO1 Permits Cytofluorometric Analysis of Programmed Cell Death (Apoptosis) Without Interfering with Cell Viability. *J. Immunol. Methods* **1995,** *185*, 249-258.

32. Barglow, K. T.; Cravatt, B. F., Discovering Disease-Associated Enzymes by Proteome Reactivity Profiling. *Chem. Biol.* **2004,** *11*, 1523-1531.

33. Weerapana, E.; Simon, G. M.; Cravatt, B. F., Disparate Proteome Reactivity Profiles Carbon Electrophiles. *Nat. Chem. Biol.* **2008,** *4* (7), 405-407.

34. Karaman, M. W.; Herrgard, S.; Treiber, D. K.; Gallant, P.; Atteridge, C. E.; Campbell, B. T.; Chan, K. W.; Ciceri, P.; Davis, M. I.; Edeen, P. T.; Faraoni, R.; Floyd, M.; Hunt, J. P.; Lockhart, D. J.; Milanov, Z. V.; Morrison, M. J.; Pallares, G.; Patel, H. K.; Pritchard, S.; Wodicka, L. M.; Zarrinkar, P. P., A Quantitative Analysis of Kinase Inhibitor Selectivity. *Nat. Biotechnol.* **2008,** *26*, 127-132.

35. Chae, H.-J.; Kang, J.-S.; Byun, J.-O.; Han, K.-S.; Kim, D.-U.; Oh, S.-M.; Kim, H.-M.; Chae, S.-W.; Kim, H.-R., Molecular Mechanism of Staurosporine-Induced Apoptosis in Osteoblasts. *Pharmacological Research* **2000,** *42*, 373-381.

36. Speers, A. E.; Adam, G. C.; Cravatt, B. F., Activity-Based Protein Profiling In Vivo Using Copper(I)-Catalyzed Azide-Alkyne [3 + 2] Cycloaddition. *J. Am. Chem. Soc.* **2003,** *125*, 4686-4687.

37. Ulukan, H.; Swaan, P. W., Camptothecins, A Review of Their Chemotherapeutical Potential. *Drugs* **2002,** *62*, 2039-2057.

38. Weerapana, E.; Speers, A. E.; Cravatt, B. F., Tandem Orthogonal Proteolysis-Activity-Based Protein Profiling (TOP-ABPP)-A General Method for Mapping Sites of Probe Modification in Proteomes. *Nature Prot.* **2007,** *2* (6), 1414-1425.

39. Hayes, J. D.; Flanagan, J. U.; Jowsey, I. R., Glutathione Transferases. *Annu. Rev. Pharmacol. Toxicol.* **2005,** *45*, 51-88.

40. Hayes, J. D.; Pulford, D. J., The Glutathione S-Transferase Supergene Family: Regulation of GST* and the Contribution of the Isoenzymes to Cancer Chemoprotection and Drug Resistance. *Crit. Rev. Biochem. Mol. Biol.* **1995,** *30*, 445-600.

41. Laborde, E., Glutathione Transferases as Mediators of Signaling Pathways Involved in Cell Proliferation and Cell Death. *Cell Death and Diff.* **2010,** *17*, 1373-1380.

42. Mannervik, B.; Awasthi, Y. C.; Board, P. G.; Hayes, J. D.; Di Ilio, C.; Ketterer, B., Nomenclature for Human Glutathione Transferases. *Biochem. J.* **1992,** *282*, 305-306; Mannervik, B.; Board, P. G.; Hayes, J. D.; Listowsky, I.; Pearson, W. R., Nomenclature for Mammalian Soluble Glutathione Transferases. *Methods Enzymol.* **2005,** *401*, 1-8.

43. Board, P. G.; Coggan, M.; Chelvanayagam, G.; Easteal, S.; Jermiin, L. S.; Schulte, G. K.; Danley, D. E.; Hoth, L. R.; Griffor, M. C.; Kamath, A. V.; Rosner, M. H.; Chrunyk, B. A.; Perregaux, D. E.; Gabel, C. A.; Geoghegan, K. F.; Pandit, J.,

Identification, Characterization, and Crystal Structure of the Omega Class Glutathione Transferases. *J. Biol. Chem.* **2000,** *275*, 24798-24806.

44. Board, P., The Omega-Class Glutathione Transferases: Structure, Function, and Genetics. *Drug Metabolism Reviews* **2011,** *43*, 226-235.

45. Whitbread, A. K.; Tetlow, N.; Eyre, H. J.; Sutherland, G. R.; Board, P. G., Characterization of the Human Omega Glutathione Transferase Genes and Associated Polymorphisms. *Pharmacogenetics* **2003,** *13*, 131-144.

46. Adam, G. C.; Burbaum, J.; Kozarich, J. W.; Patricelli, M. P.; Cravatt, B. F., Mapping Enzyme Active Sites in Complex Proteomes. *J. Am. Chem. Soc.* **2004,** *126*, 1363-1368.

47. Yan, X. D.; Pan, L. Y.; Yuan, Y.; Lang, J. H.; Mao, N., Identification of Platinum-Resistance Associated Proteins through Proteomic Analysis of Human Ovarian Cancer Cells and Their Platinum-Resistant Sublines. *J. Proteome Res.* **2007,** *6*, 772-780.

48. Piaggi, S.; Raggi, C.; Corti, A.; Pitzalis, E.; Mascherpa, M. C.; Saviozzi, M.; Pompella, A.; Casini, A. F., Glutathione Transferase Omega 1-1 (GSTO1-1) Plays an Anti-Apoptotic Role in Cell Resistance to Cisplatin Toxicity. *Carcinogenesis* **2010,** *31*, 804-811.

49. Son, J.; Lee, J.-J.; Lee, J.-S.; Schuller, A.; Chang, Y.-T., Isozyme-Specific Fluorescent Inhibitor of Glutathione S-Transferase Omega 1. *ACS Chem. Biol.* **2010,** *5*, 449-453.

50. Tsuboi, K.; Bachovchin, D. A.; Speers, A. E.; Spicer, T. P.; Fernandex-Vega, V.; Hodder, P.; Rosen, H.; Cravatt, B. F., Potent and Selective Inhibitors of Glutathione S-

Transferase Omega 1 That Impair Cancer Drug Resistance. *J. Am. Chem. Soc.* **2011,** *133*, 16605-16616.

51. Dix, M. M.; Simon, G. M.; Cravatt, B. F., Global Mapping of the Topography and Magnitude of Proteolytic Events in Apoptosis. *Cell* **2008,** *134*, 679-691.

52. Speers, A. E.; Cravatt, B. F., Profiling Enzyme Activities In Vivo Using Click Chemistry Methods. *Chem. Biol.* **2004,** *11*, 535-546.

53. Adam, G. C.; Sorensen, E. J.; Cravatt, B. F., Proteomic Profiling of Mechanistically Distinct Enzyme Classes Using a Common Chemotype. *Nat. Biotechnol.* **2002,** *20*, 805-809.

54. Bachovchin, D. A.; Brown, S. J.; Rosen, H.; Cravatt, B. F., Identification of Selective Inhibitors of Uncharacterized Enzymes by High-Throughput Screening with Fluorescent Activity-Based Probes. *Nat. Biotechnol.* **2009,** *27*, 387-394.

55. Son, J.; Lee, J. J.; Lee, J. S.; Schuller, A.; Chang, Y. T., Isozyme-Specific Fluorescent Inhibitor of Glutathione S-Transferase Omega 1. *ACS Chem. Biol.* **2010,** *5*, 449-453.

56. Edgington, L. E.; Verdoes, M.; Bogyo, M., Functional Imaging of Proteases: Recent Advances in the Design and Application of Substrate-Based and Activity-Based Probes. *Curr. Opin. Chem. Biol.* **2011,** *15*, 798-805.

57. Speers, A. E.; Cravatt, B. F., Profiling enzyme activities in vivo using click chemistry methods *Chem. Biol.* **2004,** *11*, 535-546.

58. Eng, J. K.; McCormack, A. L.; Yates III, J. R., An Approach to Correlate Tandem Mass Spectral Data of Peptides with Amino Acid Sequences in a Protein Database. *J. Am. Mass Spectrom.* **1994,** *5*, 976-989.

59. Tabb, D. L.; McDonald, W. H.; Yates III, J. R., DTASelect and Contrast: Tools for Assembling and Comparing Protein Identifications from Shotgun Proteomics. *J. Proteome res.* **2002,** *1*, 21-26.

Chapter 3

A chemical-proteomic platform to identify zinc-binding cysteine residues

A significant portion of the work described in this chapter has been published in:

Pace, N. J.; Weerapana, E. A Competitive Chemical-Proteomic Platform to Identify Zinc-Binding Cysteines. *ACS Chem. Biol.* **2014**, *9*, 258-265.

Pace, N. J.; Weerapana, E. Zinc-Binding Cysteines: Diverse Functions and Structural Motifs. *Biomolecules* **2014**, *4*, 419-434.

Qian, Y.; Martell, J.; Pace, N. J.; Ballard, T. E.; Johnson, D. S.; Weerapana, E. An Isotopically Tagged Azobenzene-Based Cleavable Linker for Quantitative Proteomics. *ChemBioChem* **2013** *14*, 1410-1414.

Introduction

Overview

Of the biologically relevant transition metals, zinc is the second most abundant found within cells, behind only iron. Zinc ions (Zn^{2+}) facilitate diverse protein functions that are essential for life. Common Zn^{2+} ligands within proteins include cysteine (S), histidine, (N), aspartate (O), and glutamate (O) residues. In particular, cysteine residues are very often observed as ligands at Zn^{2+}-binding sites. The ionization state of the thiol group of cysteine governs its ability to bind metals such as Zn^{2+}. Because the ionization state of cysteine is highly sensitive to small changes within the local protein environment,[1] the affinity of cysteine for Zn^{2+} varies accordingly for each individual cysteine within a protein scaffold. These resulting Zn^{2+}-cysteine complexes can be categorized by function: those that contribute to protein structure, catalysis, or regulation (Figure 3-1).[2, 3] Additionally, the cysteine-rich metallothioneins tightly regulate cellular Zn^{2+} levels by storing and properly redistributing Zn^{2+} throughout the cell.[4] Due to these diverse functional roles of Zn^{2+}-cysteine complexes, the development of both experimental and theoretical approaches has been paramount in the identification and characterization of Zn^{2+}-binding cysteines. Herein, we summarize key examples of functional cysteine complexes and discuss recent advances in methodologies to study them.

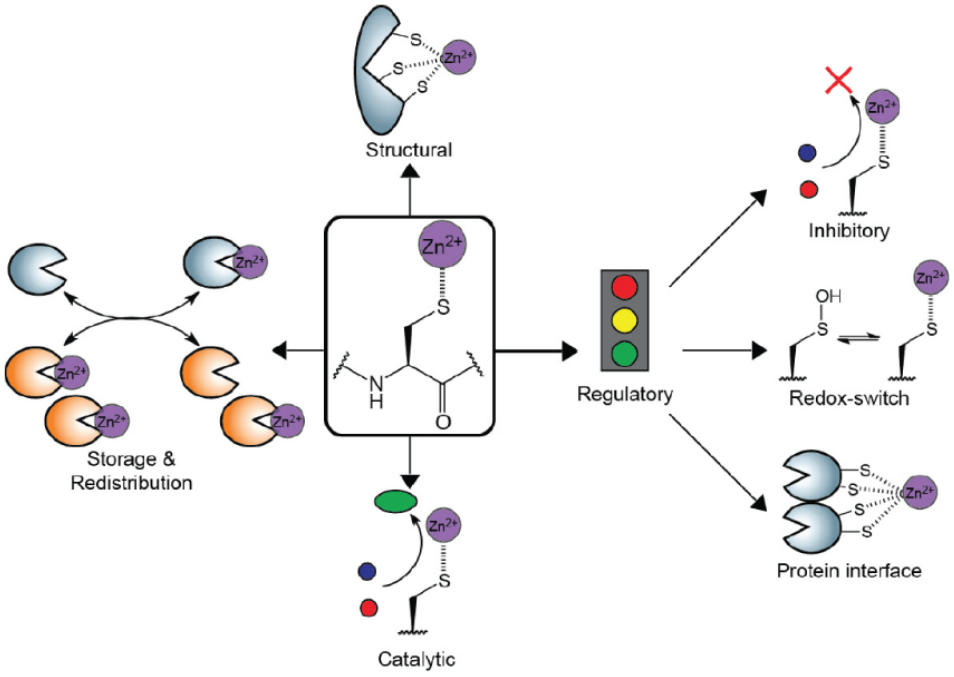

Figure 3-1. The diverse functional roles of Zn^{2+}-cysteine complexes. Figure adapted from Pace *et al*.[5]

Structural Zn^{2+}-cysteine complexes

Since zinc is a d10 transition metal, it exclusively forms a Zn^{2+} ion and lacks redox activity within cells. Zn^{2+} typically is found to assemble coordination complexes with four ligands in a tetrahedral geometry. Recent studies estimate the human proteome consists of approximately 3000 Zn^{2+}-proteins.[6] Out of all the potential Zn^{2+} ligands within proteins (cysteine, histidine, aspartate, or glutamate), the sulfur atom of cysteine transfers the most charge over to Zn^{2+}. As cysteine occupies more ligand sites, it often quenches the ability of Zn^{2+} to act as a Lewis acid, rendering these complexes relatively inert.[7] Consequently, Zn^{2+}-cysteine complexes traditionally perform structural roles within proteins with the most abundant and extensively studied of these being the zinc-finger motif.[8]

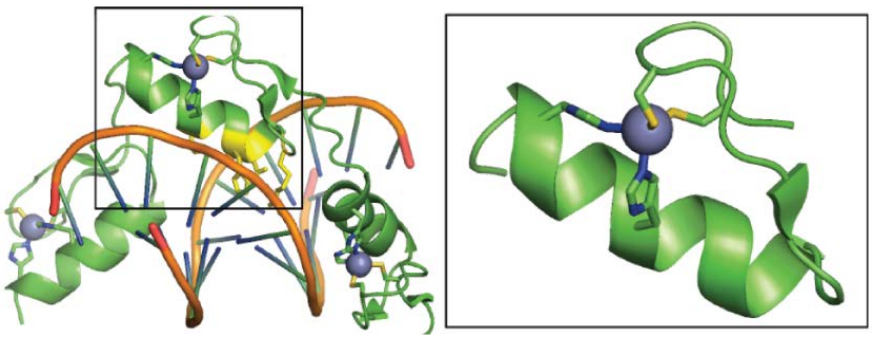

Figure 3-2. Three zinc-finger motifs bound within the major groove of a DNA strand with a single zinc-finger being highlighted (PDB ID: 1A1J). Figure adapted from Pace *et al*.[5]

Zinc-finger motifs are canonically comprised of Cys_4 or Cys_2His_2 coordination environments.[6] The classical Cys_2His_2 zinc finger chelates a single Zn^{2+} within an α-helix and antiparallel β-sheet (Figure 3-2).[9] Zinc-finger domains are typically found in clusters of four or more within a single protein, and often structurally stabilize the protein to promote interactions with other proteins and biomolecules, such as DNA and RNA. Although the functional roles of most zinc-finger proteins are poorly understand, most annotated proteins act as transcriptional activators or suppressors.[10] A single zinc finger possesses four amino acids at the -1, 2, 3, and 6 positions of the α-helix (Figure 3-2, highlighted in yellow) that participate in hydrogen-bond interactions with 3-4 nucleic acids within the major groove of DNA.[11] Differential sequences at these four positions preferentially bind to distinct nucleic acid sequences with high affinity and selectivity.[11] Consequently, this motif has been exploited in the development of zinc-finger endonucleases for genetic engineering. By conjugating specific arrays of zinc-fingers to a promiscuous FokI endonuclease, DNA can be cut at an indicated sequence to disrupt, add, or correct the gene of interest.[12] The development of a conserved linker sequence

was vital to the construction of polymeric zinc-finger endonucleases, requiring DNA sequences of up to 18 bp for recognition.[13] This advance provided enough specificity to target single genes within the human genome,[14, 15] and has extended genetic engineering to diverse gene families.[12]

Catalytic Zn^{2+}-cysteine complexes

Beyond their structural roles, cysteines bind Zn^{2+} to directly facilitate enzymatic transformations. Cysteines are less commonly observed ligands in catalytic Zn^{2+} complexes due to the steric bulk of the sulfur and greater charge transfer compared to histidine or water ligands.[7] However, catalytic Zn^{2+}-cysteine complexes have been observed across diverse enzyme classes, such as oxidoreductases, hydrolases, and transferases (Table 3-1). The exact mechanism varies within each individual enzyme, but typically is comprised of either substrate coordination or activation by the Zn^{2+}.

Protein	Enzyme Class	Function	Mechanism
Alcohol dehydrogenase	Oxidoreductase	Interconverts alcohols to aldehyde and ketones	Zn^{2+}-coordination of substrate[16]
Sorbitol dehydrogenase	Oxidoreductase	Interconverts sorbitol to fructose	Zn^{2+}-activation of nucleophilic water molecule[17]
Cytidine deaminase	Hydrolase	Irreversible hydrolytic deamination of cytidine to uridine	Zn^{2+}-activation of nucleophilic water molecule[18, 19]
GTP cyclohydrolase	Hydrolase	Converts GTP to dihydroneopterin	Zn^{2+}-activation of nucleophilic water molecule[20]
Betaine-homocysteine methyltransferase	Transferase	Transfers methyl group from betaine to homocysteine, forming dimethyl glycine and methionine	Zn^{2+}-activation of thiol of homocysteine substrate[21]
Protein farnesyltransferase	Transferase	Post-translational addition of farnesyl to cysteine residues within proteins	Zn^{2+}-activation of thiol on target protein[22, 23]

Table 3-1. Representative human proteins containing catalytic Zn^{2+}-cysteine complexes.

Alcohol dehydrogenases (ADHs) constitute a well-studied class of enzymes that were first discovered to require a Zn^{2+} for catalysis over 50 years ago.[24] These evolutionarily conserved enzymes facilitate the interconversion between alcohols and ketones or aldehydes. Humans possess six distinct classes of ADH enzymes (Figure 3-3a), each utilizing a catalytic mechanism dependent on a cysteine residue binding Zn^{2+}.[25] The active enzyme is a dimer, with each 40 kD monomer possessing a catalytic complex comprised of a Zn^{2+} bound to cysteine and an NAD^+ cofactor.[16, 26] In the case of ADH5, the Zn^{2+} is bound to Cys46 and Cys 174 (red), His66 (blue) and coordinates the alcohol substrate (cyan) adjacent to the NAD^+ (yellow). The bound Zn^{2+} coordinates the substrate in the correct geometry for the sequential proton transfer to Ser48, NAD^+, and His51, while also properly positioning the alcohol for hydride transfer to NAD^+ (Figure 3-3b). Although they do not directly interact with the substrate, these cysteine residues are essential for ADH activity and are highly conserved through human ADH enzyme classes.[25]

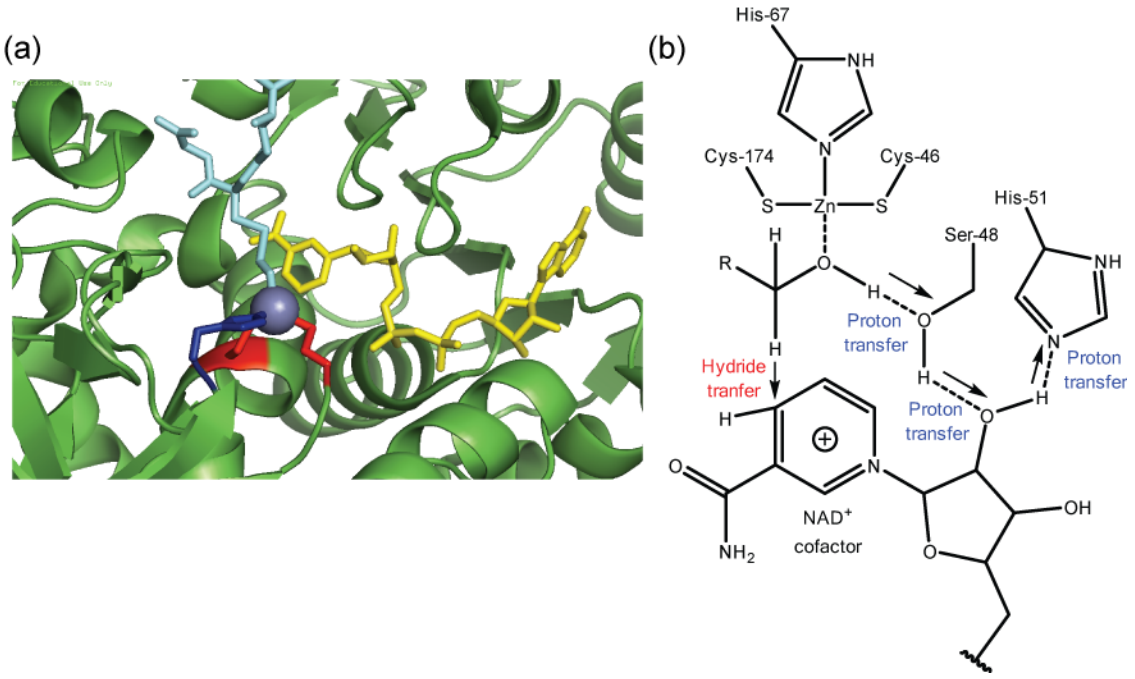

Figure 3-3. (a) The active-site of ADH5 contains a Zn^{2+} (purple) bound to two cysteines (Cys46, Cys174, red), a histidine (His66, blue), and *S*-hydroxymethyl glutathione as the alcohol substrate (cyan). This positions the alcohol in the correct geometry to the adjacent NAD^+ cofactor (yellow) (PDB ID: 1MC5). (b) The bound Zn^{2+} facilitates sequential proton transfers from the alcohol substrate to Ser48, NAD^+, and His51, while also properly positioning the alcohol for a hydride transfer to NAD^+. Figures adapted from Pace *et al*.[5]

Regulatory Zn^{2+}-cysteine complexes

Additionally, cysteine residues have also been observed to bind Zn^{2+} to modulate protein activities. In these cases, Zn^{2+}-binding must be weaker and more transient in nature to allow for the interchange between bound and apo-forms. As a result, these cysteines are often more challenging to identify. Characterized regulatory mechanisms range in complexity, and include inhibitory, redox-switches, and protein interface Zn^{2+}-

cysteine complexes (Table 3-2). Herein, we will detail each class and provide a well-characterized example.

Protein	Enzyme Class	Function	Mechanism
Dimethylarginine dimethylaminohydrolase	Hydrolase	Converts N-omega,N-omega-methyl-L-arginine to dimethylamine and L-citrulline	Inhibitory[27]
Ornithine transcarbamoylase	Transferase	Converts carbamoyl phosphate and ornithine to citrulline and phosphate	Inhibitory[28]
Cathepsin S	Protease	Lysosomal cysteine protease	Inhibitory[29, 30]
Caspase 3	Protease	Cysteine protease	Inhibitory[31, 32]
Caspase 6	Protease	Cysteine protease	Inhibitory[33]
Caspase 9	Protease	Cysteine protease	Inhibitory[34]
Aconitase 2	Isomerase	Converts citrate to iso-citrate	Inhibitory[35]
Glutathione *S*-transferase omega 1	Transferase	Conjugates glutathione to a variety of electrophiles	Inhibitory[36]
Betaine-homocysteine methyltransferase	Transferase	Transfers methyl group from betaine to homocysteine, forming dimethyl glycine and methionine	Redox-switch[37]
Protein kinase C	Kinase	Phosphorylates serines and threonines	Redox-switch[38]
Nitric oxide synthase	Oxidoreductase	Produces nitric oxide and arginine	Protein interface[39]; Redox-switch[40]
Apo2L/TRAIL	Cytokine	Induces signaling pathways to trigger apoptosis	Protein interface[41]

Table 3-2. Representative human proteins containing regulatory Zn^{2+}-cysteine complexes.

Inhibitory Zn^{2+}-cysteine complexes

Cysteine residues have been found to bind Zn^{2+} as a means of inhibiting enzymatic activities.[29] Inhibition usually occurs by chelation of Zn^{2+} to the catalytic cysteine residue (*e.g.* dimethylarginine dimethylaminohydrlase), but allosteric inhibition attributed to Zn^{2+}-binding at a cysteine distal to the active-site has also been described (*e.g.* caspase 9) (Table 3-2).

Dimethylarginine dimethylaminohydrolase (DDAH-1) is a metabolic enzyme responsible for the conversion of dimethylarginine to dimethylamine and citrulline.

Dimethylarginine is known to inhibit nitric oxide synthases to mitigate the production of nitric oxide, an important cell-signaling molecule.[42] The best studied DDAH-1 is from bovine; however, the human homologue retains 94% sequence homology. Zn^{2+} inhibits DDAH-1 activity with a K_i of 4.2 nM at pH 7.4.[27] This value is rather high when considering the physiological range of available Zn^{2+} concentrations and is suggestive of a weaker, more transient binding mode that is indicative of a regulatory role for Zn^{2+} within DDAH-1. The enzyme functions through a nucleophilic cysteine residue (Cys274) conserved in both the human and bovine forms.[43] Structural studies reveal a Zn^{2+} (purple) bound to the catalytic Cys274 (red) and His173 (blue) within the active-site of the enzyme (Figure 3-4).[44] The remaining two ligands are comprised of water molecules (white) stabilized by hydrogen-bonding to adjacent Asp79 and Glu78 (orange). DDAH-1 only possesses two Zn^{2+} ligands instead of the typical three or four, which may contribute to the weaker, more transient Zn^{2+} binding.

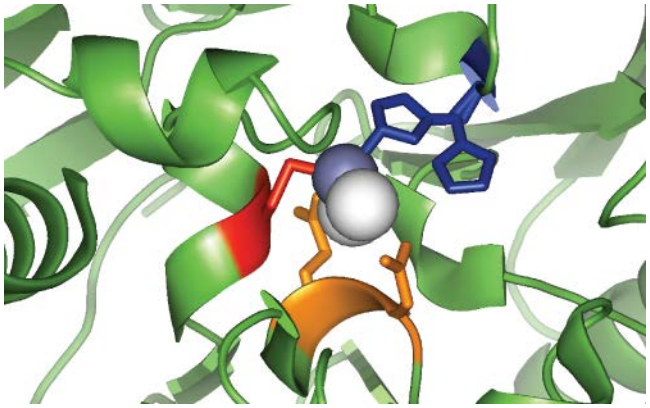

Figure 3-4. Zn^{2+} bound within the active-site of DDAH-1 (PDB ID: 2CI7).[44] Figure adapted from Pace *et al*.[5]

Although most inhibitory Zn^{2+}-cysteine complexes are found to bind directly to the nucleophilic cysteine residue, the potential for allosteric inhibition has been realized

in the case of caspase-9. Caspases are cysteine-dependent aspartate-directed proteases that play a prevalent role in signaling cascades culminating in apoptosis.[45] Zn^{2+} has been implicated as a strict mediator of apoptosis, where small fluctuations in concentration can strongly dictate cell survival and death.[46] Caspase-9 is an initiator caspase that goes on to cleave executioner caspases-3 and -7 to trigger apoptosis. When attempting to decipher the mechanism of Zn^{2+}-mediated inhibition of capase-9, two distinct Zn^{2+} binding sites were uncovered. The first, comprised of the catalytic dyad, His237 and Cys239 (red), along with the adjacent Cys287 (red), was primarily responsible for the Zn^{2+}-mediated inhibition.[34] The second binding site, which comprised Cys272, Cys230, and His224 (orange), was found distal to the active-site (Figure 3-5). Subsequent assays suggested that this distal site may have the potential for Zn^{2+}-mediated allosteric inhibition of caspase-9 activity.[34] To give precedence to this notion, Zn^{2+}-mediated allosteric inhibition has been observed in Caspase-6; however, cysteines are not Zn^{2+} ligands in this instance.[33]

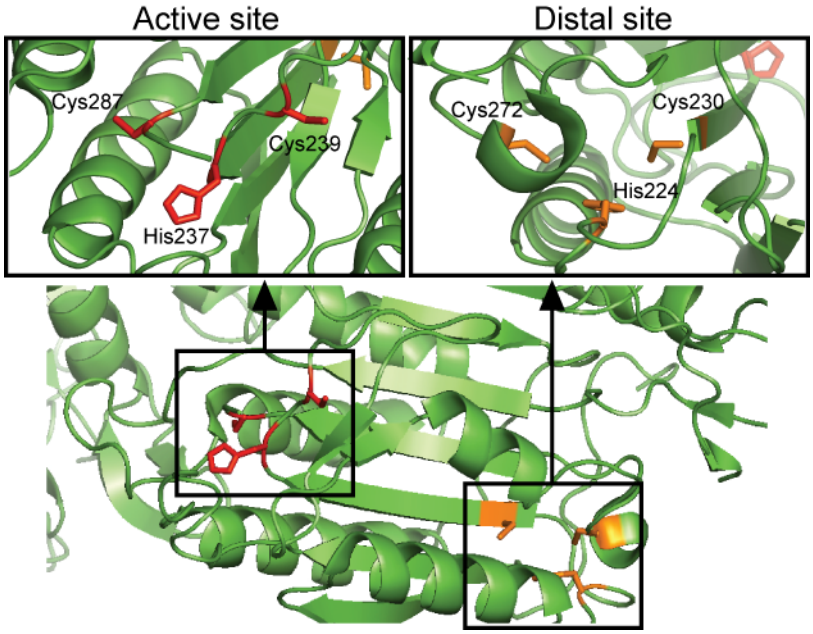

Figure 3-5. Caspase-9 structure highlighting possible Zn^{2+}-cysteine inhibitory sites. Figure adapted from Pace *et al*.[5]

Redox-switch Zn^{2+}-cysteine complexes

Cysteine residues are susceptible to a myriad of post-translational modifications including oxidation, nitrosation, and disulfide formation.[47-49] The ability of cysteine to bind Zn^{2+} is predicated upon the presence of a fully reduced, unmodified thiol. Cellular redox metabolism can therefore be coupled to Zn^{2+}-binding, giving rise to a "redox-switch" regulatory mechanism, where increase in oxidants of sulfur release Zn^{2+} and reductants restore the Zn^{2+}-binding capacity of the thiol.[50] Regulatory Zn^{2+}-cysteine complexes that function through a redox-switch mechanism have been found to modulate diverse enzymatic activities (Table 3-2). Betaine-homocysteine methyltransferase (BHMT) is an essential metabolic enzyme that contributes to the biosynthesis of glycine, serine, threonine, and methionine.[51] This transformation relies on a Zn^{2+}-cysteine complex to activate the homocysteine substrate (cyan). Under reducing conditions, Cys217, Cys299, and Cys300 (red) chelate Zn^{2+} (purple) to assemble the active form of the enzyme (Figure 3-6, left). Upon exposure to oxidative conditions, Cys217 and Cys299 (red) form a disulfide bond resulting in the release of Zn^{2+} and inactivation of the enzyme (Figure 3-6, right).[37] This interplay between Zn^{2+}-binding and disulfide formation couples the intracellular redox state to BHMT activity.

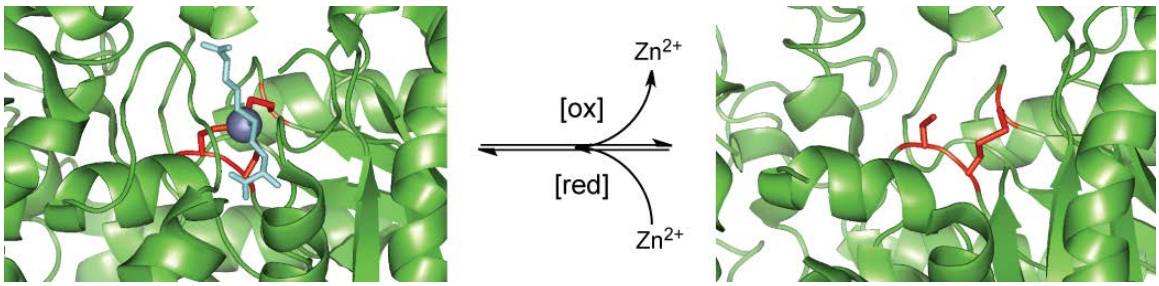

Figure 3-6. A Zn^{2+}-cysteine redox-switch regulates BHMT activity. Figure adapted from Pace *et al*.[5]

Protein interface Zn^{2+}-cysteine complexes

Zn^{2+}-cysteine complexes can also stabilize interactions between two proteins or protein-subunits. The dependence of these protein-protein interactions on available Zn^{2+} levels establishes a novel mechanism to modulate protein supramolecular assembly and subsequent enzymatic activities (Table 3-2). Nitric oxide synthases (NOS) catalyze the formation of nitric oxide and citrulline from arginine through a complex mechanism consisting of five single-electron transfers.[52] Proper dimer formation is essential for oxidoreductase activity. Structures of the endothelial NOS isoform (NOS3) revealed a Zn^{2+} bound to Cys94 and Cys99 from each monomer (Figure 3-7).[39] The Zn^{2+}-cysteine complex assists in proper dimer formation, a prerequisite for binding of the substrates and cofactors. Additionally, these Zn^{2+}-binding cysteines appeared susceptible to redox-modifications, particularly by peroxynitrite. A recent study speculates that peroxynitrite facilitates disulfide-bond formation between Cys94 and Cys99 in each monomer, allowing for subsequent release of Zn^{2+}, release of free monomers, and disruption of enzyme activity.[40] This Zn^{2+}-cysteine complex, employing both protein interface and

redox-switch mechanisms, illustrates the potential for multifaceted protein regulation by Zn^{2+}-binding cysteines.

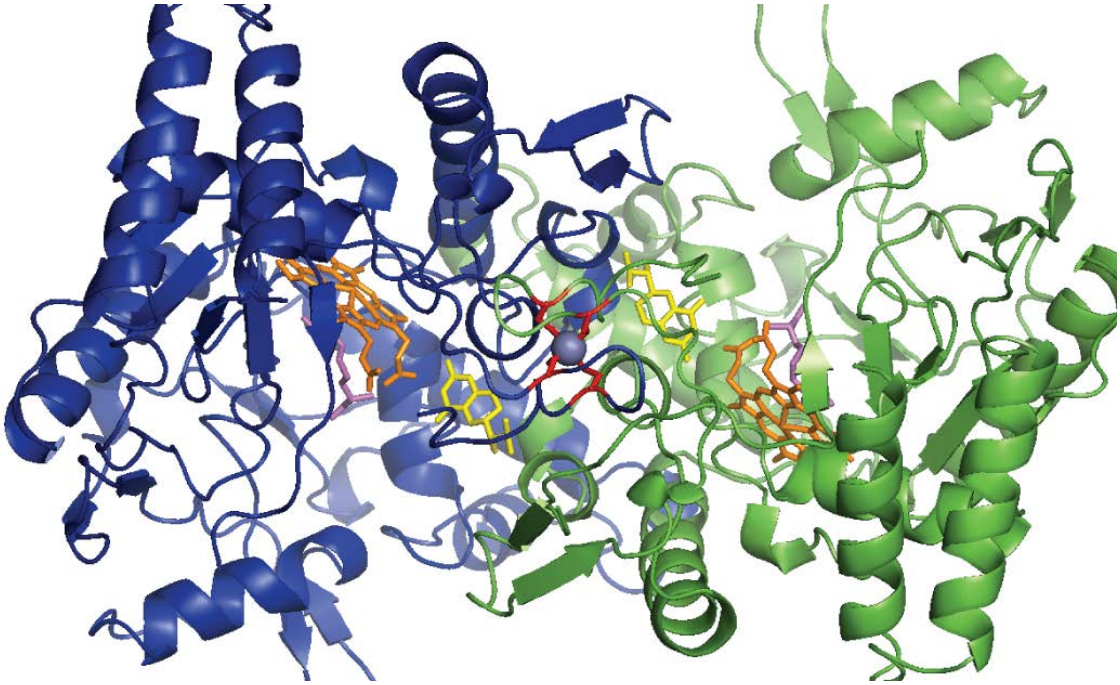

Figure 3-7. The α-subunit (green) and β-subunit (blue) of NOS3 are dependent on Zn^{2+}-binding cysteines for dimerization. Cys94 and Cys99 (red) from each subunit chelate a Zn^{2+} (purple) to stabilize dimer formation, allowing for proper binding of the heme cofactor (orange), tetrahydrobiopferin cofactor (yellow), and the homo-arginine substrate (magenta) within each active-site (PDB ID: 3NOS). Figure adapted from Pace *et al*.[5]

Zn^{2+}-cysteine complexes for Zn^{2+} transfer and cellular redistribution

Zn^{2+} readily forms stable coordination complexes, resulting in extremely low concentrations of free Zn^{2+} within cells.[53, 54] On the contrary, total cellular Zn^{2+} concentrations have been estimated on the order of 100 micromolar with Zn^{2+} being strongly buffered through a protein storage system.[55] Metallothioneins are a superfamily of low molecular weight proteins (6 – 7 kD) that possess 20 cysteine residues capable of

binding up to 7 Zn^{2+} within Zn_4Cys_{11} and Zn_3Cys_9 clusters with unique geometries. These clusters have been evaluated as thermodynamically stabile, yet kinetically labile.[56] As a result, metallothionein and the apo-form, thionein, are able to rapidly donate/accept Zn^{2+} through ligand exchange.[57] This rapid exchange allows metallothioneins to increase the pool of available Zn^{2+}, providing an adequate source of Zn^{2+} for proteins.[58] Interestingly, while Zn^{2+}-binding to metallothioneins has not been found to be cooperative, the cysteines of the Zn_4Cys_{11} bind slightly tighter than the Zn_3Cys_9 cluster, producing a more fluid buffering mechanism.[54] Zn^{2+}-complexes regulated by metallothioneins/thioneins modulate diverse protein activities such as gene expression and DNA repair.[59]

Methods of identification of Zn^{2+}-cysteine complexes

Because of the importance of Zn^{2+}-cysteine complexes to protein structure and function, strategies to identify them have been thoroughly explored. The most common methods combine experimental strategies, including structural genomics and NMR-based platforms, with computational approaches, consisting of homology searches of sequence databases.[60-62] Despite advances in both these fields, they frequently encounter a number of limitations. These structure-based approaches are reliant on a high resolution structure being available for the protein of interest or a close homologue, and the Zn^{2+}-cysteine complex must be stable to the conditions required to produce the structure. Similarly, computational methods have been successful in identifying Zn^{2+}-cysteine complexes with recognized sequence conservation, but are ineffective at predicting Zn^{2+}-cysteine complexes in which the defining structural features are unknown. For both cases, differentiation between protein-bound Zn^{2+} and other metal ions remains challenging,

thereby complicating the identification of the physiologically relevant metal species. Together, these methods prove to be well-suited to distinguish Zn^{2+}-cysteine complexes within motifs where structural features have been well-defined, such as zinc-finger domains; however, regulatory Zn^{2+}-cysteine complexes are more difficult to identify due to their necessary transient binding. By nature, these complexes must be more labile to allow for interchange between the Zn^{2+}-bound and apo-protein forms. The employment of fewer protein-based ligands (one or two instead of three or four) and the use of ligands from multiple proteins or subunits at binding interfaces contribute to this transient binding ability. As a result, regulatory Zn^{2+}-cysteine complexes are difficult to predict, and structures and homology searches fail to sufficiently detect them.

Due to their importance and the limitations of current technologies, the development of new platforms to characterize functional Zn^{2+}-cysteine complexes is vital for their expanded annotation across the entire proteome. Herein, we propose an alternative strategy for identifying Zn^{2+}-cysteine complexes within the human proteome, especially transient, regulatory complexes. Functionally important cysteine residues, including metal-binding cysteines, typically exhibit hyper-reactivity[63] and are therefore susceptible to covalent modification by small molecules containing cysteine-reactive electrophiles.[64] Our hypothesis is predicated upon the mitigated nucleophilicity of the metal-bound thiol of cysteine as compared to the free thiol; thus, Zn^{2+}-binding cysteines would show a decreased reactivity with cysteine-reactive chemical probes upon pretreatment with Zn^{2+} ions. These reactivity changes could be visualized by in-gel fluorescence and quantified using mass spectrometry (Figure 3-8).

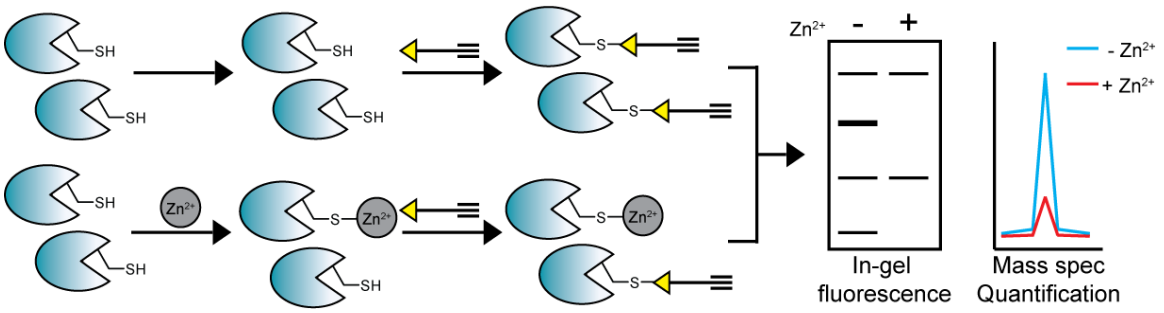

Figure 3-8. Proposed chemical-proteomic platform coupled to in-gel fluorescence or mass spectrometry for identification of Zn^{2+}-cysteine complexes and quantification of their relative affinities.

Results and Discussion

Cysteine-reactive probes can identify Zn^{2+}-cysteine complexes

Of the many cysteine-reactive probes utilized within the lab, two were selected to validate our proposed strategy based on their contrasting reactivities. The commonly used IA-alkyne (N-(hex-5-yn-1-yl)-2-iodoacetamide), a highly reactive, promiscuous probe for cysteines, was first employed for an initial gel-based evaluation (Figure 3-9a). Soluble HeLa lysates were first treated with a panel of biologically relevant divalent metal ions: Zn^{2+}, Ca^{2+}, Mg^{2+}, or Mn^{2+}. After pre-treatment, the lysates were administered IA-alkyne, fractionated on a size exclusion column to eliminate any unbound metal or probe, and visualized by in-gel fluorescence after incorporation of rhodamine azide (Rh-N_3) through click chemistry (Figure 3-9b). Although a few proteins experienced an observable reduction in fluorescence signal upon Zn^{2+}-treatment, the IA-alkyne's high reactivity resulted in conjugation to a large amount of proteins, which made distinguishing Zn^{2+}-sensitivity rather difficult.

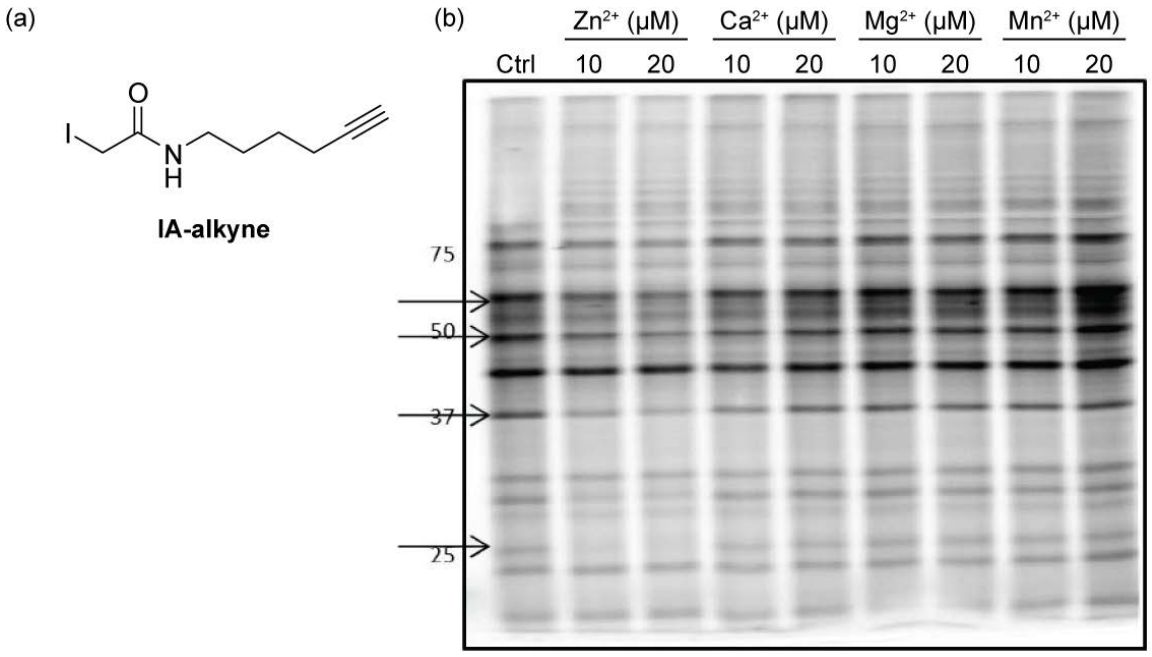

Figure 3-9. (a) Structure of IA-alkyne. (b) In-gel fluorescence analysis of HeLa lysates treated with Zn^{2+}, Ca^{2+}, Mg^{2+}, or Mn^{2+} and subsequently administered IA-alkyne.

NJP14 was also chosen to evaluate the proposed strategy. When evaluating our peptide-based library of cysteine-reactive probes, NJP14 was found to label a distinct subset of reactive cysteines from diverse protein classes as identified by LC/LC-MS/MS and detailed in Appendix II (Table 3A-1).[36] NJP14 consists of a Ser-Pro-Pra-Phe-Phe pentapeptide scaffold conjugated to a moderately-cysteine reactive chloroacetamide electrophile (Figure 3-10a). Because of its moderate-reactivity towards only a subset of reactive cysteines within the proteome, NJP14 appeared more adept to visualize potential Zn^{2+}-sensitive cysteines by in-gel fluorescence. After subjecting HeLa lysates to the same in-gel fluorescence protocol, two particular gel bands, one at ~38 kD and the other at ~28 kD, displayed a complete loss of fluorescence signal solely within the Zn^{2+}-treated samples. These bands have been arbitrarily labeled as band A and band B (Figure 3-10b).

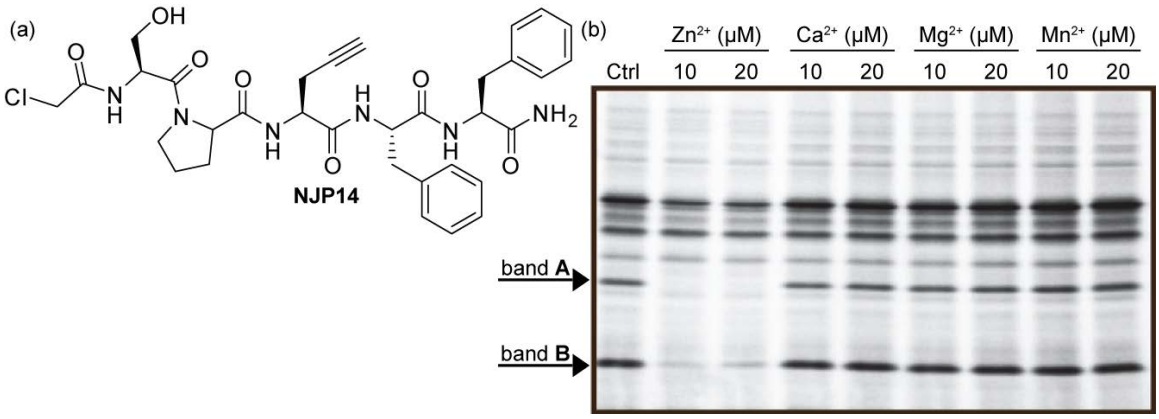

Figure 3-10. (a) Structure of NJP14. (b) In-gel fluorescence analysis of HeLa lysates treated with Zn^{2+}, Ca^{2+}, Mg^{2+}, or Mn^{2+} and subsequently administered NJP14.

Because Zn^{2+}-induced precipitation of protein has been previously observed,[65] we sought to eliminate this possibility by demonstrating the fluorescent signal for these proteins could be recovered with the addition of a Zn^{2+}-chelator, EDTA, to Zn^{2+}-treated samples (Figure 3-11a). This supports our hypothesis that reversible Zn^{2+}-binding to a reactive cysteine accounts for the mitigated fluorescent signal, as opposed to irreversible Zn^{2+}-inducted protein precipitation. Additionally, treatment with only EDTA also resulted in an increase in fluorescent signal (especially for band A), suggesting that EDTA is able to remove prebound metal ions to enhance cysteine reactivity (Figure 3-11a). This provides further support of our hypothesis that this competitive platform is selecting for endogenous Zn^{2+}-cysteine complexes.

To further demonstrate the utility of our platform, we sought to quantitatively compare the relative Zn^{2+}-affinities for band A and band B. The in-gel fluorescence platform was carried out on lysates exposed to increasing Zn^{2+} concentrations (100 nM – 10 μM). The fluorescent intensities of each band was integrated from three trials, and

plotted to calculate relative EC_{50} values (Figure 3-11b). These values ranged from 365 nM for band A to 2.1 μM for band B, illustrating the differential affinities of each cysteine residue for Zn^{2+}.

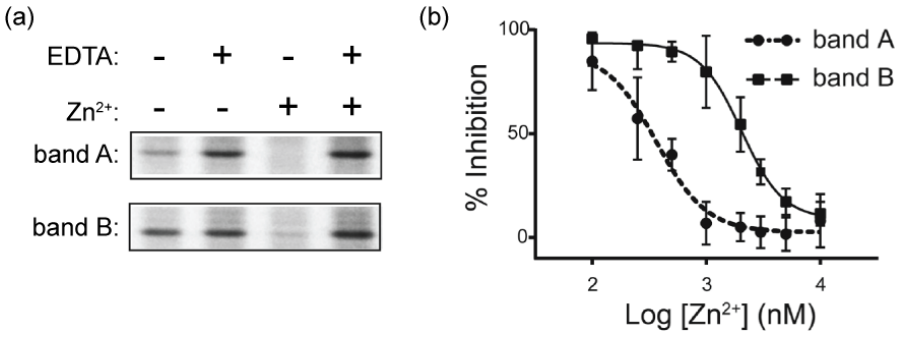

Figure 3-11. (a) The effects of Zn^{2+} (10 μM) and EDTA (1 mM) on in-gel fluorescent signals from band A and band B. (b) Integrated fluorescent signals of band A and band B from three trials were plotted to quantify relative affinities for Zn^{2+}.

We next sought to identify the proteins represented by band A and band B by adapting our platform to mass spectrometry. HeLa lysates were preincubated with Zn^{2+}, Mg^{2+}, or DMSO as a control and subsequently labeled with NJP14. The probe-labeled proteins were tagged with biotin-azide through click chemistry, enriched on streptavidin beads, and subjected to on-bead tryptic digestion, and LC/LC-MS/MS analysis.[66] Proteins identified with high spectral counts in the vehicle and Mg^{2+}-treated samples with significantly decreased spectral counts within the Zn^{2+}-treated samples were designated as putative Zn^{2+}-chelating proteins. Spectral counts refer to the total fragmentation spectra for peptides identified from a particular protein and provide a semi-quantitative measure of protein abundance across numerous proteomic samples. To best sort our dataset, for each of the proteins a % change in spectral counts was calculated for both Zn^{2+} / Mg^{2+} treatments, and the data were ranked by those that showed the largest

decrease in spectral counts (largest negative % change) in the Zn^{2+} 20 μM samples relative to the Ctrl samples (Table 3-3, Figure 3-12). The full dataset is presented in Appendix II (Table 3A-2). The majority of the proteins displayed no reduction in spectral counts due to Zn^{2+}-treatment, such as bleomycin hydrolase (BLMH); however, this analysis identified the two Zn^{2+}-sensitive proteins as visualized by gel as sorbitol dehydrogenase (SORD, band A, red point in Figure 3-12) and glutathione *S*-transferase omega 1 (GSTO1, band B, blue point in Figure 3-12) (Figure 3-13). These two proteins displayed the largest negative % change in the Zn^{2+} 20 μM samples and the molecular weights coincided with band migration during in-gel fluorescence. Interestingly, a few proteins displayed a large % decrease in spectral counts upon treatment with Mg^{2+}, with low sensitivity to Zn^{2+} (yellow points, Figure 3-12). While cysteine is not typically found as a ligand for Mg^{2+}, these could represent cysteines that are allosterically modulated by Mg^{2+} and could present interesting case studies for the future.[67]

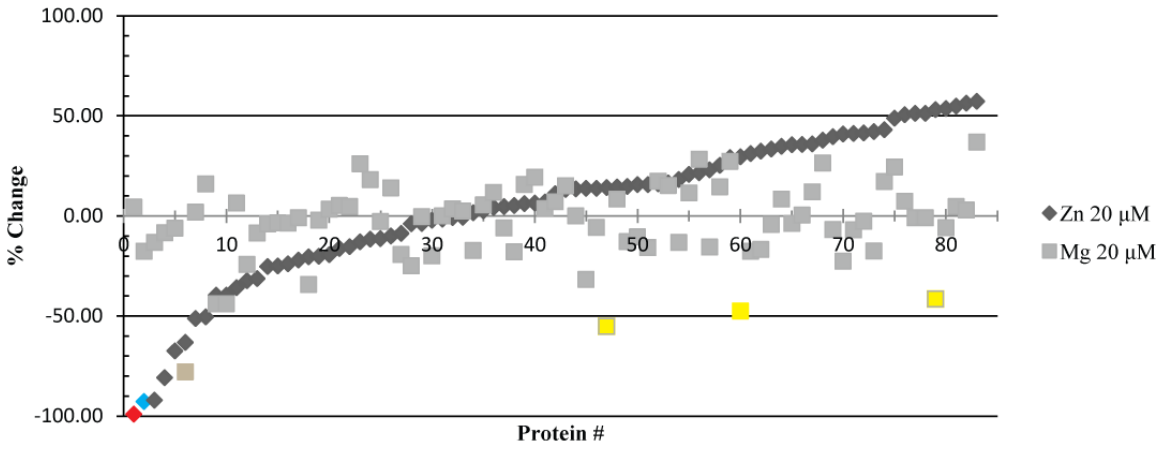

Figure 3-12. Mass spectrometry data of each protein represented as a % Change of the Zn^{2+} and Mg^{2+}-treated samples relative to the Ctrl sample.

Protein	Molecular Weight	Spectral Counts				% Change Zn^{2+} (20 μM)
		Ctrl	Zn^{2+} (10μM)	Zn^{2+} (20μM)	Mg^{2+} (20μM)	
SORD similar to sorbitol dehydrogenase	38687	250	12	3	262	-98.8
GSTO1 Glutathione transferase omega-1	27566	324	269	24	267	-92.5926
TXNRD1 thioredoxin reductase 1 isoform 3	71153	535	86	42	464	-92.1495
RRM1 Ribonucleoside-diphosphate reductase large subunit	90070	136	114	26	124	-80.8824
RPS3 40S ribosomal protein S3	26688	40	21	13	38	-67.5
EEF1A2 Elongation factor 1-alpha 2	50470	68	45	25	15	-63.2353
TUBB4 Tubulin beta-4 chain	49586	351	246	171	357	-51.2821
TGM2 Isoform 1 of Protein-glutamine gamma-glutamyltransferase 2	77329	53	27	26	63	-50.9434

Table 3-3. Mass spectrometry data using NJP14 reveals proteins containing Zn^{2+}-sensitive cysteine residues. The data were sorted by % change in spectral counts when comparing the control sample to Zn^{2+} (20 μM)-treated sample.

To corroborate our mass-spectrometry data, gel-based studies were performed to confirm the observed Zn^{2+}-sensitivity of SORD and GSTO1 and corresponding Zn^{2+}-insensitivity for BLMH (Figure 3-13). The three proteins were each overexpressed with C-terminal myc/His tags through transient transfection in HEK293T cells, and the overexpressed lysates were subjected to our in-gel fluorescence platform. As predicted by our mass spectrometry data, a reduced fluorescent signal was observed in both SORD and GSTO1 lysates upon Zn^{2+} treatment, but BLMH fluorescence was unaffected. Overexpression of SORD and GSTO1 was confirmed using an α-myc antibody, while an α-BLMH antibody had to be employed to confirm expression of BLMH because of auto-cleavage of its C-terminal tag (Figure 3-13).

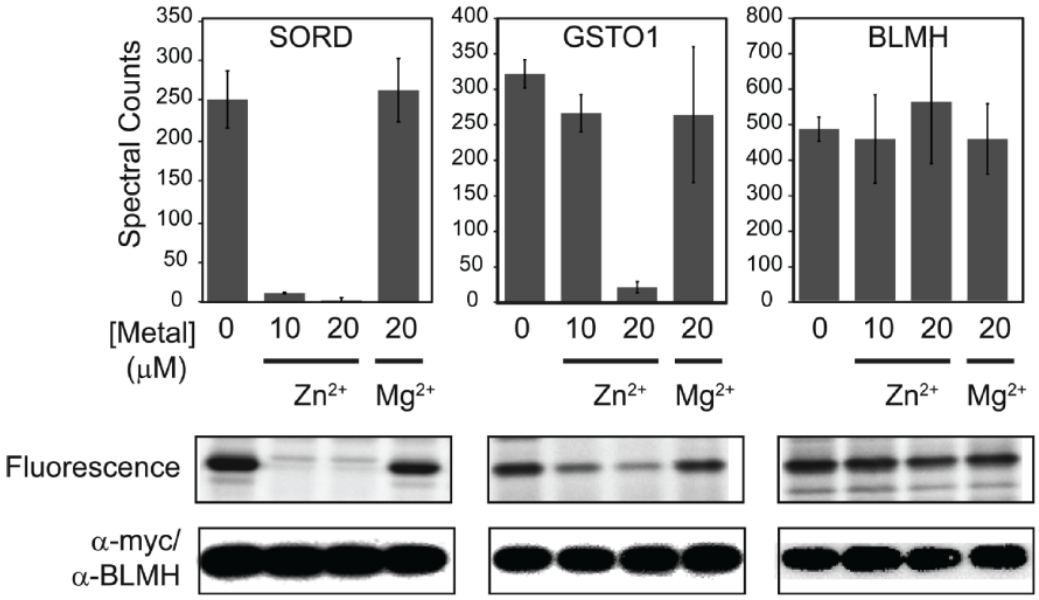

Figure 3-13. Spectral counts from mass spectrometry analysis of SORD, GSTO1, and BLMH upon Zn^{2+} or Mg^{2+} treatment. In-gel fluorescence analysis of overexpressed protein lysates confirms SORD and GSTO1 as Zn^{2+}-sensitive and BLMH as Zn^{2+}-insensitive. Overexpression was confirmed by either α-myc or α-BLMH antibody.

NJP14 modifies the catalytic Zn^{2+}-chelating cysteine of SORD

SORD is a metabolic enzyme within the polyol pathway that functions to reduce aberrantly high glucose levels. A major consequence of glucose metabolism by the polyol pathway is the production of reactive oxygen species (ROS), and this polyol pathway-induced oxidative stress is most likely an important contributing factor to diabetes mellitus (Figure 3-14). Under homeostatic conditions, glycolysis mediates the conversion of glycose to pyruvate to generate ATP and facilitate other metabolic pathways such as the tricarboxylic acid cycle. Under a state of hyperglycemia, aldose reductase first converts glucose to sorbitol, utilizing NADPH as a cofactor. As a result, the cytosolic ratio of $NADP^+$/NADPH drastically increases, preventing reduction of GSSG to GSH by

glutathione reductase, which leads to increased ROS.[68, 69] Next, sorbitol is converted to fructose by SORD, utilizing NAD^+ as a cofactor. This reaction has multiple consequences that contribute to oxidative stress. First, fructose can be converted to fructose-3-phosphate and 3-deoxyglucosone and results in an increase in advanced glycation end products (AGEs) that contribute to generation of ROS.[69] Additionally, activity by SORD produces a drastic decrease in the cytosolic NAD^+/NADH ratio. Under homeostatic conditions, the conversion of NAD^+ to NADH by SORD is balanced by the reduction of pyruvate to lactate by lactate dehydrogenase. Under hyperglycemic conditions, glyceraldehyde phosphate dehydrogenase (GAPDH) cannot convert glyceraldehyde-3-phophate to 1,3-bisphosphoglycerate because the transformation requires NAD^+.[69, 70] Instead, accumulating glyceraldehyde-3-phosphate enters alternative metabolic pathways to generate more AGEs that also contribute ROS production. Because of its impact on ROS production that likely contributes to disease pathways such as diabetes mellitus, SORD structure and enzymatic activity has been extensively studied

Structural studies have concluded that SORD is active as a tetramer, each containing a single catalytic Zn^{2+}-cysteine complex (Figure 3-15a). SORD has long been accepted to utilize a catalytic Zn^{2+}-cysteine complex within its enzymatic mechanism.[71, 72] Moreover, a recent crystal structure determined that each subunit of the tetrameric protein coordinates the Zn^{2+} to Cys44, His69, Glu70, and an activated water molecule (Figure 3-15b).[17] The mechanism has been hypothesized to occur through nucleophilic attack by this activated water molecule on sorbitol with concomitant hydride transfer to NAD^+, similar to that of ADH.[17] Importantly, this reaction is reversible; and, although to a lesser degree, SORD shows the capacity to also convert fructose back to sorbitol.

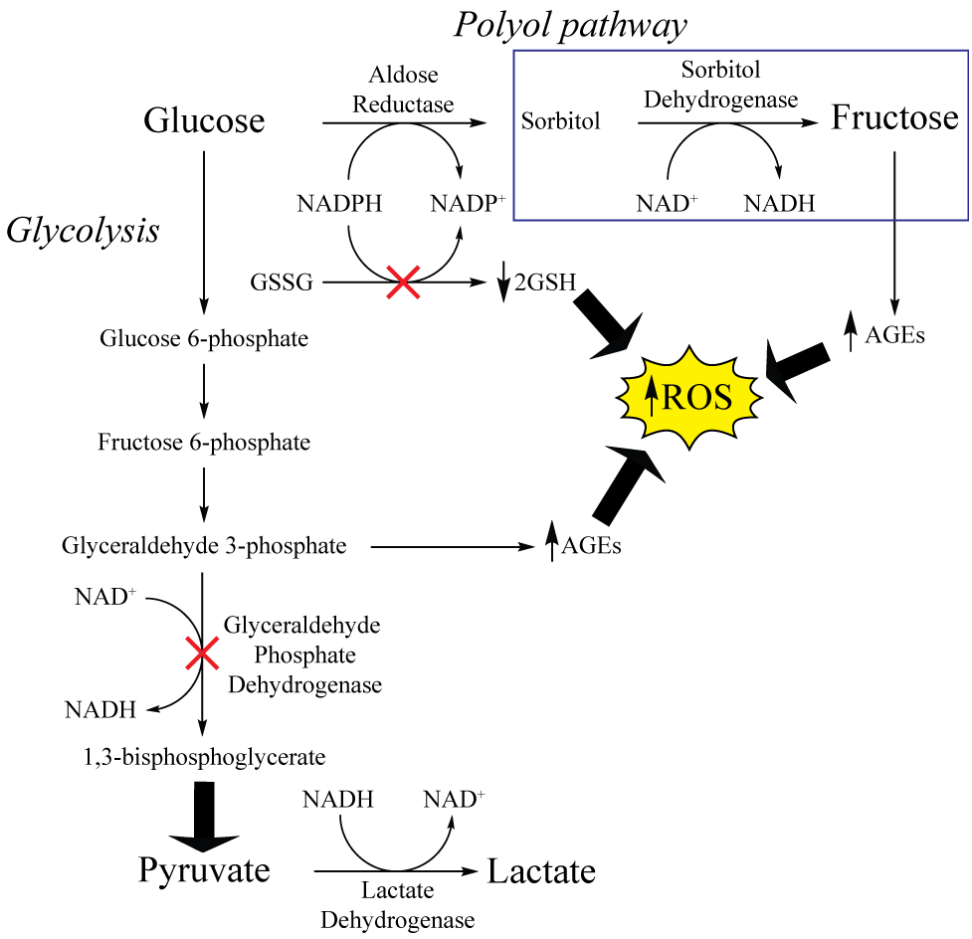

Figure 3-14. The polyol pathways functions to reduced aberrantly high glucose levels, but consequently generates significant oxidative stress. Sorbitol dehydrogenase (blue box) is a main component of this pathway and facilitates the reversible conversion of sorbitol to fructose

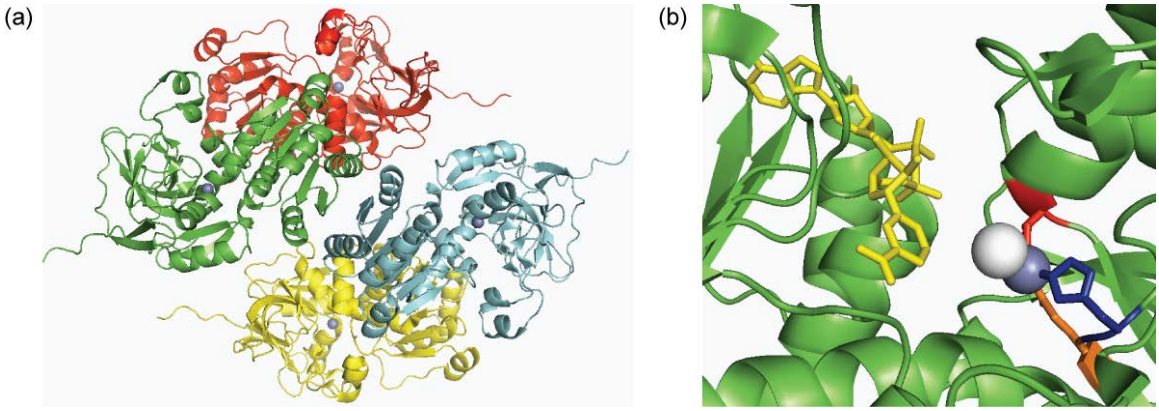

Figure 3-15. (a) Structure of SORD tetramer, each containing an active-site with a single bound Zn^{2+}. (b) The active-site of SORD contains a Zn^{2+} (purple) bound to Cys44 (red), His69 (blue), Glu70 (orange) and an activated water molecule (white). The substrate is anticipated to bind the activated water molecule and be position in the proper geometry for hydride transfer to NAD^+ (yellow).

Because of its drastic increases on ROS production observed upon SORD activity, the development of SORD inhibitors are crucial to evaluate the effect of SORD activity on contributions to cellular functions and diabetes. Inhibitor development will also allow for the assessment of SORD inhibition as a therapeutic strategy for diabetic patients. Toward this end, a very limited number of SORD inhibitors have been developed in recent years (Figure 3-16a). The first, and most well-studied, of these inhibitors is SDI-158, which has been found to inhibit SORD activity with an IC_{50} of 250 nM and K_i for SORD of 154 nM.[73] Crystal structures dosed with SDI-158 revealed that the inhibitor acts by chelating the active-site Zn^{2+} through both a pyrimidine nitrogen and the hydroxymethyl oxygen, displacing the activated water molecule and preventing nucleophilic attack on the substrate (Figure 3-16b).[17] Notably, SDI-158 is uncompetitive in respect to NAD^+, NADH, and sorbitol, meaning that the assembled enzyme-substrate

complex is required for SDI-158 binding. SDI-158 underwent stringent SAR analysis, resulting in the optimized SORD inhibitor, Compound 20, with an IC_{50} value of 4 nM and improved pharmacological properties.[74] Through the use of these inhibitors, recent attention has been directed to SORD's involvement in diabetic complications, although its role to date is still unclear. Additionally, the therapeutic potential of SORD inhibition has not been confirmed or refuted, producing conflicting results that either support or reject this strategy.[69]

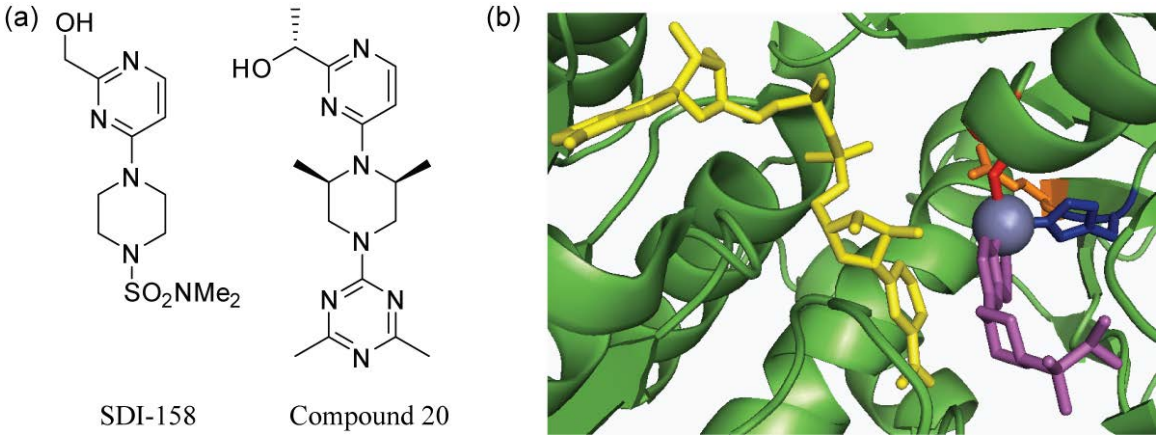

Figure 3-16. (a) Structures of SORD inhibitors SDI-158 and Compound 20. (b) SORD active-site with Zn^{2+} (purple) bound to Cys44 (red), His69 (blue), and SDI-158 (magenta). This displaces Zn^{2+}-chelation of the required water molecule (not shown) and Glu70 (orange) and prevents substrate binding. Inhibition has no effect on NAD^+ binding (yellow).

We aimed to examine the binding mode of NJP14. We hypothesized that NJP14 covalently modified this Cys44 within this predicted catalytic Zn^{2+}-cysteine complex; however, a previous proteomic study identified another cysteine within SORD (Cys179) as being hyper-reactive.[63] In order to determine the site of labeling of NJP14, SORD WT,

C44A, and C179A mutants were overexpressed by transient transfection in HEK293T cells, and these lysates were subjected to our in-gel fluorescence analysis. A complete loss of labeling was observed in the C44A sample, confirming that NJP14 does indeed target this Zn^{2+}-binding cysteine of SORD (Figure 3-17). The identification of a known Zn^{2+}-binding cysteine through our platform serves to validate our competitive cysteine-labeling strategy to identify putative Zn^{2+}-binding cysteines in the human proteome.

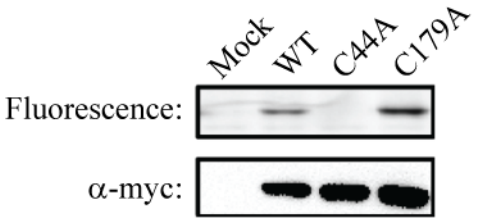

Figure 3-17. In-gel fluorescence analysis and corresponding western blots of overexpressing SORD WT, C44A, and C179 lysates compared to the mock.

To fully assess the effects of Zn^{2+}, EDTA, and NJP14 on SORD function, SORD activity assays were performed using SORD-overexpressing HEK293T lysates. We employed previously reported oxidative and reductive activity assays, in an effort to evaluate both reactions catalyzed by SORD.[75, 76] The oxidative activity assay assesses the primary conversion of sorbitol to fructose by measuring the increase in absorbance at 340 nm as the required cofactor, NAD^+, is concomitantly reduced to NADH. The reductive activity assay measures the reverse reaction, whereby fructose is converted back to sorbitol and the activity is measured by monitoring the decrease in absorbance at 340 nm as NADH is oxidized back to NAD^+.

First, lysates overexpressing SORD WT, C44A, and C179A were assessed for enzymatic activity. As expected, the C44A lysates experienced a complete loss of

oxidative and reductive activity compared to the WT and C179A lysates, confirming this Zn^{2+}-binding cysteine is required for enzymatic activity (Figure 3-18a). Upon treatment with EDTA, both oxidative and reductive SORD activities were completely abolished, corroborating the presence of the intact Zn^{2+}-cysteine complex is essential for function (Figure 3-18b). Interestingly, subsequent treatment with Zn^{2+} restored oxidative and reductive activity; however, this recovery was partial (~60%), likely due to residual EDTA remaining in the buffer (Figure 3-18b). Unlike EDTA treatment, NJP14 only partially inhibited both oxidative and reductive activity (~50%), suggesting that NJP14 can only bind the Zn^{2+}-free population of SORD and is unable to displace bound Zn^{2+} ions from the active-site (Figure 3-18b). Pretreatment with Zn^{2+} completely abolished the inhibitory effect of NJP14, confirming that saturation of the SORD active-site with Zn^{2+} prevents NJP14 binding (Figure 3-18b). Finally, SORD lysates were administered EDTA to remove the catalytic Zn^{2+}, followed by treatment with NJP14 to covalently modify the now accessible Cys44. These labeled lysates were then assayed for oxidative and reductive activities upon treatment with Zn^{2+}, revealing complete inhibition of SORD activity due to the covalently bound NJP14 preventing the reformation of the Zn^{2+}-cysteine complex (Figure 3-18b). Together, these experiments verify that NJP14 covalently modifies Cys44 of Zn^{2+}-free SORD and inhibits its activity. This inhibition is mitigated by pre-treatment with Zn^{2+} and enhanced with EDTA. Importantly, the observed labeling of SORD in non-overexpressing HeLa lysates (Figure 3-10b, Figure 3-11a) implies that a certain population of SORD endogenously exists in the Zn^{2+}-free state and is susceptible to inhibition by cysteine-reactive agents. Therefore, depending on the relative cellular concentrations of the Zn^{2+}-bound versus unbound protein, cysteine-

reactive small molecules could be utilized as potential inhibitors of SORD as well as other enzymes that rely on Zn^{2+}-cysteine complexes for activity.

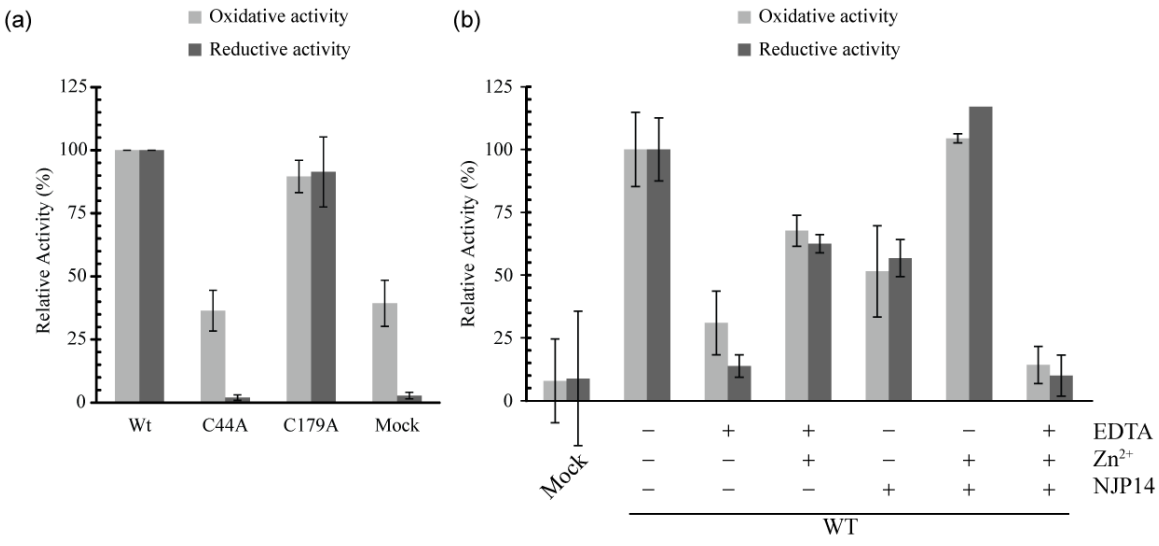

Figure 3-18. (a) SORD WT, C44A, and C179 overexpressing lysates were analyzed for oxidative (light gray) and reductive (dark gray) activities. (b) EDTA, Zn^{2+}, and NJP14 can be used in combination to regulate SORD oxidative (light gray) and reductive (dark gray) activities.

A Zn^{2+}-cysteine complex regulates GSTO1 activity

In contrast to SORD, GSTO1 has not been previously annotated as a Zn^{2+}-chelating protein. Because of the significant decrease in NJP14-labeling of GSTO1 we observed due to Zn^{2+}-treatment, we decided to further investigate the effect of Zn^{2+} on GSTO1 activity. As described in Chapter 2, GSTO1 is part of the GST superfamily that catalyzes the conjugation of GSH to endogenous and exogenous electrophiles as a mechanism of cellular defense against carcinogens, therapeutic drugs, and oxidative stress.[77] GSTO1 is unique from other GSTs in that it possesses a catalytic cysteine residue (Cys32) in place of the canonical tyrosine residue.[78] Although Cys32 has long

been characterized as the catalytic nucleophile for GSTO1 activity, its ability to bind Zn^{2+} and the functional role of this resulting Zn^{2+}-cysteine complex have never been defined. To address the role of Zn^{2+} in regulating GSTO1 function, GSTO1 WT and the C32A mutant were recombinantly expressed in *E. coli* and purified over a Ni-NTA column. A dose-dependent decrease in labeling by NJP14 was observed by in-gel fluorescence when treating GSTO1 WT with increasing Zn^{2+} concentrations (Figure 3-19). Additionally, the absence of NJP14-labeling within the GSTO1 C32A protein sample indicates that NJP14 covalently binds selectively to the catalytic cysteine (C32) of GSTO1.

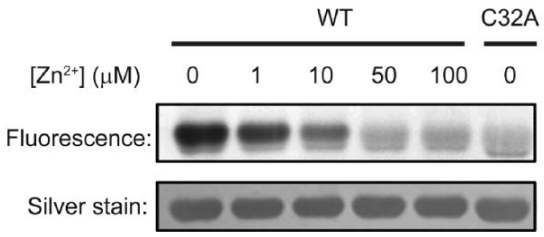

Figure 3-19. In-gel fluorescence of purified recombinant GSTO1 exposed to increasing concentrations of Zn^{2+} and labeled by NJP14.

Recombinant GSTO1 was also subjected to a previously reported activity assay that couples thioltransferase activity of GSTO1 to the oxidation of NADPH by glutathione reductase (GSR) (Figure 3-20a).[78, 79] A symmetrical disulfide, in this case 2-hydroxyethyl disulfide, must first undergo a disulfide exchange reaction with one equivalent of reduced glutathione (GSH) to form the mixed disulfide (HRS-SG). GSTO1 subsequently catalyzes another round of thioltransferase on the mixed disulfide to produce one equivalent of GS-SG. The GS-SG can now be reduced by GSR, requiring one equivalent of NADPH, and this reaction can be monitored by the absorbance of NADPH at 340 nm. At saturating concentrations of GSR, the reaction is a direct measure

of GS-SG formation and thus allows for quantification of GSTO1 activity. Importantly, the GSTO1 activity assessed here is a combination of both reactions 1 and 2 and these individual reaction rates cannot be discerned from the assay. Increasing Zn^{2+} concentrations resulted in a decrease in GSTO1 activity (Figure 3-20b) suggesting that, at least *in vitro*, GSTO1 activity is regulated by an inhibitory Zn^{2+}-cysteine complex. However, since high concentrations were necessary for complete inhibition (>10 μM), the physiological relevance of Zn^{2+}-inhibition of GSTO1 is still in question.

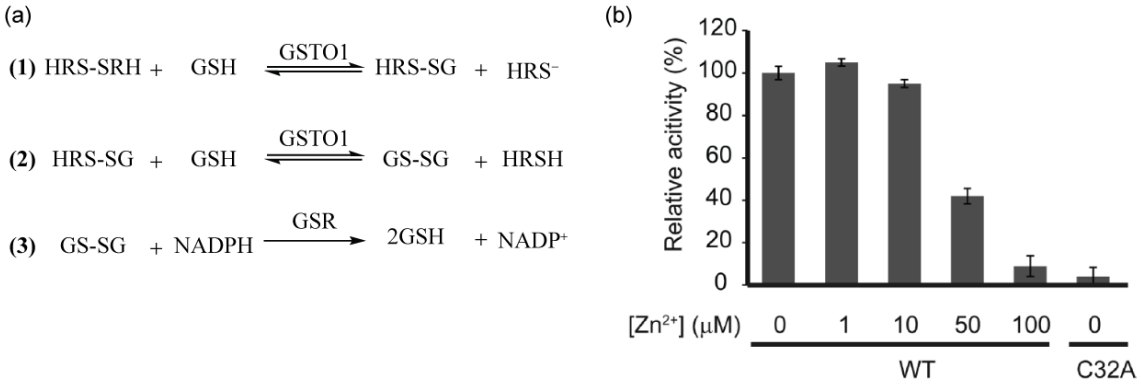

Figure 3-20. (a) Scheme of assay employed to measure GSTO1 thioltransferase activity. The first two steps were catalyzed by GSTO1 to produce GS-SG, which can subsequently be reduced by GSR. This activity can be monitored by the absorbance of NADPH at 340 nm. (b) Purified recombinant GSTO1 was treated with increasing Zn^{2+} concentrations and assayed for enzyme activity.

Quantitative mass spectrometry can globally identify Zn^{2+}-cysteine complexes

Since the previous studies conducted with NJP14 only target a subset of cysteines within the proteome, we decided to modify our platform in an effort to globally and quantitatively characterize reactive, and functional, cysteines that bind Zn^{2+}. To achieve

this, we revisited the highly promiscuous IA-alkyne probe known to react with hundreds of functional cysteines within the proteome. Although more difficult to distinguish, the gel-based studies indicated that several proteins were sensitive to Zn^{2+}-treatment (Figure 3-9b). Because the high reactivity of IA-alkyne often results in labeling of multiple cysteines within the same protein, we also needed to employ a mass spectrometry platform that specifically identifies each IA-targeted cysteine within a protein. Furthermore, we envisioned a platform that provides a more quantitative read-out relative to the semiquantitative method of spectral counting described previously. A recently developed mass-spectrometry method by our lab was modified to facilitate the identification and accurate quantification of sites of IA-alkyne labeling between two proteomes.[80] IA-alkyne labeled proteins are tagged with a linker that contains (a) an azide for click-chemistry-based conjugation to labeled proteins, (b) a biotin for enrichment on streptavidin beads, (c) an azobenzene-based cleavable moiety for release of tagged peptides upon sodium dithionite treatment, and (d) an isotopically tagged valine (light: Azo-L; heavy: Azo-H) for quantification of IA-alkyne labeled peptides across two proteomes (Figure 3-21). The Azo-L/H tags were synthesized on resin containing a PEG-linker attached to a biotin moiety under standard Fmoc-peptide coupling conditions utilizing a synthesized Fmoc-Azo-OH amino acid, an isotopic valine, and 5-azido-pentanoic acid.[80]

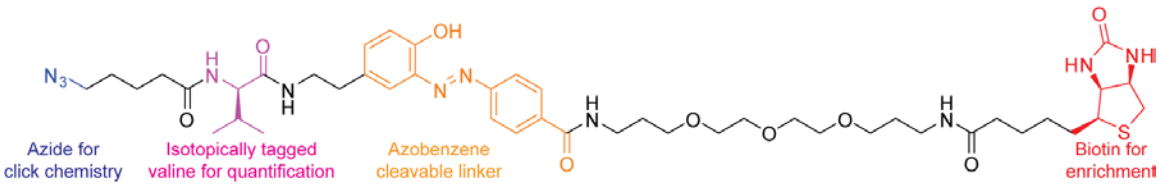

Figure 3-21. Isotopic cleavable linker for identification of site of labeling and quantitative proteomics.

In order to identify Zn^{2+}-binding cysteines and further elucidate those that endogenously bind Zn^{2+}, we performed two quantitative mass-spectrometry analyses with the IA-alkyne probe. The first compared untreated control lysates (conjugated to the Azo-H tag) to those treated with either Zn^{2+} or Mg^{2+} (conjugated to the Azo-L tag) (Figure 3-22a). A light : heavy ratio (R) was calculated for each IA-alkyne-labeled peptide. A cysteine with a R value of 1.00 is unaffected by metal-ion treatment, whereas a cysteine with $R < 0.66$ signifies a residue that demonstrated at least 1.50-fold decrease in reactivity in the presence of the metal ion. Similar to the studies using NJP14, most cysteines in the Mg^{2+}-treated sample showed ratios of ~1.00, while several cysteines in the Zn^{2+}-treated sample showed significantly reduced R values. The full dataset is presented in Appendix II (Table 3A-3). These cysteines represent those displaying affinity towards Zn^{2+}. To further filter our dataset, we employed a second round of mass spectrometry comparing untreated control lysates (conjugated to the Azo-H tag) to those treated with EDTA (conjugated to the Azo-L tag) (Figure 3-22b). In this experiment, an R value of 1.00 signifies a cysteine that is unaffected by EDTA treatment, whereas a cysteine with $R > 1.50$ possess at least 1.5-fold increase in cysteine reactivity upon EDTA treatment, implying that the innate reactivity of these cysteines is quenched by a bound-metal ion. These cysteines would represent those endogenously chelating a metal ion.

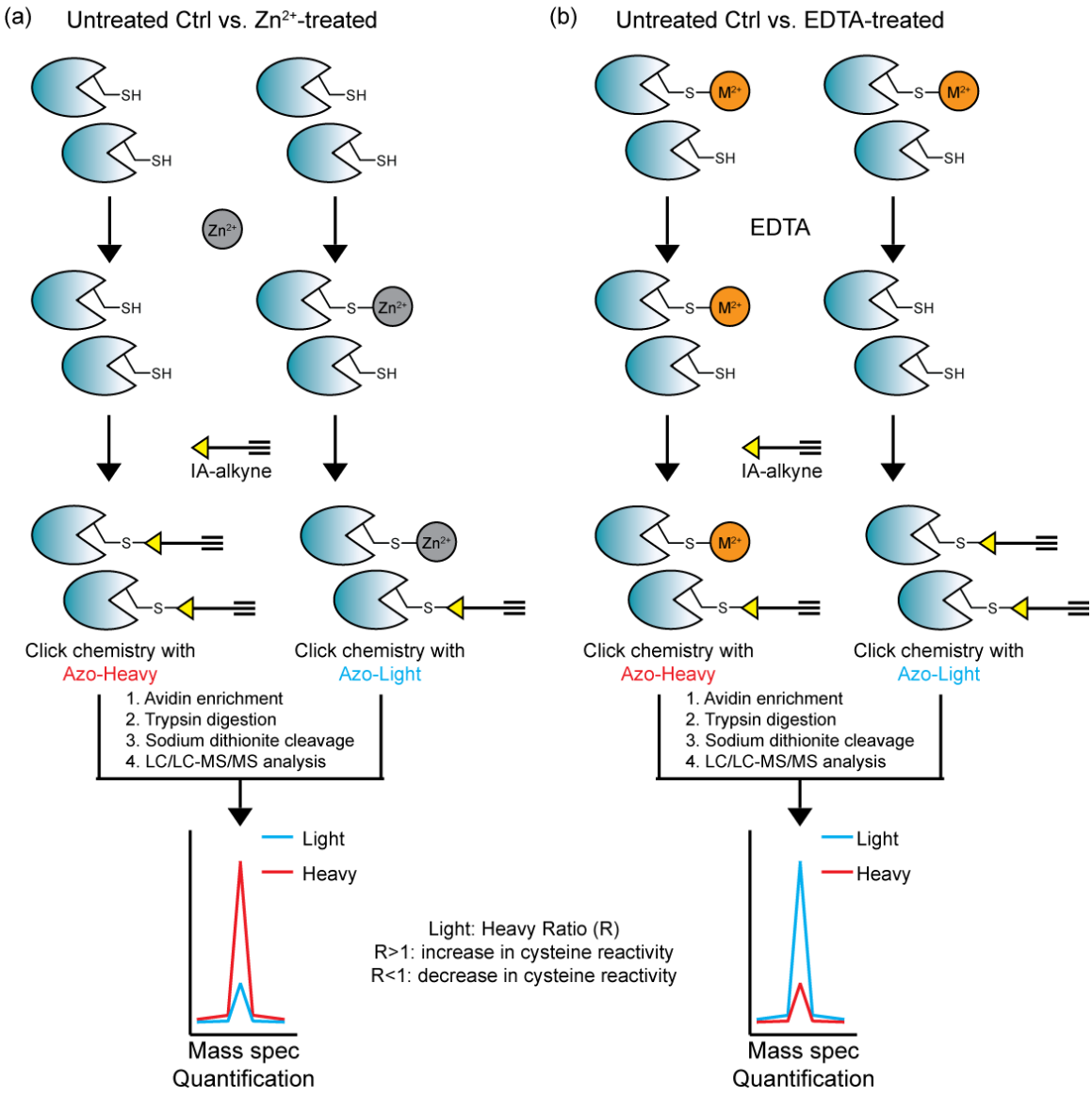

Figure 3-22. Quantitative mass spectrometry analysis of untreated control HeLa lysates compared to those pre-treated with (a) Zn^{2+} or (b) EDTA.

We therefore hypothesized that refining the data from these two mass-spectrometry analyses by focusing our attention on those cysteines that showed a ratio R < 0.66 upon Zn^{2+}-treatment and R > 1.50 upon EDTA-treatment would likely indicate a cysteine that is endogenously chelated to Zn^{2+} in these HeLa cells lysates (Figure 3-23a).

These are cysteines that show rescued reactivity upon EDTA-mediated metal removal and decreased reactivity upon addition of Zn^{2+}. The proteins that fulfilled these criteria represent diverse functional classes including oxidoreductases, metabolic enzymes, ribosomal proteins, and microtubule assembly proteins (Table 3-4). Many of these proteins have been previously annotated to bind Zn^{2+}, which helps validate our workflow. For example, our platform identified Cys174 from alcohol dehydrogenase class-3 (ADH5), which is known to bind Zn^{2+} to facilitate catalysis as described in the introduction (Figure 3-23b).[81] Additionally, bacterial ribosomal proteins are known to possess the capacity to bind up to 11 equivalents of Zn^{2+} within a single ribosome, and these interactions can account for up to 65% of the total cellular Zn^{2+}.[82] After stringent filtering of our data, 10 unique ribosomal cysteine residues were detected by our platform, confirming that this Zn^{2+} affinity extends to human ribosomes as well. The mass spectrometry platform also identified numerous cysteines in both alpha and beta-isoforms of tubulin as Zn^{2+}-binding. Tubulin-Zn^{2+} interactions have been well documented, and these interactions have proven essential for the formation of protofilament sheets and subsequent polymerization.[83, 84]

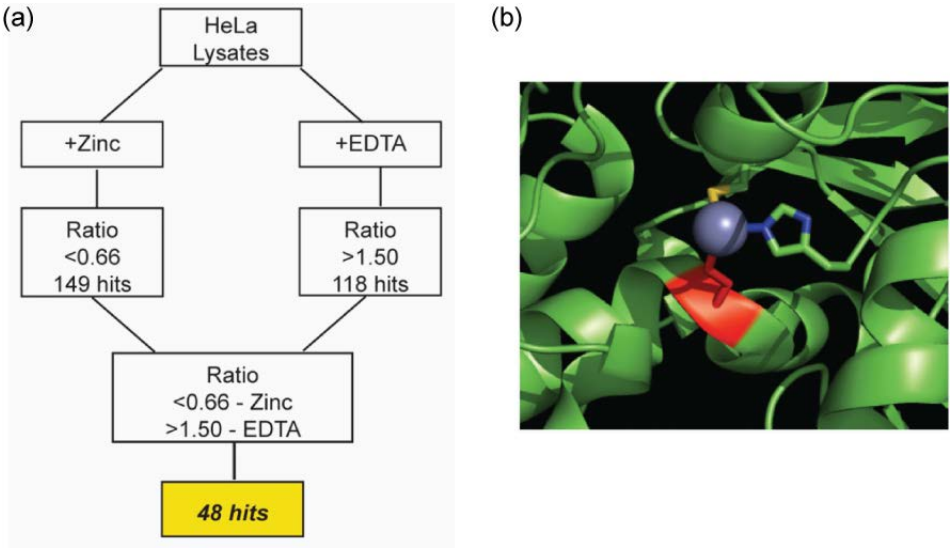

Figure 3-23. (a) Mass spectrometry data analyses filters to prioritize those putative Zn^{2+}-binding cysteines. (b) Structure of the active-site of ADH5, highlighting the identified Cys174 (red) that binds the catalytic Zn^{2+} (purple) (PDB 1MC5).

Protein	Peptide Sequence	Ratio (light: heavy)		Cellular Role
		Zn^{2+} 20uM	EDTA	
ACO2 Aconitase 2, mitochondrial	R.VGLIGSC*TNSSYEDMGR.S	0.12	1.58	Metabolic
RPS27 40S ribosomal protein S27	R.LTEGC*SFR.R	0.39	4.55	Ribosomal protein
RPS3 40S ribosomal protein S3	K.GC*EVVVSGK.L	0.44	8.83	Ribosomal protein
TUBB2C, TUBB, TUBB4, TUBB2B, TUBB8, TUBB6, Tubulin β chain	K.NMMAAC*DPR.H	0.44	1.95	Tubulin protein
TUBA4A, TUBA1B, TUBA1A, TUBA1C, Tubulin α/β chain	K.AYHEQLSVAEITNAC*FEPANQMV K.C	0.46	1.98	Tubulin protein
ADH5 Alcohol dehydrogenase class-3	K.VCLLGC*GISTGYGAAVNTAK.L	0.57	3.92	Metabolic
RPS11 40S ribosomal protein S11	R.DVQIGDIVTVGEC*RPLSK.T	0.57	4.98	Ribosomal protein
RPL23 60S ribosomal protein L23	R.ISLGLPVGAVINC*ADNTGAK.N	0.61	1.72	Ribosomal protein
USP22 Ubiquitin carboxyl-terminal hydrolase 22	K.C*DDAIITK.A	0.64	1.52	Protein Degradation
MRPS12 28S ribosomal protein S12, mitochondrial	K.GVVLC*TFTR.K	0.66	1.50	Ribosomal protein

Table 3-4. Cysteine residues identified by mass spectrometry to endogenously bind Zn^{2+} in HeLa cell lysates.

In addition to these previously characterized Zn^{2+}-binding cysteines, we identified several other putative Zn^{2+}-binding cysteines with unknown function for future exploration. For example, Cys494 of Ubiquitin carboxyl-terminal hydrolase 22 (USP22) was identified to be Zn^{2+}-binding. USP22 is the histone deubiquitinating component of the transcription regulatory histone acetylation complex SAGA (Spt-Ada-Gcn5-Acetyl transferase).[85, 86] USP22 is a putative cancer stem cell marker and was found to be highly

expressed in malignant tumor samples.[87] High levels of USP22 in tumor tissues are associated with poor clinical outcome, including high risk of recurrence, metastasis, and resistance to chemotherapy.[88-90] USP22 has another cysteine (Cys185) that acts as a catalytic nucleophile and is also thought to possess two others that assemble a structural zinc finger (Cys61 and Cys121). The role of Cys494 and its Zn^{2+}-bound complex within USP22 is currently undefined, and future studies into this cysteine residue could shed light on USP22's role in cancer progression. As a whole, these data suggest that diverse cellular pathways could potentially be modulated by fluxes in localized Zn^{2+} concentrations resulting from cellular damage or dysregulation of Zn^{2+} homeostasis.

It is also of interest to note that a small number of cysteines demonstrated an increase in reactivity upon treatment with Zn^{2+}. These cysteines were found on proteins such as ribonuclease inhibitor and inorganic pyrophosphatase (Table 3A-3). Although the relevance of these increases in cysteine reactivity is still unclear, we hypothesize that these are likely cysteines that do not directly chelate Zn^{2+} but instead are located allosteric to a Zn^{2+}-binding site, such that the metal-binding event perturbs the local environment of the cysteine and thereby affects reactivity. Future studies into such proteins are still necessary to examine the functional relevance of such cases of metal-induced increases in cysteine reactivity.

Conclusions

In summary, we report a competitive platform to identify cysteine residues that are susceptible to Zn^{2+}-binding within a complex proteome. This platform relies on monitoring a loss in cysteine nucleophilicity induced by direct chelation of Zn^{2+} to the

thiol group, as well as an increase in reactivity resulting from the removal of prebound Zn^{2+} from endogenous chelation sites in proteins. Using a mildly reactive cysteine probe, NJP14, we identified the known Zn^{2+}-binding cysteine in SORD, thereby validating the reliability of this platform. Furthermore, we also identified and characterized a cysteine disposed to Zn^{2+}-binding in GSTO1 and demonstrated the effect of Zn^{2+} in inhibiting GSTO1 activity. We then expanded our platform to apply a highly promiscuous cysteine-reactive probe, IA-alkyne, which enabled identification of potential Zn^{2+}-chelating cysteines among ~900 reactive cysteines in the human proteome. These novel Zn^{2+}-binding proteins allude to the potential regulation of a variety of cellular functions through transient fluctuations in intracellular Zn^{2+} concentrations. Since the concentrations of Zn^{2+} used in our study are significantly higher than endogenous concentrations, the physiological significance of the putative Zn^{2+}-binding sites that we identified is still unclear. However, we hypothesize that the combined identification of cysteines displaying Zn^{2+}-sensitivity (lower R value) that also show an EDTA-mediated increase in reactivity (higher R value) suggests that (1) the cysteine has high affinity to chelate to Zn^{2+}, and (2) a certain population of the protein is found to be endogenously bound to a metal ion. Therefore, combining these two analyses gives added confidence in the assignment of these cysteines as physiologically relevant Zn^{2+} binders.

Importantly, from a technological standpoint, our competitive platform can be easily expanded to examine other biologically relevant metals across diverse proteomes, thereby providing an experimental method to complement available structural and computational studies to identify both stable and transient metal-binding sites in

proteomes. Future studies should extend this platform to other metals, such as $Fe^{2+/3+}$, Cd^{2+}, and Cu^{+}, that utilize cysteine-based ligands.

Acknowledgements

I would like to acknowledge Alex Shannon for his continued help maintaining the Orbitrap mass spectrometer and also for his assistance in data analysis.

Experimental procedures

General procedures and materials

All materials were purchased from Sigma Aldrich or Fisher Scientific unless otherwise noted. Fmoc-propargylglycine (Fmoc-Pra-OH) was purchased from BaCHEM. All other Fmoc-protected amino acids, PyBOP, peptide-synthesis resin were purchased from Novabiochem. PBS buffer, DMEM/High glucose media, and penicillin streptomycin (Pen/Strep) were purchased from Thermal Scientific. Trypsin-EDTA was purchased from Invitrogen. The α-myc-tag antibody, α-mouse IgG HRP-linked antibody, and the α-rabbit IgG HRP-linked antibody were purchased from Cell Signaling. The α-BLMH antibody was purchased from Abcam. X-tremeGENE 9 DNA transfection reagent was purchased from Roche. High resolution Mass Spectra (HRMS) were obtained at the Mass Spectrometry Facility at Boston College unless otherwise noted. All metal ion solutions were composed of the appropriate concentration of MCl_2 in water. A Molecular Devices Spectramax M5 plate reader was used to read the absorbance of all activity assays. All silver staining was carried out using a ProteoSilver Silver Stain kit from

Sigma. All chemical probes were added to samples at the indicated concentration from a 50x stock in DMSO unless otherwise noted.

Synthesis of BsO-(propanamide)-Ser-Pro-Pra-Phe-Phe-NH_2 (NJP14)

The peptide was synthesized by manual solid-phase methods on Rink Amide MBHA Resin using Fmoc as the protecting group for α-amino functionalities. Amino acids were coupled using PyBOP as the activating reagent. The success of each Fmoc-deprotection and coupling reaction was qualitatively tested using the standard procedure for the Kaiser test. Fmoc-Phe-OH, Fmoc-Phe-OH, Fmoc-Pra-OH, Fmoc-Pro-OH, and Fmoc-Ser(tBu)-OH residues were added under standard coupling conditions. After Fmoc-deprotection, dry DCM was added to the resin and N_2 gas was bubbled through the reaction vessel. NEt_3 (3 eq) followed by chloroacetyl chloride (3 eq) were added dropwise to the vessel. N_2 gas was bubbled through the reaction mixture for 1 hr. Any solvent lost to evaporation was replaced. The reaction vessel was capped, sealed, and shaken for 15 hrs. The solvent was removed and the resin was washed with DCM (5 x 3 mL). After the addition of the electrophile, cleavage from the resin was performed in TFA: DCM: TIS: water (90: 5: 2.5: 2.5) solution for 2 hrs. The peptide was purified by preparative HPLC with a gradient of increasing acetonitrile-0.1% TFA (solvent) in water-0.1% TFA (solvent A) and analyzed by a Micromass LCT TOF mass spectrometer coupled to a Waters 2975 HPLC and a Waters 2996 photodiode array UV-vis detector to give the pure peptide NJP14 (23.2%). HPLC t_R = 18.60 min (C_{18}, 5-195% B in 30 mins); HRMS for NJP14 ($C_{33}H_{39}ClN_6O_7 + H^+$): *m/z* calcd 667.26; obsd [M + H^+] 667.95 (ESI+).

Cell culture and gel-based experiments

General cell culture preparation of lysates

HeLa cells were grown at 37°C under 5% CO_2 in DMEM media supplemented with 10% FCS, 2 mM glutamine, and 1% Pen/Strep. The plates were allowed to grow to 100% confluence, the cells were harvested by scraping, and the pellets were washed with PBS. The pellets were resuspended in an appropriate amount of PBS and sonicated to lyse to give whole-cell lysates. These lysates were separated by centrifugation (45 mins, 45,000 rpm) at 4°C under high vacuum to separate the soluble and membrane proteomes. The supernatant was collected as the soluble fraction and the pellet was discarded. The protein concentrations were determined using the Bio-Rad DC Protein Assay kit (Bio-Rad).

General click chemistry and fluorescent gel analysis

Protein samples (50 μL, 2 mg/mL) were subjected to click chemistry. TAMRA-N_3 (Lumiprobe, 25 μM from 50x stock in DMSO), TCEP (1 mM, from 50x fresh stock in water), TBTA ligand (100 μM, from 17x stock in DMSO: t-butanol 1:4), and copper(II) sulfate (1 mM, from 50x stock in water) were added in this order to the protein. The samples were vortexed after every addition, except TCEP, and allowed to react at room temperature for 1 hr, while being vortexed periodically. SDS-PAGE loading buffer 2x (reducing, 50 μL) was added to the samples and 25 μL of each protein solution was separated by SDS-PAGE for 217 V hrs on a 10% polyacrylamide gel. Gels were visualized for fluorescence on a Hitachi FMBIO II multiview flatbed laser-induced

fluorescent scanner. After analysis, gels underwent a typical procedure for Coomassie staining. Stained gels were visualized on a Stratagene Eagle Eye apparatus by a COHU High performance CCD camera.

Competitive metal-binding fluorescent-gel analysis: IA-alkyne

HeLa soluble protein lysates (50 μL, 2 mg/mL) were treated with either Zn^{2+}, Ca^{2+}, Mg^{2+}, Mn^{2+} (10 and 20 μM) or water as a control. The samples were allowed to sit at room temperature for 1 hr. Then IA-alkyne (1 μM) was added to the samples and they were allowed to incubate at room temperature for 1 hr. The protein samples were purified by Bio-Spin Micro-P6 size exclusion columns (Bio-Rad) according to the standard protocol. These samples were then subjected click chemistry and in-gel fluorescence analysis.

Competitive metal-binding fluorescent-gel analysis: NJP14

HeLa soluble protein lysates (50 μL, 2 mg mL^{-1}) were treated with either Zn^{2+}, Ca^{2+}, Mg^{2+}, Mn^{2+} (10 and 20 μM) or water as a control. The samples were allowed to sit at room temperature for 1 hr. Then NJP14 (50 μM) was added to the samples and they were allowed to incubate at room temperature for 1 hr. The protein samples were purified by Bio-Spin Micro-P6 size exclusion columns (Bio-Rad) according to the standard protocol. These samples were then subjected click chemistry and in-gel fluorescence analysis

EDTA treatments for gel-based analysis

HeLa soluble protein lysates underwent the competitive metal-binding fluorescent gel analysis as described above with Zn^{2+} (10 μM). Lysates were sequentially treated with EDTA (1 mM) from a 50x stock in water and NJP15 (50 μM) and were allowed to incubate at room temperature for 1 hr each time. The samples were purified by Bio-Spin Micro-P6 size exclusions columns and underwent click chemistry and in-gel fluorescence analysis as described above.

In-gel fluorescence analysis to determine Zn^{2+}-binding constants

HeLa soluble protein lysates (50 μL, 2 mg/mL) underwent the competitive metal-binding fluorescent gel analysis as described above with increasing Zn^{2+} concentrations (0, 100 nM, 250 nM, 500 nM, 1 μM, 2 μM, 3 μM, 5 μM, 10 μM). Three trials were performed and the band intensities were quantified by ImageJ and averaged from the trials. EC_{50} values were generated using prims software. The full gels are presented within Appendix III (Figure 3A-1).

Overexpression of SORD, GSTO1, and BLMH in HEK293T cells

The cDNA constructs for each protein were purchased as full-length expressed sequence tags (Open Biosystems) and subcloned into a pcDNA3.1-myc/His mammalian expression vector. HEK293T cells were grown at 37 °C under 5% CO_2 in DMEM media supplemented with 10% FCS, 2 mM glutamine, and 1% Pen/Strep. Transfections were performed on 15 cm plates of ~50% confluence. DMEM media serum free (600 μL) and

X-tremeGENE DNA transfection reagent (20 μL) were combined and vortexed. Plasmids for each protein (6 μg) were added and the samples were vortexed and remained at room temperature for 15 mins. This plasmid solution was added dropwise to a plate of HEK293T cells. The plate was incubated at 37 °C under 5% CO_2 for 48 hrs. HEK293T cells transfected with the pcDNA3.1-myc/His plasmid was used as a mock negative control. The lysates were prepared as before and underwent competitive metal-binding fluorescent-gel analysis with Zn^{2+} and Mg^{2+} as described above.

Western blot analysis

The SDS-PAGE gels from above were transferred by electroblotting onto nitrocellulose membranes for 150 volt hours. The membranes were blocked in TBS-T and 5% (w/v) non-fat dry milk at room temperature for 2 hrs. The blot was washed with TBS-T three times (5 min per wash), and the SORD and GSTO1 blots were treated with α-myc tag rabbit antibody (1:1000) overnight at 4 °C. The BLMH blot was treated with α-BLMH mouse antibody (1:1000), since self-processing of the enzyme results in the removal of the C-terminal myc tag. The blots were washed with TBS-T three times (5 mins per wash). The blots were treated with the appropriate secondary antibody (α-rabbit or α-mouse, 1:3333) for 2 hrs at room temperature. The blots were washed three times with TBS-T (5 mins per wash), treated with HRP super signal chemiluminescence reagents and exposed to film for 1-10 mins before development. Development took place using a Kodak X-OMAT 2000A processor.

Site-directed mutagenesis and fluorescent gel analysis of SORD mutants

The SORD C44A and C179A mutants were generated using the Quickchange kit (Stratagene) using the following primers:

SORD-C44A Sense: 5'-GAAAAGCTTATGCTGCGCCGC-3'

Antisense: 5'-GCATCTAGACAGTTCATCTTTCACAGCTT-3'

SORD-C179A Sense: 5'-GAAAAGCTTATGAGGGAAATCGTGCACAT-3'

Antisense: 5'-GAACTCGAGGGCCTCCTCTTC-3'

The mutant cDNA was sequenced and found to contain only the desired mutation. The SORD WT, C44A, and C179A mutants were overexpressed in HEK293T cells and lysates were collected as described above. The lysates were subjected to in-gel fluorescence studies after labeling with NJP14 and subsequently underwent western blotting as described above to confirm the site of labeling of NJP14.

General mass spectrometry experiments

Click chemistry and streptavidin enrichment of protein for mass spectrometry

HeLa soluble protein lysates treated were prepared as described above. These protein samples (500 μL, 2 mg/mL) were aliquoted to undergo click chemistry. Biotin azide[66] (200 μM from 5 mM DMSO stock), TCEP (1 mM, from fresh 50x stock in water), ligand (100 μM, from 17x stock of DMSO: t-butanol 1:4), and copper(II) sulfate (1 mM, from 50x stock in water) were added to the protein samples. The samples were allowed to react at room temperature for 1 hr and were vortexed periodically. Tubes were centrifuged (10 mins, 4 °C) to pellet the precipitated proteins. The pellets were resuspended in cold MeOH (500 μL) by sonication, centrifuged (10 mins, 4 °C), and the

supernatants were removed. Following a second MeOH wash, the pelleted protein was solubilized in a 1.2% SDS in PBS solution (1 mL) by sonication and heating (5 mins, 80 °C). These solubilized samples were diluted with PBS (5 mL) to give a final SDS concentration of 0.2%. The solutions were incubated with streptavidin-agarose beads (100 μL, Thermo Scientific) at 4 °C for 16 hrs and then at room temperature for 2.5 hrs. The beads were washed with 0.2% SDS in PBS (5 mL), PBS (3 x 5 mL), and water (3 x 5 mL). The beads were pelleted by centrifugation (3 mins, 1400 x g) between washes.

On-bead trypsin digestion

The washed beads were suspended in a 6 M urea in PBS solution (500 μL). DTT (10 mM, from 20x stock in water) was added to the samples and they were reduced by heating to 65 °C for 15 mins. Iodoacetamide (20 mM, from 50x stock in water) was added and the samples were placed in the dark and alkylation was allowed to proceed at room temperature for 30 mins. Following reduction and alkylation, the beads were pelleted by centrifugation (2 mins, 1400 x g) and resuspended in 200 μL of urea (2 mM), $CaCl_2$ (1 mM, from 100x stock in water), and trypsin (2 μg, from a 20 μg in 40 μL of trypsin buffer) in PBS. The digestion was allowed to proceed overnight at 37 °C. The digestion was separated from the beads using a Micro Bio-Spin column (Bio-Rad). The beads were washed with water (2 x 50 μL) and the washes were combined with the eluted peptides. Formic acid (15 μL) was added to the samples, and they were stored at -20 °C until analyzed by mass spectrometry.

Liquid chromatography/mass spectrometry (LC/MS) analysis

LC/MS analysis was performed on an LTQ Orbitrap Discovery mass spectrometer (ThermoFisher) coupled to an Agilent 1200 series HPLC. Digest were pressure loaded onto a 250 μm fused silica desalting column packed with 4 cm of Aqua C18 reverse phase resin (Phenomenex). The peptides were eluted onto a biphasic column (100 μm fused silica with a 5 μm tip, packed with 10 cm C18 and 3 cm Partisphere SCX (Whatman)). Using a gradient 5-100% Buffer B in Buffer A (Buffer A: 95% water, 5 % acetonitrile, 0.1% formic acid; Buffer B: 20% water, 80% acetonitrile, 0.1% formic acid). The peptides were eluted from the SCX onto the C18 resin and into the mass spectrometer following the four salt steps outlined previously.[66] The flow rate through the column was set to ~0.25 μL/min and the spray voltage was set to 2.75 kV. One full MS scan (400-1800 MW) was followed by 8 data dependent scans of the n^{th} most intense ions with dynamic exclusion enabled.

NJP14 mass spectrometry experiments

Mass spectrometry Data Analysis: +/- NJP14

HeLa soluble protein lysates (2 x 500 μL, 2 mg/mL) in PBS were aliquoted as 6 samples (three neg. ctrl, three +NJP14). NJP14 (25 μM) was added to the appropriate samples and the corresponding volume of DMSO was added to the negative controls. These samples were subjected to click chemistry, streptavidin enrichment, on-bead trypsin digestion, and LC/LC-MS/MS as described above. The generated tandem MS data were searched using SEQUEST[91] algorithm against the human IPI database. A static modification of +57 on Cys was specified to account for iodoacetamide alkylation. The

SEQUEST output files generated from the digests were filtered using DTASelect 2.0[92] to generate a list of protein hits with a peptide false-discovery rate of <5%. The resulting identified peptides were further filtered to display proteins identified in all three NJP14 samples with spectral counts >25. For each of these proteins, a % change in spectral counts was calculated and the data were ranked by those proteins displaying the highest % change in spectral counts in the NJP14 samples relative to the Ctrl samples. All proteins with a 50% change in spectral counts (2-fold increase in NJP14 vs Ctrl) are displayed within the Table 3A-1 of Appendix II.

Mass spectrometry analysis: Zn^{2+}/Mg^{2+} + NJP14

HeLa soluble protein lysates (1 x 500 μL, 4 mg/mL) in PBS were aliquoted as 8 samples (two neg. ctrl, two 10 μM Zn^{2+}, two 20 μM Zn^{2+}, and two 20 μM Mg^{2+}). Zn^{2+}/Mg^{2+} were added to the appropriate samples at the designated concentration, and an equal volume of water was added to the control samples. The samples were allowed to sit at room temperature for 1 hr. NJP14 (100 μM) was added to all the samples, and they were allowed to sit at room temperature for 1 hr. Each sample was passed through a Nap-5 column (GE Healthcare) according to standard protocol, and eluents (2 x 500 μL, 2 mg/mL protein for each sample) were collected. These samples were subjected to click chemistry, streptavidin enrichment, on-bead trypsin digestion, and LC/LC-MS/MS as described above. The generated tandem MS data were searched using the SEQUEST[91] algorithm against the human IPI database. A static modification of +57 on Cys was specified to account for iodoacetamide alkylation. The SEQUEST output files were filtered using DTASelect 2.0[92] to generate a list of protein hits with a peptide false-

discovery rate of <5%. The resulting peptides were further filtered to display proteins identified in both the Ctrl samples with spectral counts > 25. For each of these proteins, a % change in spectral counts was calculated for both Zn^{2+}/Mg^{2+} samples, and the data were ranked by those that showed the highest decrease in spectral counts (large negative % change) in the Zn^{2+} 20 μM samples relative to the Ctrl samples. A partial dataset is presented as Table 3-1, and the full dataset in Appendix II as Table 3A-2.

SORD activity assays

Generalized procedure for the SORD oxidative activity assay

An oxidative assay buffer (OAB) stock consisted of glycine (50 mM) and the pH was adjusted to 9.9. OAB, sorbitol (10 mM), NAD^+ (18.0 μM), and HEK293T SORD soluble protein lysates (15 μg, prepared as described above) were combined and aliquoted into a clear 96-well plate at 100 μL per well. The increase in absorbance at 340 nm was monitored and activities were calculated as the initial change in absorbance.

Generalized procedure for SORD reductive activity assay

A reductive assay buffer (RAB) stock consisted of sodium phosphate (10 mM) and the pH was adjusted to 7.0. RAB, fructose (100 mM), NADH (46 μM), and HEK293T SORD soluble protein lysates (15 μg, prepared as described above) were combined and aliquoted into a clear 96-well plate, 100 μL per well. The decrease in

absorbance at 340 nm was read and activities were calculated as the initial change in absorbance.

SORD WT vs Mutants

HEK293T mock and SORD WT, C44A, and C179A lysates were subjected to both the SORD oxidative and reductive activity assays. The activities were determined as replicates of 3 separate trails.

Effect of Zn^{2+}, and NJP14 competition on SORD activity

SORD WT overexpressed HEK293T lysates (75 μL, 2 mg/mL) in PBS were aliquoted (4 aliquots). Zn^{2+} (5 μM) was added to two of the aliquots and water added to the other two as a control. The samples were incubated at room temperature for 1 hr. NJP14 (50 μM) was added to a + and – Zn^{2+} sample, while DMSO as a control was added to the remaining two samples. The samples were incubated at room temperature for 1 hr. These samples were subjected to both SORD oxidative and reductive activity assays. Activities were determined as replicates of 3 separate trials and normalized relative to the untreated Ctrl sample.

Effect of EDTA, NJP14, and Zn^{2+} on SORD activity

SORD WT overexpressed HEK293T lysates (50 μL, 2 mg/mL) in PBS were aliquoted (4 samples) and designated as follows: SORD; SORD-EDTA; SORD-EDTA-Zn^{2+}; SORD-EDTA-NJP14-Zn^{2+}. EDTA (1 mM) was added to the appropriate samples and they were allowed to incubate at room temperature for 1 hr. All samples underwent size exclusion chromatography as described previously. NJP14 (100 μM) or DMSO vehicle were added to the appropriate samples and they were allowed to incubate at room temperature for 1 additional hour. Zn^{2+} (1 mM) was added to the appropriate samples and they were allowed to incubate at room temperature for 1 hr. These samples underwent both the oxidative and reductive SORD activity assays as described above. Activities were determined as replicates of 3 separate trials and normalized relative to the untreated Ctrl sample.

GSTO1 WT and C32A recombinant expression, activity, and binding assays

Recombinant expression

The cDNA for both the GSTO1 WT and C32A mutant were amplified by PCR (sense primer 5'-TATGGATCCGCCATGTCCGGGGGAGTCA-3', antisense primer 5'-GCACTCGAGGAGCCCATAGTCACAGGC-3'), added between the *BamHI* and *XhoI* sites of a bacterial pET-23a(+) expression vector, and transformed into BL21 cells. Overnight cultures were seeded, scaled up, and grown to OD_{600} of 0.8. The cultures were induced with isopropyl β-D-1-thiogalactopyranoside (IPGT, 1 mM) and grown for 4 hrs further. The soluble protein fractions for each protein were collected and purified on

nickel agarose resin (Thermo). The resin was washed with 50 mM imidazole in PBS and protein was eluted with 500 mM imidazole in PBS. The purity of the fractions was judged by silver-stained SDS-PAGE gels and the fractions containing purified enzyme were combined. The imidazole was removed by running the protein through a NAP-5 size exclusion column according to the standard protocol. The protein was subsequently used for the assays and stored on ice.

NJP14 labeling of recombinant GSTO1 in the presence of Zn^{2+}

The recombinant purified GSTO1 WT or C32A mutant was diluted (2 : 3; protein : PBS) and 50 μL aliquots were made. Zn^{2+} was added to the samples at 0, 1, 10, 50, or 100 μM. The samples were incubated at room temperature for 30 mins. NJP14 (1 μM) was added to all the samples and they were vortexed and allowed to sit at room temperature for an additional hour. Bio-Spin Micro-6 columns (Bio-Rad) were equilibrated and each sample was passed through a column. The eluents underwent click chemistry and in-gel fluorescence as described previously and were subsequently silver-stained according to the standard protocol. The fluorescent signals were integrated using ImageJ software and these values were plotted.

General procedures for assay of GSTO1 activity

The procedure for a previously described thioltransferase activity assay was employed.[78] Tris (100 mM) pH 8.0, bovine serum albumin (0.1 mg/mL), GSH (1 mM),

glutathione reductase (~2 units), and NADPH (0.3 mM) were combined for each sample. Hydroxyethyl disulfide (HEDS, 0.75 mM) was added to each sample and they were allowed to sit at room temperature for about 2 mins in order for the disulfides to equilibrate. The protein was added to each sample and they were subsequently aliquoted into a clear 96-well plate, 100 μL per well. The plate was read for absorbance at 340 nm and activities were calculated as the initial change in absorbance.

Effect of increasing [Zn^{2+}] on GSTO1 activity

Aliquots of PBS, recombinant purified GSTO1 WT or C32A protein were treated with Zn^{2+} at 0, 1, 10, 20, 50, or 100 μM. The protein samples were allowed to incubate at room temperature for 30 mins. The protein was then utilized in the previously described GSTO1 activity assay and the activities were determined as an average from 3 trials.

Quantitative mass spectrometry with IA-alkyne and azo-tags

Synthesis of light and heavy azobenzene tags (Azo-L and Azo-H)

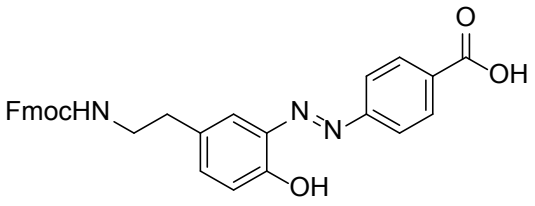

Fmoc-Azo-OH

Azo-L and Azo-H tags were synthesized by manual solid-phase methods on Biotin-PEG NovaTag resin using Fmoc as the protecting group for the α-amino functionalities. All reactions were performed in the dark. Amino acids were coupled using PyBOP (2 eq) as the activating agent and DIPEA (4 eq). Fmoc-Azo-OH ((E)-4-((5-(Fmoc-2-aminoethyl)-2-hydroxyphenyl)diazenyl)benzoic acid, synthesized accord to Qian et al),[80] valine, and 5-azido-pentanoic acid (2 eq each) were added under standard coupling conditions. Cleavage from the resin was performed in TFA : DCM : TIS : water (90 : 5 : 2.5 : 2.5) solution for 2 hrs. All peptides were purified by preparative HPLC with a gradient of increasing acetonitrile-0.1% TFA (solvent B) in water -0.1% TFA (solvent A). All peptides were analyzed by a Micromass LCT TOF mass spectrometer coupled to a Waters 2975 HPLC and a Waters 2996 photodiode array UV-vis detector and HRMS were determined using an LTQ Orbitrap Discovery mass spectrometer (ThermoFisher) coupled to an Agilent 1200 series HPLC. Azo-L (48.49%), HPLC t_R = 28.50 min (C18, 5-100% B in 30 mins); HRMS ($C_{45}H_{67}N_{11}O_9S$): m/z calcd 937.48; obsd $[M + H]^+$ 938.49 (ESI+); Azo-H (38.23%), HPLC t_R = 28.50 min (C18, 5-100% B in 30 mins); HRMS ($C_{45}H_{67}N_{11}O_9S$): m/z calcd 943.88; obsd $[M + H]^+$ 944.51 (ESI+).

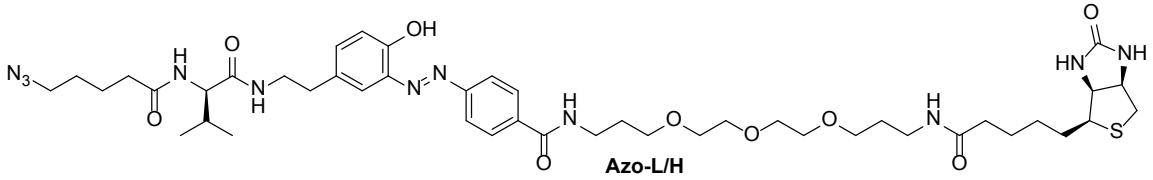

Azo-L/H

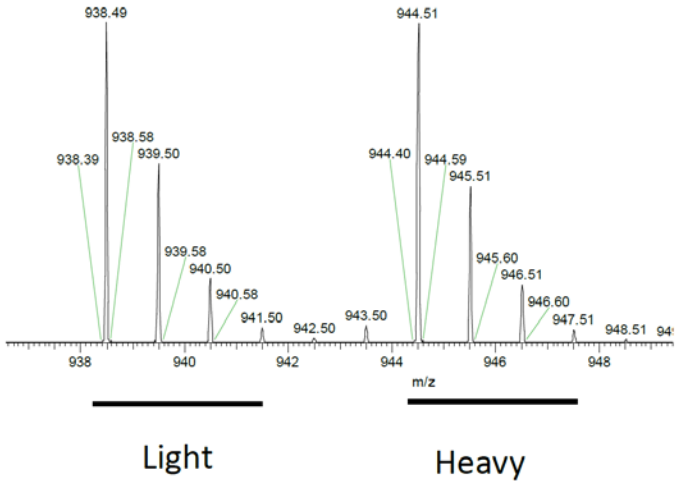

Quantitative mass spectrometry using Azo-tags: Zn^{2+} + IA-alkyne

HeLa soluble protein lysates (500 µL, 2 x 4 mg/mL) in PBS for each proteome were aliquoted. One set underwent treatment with Zn^{2+} 10 µM / Zn^{2+} 20 µM / Mg^{2+} 20 µM while the other set was treated with an equal volume of water for 1 hr. All samples were then treated with IA-alkyne (100 µM from 100x stock in DMSO) and allowed to sit at room temperature for 1 hr. After purification by size exclusion chromatography, the Azo-L tag (100 µM) was added to the variable samples, while the Azo-H tag (100 µM) was conjugated to the control samples through standard procedure for click chemistry. The samples were combined pairwise and washed with MeOH as described above. Streptavidin enrichment and trypsin digestion was also performed as described above. The beads were washed with PBS (3 x 600 µL) and water (3 x 600 µL) and subsequently transferred to Eppendorf tubes. The azobenzene cleavage was carried out by incubating the beads with fresh 25 mM sodium dithionite in PBS (25 mM) for 1 hr at room temperature on a rotator. After centrifugation, the supernatant was transferred to new

eppendorf tubes. The cleavage process was repeated twice more with dithionite solution (75 μL, 25 mM; 75 μL, 50 mM) to ensure completion and the supernatants were combined each time in the eppendorf. The beads were additionally washed twice with water (75 μL). Formic acid (15 μL) was added to the samples, and they were stored at -20 °C until mass spectrometry analysis. Mass spectrometry analysis was performed as described previously using a biphasic chromatography column. The peptides were eluted from the strong cation exchange (SCX) onto the C18 resin and into the mass spectrometer following the four salt steps outline in Weerapana et al for the TEV samples.[66] The flow rate through the column was set to ~0.25 μL/min and the spray voltage was set to 2.75 kV. One full MS scan (400-1800 MW) was followed by 18 data dependent scans of the n^{th} most intense ions with dynamic exclusion disabled.

Quantitative mass spectrometry using Azo-tags: EDTA + IA-alkyne

Protein samples underwent the same procedure described above, except metal ions were substituted with EDTA (100 mM).

Combined data analysis

The generated tandem MS data from each sample were searched using the SEQUEST[91] algorithm against the human IPI database. A static modification of +57 on Cys was specified to account for iodoacetamide alkylation and differential modifications of +456.2849 (Azo-L) and +462.2987 (Azo-H) were specified on cysteine to account for probe modifications. The SEQUEST output files generated from the digests were filtered

using DTASelect 2.0.[92] Reported peptides were required to be fully tryptic and contain the desired probe modification and discriminant analyses were performed to achieve a peptide false-discovery rate below 5%. Quantification of light/heavy ratios "R" was performed using the CIMAGE quantification package as described previously.[63] Data from the Zn^{2+}-treated samples were sorted to identify peptides with $R < 0.66$ (149 hits), while data from the EDTA-treated samples were sorted to identify peptides with $R > 1.50$ (118 hits). These full datasets are presented in the Appendix as Table 3A-3 and Table 3A-4 respectively. These datasets were combined and sorted to obtain peptides that fit both criteria (48 hits) and these are presented in Table 3-2.

References

1. Harris, T. K.; Turner, G. J., Structural Basis of Perturbed pKa Values of Catalytic Groups in Enzyme Active Sites. *IUBMB Life* 2002, 53, 85-98.

2. Giles, N. M.; Watts, A. B.; Giles, G. I.; Fry, F. H.; Littlechild, J. A.; Jacob, C., Metal and Redox Modulation of Cysteine Protein Function. *Chem. Biol.* 2003, 10, 677-693.

3. Tainer, J. A.; Roberts, V. A.; Getzoff, E. D., Metal-Binding Sites in Proteins. *Curr. Opin. Biotechnol.* 1991, 2, 582-591.

4. Maret, W.; Yetman, C. A.; Jiang, L.-J., Enzyme regulation by reversible zinc inhibition: glycerol phosphate dehydrogenase as an example. *Chemico-Biological Interactions* 2001, 130-132, 891-901.

5. Pace, N. J.; Weerapana, E., Zinc-Binding Cysteines: Diverse Functions and Structural Motifs. *Biomolecules* 2014, 4, 419-434.

6. Andreini, C.; Banci, L.; Bertini, I.; Rosato, A., Counting the Zinc-Proteins Encoded in the Human Genome. *J. Proteome Res.* 2006, 5, 196-201.

7. Lee, Y.-M.; Lim, C., Physical Basis of Structural and Catalytic Zn-Binding Sites in Proteins. *J. Mol. Biol.* 2008, 379, 545-553.

8. Krishna, S. S.; Majumdar, I.; Grishin, N. V., Structural Classification of Zinc Fingers: Survey and Summary. 2003, 31, 532-550.

9. Lee, M. S.; Gippert, G. P.; Soman, K. V.; Case, D. A.; Wright, P. E., Three-Dimensional Solution Structure of a Single Zinc Finger DNA-Binding Domain. *Science* 1989, 245, 635-637.

10. Razin, S. V.; Borunova, V. V.; Maksimenko, O. G.; Kantidze, O. L., Cys_2His_2 Zinc Finger Protein Family: Classification, Functions, and Major Members. *Biochemistry (Moscow)* 2011, 77, 217-226.

11. Wolfe, S. A.; Nekludova, L.; Pabo, C. O., DNA Recognitions by Cys_2His_2 Zinc Finger Proteins. *Annu. Rev. Biophys. Biomol. Struct.* 1999, 3, 183-212.

12. Gaj, T.; Gersbach, C. A.; Barbas II, C. F., ZFN, TALEN, adn CRISPR/Cas-Based Methods for Genome Engineering. *Trends in Biotechnology* 2013, 31, 397-405.

13. Liu, Q.; Segal, D. J.; Ghiara, J. B.; Barbas III, C. F., Design of Polydactyl Zinc-Finger Proteins for Unique Addressing Within Complex Genomes. *Proc. Natl. Acad. Sci. USA* 1997, 94, 5525-5530.

14. Beerli, R. R.; Segal, D. J.; Birgit, D.; Barbas, C. F. I., Toward Controlling Gene Expression at Will: Specific Regulation of the erb-2/HER-2 Promoter by Using Polydactyl Zinc Finger Proteins Constructed from Modular Building Blocks. *Proc. Natl. Acad. Sci. USA* 1998, 95, 14628-14633.

15. Beerli, R. R.; Dreier, B.; Barbas III, C. F., Positive and Negative Regulation of Endogenous Genes by Designed Transcription Factors. *Proc. Natl. Acad. Sci. USA* 1999, 97, 1495-1500.

16. Klinman, J. P., Probes of Mechanism and Transition-State Structure in the Alcohol Dehydrogenase Reaction. *Crit. Rev. Biochem.* 1981, 10, 39-78.

17. Pauly, T. A.; Ekstrom, J. L.; Beebe, D. A.; Chrunyk, B.; Cunningham, D.; Griffor, M.; Kamath, A.; Lee, S. E.; Madura, R.; Mcguire, D.; Subashi, T.; Wasilko, D.; Watts, P.; Mylari, B. L.; Oates, P. J.; Adams, P. D.; Rath, V. L., X-Ray Crystallographic and Kinetic Studies of Human Sorbitol Dehydrogenase. *Structure* 2003, 11, 1072-1085.

18. Carter Jr., C. W., The Nucleoside Deaminases for Cytidine and Adenosine: Structure, Transistion State Stabilization, Mechanism, and Evolution. *Biochimie* 1995, 77, 92-98.

19. Xiang, S.; Short, S. A.; Wolfenden, R.; Carter Jr., C. W., Transition-State Selectivity for a Single Hydroxyl Group During Catalysis by Cytidine Deaminase. *Biochemistry* 1995, 34, 4516-4523.

20. Auerbach, G.; Herrmann, A.; Bracher, A.; Bader, G.; Gutlich, M.; Fischer, M.; Neikamm, M.; Garrido-Franco, M.; Richarson, J.; Nar, H.; Huber, R.; Bacher, A., Zinc Plays a Key Role in Human and Bacterial GTP Cyclohydrolase I. *Proc. Natl. Acad. Sci. USA* 2000, 97, 13567-13572.

21. Evans, J. C.; Huddler, D. P.; Jiracek, J.; Castro, C.; Millian, N. S.; Garrow, T. A.; Ludwig, M. L., Betain-Homocysteine Methyltransferase: Zinc in a Distored Barrel. *Structure* 2002, 10, 1159-1171.

22. Long, S. B.; Casey, P. J.; Beese, L. S., Reaction Path of Protein Farnesyltransferase at Atomic Resolution. *Nature* 2002, 419, 645-650.

23. Sousa, S. F.; Fernandes, P. A.; Ramos, M. J., Unraveling the Mechanism of the Farnesyltransferase Enzyme. *J. Biol. Inorg. Chem.* 2004, 10, 3-10.

24. Theorell, H.; McKinley McKee, J. S., Mechanism of Action of Liver Alcohol Dehydrogenase. *Nature* 1961, 192, 47-50.

25. Hoog, J.-O.; Ostberg, L. J., Mammalian Alcohol Dehydrogenases - A Comparative Investigation at Gene and Protein Levels. *Chemico-Biological Interactions* 2011, 191, 2-7.

26. Pettersson, G., Liver Alcohol Dehydrogenase. *Crit. Rev. Biochem.* 1987, 21, 349-388.

27. Knipp, M.; Charnock, J. M.; Garner, C. D.; Vasak, M., Structural and Functional Characterization of the Zn(II) Site in Dimethylargininase-1 (DDAH-1) from Bovine Brain. *J. Biol. Chem.* 2001, 276, 40449-40456.

28. Lee, S.; Shen, W.-H.; Miller, A.; Kuo, L. C., Zn^{2+} Regulation of Ornithine Transcarbamoylase. *J. Mol. Biol.* 1990, 211, 255-269.

29. Maret, W., Inhibitory Zinc Sites in Enzymes. *Biometals* 2013, 2, 197-204.

30. Tully, D. C.; Liu, H.; Chatterjee, A. K.; Alper, P. B.; Epple, R.; Williams, J. A.; Roberts, M. J.; Woodmansee, D. H.; Masick, B. T.; Tumanut, C.; Li, J.; Spraggon, G.; Hornsby, M.; Chang, J.; Tuntland, T.; Hollenbeck, T.; Gordon, P.; Harris, J. L.; Karanewsky, D. S., Synthesis and SAR of Arylaminoethyl Amides as Noncovalent Inhibitors of Cathepsin S: P3 Cyclic Ethers. *Bioorg. Med. Chem. Lett.* 2006, 16, 5112-5117.

31. Perry, D. K.; Smyth, M. J.; Stennicke, H. R.; Salvesen, G. S.; Duriez, P.; Poirier, G. G.; Hannun, Y. A., Zinc is a Potent Inhibitor of the Apoptotic Protease, Caspase-3: A Novel Target for Zinc in the Inhibition of Apoptosis. *J. Biol. Chem.* 1997, 272, 18530-18533.

32. Peterson, Q. P.; Goode, D. R.; West, D. C.; Ramsey, K. N.; Lee, J. J. Y.; Hergenrother, P. J., PAC-1 Activates Procaspase-3 In Vitro Through Relief of Zinc-Mediated Inhibition. *J. Mol. Biol.* 2009, 388, 144-158.

33. Velazquez-Delgado, E. M.; Hardy, J. A., Zinc-Mediated Allosteric Inhibition of Caspase-6. *J. Biol. Chem.* 2012, 287, 36000-36011.

34. Huber, K. L.; Hardy, J. A., Mechanism of Zinc-Mediated Inhibition of Caspase-9. *Protein Sci.* 2012, 21, 1056-1065.

35. Costello, L. C.; Liu, Y.; Franklin, R. B.; Kennedy, M. C., Zinc Inhibition of Mitochondrial Aconitase and Its Importance in Citrate Metabolism of Prostate Epithelial Cells. *J. Biol. Chem.* 1997, 272, 28875.

36. Pace, N. J.; Weerapana, E., A Competitive Chemical-Proteomic Platform to Identify Zinc-Binding Cysteines. *ACS Chem. Biol.* 2014, 9, 258-265.

37. Evans, J. C.; Huddler, D. P.; Jiracek, J.; Castro, C.; Millian, N. S.; Garrow, T. A.; Ludwig, M. L., Betaine-Homocysteine Methyltransferase: Zinc in a Distored Barrel. *Structure* 2002, 10, 1159-1171.

38. Korichneva, I.; Hoyos, B.; Chua, R.; Levi, E.; Hammerling, U., Zinc Release from Protein Kinase C as the Common Event During Activation by Lipid Second Messenger or Reactive Oxygen. *J. Biol. Chem.* 2002, 277, 44327-44331.

39. Fischmann, T. O.; Hruza, A.; Da Niu, X.; Fossetta, J. D.; Lunn, C. A.; Dolphin, E.; Prongay, A. J.; Reichert, P.; Lundell, D. J.; Narula, S. K.; Weber, P. C., Structural Characterization of Nitric Oxide Synthase Isoforms Reveals Striking Active-Site Conservation. *Nat. Struc. Biol.* 1999, 6, 233-242.

40. Zou, M.-H.; Shi, C.; Cohen, R. A., Oxidation of Zinc-Thiolate Complex and Uncoupling of Endothelial Nitric Oxide Synthase by Peroxynitrite. *J. Clin. Invest.* 2002, 109, 817-826.

41. Hymowitz, S. G.; O'Connell, M. P.; Ultsch, M. H.; Hurst, A.; Totpal, K.; Ashkenazi, A.; de Vos, A. M.; Kelley, R. F., A Unique Zinc-Binding Site Revealed by a High-Resolution X-Ray Structure of Homotrimeric Apo2L/TRAIL. *Biochemistry* 2000, 39, 633-640.

42. MacAllister, R. J.; Parry, H.; Kimoto, M.; Ogawa, T.; Russell, R. J.; Hodson, H.; Whitley, G. S. J.; Vallance, P., Regulation of Nitric Oxide by Dimethylarginine Dimethylaminohydrolase. *Br. J. Pharmacol.* 1996, 119, 1533-1540.

43. Wang, Y.; Monzingo, A. F.; Hu, S.; Schaller, T. H.; Robertus, J. D.; Fast, W., Developing Dual and Specific Inhibitors of Dimethylarginine Dimethylaminohydrolase-1 and Nitric Oxide Synthase: Toward a Targeted Polypharmacology to Control Nitric Oxide. *Biochemistry* 2009, 48, 8624-8635.

44. Frey, D.; Braun, O.; Briand, C.; Vasak, M.; Grutter, M. G., Structure of the Mammalian NOS Regulator Dimethylarginine Dimethylaminohydrolase: A Basis for the Design of Specific Inhibitors. *Structure* 2006, 14, 901-911.

45. Thornberry, N. A., The Caspase Family of Cysteine Proteases. *Br. Med. Bull.* 1997, 53, 478-490.

46. Zalewski, P. D.; Forbes, I. J.; Betts, W. H., Correlation of Apoptosis with Change in Intracellular Labile Zn(II) Using Zinquin [(2-Methyl-8-p-Toluenesulphonamido-6-Quinolyloxy)Acetic Acid], a New Specific Fluorescent Probe for Zn(II). *Biochem. J.* 1993, 296, 403-408.

47. Paulsen, C. E.; Carroll, K. S., Orchestrating Redox Signaling Networks Through Regulatory Cysteine Switches. *ACS Chem. Biol.* 2010, 5, 47-62.

48. Klomsiri, C.; Karplus, P. A.; Poole, L. B., Cysteine-Based Redox Switches in Enzymes. *Antioxid. Redox Signaling* 2011, 14, 1065-1077.

49. Hess, D. T.; Matsumoto, A.; Kim, S. O.; Marshall, H. E.; Stamler, J. S., Protein S-Nitrosylation: Purview and Parameters. *Nat. Rev. Mol. Cell. Biol.* 2005, 6, 150-166.

50. Maret, W., Zinc Coordination Environments in Proteins Determine Zinc Functions. *J Trace Elem in Med and Biol* 2005, 19, 7-12.

51. Pajares, M. A.; Perez-Sala, D., Betaine Homocysteine S-Methyltransferase: Just a Regulator of Homocysteine Metabolism? *Cell. Mol. Life Sci.* 2006, 63, 2792-2803.

52. Stuehr, D. J., Mammalian Nitric Oxide Synthases. *Biochim. et Biophys. Acta* 1999, 1411, 217-230.

53. Irving, H.; Williams, R. J. P., Order of Stability of Metal Complexes. *Nature* 1948, 162, 746-747.

54. Krezel, A.; Maret, W., Dual Nanomolar and Picomolar Zn(II) Binding Properties of Metallothionein. *J. Am. Chem. Soc.* 2007, 129, 10911-10921.

55. Krezel, A.; Maret, W., Zinc-Buffering Capacity of a Eukaryotic Cell at Physiological pZn. *J. Biol. Inorg. Chem.* 2006, 11, 1049-1062.

56. Romero-Isart, N.; Vasak, M., Advances in the Structure and Chemistry of Metallothioneins. *J. Inorg. Biochem.* 2002, 88, 388-396.

57. Maret, W.; Larsen, K. S.; Vallee, B. L., Coordination Dynamics of Biological Zinc "Clusters" in Metallothioneins and in the DNA-Binding Domain of Transcription Factor Gal4. *Proc. Natl. Acad. Sci. USA* 1997, 94, 2233-2237.

58. Heinz, U.; Kiefer, M.; Tholey, A.; Adolph, H.-W., On the Competition for Available Zinc. *J. Biol. Chem.* 2005, 280, 3197-3207.

59. Babula, P.; Masarik, M.; Adam, V.; Eckschlager, T.; Stiborova, M.; Trnkova, L.; Skutkova, H.; Provaznik, I.; Hubalek, J.; Kizek, R., Mammalian Metallothioneins: Properties and Functions. *Metallomics* 2012, 4, 739-750.

60. Maret, W., Metalloproteomics, Metalloproteomes, and the Annotation of Metalloproteins. *Metallomics* 2010, 2, 117-125.

61. Bertini, I.; Decaria, L.; Rosato, A., The Annotation of Full Zinc Proteomes. *J. Biol. Inorg. Chem.* 2010, 15, 1071-1078.

62. Kornhaber, G. J.; Snyder, D.; Moseley, H. N.; Montelione, G. T., Identification of Zinc-Ligated Cysteine Residues based on 13Cα and 13Cβ Chemical Shift Data. *Journal of Biomolecular NMR* 2006, 34, 259-269.

63. Weerapana, E.; Wang, C.; Simon, G. M.; Richter, F.; Khare, S.; Dillon, M. B. D.; Bachovchin, D. A.; Mowen, K.; Baker, D.; Cravatt, B. F., Quantitative Reactivity Profiling Predicts Functional Cysteines in Proteomes. *Nature* 2010, 468, 790-795.

64. Weerapana, E.; Simon, G. M.; Cravatt, B. F., Disparate Proteome Reactivity Profiles Carbon Electrophiles. *Nat. Chem. Biol.* 2008, 4, 405-407.

65. Zaworski, P. G.; Gill, G. S., Precipitation and Recovery of Proteins from Culture Supernatants Using Zinc. *Anal. Biochem.* 1988, 173, 440-444.

66. Weerapana, E.; Speers, A. E.; Cravatt, B. F., Tandem Orthogonal Proteolysis-Activity-Based Protein Profiling (TOP-ABPP)-A General Method for Mapping Sites of Probe Modification in Proteomes. *Nature Prot.* 2007, 2, 1414-1425.

67. Dudev, T.; Lim, C., Principles Governing Mg, Ca, and Zn Binding and Selectivity in Proteins. *Chem. Rev.* 2003, 103, 773-787.

68. Engerman, R. L.; Kern, T. S.; Larson, M. E., Nerve Conduction and Aldose Reductase Inhibition During 5 Years of Diabetes or Galactosemia in Dogs. *Diabetologia* 1994, 37, 141-4.

69. El-Kabbani, O.; Darmanin, C.; Chung, R. P.-T., Sorbitol Dehydrogenase: Structure, Function, and Ligand Design. *Curr. Med. Chem.* 2004, 11.

70. Rose, I. A.; Warms, J. V. B., Control of Glycolysis in the Human Red Blood Cell. *J. Biol. Chem.* 1966, 241, 4848-54.

71. Jeffrey, J.; Chesters, J.; Mills, C.; Sadler, P. J.; Jornvall, H., Sorbitol Dehydrogenase is a Zinc Enzyme. *EMBO J.* 1984, 3.

72. Maret, W., Human Sorbitol Dehydrogenase - A Secondary Alcohol Dehydrogenase with Distinct Pathophysiological Roles: pH-Dependent Kinetic Studies. *Adv. Exp. Med. Biol.* 1996, 414, 383-393.

73. Geisen, K.; Utz, R.; Groetsch, H.; Lang, H. J.; Nimmesgern, H., Sorbitol-Accumulating Pyrimidine Derivatives. *Arzneim.-Forsch.* 1994, 44, 1032-43.

74. Mylari, B. L.; Oates, P. J.; Zembrowski, W. J.; Beebe, D. A.; Conn, E. L.; Coutcher, J. B.; O'Gorman, M. T.; Linhares, M. C.; Withbroe, G. J., A Sorbitol

Dehydrogenase Inhibitor of Exceptional in Vivo Potency with a Long Duration of Action: 1-(R)-{4-[4-(4,6-Dimethyl[1,3,5]triazin-2-yl)- 2R,6S-dimethylpiperazin-1-yl]pyrimidin-2- yl}ethanol. *J. Med. Chem.* 2002, 45, 4398-4401.

75. Rose, C. I.; Henderson, A. R., Reaction-Rate Assay of Serum Sorbitol Dehydrogenase Activity at 37 °C. *Clin. Chem.* 1975, 21, 1619-1626.

76. Lindstad, R. I.; McKinley-McKee, J. S., Reversible Inhibition of Sheep Liver Sorbitol Dehydrogenase by the Antidiabetogenic Drug 2-hydroxymethyl-4-(4-*N,N*-dimethylaminosulfonyl-1-piperazino) pyrimidine. *FEBS Lett.* 1997, 408, 57-61.

77. Hayes, J. D.; Pulford, D. J., The Glutathione S-Transferase Supergene Family: Regulation of GST* and the Contribution of the Isoenzymes to Cancer Chemoprotection and Drug Resistance. *Crit. Rev. Biochem. Mol. Biol.* 1995, 30, 445-600.

78. Board, P. G.; Coggan, M.; Chelvanayagam, G.; Easteal, S.; Jermiin, L. S.; Schulte, G. K.; Danley, D. E.; Hoth, L. R.; Griffor, M. C.; Kamath, A. V.; Rosner, M. H.; Chrunyk, B. A.; Perregaux, D. E.; Gabel, C. A.; Geoghegan, K. F.; Pandit, J., Identification, Characterization, and Crystal Structure of the Omega Class Glutathione Transferases. *J. Biol. Chem.* 2000, 275, 24798-24806.

79. Axelsson, K.; Eriksson, S.; Mannervik, B., Purification and Characterization of Cytoplasmic Thioltransferase (Glutathione:Disulfide Oxidoreductase) From Rat Liver. *Biochemistry* 1978, 17, 2978-84.

80. Qian, Y.; Martell, J.; Pace, N. J.; Ballard, T. E.; Johnson, D. S.; Weerapana, E., An Isotopically Tagged Azobenzene-Based Cleavable Linker for Quantitative Proteomics. *Chem. Bio. Chem.* 2013, 14, 1410-1414.

81. Sanghani, P. C.; Bosron, W. F.; Hurley, T. D., Human Glutathione-Dependent Formaldehyde Dehydrogenase. Structural Changes Associated with Ternary Complex Formation. *Biochemistry* 2002, 41, 15189-15194.

82. Hensley, M. P.; Tierney, D. L.; Crowder, M. W., Zn(II) Binding to *Escherichia* C*oli* 70S Ribosomes. *Biochemistry* 2011, 50, 9937-9939.

83. Gaskin, F.; Kress, Y., Zinc Ion-Induced Assembly of Tubulin. *J. Biol. Chem.* 1977, 252, 6918-6924.

84. Eagle, G. R.; Zombola, R. R.; Himes, R. H., Tubulin-Zinc Interactions: Binding and Polymerization Studies. *Biochemistry* 1983, 22, 221-228.

85. Samara, N. L.; Ringel, A. E.; Wolberger, C., A Role for Intersubunit Interactions in Maintaining SAGA Deubiquitinating Module Structure and Activity. *Structure* 2012, 20, 1414-1424.

86. Lang, G.; Bonnet, J.; Umlauf, D.; Karmodiya, K.; Koffler, J.; Stierle, M.; Devys, D.; Tora, L., The Tightly Controlled Deubiquitination Activity of the Human SAGA Complex Differentially Modifies Distinct Gene Regulatory Elements. *Mol. and Cell. Biol.* 2011, 31, 3734-3744.

87. Cao, J.; Yan, Q., Histone Ubiquitination and Deubiquitination in Transcription, DNA Damage Response, ,and Cancer. *Frontier in Oncology* 2012, 2, 1-9.

88. Glinsky, G. V., Death-From-Cancer Signatures and Stem Cell Contribution to Metastatic Cancer. *Cell Cycle* 2005, 4, 1171-1175.

89. Glinsky, G. V.; Berezovska, O.; Glinskii, A. B., Microarray Analysis Identifies a Death-From-Cancer Signature Predicting Therapy Failure in Patients with Multiple Types of Cancer. *J. Clin. Invest.* 2005, 115, 1503-1521.

90. Zhang, Y. X.; Yao, L.; Zhang, X. Y.; Ji, H. F.; Wang, L. H.; Sun, S. S.; Pang, D., Elevated Expression of USP22 in Correlation with Poor Prognosis in Patients with Invasive Breast Cancer. *J. Cancer Res. Clin. Oncol.* 2011, 137, 1245-1253.

91. Eng, J. K.; McCormack, A. L.; Yates III, J. R., An Approach to Correlate Tandem Mass Spectral Data of Peptides with Amino Acid Sequences in a Protein Database. *J. Am. Mass Spectrom.* 1994, 5, 976-989.

92. Tabb, D. L.; McDonald, W. H.; Yates III, J. R., DTASelect and Contrast: Tools for Assembling and Comparing Protein Identifications from Shotgun Proteomics. *J. Proteome res.* 2002, 1, 21-26.

Chapter 4

Selective covalent inhibitors to interrogate the role of protein disulfide isomerase in cancer progression

Introduction

Overview

Protein disulfide isomerase A1 (PDIA1), a 57-kD dithiol-disulfide oxidoreductase and molecular chaperone, is one of the most abundant soluble proteins in the endoplasmic reticulum (ER) and accounts for up to 0.8% of total cellular protein.[1, 2] PDIA1 was the first endogenous protein-folding catalyst discovered in 1963,[3, 4] and was given its name the following decade.[5] At least 21 other members have been subsequently identified, giving rise to the PDI protein family (Table 4-1).[6] While many vary in size, structure, and function, the majority of PDIs possess at least one, but often multiple, conserved thioredoxin-like domains (CXXC) that facilitate catalysis and have thus been characterized as members of the thioredoxin super family. Thioredoxin domains are recognized by a canonical protein fold and are often comprised of a pair of redox-catalytic cysteines (CXXC) that catalyzes oxidative protein folding and the formation of native disulfide bonds.[7] It's this structural similarity that defines the PDI protein family; however, only about half of PDIs possess the CXXC active-site domain, suggesting that the others likely do not have catalytic activity. These 21 isoforms have been studied in varying detail, but the majority of this thesis will focus on protein disulfide isomerase A1 (PDIA1) henceforward.

Name	Length	Domain composition	# a-type domains	Active-site sequence
PDIA1 (PDI)	508	a-b-b'-a'	2	CGHC, CGHC
PDIA2 (PDIp)	525	a-b-b'-a'	2	CGHC, CTHC
PDIA3 (ERp57)	505	a-b-b'-a'	2	CGHC, CGHC
PDIA4 (ERp72)	645	a°-a-b-b'-a'	3	CGHC, CGHC, CGHC
PDIA5 (PDIr)	519	b-a°-a-a'	3	CSMC, CGHC, CPHC
PDIA6 (P5)	440	a°-a-b	2	CGHC, CGHC

PDIA7 (PDILT)	584	a-b-b'-a'	2	SKQS, SKKC
PDIA8 (ERp27)	273	b-b'	0	N/A
PDIA9 (ERp28)	261	b-D	0	N/A
PDIA10 (ERp44)	406	a-b-b'	1	CRFS
PDIA11 (TMX1)	280	a	1	CPAC
PDIA12 (TMX2)	296	a	1	SNDC
PDIA13 (TMX3)	454	a-b-b'	1	CGHC
PDIA14 (TMX4)	349	a	1	CPSC
PDIA15 (ERp46)	432	a°-a-a'	3	CGHC, CGHC, CGHC
PDIA16 (ERp18)	172	a	1	CGAC
PDIA17 (HAG-2)	175	a	1	CPHS
PDIA18 (HAG-3)	165	a	1	CQYS
PDIA19 (ERdj5)	793	J-a''-b-a°-a-a'	4	CSHC, CPPC, CHPC, CGPC
PDIB1 (CASQ1)	396	Unknown	N/A	N/A
PDIB2 (CASQ2)	399	Unknown	N/A	N/A

Table 4-1. PDI protein family consists of 21 members with varying structures.

Cellular functions of PDIA1

PDIA1 primarily mediates oxidative protein folding within the ER as a dithiol-disulfide reductase, oxidase, and isomerase, and also displays general molecular chaperone activity. Disulfide-bond formation occurs in approximately 30% of all proteins and is essential for assembly of native structures required for bioactivity.[2] In addition, PDIA1 performs other diverse and essential cellular functions. It binds and stabilizes the major histocompatibility complex (MHC) class I peptide-loading complex that mediates MHC class I folding and peptide loading.[8] PDIA1 also binds NAD(P)H oxidase subunits and regulates NAD(P)H oxidase activity in vascular smooth muscle cells.[9] Finally, PDIA1 has also been observed to be a subunit of prolyl-4 hydroxylase,[10] an essential enzyme for the synthesis of collagens and microsomal triglyceride transfer protein, a central enzyme for the assembly of apoliprotein B-containing lipoproteins.[11]

Besides its primary location in the ER as a soluble oxidoreductase, PDIA1 is also present on the extracellular side of the plasma membrane.[12, 13] Although the mechanism of PDIA1 secretion or translocation to the cell surface is unresolved, some evidence suggests that it interacts with the cell membrane via electrostatic charges.[14] PDIA1 mainly functions as a reductase[15] or an isomerase[16] at the cell surface and has been shown to regulate multiple important biological processes, including coagulation,[17] injury response,[18] platelet activation[19-21] and thrombus formation,[22-24] T cell migration,[15] glioma cell migration,[25] gamete fusion,[26] and nitric oxide internalization from extracellular *S*-nitrosothiols.[27] PDIA1 has also been shown to facilitate viral infection,[28] as exemplified by its involvement in HIV-1 fusogenic events. Cell surface PDIA1 catalyzes the reduction of at least two disulfide bonds in an HIV-1 envelope glycoprotein, gp120, resulting in a conformation change that enhances binding to chemokine (C-X-C motif) receptor 4 (CXCR4) and C-C chemokine receptor type 5 (CCR5).[29-31] Besides the ER and cell surface, PDIA1 has also been speculated to reside within other organelles, such as the mitochondria and nucleus; however, no conclusive evidence confirms the presence of PDIA1 within these subcellular locations and potential biological functions of PDIA1 within these organelles remain unclear.[32, 33]

Structural properties of PDIA1

The full-length PDIA1 contains 508 amino acids, including a 17-amino-acid N-terminal signal peptide that undergoes cleavage upon maturation. PDIA1 is organized into four thioredoxin-like domains: **a**, **b**, **b'**, **a'**, and a highly acidic C-terminal extension **c** domain (Figure 4-1). The **a**-type domains each contain a thioredoxin-like active-site

motif (CGHC) to facilitate thiol-disulfide oxidoreductase activity. These cysteines typically convert between reduced dithiols and an oxidized disulfide. In contrast, the **b**-type domains exhibit no catalytic activity and solely contribute to substrate binding. The **c** domain possesses a canonical ER signaling sequence (KDEL) at the C-terminus, which sequesters the protein to the lumen of the ER, an oxidizing environment that promotes disulfide-bond formation.

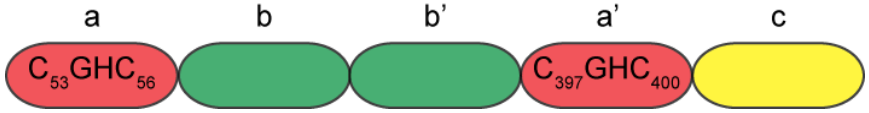

Figure 4-1. Domain organization of PDIA1.

Although the structure of full-length human PDIA1 has not yet been resolved, a high resolution structure of human PDIA1 **a-b-b'-a'** within both its reduced and oxidized states revealed that the **a-b-b'-a'** domains arrange in a horseshoe-like shape with the active-sites of the **a**-type domains facing each other (Figure 4-2).[34] Importantly, PDIA1 is found to undergo significant conformational changes upon reduction/oxidation. In the reduced PDIA1, the open side of the cleft formed by the **a-b-b'-a'** domains for accommodating a substrate is narrow (~15 Å) and the volume of the cleft is smaller (~6,816 $Å^3$), which is estimated to be sufficient to accommodate a small folded protein of ~50 residues. However, in the oxidized PDIA1, the open side of the cleft becomes wider (~30 Å), and the volume of the cleft becomes much larger (~14,453 $Å^3$) allowing for accommodation of larger proteins of ~100 residues.[34] These conformational changes are thought to help facilitate the oxidoreductase activity of PDIA1.

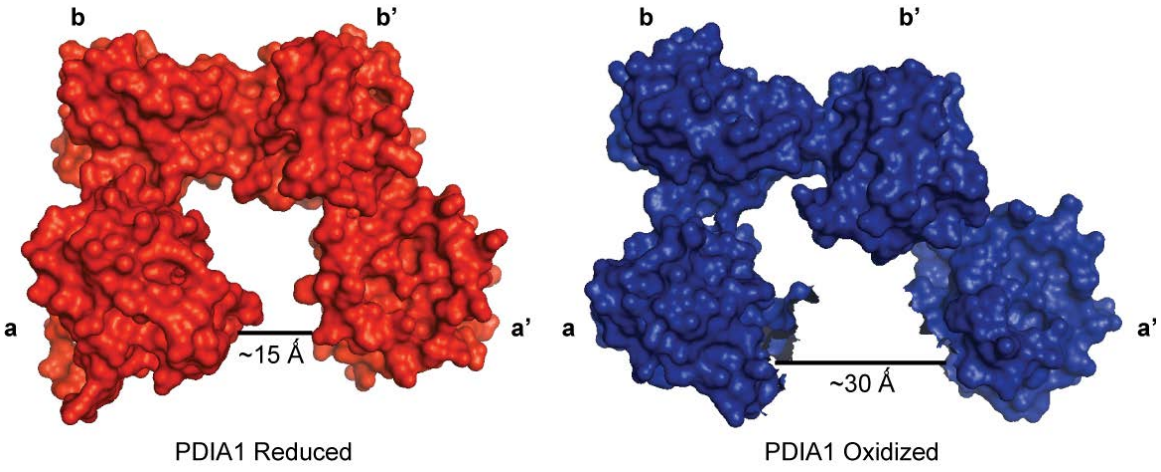

Figure 4-2. Crystal structures of the oxidized (PDB ID 4EL1) and reduced (PDB ID 4EKZ) **a-b-b'-a'** domains of PDIA1 show conformational changes.

PDIA1 is a structurally unique enzyme, as it contains two functional active-sites, each relying on a pair of redox-catalytic cysteine residues (Cys53 and Cys56 within **a**; Cys397 and Cys400 within **a'**) for activity (Figure 4-1). The cysteines nearer the N-terminus (Cys53 & Cys397) have a pK_a-value in the range of 4.5-5.6 and are readily deprotonated at physiological pH.[35, 36] These nucleophilic cysteines are exposed to solvent and able to react with substrates, while the more C-terminal cysteines (Cys56, Cys400) possess a higher pK_a, calculated to be about 12.8,[37] and are found to be buried within the active-sites.[38] Some studies have suggested that during certain chemical transformations, the **a**-type domains undergo conformational changes that cause a shift in the pK_a of the C-terminal cysteine from 12.8 to 6.1.[37, 39] The interplay between these cysteine residues facilitates disulfide bond reduction, oxidation, and isomerization.

While each retain the highly conserved CGHC domains that are required for activity, the **a** and **a'** domains of PDIA1 share only 33.6% sequence homology and have been observed to be functionally nonequivalent. A detailed analysis of the oxidase

activity of PDIA1 WT and mutants of the redox-catalytic cysteines within the **a** and **a'** site revealed that while both sites contribute to the overall enzyme kinetics, the two sites may play complementary rather than identical roles. The **a** site was found to contribute more to catalysis (higher k_{cat}) within the enzyme-substrate complex, while the **a'** site improves the binding interactions between the enzyme and substrate (lower K_m).[40] The **a** and **a'** site are also found to possess different structural characteristics. Almost no interactions exists between the **a** and **b** site, which renders these domains as structurally rigid. Alternatively, the **a'** and **b'** exhibit extensive interactions, which are thought to be facilitated by a "**x** linker" located between these domains. This bestows an increased flexibility to the **a'** site and allows for a very elastic structure.[34] Upon oxidation/reduction, the **a** and **a'** site also experience distinct conformational changes. Within the reduced state, the **a**, **b**, and **b'** domains are found to be within the same plane, whereas the **a'** domain is twisted ~45° out of this plane and is found to be 27.6 Å from the **a** site. Upon oxidation, the **a'** site arranges in the same plane as the **a**-**b**-**b'** domains, and the distance between the two active sites increases to 40.3 Å.[34] Together, it's clear that the **a** and **a'** sites display functional nonequivalence, and we believe that site-selective inhibitors would help uncover the specific contribution from each active-site to PDIA1 function.

In contrast, the **b** and **b'** domains do not possess catalytically-active sites and instead contribute to substrate binding. Within PDIA1, the **b** and **b'** domains only share 16.5% sequence identity, and vary greatly amongst other PDI family members. For PDIA1, the **b'** domain has been shown to be especially important, as it constitutes the principal substrate-binding site and displays high affinity and broad specificity.[41] The **b'**

domain is essential for sufficient binding of smaller peptides through hydrophobic interactions,[42] but not for binding of larger peptides or proteins.[41] Additionally, substrate binding for general chaperone activity,[43] as well as the interactions with the α-subunit of prolyl-4-hydroxylase also occur at the **b'** site.[44]

Thiol-exchange reactions of PDIA1

PDIA1 possesses two pairs of redox-catalytic cysteines that facilitate oxidation, reduction, and isomerization of disulfide bonds within proteins. During transfer of oxidizing or reducing equivalents to substrates, the cysteine pairs within PDIA1 cycle between the oxidized (disulfide) and reduced (dithiol) states. Sequence characteristics, especially the traversing XX within the CXXC motif, influence the relative stabilities of these two states and dictate how easily the active-site disulfide can be formed or reduced. Active-sites that are good oxidants possess a disulfide that is less stable, more difficult to assemble, and is more easily transferred to the substrate. On the contrary, active sites that are good reductants possess a disulfide that is more stable, easier to assemble, and is difficult to transfer to substrates.[45] Notably, PDIA1 is one of the best oxidants of the entire PDI family,[46] and therefore primarily functions in the formation of disulfide bonds. This oxidase activity of PDIA1 inserts disulfides into protein substrates, while consequently reducing the disulfide within the PDIA1 active-site (Figure 4-3a). Mechanistically, a thiolate from the dithiol substrate will attack a disulfide bond of PDIA1, forming an intermolecular disulfide bond. Subsequent nucleophilic attack by the remaining thiolate generates the desired disulfide bond within the substrate and generates a reduced dithiol within PDIA1 (Figure 4-3b). Subsequently, oxidants, such as

glutathione disulfide (GSSG) and H_2O_2 act as terminal electron acceptors to oxidize the dithiol back to the disulfide state and complete the catalytic cycle. Additionally, enzymatic regeneration of disulfide bonds in PDIA1 has been observed by endoplasmic reticulum oxidoreductin 1 (Ero1). During this reaction, Ero1 transfers electrons to O_2, producing one equivalent of H_2O_2 per disulfide bond.[47]

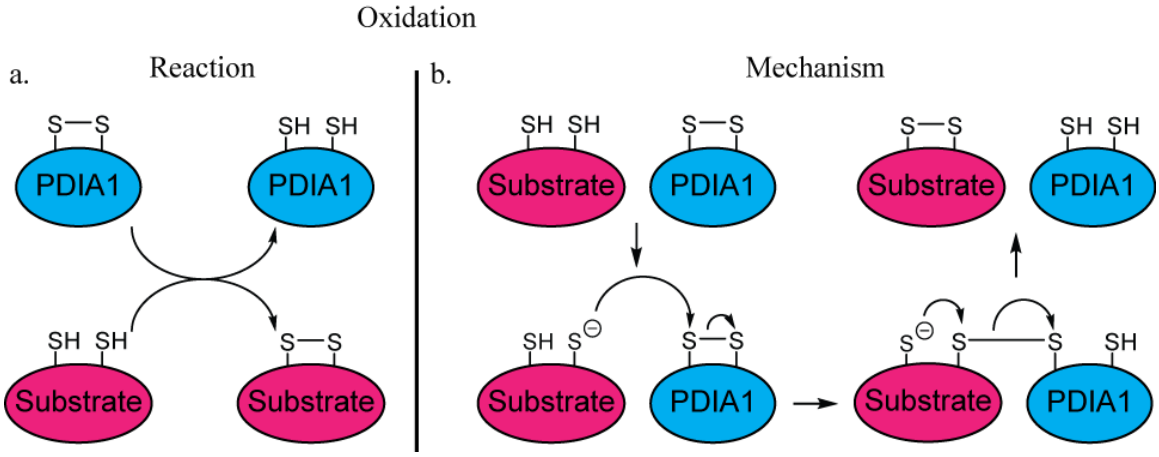

Figure 4-3. (a) PDIA1 oxidase activity promotes the formation of disulfide bonds. (b) Mechanistically, a nucleophilic cysteine within the substrate attacks the disulfide bond of PDIA1, resulting in an intermolecular disulfide. An adjacent cysteine within the substrate is then activated, and assembles the intramolecular disulfide bond, breaking the intermolecular disulfide and generating the dithiols within PDIA1.

A less common activity of PDIA1, compared to its other family members, is its ability to act as a reductase. Contrary to oxidation, PDIA1 within its reduced state utilizes its dithiols to reduce disulfides within protein substrates (Figure 4-4a). These thiol-disulfide reactions proceed through the formation of a transient mixed disulfide between the N-terminal cysteine residue of either pair (Cys53 or Cys397) of PDIA1 and the substrate (Figure 4-4b). Upon activation, the C-terminal cysteine residue within PDIA1

(Cys56 or Cys400) will cleave the intermolecular disulfide generating the reduced substrate and oxidized PDIA1. The resulting intramolecular disulfides within PDIA1 are reduced by terminal electron donors, such as reduced glutathione (GSH) and NADPH back to the dithiol state to complete the catalytic cycle. Interestingly, since reduction requires the C-terminal cysteine to resolve the mixed disulfide with the substrate, mutation of this residue leads to the accumulation of covalent substrate-enzyme complexes through an intermolecular disulfide.[38, 48]

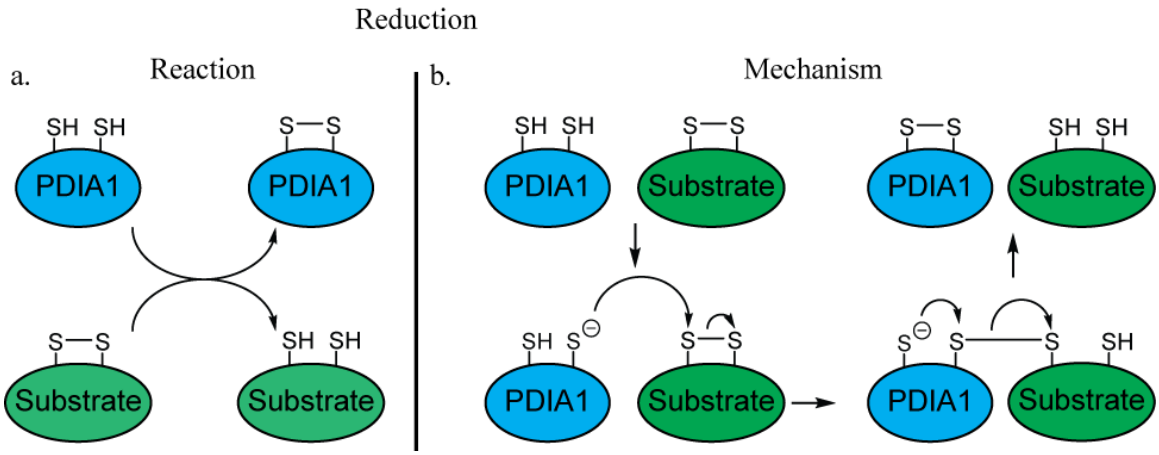

Figure 4-4. (a) PDIA1 reductase activity promotes cleavage of disulfide bonds. (b) Mechanistically, a nucleophilic cysteine (Cys53 or Cys397) within PDIA1 attacks the disulfide bond of substrate, resulting in an intermolecular disulfide. The adjacent cysteine (Cys56 or Cys400) within PDIA1 is then activated, and forms the intramolecular disulfide bond, breaking the intermolecular disulfide and generating the dithiols within the substrate.

Additionally, PDIA1 has the ability to isomerize wrongly formed disulfide bonds,[49] an activity unique to only a few protein disulfide isomerases (Figure 4-5a). Non-native disulfides that assemble during folding prevent the formation of the native

structure for proper function and necessitate isomerization activity by PDIA1 to promote conventional folding.[49] First, the N-terminal nucleophilic cysteine attacks a mismatched disulfide bond, forming a covalent complex between the substrate and PDIA1 (Figure 4-5b). At this point, a "mechanistic decision" must occur: either the original substrate cysteine will attack the intermolecular disulfide releasing the substrate without isomerization (dashed black line) or another cysteine and assemble the native protein structure (solid black line).[45] Importantly, the C-terminal cysteine within the PDIA1 active site can react with its adjacent cysteine to reduce the intermolecular disulfide bond (dashed red line) (Figure 4-5b). This mechanism instills a set amount of time the substrate has to succeed in an intramolecular isomerization, which increases the likelihood of attaining the native protein structure.[48] In addition, if the PDIA1 escapes and reduces the substrate, subsequent reoxidation may achieve the desired isomerization. PDIA1 does not experience any net reduction/oxidation upon isomerization, and can readily participate in additional catalytic cycles. Together, these PDIA1 thioltransferase activities assist in promoting proper disulfide-bond formation and native protein structures.

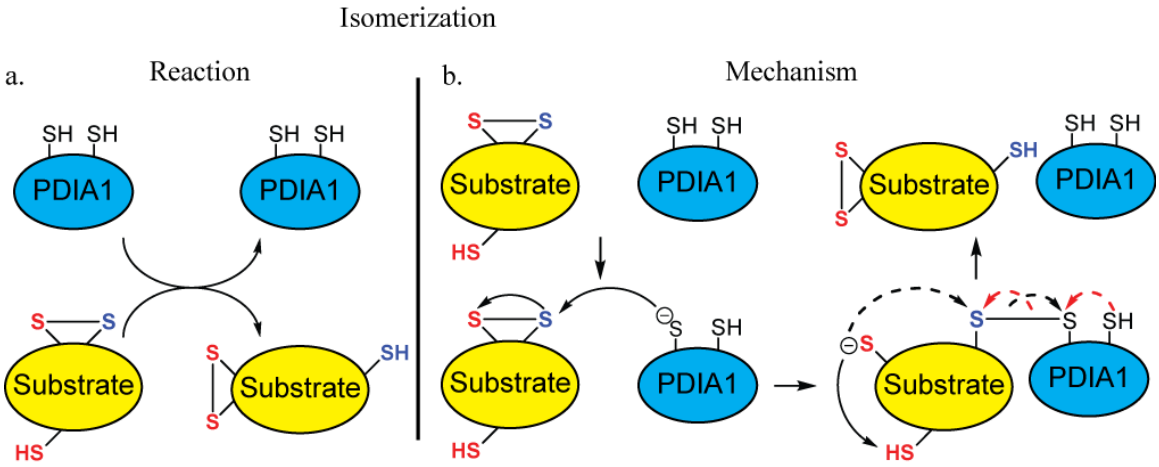

Figure 4-5. (a) PDIA1 isomerase activity assembles native protein structures. (b) Mechanistically, a nucleophilic cysteine (Cys53 or Cys397) within PDIA1 attacks the misfolded disulfide bond of substrate, breaking this bond and assembling an intermolecular disulfide. At this point, either the correct substrate disulfide can form (solid black arrows), the substrate can reassemble the incorrect disulfide (dashed black arrows), or the adjacent cysteine in PDIA1 (Cys56 or Cys400) can break the intermolecular disulfide and release the unfolded substrate (dashed red arrows).

Regulation of PDIA1 activity

Because proper protein folding is necessary for virtually all cellular functions, mechanisms have evolved to regulate activities of proteins such as PDIA1 (Figure 4-6). To mediate oxidative protein folding, PDIA1 exhibits oxidase activity to assemble disulfide bonds in nascent proteins, but the required active-site disulfides within PDIA1 are simultaneously reduced. At this point, these reduced disulfides can function in isomerization reactions within the ER, but these cysteines need to be reoxidized back to a disulfide bond in order to participate in multiple rounds oxidase activity. Small molecules, such as GSSG and H_2O_2, have long been known to carry out this process, but recently an enzyme, Ero1, was found to preferentially interact with and oxidize PDIA1.[50, 51] In particular, Ero1 was found to possess high affinity for the cysteines within the **a'** site.[52] Other mechanisms of PDIA1 reoxidation, such as those utilizing peroxiredoxin 4 (Prdx4), docosahexaenoic acid (DHA) and vitamin K, have also been described but are less common.[53]

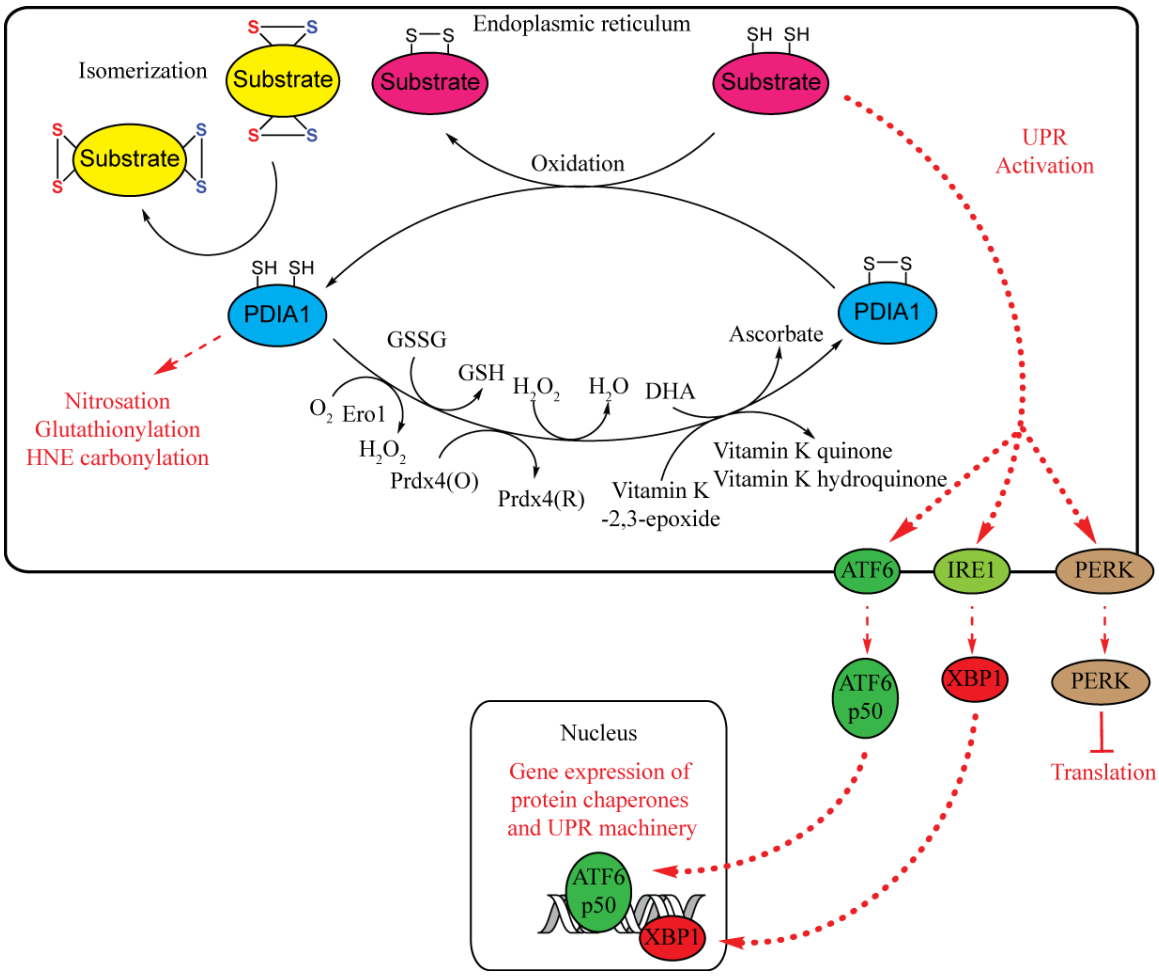

Figure 4-6. Regulatory mechanisms of PDIA1 activity within the ER. PDIA1 primarily acts as an oxidase to assemble disulfide bonds within its protein substrates. This results in dithiol formation in the active-site of PDIA1, which can be used to facilitate disulfide bond isomerizations or be oxidized back to the requisite disulfide to perform multiple rounds of oxidase activity. Reduced PDIA1 can also be post-translationally modified and rendered inactive, which results in an accumulation of misfolded and unfolded proteins that contribute to significant ER stress. To account for this ER stress, the cell activates an Unfolded Protein Response (UPR). ER transmembrane proteins ATF6, IRE1, and PERK translocate to the cytosol to suppress protein translation and upregulate expression of protein chaperones and UPR machinery.

Beyond, oxidation, the reduced redox-catalytic cysteines of PDIA1 are also susceptible to post-translational modifications, with the N-terminal cysteines (Cys53 and Cys397) being especially vulnerable (Figure 4-6). A reduced, nucleophilic thiol is preferential for post-translational modifications; thus, once PDIA1 performs a disulfide bond oxidation, modifications to the resulting dithiols are able to "trap" and inactivate PDIA1, preventing the reoxidation of its redox-catalytic cysteine pairs back to the required disulfides. These cysteines have been observed to undergo *S*-glutathionylation,[54-56] *S*-nitrosation,[57] and carbonylation by 4-hydroxynonenal (HNE),[58] which results in disruption of enzymatic activity, activation of the unfolded protein response, and induction of ER stress that can ultimately lead to apoptosis.

Because PDIA1 serves as one of the most abundant and essential enzymes in disulfide-bond formation and protein folding, its dysfunction results in rapid accumulation of unfolded and misfolded proteins in the lumen of the ER. These proteins typically expose hydrophobic residues at their surface and aggregate, which triggers significant ER stress. To account for this ER stress, cells have evolved a stress responsive signaling pathway termed the Unfolded Protein Response (UPR) to maintain ER proteostasis (Figure 4-6).[59, 60] UPR signaling emanates from three ER transmembrane proteins, activating transcription factor 6 (ATF6), Inositol-requiring protein 1 (IRE1), and protein kinase RNA-like endoplasmic reticulum kinase (PERK).[59] Once activated, PERK migrates to the cytosol and phosphorylates E74-like factor 2 (eIF2), a regulator of initiator mRNA translation, which results in cessation of protein translation, decreasing protein influx to the ER.[61] Activated IRE1, a site-specific endonuclease, removes an

intron from X-box binding protein 1 (XBP1) mRNA, which results in mRNA stabilization and an increase in XBP1 levels.[62] ATF6 translocates to the Golgi and is cleaved to form the activated subunit, ATF6 p50.[63] XBP1 and ATF6 p50 subsequently translocate to the nucleus and bind to promoters that upregulate expression of general protein chaperones and UPR machinery. The combined increase in protein folding machinery signaled by XBP1 and ATF6 with the decreased influx of proteins to the ER accomplished by PERK provides a mechanism to rescue the cell from ER stress; however, if this pro-survival mechanism does not restore ER homeostasis, the cell will enter apoptosis.

PDIA1 as a potential drug target for cancer treatment

Although PDIA1 has been studied extensively, its role in cancer has not yet been established. Gene expression microarray studies have observed an increase in PDIA1 expression in a variety of cancer types, including brain and central nervous system cancers,[64-69] lymphoma,[70-72] kidney,[73-75] ovarian,[76, 77] prostate,[78, 79] lung,[80] and male germ cell tumors.[81] Additionally, upregulation of PDIA1 has also been shown in MALDI/TOF proteome analyses of human cancers.[82, 83] Increased PDIA1 levels have also been shown to correlate with cancer metastasis and invasion, as evidenced by significantly higher PDIA1 protein levels observed in axillary lymph node metastatic breast tumor compared to primary breast tumor.[84] Lower PDIA1 expression levels have also been associated with higher survival rates of patients with glioblastoma and breast cancer.[66, 67, 85] These combined studies indicate PDIA1 has the potential to be a biomarker of cancer and could be used to assess patient prognosis. Monitoring PDIA1 levels as a biomarker for clinical

detection of cancers has the potential to be a powerful and noninvasive strategy because PDIA1 is both abundant and secreted into the extracellular environment.

Additionally, chemotherapeutic resistance is a major obstacle in cancer treatment, and PDIA1 has been recently thought to play a role in resistance mechanisms. A recent study evaluated the levels of PDIA1 in HeLa cells resistant to aplidin, a cyclic depsipeptide currently in clinical trials for anti-tumor activity. Compared to aplidin-sensitive HeLa cells, aplidin-resistant HeLa cells expressed significantly higher levels of PDIA1, and inhibition of PDIA1 by bacitracin sensitized aplidin-resistant HeLa cells to the drug.[86] Similarly, a class of PDIA1 inhibitors was found to sensitize cancer cells towards etoposide-induced apoptosis at subtoxic concentrations.[87] These data suggest that combining PDIA1 inhibitors with traditional anticancer therapies could achieve synergistic effects and overcome chemotherapeutic resistance.

Inhibitors of PDIA1 show promise as therapeutic drugs

Towards this end, inhibitors of PDIA1 have been designed with various efficacies (Table 4-2).[2] It is important to note that different activity assays have been designed to assess oxidase, reductase, isomerase, and general chaperone activity, and many of the described PDIA1 inhibitors have only been evaluated to inhibit a single PDIA1 function, most often reductase activity. These inhibitors are both reversible and irreversible (often covalently binding the redox-catalytic cysteines) and display a wide-range of potencies and specificities.

Name	IC_{50} (μM)	PDIA1 Activity	Selectivity	Reversibility	Membrane Permeable?
Juniferdin[94]	0.156	Reductase	Nonspecific	Reversible	Unknown
P1[91]	1.7	Reductase	Moderate selectivity	Irreversible (Cys397)	Yes
Quercetin-3-rutinoside	6.1	Reductase	Selective for PDIA1 over other family members	Reversible	No
NEM[93]	8	Reductase	Nonspecific	Irreversible	Yes
Iodoacetamide[93]	8***	Reductase	Nonspecific	Irreversible	Yes
PACMA 31[88]	10	Reductase	Selective for PDIA1 over other proteins such as BSA and Grp78	Irreversible (Cys397)	Yes
Acrolein[93]	10	Reductase	Nonspecific	Irreversible	Yes
JP04-42[87]	15	Reductase	Moderate selectivity	Reversible	Yes
Thiomuscimol[15]	23	Reductase	Nonspecific	Irreversible	Yes
RB-11-ca[90]	40	Reductase	N/A	Irreversible (Cys53)	Yes
16F16[89]	63	Reductase	N/A	Irreversible	Yes
Cystamine[53]	66	Reductase	Nonspecific	Irreversible	Yes
PS89[87]	78	Reductase	Moderate selectivity	Reversible	Yes
PAO[88]*	85	Reductase	Reacts readily with CxxC motif	Irreversible	Yes
Bacitracin[95]	90	Reductase	Nonspecific	Irreversible	No
DTNB[92]**	100	Reductase	Nonspecific	Irreversible	No
Ribostamycin[96]	N/A****	Chaperone	Nonspecific	Reversible	Yes

Table 4-2. Previously reported PDIA1 inhibitors sorted by potency. Table adapted from Xu et al.[2] First generation PDIA1 inhibitors are shaded white; second generation PDIA1 inhibitors are shaded gray. (*PAO: phenylarsine oxide **DTNB: 5′5-dithio-bis(2-nitrobenzoic acid); ***At pH 6; ****Sufficient inhibition at 100:1 molar ratio of ribostamycin to PDIA1.)

The first inhibitor of PDIA1, bacitracin, was first reported in 1981 and was found to inhibit PDI activities in a variety of cellular processes.[95] However bacitracin required high micromolar concentrations for inhibition of reductase activity, displayed minimal inhibition of oxidase or isomerase activity, possessed low specificity for PDIA1, and was membrane impermeable, making it a fairly weak and ineffective inhibitor of PDIA1.[42]

Similarly, the majority of these initial PDIA1 inhibitors lacked specificity for PDIA1, failed to inhibit PDIA1 oxidase activity, and possessed poor pharmacological properties, rendering them relatively ineffective as tools to deconvolute the role of PDIA1 in cancer or in the development of potential drug candidates. Towards this end, a second-generation of potent and selective PDIA1 inhibitors has been developed in recent years: PACMA 31, 16F16, Juniferdin, JP04-42 and PS89, P1, and RB-11-ca (Figure 4-7).

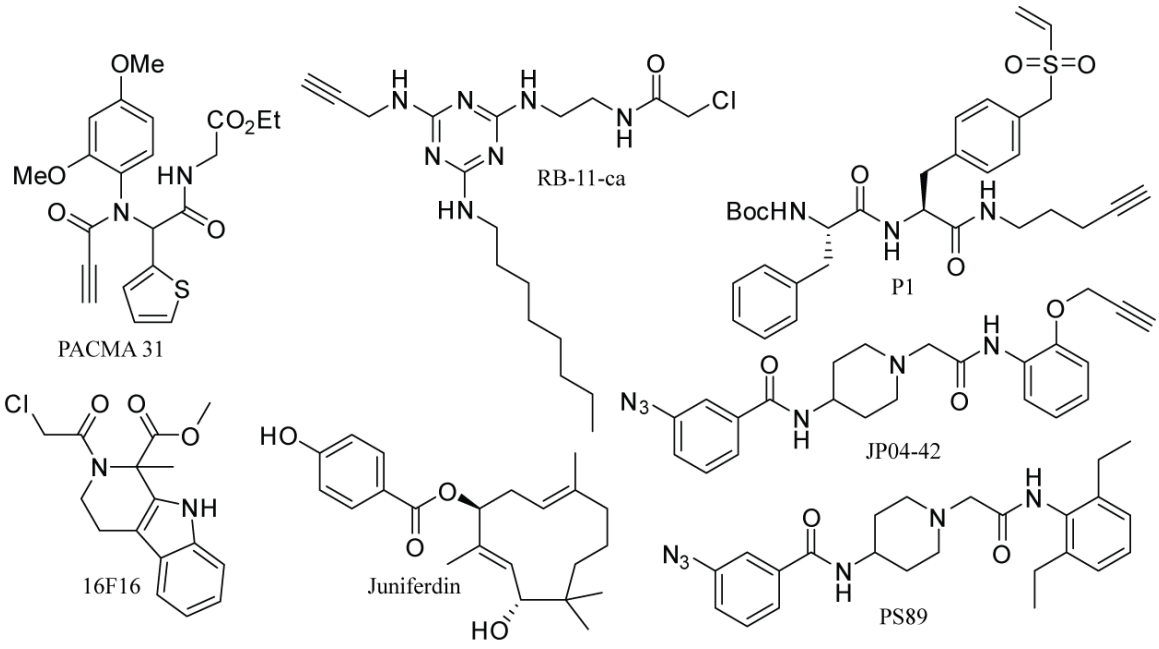

Figure 4-7. Structures of second-generation PDIA1 inhibitors.

16F16 was discovered through a high-throughput screen of 68,887 compounds as an irreversible inhibitor of PDIA1.[89] 16F16 contains a cysteine-reactive chloroacetamide electrophile, but the specific site (**a** or **a'**) and cysteine it binds are not currently known. Through the use of an alkyne handle, 16F16 was found to bind PDIA1 and PDIA3, but also displayed cytotoxicity in cells at concentrations above 12 μM, hinting at significant off-target binding. While 16F16 was never tested in a cancer model, it showed the ability

to rescue cells from apoptosis in an *in vitro* PC12 cell-based model of Huntington's disease.[89]

Juniferdin was discovered as a PDIA1 inhibitor through a high-throughput screen of natural product libraries.[94] Juniferdin was found to be a noncovalent inhibitor of PDIA1, but the binding mode has not been described. Although Juniferdin was never studied in cancer models, it was found to block PDIA1-catalyzed reduction of disulfide bonds in the HIV-1 envelope glycoprotein gp120, thereby inhibiting the entry of HIV-1 virus into cells.[94] Although it was found to be a potent inhibitor of PDIA1 reductase activity, which is the primary activity of extracellular PDIA1, Juniferdin displayed little inhibition of PDIA1 oxidase activity, the primary activity of PDIA1 within the ER. Furthermore, because studies with Juniferdin have been on extracellular PDIA1, its cell permeability and stability within cells is still unclear.[94]

A previous member within the Weerapana lab synthesized a library of cysteine-reactive covalent inhibitors from a trifunctionalized 1,3,5-triazine scaffold. Each library member was evaluated in HeLa cells, and one inhibitor, RB-11-ca, was determined to selectively bind PDIA1.[90] Interestingly, RB-11-ca was shown to exhibit high specificity for Cys53 of the **a** site, with virtually no binding observed to Cys56 or either redox-catalytic cysteine within the **a'** site. The ability of RB-11-ca to inhibit PDIA1 reductase activity was determined to be comparable to that of 16F16, and mitigated HeLa cell proliferation with an EC_{50} value of 23.9 μM.[90]

Because the most effective PDIA1 inhibitors possess cysteine-reactive electrophiles, recent efforts have focused on screening libraries of compounds comprised of similar moieties, including vinyl sulfones and sulfonates. The screen resulted in the

discovery of P1, a phenyl vinyl sulfonate-containing small molecule.[91] This vinyl sulfonate electrophile was found to covalently bind Cys397 within the **a'** site to inhibit PDIA1 activity at potencies not yet achieved by this new generation of selective PDIA1 inhibitors (1.7 μM). P1 represents one of the more potent, cell-permeable small molecule PDIA1 inhibitors discovered to date.[91]

PACMA 31 was recently reported as an irreversible inhibitor of PDIA1 with potency in both *in vitro* and *in vivo* models of ovarian cancer.[88] The molecule contains a cysteine-reactive electrophile in the form of the terminal propionic group and inhibits PDIA1 through covalent modification of a cysteine residue. Mass spectrometry and modeling studies predict binding of PACMA 31 to the nucleophilic Cys397 within the **a'** site. Importantly, PACMA 31 showed tumor targeting ability and significantly suppressed ovarian tumor growth without causing toxicity to normal tissues, implicating PDIA1 as a potential target for cancer therapeutics.[88]

Because most of the second-generation PDIA1 inhibitors are covalent modifiers, recent efforts have sought to develop inhibitors that function through noncovalent interactions, which are thought to be more pharmacologically desirable. Through a screen of a commercial compound library and upon further structure-activity relationship (SAR) optimization, JP04-42 and PS89 were identified through proteomic analyses to be potent reversible inhibitors of PDIA1 reductase activity.[87] These inhibitors were shown to sensitize cancer cells to etoposide treatment at subtoxic concentrations, providing further evidence that PDIA1 plays a role in chemotherapeutic resistance.[87]

This second-generation of PDIA1 inhibitors represents a significant improvement; however, these inhibitors are limited by their potency, selectivity, and poor

pharmacological properties. We aimed to utilize cysteine-reactive electrophiles and proteomic analyses to access improved second-generation inhibitors of PDIA1 to be employed as tools to better understand the role of PDIA1 in cancer progression and chemotherapeutic resistance. Importantly, we believe that the current strategies employed to evaluate PDIA1 inhibitors as tools to interrogate the enzyme's role in cancer are flawed. PDIA1 is an extremely unique and complex enzyme, since it possesses two non-equivalent active sites, is localized within the ER and at the cell surface, and is multifunctional, performing oxidase, reductase, isomerase, and general chaperone activities. Increased PDIA1 oxidase and isomerase activities within the ER are thought to be essential for cancer cells to produce the elevated levels of protein to facilitate the biological activities that promote their rapid growth. Because healthy cells do not require the higher levels of PDIA1 activity, cancerous cells should display an increased sensitivity to PDIA1 inhibition. To date, all of the second-generation PDIA1 inhibitors described have only been tested against PDIA1 reductase activity, which is thought to be of little importance to PDIA1's role cancer. When evaluating PDIA1 inhibitors as cancer therapeutics, activity assays to assess PDIA1's oxidase and isomerase activity, which appear to be most important to cancer progression, should be employed.

Furthermore, we sought to evaluate the binding affinities of each PDIA1 inhibitor for both the **a** and **a'** site, as inhibitors may display differential affinities for each site. The endogenous functions of each active-site (**a** or **a'**) are still unknown, but we believe that site-selective inhibitors may help clarify the redundancy and unique properties of each active-site. Additionally, site-selective inhibitors are likely to display a better therapeutic index because they are not completely shutting down all PDIA1 activity, but

only those activities attributed to a single active-site. PDIA1 is essential for normal cell growth and maintenance, so complete abolition of PDIA1 activity is likely to be detrimental. Inhibition of a single active site will likely have a larger effect on cancer cells due to their increased reliance on PDIA1 activity, while still allowing for enough activity in healthy cells to prevent cytotoxicity.

In conclusion, we believe that the expansion of cysteine-reactive inhibitors and the revised methodologies taken to evaluate them will lead to 1) a potent and selective inhibitor of the **a** site of PDIA1, 2) a potent and selective inhibitor of the **a'** site of PDI, and 3) a potent and selective pan-inhibitor for both the **a** and **a'** site of PDIA1. These optimized second-generation inhibitors will deconvolute the function of each individual active site, including their substrate scopes and contribution to various cellular PDIA1 activities. Successful inhibitors will then be evaluated for inhibition of PDIA1 oxidase and isomerase activity, and for cytotoxicity in cancer cells. We hope that these inhibitors aid in uncovering the role of PDIA1 in cancer progression and may serve as a starting point for PDIA1-based cancer therapeutics.

Results and Discussion

Validation of PDIA1 as a potential target for cancer therapeutics

We first sought to assess PDIA1 as a therapeutic target for cancer, and chose a well-characterized ovarian cancer cell line, SKOV3, as a model system. We aimed to engineer stable cell lines through lentiviral transduction containing a PDIA1 knockdown or a PDIA1 overexpression and perform cancer phenotypic assays on these cell lines to

measure the effect of PDIA1 on the capacity of cancer cells for proliferation, survival, migration, and invasion. For the knockdown, a PDIA1 shRNA within a pLKO.1 vector was purchased (Figure 4-8a). For the overexpression, the PDIA1 sequence within a pDONR2233 vector was subcloned into a pLenti CMV Puro DEST viral overexpression vector through an LR Clonase reaction standard to Gateway cloning (Figure 4-8b). HEK293T cells were first transfected with vsvg and pspax2 viral constructs and either the shRNA-pLKO.1 viral knockdown plasmid, the PDIA1-pLenti CMV Puro DEST viral overexpression plasmid, or a shGFP-pLKO.1 control. The shGFP-pLKO.1 contains an shGFP sequence that will result in no proteomic effect (since the SKVO3 cells do not synthesize GFP) and will therefore serve as a control for PDIA1 mRNA and protein levels.

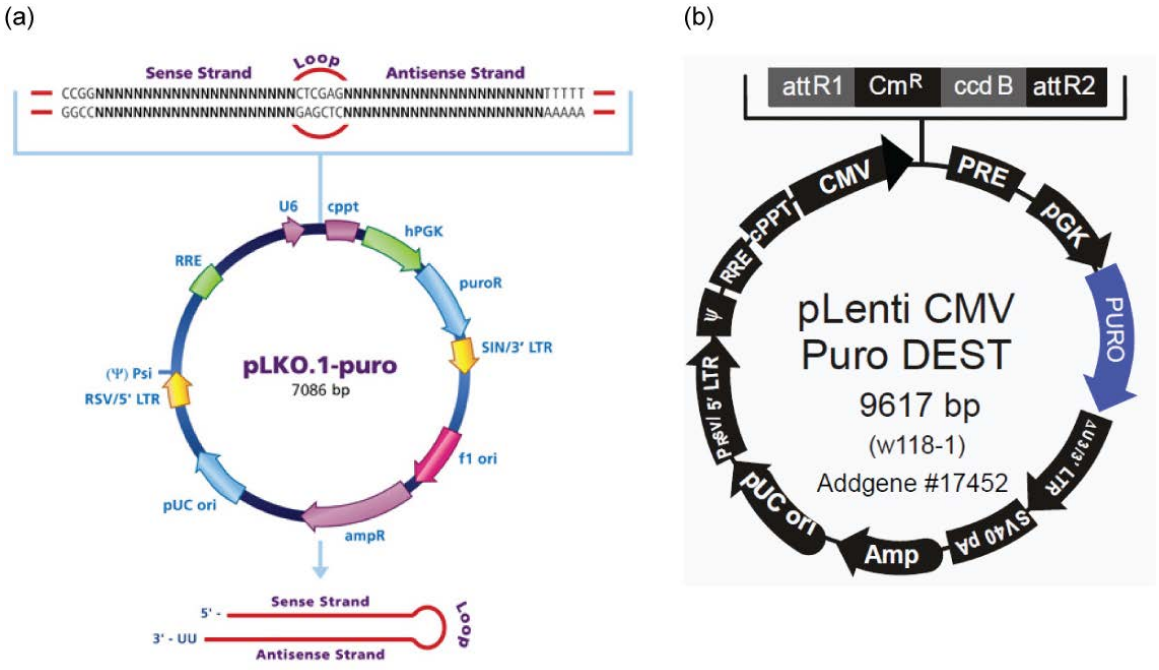

Figure 4-8. Vector maps for (a) pLKO.1-Puro (Figure from Sigma Aldrich) and (b) pLenti CMV Puro Dest (Figure from Eric Campeau).

After two days, the presence of virus was confirmed and harvested within the media. This media was utilized to infect SKOV3 cells to incorporate either the PDIA1 shRNA or overexpression sequence stably within the genome. After a round of puromycin selection, the PDIA1 knockdown (SKOV3-PDIA1-) and overexpression (SKOV3-PDIA1+) were confirmed using RT-PCR (Figure 4-9a/b) and western blot (Figure 4-9c) by comparing to the GFP knockdown (SKOV3-Ctrl). RT-PCR revealed a ~75% decrease in mRNA levels for the PDIA1 knockdown, while the overexpression saw an increase of ~75%. The gel band intensities were integrated and averaged from an n = 2 from two biological replicates (Figure 4-9b). The western blot confirmed that this decrease in RNA extends to PDIA1 protein levels as well. Interestingly, a higher band also appeared on the western blot, and we hypothesize this band is the nascent PDIA1, containing the additional N-terminal 18 amino acid sequence to account for the additional molecular weight.

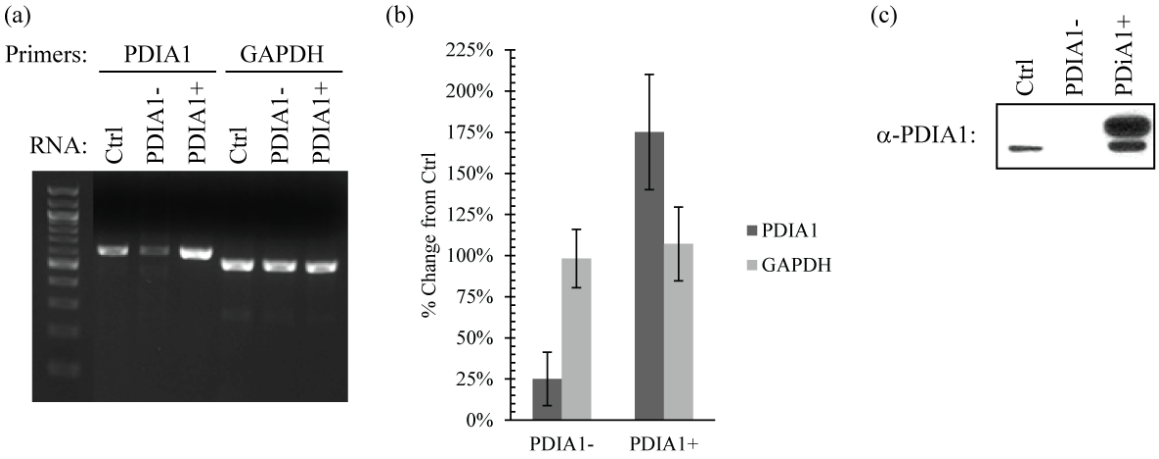

Figure 4-9. (a) Confirmation of PDIA1 knockdown by RT-PCR. (b) Gel bands were integrated with an n = 2 from two biological replicates. (c) Western blot with a α-PDIA1 antibody confirms almost complete PDIA1 knockdown at protein levels.

The SKOV3-Ctrl and SKOV3-PDIA1+ cell lines could be cultured over multiple passages, but the PDIA1 knockdown was found to be lethal after approximately one week post-selection, likely due to the inability to support protein folding and homeostasis upon complete PDIA1 knockdown. Consequently, the SKOV3-PDIA1- cells underwent the cancer phenotypic assays immediately after coming off selection. The cell lines were first assessed for SKOV3 cell proliferation and survival by comparing the PDIA1- and PDIA1+ to the Ctrl. Proliferation assays necessitate serum-containing media that promotes rapid growth. These conditions allow for assessment of the cell viability of readily propagating cells compared to the SKOV3-Ctrl. Survival assays require serum-free media, which generates environmental stress and prevents cellular growth. These conditions allow for the evaluation of solely the plated cells' ability to survive compared to the SKOV3-Ctrl. The three cell lines were suspended in both media and plated into four 96-well plates. To evaluate cell viability, cells were treated with WST-1. WST-1 is cleaved to form formazan by a complex cellular mechanism that occurs primarily at the cell surface via plasma membrane electron transport.[97] Consequently, this bioreduction is largely dependent on the glycolytic production of NAD(P)H in viable cells.[97] Therefore, the amount of formazan dye formed directly correlates to the number of metabolically active cells in the culture. The transition from WST-1 to formazan generates a sharp increase in absorbance at 450 nm and directly correlates to cell viability (Figure 4-10).[97]

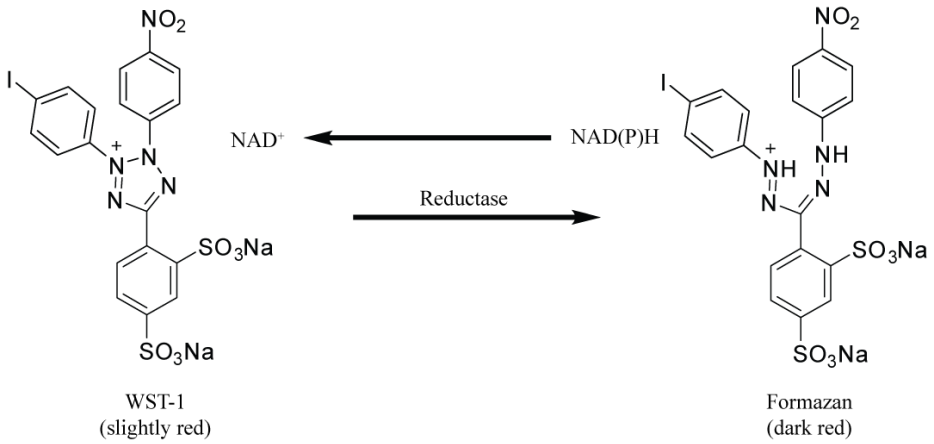

Figure 4-10. WST-1 salt is reduced to formazan by plasma membrane reductases and provides a direct correlation to cell viability.

One of the four plates is immediately treated with WST-1 after plating to assess initial cell viability at Time 0. After the appropriate time points, the other plates of cells were also administered WST-1 and the changes in cell viabilities were compared to the initial measurements at Time 0. The relative changes in proliferation/survival for SKOV3-PDIA1- and SKOV3-PDIA+ were compared relative to the SKOV3-Ctrl. After 72 hrs, the rate of proliferation had decreased by ~50%, and after 120 hrs the cells had all but completely stopped growing (Figure 4-11a). These observations all extended to cancer cell survival, as the cells were almost completely dead at 120 hrs (Figure 4-11b). We anticipated no significant change in the SKOV3-PDIA+ because PDIA1 is already a highly abundant enzyme, and further increasing the levels are unlikely to be beneficial. Notably, the SKOV3-PDIA1+ did display a slight decrease, although this decrease remained stable throughout the timeframe of the experiment, in both cell proliferation and survival compared to SKOV3-Ctrl and could make for an interesting future case study.

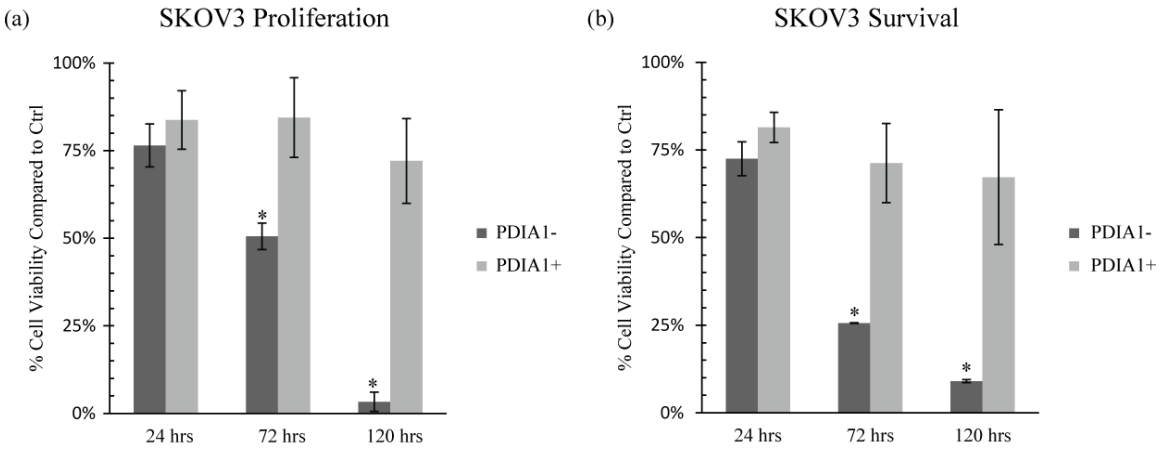

Figure 4-11. SKOV3-PDIA1- and SKOV3-PDIA1+ cell lines (a) proliferation and (b) survival were compared to that of the SKOV3-Ctrl. Data are presented as a mean of n = 5 replicates from two biological samples +/- SEM with significance expressed as * $p < 0.01$.

The SKOV3-Ctrl, SKOV3-PDIA1-, and SKOV3-PDIA1+ cell lines were also assessed for their migration and invasion capacities, both essential phenotypes of aggressive metastatic cancers. Metastasis is defined as the dissemination of cancer cells from the primary tumor to a distant organ and is often the leading cause of death among patients with cancer.[98] The particular molecular mechanisms of metastasis are poorly understood as a result of their inherent complexity. Cancer cell migration and invasion in adjacent tissues and intravasation into blood/lymphatic vessels are required for metastasis in most human cancers.[99, 100] Cancer cell migration and invasion are typically complementary to each other. Invasive cancer cells acquire a migratory phenotype that involves increased expression of several genes that contribute to cell motility.[101, 102] Once moving, this allows cancer cells to respond to cues from the tumor microenvironment and trigger invasion.

Migration is often used as a general term in cell biology to describe any directed cell movement throughout the body. This phenotype was assessed using a transwell assay to measure a cell movement through a 2D porous surface without any obstructive fiber network (in this case, a collagen I network was employed).[103] Invasion is defined as the penetration of tissue barriers and is increasingly more complex than migration.[103] Invasion requires adhesion, proteolysis of extracellular matrix components, and migration.[104] A similar transwell assay to measure cell movement was employed; however the transwell will be coated with a 3D extracellular matrix environment.[103] For both assays, the transwells will be stained and measured by cell counting.

At 24 hrs post-selection, the SKOV3-PDIA1- cells underwent both migration and invasion assays and were compared to SKOV3-Ctrl and SKOV3-PDIA1+. The SKOV3-PDIA1- cell line displayed an approximately 20% decrease in migration (Figure 4-12a) and 45% decrease in invasion phenotypes (Figure 4-12b), both of which were found to be statistically significant. Alternatively, SKOV3-PDIA1+ showed no significant change in migration and invasion phenotypes, which was expected since PDIA1+ is already a highly abundant protein. Importantly, these assays were carried out at a point when the cells are still living according to the proliferation and survival assays, so cell viability should only have minimal effect on these phenotypes. This effect of the PDIA1 knockdown provides continued support that PDIA1 plays a role in cancer progression and aggressiveness.

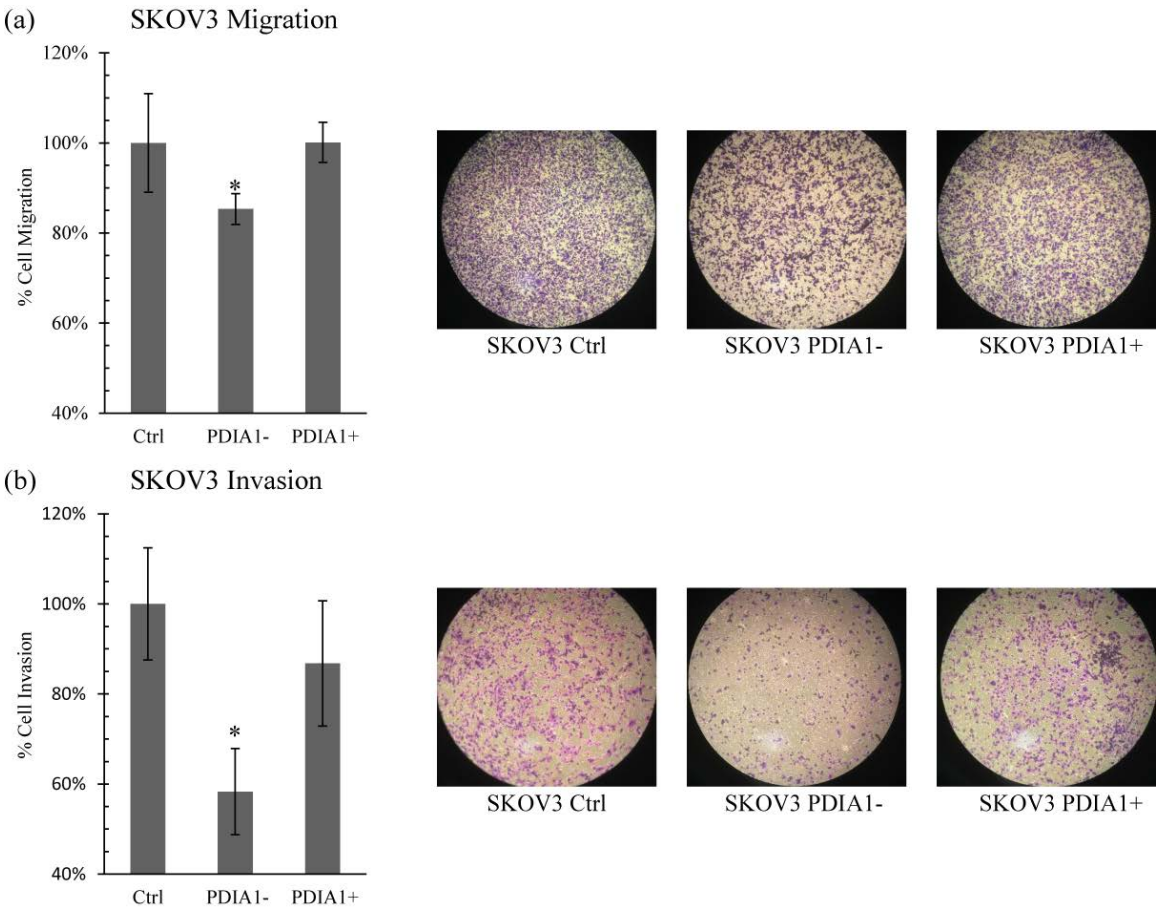

Figure 4-12. SKOV3-PDIA1- and SKOV3-PDIA1+ cell lines (a) migration and (b) invasion phenotypes were compared to that of the SKOV3-Ctrl. Data are presented as a mean of n = 3 replicates from two biological samples +/- SEM with significance expressed as * $p < 0.01$. A representative image from each sample is included.

Evaluation of PDIA1 oxidase activity

Of the many cellular functions PDIA1 performs, its oxidative protein folding within the ER is of most significant interest when developing PDIA1 inhibitors as cancer therapeutics. In order to assess PDIA1 oxidase activity, we employed a previously reported ribonuclease (RNase) oxidation assay on recombinantly expressed and purified PDIA1.[40, 107] RNase catalyzes the hydrolysis of phosphodiester bonds within RNA. In

this assay, PDIA1 catalyzes the oxidative renaturation of active RNase from its inactive reduced form. The active RNase subsequently catalyzes the hydrolysis of cyclic cytidine monophosphate (cCMP), leading to an increase in absorbance at 296 nm. This rate of cCMP hydrolysis correlates to the oxidase activity of PDIA1 (Figure 4-13). PDIA1 oxidase activity was determined by subtracting each measurement from a corresponding sample without PDIA1 to account for spontaneous regeneration of active RNase. Lags are common observations in both the catalyzed and uncatalyzed regeneration of RNase A and have been attributed to the prerequisite formation of RNase redox isomers that can be converted to the native protein.[107]

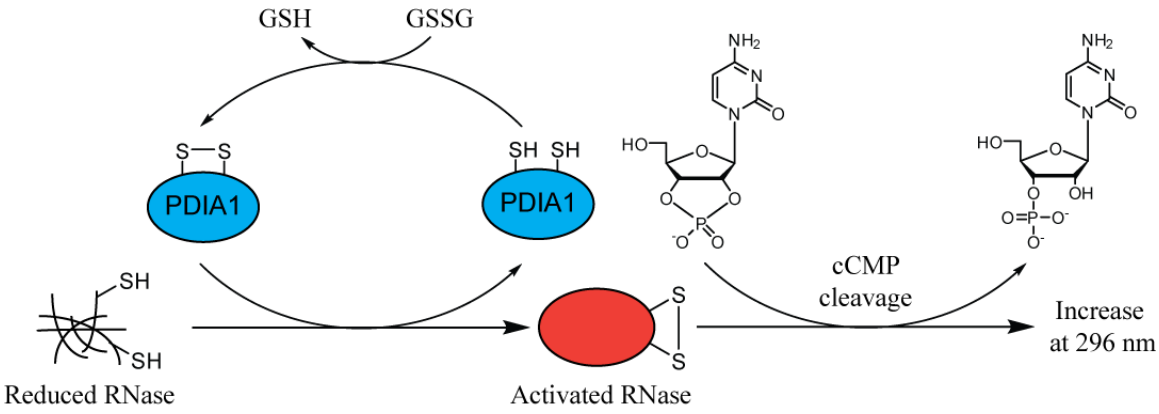

Figure 4-13. PDIA1 oxidase activity is measured by the rate of oxidation of reduced RNase to active RNase by coupling this oxidase reaction to the hydrolysis of cCMP by activated RNase.

We wanted to evaluate the effect of each cysteine residue on PDIA1 oxidase activity. Previous studies have reported the contribution of each active-site (**a** and **a'**) to reoxidation of RNase by comparing PDIA1 WT to PDI C53/56A and PDIA1 C397/400A. At saturating concentrations of reduced RNase, the PDIA1 C397/400A mutant (k_{cat} ~

0.72 min^{-1}) was found to retain activity near that of the PDIA1 WT (k_{cat} ~0.76 min^{-1}), while the PDIA1 C53/56A exhibited a significantly lower k_{cat} (~0.24 min^{-1}). The K_m for reduced RNase is elevated for PDIA1 C397/400A mutant (K_m ~29 μM), while the PDI 53/56A mutant (K_m ~ 7.1 μM) exhibits a near PDIA1 WT K_m (~6.9 μM). The larger K_m for the PDIA1 C397/400A mutant (4.2x of PDIA1 WT) and the lower k_{cat} of PDIA1 C53/56A (one third that of PDIA1 WT) suggest that the **a'** site contributes more to apparent steady-state substrate binding, and the **a** site contributes more to catalysis at saturating concentrations of substrate.[40]

While these data adequately illustrate the contribution of each active-site to oxidase activity, we looked to perform the assay on our single cysteine mutants (PDIA1 C53A, C56A, C397A, C400A) in order to examine the contribution of each cysteine residue within the redox-catalytic pairs to oxidase activity. Recombinant PDIA1 WT and cysteine mutants were assayed for oxidase activity (Figure 4-14a). These data suggest that the N-terminal cysteine within each pair (Cys53 and Cys397) contributes significantly more to activity than the C-terminal cysteine (Cys56 and Cys400). Both PDIA1 C53A and PDIA1 C397A displayed a ~50% drop in V_{max} and k_{cat} compared to the WT, indicating that mutation of these residues completely abolishes activity at these sites (Figure 4-14b). Additionally, a double-mutant of both N-terminal cysteines (PDIA1 C53/397A) displayed only minimal activity, confirming our claim. The PDIA1 C56A and C400A mutants exhibited a slight decrease in activity as compared to the WT; however, oxidase activity still occurs in each active-site even without these cysteines present, indicating that they may be non-essential for activity. The assay requires glutathione, and it's possible that the nucleophilic cysteines (Cys53 and Cys397) could assemble the

necessary disulfide bond for oxidation intermolecularly. Together, we conclude that under our assay conditions both active-sites display near equal affinities for RNase and similar oxidative activity as indicate by their comparable k_{cat}/K_m values.

(a)

Isoform	V_{max} (μM/min)	K_m (μM^{-1})	k_{cat} (min^{-1})	k_{cat}/K_m (μM/min)
WT	0.5052	4.595	0.3558	7.74×10^4
C53A	0.2957	2.687	0.2082	7.75×10^4
C56A	0.4376	4.659	0.3082	6.62×10^4
C397A	0.2427	1.827	0.1709	9.35×10^4
C400A	0.3408	2.759	0.2400	8.70×10^4
C53/397A	0.01505	-	-	-

(b)

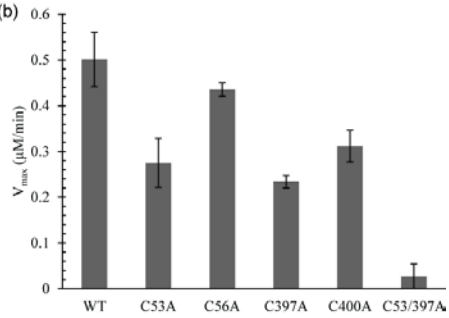

Figure 4-14. (a) PDIA1 WT and cysteine mutants were assayed for oxidase activity to compare V_{max}, k_{cat}, K_m and k_{cat}/K_m. (b) V_{max} values revealed loss of activity within each active-site upon mutation to nucleophilic cysteine residue (Cys53 or Cys397), with only minimal activity observed in double-mutant.

Evaluation of inhibitor affinities for each active-site within PDIA1

From previous work within our lab, RB-11-ca was identified as a cysteine-reactive probe that appeared to target Cys53 of PDIA1,[90] and SMC-9 was also found to target PDIA1 through a screen of a 4-aminopiperidine library.[105] Additionally, NJP15, a peptide-based cysteine-reactive small molecule, was also found to bind PDIA1. We decided to take RB-11-ca, SMC-9, and NJP15 along with the 16F16, since it's commercially available, and assess their affinities for each active-site cysteine residue (Cys53 or Cys397) within PDIA1 (Figure 4-15).

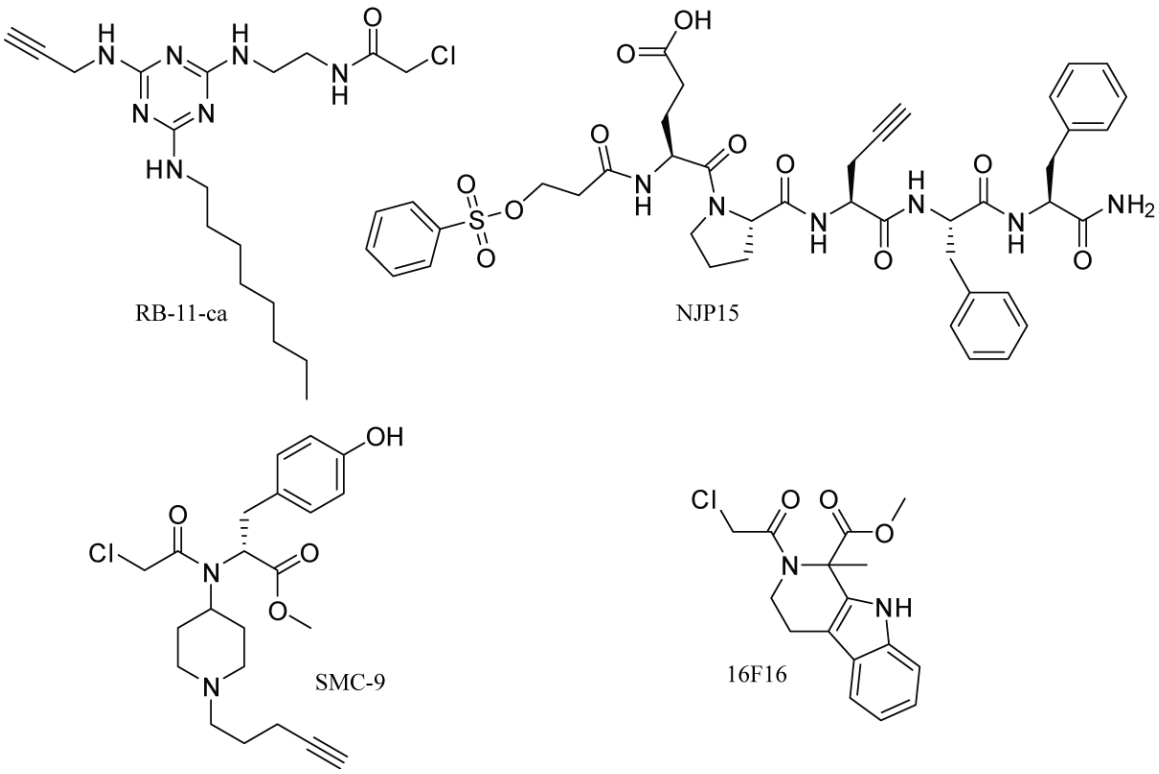

Figure 4-15. Structures of the panel of potential site-selective PDIA1 inhibitors: RB-11-ca, NJP15, SMC-9, and 16F16.

In order to individually assess each active site, the nucleophilic cysteines within each redox-catalytic pair from the **a** and **a'** site (Cys53 and Cys397) were mutated to alanine through site-directed mutagenesis. As a result, PDIA1 C53A will allow us to assess affinity for Cys397 in the **a'** site and vice versa (Figure 4-16).

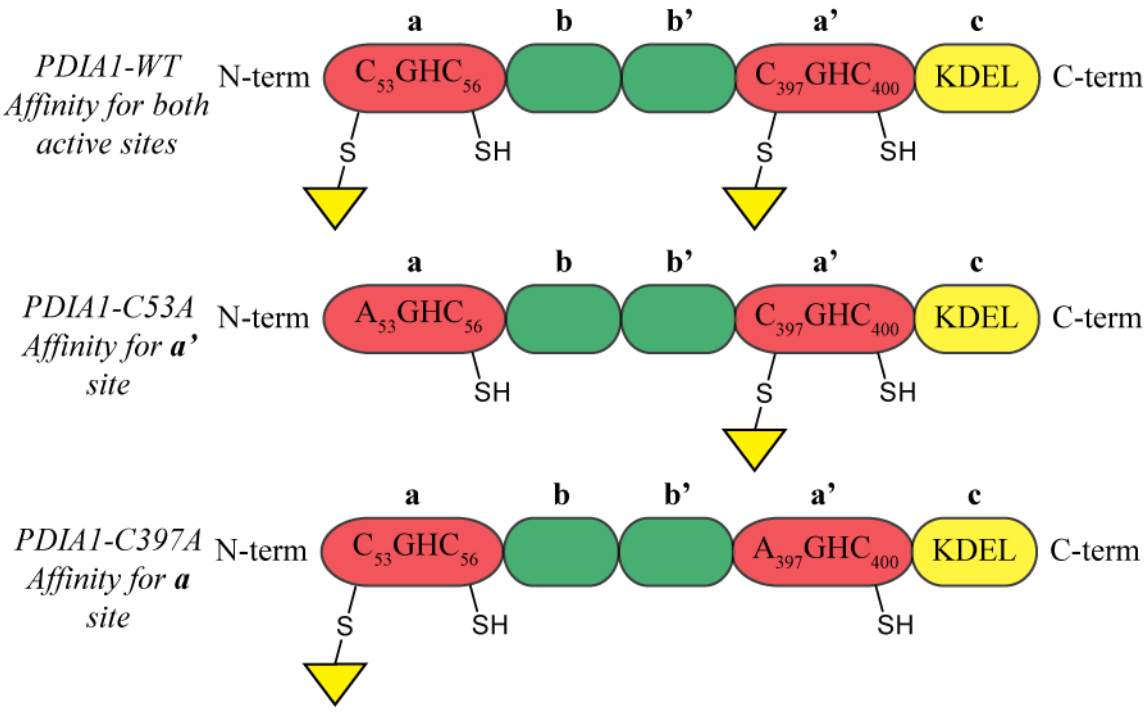

Figure 4-16. PDIA1 WT, C53A, and C397A structures allow for isolation of each active-site to determine differential affinities of each potential inhibitor for the **a** and **a'** site.

We employed a competitive in-gel fluorescence platform on each PDIA1 mutant to assess the potential inhibitors' affinities for each active-site. Since all of these potential inhibitors function through a covalent, irreversible mechanism, we employed a chloroacetamide rhodamine (CA-Rh) to measure residual cysteine reactivity upon inhibitor competition (Figure 4-17). CA-Rh can be easily synthesized and displays near-equal affinities for Cys53 and Cys397.[106] Those potential inhibitors that mitigate CA-Rh binding within either the **a** or **a'** site, represent strong binders to that particular active-site.

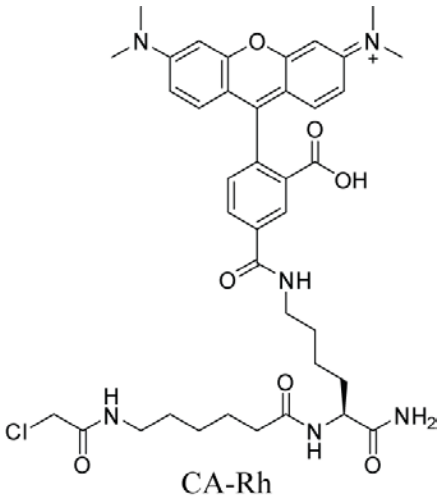

Figure 4-17. Structure of CA-Rh used to measure residual PDIA1 binding.

HeLa lysates spiked with recombinantly expressed and purified PDIA1 C53A or C397A were exposed to increasing concentrations of each of the four potential inhibitors (Figure 4-18). Notably, no binding occurs to solely purified PDIA1 unless additional protein (HeLa lysates) is added. This additional protein may be required for proper PDIA1 folding or to prevent aggregation; however, the exact reasoning is still unclear. RB-11-ca and 16F16 displayed similar potencies, with complete inhibition of the **a** site requiring less than 100 μM. SMC-9 and NJP15 were significantly less potent, requiring higher concentrations (upwards of 1,000 μM) to achieve near complete inhibition. For each inhibitor/active-site combination, at least two trials were performed. Gel band intensities were integrated, subtracted away from a PDIA1 C53/397A sample that served to measure the background fluorescence of the protein in the absence of CA-Rh binding to Cys53 or Cys397, normalized to the vehicle-treated sample, and pEC_{50} values were generated through non-linear regression (Figure 4-19). While the potencies of these inhibitors are suboptimal, we were much more interested in their selectivities for each

active-site. RB-11-ca remarkably displays 10-fold selectivity for the **a** site (EC_{50} = 47.4 μM) over the **a'** site (EC_{50} = 560.2 μM). 16F16, while displaying similar potency as RB-11-ca for the **a** site (35.4 μM), only produced 2-fold selectivity over the **a'** site (65.4 μM). For SMC-9, similar affinities for both the a (172.2 μM) and **a'** sites (258.1 μM) were observed. NJP15 displayed almost 10-fold selectivity for the **a'** site (396.4 μM) over the **a** site (3,172.0 μM). From these data, we believe we have an inhibitor toolbox that, upon optimization, could lead to an inhibitor selective for the **a** site (RB-11-ca), an inhibitor selective for the **a'** site (NJP15), and a pan-active-site inhibitor (SMC-9) (Figure 4-19, corner circles). Notably, because this approach is competitive, these EC_{50} values are dependent on the potency of CA-Rh and should be recognized as relative to the assay.

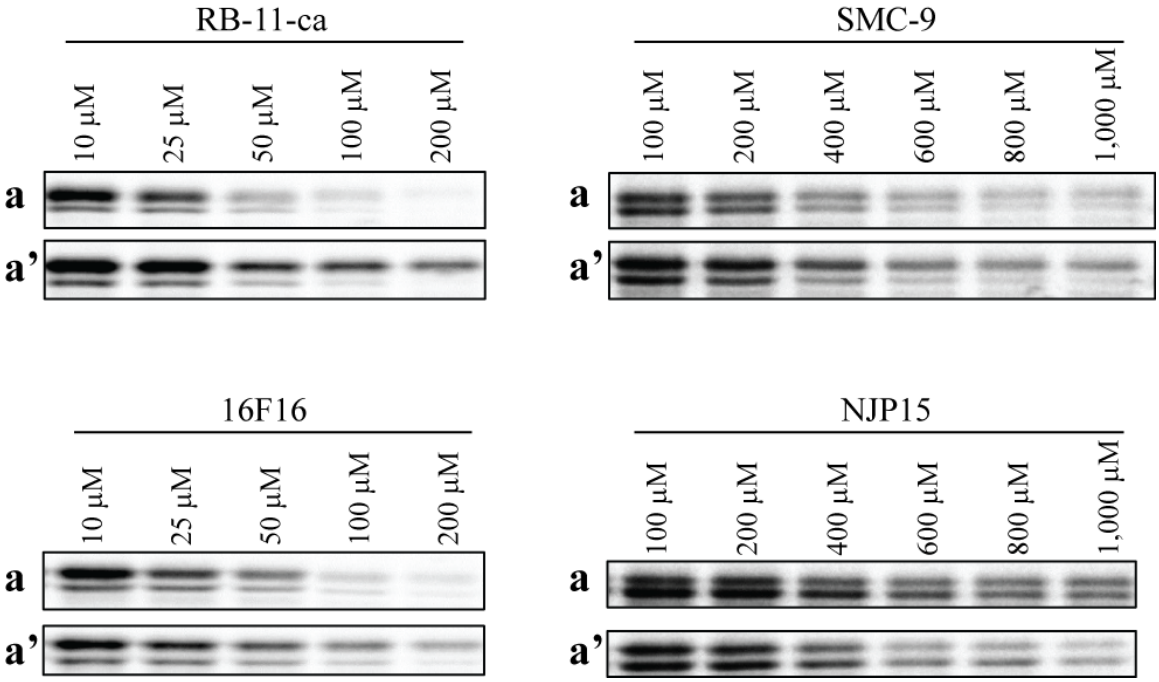

Figure 4-18. Affinity for each of the PDIA1 inhibitors for each active-site (**a** or **a'**). Concentrations for RB-11-ca and 16F16 ranged from 10 – 200 μM while those for SMC-9 and NJP15 ranged from 100 μM – 1,000 μM.

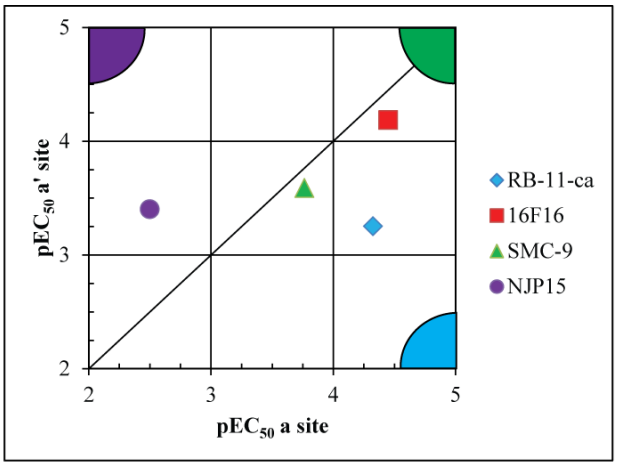

	EC_{50} **a** site (μM)	EC_{50} **a'** site (μM)
RB-11-ca	47.4	560.2
16F16	35.4	65.4
SMC-9	172.2	258.1
NJP15	3172.0	396.4

Figure 4-19. pEC_{50} values for each active-site of PDIA1 were calculated for each of the four inhibitors. The colored circles represent the optimal potencies/selectivities for our inhibitors

Evaluation of the effect of cysteine-reactive inhibitors on PDIA1 oxidase activity

Next, we looked to assess the effect of our PDIA1 inhibitors on oxidase activity. Enzyme kinetics for covalent inhibitors is assumed to be a two-step process (Figure 4-20). Inhibitor must first bind and associate within the enzyme noncovalently, and this rate of association is represented as k_{on}. This first-step is reversible, with the rate of dissociation represented as k_{off}. K_I, which represents the overall binding affinity for the inhibitor for the enzyme, is calculated by comparing the relative rates of association (k_{on}) and dissociation (k_{off}). Once the transient enzyme-inhibitor complex is generated, the electrophilic warhead can covalently bind to the enzyme. This irreversible reaction produces the permanently inactivated enzyme-inhibitor complex, and this rate of enzyme inactivation is measured as k_{inact}. For covalent inhibition, the electrophilic warhead alone is not the sole determinant of potency; covalent inhibitors must possess a balance

between binding and reactivity. To account for both properties, covalent inhibitors are typically evaluated by their k_{inact}/K_I. Notably, a certain population of inhibitor may covalently bind to other nucleophilic species in the system and be inactivated, lowering the effective inhibitor concentration.

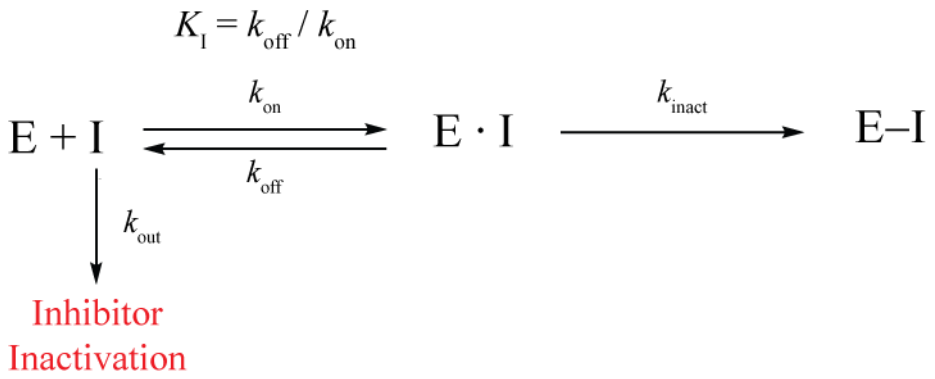

Figure 4-20. Enzyme kinetics of covalent inhibition is a two-step process. The first step is reversible and involves inhibitor binding to the enzyme. Once bound, the inhibitor can covalently bind and permanently inactivate the enzyme.

The majority of existing PDIA1 inhibitors have only been assessed for PDIA1 reductase activity, including 16F16[89] and RB-11-ca.[90] Aliquots of PDIA1 WT and casein (excess protein required for inhibitor binding) in PBS were treated with inhibitor at increasing concentrations (10, 25, 50, 75, 100, 200 μM) for various time points (5, 15, 30, 45 and 60 mins). These inhibitor-treated PDIA1 samples were assayed for oxidase activity of the reduced RNase substrate (25 μM). Data were analyzed to generate k_{inact}/K_I values for 16F16 and RB-11-ca (Figure 4-21). RB-11-ca and 16F16 both displayed similar k_{inact}/K_I values, which was consistent with data from the in-gel fluorescence platform and affinity for each site. Furthermore, the ability of 16F16 to bind both active-sites with similar potencies likely accounts for its higher k_{inact} value, since RB-11-ca is

only binding the **a** site and will eventually reach a limit of inactivation rate. The combined potency of 16F16 renders it a better inhibitor of overall PDIA1 WT oxidase activity. Because these PDIA1 inhibitors mitigate PDIA1 oxidase activity, they show promise as starting points in the development of cancer therapeutic agents.

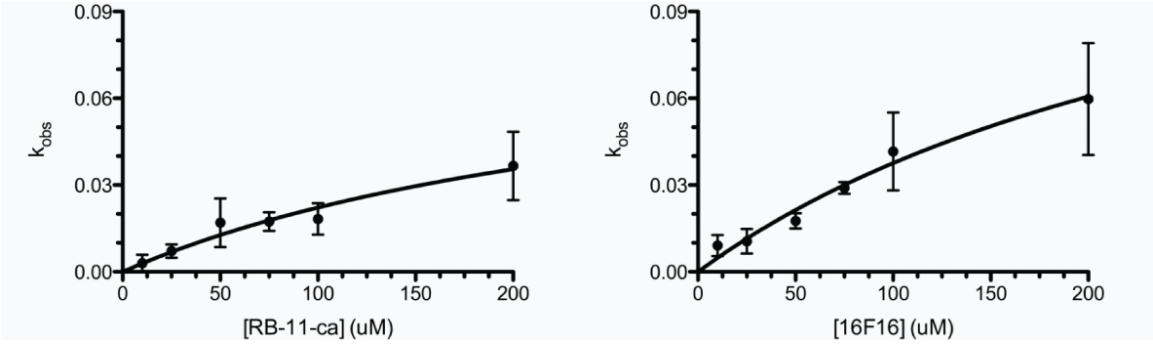

Probe	k_{inact}	K_I	k_{inact}/K_I
RB-11-ca	0.0630 min^{-1}	297 μM	212.3 M^{-1} min^{-1}
16F16	0.1114 min^{-1}	315 μM	353.9 M^{-1} min^{-1}

Figure 4-21. PDIA1 oxidase activity upon treatment with RB-11-ca and 16F16.

Effects of PDIA1 inhibition on cancer cell survival and proliferation

Next, we wanted to evaluate the effect of PDIA1 inhibitor treatment on cell proliferation. SKOV3 cells were dosed with increasing concentrations of RB-11-ca or 16F16 and assayed for cell proliferation after 24 hrs (Figure 4-22). This produced IC_{50} values of 32.97 and 9.98 μM respectively. Importantly, IC_{50} (32.97 and 9.98 μM respectively) are close to the concentrations required for inhibitor binding to PDIA1 (47.4 μM for RB-11-ca binding to the **a** site; 35.4 μM for 16F16 binding to the **a** site; 65.4 μM for 16F16 binding to the **a'** site) and in the range of those used to inhibit oxidase activity, hinting that inhibition of PDIA1 oxidase activity is triggering cellular death.

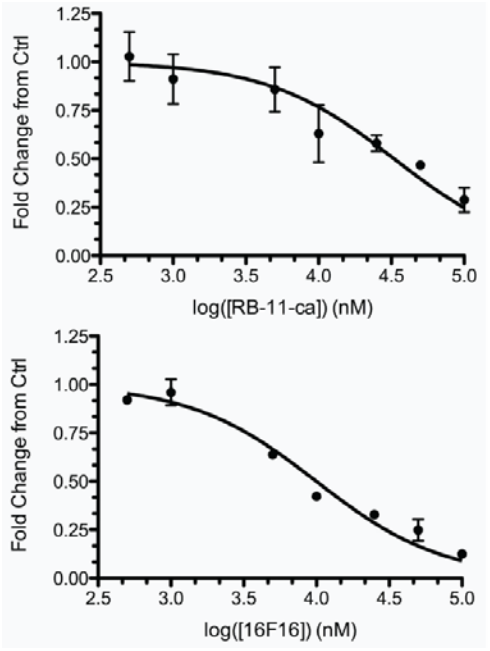

	IC_{50} (μM)
RB-11-ca	32.97
16F16	9.98

Figure 4-22. RB-11-ca and 16F16 show dose-dependent inhibition of SKOV3 proliferation.

As described earlier, PDIA1 inhibition causes a great deal of ER stress, which results in the activation of the unfolded protein response (UPR) (Figure 4-6). To corroborate that cytotoxicity is due to PDIA1 inhibition, we hypothesized that an upregulated UPR should provide a certain degree of protection to cells treated with PDIA1 inhibitors. A HEK293^{DAX} cell line was engineered to stably overexpress ATF6 and XBP1 within an inducible expression system.[108] Tetracycline (tet)-repressor technology was applied to allow doxycycline(dox)-dependent control of XBP1 levels within a physiological range.[109] Additional tet-repressor regulation of ATF6 activity produced non-physiological levels of ATF6 expression and significant off-target effects including strong upregulation of established XBP1 target genes. Instead, a destabilized domain technology was employed as a dosable and orthogonal system to tet-repressor

technology.[110, 111] A destabilized variant of *E. coli* dihydrofolate reductase (DHFR) was fused to the N-terminus of ATF6 via a short Gly-Ser linker. The poorly folded DHFR domain directs the entirely constitutively expressed DHFR-ATF6 fusion protein towards rapid proteasomal degradation. Administration of the DHFR-specific chaperone, trimethoprim (TMP), stabilizes the folded DHFR conformation, increasing the initially poorly populated folded DHFR population, attenuating proteomsomal degradation and inducing the ATF6 transcriptional program.[108] Recent studies on the HEK293^{DAX} cell line demonstrated that activation of XBP1 and ATF6 influences folding, trafficking, and degradation of destabilized ER proteins without globally effecting the endogenous proteome.[108] HEK293^{DAX} cells appear to be the perfect system to confirm that ER stress arising from PDIA1 inhibition is the cause of cellular death.

HEK293^{DAX} were grown within selection media and both dox and TMP were added to media to induce expression of XBP1 and ATF6 and activate UPR. After 12 hours, both the UPR-activated HEK293^{DAX} cells and inactivated controls were treated with increasing concentrations of RB-11-ca or 16F16 and assayed for cell proliferation after 24 hrs (Figure 4-23). For each inhibitor, three biological replicates were performed at an n = 3. Importantly, RB-11-ca showed in increase in inhibitor tolerance of 1.91-fold upon activation of UPR, while 16F16 only showed an increase in inhibitor tolerance of 1.35-fold. In both cases, the chemotherapeutic resistance achieved upon UPR activations signals that these inhibitors function, at least partially, by cytotoxicity induced by ER stress arising from PDIA1 inhibition. However, the lower degree of tolerance achieved by 16F16 compared to RB-11-ca signifies that 16F16 may suffer from off-target binding that also contributes to cytotoxicity.

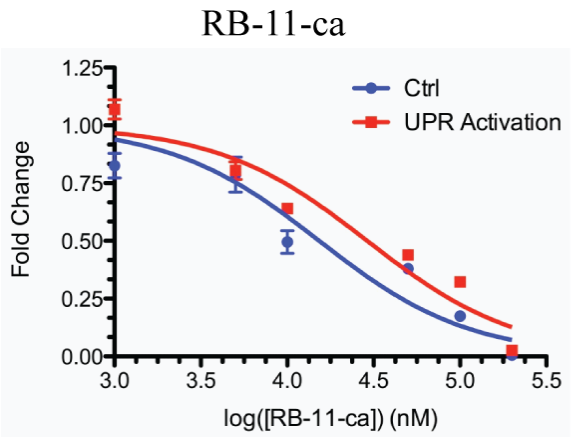

	EC_{50} (μM)			
	Trial 1	*Trial 2*	*Trial 3*	*Average*
Ctrl	15.322	38.446	10.281	21.350 +/- 15.019
Dox/TMP	29.037	62.542	22.626	38.068 +/- 21.435
Fold Increase	1.90	1.63	2.20	1.91 +/- 0.28

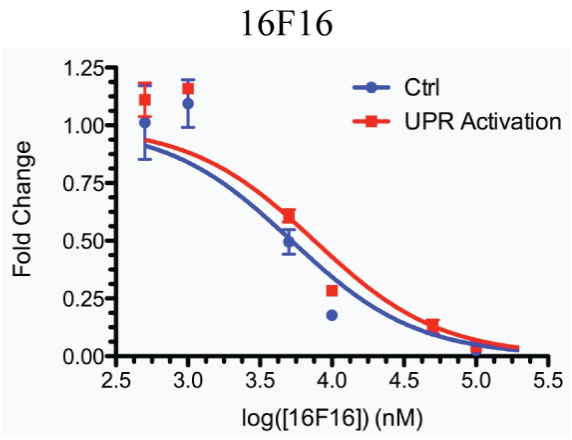

	EC_{50} (μM)			
	Trial 1	*Trial 2*	*Trial 3*	*Average*
Ctrl	15.696	5.235	2.860	7.930 +/- 6.829
Dox/TMP	19.240	7.554	3.965	10.253 +/- 7.987
Fold-Increase	1.23	1.44	1.39	1.35 +/- 0.11

Figure 4-23. UPR activation provides cytoprotection from cytotoxicity resulting from PDIA1 inhibition by RB-11-ca and 16F16.

Conclusions

We believe that our novel approach will ultimately lead to the development of a PDIA1 inhibitor toolbox to help deconvolute the role of PDIA1 in cellular functions and disease pathways. First, an engineered PDIA1 knockdown into an ovarian cancer cell line (SKOV3) significantly diminished cell proliferation, survival, migration and invasion, which validates PDIA1 inhibition as a therapeutic pathway for cancer treatment. We sought to examine a panel of PDIA1 inhibitors, and enact our new approach to assess their effectiveness as anticancer agents. This strategy first employed a competitive in-gel fluorescence assay to evaluate inhibitor binding affinities for each individual active-site (**a** vs **a'**). At this point, we have designed PDIA1 inhibitors with potential of being 1) selective for the **a** site (RB-11-ca), 2) selective for the **a'** site (NJP15), and 3) a pan-PDIA1 inhibitor (SMC-9). These site-selective inhibitors should help uncover the roles of

each active-site in PDIA1 function. Site-selective inhibitors could be extremely important for PDIA1-based anticancer therapies. Because PDIA1 function is essential for healthy and cancer cells, only inhibiting a single active-site may result in cytotoxicity solely to cancer cells due to their increased reliance on PDIA1. Furthermore, inhibitors that displayed successful binding to PDIA1 underwent an activity assay to determine their ability to inhibit PDIA1 oxidase activity, since that activity is thought to be most important to cancer progression. While inhibition of PDIA1 oxidase activity was observed upon RB-11-ca and 16F16 treatment, these inhibitors all unfortunately lacked sufficient potencies. Currently, other members of the Weerapana lab are examining SAR of all PDIA1 inhibitors for each active-site in the hopes of developing more potent derivatives that maintain site-selectivity. Furthermore, other PDIA1 family members, in particular PDIA3, PDIA4, and PDIA6, should be examined for a role in cancer pathogenesis. The design of selective inhibitors for other members of the PDIA1 family should continue to aid efforts to deconvolute their cellular roles and contribution to disease.

Acknowledgements

Dr. Ranjan Banerjee synthesized and initially discovered the PDIA1 inhibitory potential of RB-11-ca. Shalise Couvertier synthesized and initially discovered the PDIA1 inhibitory potential of SMC-9. I would like to thank Kyle Cole for synthesizing additional stocks of RB-11-ca and CA-Rh and continued work on PDIA1. Special thanks to Emily Witsberger for her synthesis of NJP15, optimization of peptide synthesis, and continued efforts to synthesize derivatives of NJP15. I would also like to thank Omar

Khan for taking over for Emily Witsberger and continuing synthesizing derivatives of NJP15. Special thanks to Sharon Louie, Dr. Mela Mulvihill, Dr. Dan Nomura, and the entire Nomura lab at University of California Berkeley for hosting me in their laboratory and teaching me lentiviral transduction and the cancer phenotypic assays. I would also like to thank Kimberly Miller from the biology department at Boston College for all her knowledge of RT-PCR. Special thanks to Tyler Bechtel and Kyle Cole for continuing with this project.

Experimental procedures

General procedures and materials

All materials were purchased from Sigma Aldrich or Fisher Scientific unless otherwise noted. Fmoc-propargylglycine (Fmoc-Pra-OH) was purchased from BaCHEM. All other Fmoc-protected amino acids, PyBOP, peptide-synthesis resin were purchased from Novabiochem. PBS buffer, DMEM/High glucose media, and penicillin streptomycin (Pen/Strep) were purchased from Thermal Scientific. Trypsin-EDTA was purchased from Invitrogen. X-tremeGENE 9 DNA transfection reagent was purchased from Roche. High resolution Mass Spectra (HRMS) were obtained at the Mass Spectrometry Facility at Boston College unless otherwise noted. A Molecular Devices Spectramax M5 plate reader was used to read the absorbance of all activity assays. All silver staining was carried out using a ProteoSilver Silver Stain kit from Sigma. The α-PDI antibody was purchased from cell signaling. All work with RNA was performed under RNase free conditions (filtered pipet tips and decontaminating with RNase away).

DEPC-water and pLenti Go-Stix were purchased from ClonTech. All sequencing was performed by Genewiz with the appropriate primers.

Synthesis of BsO-(propanamide)-Glu-Pro-Pra-Phe-Phe-NH_2 (NJP15)

The peptide was synthesized by manual solid-phase methods on Rink Amide MBHA Resin using Fmoc as the protecting group for α-amino functionalities. Amino acids were coupled using PyBOP as the activating reagent. The success of each Fmoc-deprotection and coupling reaction was qualitatively tested using the standard procedure for the Kaiser test. Fmoc-Phe-OH, Fmoc-Phe-OH, Fmoc-Pra-OH, Fmoc-Pro-OH, and Fmoc-Glu(OtBu)-OH residues were added under standard coupling conditions. After Fmoc-deprotection, 3-(trityloxy)propanoic acid (NJP12, synthesis detailed in Chapter 2) (2 eq) and PyBOP (2 eq) were dissolved in DMF and this solution was added to the resin. DIPEA (4 eq) was added to the resin, and the reaction was shaken at room temperature for 2 hrs. The solvent was removed by vacuum and the resin was washed with DMF (5 x 3 mL) and DCM (3 x 3 mL). The resin was shaken in a 1% TFA, 2% TIS in DCM solution to remove the trityl group (3 x 5 mins). Dry DCM was added to the resin and N_2 gas was bubbled through the reaction vessel. NEt_3 in large excess (~100 eq) followed by benzene sulfonylchloride in large excess (~100 eq) were added to the resin. N_2 gas was bubbled through the reaction mixture for 1 hr, and any solvent lost was replaced. The reaction vessel was capped, sealed with parafilm, and shaken for 15 hrs. The solvent was removed and the resin was washed with DCM (5 x 3 mL). After the addition of the electrophile, cleavage from the resin was performed in TFA: DCM: TIS: water (90: 5: 2.5: 2.5) solution for 2 hrs. The peptide was purified by preparative HPLC with a gradient

of increasing acetonitrile-0.1% TFA (solvent) in water-0.1% TFA (solvent A) and analyzed by a Micromass LCT TOF mass spectrometer coupled to a Waters 2975 HPLC and a Waters 2996 photodiode array UV-vis detector to give the pure peptide NJP15 (5.71%). HPLC t_R = 20.48 min (C_{18}, 5-195% B in 30 mins); HRMS for NJP14 ($C_{42}H_{48}N_6O_{11}S + Na^+$): *m/z* calcd 844.31; obsd [M + Na^+] 867.3 (ESI+).

Generation of stable cell lines

General cell culture and preparation of protein lysates

All SKOV3 cell lines were grown in the cell incubator at 37°C under 5% CO_2 in RPMI media supplemented with 10% FCS, 2 mM glutamine, and 1% Pen/Strep (RPMI+FBS). HEK293T and HeLa cells were grown in the cell incubator at 37°C under 5% CO_2 in DMEM media supplemented with 10% FCS, 2 mM glutamine, and 1% Pen/Strep (DMEM+FCS). The plates were allowed to grow to 100% confluence, the cells were harvested by scraping, and the pellets were washed with PBS. The pellets were resuspended in an appropriate amount of PBS and sonicated to lyse to give whole-cell lysates. These lysates were separated by centrifugation (45 mins, 45,000 rpm) at 4°C under high vacuum to separate the soluble and membrane proteomes. The supernatant was collected as the soluble fraction and the pellet was discarded. The protein concentrations were determined using the Bio-Rad DC Protein Assay kit (Bio-Rad). In some cases serum free RPMI or DMEM media supplemented with 2 mM glutamine and 1% Pen//Strep are utilized (RPMI-SF or DMEM-SF).

Heat Inactivated Serum

An aliquot of FCS (50 mL) was removed from the -20 °C freezer and was thawed. The FCS was heated in a 55 °C water bath for at least 30 mins, and was then added to either RPMI media supplemented with 2 mM glutamine and 1% Pen/Strep (RPMI+HIS) or DMEM media supplemented with 2 mM glutamine and 1% Pen/Strep (DMEM+HIS).

Gateway cloning of PDIA1 sequence into viral expression vector

PDIA1-pDONR2233 plasmid (1.0 µL, 100 ng/µL = 100 ng; GE Healthcare) and the destination pLenti CMV Puro Dest expression vector (1.0 µL, 150 ng/µL), TE buffer pH 8.0 (6.0 µL, purchased from Fisher) were combined in an eppendorf tube. LR clonase II enzyme mix (Life Technologies) was thawed on ice and briefly vortexed. This solution (2.0 µL) was added to the eppendorf. The reaction was vortexed and allowed to proceed at room temperature for 1 hr. Proteinase K (1.0 µL; Life Technologies) was added to the reaction and it was vortexed and allowed to proceed at room temperature for an addition 10 mins. The reaction mixture was transformed into DH5α chemically competent cells, colonies were cultured, and plasmid was isolated and confirmed by sequencing.

Lentiviral transduction of shGFP, shPDIA1, and PDIA1 overexpression sequence

The following procedure is for one 10 cm plate HEK293T cells to produce one 10 cm plate of infected SKOV3 cells. (If performing in a 15 cm plate, multiply all amounts by 4). DMEM-SF (1.160 mL) and X-tremeGENE 9 DNA transfection reagent (40 µL) were combined and briefly shaken. VSVG-pCMV (1 µg), pspax2-pCMV (1 µg), and the

shRNA or viral overexpression construct (2 μg) were added to the solution. The sample was briefly shaken and allowed to sit at room temperature for about 15-20 mins. A 10 cm plate of HEK293T cells at ~75% confluence, grown in DMEM-HIS were removed from the cell incubator, and the plasmid solution was added dropwise to the plate. The plate returned to the cell incubator for approximately 16-24 hrs. The media was removed by vacuum, and fresh DMEM-HIS (5 mL) was added to the transfected plate to concentrate the virus, and the plate was returned to the cell incubator for an additional 16-24 hrs. The presence of virus was confirmed using Lenti-X GoStix. For each sample, RPMI+HIS (5 mL) and polybrene in water (10 μL, 10 mg/mL) were combined in a 15 mL conical tube. The virus-containing DMEM+HIS (5 mL) was removed from the HEK293T cells and was filtered through a 0.4 μm filter into the 15 mL conical tubes. In addition, a negative control was made by using DMEM+HIS. SKOV3 cells at ~50% confluence grown in RPMI+HIS were removed from the cell incubator and the media was removed by vacuum. Each of the virus containing media solutions (~10 mL) was added to the plates, and the plates were returned to the cell incubator for 16-24 hrs. The plates were removed from the cell incubator and the media was removed by vacuum. RPMI+FBS (10 mL) and puromycin (10.0 μL, 1 mg/mL) were added to the plates and they were returned to the cell incubator. The selection was carried out until all the cells were dead within the negative control (approx. 72 hrs for SKOV3 cells). The media was removed from all the plates by vacuum and replaced with fresh RPMI+FBS.

Evaluation of mRNA levels of SKOV3-Ctrl, SKOV3-PDIA1-, SKOV3-PDIA1+

RNA extraction

TRIzol reagent (1.00 mL; Life Technologies) was added to a 10 cm plates of 100% confluent SKOV3 cells and allowed to incubate at room temperature for 5 mins. The TRIzol solution was transferred to an eppendorf tube and chloroform (200 µL) was added to the tube. The tube was briefly shaken and centrifuged (12 mins, 4 °C). The top layer was carefully transferred to another eppendorf tube. Isopropanol (400 µL) was added, the tube was vortexed, and it was allowed to sit at room temperature for ~5-10 mins. The samples were centrifuged (10 mins, 4 °C) and the supernatants were carefully discarded. A 75% EtOH in DEPC-water solution (400 µL) was added to wash the pellets. The sample was vortexed rigorously, centrifuged (5 mins, 4 °C), and the supernatant was carefully removed. The sample was allowed to briefly air dry and was resuspended in DEPC-water (25-35 µL). The RNA can be stored at -80 °C and concentrations can be taken using the Nanodrop.

cDNA formation

RNA stocks were diluted to 500 ng/µL. DEPC-water (9.5 µL), RNA (1.0 µL, 500 ng/µL = 500 ng), and Oligo-dT's (2.0 µL, 100 µM) were combined in a PCR tube. The tube was incubated in at 65 °C for 2 mins and was then chilled on ice for 1 min. M MuLV Reverse Transcriptase 10x Reaction Buffer (2.0 µL; New England Biolabs), dNTP mix (2.0 µL, 10 mM), DTT (2.0 µL, 100 mM), RNase Inhibitor (0.5 µL; New England Biolabs), and M MuLV Reverse Transcriptase (1.0 µL; New England Biolabs) were added to the sample to give a total volume of 20.0 µL. The tubes were briefly mixed and

were incubated at 37 °C for 60 mins, then 85 °C for 5 mins to terminate the reaction. The tubes were allowed to sit on ice for 1 min, and can be stored at -80 °C.

RT-PCR

The following primers were designed to evaluate PDIA1 mRNA levels and GAPDH levels. GAPDH was used as a housekeeper gene. For each gene, the primers were prepared as a mixture of both forward and reverse (10 μM each) in DEPC-water. The primers were evaluated for the capacity to dimerize.

PDIA1_Forward: 5'-TTTGGAGGTGAAATCAAGACTCA-3'

PDIA1_Reverse: 5'-GAAAGAACTTGAGTGTGGGG-3'

GAPDH_Forward: 5'-GATTTGGTCGTATTGGGCGC-3'

GAPDH_Reverse: 5'-AGTGATGGCATGGACTGTGG-3'

For each sample, DEPC-water (16.8 μL), 5x HF Buffer (5.0 μL; Finnzyme), primer mix (1.50 μL), cDNA (1.00 μL), dNTPs (0.50 μL, 10 mM), and Phusion polymerase (0.25 μL; Finnzyme). The following PCR conditions were used:

	30 cycles				
Initial	Denature	Anneal	Elongation	Final	
95 °C	95 °C	55 °C	68 °C	72 °C	4 °C
2 mins	15 sec	30 sec	30 sec	10 mins	End

Xylene cyanol (5.0 μL) was added to the samples and each sample (5.0 μL) and a Tri-Dye 100 bp DNA ladder (New England Biolabs) ware loaded onto a 2% agarose gel. The gel was run at 155 volts for 15 mins and visualized under UV light. Band quantification was performed using ImageJ software, and values were calculated from two technical replicates of two biological replicates.

Western blot

Protein lysates were collected for the SKOV3-Ctrl, SKOV3-PDIA1-, and SKOV3-PDIA1+ cell lines. The protein lysates (15 μL) and 2x gel loading dye (15 μL) were combined and loaded onto a 10% polyacrylamide gel. The gel was run for 217 volt hrs. These SDS-PAGE gels were transferred by electroblotting onto nitrocellulose membranes for 150 volt hours. The membranes were blocked in TBS-T and 5% (w/v) non-fat dry milk at room temperature for 2 hrs. The blot was washed with TBS-T three times (5 min per wash), and the blot was treated with α-PDIA1 rabbit antibody (1:1000) overnight at 4 °C. The blots were washed with TBS-T three times (5 mins per wash). The blots were treated with the appropriate secondary antibody (α-rabbit, 1:3333) for 2 hrs at room temperature. The blots were washed three times with TBS-T (5 mins per wash), treated with HRP super signal chemiluminescence reagents and exposed to film for 1-10 mins before development. Development took place using a Kodak X-OMAT 2000A processor.

Cancer phenotypic assays

Proliferation and survival

A 10 cm plate of each cell type (SKOV3-Ctrl, SKOV3-PDIA1-, SKOV3-PDIA1+) was removed from the cell incubator and the media was removed. The plates were washed with PBS (5 mL). RPMI-SF (5 mL) was added to the plates and they were returned to the cell incubator for ~2 hrs to serum starve cells.

The serum-starved plates were removed and the media was removed. The plates were washed with PBS (5 mL). The cells were incubated in Trypsin-EDTA (1.25 mL) for an appropriate time point. The suspension were diluted 10x with RPMI-SF (12.5 mL), transferred to 15 mL conical tubes, centrifuged (5 mins, 3500 rpm, 4°C), and the supernatants were removed. The pellets were resuspended in RPMI-SF and were counted using a hemocytometer.

Four, clear, 96-well plates were designated as Day 0, Day 1, Day 3, Day 5. For proliferation, SKOV3 cells (10,000 cells/well) in RPMI+FBS (150 µL total volume) were added to five wells of each of the four plates. For survival, SKOV3 cells (20,000 cells/well) in RPMI-SF (150 µL total volume) were added to five wells of each of the four plates. WST-1 proliferation agent (10.0 µL; Roche) was immediately added to each well of the Day 0 plates. The plates were placed in the cell incubator for 1 hr and the absorbance at 450 nm was recorded for each well. After the appropriate time points (24, 72, and 120 hrs), WST-1 proliferation agent (10 µL) was added to plate and the process was repeated. Data were subtracted from a media blank and taken as n = 5 from two biological replicates.

Migration

A 10 cm plate of each cell type (SKOV3-Ctrl, SKOV3-PDIA1-, SKOV3-PDIA1+) was removed from the cell incubator and the media was removed. The plates were washed with PBS (5 mL). RPMI-SF (5 mL) was added to the plates and they were returned to the cell incubator for ~2 hrs to serum starve cells. PBS (13 mL) and collagen from rat tail (35 µL; Life Technologies) were combined and this solution (750 µL) was

added to 12 wells of a Corning Transwell Permeable Support (24-well plate with 12 inserts). The inserts were placed in these collagen filled wells, and the plate was placed in the cell incubator for ~2 hrs.

The serum-starved plates were removed and the media was removed. The plates were washed with PBS (5 mL). The cells were incubated in Trypsin-EDTA (1.25 mL) for an appropriate time point. The suspension were diluted 10x with RPMI-SF (12.5 mL), transferred to 15 mL conical tubes, centrifuged (5 mins, 3500 rpm, 4°C), and the supernatants were removed. The pellets were resuspended in RPMI-SF and were counted using a hemocytometer.

The migration chamber was removed from the cell incubator and RPMI-SF (750 μL) was added to the remaining 12 wells. The inserts were moved to these wells, and SKOV3 cells (50,000 cells/well) in RPMI-SF (200 μL) were added to these inserts. The migration chamber was placed in the cell incubator for 5 hrs. The migration chamber was removed and the inserted wells were removed, dried, and stained using Diff-Quik Stain Set (Siemens). Images were captured for each well under a 20x and 40x optical microscope. The amount of cells on the 40x images were counted, and the results were displayed as an average and SEM from n = 3 from two biological samples. The data were displayed relative to the SKOV3-Ctrl cell line.

Invasion

A 10 cm plate of each cell type (SKOV3-Ctrl, SKOV3-PDIA1-, SKOV3-PDIA1+) was removed from the cell incubator and the media was removed. The plates were washed with PBS (5 mL). RPMI-SF (5 mL) was added to the plates and they were

returned to the cell incubator for ~2 hrs to serum starve cells. RPMI-SF (750 μL) was added to 12 wells of a Corning BioCoat Matrigel Invasion Chamber (24-well plate with 12 inserts). The inserts were placed in these media filled wells for re-hydration, and the plate was placed in the cell incubator for ~2 hrs.

The serum-starved plates were removed and the media was removed. The plates were washed with PBS (5 mL). The cells were incubated in Trypsin-EDTA (1.25 mL) for an appropriate time point. The suspension were diluted 10x with RPMI-SF (12.5 mL), transferred to 15 mL conical tubes, centrifuged (5 mins, 3500 rpm, 4°C), and the supernatants were removed. The pellets were resuspended in RPMI-SF and were counted using a hemocytometer.

The invasion chamber was removed from the cell incubator and RPMI-SF (750 μL) was added to the remaining 12 wells. The inserts were moved to these wells, and SKOV3 cells (50,000 cells/well) in RPMI-SF (500 μL) were added to these inserts. The migration chamber was placed in the cell incubator for 24 hrs. The invasion chamber was removed and the inserted wells were removed, dried, and stained using Diff-Quik Stain Set (Siemens). Images were captured for each well under a 20x and 40x optical microscope. The amount of cells on the 40x images were counted, and the results were displayed as an average and SEM from n = 3 from two biological samples. The data were displayed relative to the SKOV3-Ctrl cell line.

PDIA1 recombinant protein expression

Cloning of PDIA1 WT and cysteine mutants into mammalian overexpression vector pcDNA3.1+(myc/His) bacterial expression vector (pET)

The PDIA1 WT cDNA was initially subcloned into pcDNA3.1+(myc/His) mammalian expression vector through the *HindIII* and *XbaI* restriction sites. The PDIA1 C53A, C56A, C397A, C400A, and C53/397A mutants were generated through site-directed mutagenesis (Quik-Change, Stratagene) using the following primers:

PDIA1 C53A-For: 5'-CATGCCCCCTGGGCTGGCCACTGCAAG-3'

PDIA1 C53A-Rev: 5'- CTTGCAGTGGCCAGCCCAGGGGGCATG-3'

PDIA1 C56A-For: 5'- GGTGTGGCCACGCCAAGGCTCTGGC-3'

PDIA1 C56A-For: 5'- GCCAGAGCCTTGGCGTGGCCACACC-3'

PDIA1 C397A-For: 5'- CTATGCCCCATGGGCTGGTCACTGCAAAC-3'

PDIA1 C397A-Rev: 5'- GTTTGCAGTGACCAGCCCATGGGGCATAG-3'

PDIA1 C400A-For: 5'- CATGGTGTGGTCACGCCAAACAGTTGGCTC-3'

PDIA1 C400A-Rev: 5'- GAGCCAACTGTTTGGCGTGACCACACCATG-3'

The PDIA1 C53/397A was made through two rounds of mutagenesis. All constructs were verified by sequencing.

Cloning of PDIA1 WT and cysteine mutants into bacterial expression vector (pET-a-d(+))

The PDIA1 WT, C53A, C56A, C397A, C400A, C53/397A constructs were subcloned into pET-a-d(+) through the *BamHI* and *HindIII* restriction sites. For all constructs, the first 51 bases were removed and replaced by an ATG sequence in the forward primer to account for the loss of the 18 amino acid signaling sequence that is

cleaved upon PDIA1 maturation. Constructs were verified by sequencing and contained a His-tag for purification.

Bacterial protein expression

Starting from a 5 mL overnight BL21 *E. coli* culture, PDIA1 WT, C53A, C56A, C397A, C400A, and C53/397A were grown at 37°C in LB broth (500 mL) to an OD_{600} of ~0.8. The cultures were induced with IPTG (0.4 mM) and were shaken at 37°C for 4 additional hours. The cells were harvested by centrifugation (5 mins, 5000 rpm) and pellets were frozen at -80°C until needed.

Protein purification

E. coli pellets were thawed on ice and resuspended in PBS (10 mL). The suspensions were sonicated to lyse to form whole cell lysates. These lysates were separated by centrifuging at 45,000 rpm for 45 mins at 4 °C to yield soluble and membrane proteomes. The supernatant was collected as the soluble crude fraction and the pellet was discarded. The crude lysates were loaded onto a Ni-NTA column equilibrated with PBS. The column was washed with 3 - 6 column volumes of a 25 mM imidazole in PBS solution, and the purified protein was eluted with 2 column volumes of 500 mM imidazole in PBS solution. Each fraction was analyzed by SDS-PAGE and silver stain, and purified fractions were combined and further purified by a PD-10 size exclusion column (GE Life Sciences) to remove imidazole. The protein concentrations were determined using the Bio-Rad DC Protein Concentration Assay, and the lysates were

stored on ice in GSH (1 mM) and GSSG (0.2 mM) in PBS. The protein retained activity for approximately 2 – 4 weeks.

Competitive in-gel fluorescence to assay affinity to the a and a' site of PDIA1

Recombinant PDIA1 C53A, C397A, or C53/397A (1.25 μg) and HeLa lysates (1.00 mg/mL) were combined and diluted with PBS to a total volume of 25 μL. DMSO or inhibitor (from a 50x stock in DMSO) was added to each of the protein samples to give the following concentrations:

RB-11-ca/16F16: 10, 25, 50, 100, 200 (μM)

SMC-9/NJP15: 100, 200, 400, 600, 800, 1,000 (μM)

Additionally, a PDIA1 C53/397A sample plus DMSO was added as a negative control. The samples were vortexed and allowed to sit at room temperature for 1 hr. CA-Rh (8 μM, from a 50x stock in DMSO) was added to all the samples, they were vortexed and incubated at room temperature for an additional hour. Loading dye 2x (25 μL) was added to the samples, and each sample (25 μL) was loaded onto a 10% polyacrylamide gel. The gel was run for 217 volt hrs, fluorescent scanned, and coomassie stained. The gel band intensities were integrated using ImageJ from at least three trials. For each sample, the band intensity was subtracted from the PDIA1 C53/397A sample, which served to measure background protein fluorescence. The full gels are presented within Appendix III (Figure 4A-1, Figure 4A-2, Figure 4A-3, ,and Figure 4A-3).

PDIA1 oxidative activity assays

General assay protocol

To prepare the reduced RNase substrate (rRNase), guanidine HCl (6 M), DTT (1.4 mM from 100x stock), and RNase A (10 mg/mL) were combined and shaken at 37°C overnight. The rRNase was purified on a Nap-5 size exclusion column (GE Life Sciences) immediately before use. GSH (1 mM, from 100x stock), GSSG (0.2 mM from 100x stock), and cytidine 2'3'-cyclic monophosphate (4.5 mM from 100x stock; cCMP) were combined in a 100 mM Tris-acetic acid, 2 mM EDTA, pH 8.0 buffer (PDIA1 buffer) to form an assay stock solution. Recombinant PDIA1 (1.4 μM) was added to the stock solution and aliquoted to wells of a UV-capable 96-well plate (Greiner). rRNase (1, 5, 10, 25, or 50 μM) was added and the absorbance at 296 nm was recorded every 30 seconds for 15-30 mins to measure the amount of product, activated RNase (aRNase).

Oxidative activity assays of PDIA1 WT and cysteine mutants

The rRNase substrate was prepared as described above. A stock solution of PDIA1 buffer, GSH, GSSG, cCMP, and PDIA1 was prepared as described above and aliquoted (86.4 μL) to each well. Purified rRNase solution (13.6 μL, 1, 5, 10, 25, 50 μM from a 0.1 mg/mL, 0.5 mg/mL, 1.0 mg/mL, 2.5 mg/mL, and 5.0 mg/mL stock respectively) was added to each well, and the absorbance at 296 nm was recorded every 30 seconds for 15 mins. Data analysis was performed to generate curves of [Product] formed / Time vs. [Substrate]. The derivative of each A vs. Time plot gave dA vs. Time, which was converted to [aRNase] vs. Time (769 A = 1 μM aRNase). Linear regression for each [rRNase] was performed to give a final plot of [aRNase]/Time vs. [rRNase].

Oxidative activity assays of PDIA1 WT treated with 16F16 or RB-11-ca

PDIA1 WT (0.29 mg/mL, 5.09 μM), casein in PBS (0.057 mg/mL), GSH (100 mM), GSSG (0.2 mM) and PBS were combined and aliquoted as 30.0 μL samples. Inhibitor in DMSO (1.00 μL at the appropriate 30x concentration) was added to each sample for either 10, 20, 30, 40, or 50 mins. The samples were briefly vortexed and spun down. PDIA1 buffer, GSH (1 mM), GSSG (0.2 mM) and cCMP (will be 4.5 mM once diluted) were combined as a substrate stock solution. This solution (65.8 μL) was added to each well of a 96-well plate. Each inhibitor-treated protein sample (27.4 μL) was added to the appropriate wells. A sample without PDIA1 was used as a blank control. Purified rRNase (6.9 μL, 5 mg/mL) was added to the samples. This gives final concentrations of PDIA1 WT (1.4 μM), GSH (1 mM), GSSG (0.2 mM), cCMP (4.5 mM), and rRNase (25 μM). The plate was read for absorbance at 296 every 30 seconds for 30 mins. For data analysis, each well was subtracted from the average of the –PDIA1 samples at each respective time point. The derivatives (dA) of each concentration at each precincubation time were calculated as dA vs Time. The dA vs Time plots were converted to [aRNase] vs Time (769 A = 1 μM aRNase). Linear regressions for each preincubation time point at each [Inhibitor] were performed to give 5 slopes (5 preincubation times) for each [Inhibitor]. For each [Inhibitor], the Rate of Activity ([aRNase] / Time) vs Preincubation time was plotted. These were all normalized to the samples without Inhibitor, to give % Rate of Ctrl vs Preincubation time. One phase nonlinear regression was performed for each [Inhibitor] to produce a rate constant for inhibition. These rate constants were plotted as k_{obs} vs [I], and another nonlinear regression was performed to calculate K_I and k_{inact}.

PDIA1 cytotoxicity assays

Proliferation assay: SKOV3 + PDIA1 inhibitors

A 10 cm plate of SKOV3 cells was removed from the cell incubator and the media was removed. The plates were washed with PBS (5 mL). RPMI-SF (5 mL) was added to the plates and they were returned to the cell incubator for ~2 hrs to serum starve cells.

The serum-starved plates were removed and the media was removed. The plates were washed with PBS (5 mL). The cells were incubated in Trypsin-EDTA (1.25 mL) for an appropriate time point. The suspension were diluted 10x with RPMI-SF (12.5 mL), transferred to 15 mL conical tubes, centrifuged (5 mins, 3500 rpm, 4°C), and the supernatants were removed. The pellets were resuspended in RPMI-SF and were counted using a hemocytometer.

Two, clear, 96-well plates were designated as Day 0 and Day 1. SKOV3 cells (10,000 cells/well) and inhibitor (0, 0.5 1.0, 5.0, 10.0, 25.0, 50.0, 100.0 μM) in RPMI+FCS (150 μL total volume) stocks (6x) were made and each solution (150 μL) added to three wells of each of the two plates. WST-1 proliferation agent (10.0 μL; Roche) was immediately added to each well of the Day 0 plates. The plates were placed in the cell incubator for 1 hr and the absorbance at 450 nm was recorded for each well. After 24 hrs, WST-1 proliferation agent (10 μL) was added to the Day 1 plate and the process was repeated. Data were taken as n = 3 from 3 biological replicates.

Proliferation assay: HEK293DAX + PDIA1 inhibitors

Two 10 cm plates of HEK293^{DAX} cells at ~80% confluence were removed from the cell incubator and the media was replaced with fresh DMEM+FBS (10 mL). Dox in water (1.00 µL, 10 mg/mL = 1.0 µg/mL) and TMP in DMSO (1.00 µL, 10 mg/mL = 10 µM) were added to one of the plates to activate UPR. DMSO (1.00 µL) and water (1.00 µL) was added to the other plate as a control. The plates were returned to the cell incubator for 12 hours.

The plates were removed from the cell incubator and the media was removed. The plates were washed with PBS (5 mL). The cells were incubated in Trypsin-EDTA (1.25 mL) for an appropriate time point. The suspension were diluted 10x with DMEM-SF (12.5 mL), transferred to 15 mL conical tubes, centrifuged (5 mins, 3500 rpm, 4°C), and the supernatants were removed. UPR-Media was made by combining DMEM+FBS (15.0 mL), dox in water (1.00 µL, 10 mg/mL = 1 µg/mL), and TMP in DMSO (1.00 µL, 100 mM = 10 µM) in a conical tube. Ctrl-Media was made by combining DMEM+FBS (15.0 mL), water (1.00 µL), and DMSO (1.00 µL) in a conical tube. The HEK293^{DAX} pellets were resuspended in the appropriate media (Ctrl or UPR) and were counted using a hemocytometer.

For both Ctrl and UPR HEK293^{DAX} cells, 7x stocks were made by combining cells (20,000 cells/well) and inhibitor (0, 0.5, 1.0, 5.0, 10.0, 50.0, 100.0 µM from 100x stock in DMSO) in the appropriate media (Ctrl or UPR). Each suspension was aliquoted to three wells of two 96-well plates (150 µl/well) designated as Day 0 and Day 1. WST-1 proliferation agent (10.0 µL; Roche) was immediately added to each well of the Day 0 plates. The plates were placed in the cell incubator for 1 hr and the absorbance at 450 nm

was recorded for each well. After 24 hrs, WST-1 proliferation agent (10 μL) was added to the Day 1 plate and the process was repeated. Data were taken as n = 3 from 3 biological replicates.

References

1. Ferrari, D. M.; Soling, H. D., The Protein Disulphide-Isomerase Family: Unravelling a String of Folds. *Biochem. J.* 1999, 339, 1-10.

2. Xu, S.; Sankar, S.; Neamati, N., Protein Disulfide Isomerase: A Promising Target for Cancer Therapy. *Drug. Discov. Today* 2014, 19, 222-240.

3. Venetianer, P.; Straub, F. B., The Enzymatic Reactivation of Reduced Ribonuclease. *Biochim. Biophys. Acta* 1963, 67, 166-168.

4. Goldberger, R. F.; Epstein, C. J.; Anfinsen, C. B., Acceleration of Reactivation of Reduced Bovine Pancreatic Ribonuclease by a Microsomal System from Rat Liver. *J. Biol. Chem.* 1963, 238, 628-635.

5. Hawkins, H. C.; Freedman, R. B., Randomly Reoxidised Soybean Trypsin Inhibitor and the Possibility of Conformational Barriers to Disulphide Isomerization in Proteins. *FEBS Lett.* 1975, 58, 7-11.

6. Appenzeller-Herzog, C.; Ellgaard, L., The Human PDI Family: Versatility Packed into a Single Fold. *Biochimica et Biophysica Acta* 2008, 1783, 535-548.

7. Lu, J.; Holmgren, A., The Thioredoxin Superfamily in Oxidative Protein Folding. *Antioxid. Redox Signaling* 2014, 21, 457-470.

8. Peaper, D. R.; Cresswell, P., Regulation of MHC Class I Assembly and Peptide Binding. *Annu. Rev. Cell Dev. Biol.* 2008, 24, 343-368.

9. Janiszewski, M.; Lopes, L. R.; Carmo, A. O.; Pedro, M. A.; Brandes, R. P.; Santos, C. X. C.; Laurindo, F. R. M., Regulatio of NAD(P)H Oxidase by Associated Protein Disulfide Isomerase in Vascular Smooth Muscle Cells. *J. Biol. Chem.* 2005, 280, 40813-40819.

10. Koivu, J.; Myllyla, R.; Helaakoski, T.; Pihlajaniemi, T.; Tasanen, K.; Kivirkko, K. I., A Single Polypeptide Acts Both as the B Subunit of Prolyl-5-Hydrolase and as a Protein Disulfide-Isomerase. *J. Biol. Chem.* 1987, 262, 6447-6449.

11. Wetterau, J. R.; Combs, K. A.; McLean, L. R.; Spinner, S. N.; Aggerbeck, L. P., Protein Disulfide Isomerase Appears Necessary to Maintain Catalytically Active Structure of Microsomal Triglyceride Transfer Protein. *Biochemistry* 1991, 30, 9728-9735.

12. Jiang, X.-M.; Fitzgerald, M.; Grant, C. M.; Hogg, P. J., Redox Control of Exofacial Protein Thiols/Disulfides by Protein Disulfide Isomerase. *J. Biol. Chem.* 1999, 274, 2416-2423.

13. Donoghue, N.; Yam, P. T. W.; Jiang, X.-M.; Hogg, P. J., Presence of Closely Spaced Protein Thiols on the Surface of Mammalian Cells. *Protein Sci.* 2000, 9, 2436-2445.

14. Terada, K.; Manchikalapudi, P.; Noiva, R.; Jauregui, H. O.; Stockert, R. J.; Schilsky, M. L., Secretion Surface Localization, Turnover, and Steady State Expression of Protein Disulfide Isomerase in Rat Hepatocytes. *J. Biol. Chem.* 1995, 270, 20410-20416.

15. Bi, S.; Hong, P. W.; Lee, B.; Baum, L. G., Galectin-9 Binding to Cell Surface Protein Disulfide Isomerase Regulates the Redox Environment to Enhance T-Cell Migration and HIV Entry. *Proc. Natl. Acad. Sci. U. S. A.* 2011, 108, 10650-10655.

16. Willems, S. H.; Tape, C. J.; Stanley, P. L.; Taylor, N. A.; Mills, I. G.; Neal, D. E.; McCafferty, J.; Murphy, G., Thiol Isomerases Negatively Regulate the Cellular Shedding Activity of ADAM17. *Biochem. J.* 2010, 428, 439-450.

17. Popescu, N. I.; Lupu, C.; Lupu, F., Extracellular Protein Disulfide Isomerase Regulates Coagulation of Endothelial Cells Through Modulation of Phosphatidylserine Exposure. *Blood* 2010, 116, 993-1001.

18. Reinhardt, C.; von Bruehl, M.-L.; Manukyan, D.; Grahl, L.; Lorenz, M.; Altmann, B.; Dlugai, S.; Hess, S.; Korand, I.; Orschiedt, L.; Mackman, N.; Ruddock, L.; Massberg, S.; Engelmann, B., Protein Disulfide Isomerase Acts As An Injury Response Signal that Enhances Fibrin Generation Via Tissue Factor Activation. *J. Clin. Invest.* 2008, 118, 1110-1122.

19. Lahav, J.; Wijnen, E. M.; Hess, O.; Hamaia, S. W.; Griffiths, D.; Makris, M.; Knight, C. G.; Essex, D. W.; Farndale, R. W., Enzymatically Catalyzed Disulfide Exchange is Required for Platelet Adhesion to Collagen Via Integrin a2B1. *Blood* 2003, 102, 2085-2092.

20. Essex, D. W.; Li, M., Protein Disulphide Isomerase Mediates Platelet Aggregation and Secretion. *Br. J. Haematol.* 1999, 104, 448-454.

21. Essex, D. W.; Li, M.; Miller, A.; Feinman, R. D., Protein Disulfide Isomerase and Sulfhydryl-Dependent Pathways in Platelet Activation. *Biochemistry* 2001, 40, 6070-6075.

22. Cho, J.; Furie, B. C.; Coughlin, S. R.; Furie, B., A Critical Role for Extracellular Protein Disulfide Isomerase During Thrombus Formation in Mice. *J. Clin. Invest.* 2008, 118, 1123-1131.

23. Raturi, A.; Ruf, W., Effect of Protein Disulfide Isomerase Chaperone Activity Inhibition on Tissue Factor Activity. *J. Thromb. Haemost.* 2010, 8, 1863-1865.

24. Flaumenhaft, R., Protein Disulfide Isomerase as an Antithrombotic Target. *Trends Cardiovasc. Med.* 2013, 23, 264-268.

25. Goplen, D.; Wang, J.; Enger, P. O.; Tysnes, B. B.; Terzis, A. J. A.; Laerum, O. D.; Bjerkvig, R., Protein Disulfide Isomerase Expression Is Related to the Invasive Properties of Malignant Glioma. *Cancer Res.* 2006, 66, 9895-9902.

26. Jain, S.; McGinnes, L. W.; Morrison, T. G., Thiol/Disulfide Exchange is Required for Membrane Fusion Directed by the Newcastle Disease Virus Fusion Protein. *J. Virol.* 2007, 81, 2328-2339.

27. Ramachandran, N.; Root, P.; Jiang, X.-M.; Hogg, P. J.; Mutus, B., Mechanism of Transfer of NO From Extracellular S-Nitrosothiols into the Cytosol by Cell-Surface Protein Disulfide Isomerase. *Proc. Natl. Acad. Sci. U. S. A.* 2001, 98, 9539-9544.

28. Stolf, B. S.; Ioannis, S.; Lopes, L. R.; Vendramin, A.; Goto, H.; Laurindo, F. R. M.; Shah, A. M.; Santos, C. X. C., Protein Disulfide Isomerase and Host-Pathogen Interaction.

29. Gallina, A.; Hanley, T. M.; Mandel, R.; Trahey, M.; Broder, C. C.; Viglianti, G. A.; Ryser, H. J.-P., Inhibitors of Protein-Disulfide Isomerase Prevent Cleavage of Disulfide Bonds in Receptor-Bound Glycoprotein 120 and Prevent HIV-1 Entry. *J. Biol. Chem.* 2002, 277, 50579-50588.

30. Barbouche, R.; Miquelis, R.; Jones, I. M.; Fenoillet, E., Protein-Disulfide Isomerase-Mediated Reduction of Two Disulfide Bonds in HIV Envelope Glycoprotein 120 Occurs Post-CXCR4 and Is Required for Fusion. *J. Biol. Chem.* 2003, 278, 3131-3136.

31. Ryser, H. J.-P.; Fluckiger, R., Progress In Targeting HIV-1 Entry. *Drug Discov. Today* 2005, 10, 1085-1094.

32. Rigobello, M. P.; Donella-Deana, A.; Cesaro, L.; Bindoli, A., Distribution of Protein Disulfide Isomerase in Rat Liver Mitochondria. *Biochem. J.* 2001, 356, 567-570.

33. Turano, C.; Coppari, S.; Altieri, F.; Ferraro, A., Proteins of the PDI Family: Unpredicted Non-ER Locations and Functions. *J. Cell. Physiol.* 2002, 193, 154-163.

34. Wang, C.; Li, W.; Ren, J.; Fang, J.; Ke, H.; Gong, W.; Feng, W.; Wang, C.-C., Structural Insights Into the Redox-Regulated Dynamic Conformations of Human Protien Disulfide Isomerase. *Antioxid. Redox Signal.* 2013, 19, 36-45.

35. Ruddock, L. W.; Hirst, T. R.; Freedman, R. B., pH-Dependence of the Dithiol-Oxidizing Activity of DsbA (A Periplasmic Protein Thiol:Disulfide Oxidoreductase) and Protein Disulfide-Isomerase: Studies With a Novel Simple Peptide Substrate. *Biochem. J.* 1996, 315, 1001-1005.

36. Kortemme, T.; Darby, N. J.; Creighton, T. E., Electrostatic Interactions In the Active Site of the N-Terminal Thioredoxin-Like Domain of Protein Disulfide Isomerase. *Biochemistry* 1996, 35, 14503-14511.

37. Lappi, A. K.; Lensink, M. F.; Alanen, H. I.; Salo, K. E. H.; Lobell, M.; Juffer, A. H.; Ruddock, L. W., A Conserved Arginine Plays a Role in the Catalytic Cycle of the Protein Disulphide Isomerases. *J. Mol. Biol.* 2003, 335, 283-295.

38. Walker, K. M.; Lyles, M. M.; Gilbert, H. F., Catalysis of Oxidative Protein Folding by Mutants of Protein Disulfide Isomerase with a Single Active-Site Cysteine. *Biochemistry* 1996, 35, 1972-1980.

39. Karala, A.-R.; Lappi, A.-K.; Ruddock, L. W., Modulation of an Active-Site Cysteine pKa Allows PDI to Act as a Catalyst of Both Disulfide Bond Formation and Isomerization. *J. Mol. Biol.* 2010, 396, 883-892.

40. Lyles, M. M.; Gilbert, H. F., Mutations in the Thioredoxin Sites of Protein Disulfide Isomerase Reveal Functional Nonequivalence of the N- and C-terminal Domains. *J. Biol. Chem.* 1994, 269, 30946-30952.

41. Klappa, P.; Ruddock, L. W.; Darby, N. J.; Freedman, R. B., The b' Domain Provides the Principal Peptide-Binding Site of Protein Disulfide Isomerase But All Domains Contribute to Binding of Misfolded Proteins. *EMBO J.* 1998, 17, 927-935.

42. Karala, A. R.; Ruddock, L. W., Bacitracin is Not a Specific Inhibitor of Protein Disulfide Isomerase. *FEBS J.* 2010, 277, 2454-2462.

43. Quan, H.; Fan, G.; Wang, C.-C., Independence of the Chaperone Activity of Protein Disulfide Isomerase From Its Thioredoxin-Like Active Site. *J. Biol. Chem.* 1995, 270, 17078-17080.

44. Pirneskoski, A.; Ruddock, L. W.; Klappa, P.; Freedman, R. B.; Kivirikko, K. I.; Koivunen, P., Domains B' and A' of Protein Disulfide Isomerase Fulfill the Minimum Requirement for Function as a Subunit of Prolyl-4-Hydroxylase. The N-Terminal Domains A and B Enhance This Function and Can Be Substituted In Part By Those of ERp57. *J. Biol. Chem.* 2001, 276, 11287-11293.

45. Wilkinson, B.; Gilbert, H. F., Protein Disulfide Isomerase. *Biochim. et Biophys. Acta* 2004, 1699, 35-44.

46. Gilbert, H. F., Thiol/Disulfide Exchange and Redox Potentials of Proteins. In *Bioelectrochemistry of Biomacromolecules*, Lenaz, G.; Milazzo, G., Eds. Birkhauser Verlag: Basel, Switzerland, 1997; pp 256-324.

47. Gross, E.; Sevier, C. S.; Heldman, N.; Vitu, E.; Bentzur, M.; Kaiser, C. A.; Thorpe, C.; Fass, D., Generating Disulphides Enzymatically: Reaction Products and Electron Acceptors of the Endoplasmic Reticulum Thiol Oxidase Ero1p. *Proc. Natl. Acad. Sci. U.S.A.* 2006, 103, 299-304.

48. Walker, K. W.; Gilbert, H. F., Scanning and Escape During Protein Disulfide Isomerase-Assisted Protein Folding. *J. Biol. Chem.* 1997, 272, 8845-8848.

49. Jansens, A.; van Duijn, E.; Braakman, I., Coordinated Nonvectorial Folding in a Newly Synthesized Multidomain Protein. *Science* 2002, 298, 2401-2403.

50. Mezghrani, A.; Fassio, A.; Benham, A.; Simmen, T.; Braakman, I.; Sitia, R., Manipulation of Oxidative Protein Folding and PDI Redox State In Mammalian Cells. *EMBO J.* 2001, 20, 6288-6296.

51. Appenzeller-Herzog, C.; Riemer, J.; Zito, E.; Chin, K.-T.; Ron, D.; Spiess, M.; Ellgaard, L., Disulphide Production By Ero1a-PDI Relay is Rapid and Effectively Regulated. *EMBO J.* 2010, 29, 3318-3329.

52. Wang, L.; Li, S.-J.; Sidhu, A.; Zhu, L.; Liang, Y.; Freedman, R. B.; Wang, C.-C., Reconstitution of Human Ero1-La/Protein-Disulphide Isomerase Oxidative Folding Pathway In Vitro: Position-Dependent In Role Between the A and A' Domains of Protein-Disulphide Isomerase. *J. Biol. Chem.* 2009, 284, 199-206.

53. Laurindo, F. R. M.; Pescatore, L. A.; Fernandes, D. C., Protein Disulfide Isomerase In Redox Cell Signaling and Homeostasis. *Free Radic. Biol. Med.* 2012, 52, 1954-1969.

54. Townsend, D. M.; Manevich, Y.; He, L.; Xiong, Y.; Bowers Jr, R. R.; Hutchens, S.; Tew, K. D., Nitrosative Stress-Induced S-Glutathionylation of Protein Disulfide Isomerase Leads to Activation of the Unfolded Protein Response. *Cancer Res.* 2009, 69, 7626-7634.

55. Xiong, Y.; Manevich, Y.; Tew, K. D.; Townsend, D. M., S-Glutathionylation of Protein Disulfide Isomerase Regulates Estrogen Receptor A Stability and Function. *Int. J. Cell Biol.* 2012, 273549.

56. Uys, J. D.; Xiong, Y.; Townsend, D. M., Nitrosative Stress-Induced S-Glutathionylation of Protien Disulfide Isomerase. *Methods Enzymol.* 2011, 490, 321-332.

57. Uehara, T.; Nakamura, T.; Yao, D.; Shi, Z.-Q.; Gu, Z.; Ma, Y.; Masliah, E.; Nomura, Y.; Lipton, S. A., S-Nitrosylated Protien-Disulphide Isomerase Links Protein Misfolding to Neurodegeneration. *Nature* 2006, 441, 513-517.

58. Muller, C.; Bandemer, J.; Vindis, C.; Camare, C.; Mucher, E.; Gueraud, F.; Larroque-Cardoso, P.; Bernis, C.; Auge, N.; Salvayre, R.; Negre-Salvayre, A., Protein Disulfide Isomerase Modification and Inhibition to ER Stress and Apoptosis Induced by Oxidized Low Densisty Lipoproteins. *Antioxid. Redox Signal.* 2013, 18, 731-742.

59. Schroder, M.; Kaufman, R. J., The Mammalian Unfolded Protein Response. *Annu. Rev. Biochem.* 2005, 74, 739-789.

60. Hotamisligil, G. S., Endoplasmic Reticulum Stress and the Inflammatory Basis of Metabolic Disease. *Cell* 2010, 140, 900-917.

61. Harding, H. P.; Zhang, Y.; Bertolotti, A.; Zeng, H.; Ron, D., Perk is Essential for Translational Regulation and Cell Survival During the Unfolded Protein Response. *Mol. Cell* 2000, 5, 897-904.

62. Yoshida, H.; Matsui, T.; Yamamoto, A.; Okada, T.; Mori, K., XBP1 mRNA is Induced By ATF6 and Spliced By IRE1 In Response to ER Stress to Produce a Highly Active Transcription Factor. *Cell* 2001, 107, 881-891.

63. Schindler, A. J.; Schekman, R., In Vitro Reconstitution of ER-Stress Induced ATF6 Transport in COPII Vesicles. *Proc. Natl. Acad. Sci. U.S.A.* 2009, 106, 17775-17780.

64. Rickman, D. S.; Bobek, M. P.; Misek, D. E.; Kuick, R.; Blaivas, M.; Kurnit, D. M.; Taylor, J.; Hanash, S. M., Distinctive Molecular Profiles of High-Grade and Low-Grade Gliomas Based on Oligonucleotide Microarray Analysis. *Cancer Res.* 2001, 61, 6885-6891.

65. Gutmann, D. H.; Hedrick, N. M.; Li, J.; Nagarajan, R.; Perry, A.; Watson, M. A., Comparative Gene Expression Profile Analysis of Neurofibromatosis 1-Associated Sporadic Astrocytomas. *Cancer Res.* 2002, 62, 2085-2091.

66. Network, C. G. A. R., Comprehensive Genomic Characterization Defines Human Glioblastoma Genes and Core Pathways. *Nature* 2008, 455, 1061-1068.

67. Shai, R.; Shi, T.; Kremen, T. J.; Horvath, S.; Liau, L. M.; Cloughesy, T. F.; Mischel, P. S.; Nelson, S. F., Gene Expression Profiling Identifies Molecular Subtypes of Gliomas. *Oncogene* 2003, 22, 4918-4923.

68. Sun, L.; Hui, A.-M.; Su, Q.; Vortmeyer, A.; Kotliarov, Y.; Pastorino, S.; Passaniti, A.; Menon, J.; Walling, J.; Bailey, R.; Rosenblum, M.; Mikkelsen, T.; Fine, H.

A., Neuronal and Glioma-Derived Stem Cell Factor Induces Angiogenesis Within the Brain. *Cancer Cell* 2006, 9, 287-300.

69. Bredel, M.; Bredel, C.; Juric, D.; Harsh, G. R.; Vogel, H.; Recht, L. D.; Sikic, B. I., Functional Network Analysis Reveals Extended Gliomagenesis Pathway Maps and Three Novel MYC-Interacting Genes in Human Gliomas. *Cancer Res.* 2005, 65, 8679-8689.

70. Basso, K.; Margolin, A. A.; Stolovitzky, G.; Klein, U.; Dalla-Favera, R.; Califano, A., Reverse Engineering of Regulatory Networks in Human B Cells. *Nat. Genet.* 2005, 37, 382-390.

71. Compagno, M.; Lim, W. K.; Grunn, A.; Nandula, S. V.; Brahmachary, M.; Shen, Q.; Bertoni, F.; Ponzoni, M.; Scandurra, M.; Califano, A.; Bhagat, G.; Chadburn, A.; Dalla-Favera, R.; Pasqualucci, L., Mutations of Multiple Genes Cause Deregulation of NF-κB in Diffuse Large B-Cell Lymphoma. *Nature (London, U. K.)* 2009, 459, 717-721.

72. Piccaluga, P. P.; Agostinelli, C.; Califano, A.; Rossi, M.; Basso, K.; Zupo, S.; Went, P.; Klein, U.; Zinzani, P. L.; Baccarani, M.; Dalla Favera, R.; Pileri, S. A., Gene Expression Analysis of Peripheral T Cell Lymphoma, Unspecified, Reveals Distinct Profiles and New Potential Therapeutic Targets. *J. Clin. Invest.* 2007, 117, 823-834.

73. Yusenko, M. V.; Kuiper, R. P.; Boethe, T.; Ljungberg, B.; van, K. A. G.; Kovacs, G., High-Resolution DNA Copy Number and Gene Expression Analyses Distinguish Chromophobe Renal Cell Carcinomas and Renal Oncocytomas. *BMC Cancer* 2009, 9, 152.

74. Beroukhim, R.; Brunet, J.-P.; Di Napoli, A.; Mertz, K. D.; Seeley, A.; Pires, M. M.; Linhart, D.; Worrell, R. A.; Moch, H.; Rubin, M. A.; Sellers, W. R.; Meyerson, M.;

Linehan, W. M.; Kaelin, W. G., Jr.; Signoretti, S., Patterns of Gene Expression and Copy-Number Alterations in von-Hippel Lindau Disease-Associated and Sporadic Clear Cell Carcinoma of the Kidney. *Cancer Res.* 2009, 69, 4674-4681.

75. Jones, J.; Otu, H.; Spentzos, D.; Kolia, S.; Inan, M.; Beecken, W. D.; Fellbaum, C.; Gu, X.; Joseph, M.; Pantuck, A. J.; Jonas, D.; Libermann, T. A., Gene Signatures of Progression and Metastasis in Renal Cell Cancer. *Clin. Cancer Res.* 2005, 11, 5730-5739.

76. Bonome, T.; Levine, D. A.; Shih, J.; Randonovich, M.; Pise-Masison, C. A.; Bogomolniy, F.; Ozbun, L.; Brady, J.; Barrett, J. C.; Boyd, J.; Birrer, M. J., A Gene Signature Predicting for Survival in Suboptimally Debulked Patients with Ovarian Cancer. *Cancer Res.* 2008, 68, 5478-5486.

77. Welsh, J. B.; Zarrinkar, P. P.; Sapinoso, L. M.; Kern, S. G.; Behling, C. A.; Monk, B. J.; Lockhart, D. J.; Burger, R. A.; Hampton, G. M., Analysis of Gene Expression Profiles in Normal and Neoplastic Ovarian Tissue Samples Identifies Candidate Molecular Markers of Epithelial Ovarian Cancer. *Proc. Natl. Acad. Sci. U. S. A.* 2001, 98, 1176-1181.

78. Welsh, J. B.; Sapinoso, L. M.; Su, A. I.; Kern, S. G.; Wang-Rodriguez, J.; Moskaluk, C. A.; Frierson, H. F., Jr.; Hampton, G. M., Analysis of Gene Expression Identifies Candidate Markers and Pharmacological Targets in Prostate Cancer. *Cancer Res.* 2001, 61, 5974-5978.

79. Singh, D.; Febbo, P. G.; Ross, K.; Jackson, D. G.; Manola, J.; Ladd, C.; Tamayo, P.; Renshaw, A. A.; D'Amico, A. V.; Richie, J. P.; Lander, E. S.; Loda, M.; Kantoff, P. W.; Golub, T. R.; Sellers, W. R., Gene Expression Correlates of Clinical Prostate Cancer Behavior. *Cancer Cell* 2002, 1, 203-209.

80. Beer, D. G.; Kardia, S. L. R.; Huang, C.-C.; Giordano, T. J.; Levin, A. M.; Misek, D. E.; Lin, L.; Chen, G.; Gharib, T. G.; Thomas, D. G.; Lizyness, M. L.; Kuick, R.; Hayasaka, S.; Taylor, J. M. G.; Iannettoni, M. D.; Orringer, M. B.; Hanash, S., Gene-Expression Profiles Predict Survival of Patients with Lung Adenocarcinoma. *Nat. Med. (N. Y., NY, U. S.)* 2002, 8, 816-824.

81. Korkola, J. E.; Houldsworth, J.; Chadalavada, R. S. V.; Olshen, A. B.; Dobrzynski, D.; Reuter, V. E.; Bosl, G. J.; Chaganti, R. S. K., Down-Regulation of Stem Cell Genes, Including Those in a 200-kb Gene Cluster at 12p13.31, Is Associated with In Vivo Differentiation of Human Male Germ Cell Tumors. *Cancer Res.* 2006, 66, 820-827.

82. Chahed, K.; Kabbage, M.; Ehret-Sabatier, L.; Lemaitre-Guillier, C.; Remadi, S.; Hoebeke, J.; Chouchane, L., Expression of Fibrinogen E-Fragment and Fibrin E-Fragment is Inhibited in the Human Infiltrating Ductal Carcinoma of the Breast: The Two-Dimensional Electrophoresis and MALDI-TOF-Mass Spectrometry Analyses. *Int. J. Oncol.* 2005, 27, 1425-1431.

83. Chahed, K.; Kabbage, M.; Hamrita, B.; Guillier, C. L.; Trimeche, M.; Remadi, S.; Ehret-Sabatier, L.; Chouchane, L., Detection of Protein Alterations in Male Breast Cancer Using Two Dimensional Gel Electrophoresis and Mass Spectrometry: The Involvement of Several Pathways in Tumorigenesis. *Clin. Chim. Acta* 2008, 388, 106-114.

84. Thongwatchara, P.; Promwikorn, W.; Srisomsap, C.; Chokchaichamnankit, D.; Boonyaphiphat, P.; Thongsuksai, P., Differential Protein Expression in Primary Breast Cancer and Matched Axillary Node Metastasis. *Oncol. Rep.* 2011, 26, 185-191.

85. van de Vijver, M. J.; He, Y. D.; van 't Veer, L.; Dai, H.; Hart, A. A. M.; Voskuil, D. W.; Schreiber, G. J.; Peterse, J. L.; Roberts, C.; Marton, M. J.; Parrish, M.; Atsma, D.; Witteveen, A.; Glas, A.; Delahaye, L.; van der Velde, T.; Bartelink, H.; Rodenhuis, S.; Rutgers, E. T.; Friend, S. H.; Bernards, R., A Gene-Expression Signature As a Predictor of Survival in Breast Cancer. *N. Engl. J. Med.* 2002, 347, 1999-2009.

86. Gonzalez-Santiago, L.; Alfonso, P.; Suarez, Y.; Nunez, A.; Garcia-Fernandez, L. F.; Alvarez, E.; Munoz, A.; Casal, J. I., Proteomic Analysis of the Resistance to Aplidin in Human Cancer Cells. *J. Proteome Res.* 2007, 6, 1286-1294.

87. Eirich, J.; Braig, S.; Schyschka, L.; Servatius, P.; Hoffmann, J.; Hecht, S.; Fulda, S.; Zahler, S.; Antes, I.; Kazmaier, U.; Sieber, S. A.; Vollmar, A. M., A Small Molecule Inhibits Protein Disulfide Isomerase and Triggers the Chemosensitization of Cancer Cells. *Angew. Chem., Int. Ed.* 2014, 53, 12960-12965.

88. Xu, S.; Butkevich, A. N.; Yamada, R.; Zhou, Y.; Debnath, B.; Duncan, R.; Zandi, E.; Petasis, N.; Neamati, N., Discovery of an Orally Active Small-Molecule Irreversible Inhibitor of Protein Disulfide Isomerase for Ovarian Cancer Treatment. *Proc. Natl. Acad. Sci. USA* 2012, 109, 16348-16353.

89. Hoffstrom, B. G.; Kaplan, A.; Letso, R.; Schmid, R. S.; Turmel, G. J.; Lo, D. C.; Stockwell, B. R., Inhibitors of Protein Disulfide Isomerase Suppress Apoptosis Induced by Misfolded Proteins. *Nat. Chem. Biol.* 2010, 6, 900-906.

90. Banerjee, R.; Pace, N. J.; Brown, D. R.; Weerapana, E., 1,3,5-Triazine As a Modular Scaffold For Covalent Inhibitors With Streamlined Target Identification. *J. Am. Chem. Soc.* 2013, 135, 2497-2500.

91. Ge, J.; Zhang, C.-J.; Li, L.; Chong, L. M.; Wu, X.; Hao, P.; Sze, S. K.; Yao, S. Q., Small Molecule Probe suitable For In Situ Profiling and Inhibition of Protein Disulfide Isomerase. *ACS Chem. Biol.* 2013, 8, 2577-2585.

92. Mandel, R.; Ryser, H. J.; Ghani, F.; Wu, M.; Peak, D., Inhibition of a Reductive Function of the Plasma Membrane by Bacitracin and Antibodies Against Protein Disulfide-Isomerase. *Proc. Natl. Acad. Sci. U. S. A.* 1993, 90, 4112-16.

93. Liu, X.-W.; Sok, D.-E., Inactivation of Protein Disulfide Isomerase By Alkylators Including α,β-Unsaturated Aldehydes at Low Physiological pHs. *Biol. Chem.* 2004, 385, 633-637.

94. Khan, M. M. G.; Simizu, S.; Lai, N.-S.; Kawatani, M.; Shimizu, T.; Osada, H., Discovery of a Small Molecule PDI Inhibitor That Inhibits Reduction of HIV-1 Envelope Glycoprotein gp120. *ACS Chem. Biol.* 2011, 6, 245-251.

95. Roth, R. A.; Mesirow, M. L., Bacitracin: An Inhibitor of the Insulin Degrading Activity of Glutathione-Insulin Transhydrogenase. *Biochem. Biophys. Res. Commun.* 1981, 98, 431-8.

96. Horibe, T.; Nagai, H.; Sakakibara, K.; Hagiwara, Y.; Kikuchi, M., Ribostamycin Inhibits the Chaperone Activity of Protein Disulfide Isomerase. *Biochem. Biophys. Res. Commun.* 2001, 289, 967-972.

97. Berridge, M. V.; Herst, P. M.; Tan, A. S., Tetrazolium Dyes As Tools in Cell biology: New Insights Into Their Cellular Reduction. *Biotechnol. Annu. Rev.* 2005, 11, 127-152.

98. Yamaguchi, H.; Wyckoff, J.; Condeelis, J., Cell Migration In Tumors. *Curr. Opin. Cell Biol.* 2005, 17, 559-564.

99. Chambers, A. F.; Groom, A. C.; MacDonald, I. C., Metastasis: Dissemination and Growth of Cancer Cells in Metastatic Sites. *Nat. Rev. Cancer* 2002, 2, 563-572.

100. Friedl, P.; Wolf, K., Tumor-Cell Invasion and Migration: Diversity and Escape Mechanisms. *Nat. Rev. Cancer* 2003, 3, 362-374.

101. Wang, W.; Goswami, S.; Lapidus, K.; Wells, A. L.; Wyckoff, J. B.; Sahai, E.; Singer, R. H.; Segall, J. E.; Condeelis, J. S., Identification and Testing of a Gene Expression Signature of Invasive Carcinoma Cells Within Primary Mammary Tumors. *Cancer Res.* 2004, 64, 8585-8594.

102. Wang, W.; Goswami, S.; Sahai, E.; Wyckoff, J. B.; Segall, J. E.; Condeelis, J. S., Tumor Cells Caught In the Act of Invading: Their Strategy For Enhanced Cell Motility. *Trends Cell Biol.* 2005, 15, 138-145.

103. Kramer, N.; Walzl, A.; Unger, C.; Rosner, M.; Krupitza, G.; Hengstschlaeger, M.; Dolznig, H., *In Vitro* Cell Migration and Invasion Assays. *Mutat. Res., Rev. Mutat. Res.* 2013, 752, 10-24.

104. Friedl, P.; Wolf, K., Plasticity of Cell Migration: A Multiscale Tuning Model. *J. Cell Biol.* 2010, 188, 11-19.

105. Couvertier, S. M.; Weerapana, E., Cysteine-Reactive Chemical Probes Based On a Modular 4-Aminopiperidine Scaffold. *MedChemComm* 2014, 5, 358-362.

106. Bachovchin, D. A.; Zuhl, A. M.; Speers, A. E.; Wolfe, M. R.; Weerapana, E.; Brown, S. J.; Rosen, H.; Cravatt, B. F., Discovery and Optimization of Sulfonyl Acrylonitriles as Selective, Covalent Inhibitors of Protein Phosphatase Methylesterase-1. *J. Med. Chem.* 2011, 54, 5229-5236.

107. Lyles, M. M.; Gilbert, H. F., Catalysis of the Oxidative Folding of Ribonuclease A by Protein Disulfide Isomerase: Dependence of the Rate on the Composition of the Redox Buffer. *Biochemistry* 1991, 30, 613-19.

108. Shoulders, M. D.; Ryno, L. M.; Genereux, J. C.; Moresco, J. J.; Tu, P. G.; Wu, C.; Yates III, J. R.; Su, A. I.; Kelly, J. W.; Wiseman, R. L., Stress-Independent Activation of XBP1s and/or ATF6 Reveals Three Functionally Diverse ER Proteostasis Environments. *Cell Reports* 2013, 3, 1279-1292.

109. Lee, A.-H.; Iwakoshi, N. N.; Glimcher, L. H., XBP-1 Regulates a Subset of Endoplasmic Reticulum Resident Chaperone Genes In the Unfolded Protein Response. *Mol. Cell. Biol.* 2003, 23, 7448-7459.

110. Banaszynski, L. A.; Chen, L.-c.; Maynard-Smith, L. A.; Ooi, A. G. L.; Wandless, T. J., A Rapid, Reversible, and Tunable Method to Regulate Protein Function in Living Cells Using Synthetic Small Molecules. *Cell (Cambridge, MA, U. S.)* 2006, 126, 995-1004.

111. Iwamoto, M.; Bjoerklund, T.; Lundberg, C.; Kirik, D.; Wandless, T. J., A General Chemical Method to Regulate Protein Stability in the Mammalian Central Nervous System. *Chem. Biol. (Cambridge, MA, U. S.)* 2010, 17, 981-988.

Appendix I

NMR Data

3-(trityloxy)propan-1-ol (NJP11)

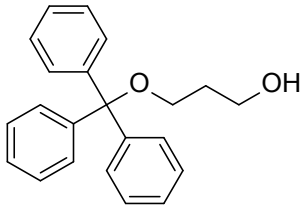

^{1}H-NMR

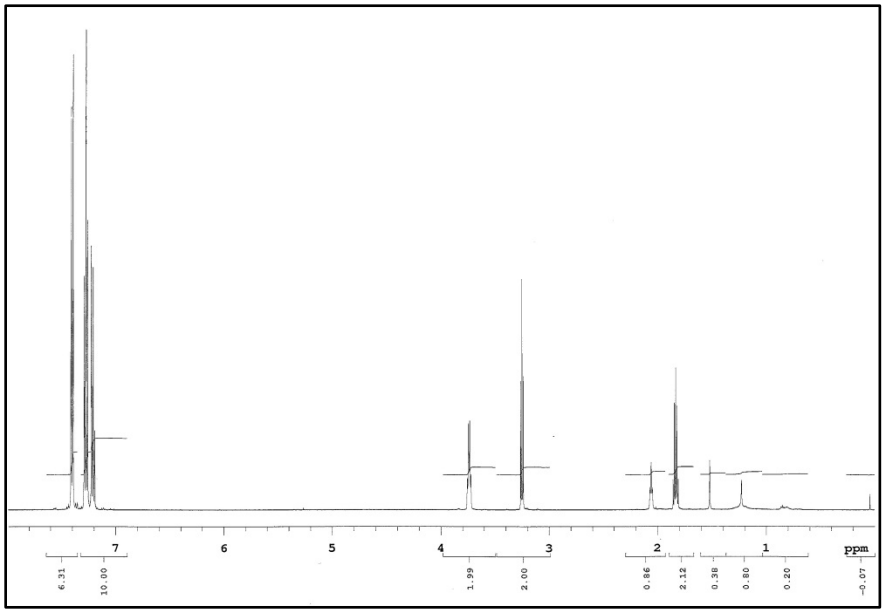

^{13}C-NMR

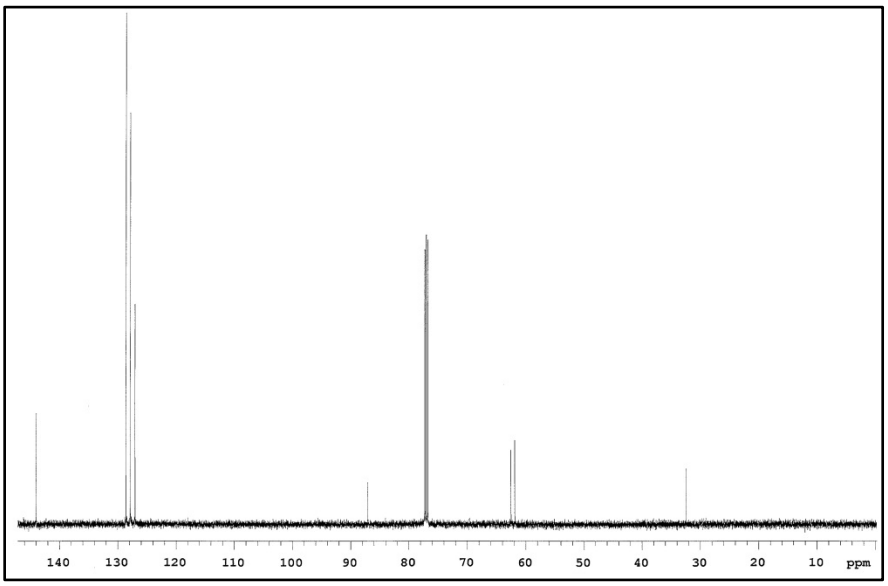

3-(trityloxy)propanoic acid (NJP12)

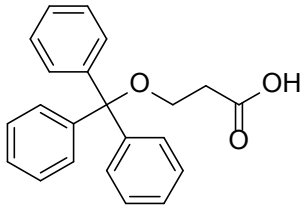

^{1}H-NMR

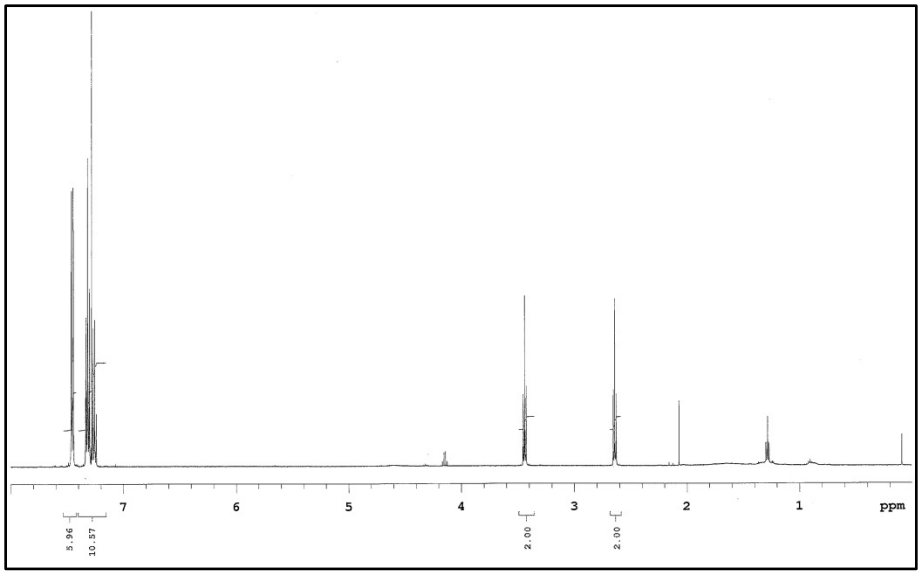

^{13}C-NMR

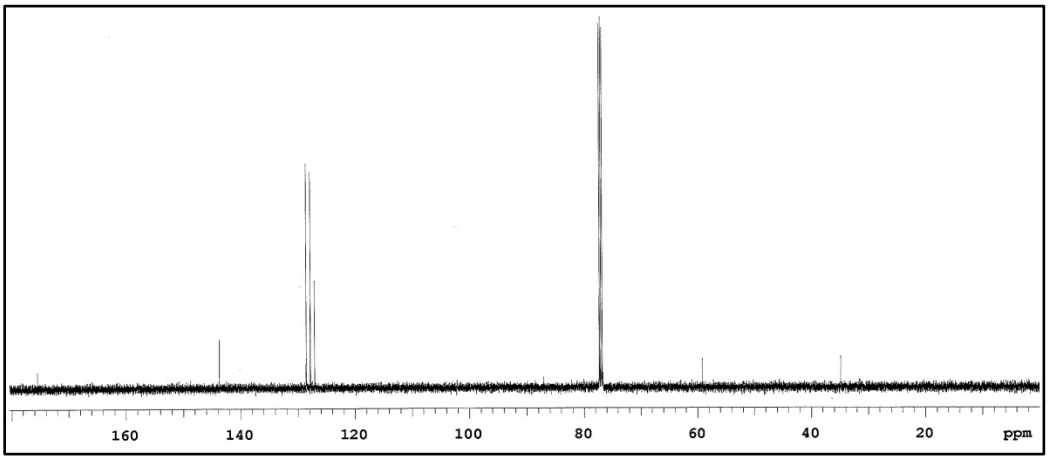

Appendix II

Mass spectrometry tables

Table 3A-1. Tryptic digests of HeLa lysates treated +/- NJP14.

Protein	Mol Weight (Da)	Average Spectral counts		% Change
		Ctrl	NJP14	
IPI00793953 - Gene_Symbol=TUBA8 Putative uncharacterized protein DKFZp686L04275 (Fragment)	53969	0.00	146.33	100.00
IPI00787158 - Gene_Symbol=SORD similar to sorbitol dehydrogenase	38687	0.00	126.00	100.00
IPI00023598 - Gene_Symbol=TUBB4 Tubulin beta-4 chain	49586	0.00	124.00	100.00
IPI00019755 - Gene_Symbol=GSTO1 Glutathione transferase omega-1	27566	0.00	76.00	100.00
IPI00013871 - Gene_Symbol=RRM1 Ribonucleoside-diphosphate reductase large subunit	90070	0.00	43.00	100.00
IPI00303568 - Gene_Symbol=PTGES2 Prostaglandin E synthase 2	41943	0.00	39.00	100.00
IPI00009904 - Gene_Symbol=PDIA4 Protein disulfide-isomerase A4 precursor	72933	0.00	28.00	100.00
IPI00219575 - Gene_Symbol=BLMH Bleomycin hydrolase	52562	0.67	164.67	99.60
IPI00010796 - Gene_Symbol=P4HB Protein disulfide-isomerase precursor	57116	4.67	453.67	98.97
IPI00025252 - Gene_Symbol=PDIA3 Protein disulfide-isomerase A3 precursor	56782	3.00	118.67	97.47
IPI00022977 - Gene_Symbol=CKB Creatine kinase B-type	42644	1.67	38.00	95.61
IPI00783641 - Gene_Symbol=TXNRD1 thioredoxin reductase 1 isoform 3	71153	7.67	145.67	94.74
IPI00299571 - Gene_Symbol=PDIA6 Isoform 2 of Protein disulfide-isomerase A6 precursor	53901	3.67	57.00	93.57
IPI00218343 - Gene_Symbol=TUBA1C Tubulin alpha-1C chain	49895	13.33	171.33	92.22
IPI00171438 - Gene_Symbol=TXNDC5;MUTED Thioredoxin domain-containing protein 5 precursor	47629	3.67	46.33	92.09
IPI00180675 - Gene_Symbol=TUBA1A Tubulin alpha-1A chain	50136	15.67	194.00	91.92
IPI00477531 - Gene_Symbol=DYNC1H1 532 kDa protein	532371	5.00	40.00	87.50
IPI00031370 - Gene_Symbol=TUBB2B Tubulin beta-2B chain	49953	25.67	184.00	86.05
IPI00007750 - Gene_Symbol=TUBA4A Tubulin alpha-4A chain	49924	27.67	189.67	85.41
IPI00646779 - Gene_Symbol=TUBB6 TUBB6 protein	50090	24.67	164.67	85.02
IPI00387144 - Gene_Symbol=TUBA1B Tubulin alpha-1B chain	50152	32.00	202.00	84.16
IPI00011654 - Gene_Symbol=TUBB Tubulin beta chain	49671	74.33	460.33	83.85
IPI00007752 - Gene_Symbol=TUBB2C Tubulin beta-2C chain	49831	39.33	241.33	83.70
IPI00296337 - Gene_Symbol=PRKDC Isoform 1 of DNA-dependent protein kinase catalytic subunit	469093	10.67	59.67	82.12
IPI00152453 - Gene_Symbol=TUBB3 Tubulin, beta, 4	88382	29.00	155.33	81.33
IPI00026781 - Gene_Symbol=FASN Fatty acid synthase	273397	15.33	65.67	76.65
IPI00186711 - Gene_Symbol=PLEC1 plectin 1 isoform 6	531796	9.00	35.00	74.29
IPI00472102 - Gene_Symbol=HSPD1 61 kDa protein	61213	22.67	72.00	68.52
IPI00021290 - Gene_Symbol=ACLY ATP-citrate synthase	120839	14.00	44.00	68.18
IPI00186290 - Gene_Symbol=EEF2 Elongation factor 2	95338	18.33	56.67	67.65
IPI00643920 - Gene_Symbol=TKT Transketolase	67878	16.00	49.00	67.35
IPI00480131 - Gene_Symbol=FLNB Uncharacterized protein FLNB	278188	28.00	68.00	58.82
IPI00019502 - Gene_Symbol=MYH9 Myosin-9	226530	47.33	114.67	58.72
IPI00396485 - Gene_Symbol=EEF1A1 Elongation factor 1-alpha 1	50141	30.33	68.00	55.39
IPI00472724 - Gene_Symbol=- Elongation factor 1-alpha	50185	30.33	68.00	55.39
IPI00009342 - Gene_Symbol=IQGAP1 Ras GTPase-activating-like protein IQGAP1	189251	13.00	28.00	53.57

IPI00024067 - Gene_Symbol=CLTC Isoform 1 of Clathrin heavy chain 1	191613	24.00	51.00	52.94
IPI00333541 - Gene_Symbol=FLNA Filamin-A	280737	92.00	192.33	52.17
IPI00465248 - Gene_Symbol=ENO1 Isoform alpha-enolase of Alpha-enolase	47169	22.00	44.67	50.75
IPI00848058 - Gene_Symbol=ACTB Actin, cytoplasmic 2	45086	93.33	188.67	50.53
IPI00294578 - Gene_Symbol=TGM2 Isoform 1 of Protein-glutamine gamma-glutamyltransferase 2	77329	17.33	34.67	50.00

Table 3A-2. Tryptic digests of HeLa lysates treated with +/- Zn^{2+}/Mg^{2+} followed by NJP14.

Protein	Average Spectral Counts				% Change Zn	% Change Mg
	Ctrl	Zn^{2+} 10μM	Zn^{2+} 20μM	Mg^{2+} 20μM		
IPI00787158 - Gene_Symbol=SORD similar to sorbitol dehydrogenase ENSG00000140263 IPI00216057 IPI00791243 IPI00787158 xxxxx	250	11.5	2.5	261.5	-99.00	4.40
IPI00019755 - Gene_Symbol=GSTO1 Glutathione transferase omega-1 ENSG00000148834 IPI00513927 IPI00019755 IPI00642936 xxxxx	324	268.5	23.5	266.5	-92.75	-17.75
IPI00783641 - Gene_Symbol=TXNRD1 thioredoxin reductase 1 isoform 3 ENSG00000198431 IPI00783641 IPI00743646 IPI00554786 IPI00847482 IPI00796750 IPI00797831 IPI00816732 xxxxx	535	86	42	463.5	-92.15	-13.36
IPI00013871 - Gene_Symbol=RRM1 Ribonucleoside-diphosphate reductase large subunit ENSG00000167325 IPI00013871 xxxxx	135.5	114	26	124	-80.81	-8.49
IPI00011253 - Gene_Symbol=RPS3 40S ribosomal protein S3 ENSG00000149273 IPI00011253 xxxxx	40	21	13	37.5	-67.50	-6.25
IPI00014424 - Gene_Symbol=EEF1A2 Elongation factor 1-alpha 2 ENSG00000101210 IPI00014424 xxxxx	68	44.5	25	15	-63.24	-77.94
IPI00023598 - Gene_Symbol=TUBB4 Tubulin beta-4 chain ENSG00000104833 IPI00023598 xxxxx	351	245.5	171	357.5	-51.28	1.82
IPI00294578 - Gene_Symbol=TGM2 Isoform 1 of Protein-glutamine gamma-glutamyltransferase 2 ENSG00000198959 IPI00218252 IPI00218251 IPI00294578 xxxxx	52.5	26.5	26	62.5	-50.48	16.00
IPI00396485 - Gene_Symbol=EEF1A1 Elongation factor 1-alpha 1 ENSG00000156508 IPI00853600 IPI00396485 IPI00641459 IPI00847435 IPI00431701 IPI00431441 IPI00382804 IPI00025447 xxxxx	219.5	180	132.5	123	-39.64	-43.96
IPI00472724 - Gene_Symbol=- Elongation factor 1-alpha ENSG00000185637 IPI00472724 xxxxx	219.5	180	132.5	123	-39.64	-43.96
IPI00010796 - Gene_Symbol=P4HB Protein disulfide-isomerase precursor ENSG00000185624 IPI00010796 IPI00386460 xxxxx	677	376.5	433.5	723	-35.97	6.36
IPI00329633 - Gene_Symbol=TARS Threonyl-tRNA synthetase, cytoplasmic ENSG00000113407 IPI00329633 xxxxx	37	31.5	25	28	-32.43	-24.32
IPI00026328 - Gene_Symbol=TXNDC12 Thioredoxin domain-containing protein 12 precursor ENSG00000117862 IPI00026328 xxxxx	35	39.5	24	32	-31.43	-8.57
IPI00025252 - Gene_Symbol=PDIA3 Protein disulfide-isomerase A3 precursor ENSG00000167004 IPI00657680 IPI00025252 IPI00796177 IPI00796736 IPI00790740 IPI00791418 xxxxx	321	263.5	239.5	308	-25.39	-4.05
IPI00171438 - Gene_Symbol=TXNDC5;MUTED Thioredoxin domain-containing protein 5 precursor ENSG00000188428 IPI00154778 IPI00395646 IPI00171438 IPI00646720 xxxxx	85.5	59	64	82.5	-25.15	-3.51

IPI00000875 - Gene_Symbol=EEF1G Elongation factor 1-gamma ENSG00000186676 IPI00000875 IPI00747497 IPI00738381 xxxxx	27	24.5	20.5	26	-24.07	-3.70
IPI00303568 - Gene_Symbol=PTGES2 Prostaglandin E synthase 2 ENSG00000148334 IPI00472496 IPI00303568 IPI00395565 IPI00514138 xxxxx	106	99	82.5	105	-22.17	-0.94
IPI00180730 - Gene_Symbol=- Uncharacterized protein ENSP00000333488 ENSG00000183920 IPI00180730 xxxxx	36.5	42	29	24	-20.55	-34.25
IPI00478758 - Gene_Symbol=C10orf119 Uncharacterized protein C10orf119 ENSG00000197771 IPI00478758 IPI00414458 IPI00552546 xxxxx	44.5	44.5	35.5	43.5	-20.22	-2.25
IPI00007750 - Gene_Symbol=TUBA4A Tubulin alpha-4A chain ENSG00000127824 IPI00335314 IPI00007750 IPI00794663 IPI00797717 IPI00794009 xxxxx	554	393	446.5	572.5	-19.40	3.23
IPI00216694 - Gene_Symbol=PLS3 plastin 3 ENSG00000102024 IPI00848312 IPI00216694 xxxxx	27.5	32	23	29	-16.36	5.17
IPI00013723 - Gene_Symbol=PIN1 Peptidyl-prolyl cis-trans isomerase NIMA-interacting 1 ENSG00000127445 IPI00013723 IPI00644298 IPI00446477 xxxxx	52	49	44	54.5	-15.38	4.59
IPI00301263 - Gene_Symbol=CAD CAD protein ENSG00000084774 IPI00301263 xxxxx	38.5	43	33.5	52	-12.99	25.96
IPI00477531 - Gene_Symbol=DYNC1H1 532 kDa protein ENSG00000197102 IPI00456969 IPI00477531 IPI00440177 xxxxx	76.5	83.5	67.5	93.5	-11.76	18.18
IPI00169383 - Gene_Symbol=PGK1 Phosphoglycerate kinase 1 ENSG00000102144 IPI00169383 xxxxx	35	32.5	31	34	-11.43	-2.86
IPI00793953 - Gene_Symbol=TUBA8 Putative uncharacterized protein DKFZp686L04275 (Fragment) ENSG00000183785 IPI00646909 IPI00743964 IPI00816098 IPI00792478 IPI00791613 IPI00853556 IPI00793953 xxxxx	346	248.5	311	402.5	-10.12	14.04
IPI00796333 - Gene_Symbol=ALDOA 45 kDa protein ENSG00000149925 IPI00465439 IPI00640568 IPI00642546 IPI00796333 xxxxx	28.5	35	26	23	-8.77	-19.30
IPI00784459 - Gene_Symbol=CFL1 Uncharacterized protein CFL1 ENSG00000172757 IPI00784459 IPI00012011 xxxxx	38	38	36.5	28.5	-3.95	-25.00
IPI00180675 - Gene_Symbol=TUBA1A Tubulin alpha-1A chain ENSG00000167552 IPI00180675 xxxxx	588	389	565.5	585	-3.83	-0.51
IPI00643920 - Gene_Symbol=TKT Transketolase ENSG00000163931 IPI00643920 IPI00793119 IPI00792641 IPI00789310 IPI00788802 xxxxx	110	105	107.5	88	-2.27	-20.00
IPI00011062 - Gene_Symbol=CPS1 Isoform 1 of Carbamoyl-phosphate synthase [ammonia], mitochondrial precursor ENSG00000021826 IPI00011062 IPI00397498 IPI00447499 xxxxx	60.5	61	59.5	60.5	-1.65	0.00
IPI00387144 - Gene_Symbol=TUBA1B Tubulin alpha-1B chain ENSG00000123416 IPI00387144 IPI00792677 IPI00793930 xxxxx	613.5	437	608	635.5	-0.90	3.46
IPI00418169 - Gene_Symbol=ANXA2 annexin A2 isoform 1 ENSG00000182718 IPI00418169 IPI00455315 IPI00795925 IPI00797556 IPI00798111 IPI00797581 IPI00790111 xxxxx	64	74	63.5	65.5	-0.78	2.29
IPI00019502 - Gene_Symbol=MYH9 Myosin-9 ENSG00000100345 IPI00019502 IPI00395772 IPI00556012 IPI00742780 xxxxx	231.5	267.5	235	191.5	1.49	-17.28
IPI00031370 - Gene_Symbol=TUBB2B Tubulin beta-2B chain ENSG00000137285 IPI00031370 IPI00748943 xxxxx	314.5	232.5	322.5	332.5	2.48	5.41
IPI00024067 - Gene_Symbol=CLTC Isoform 1 of Clathrin heavy chain 1 ENSG00000141367 IPI00024067 IPI00455383 xxxxx	68	92	71	77	4.23	11.69
IPI00645078 - Gene_Symbol=UBE1 Ubiquitin-activating enzyme E1 ENSG00000130985 IPI00645078 IPI00026119 IPI00641319 IPI00644183 IPI00647463 IPI00646990 IPI00552452 IPI00383182 xxxxx	41	46	43	38.5	4.65	-6.10
IPI00333541 - Gene_Symbol=FLNA Filamin-A ENSG00000196924 IPI00553169 IPI00302592 IPI00644576 IPI00333541 IPI00552858 IPI00552416 xxxxx	442.5	436.5	466.5	363	5.14	-17.97
IPI00480131 - Gene_Symbol=FLNB Uncharacterized protein FLNB ENSG00000136068 IPI00480131	85.5	112.5	91	101.5	6.04	15.76

IPI00382697 IPI00289334 IPI00382698 IPI00477536 IPI00382696 IPI00382699 IPI00382700 IPI00798140 IPI00797598 IPI00794125 IPI00798186 IPI00816637 xxxxx						
IPI00186711 - Gene_Symbol=PLEC1 plectin 1 isoform 6 ENSG00000178209 IPI00186711 IPI00398779 IPI00398777 IPI00420096 IPI00398775 IPI00398002 IPI00398778 IPI00398776 IPI00014898 xxxxx	44	44.5	47	54.5	6.38	19.27
IPI00218343 - Gene_Symbol=TUBA1C Tubulin alpha-1C chain ENSG00000167553 IPI00478908 IPI00218343 IPI00166768 IPI00795002 xxxxx	488.5	320.5	524.5	506.5	6.86	3.55
IPI00007752 - Gene_Symbol=TUBB2C Tubulin beta-2C chain ENSG00000188229 IPI00007752 xxxxx	470.5	333.5	529	506	11.06	7.02
IPI00329200 - Gene_Symbol=RANBP5 127 kDa protein ENSG00000065150 IPI00329200 IPI00793443 IPI00514205 IPI00639960 xxxxx	39.5	58.5	45.5	46.5	13.19	15.05
IPI00334775 - Gene_Symbol=HSP90AB1 85 kDa protein ENSG00000096384 IPI00414676 IPI00334775 IPI00411633 IPI00640129 IPI00515119 IPI00746291 IPI00514659 IPI00514027 xxxxx	103	105	119	103	13.45	0.00
IPI00419585 - Gene_Symbol=PPIA;LOC654188;PPIAL3 Peptidyl-prolyl cis-trans isomerase A ENSG00000196262 IPI00472718 IPI00419585 Tax_Id=9606 Gene_Symbol=PPIA;LOC654188;PPIAL3 Peptidyl-prolyl cis-trans isomerase A ENSG00000198618 IPI00419585 xxxxx	31.5	30	36.5	21.5	13.70	-31.75
IPI00219575 - Gene_Symbol=BLMH Bleomycin hydrolase ENSG00000108578 IPI00219575 IPI00794082 xxxxx	483	455	560	455	13.75	-5.80
IPI00006510 - Gene_Symbol=TUBB1 Tubulin beta-1 chain ENSG00000101162 IPI00006510 xxxxx	33.5	0	39	15	14.10	-55.22
IPI00011654 - Gene_Symbol=TUBB Tubulin beta chain ENSG00000183311 IPI00011654 Tax_Id=9606 Gene_Symbol=TUBB Tubulin beta chain ENSG00000137379 IPI00011654 Tax_Id=9606 Gene_Symbol=TUBB Tubulin beta chain ENSG00000196230 IPI00647896 IPI00011654 IPI00645452 xxxxx	839.5	627	980.5	916	14.38	8.35
IPI00298994 - Gene_Symbol=TLN1 Uncharacterized protein TLN1 ENSG00000137076 IPI00298994 IPI00385946 IPI00642355 IPI00784273 xxxxx	58	64	68	50.5	14.71	-12.93
IPI00026781 - Gene_Symbol=FASN Fatty acid synthase ENSG00000169710 IPI00026781 IPI00847250 IPI00792768 IPI00793768 IPI00795589 IPI00795588 xxxxx	220	211	260.5	197	15.55	-10.45
IPI00848058 - Gene_Symbol=ACTB Actin, cytoplasmic 2 ENSG00000075624 IPI00021439 IPI00848058 IPI00844533 xxxxx	259	216	307	218	15.64	-15.83
IPI00001159 - Gene_Symbol=GCN1L1 GCN1-like protein 1 ENSG00000089154 IPI00001159 IPI00789420 IPI00788818 xxxxx	47.5	63	56.5	57.5	15.93	17.39
IPI00646779 - Gene_Symbol=TUBB6 TUBB6 protein ENSG00000176014 IPI00646779 IPI00641706 IPI00643158 IPI00647682 IPI00646972 xxxxx	229	190.5	274	270	16.42	15.19
IPI00186290 - Gene_Symbol=EEF2 Elongation factor 2 ENSG00000167658 IPI00186290 xxxxx	117	108	143	101.5	18.18	-13.25
IPI00009342 - Gene_Symbol=IQGAP1 Ras GTPase-activating-like protein IQGAP1 ENSG00000140575 IPI00009342 xxxxx	38.5	57.5	48.5	43.5	20.62	11.49
IPI00296337 - Gene_Symbol=PRKDC Isoform 1 of DNA-dependent protein kinase catalytic subunit ENSG00000121031 IPI00296337 IPI00376215 xxxxx	62	78.5	79	86.5	21.52	28.32
IPI00465248 - Gene_Symbol=ENO1 Isoform alpha-enolase of Alpha-enolase ENSG00000074800 IPI00465248 IPI00759806 xxxxx	38.5	51	50	32.5	23.00	-15.58
IPI00013452 - Gene_Symbol=EPRS glutamyl-prolyl tRNA synthetase ENSG00000136628 IPI00013452 xxxxx	35.5	40	47.5	41.5	25.26	14.46
IPI00178352 - Gene_Symbol=FLNC Isoform 1 of Filamin-C ENSG00000128591 IPI00178352 IPI00413958 IPI00783128 xxxxx	41.5	55	58.5	57	29.06	27.19
IPI00009865 - Gene_Symbol=KRT10 Keratin, type I cytoskeletal 10 ENSG00000186395 IPI00383111	51.5	50	73	27	29.45	-47.57

IPI00009865 xxxxx						
IPI00013808 - Gene_Symbol=ACTN4 Alpha-actinin-4 ENSG00000130402 IPI00013808 IPI00793285 xxxxx	31	29.5	45	25.5	31.11	-17.74
IPI00219757 - Gene_Symbol=GSTP1 Glutathione S-transferase P ENSG00000084207 IPI00219757 IPI00793319 xxxxx	53.5	45	79	44.5	32.28	-16.82
IPI00382470 - Gene_Symbol=HSP90AA1 heat shock protein 90kDa alpha (cytosolic), class A member 1 isoform 1 ENSG00000080824 IPI00784295 IPI00382470 IPI00604607 IPI00795108 IPI00796865 IPI00796844 IPI00796258 xxxxx	57	66	85.5	54.5	33.33	-4.39
IPI00011200 - Gene_Symbol=PHGDH D-3-phosphoglycerate dehydrogenase ENSG00000092621 IPI00642548 IPI00011200 xxxxx	33	35.5	50.5	36	34.65	8.33
IPI00026216 - Gene_Symbol=NPEPPS Puromycin-sensitive aminopeptidase ENSG00000141279 IPI00026216 xxxxx	52.5	53	81.5	50.5	35.58	-3.81
IPI00783061 - Gene_Symbol=PKM2 Uncharacterized protein PKM2 ENSG00000067225 IPI00783061 IPI00784179 IPI00607698 IPI00604528 IPI00479186 IPI00220644 IPI00847989 IPI00788663 IPI00789727 IPI00792817 IPI00797668 IPI00798295 xxxxx	143.5	145	223	144	35.65	0.35
IPI00024580 - Gene_Symbol=MCCC1 Methylcrotonoyl-CoA carboxylase subunit alpha, mitochondrial precursor ENSG00000078070 IPI00024580 IPI00792499 IPI00792968 IPI00789136 xxxxx	102.5	128.5	160	116.5	35.94	12.02
IPI00009904 - Gene_Symbol=PDIA4 Protein disulfide-isomerase A4 precursor ENSG00000155660 IPI00009904 IPI00852730 IPI00852792 xxxxx	86.5	105	139	117.5	37.77	26.38
IPI00396015 - Gene_Symbol=ACACA Isoform 4 of Acetyl-CoA carboxylase 1 ENSG00000132142 IPI00745874 IPI00396015 IPI00847501 IPI00011569 IPI00396018 IPI00472339 IPI00796495 IPI00798329 IPI00796157 IPI00793409 IPI00816085 IPI00396017 xxxxx	701.5	664	1159	653.5	39.47	-6.84
IPI00022977 - Gene_Symbol=CKB Creatine kinase B-type ENSG00000166165 IPI00022977 IPI00794730 IPI00789218 xxxxx	174	131	294.5	134.5	40.92	-22.70
IPI00021290 - Gene_Symbol=ACLY ATP-citrate synthase ENSG00000131473 IPI00021290 IPI00394838 xxxxx	170.5	190	289.5	158.5	41.11	-7.04
IPI00788737 - Gene_Symbol=GAPDH 39 kDa protein ENSG00000111640 IPI00789134 IPI00219018 IPI00788737 IPI00796735 IPI00797221 IPI00795622 IPI00796111 IPI00794508 IPI00794991 IPI00793922 IPI00794605 IPI00795257 xxxxx	56	53.5	95.5	54.5	41.36	-2.68
IPI00220327 - Gene_Symbol=KRT1 Keratin, type II cytoskeletal 1 ENSG00000167768 IPI00220327 xxxxx	57	48.5	98.5	47	42.13	-17.54
IPI00152453 - Gene_Symbol=TUBB3 Tubulin, beta, 4 ENSG00000198211 IPI00152453 IPI00013683 IPI00640115 IPI00644620 xxxxx	209.5	148	368	253	43.07	17.19
IPI00472102 - Gene_Symbol=HSPD1 61 kDa protein ENSG00000144381 IPI00472102 IPI00784154 IPI00795445 IPI00790763 IPI00794769 xxxxx	52.5	71.5	102.5	69.5	48.78	24.46
IPI00796978 - Gene_Symbol=PCCA 80 kDa protein ENSG00000175198 IPI00749503 IPI00553145 IPI00553241 IPI00552419 IPI00744115 IPI00796978 IPI00552081 IPI00647500 IPI00383473 xxxxx	95	126.5	192	102.5	50.52	7.32
IPI00008603 - Gene_Symbol=ACTA2 Actin, aortic smooth muscle ENSG00000107796 IPI00008603 IPI00645534 IPI00816229 xxxxx	52.5	69.5	107.5	52	51.16	-0.95
IPI00023006 - Gene_Symbol=ACTC1 Actin, alpha cardiac muscle 1 ENSG00000159251 IPI00023006 xxxxx	52.5	69.5	107.5	52	51.16	-0.95
IPI00021304 - Gene_Symbol=KRT2 Keratin, type II cytoskeletal 2 epidermal ENSG00000172867 IPI00021304 IPI00791653 IPI00792970 xxxxx	26.5	26	56.5	15.5	53.10	-41.51
IPI00299402 - Gene_Symbol=PC Pyruvate carboxylase, mitochondrial precursor ENSG00000173599 IPI00299402 xxxxx	505.5	787	1087.5	475.5	53.52	-5.93
IPI00299571 - Gene_Symbol=PDIA6 Isoform 2 of Protein disulfide-isomerase A6 precursor ENSG00000143870 IPI00644989 IPI00299571 xxxxx	94	77.5	208	98.5	54.81	4.57

IPI00009790 - Gene_Symbol=PFKP 6-phosphofructokinase type C ENSG00000067057 IPI00642664 IPI00643196 IPI00552617 IPI00009790 IPI00552290 IPI00645848 IPI00646468 IPI00639981 xxxxx	33	41.5	75.5	34	56.29	2.94
IPI00027223 - Gene_Symbol=IDH1 Isocitrate dehydrogenase [NADP] cytoplasmic ENSG00000138413 IPI00027223 IPI00023029 xxxxx	26.5	39.5	62	42	57.26	36.90

Table 3A-3. Mass-spectrometry results of global competitive zinc-binding treatment of HeLa cell with zinc and IA-alkyne utilizing the quantitative isotopic Azo-tags. Two replicates of each metal ion concentration were performed and if the peptide was found in both runs it is represented as an average of the two R ratios. Data were sorted to present those with the lowest R ratio within the Zn^{2+} 20μM runs (i.e. largest decrease in IA-labeling upon zinc treatment). A '0' indicates that the peptide was not identified in those samples. Peptides with a R < 0.66 for the Zn^{2+} 20μM runs are highlighted in grey and represent cysteines that are most sensitive to Zn^{2+} (show a 1.5-fold decrease in labeling upon zinc treatment).

ipi	description	symbol	sequence	Reactivity Ratios (R)		
				Zn^{2+} 10μM	Zn^{2+} 20μM	Mg^{2+} 20μM
IPI00017799.5	TXN2 Thioredoxin, mitochondrial precursor ENSG0000	TXN2	R.VVNSETPVVVDF HAQWC*GPCK.I	0.605	0.05	1.045
IPI00216298.6	TXN Thioredoxin ENSG00000136810 IPI00552768 IPI002	TXN	K.LVVVDFSATWC* GPCK.M	0.695	0.085	1.03
IPI00790739.1	ACO2 Aconitase 2, mitochondrial ENSG00000100412 IP	ACO2	R.VGLIGSC*TNSSY EDMGR.S	0.46	0.115	1.03
IPI00007102.3	GLOD4 Uncharacterized protein C17orf25 ENSG0000016	GLOD 4	K.AAC*NGPYDGK. W	0.68	0.13	0.92
IPI00641743.2	HCFC1 Uncharacterized protein HCFC1 ENSG0000017253	HCFC 1	R.VAGINAC*GR.G	0.84	0.165	0.975
IPI00163085.2	AMOT Isoform 1 of Angiomotin ENSG00000126016 IPI00	AMOT	R.QGNC*QPTNVSE YNAAALMELLR.E	0.875	0.19	1.08
IPI00430812.4	CNBP Zinc finger protein 9 ENSG00000169714 IPI0043	CNBP	R.C*GESGHLAK.D	0.1	0.19	0.125
IPI00041127.6	ASF1B Histone chaperone ASF1B ENSG00000105011 IPI0	ASF1B	K.GLGLPGC*IPGLL PENSMDCI.-	0.965	0.2	1.035
IPI00844388.1	HELLS 103 kDa protein ENSG00000119969 IPI00012073	HELL S	K.ILENSEDSSPEC*L F.-	0.855	0.21	0.45
IPI00797038.1	PCK2 mitochondrial phosphoenolpyruvate carboxykina	PCK2	R.YVAAAFPSAC*G K.T	0.81	0.22	1.245
IPI00014589.1	CLTB Isoform Brain of Clathrin light chain B ENSG0	CLTB	K.VAQLC*DFNPK.S	0.74	0.24	1.005
IPI00299214.6	TK1 thymidine kinase 1, soluble ENSG00000167900 IP	TK1	R.YSSSFC*THDR.N	0.51	0.25	1.035

Reverse_IPI00376429.3	LOC391370 Uncharacterized protein ENSP00000352557	LOC391370	K.C*LGVWEGLK.K	0.905	0.26	0.985
IPI00032900.1	BOLA1 BolA-like protein 1 ENSG00000178096 IPI00032	BOLA1	R.VCLC*QGSAGSGAIGPVEAAIR.T	0.655	0.275	0.975
IPI00183626.8	PTBP1 polypyrimidine tract-binding protein 1 isofo	PTBP1	K.LSLDGQNIYNAC*CTLR.I	0	0.28	0.73
IPI00016610.2	PCBP1 Poly(rC)-binding protein 1 ENSG00000169564 I	PCBP1	R.VMTIPYQPMPASSPVIC*AGGQDR.C	0.54	0.28	0.945
IPI00013847.4	UQCRC1 Ubiquinol-cytochrome-c reductase complex co	UQCRC1	R.NALVSHLDGTTPVC*EDIGR.S	0.73	0.28	1.005
IPI00797038.1	PCK2 mitochondrial phosphoenolpyruvate carboxykina	PCK2	R.QC*PIMDPAWEAPEGVPIDAIIFGGR.R	0.66	0.29	1.06
IPI00216230.3	TMPO Lamina-associated polypeptide 2 isoform alpha	TMPO	K.SGIQPLC*PER.S	0.945	0.29	1.02
IPI00376429.3	LOC391370 Uncharacterized protein ENSP00000352557	LOC391370	K.LGEWVGLC*K.T	0.885	0.29	0.995
IPI00024623.3	ACADSB Short/branched chain specific acyl-CoA dehy	ACADSB	R.ASSTC*PLTFENVK.V	0.69	0.3	1.01
IPI00008982.1	ALDH18A1 Isoform Long of Delta-1-pyrroline-5-carbo	ALDH18A1	K.CEYPAAC*NALETLLIHR.D	0.94	0.31	1.095
IPI00742905.1	DHX9 146 kDa protein ENSG00000135829 IPI00742905 I	DHX9	K.SSVNC*PFSSQDMK.Y	0.75	0.31	0.895
IPI00103994.4	LARS Leucyl-tRNA synthetase, cytoplasmic ENSG00000	LARS	R.NFEATLGWLQEHAC*SR.T	0	0.31	0
IPI00377005.2	_ Uncharacterized protein ENSP00000340627 ENSG0000	–	K.EEHLC*TQR.M	0.815	0.31	0.95
IPI00025273.1	GART Isoform Long of Trifunctional purine biosynth	GART	R.FGDPEC*QVILPLLK.S	0.74	0.315	1.055
IPI00021277.1	NUBP1 Nucleotide-binding protein 1 ENSG00000103274	NUBP1	R.LC*ASGAGATPDTAIEEIKEK.M	0.875	0.32	1.12
IPI00030702.1	IDH3A Isoform 1 of Isocitrate dehydrogenase [NAD]	IDH3A	K.C*SDFTEEICR.R	0	0.32	1.16
IPI00217952.6	GFPT1 Isoform 1 of Glucosamine--fructose-6-phospha	GFPT1	R.VDSTTC*LFPVEEK.A	0.82	0.33	1.08
IPI00217952.6	GFPT1 Isoform 1 of Glucosamine--fructose-6-phospha	GFPT1	K.C*QNALQQVVAR.Q	0.575	0.335	1.015
IPI00026781.2	FASN Fatty acid synthase ENSG00000169710 IPI000267	FASN	R.LGMLSPEGTC*K.A	0.7	0.34	1
IPI00015262.10	CNN2 Calponin-2 ENSG00000064666 IPI00015262 IPI003	CNN2	K.AGQC*VIGLQMGTNK.C	0.875	0.34	1.12
IPI00220503.9	DCTN2 dynactin 2 ENSG00000175203 IPI00220503 IPI00	DCTN2	R.C*DQDAQNPLSAGLQGAC*LMETVELLQAK.V	0.77	0.34	1.155
IPI00641950.3	GNB2L1 Lung cancer oncogene 7 ENSG00000204628 IPI0	GNB2L1	K.VWNLANC*K.L	0.7	0.345	0.87
IPI00150269.1	PRPF4 Isoform 1 of U4/U6 small nuclear ribonucleop	PRPF4	K.DVNLASC*AADGSVK.L	0.51	0.35	0.965
IPI00306301.2	PDHA1 Mitochondrial PDHA1 ENSG00000131828 IPI00642	PDHA1	R.GFC*HLCDGQEACCVGLEAGINPTDHLITAYR.A	1.39	0.35	0
IPI00026496.3	NPM3 Nucleoplasmin-3 ENSG00000107833 IPI00026496	NPM3	K.LSC*QPMLSLDDFQLQPPVTFR.L	0	0.365	1.35
IPI00647337.1	_ OTTHUMP00000016411 ENSG00000181524 IPI00647337	–	K.VELC*SFSGYK.I	0.77	0.37	0.95
IPI00024163.1	POLR3A DNA-directed RNA polymerase III subunit RPC	POLR3A	K.LQQQPGC*TAEETLEALILK.E	0.79	0.37	1.05
IPI00759493.3	SUCLG1 succinate-CoA ligase, GDP-forming, alpha su	SUCLG1	K.IIC*QGFTGK.Q	0.84	0.375	1.04
IPI00301994.6	FAHD2B Fumarylacetoacetate hydrolase domain-contai	FAHD2B	K.TFDTFC*PLGPALVTK.D	0.735	0.375	0.99
IPI00025273.1	GART Isoform Long of Trifunctional purine biosynth	GART	K.AFTKPEEAC*SFILSADFPALVVK.A	0.81	0.375	1.035
IPI00016862.1	GSR Isoform Mitochondrial of Glutathione reductase	GSR	K.LGGTC*VNVGCVPK.K	0.75	0.38	1.01
IPI00745568.1	TIPRL Uncharacterized protein TIPRL ENSG0000014315	TIPRL	K.VAC*AEEWQESR.T	0.795	0.38	1.15

IPI00072534.2	UNC45A Isoform 1 of UNC45 homolog A ENSG0000014055	UNC45A	K.LLAAGVVSAMVC*MVK.T	0	0.38	0.87
IPI00012433.2	F8A1 F8A2 F8A3 Factor VIII intron 22 protein ENSG0	F8A1	R.LVC*PAAYGEPLQAAASALGAAVR.L	0.7	0.38	0.915
IPI00024317.1	GCDH Isoform Long of Glutaryl-CoA dehydrogenase, m	GCDH	R.ASATGMIIMDGVEVPEENVLPGASSLGGPFGC*LNNAR.Y	0.715	0.385	1.005
IPI00397963.3	_ Uncharacterized protein ENSP00000301828 ENSG0000	_	R.LTEGC*SFR.R	0.735	0.385	0.985
IPI00552569.1	ERCC6L excision repair protein ERCC6-like ENSG0000	ERCC6L	K.GFGSVEELC*TNSSLGMEK.S	0.82	0.39	1.135
IPI00328319.8	RBBP4 Histone-binding protein RBBP4 ENSG0000016252	RBBP4	R.YMPQNPC*IIATK.T	0.72	0.39	1.04
IPI00220301.5	PRDX6 Peroxiredoxin-6 ENSG00000117592 IPI00220301	PRDX6	R.DFTPVC*TTELGR.A	0.94	0.4	1.04
IPI00297455.4	AKAP8L A-kinase anchor protein 8-like ENSG00000011	AKAP8L	R.GQC*MSGASR.L	0.865	0.4	1.04
IPI00301609.8	NEK9 Serine/threonine-protein kinase Nek9 ENSG0000	NEK9	R.LNPAVTC*AGK.G	0.82	0.4	0.985
IPI00513827.3	ACADM Putative uncharacterized protein DKFZp686M24	ACADM	R.MTEEPLMC*AYCVTEPGAGSDVAGIK.T	0.38	0.4	0.685
IPI00144171.2	hCG_2015956 similar to 60S ribosomal protein L7 is	hCG_2015956	K.YGIIC*MEDLIHEIYTVGK.R	0	0.4	1.06
IPI00013774.1	HDAC1 Histone deacetylase 1 ENSG00000116478 IPI005	HDAC1	R.FNVGEDC*PVFDGLFEFCQLSTGGSVASAVK.L	0.65	0.4	0
IPI00299214.6	TK1 thymidine kinase 1, soluble ENSG00000167900 IP	TK1	K.LFAPQQILQC*SPAN.-	0.965	0.405	1.11
IPI00003918.6	RPL4 60S ribosomal protein L4 ENSG00000174444 IPI0	RPL4	R.SGQGAFGNMC*R.G	0.76	0.405	0.98
IPI00011107.2	IDH2 Isocitrate dehydrogenase [NADP], mitochondria	IDH2	K.DLAGC*IHGLSNVK.L	1.08	0.405	1.185
IPI00646105.3	PYCRL Pyrroline-5-carboxylate reductase ENSG000001	PYCRL	R.SDVC*TPGGTTIYGLHALEQGGLR.A	0.71	0.405	0.96
IPI00164672.6	DCP1A mRNA-decapping enzyme 1A ENSG00000162290 IPI	DCP1A	K.QHDPYITSIADLTGQVALYTFC*PK.A	0.9	0.405	0.98
IPI00216725.2	PHKA1 Uncharacterized protein PHKA1 ENSG0000006717	PHKA1	K.KVEALDEAC*TDLLSHQK.H	0.56	0.405	0.95
IPI00640364.2	OTUD5 Isoform 1 of OTU domain-containing protein 5	OTUD5	R.ATSPLVSLYPALEC*R.A	0.92	0.41	0.97
IPI00010810.1	ETFA Electron transfer flavoprotein subunit alpha,	ETFA	R.LGGEVSC*LVAGTK.C	0.91	0.41	1.02
IPI00007752.1	TUBB2C Tubulin beta-2C chain ENSG00000188229 IPI00	TUBB2C	K.LTTPTYGDLNHLVSATMSGVTTC*LR.F	0.745	0.415	0.985
IPI00145260.3	C1orf69 Putative transferase C1orf69, mitochondria	C1orf69	R.VWAVLPSSPEAC*GAASLQER.A	1.02	0.415	0.965
IPI00025273.1	GART Isoform Long of Trifunctional purine biosynth	GART	R.SAGVQC*FGPTAEAAQLESSKR.F	0.83	0.415	1.03
IPI00456664.1	NIT1 Isoform 4 of Nitrilase homolog 1 ENSG00000158	NIT1	K.IGLAVC*YDMR.F	0.765	0.415	0.995
IPI00394788.4	AARS2 Probable alanyl-tRNA synthetase, mitochondri	AARS2	K.HSTYDTDLFSPLLNAIQQGC*R.A	0.83	0.415	1.1
IPI00296053.3	FH Isoform Mitochondrial of Fumarate hydratase, mi	FH	K.FEALAAHDALVELSGAMNTTAC*SLMK.I	0.735	0.42	0.985
IPI00018350.3	MCM5 DNA replication licensing factor MCM5 ENSG000	MCM5	K.C*SPIGVYTSGK.G	0.9	0.42	0.975
IPI00217952.6	GFPT1 Isoform 1 of Glucosamine--fructose-6-phospha	GFPT1	R.QGRPVVIC*DKEDTETIK.N	0	0.42	1.035
IPI00848058.1	ACTB Actin, cytoplasmic 2 ENSG00000075624 IPI00021	ACTB	K.C*DVDIRK.D	0.825	0.425	1.055
IPI00024317.1	GCDH Isoform Long of Glutaryl-CoA dehydrogenase, m	GCDH	K.GYGC*AGVSSVAYGLLAR.E	0.765	0.425	1.2
IPI00743416.1	IKBKAP inhibitor of kappa light polypeptide gene e	IKBKAP	R.GDGQFFAVSVVC*PETGAR.K	0.95	0.43	0.83

IPI00292771.4	NUMA1 Isoform 1 of Nuclear mitotic apparatus prote	NUMA1	R.QFC*STQAALQAMER.E	0.805	0.43	0.905
IPI00556494.3	MED4 Mediator of RNA polymerase II transcription s	MED4	R.ISASNAVC*APLTWVPGDPR.R	0	0.43	0.885
IPI00301421.5	ZC3HC1 Isoform 1 of Nuclear-interacting partner of	ZC3HC1	R.LC*SSSSSDTSSR.S	0.925	0.43	1.05
IPI00007750.1	TUBA4A Tubulin alpha-4A chain ENSG00000127824 IPI0	TUBA4A	K.AYHEQLSVAEITNAC*FEPANQMVK.C	0.74	0.43	0.98
IPI00018009.2	EDC3 Enhancer of mRNA-decapping protein 3 ENSG0000	EDC3	K.SQDVAVSPQQQQC*SK.S	0.925	0.43	1.055
IPI00025273.1	GART Isoform Long of Trifunctional purine biosynth	GART	R.LLEGDGGPNTGGMGAYC*PAPQVSNDLLLK.I	0.805	0.43	1.01
IPI00550882.2	PYCR1 Pyrroline-5-carboxylate reductase 1 ENSG0000	PYCR1	R.C*MTNTPVVVR.E	0.745	0.435	1.04
IPI00441473.3	PRMT5 Protein arginine N-methyltransferase 5 ENSG0	PRMT5	R.DLNC*VPEIADTLGAVAK.Q	0.85	0.435	0.965
IPI00011253.3	RPS3 40S ribosomal protein S3 ENSG00000149273 IPI0	RPS3	K.GC*EVVVSGK.L	0.735	0.435	0.925
IPI00296337.2	PRKDC Isoform 1 of DNA-dependent protein kinase ca	PRKDC	R.VEQLFQVMNGILAQDSAC*SQR.A	0.765	0.44	0.955
IPI00029485.2	DCTN1 Isoform p150 of Dynactin subunit 1 ENSG00000	DCTN1	K.VTFSC*AAGFGQR.H	0.87	0.44	0.99
IPI00748696.1	AP3S2 44 kDa protein ENSG00000157823 IPI00025115 I	AP3S2	K.C*NFTGDGK.T	0.91	0.44	1.05
IPI00218728.4	PAFAH1B1 Isoform 1 of Platelet-activating factor a	PAFAH1B1	K.LWDFQGFEC*IR.T	0	0.44	1.07
IPI00784194.1	SART1 Uncharacterized protein SART1 ENSG0000017546	SART1	R.GLAAALLLC*QNK.G	0.94	0.44	0.995
IPI00746165.2	WDR1 Isoform 1 of WD repeat-containing protein 1 E	WDR1	R.MTVDESGQLISC*SMDDTVR.Y	1.035	0.44	1.025
IPI00004459.1	DIMT1L Probable dimethyladenosine transferase ENSG	DIMT1L	K.TDLPFFDTC*VANLPYQISSPFVFK.L	0.6	0.44	0.72
IPI00787501.1	LOC727737 similar to APG4 autophagy 4 homolog B is	LOC727737	R.TSVPC*AGATAFPADSDR.H	1.005	0.44	0
IPI00479385.3	ASMTL Uncharacterized protein ASMTL ENSG0000016909	ASMTL	K.LTAC*QVATAFNLSR.F	0.995	0.445	1.095
IPI00014177.3	SEPT2 Septin-2 ENSG00000168385 IPI00014177	41519	R.LTVVDTPGYGDAINC*R.D	0.64	0.445	0.915
IPI00017726.1	HSD17B10 Isoform 1 of 3-hydroxyacyl-CoA dehydrogen	HSD17B10	K.LGNNC*VFAPADVTSEKDVQTALALAK.G	0.8	0.445	0.935
IPI00007750.1	TUBA4A Tubulin alpha-4A chain ENSG00000127824 IPI0	TUBA4A	R.AVC*MLSNTTAIAEAWAR.L	0.755	0.445	0.995
IPI00218343.4	TUBA1C Tubulin alpha-1C chain ENSG00000167553 IPI0	TUBA1C	K.AYHEQLTVAEITNAC*FEPANQMVK.C	0.755	0.445	0.98
IPI00025366.4	CS Citrate synthase, mitochondrial precursor ENSG0	CS	R.GFSIPEC*QK.L	0.75	0.445	0.99
IPI00018206.3	GOT2 Aspartate aminotransferase, mitochondrial pre	GOT2	K.TC*GFDFTGAVEDISK.I	0.795	0.445	1.06
IPI00398057.1	LOC389342 Uncharacterized protein ENSP00000353659	LOC389342	R.LIPDGC*GVK.Y	0.82	0.45	1.04
IPI00646512.1	RBBP7 Retinoblastoma binding protein 7 ENSG0000010	RBBP7	R.VHIPNDDAQFDASHC*DSDKGEFGGFGSVTGK.I	0.925	0.45	0.99
IPI00219445.1	PSME3 Isoform 2 of Proteasome activator complex su	PSME3	R.LDEC*EEAFQGTK.V	0.975	0.45	1.04
IPI00030363.1	ACAT1 Acetyl-CoA acetyltransferase, mitochondrial	ACAT1	K.DGLTDVYNKIHMGSC*AENTAK.K	0.77	0.45	1.025
IPI00018931.6	VPS35 Vacuolar protein sorting-associated protein	VPS35	R.TQC*ALAASK.L	0.91	0.45	1.065
IPI00003918.6	RPL4 60S ribosomal protein L4 ENSG00000174444 IPI0	RPL4	R.YAIC*SALAASALPALVMSK.G	0.695	0.45	0.915
IPI00163085.2	AMOT Isoform 1 of Angiomotin ENSG00000126016 IPI00	AMOT	R.C*LDMEGR.I	0.845	0.455	0.965

IPI00007750.1	TUBA4A Tubulin alpha-4A chain ENSG00000127824 IPI0	TUBA4A	K.RSIQFVDWC*PTGFK.V	0.82	0.455	1.04
IPI00021435.3	PSMC2 26S protease regulatory subunit 7 ENSG000001	PSMC2	R.LC*PNSTGAEIR.S	0.805	0.46	1.025
IPI00007752.1	TUBB2C Tubulin beta-2C chain ENSG00000188229 IPI00	TUBB2C	K.NMMAAC*DPR.H	0.78	0.46	1.01
IPI00218343.4	TUBA1C Tubulin alpha-1C chain ENSG00000167553 IPI0	TUBA1C	R.AVC*MLSNTTAVAEAWAR.L	0.865	0.465	1.2
IPI00027107.5	TUFM Tu translation elongation factor, mitochondri	TUFM	K.KGDEC*ELLGHSK.N	0.74	0.465	0.975
IPI00397383.2	KIF1B Isoform 4 of Kinesin-like protein KIF1B ENSG	KIF1B	R.ASSPC*PEFEQFQIVPAVETPYLAR.A	1.06	0.465	0
IPI00012866.2	AKT1 RAC-alpha serine/threonine-protein kinase ENS	AKT1	K.TFC*GTPEYLAPEVLEDNDYGR.A	0.87	0.47	1.075
IPI00297579.4	CBX3 LOC653972 Chromobox protein homolog 3 ENSG000	CBX3	R.LTWHSC*PEDEAQ.-	0.825	0.47	1.06
IPI00007752.1	TUBB2C Tubulin beta-2C chain ENSG00000188229 IPI00	TUBB2C	K.TAVC*DIPPR.G	0.805	0.47	1.025
IPI00472102.3	HSPD1 61 kDa protein ENSG00000144381 IPI00472102 I	HSPD1	R.C*IPALDSLTPANEDQK.I	0.855	0.47	0.99
IPI00025273.1	GART Isoform Long of Trifunctional purine biosynth	GART	K.ISNTAISISDHTALAQFC*K.E	0.79	0.47	1.035
IPI00646493.1	COPA coatomer protein complex, subunit alpha isofo	COPA	R.MC*TLIDKFDEHDGPVR.G	0	0.47	1.07
IPI00107693.4	MED15 Isoform 1 of Mediator of RNA polymerase II t	MED15	K.QQYLC*QPLLDAVLANIR.S	1.34	0.475	0.905
IPI00180675.4	TUBA1A Tubulin alpha-1A chain ENSG00000167552 IPI0	TUBA1A	R.TIQFVDWC*PTGFK.V	0.825	0.475	1.04
IPI00019994.3	CXorf15 Gamma-taxilin ENSG00000086712 IPI00019994	CXorf15	R.TDPPDGQQDSEC*NR.N	0.82	0.475	0.985
IPI00844388.1	HELLS 103 kDa protein ENSG00000119969 IPI00012073	HELLS	K.C*NGQPVPFQQPK.H	0	0.475	1.03
IPI00045051.3	PURB Transcriptional activator protein Pur-beta EN	PURB	R.GGGGGPC*GFQPASR.G	0.96	0.48	1.18
IPI00030363.1	ACAT1 Acetyl-CoA acetyltransferase, mitochondrial	ACAT1	R.QAVLGAGLPISTPC*TTINK.V	0.82	0.48	1.025
IPI00024919.3	PRDX3 Thioredoxin-dependent peroxide reductase, mi	PRDX3	K.AFQYVETHGEVC*PANWTPDSPTIKPSPAASK.E	0	0.48	0
IPI00295851.4	COPB1 Coatomer subunit beta ENSG00000129083 IPI002	COPB1	K.ALSGYC*GFMAANLYAR.S	0.98	0.485	1.075
IPI00184523.1	ARNT Putative uncharacterized protein DKFZp547B061	ARNT	K.MTAYITELSDMVPTC*SALAR.K	0.76	0.485	0.85
IPI00789740.1	GEMIN4 Gem (Nuclear organelle) associated protein	GEMIN4	R.SDPDAC*PTMPLLAMLLR.G	1.51	0.485	1.43
IPI00006663.1	ALDH2 Aldehyde dehydrogenase, mitochondrial precur	ALDH2	K.LLC*GGGIAADR.G	0.83	0.485	1.015
IPI00157304.1	SSBP3 Isoform 1 of Single-stranded DNA-binding pro	SSBP3	R.DTC*EHSSEAK.A	0	0.49	0
IPI00218728.4	PAFAH1B1 Isoform 1 of Platelet-activating factor a	PAFAH1B1	R.MVRPNQDGTLIASC*SNDQTVR.V	0.835	0.49	0.99
IPI00008982.1	ALDH18A1 Isoform Long of Delta-1-pyrroline-5-carbo	ALDH18A1	K.LGSAVVTRGDEC*GLALGR.L	0.91	0.495	1.07
IPI00641743.2	HCFC1 Uncharacterized protein HCFC1 ENSG0000017253	HCFC1	R.AC*AAGTPAVIR.I	1.09	0.495	1.03
IPI00004860.2	RARS Isoform Complexed of Arginyl-tRNA synthetase,	RARS	K.NC*GC*LGASPNLEQLQEENLK.L	0	0.495	0.98
IPI00062419.2	SDSL Serine dehydratase-like ENSG00000139410 IPI00	SDSL	R.MLVEPAC*GAALAAIYSGLLR.R	0	0.495	0
IPI00030363.1	ACAT1 Acetyl-CoA acetyltransferase, mitochondrial	ACAT1	K.QGEYGLASIC*NGGGGASAMLIQK.L	0.795	0.5	1.03
IPI00031370.3	TUBB2B Tubulin beta-2B chain ENSG00000137285 IPI00	TUBB2B	K.ESESC*DCLQGFQLTHSLGGGTGSGMGTLLISK.I	0.725	0.5	0.94
IPI00455607.3	_ Uncharacterized protein ENSP00000329518 ENSG0000	–	R.AQYYHSC*GRESVIWEITPPALFR.Q	0	0.5	0

IPI00011916.1	JTV1 Multisynthetase complex auxiliary component p	JTV1	R.VELPTC*MYR.L	0.9	0.505	1.06
IPI00025178.3	BCAS2 Breast carcinoma amplified sequence 2 ENSG00	BCAS2	K.NDITAWQEC*VNNSMAQLEHQAVR.I	0.77	0.505	1.02
IPI00009342.1	IQGAP1 Ras GTPase-activating-like protein IQGAP1 E	IQGAP1	K.QIPAITC*IQSQWR.G	0	0.505	1.09
IPI00011107.2	IDH2 Isocitrate dehydrogenase [NADP], mitochondria	IDH2	K.NYDGDVQSDILAQGFGSLGLMTSVLVC*PDGK.T	0	0.505	1.46
IPI00025366.4	CS Citrate synthase, mitochondrial precursor ENSG0	CS	K.LPC*VAAK.I	0.815	0.51	0.96
IPI00007752.1	TUBB2C Tubulin beta-2C chain ENSG00000188229 IPI00	TUBB2C	K.VSDTVVEPYNATLSVHQLVENTDETYC*IDNEALYDICFR.T	0.805	0.51	1.01
IPI00655631.1	POLD1 DNA polymerase ENSG00000062822 IPI00002894 I	POLD1	R.DNC*PLVANLVTASLR.R	0	0.51	1.195
IPI00025091.3	RPS11 40S ribosomal protein S11 ENSG00000142534 IP	RPS11	K.C*PFTGNVSIR.G	0.84	0.51	0.95
IPI00170877.2	MRPL10 mitochondrial ribosomal protein L10 isoform	MRPL10	R.TVPFLPLLGGC*IDDTILSR.Q	0	0.51	1.18
IPI00470610.3	PYCR2 Pyrroline-5-carboxylate reductase 2 ENSG0000	PYCR2	R.SLLINAVEASC*IR.T	0.815	0.515	1.06
IPI00295388.2	GLDC Glycine dehydrogenase ENSG00000178445 IPI0074	GLDC	K.MEDPVC*ENEILATLHAISSK.N	0.92	0.515	0.96
IPI00291419.5	ACAT2 Acetyl-CoA acetyltransferase, cytosolic ENSG	ACAT2	R.QASVGAGIPYSVPAWSC*QMICGSGLK.A	0.91	0.52	0.905
IPI00790757.1	DUSP3 23 kDa protein ENSG00000108861 IPI00018671 I	DUSP3	R.EIGPNDGFLAQLC*QLNDR.L	3.96	0.52	2.34
IPI00845348.1	ZRANB2 Putative uncharacterized protein DKFZp686N0	ZRANB2	K.C*GNVNFAR.R	0.74	0.52	1.015
IPI00759493.3	SUCLG1 succinate-CoA ligase, GDP-forming, alpha su	SUCLG1	R.LIGPNC*PGVINPGECK.I	0.79	0.52	1.07
IPI00641950.3	GNB2L1 Lung cancer oncogene 7 ENSG00000204628 IPI0	GNB2L1	K.LWNTLGVC*K.Y	0.775	0.525	1.01
IPI00479743.3	POTE2 protein expressed in prostate, ovary, testis	POTE2	K.EKLC*YVALDFEQEMATAASSSSLEK.S	0.85	0.525	1.02
IPI00787158.1	SORD similar to sorbitol dehydrogenase ENSG0000014	SORD	R.YNLSPSIFFC*ATPPDDGNLCR.F	0.8	0.525	1
IPI00386591.5	C14orf149 Probable proline racemase ENSG0000012679	C14orf149	R.IVLAGC*PEVSGPTLLAK.R	0	0.53	1.02
IPI00064765.3	RPL10L 60S ribosomal protein L10-like ENSG00000165	RPL10L	K.MLSC*AGADR.L	0.675	0.535	0.82
IPI00022334.1	OAT Ornithine aminotransferase, mitochondrial prec	OAT	K.VLPMNTGVEAGETAC*K.L	0.81	0.535	0.935
IPI00031820.3	FARSA Phenylalanyl-tRNA synthetase alpha chain ENS	FARSA	K.VNLQMVYDSPLC*R.L	0.835	0.535	1.01
IPI00787158.1	SORD similar to sorbitol dehydrogenase ENSG0000014	SORD	R.YC*NTWPVAISMLASK.S	0.885	0.535	0.975
IPI00290142.5	CTPS CTP synthase 1 ENSG00000171793 IPI00290142	CTPS	R.LLETC*SIALVGK.Y	0.795	0.535	1.065
IPI00450975.1	RPS16 RPS16 protein ENSG00000105193 IPI00221092 IP	RPS16	K.TATAVAHC*K.R	0.925	0.535	1.075
IPI00291646.2	MTHFD1L methylenetetrahydrofolate dehydrogenase (N	MTHFD1L	R.SSC*SPGGR.T	0.925	0.54	1.045
IPI00025746.5	ANKRD54 Isoform 1 of Ankyrin repeat domain-contain	ANKRD54	R.LDDLC*TR.L	0.81	0.545	1
IPI00014424.1	EEF1A2 Elongation factor 1-alpha 2 ENSG00000101210	EEF1A2	K.SGDAAIVEMVPGKPMC*VESFSQYPPLGR.F	1.08	0.545	1.18
IPI00291570.9	CASP2 Isoform ICH-1L of Caspase-2 precursor ENSG00	CASP2	R.SDMICGYAC*LK.G	1.19	0.545	1

IPI00015911.1	DLD Dihydrolipoyl dehydrogenase, mitochondrial pre	DLD	K.NETLGGTC*LNV GCIPSK.A	0.885	0.55	0.82
IPI00018350.3	MCM5 DNA replication licensing factor MCM5 ENSG000	MCM5	K.AIAC*LLFGGSR.K	0.79	0.55	1.01
IPI00001539.8	ACAA2 3-ketoacyl-CoA thiolase, mitochondrial ENSG0	ACAA 2	R.IVGYFVSGC*DPSI MGIGPVPAISGALK. K	0	0.55	0
IPI00016912.1	TTC1 Tetratricopeptide repeat protein 1 ENSG000001	TTC1	K.VTDTQEAEC*AG PPVPDPK.N	1.105	0.555	1.12
IPI00008240.2	MARS Methionyl-tRNA synthetase, cytoplasmic ENSG00	MARS	R.LFVSDGVPGC*LP VLAAAGR.A	0	0.56	0
IPI00641384.2	SEC16A SEC16 homolog A ENSG00000148396 IPI00641384	SEC16 A	R.ANNNAAVAPTTC *PLQPVTDPFAFSR. Q	0.94	0.565	1.06
IPI00096066.2	SUCLG2 Succinyl-CoA ligase [GDP-forming] beta-chai	SUCL G2	K.IDATQVEVNPFGE TPEGQVVC*FDAK.I	0.91	0.565	0.94
IPI00001890.8	COPG 98 kDa protein ENSG00000181789 IPI00001890 IP	COPG	R.ALC*QITDSTMLQ AIER.Y	0.835	0.565	1.15
IPI00291006.1	MDH2 Malate dehydrogenase, mitochondrial precursor	MDH2	K.TIIPLISQC*TPK.V	0.84	0.57	0.98
IPI00453476.2	_ Uncharacterized protein ENSP00000348237 ENSG0000	–	R.YADLTEDQLPSC* ESLK.D	0.9	0.57	0.985
IPI00746777.3	ADH5 Alcohol dehydrogenase class-3 ENSG00000197894	ADH5	K.IDPLAPLDKVCLL GC*GISTGYGAAVN TAK.L	0.71	0.57	1.055
IPI00220503.9	DCTN2 dynactin 2 ENSG00000175203 IPI00220503 IPI00	DCTN 2	R.C*DQDAQNPLSA GLQGACLMETVELL QAK.V	0.795	0.57	0.995
IPI00025091.3	RPS11 40S ribosomal protein S11 ENSG00000142534 IP	RPS11	R.DVQIGDIVTVGEC *RPLSK.T	0.84	0.57	1.025
IPI00029629.3	TRIM25 Tripartite motif-containing protein 25 ENSG	TRIM2 5	K.NTVLC*NVVEQF LQADLAR.E	0.88	0.575	1.06
IPI00554777.2	ASNS Asparagine synthetase ENSG00000070669 IPI0055	ASNS	R.IGC*LLSGGLDSSL VAATLLK.Q	0.845	0.575	0.95
IPI00641950.3	GNB2L1 Lung cancer oncogene 7 ENSG00000204628 IPI0	GNB2 L1	K.AEPPQC*TSLAWS ADGQTLFAGYTDN LVR.V	0.8	0.575	1.09
IPI00024381.1	CLP1 Pre-mRNA cleavage complex II protein Clp1 ENS	CLP1	K.VGAPTIPDSC*LPL GMSQEDNQLK.L	0.86	0.58	0.915
IPI00146935.4	DNM1L Isoform 1 of Dynamin-1-like protein ENSG0000	DNM1 L	K.YIETSELC*GGAR. I	0	0.58	0
IPI00033025.8	SEPT7 Isoform 1 of Septin-7 ENSG00000122545 IPI008	41524	K.ADTLTPEEC*QQF KK.Q	0.87	0.58	1.055
IPI00141933.3	BUB1B Mitotic checkpoint serine/threonine-protein	BUB1 B	K.IPGMTLSSSVCQV NCC*AR.E	0	0.58	1.06
IPI00218342.10	MTHFD1 C-1-tetrahydrofolate synthase, cytoplasmic	MTHF D1	K.GC*LELIKETGVPI AGR.H	0.95	0.58	1.155
IPI00013214.1	MCM3 DNA replication licensing factor MCM3 ENSG000	MCM3	R.SVHYC*PATK.K	0.935	0.585	1.065
IPI00784131.1	AARS Uncharacterized protein AARS ENSG00000090861	AARS	K.AVYTQDC*PLAA AK.A	0.955	0.585	1.075
IPI00794575.1	DNM2 98 kDa protein ENSG00000079805 IPI00215974 IP	DNM2	K.LQDAFSSIGQSC* HLDLPQIAVVGGQS AGK.S	0	0.585	0.97
IPI00641950.3	GNB2L1 Lung cancer oncogene 7 ENSG00000204628 IPI0	GNB2 L1	R.FSPNSSNPIIVSC* GWDK.L	0.825	0.59	0.985
IPI00029468.1	ACTR1A Alpha-centractin ENSG00000138107 IPI0002946	ACTR 1A	R.AC*YLSINPQKDE TLETEK.A	1.095	0.59	1.09
IPI00646493.1	COPA coatomer protein complex, subunit alpha isofo	COPA	R.TTYQALPC*LPSM YGYPNR.N	0	0.59	1.02
IPI00301058.5	VASP Vasodilator-stimulated phosphoprotein ENSG000	VASP	K.SSSSVTTSETQPC* TPSSSDYSDLQR.V	0.985	0.595	1.03
IPI00152998.3	LRRC40 Leucine-rich repeat-containing protein 40 E	LRRC 40	R.FLPEFPSC*SLLK.E	0.78	0.595	1.01
IPI00220158.1	ADD1 Isoform 3 of Alpha-adducin ENSG00000087274 IP	ADD1	K.YSDVEVPASVTG YSFASDGDSGTC*SP LR.H	1.08	0.595	0.95

IPI00186290.6	EEF2 Elongation factor 2 ENSG00000167658 IPI001862	EEF2	R.TFC*QLILDPIFK.V	0.885	0.595	1.115
IPI00018206.3	GOT2 Aspartate aminotransferase, mitochondrial pre	GOT2	K.EYLPIGGLAEFC*K.A	0.91	0.6	1.02
IPI00028091.3	ACTR3 Actin-like protein 3 ENSG00000115091 IPI0002	ACTR3	K.LGYAGNTEPQFIIPSC*IAIK.E	0.825	0.605	0.93
IPI00302112.1	MAP2K7 Isoform 2 of Dual specificity mitogen-activ	MAP2K7	K.LC*DFGISGR.L	0.89	0.605	1.01
IPI00022744.5	CSE1L Isoform 1 of Exportin-2 ENSG00000124207 IPI0	CSE1L	K.IC*AVGITK.L	0.945	0.605	1.06
IPI00007750.1	TUBA4A Tubulin alpha-4A chain ENSG00000127824 IPI0	TUBA4A	K.YMAC*CLLYR.G	0.895	0.605	1.015
IPI00746806.1	CTTN CTTN protein ENSG00000085733 IPI00029601 IPI0	CTTN	K.C*ALGWDHQEK.L	1.02	0.605	1.105
IPI00556451.2	ETFB Isoform 2 of Electron transfer flavoprotein s	ETFB	K.HSMNPFC*EIAVEEAVR.L	0.92	0.61	0.74
IPI00646689.1	TXNDC17 Thioredoxin domain-containing protein 17 E	TXNDC17	K.DAGGKSWC*PDCVQAEPVVR.E	1.06	0.61	1.03
IPI00015956.3	EXOSC3 Exosome complex exonuclease RRP40 ENSG00000	EXOSC3	K.LLAPDC*EIIQEVGK.L	0.96	0.61	1.11
IPI00644674.1	NUBP2 Nucleotide-binding protein 2 ENSG00000095906	NUBP2	K.ILDATPAC*LP.-	0.855	0.61	0.87
IPI00005011.1	CNOT2 Isoform 1 of CCR4-NOT transcription complex	CNOT2	R.SSPSIIC*MPK.Q	0.81	0.61	0.765
IPI00796337.1	PCBP2 poly(rC)-binding protein 2 isoform a ENSG000	PCBP2	R.YSTGSDSASFPHTTPSMC*LNPDLEGPPLEAYTIQGQYAIPQPDLTK.L	0.975	0.61	1.035
IPI00010153.5	RPL23 60S ribosomal protein L23 ENSG00000125691 IP	RPL23	R.ISLGLPVGAVINC*ADNTGAK.N	0.84	0.61	1.01
IPI00604527.2	TARS2 Threonyl-tRNA synthetase, mitochondrial prec	TARS2	R.LALSTRPSGFLGDPC*LWDQAEQVLK.Q	0	0.61	0.66
IPI00291006.1	MDH2 Malate dehydrogenase, mitochondrial precursor	MDH2	K.GYLGPEQLPDC*LK.G	0.51	0.61	0.955
IPI00011062.1	CPS1 Isoform 1 of Carbamoyl-phosphate synthase [am	CPS1	K.TSAC*FEPSLDYMVTK.I	0.79	0.61	0
IPI00177743.5	ZNF318 zinc finger protein 318 ENSG00000171467 IPI	ZNF318	K.TINSAGLGPSPC*LPDLVDFVTR.T	0	0.61	0
IPI00216383.1	RAD51L3 Isoform 5 of DNA repair protein RAD51 homo	RAD51L3	R.VGLC*PGLTEEMIQLLR.S	0	0.61	0
IPI00793696.1	RPL24 19 kDa protein ENSG00000114391 IPI00306332 I	RPL24	K.C*ESAFLSK.R	0.905	0.61	1.03
IPI00646105.3	PYCRL Pyrroline-5-carboxylate reductase ENSG000001	PYCRL	R.AATMSAVEAATC*R.A	0.78	0.615	1.035
IPI00018465.1	CCT7 T-complex protein 1 subunit eta ENSG000001356	CCT7	R.QLC*DNAGFDATNILNK.L	0.735	0.615	0.93
IPI00464979.4	SUCLA2 Isoform 1 of Succinyl-CoA ligase [ADP-formi	SUCLA2	K.YDATMIEINPMVEDSDGAVLC*MDAK.I	0.975	0.615	1.225
IPI00008240.2	MARS Methionyl-tRNA synthetase, cytoplasmic ENSG00	MARS	K.VPVLQLDSGNYLFSTSAIC*R.Y	0.84	0.615	0
IPI00018206.3	GOT2 Aspartate aminotransferase, mitochondrial pre	GOT2	R.VGAFTMVC*K.D	0.905	0.62	1.025
IPI00748490.1	AARSD1 Alanyl-tRNA synthetase, class IIc family pr	AARSD1	R.VVNIEGVDSNMC*CGTHVSNLSDLQVIK.I	0.66	0.62	0
IPI00294739.1	SAMHD1 SAM domain and HD domain-containing protein	SAMHD1	R.C*DDSPR.T	0	0.62	0
IPI00017552.2	MED9 Mediator of RNA polymerase II transcription s	MED9	K.SLC*MFEIPKE.-	0	0.62	0.96
IPI00018206.3	GOT2 Aspartate aminotransferase, mitochondrial pre	GOT2	R.HFIEQGINVC*LCQSYAK.N	0.92	0.62	1.07

IPI00106642.4	SDF2L1 Dihydropyrimidinase-like 2 ENSG00000128228	SDF2L1	R.FQLTDC*QIYEVLSVIR.D	0	0.62	1.225
IPI00021808.3	HARS Histidyl-tRNA synthetase, cytoplasmic ENSG000	HARS	R.TGQPLC*IC.-	0.97	0.625	1.125
IPI00217442.2	MASK-BP3 EIF4EBP3 MASK-4E-BP3 protein ENSG00000131	MASK-BP3	R.LTSSVSC*ALDEAAAALTR.M	1.01	0.625	1.215
IPI00030328.1	SRR Serine racemase ENSG00000167720 IPI00030328	SRR	K.LEGIPAYIVVPQTAPDC*K.K	1.025	0.625	1.04
IPI00444329.1	BCKDHA CDNA FLJ45695 fis, clone FEBRA2013570, high	BCKDHA	R.DYPLELFMAQC*YGNISDLGK.G	0.65	0.625	1.04
IPI00387130.1	CIAPIN1 Isoform 1 of Anamorsin ENSG00000005194 IPI	CIAPIN1	R.AASC*GEGK.K	0.87	0.625	1.005
IPI00783061.1	PKM2 Uncharacterized protein PKM2 ENSG00000067225	PKM2	R.GIFPVLC*KDPVQEAWAEDVDLR.V	0.935	0.625	1.175
IPI00641950.3	GNB2L1 Lung cancer oncogene 7 ENSG00000204628 IPI0	GNB2L1	K.HLYTLDGGDIINALC*FSPNR.Y	0.92	0.625	1.22
IPI00026781.2	FASN Fatty acid synthase ENSG00000169710 IPI000267	FASN	K.AFDTAGNGYC*R.S	0.96	0.63	1.04
IPI00069693.4	_ Uncharacterized protein ENSP00000350479 ENSG0000	–	R.ALVDGPC*TQVR.R	0.84	0.63	1.01
IPI00216298.6	TXN Thioredoxin ENSG00000136810 IPI00552768 IPI002	TXN	K.C*MPTFQFFK.K	0.7	0.63	1.125
IPI00478208.2	hCG_2004593 hypothetical protein LOC645296 ENSG000	hCG_2004593	R.INPYMSSPC*HIEMILTEK.E	0.77	0.63	0.9
IPI00013485.3	RPS2 40S ribosomal protein S2 ENSG00000140988 IPI0	RPS2	R.GC*TATLGNFAK.A	0.93	0.63	1
IPI00006164.4	ILKAP Integrin-linked kinase-associated serine/thr	ILKAP	R.FILLAC*DGLFK.V	0.53	0.63	0
IPI00301107.5	IPO11 Importin-11 ENSG00000086200 IPI00783526 IPI0	IPO11	R.LKQFLEC*SR.S	0	0.63	0.92
IPI00784614.1	SEPT9 Isoform 1 of Septin-9 ENSG00000184640 IPI007	41526	K.LTVIDTPGFGDHINNENC*WQPIMK.F	1.165	0.63	0.99
IPI00219077.4	LTA4H Isoform 1 of Leukotriene A-4 hydrolase ENSG0	LTA4H	R.AILPC*QDTPSVK.L	0	0.63	0.99
IPI00020599.1	CALR Calreticulin precursor ENSG00000179218 IPI007	CALR	K.LFPNSLDQTDMHGDSEYNIMFGPDIC*GPGTK.K	0.52	0.63	0.96
IPI00028091.3	ACTR3 Actin-like protein 3 ENSG00000115091 IPI0002	ACTR3	R.YSYVC*PDLVK.E	1.02	0.635	1.15
IPI00217030.10	RPS4X 40S ribosomal protein S4, X isoform ENSG0000	RPS4X	R.EC*LPLIIFLR.N	0.92	0.635	1.12
IPI00396627.1	ELAC2 Isoform 1 of Zinc phosphodiesterase ELAC pro	ELAC2	K.VC*FGDFPTMPK.L	0.955	0.635	1.18
IPI00186290.6	EEF2 Elongation factor 2 ENSG00000167658 IPI001862	EEF2	R.YVEPIEDVPC*GNIVGLVGVDQFLVK.T	0.85	0.635	0.97
IPI00029091.1	_ Putative nucleoside diphosphate kinase ENSG00000	_	R.GDFC*IQVGR.N	1.265	0.64	0.86
IPI00396485.3	EEF1A1 Elongation factor 1-alpha 1 ENSG00000156508	EEF1A1	K.PMC*VESFSDYPPLGR.F	0.885	0.64	1.005
IPI00852960.1	USP22 Ubiquitin carboxyl-terminal hydrolase 22 ENS	USP22	K.C*DDAIITK.A	0	0.64	0
IPI00398009.2	IPO4 Isoform 2 of Importin-4 ENSG00000196497 IPI00	IPO4	R.APAALPALC*DLLASAADPQIR.Q	0.96	0.65	0.92
IPI00019755.3	GSTO1 Glutathione transferase omega-1 ENSG00000148	GSTO1	R.FC*PFAER.T	1.05	0.65	1.005
IPI00018235.3	PEF1 Peflin ENSG00000162517 IPI00018235	PEF1	K.QALVNC*NWSSFNDETCLMMINMFDK.T	0	0.65	0.95
IPI00419237.3	LAP3 Isoform 1 of Cytosol aminopeptidase ENSG00000	LAP3	R.SAGAC*TAAAFLK.E	1.065	0.65	1.005
IPI00739117.3	BAT2D1 HBxAg transactivated protein 2 ENSG00000117	BAT2D1	R.IAC*GPPQAK.L	0.93	0.65	1.07
IPI00412771.1	CD2AP CD2-associated protein ENSG00000198087 IPI00	CD2AP	K.DTC*YSPKPSVYLSTPSSASK.A	0.965	0.655	1
IPI00748256.1	PSME1 Uncharacterized protein PSME1 ENSG0000009201	PSME1	K.VDVFREDLC*TK.T	0.845	0.655	0.99

IPI00790530.1	NUP85 nucleoporin 85 ENSG00000125450 IPI00790530 I	NUP85	R.GC*FSDLDLIDNL GPAMMLSDR.L	0.85	0.655	0.92
IPI00218606.7	RPS23 40S ribosomal protein S23 ENSG00000186468 IP	RPS23	K.ITAFVPNDGC*LN FIEENDEVLVAGFG R.K	0.925	0.655	1.06
IPI00001890.8	COPG 98 kDa protein ENSG00000181789 IPI00001890 IP	COPG	K.ELAPAVSVLQLFC *SSPK.A	0.815	0.655	1.125
IPI00329260.3	C13orf23 Uncharacterized protein KIAA2032 ENSG0000	C13orf 23	K.DGEEC*TNEGK.G	0.73	0.66	1.065
IPI00852816.1	SMARCD1 SWI/SNF-related matrix-associated actin-de	SMAR CD1	R.AEFYFQPWAQEA VC*R.Y	0	0.66	1.14
IPI00025273.1	GART Isoform Long of Trifunctional purine biosynth	GART	K.QVLVAPGNAGTA C*SEK.I	1.005	0.66	0.965
IPI00220150.4	IDH3G Isocitrate dehydrogenase [NAD] subunit gamma	IDH3G	R.TSLDLYANVIHC* K.S	1.12	0.66	0
IPI00005692.1	MRPS12 28S ribosomal protein S12, mitochondrial pr	MRPS 12	K.GVVLC*TFTR.K	0	0.66	1.32
IPI00011253.3	RPS3 40S ribosomal protein S3 ENSG00000149273 IPI0	RPS3	R.GLC*AIAQAESLR. Y	0.95	0.66	0.98
IPI00743871.1	INTS7 Uncharacterized protein INTS7 ENSG0000014349	INTS7	R.IDLLQAFSQLIC*T CNSLK.T	0	0.66	0
IPI00298887.5	STAT3 88 kDa protein ENSG00000168610 IPI00298887 I	STAT3	R.QQIAC*IGGPPNIC LDR.L	0	0.66	0
IPI00031563.4	C19orf58 Uncharacterized protein C19orf58 ENSG0000	C19orf 58	R.FHADSVC*K.A	1.05	0.665	1.01
IPI00027107.5	TUFM Tu translation elongation factor, mitochondri	TUFM	K.GEETPVIVGSALC *ALEGR.D	0.86	0.665	1.01
IPI00025746.5	ANKRD54 Isoform 1 of Ankyrin repeat domain-contain	ANKR D54	K.LNILQEGHAQC*L EAVR.L	1.24	0.67	0.91
IPI00219217.3	LDHB L-lactate dehydrogenase B chain ENSG000001117	LDHB	K.GMYGIENEVFLSL PC*ILNAR.G	0.875	0.67	0.725
IPI00027251.1	STK38 Serine/threonine-protein kinase 38 ENSG00000	STK38	K.LSDFGLC*TGLK. K	0.865	0.67	0.98
IPI00219160.3	RPL34 60S ribosomal protein L34 ENSG00000109475 IP	RPL34	K.SACGVC*PGR.L	0.79	0.67	1.055
Reverse_IPI00303 343.7	SCAF1 Splicing factor, arginine/serine-rich 19 ENS	SCAF1	K.AAREEGSWSTEE AGKTGAAQSC*SDA KSKK.L	1.23	0.67	0.92
IPI00303882.2	M6PRBP1 Isoform B of Mannose-6-phosphate receptor-	M6PR BP1	R.VASMPLISSTC*D MVSAAYASTK.E	0	0.67	1.24
IPI00257508.4	DPYSL2 Dihydropyrimidinase-related protein 2 ENSG0	DPYS L2	R.GLYDGPVC*EVS VTPK.T	0.975	0.675	1.135
IPI00006754.1	WDR68 WD repeat-containing protein 68 ENSG00000136	WDR6 8	R.VPC*TPVAR.L	0.91	0.675	1.085
IPI00003881.5	HNRPF Heterogeneous nuclear ribonucleoprotein F EN	HNRP F	R.DLSYC*LSGMYD HR.Y	0.89	0.68	0.9
IPI00291646.2	MTHFD1L methylenetetrahydrofolate dehydrogenase (N	MTHF D1L	K.IDRYTQQGFGNLP IC*MAK.T	0	0.68	0.89
IPI00008453.3	CORO1C Coronin-1C ENSG00000110880 IPI00008453 IPI0	CORO 1C	K.C*DLISIPK.K	1	0.685	1.03
IPI00008530.1	RPLP0 60S acidic ribosomal protein P0 ENSG00000089	RPLP0	R.AGAIAPC*EVTVP AQNTGLGPEK.T	0.93	0.685	1.055
IPI00514501.1	C1orf57 Chromosome 1 open reading frame 57 ENSG000	C1orf5 7	R.NADC*SSGPGQR. V	0.9	0.685	0.945
IPI00013871.1	RRM1 Ribonucleoside-diphosphate reductase large su	RRM1	R.DECLMC*GS.-	0.815	0.69	1.03
IPI00787501.1	LOC727737 similar to APG4 autophagy 4 homolog B is	LOC72 7737	K.NFPAIGGTGPTSD TGWGC*MLR.C	0.955	0.69	1.05
IPI00100160.3	CAND1 Isoform 1 of Cullin-associated NEDD8-dissoci	CAND 1	K.NC*IGDFLK.T	0	0.69	1.085
IPI00018768.1	TSN Translin ENSG00000211460 IPI00018768	TSN	K.ETAAAC*VEK.-	0.905	0.69	1.015
IPI00013871.1	RRM1 Ribonucleoside-	RRM1	R.NTAAMVC*SLEN	0.815	0.69	1.03

	diphosphate reductase large su		RDECLMCGS.-			
IPI00303207.3	ABCE1 ATP-binding cassette sub-family E member 1 E	ABCE1	R.YC*ANAFK.L	0.845	0.69	1.08
IPI00152998.3	LRRC40 Leucine-rich repeat-containing protein 40 E	LRRC40	R.DC*GTSVPQGLLK.A	0.89	0.69	1.13
IPI00306017.2	C15orf44 Isoform 1 of UPF0464 protein C15orf44 ENS	C15orf44	R.LIDLNNGEGQIFTIDGPLC*LK.N	0.89	0.7	1.025
IPI00016802.1	SIRT1 NAD-dependent deacetylase sirtuin-1 ENSG0000	SIRT1	R.GC*PGAAAAALWR.E	0	0.7	0.94
IPI00015911.1	DLD Dihydrolipoyl dehydrogenase, mitochondrial pre	DLD	R.VLGAHILGPGAGEMVNEAALALEYGASC*EDIAR.V	0	0.7	1.02
IPI00186290.6	EEF2 Elongation factor 2 ENSG00000167658 IPI001862	EEF2	R.LMEPIYLVEIQC*PEQVVGGIYGVLNR.K	0.82	0.7	1.11
IPI00301139.5	MED17 Isoform 1 of Mediator of RNA polymerase II t	MED17	K.MELLMSALSPC*LL.-	1.08	0.71	1.04
IPI00008247.2	ANAPC5 Isoform 1 of Anaphase-promoting complex sub	ANAPC5	K.LIEESC*PQLANSVQIR.I	0.92	0.71	0.96
IPI00396086.1	RPS21 8.2 kDa differentiation factor ENSG000001718	RPS21	R.KC*SASNR.I	1.045	0.715	1.02
IPI00008433.4	RPS5 40S ribosomal protein S5 ENSG00000083845 IPI0	RPS5	K.AQC*PIVER.L	1	0.715	0.995
IPI00022977.1	CKB Creatine kinase B-type ENSG00000166165 IPI0002	CKB	K.DYEFMWNPHLGYILTC*PSNLGTGLR.A	0	0.715	0
IPI00099986.5	FN3KRP Ketosamine-3-kinase ENSG00000141560 IPI0009	FN3KRP	R.ATGHSGGGC*ISQGR.S	0.985	0.72	1.035
IPI00019376.6	SEPT11 Septin-11 ENSG00000138758 IPI00019376	41528	K.STSQGFC*FNILCVGETGIGK.S	0.985	0.72	1.065
IPI00103925.2	IRGQ Immunity-related GTPase family Q protein ENSG	IRGQ	R.TDGEGEDPEC*LGEGK.M	1.17	0.72	0.96
IPI00788737.1	GAPDH 39 kDa protein ENSG00000111640 IPI00789134 I	GAPDH	K.IISNASC*TTNCLAPLAK.V	1	0.72	1.015
IPI00011253.3	RPS3 40S ribosomal protein S3 ENSG00000149273 IPI0	RPS3	R.AC*YGVLR.F	0.885	0.72	0.975
IPI00005780.3	OGT Isoform 3 of UDP-N-acetylglucosamine--peptide	OGT	K.VMAEANHFIDLSQIPC*NGK.A	0.98	0.725	0.96
IPI00419880.6	RPS3A 40S ribosomal protein S3a ENSG00000145425 IP	RPS3A	R.DKMC*SMVK.K	0.95	0.725	1
IPI00062839.4	MARS2 Methionyl-tRNA synthetase, mitochondrial pre	MARS2	R.INPSETYPAFC*TTCFPSEPGLVGPSVR.A	0.94	0.725	1.135
IPI00289773.3	CEBPB CCAAT/enhancer-binding protein beta ENSG0000	CEBPB	K.APPTAC*YAGAAPAPSQVK.S	0	0.725	1.05
IPI00096066.2	SUCLG2 Succinyl-CoA ligase [GDP-forming] beta-chai	SUCLG2	R.SC*NGPVLVGSPQGGVDIEEVAASNPELIFK.E	0.9	0.73	1.03
IPI00306290.4	XPOT Uncharacterized protein XPOT ENSG00000184575	XPOT	R.QASLADC*LNHAVGFASR.T	0.9	0.73	0
IPI00146935.4	DNM1L Isoform 1 of Dynamin-1-like protein ENSG0000	DNM1L	R.IC*YIFHETFGR.T	0	0.73	0
IPI00026781.2	FASN Fatty acid synthase ENSG00000169710 IPI000267	FASN	K.LTPGC*EAEAETEAICFFVQQFTDMEHNR.V	0.94	0.735	1.045
IPI00011631.6	ZW10 Centromere/kinetochore protein zw10 homolog E	ZW10	R.LAPILC*DGTATFVDLVPGFR.R	0.965	0.735	0.92
IPI00013871.1	RRM1 Ribonucleoside-diphosphate reductase large su	RRM1	K.IIDINYYPVPEAC*LSNKR.H	0.86	0.735	0.99
IPI00465260.4	GARS Glycyl-tRNA synthetase ENSG00000106105 IPI004	GARS	R.SCYDLSC*HAR.A	0.6	0.735	1.01
IPI00018465.1	CCT7 T-complex protein 1 subunit eta ENSG000001356	CCT7	R.YNFFTGC*PK.A	1.22	0.735	0.82
IPI00005791.1	NDC80 Kinetochore protein Hec1 ENSG00000080986 IPI	NDC80	K.FNPEAGANC*LVK.Y	0	0.735	1.15
IPI00783061.1	PKM2 Uncharacterized protein PKM2 ENSG00000067225	PKM2	R.AEGSDVANAVLDGADC*IMLSGETAK.	0.725	0.735	0.955

			G			
IPI00329638.10	ZAK Isoform 1 of Mitogen-activated protein kinase	ZAK	K.FDDLQFFENC*GGGSFGSVYR.A	0	0.74	0.84
IPI00007818.3	CPSF3 Cleavage and polyadenylation specificity fac	CPSF3	R.NFNYHILSPC*DLSNYTDLAMSTVK.Q	0.97	0.74	0.97
IPI00016580.6	DSN1 Isoform 1 of Kinetochore-associated protein D	DSN1	K.VFDC*MELVMDELQGSVK.Q	1.04	0.74	1.14
IPI00641635.1	FTO 64 kDa protein ENSG00000140718 IPI00028277 IPI	FTO	K.ANEDAVPLC*MSADFPR.V	0.985	0.74	0.945
IPI00023919.4	PSMC5 26S protease regulatory subunit 8 ENSG000000	PSMC5	K.FVVDVDKNIDINDVTPNC*R.V	0.94	0.74	0.94
IPI00011200.5	PHGDH D-3-phosphoglycerate dehydrogenase ENSG00000	PHGDH	K.NAGNC*LSPAVIVGLLK.E	0.94	0.745	0.91
IPI00301051.3	NHLRC2 NHL repeat-containing protein 2 ENSG0000019	NHLRC2	K.AILFSQPLQITDTQQGC*IAPVELR.Y	0.965	0.745	0.92
IPI00004358.4	PYGB Glycogen phosphorylase, brain form ENSG000001	PYGB	R.LAAC*FLDSMATLGLAAYGYGIR.Y	0	0.745	0.85
IPI00002966.1	HSPA4 Heat shock 70 kDa protein 4 ENSG00000170606	HSPA4	R.GC*ALQCAILSPAFK.V	1.07	0.75	1.085
IPI00026230.1	HNRPH2 Heterogeneous nuclear ribonucleoprotein H	HNRPH2	R.DLNYC*FSGMSDHR.Y	0.91	0.75	0.955
IPI00215719.6	RPL18 60S ribosomal protein L18 ENSG00000063177 IP	RPL18	K.GC*GTVLLSGPR.K	0.88	0.75	0.96
IPI00012828.3	ACAA1 3-ketoacyl-CoA thiolase, peroxisomal precurs	ACAA1	R.DC*LIPMGITSENVAER.F	0.97	0.75	0
IPI00643920.2	TKT Transketolase ENSG00000163931 IPI00643920 IPI0	TKT	R.TVPFC*STFAAFFTR.A	0	0.75	1.01
IPI00011511.1	CECR5 Isoform 2 of Cat eye syndrome critical regio	CECR5	K.AQELSALLGC*EVDADQVILSHSPMK.L	1.1	0.755	1.145
IPI00028091.3	ACTR3 Actin-like protein 3 ENSG00000115091 IPI0002	ACTR3	R.LPACVVDC*GTGYTK.L	0.945	0.755	1.07
IPI00844375.1	PSMB2 Proteasome beta 2 subunit variant (Fragment)	PSMB2	R.NLADC*LR.S	0.92	0.76	0.985
IPI00176655.5	_ Uncharacterized protein ENSP00000348430 ENSG0000	_	K.TPC*GEGSK.T	0.99	0.76	1.03
IPI00641582.1	BAG3 BAG family molecular chaperone regulator 3 EN	BAG3	R.SQSPAASDC*SSSSSSASLPSSGR.S	1.05	0.76	0
IPI00013847.4	UQCRC1 Ubiquinol-cytochrome-c reductase complex co	UQCRC1	K.YIYDQC*PAVAGYGPIEQLPDYNR.I	0	0.76	0.975
IPI00290566.1	TCP1 T-complex protein 1 subunit alpha ENSG0000012	TCP1	K.VLC*ELADLQDKEVGDGTTSVVIIAAELLK.N	1.27	0.76	1.02
IPI00021926.2	PSMC6 26S protease regulatory subunit S10B ENSG000	PSMC6	K.GC*LLYGPPGTGK.T	0.71	0.76	0.925
IPI00219156.7	RPL30 60S ribosomal protein L30 ENSG00000156482 IP	RPL30	R.VC*TLAIIDPGDSDIIR.S	0.97	0.765	1.075
IPI00176574.1	LOC284230 Uncharacterized protein ENSP00000351550	LOC284230	R.LECVEPNC*R.S	0.895	0.765	1
IPI00065671.1	UCK2 Isoform 1 of Uridine-cytidine kinase 2 ENSG00	UCK2	R.QTNGC*LNGYTPSR.K	1.04	0.77	1.005
IPI00020898.1	RPS6KA3 Ribosomal protein S6 kinase alpha-3 ENSG00	RPS6KA3	K.AYSFC*GTVEYMAPEVVNR.R	0.88	0.77	1.08
IPI00023530.6	CDK5 Cell division protein kinase 5 ENSG0000016488	CDK5	R.ISAEEALQHPYFSDFC*PP.-	0.98	0.77	0.98
IPI00026781.2	FASN Fatty acid synthase ENSG00000169710 IPI000267	FASN	R.DPETLVGYSMVGC*QR.A	1.03	0.775	0.945
IPI00026781.2	FASN Fatty acid synthase ENSG00000169710 IPI000267	FASN	K.ADEASELAC*PTPK.E	0.96	0.775	1.11
IPI00027107.5	TUFM Tu translation elongation factor, mitochondri	TUFM	K.NMITGTAPLDGC*ILVVAANDGPMPQTR.E	0.84	0.775	1.045
IPI00013214.1	MCM3 DNA replication licensing factor MCM3 ENSG000	MCM3	R.TLTSC*FLSCVVCVEGIVTK.C	0	0.775	1.41
IPI00008994.2	NDRG2 Isoform 1 of Protein NDRG2 ENSG00000165795 I	NDRG2	K.YFLQGMGYMASSC*MTR.L	0.84	0.78	0.91

IPI00291939.1	SMC1A Structural maintenance of chromosomes protei	SMC1A	K.AESLIGVYPEQGDC*VISK.V	0.88	0.78	1.04
IPI00220373.4	IDE Insulin-degrading enzyme ENSG00000119912 IPI00	IDE	R.EMDSC*PVVGEFPCQNDINLSQAPALPQPEVIQNMTEFKR.G	1.12	0.785	1.005
IPI00383460.7	GRSF1 G-rich RNA sequence binding factor 1 isoform	GRSF1	R.YIELFLNSC*PK.G	1.135	0.79	1.115
IPI00478758.1	C10orf119 Uncharacterized protein C10orf119 ENSG00	C10orf119	R.DASALLDPMEC*TDTAEEQR.V	1.045	0.79	1.03
IPI00021840.1	RPS6 40S ribosomal protein S6 ENSG00000137154 IPI0	RPS6	K.LNISFPATGC*QK.L	0.965	0.79	0.985
IPI00375704.1	PSMB5 Putative uncharacterized protein DKFZp686I01	PSMB5	K.KVIEINPYLLGTMAGGAADC*SFWER.L	0.91	0.79	1
IPI00745793.1	CCNB1 G2/mitotic-specific cyclin-B1 ENSG0000013405	CCNB1	R.FMQNNC*VPK.K	1.1	0.79	1.175
IPI00008422.5	SMARCAD1 Isoform 2 of SWI/SNF-related matrix-assoc	SMARCAD1	K.NTEMC*NVMMQLR.K	1.01	0.795	1.03
IPI00796337.1	PCBP2 poly(rC)-binding protein 2 isoform a ENSG000	PCBP2	R.AITIAGIPQSIIEC*VK.Q	1.015	0.795	1.06
IPI00301609.8	NEK9 Serine/threonine-protein kinase Nek9 ENSG0000	NEK9	R.LLTFGC*NK.C	1.015	0.8	1.14
IPI00292753.7	GAPVD1 GTPase activating protein and VPS9 domains	GAPVD1	R.LQELESC*SGLGSTSDDTDVR.E	1.035	0.8	1.105
IPI00182533.5	RPL28 60S ribosomal protein L28 ENSG00000108107 IP	RPL28	R.NC*SSFLIK.R	0.99	0.8	1.055
IPI00449197.1	GMPR2 GMPR2 protein ENSG00000100938 IPI00385158 IP	GMPR2	K.VGIGPGSVC*TTR.K	1.38	0.8	0.955
IPI00472102.3	HSPD1 61 kDa protein ENSG00000144381 IPI00472102 I	HSPD1	K.C*EFQDAYVLLSEK.K	0.95	0.8	0.985
IPI00219669.5	CA8 Carbonic anhydrase-related protein ENSG0000017	CA8	K.GAELVEGC*DGILGDNFRPTQPLSDR.V	0.905	0.8	0
IPI00241841.8	KRT79 keratin 6L ENSG00000185640 IPI00241841	KRT79	K.KQC*QQLQTAIAEAEQR.G	0.9	0.8	0
IPI00018009.2	EDC3 Enhancer of mRNA-decapping protein 3 ENSG0000	EDC3	K.DLPTSPVDLVINC*LDCPENVFLR.D	0.935	0.805	0.97
IPI00003768.1	PES1 Isoform 1 of Pescadillo homolog 1 ENSG0000010	PES1	K.AGEGTYALDSESC*MEK.L	0.89	0.805	0.86
IPI00099996.2	RG9MTD1 RNA (guanine-9-) methyltransferase domain-	RG9MTD1	K.SSVQEEC*VSTISSSKDEDPLAATR.E	1.02	0.805	0.845
IPI00216975.1	TPM4 Isoform 2 of Tropomyosin alpha-4 chain ENSG00	TPM4	K.EENVGLHQTLDQTLNELNC*I.-	1.195	0.805	0.94
IPI00147874.1	NANS Sialic acid synthase ENSG00000095380 IPI00147	NANS	K.QLLPCEMAC*NEK.L	0.98	0.81	1.045
IPI00640703.3	XPO5 Isoform 1 of Exportin-5 ENSG00000124571 IPI00	XPO5	R.AVMEQIPEIQKDSLDQFDC*K.L	0.98	0.81	1.07
IPI00006167.1	PPM1G Protein phosphatase 1G ENSG00000115241 IPI00	PPM1G	R.GTEAGQVGEPGIPTGEAGPSC*SSASDKLPR.V	1.045	0.815	1.005
IPI00019380.1	NCBP1 Nuclear cap-binding protein subunit 1 ENSG00	NCBP1	K.SAC*SLESNLEGLAGVLEADLPNYK.S	0	0.815	0
IPI00025087.1	TP53 Isoform 1 of Cellular tumor antigen p53 ENSG0	TP53	R.C*SDSDGLAPPQHLIR.V	0.99	0.82	1.23
IPI00299524.1	NCAPD2 Condensin complex subunit 1 ENSG00000010292	NCAPD2	K.VACC*PLER.C	1.065	0.82	0.97
IPI00220301.5	PRDX6 Peroxiredoxin-6 ENSG00000117592 IPI00220301	PRDX6	K.DINAYNC*EEPTEK.L	0.975	0.82	0.995
IPI00747722.1	GALK1 Uncharacterized protein GALK1 ENSG0000010847	GALK1	K.GHALLIDC*R.S	1.03	0.82	0.925
IPI00448095.3	DCXR L-xylulose reductase ENSG00000169738 IPI00448	DCXR	R.GVPGAIVNVSSQC*SQR.A	0.985	0.825	1.27
IPI00514983.3	HSPH1 Isoform Alpha of Heat shock protein 105 kDa	HSPH1	R.C*TPSVISFGSK.N	1.105	0.825	1.04
IPI00010157.1	MAT2A S-adenosylmethionine synthetase isoform type	MAT2A	K.VAC*ETVAK.T	0.965	0.825	1.005
IPI00025273.1	GART Isoform Long of	GART	R.SGC*KVDLGGFA	0	0.825	1.12

	Trifunctional purine biosynth		GLFDLK.A			
IPI00009668.3	CENPH Centromere protein H ENSG00000153044 IPI0000	CENPH	R.AGGPPQVAGAQAAC*SEDR.M	1.055	0.83	1.11
IPI00788737.1	GAPDH 39 kDa protein ENSG00000111640 IPI00789134 I	GAPDH	R.VPTANVSVVDLTC*R.L	1	0.83	1
IPI00304596.3	NONO Non-POU domain-containing octamer-binding pro	NONO	R.C*SEGSFLLTTFPRPVTVEPMDQLDDEEGLPEK.L	1.19	0.83	1.19
IPI00166130.1	D15Wsu75e DJ347H13.4 protein ENSG00000100418 IPI00	D15Wsu75e	R.GEAYNLFEHNC*NTFSNEVAQFLTGR.K	0.95	0.83	0.935
IPI00555734.3	ASRGL1 asparaginase-like 1 protein ENSG00000162174	ASRGL1	K.GAQKTDC*QK.N	1.085	0.83	1.05
IPI00220766.5	GLO1 Lactoylglutathione lyase ENSG00000124767 IPI0	GLO1	K.C*DFPIMK.F	0.91	0.83	0.955
IPI00016610.2	PCBP1 Poly(rC)-binding protein 1 ENSG00000169564 I	PCBP1	R.AITIAGVPQSVTEC*VK.Q	0	0.83	0.985
IPI00026781.2	FASN Fatty acid synthase ENSG00000169710 IPI000267	FASN	K.AINC*ATSGVVGLVNCLR.R	1.2	0.835	1.125
IPI00022228.1	HDLBP Vigilin ENSG00000115677 IPI00022228 IPI00443	HDLBP	K.AAC*LESAQEPAGAWGNK.I	1	0.835	0.925
IPI00021766.4	RTN4 Isoform 1 of Reticulon-4 ENSG00000115310 IPI0	RTN4	K.YSNSALGHVNC*TIK.E	0.62	0.835	1.005
IPI00290566.1	TCP1 T-complex protein 1 subunit alpha ENSG0000012	TCP1	R.SLHDALC*VVK.R	1.075	0.835	0.94
IPI00607557.1	ELF2 Isoform 5 of ETS-related transcription factor	ELF2	K.IITIPATQLAQC*QLQTK.S	0.96	0.835	1.135
IPI00292771.4	NUMA1 Isoform 1 of Nuclear mitotic apparatus prote	NUMA1	K.APVPSTC*SSTFPEELSPPSHQAK.R	0	0.835	0.74
IPI00556027.1	BAG5 BCL2-associated athanogene 5 isoform a ENSG00	BAG5	K.TELQGLIGQLDEVSLEKNPC*IR.E	0.88	0.835	0.99
IPI00220158.1	ADD1 Isoform 3 of Alpha-adducin ENSG00000087274 IP	ADD1	R.VSMILQSPAFC*EELESMIQEQFKK.G	0.94	0.84	0.97
IPI00290566.1	TCP1 T-complex protein 1 subunit alpha ENSG0000012	TCP1	R.DC*LINAAK.T	0.915	0.84	1.01
IPI00307755.3	PRKAA2 5-AMP-activated protein kinase catalytic s	PRKAA2	R.TSC*GSPNYAAPEVISGR.L	1	0.84	1.02
IPI00221091.9	RPS15A 40S ribosomal protein S15a ENSG00000134419	RPS15A	K.C*GVISPR.F	0.97	0.84	1.085
IPI00304742.4	STK10 Uncharacterized protein STK10 ENSG0000007278	STK10	K.LSEEAEC*PNPSTPSK.A	0	0.84	0
IPI00299263.5	ARFGAP3 ADP-ribosylation factor GTPase-activating	ARFGAP3	K.LANTC*FNEIEK.Q	1.085	0.845	1.005
IPI00336008.1	ALDH5A1 aldehyde dehydrogenase 5A1 precursor, isof	ALDH5A1	R.NTGQTC*VCSNQFLVQR.G	1.02	0.845	0.895
IPI00302673.3	ATPAF1 ATP synthase mitochondrial F1 complex assem	ATPAF1	K.C*AQNQNKT.-	1.05	0.845	1
IPI00018465.1	CCT7 T-complex protein 1 subunit eta ENSG000001356	CCT7	R.INALTAASEAAC*LIVSVDETIKNPR.S	0	0.845	0.815
IPI00163085.2	AMOT Isoform 1 of Angiomotin ENSG00000126016 IPI00	AMOT	R.DC*STQTER.G	1.035	0.845	0.97
IPI00024579.1	RAD18 E3 ubiquitin-protein ligase RAD18 ENSG000000	RAD18	K.TQCPTCC*VTVTEPDLK.N	1.085	0.85	0.775
IPI00748353.1	WDHD1 126 kDa protein ENSG00000198554 IPI00748353	WDHD1	K.NVLSETPAIC*PPQNTENQRPK.T	1.03	0.85	1.05
IPI00024719.1	HAT1 Histone acetyltransferase type B catalytic su	HAT1	K.VDENFDC*VEADDVEGK.I	0.97	0.85	1.05
IPI00644290.1	NDRG3 NDRG family member 3 ENSG00000101079 IPI0021	NDRG3	R.FALNHPELVEGLVLINVDPC*AK.G	0	0.85	0
Reverse_IPI00376572.2	LOC391722 similar to myosin regulatory light chain	LOC391722	K.CCC*NQSPPSSASSVPAMNRNKNVNRQER.F	0	0.85	0
IPI00552897.2	MDC1 Isoform 1 of Mediator of DNA damage checkpoin	MDC1	R.C*NVEPVGR.L	0.99	0.85	0.98

IPI00025815.2	TARDBP TDP43 ENSG00000120948 IPI00025815 IPI006398	TARDBP	R.VTEDENDEPIEIPSEDDGTVLLSTVTAQFPGAC*GLR.Y	0	0.85	0.93
IPI00302688.7	ECHDC1 Isoform 1 of Enoyl-CoA hydratase domain-con	ECHDC1	K.SLGTPEDGMAVC*MFMQNTLTR.F	0.985	0.855	1.29
IPI00329321.3	LYRM7 LYR motif-containing protein 7 ENSG000001866	LYRM7	R.KDLLVENVPYC*DAPTQK.Q	0.96	0.855	0.98
IPI00022827.1	SLK Isoform 1 of STE20-like serine/threonine-prote	SLK	K.MTGESEC*LNPSTQSR.I	1.03	0.855	0.905
IPI00410067.1	ZC3HAV1 Isoform 1 of Zinc finger CCCH type antivir	ZC3HAV1	K.NSNVDSSYLESLYQSC*PR.G	1.135	0.855	0.965
IPI00013452.8	EPRS glutamyl-prolyl tRNA synthetase ENSG000001366	EPRS	K.LGVENC*YFPMFVSQSALEK.E	1	0.855	0.995
IPI00017963.1	SNRPD2 Small nuclear ribonucleoprotein Sm D2 ENSG0	SNRPD2	K.NNTQVLINC*R.N	0.885	0.855	1.01
IPI00029079.5	GMPS GMP synthase ENSG00000163655 IPI00029079	GMPS	K.AC*TTEEDQEK.L	1.145	0.855	0.955
IPI00479877.4	ALDH9A1 aldehyde dehydrogenase 9A1 ENSG00000143149	ALDH9A1	K.GALMANFLTQGQVC*CNGTR.V	1.045	0.86	1.005
IPI00455153.2	NFU1 HIRA interacting protein 5 isoform 2 ENSG0000	NFU1	K.LQGSCTSC*PSSIITLK.N	1.145	0.86	1.085
IPI00215610.2	MPP1 55 kDa erythrocyte membrane protein ENSG00000	MPP1	R.VASMAQSAPSEAPSC*SPFGK.K	1.075	0.86	1.02
IPI00010860.1	PSMD9 Isoform p27-L of 26S proteasome non-ATPase r	PSMD9	K.GIGMNEPLVDC*EGYPR.S	0.95	0.86	0.87
IPI00220906.4	ACOT2 Isoform 1 of Acyl-coenzyme A thioesterase 2,	ACOT2	K.SEFYANEAC*KR.L	0.81	0.86	1.065
IPI00386755.2	ERO1L ERO1-like protein alpha precursor ENSG000001	ERO1L	K.HDDSSDNFC*EADDIQSPEAEYVDLLLNPER.Y	1.03	0.865	0.95
IPI00479385.3	ASMTL Uncharacterized protein ASMTL ENSG0000016909	ASMTL	K.VDASAC*GMER.L	1.105	0.865	1.05
IPI00001287.1	C20orf72 Uncharacterized protein C20orf72 ENSG0000	C20orf72	R.GVAQTPGSVEEDALLC*GPVSK.H	1.05	0.865	1.135
IPI00294008.4	ZWINT ZW10 interactor ENSG00000122952 IPI00646553	ZWINT	K.LLC*SQLQVADFLQNILAQEDTAK.G	0.9	0.865	1.025
IPI00017184.2	EHD1 EH domain-containing protein 1 ENSG0000011004	EHD1	R.FMC*AQLPNPVLDSISIIDTPGILSGEK.Q	0	0.865	0
IPI00015141.4	CKMT2 Creatine kinase, sarcomeric mitochondrial pr	CKMT2	R.LGYILTC*PSNLGTGLR.A	1.06	0.87	1.015
IPI00090720.4	QRSL1 Glutaminyl-tRNA synthase-like protein 1 ENSG	QRSL1	K.QVQFPVIQLQELMDDC*SAVLENEK.L	0.825	0.87	0.935
IPI00550365.2	PCBP3 Poly(RC) binding protein 3 ENSG00000183570 I	PCBP3	R.LVVPASQC*GSLIGK.G	0.93	0.87	1
IPI00480131.1	FLNB Uncharacterized protein FLNB ENSG00000136068	FLNB	R.SSTETC*YSAIPK.A	0.975	0.87	0.97
IPI00300371.5	SF3B3 Isoform 1 of Splicing factor 3B subunit 3 EN	SF3B3	R.SEHPPLC*GR.D	0	0.87	0.895
IPI00333763.7	GLRX5 Glutaredoxin-related protein 5 ENSG000001825	GLRX5	K.GTPEQPQC*GFSNAVVQILR.L	0.95	0.875	1.01
IPI00374272.3	LOC285636 hypothetical protein LOC285636 ENSG00000	LOC285636	R.C*PIQLNEGVSFQDLDTAK.L	0.905	0.875	1.095
IPI00639841.2	PECI Peroxisomal 3,2-trans-enoyl-CoA isomerase ENS	PECI	R.WLSDEC*TNAVVNFLSR.K	0.92	0.875	1.005
IPI00748935.1	ELP4 59 kDa protein ENSG00000109911 IPI00847770 IP	ELP4	K.VEPC*SLTPGYTK.L	1.135	0.875	1.08
IPI00294536.1	STRAP Serine-threonine kinase receptor-associated	STRAP	K.IGFPETTEEELEEIASENSDC*IFPSAPDVK.A	0.99	0.875	1.01
IPI00746351.1	DIS3 Uncharacterized protein DIS3 ENSG00000083520	DIS3	R.LAC*LSEEGNEIESGK.I	1.195	0.875	1.21
IPI00848058.1	ACTB Actin, cytoplasmic 2 ENSG00000075624 IPI00021	ACTB	R.C*PEALFQPSFLGMESCGIHETTFNSIMK.C	0	0.875	0

IPI00012197.1	XTP3TPA XTP3-transactivated gene A protein ENSG000	XTP3TPA	K.YTELPHGAISEDQAVGPADIPC*DSTGQTST.-	0.995	0.88	1.005
IPI00514983.3	HSPH1 Isoform Alpha of Heat shock protein 105 kDa	HSPH1	K.LMSSNSTDLPLNIEC*FMNDKDVSGK.M	1.005	0.88	0.935
IPI00332499.1	NASP nuclear autoantigenic sperm protein isoform 1	NASP	R.KPTDGASSSNC*VTDISHLVR.K	0.96	0.88	1.06
IPI00101652.4	SCLY Selenocysteine lyase ENSG00000132330 IPI00101	SCLY	R.DAPAPAASQPSGC*GK.H	1.06	0.88	1.055
IPI00003814.1	MAP2K6 Isoform 1 of Dual specificity mitogen-activ	MAP2K6	K.AC*ISIGNQNFEVK.A	0	0.88	1.07
IPI00021320.2	MEPCE 7SK snRNA methylphosphate capping enzyme ENS	MEPCE	R.SC*FPASLTASR.G	0.78	0.88	1.165
IPI00007935.4	PDLIM5 PDZ and LIM domain protein 5 ENSG0000016311	PDLIM5	R.QPTVTSVC*SETSQELAEGQR.R	1.055	0.88	0.945
IPI00103925.2	IRGQ Immunity-related GTPase family Q protein ENSG	IRGQ	R.EKC*SAGSQK.A	1.27	0.88	1.15
IPI00009654.1	TRAPPC1 Trafficking protein particle complex subun	TRAPPC1	K.NPLC*PLGQTVQSELFR.S	0	0.88	0
IPI00027443.5	CARS cysteinyl-tRNA synthetase isoform c ENSG00000	CARS	R.VQPQWSPPAGTQPC*R.L	1.08	0.885	1.09
IPI00021347.1	UBE2L3 Ubiquitin-conjugating enzyme E2 L3 ENSG0000	UBE2L3	K.GQVC*LPVISAENWKPATK.T	0.36	0.885	1.225
IPI00807364.1	FNBP1L Isoform 1 of Formin-binding protein 1-like	FNBP1L	R.FTSC*VAFFNILNELNDYAGQR.E	0	0.885	0
IPI00658023.1	PTPN11 Isoform 1 of Tyrosine-protein phosphatase n	PTPN11	K.YSLADQTSGDQSPLPPCTPTPPC*AEMR.E	0.83	0.89	1.02
IPI00030876.6	DIAPH1 Diaphanous 1 ENSG00000131504 IPI00030876 IP	DIAPH1	K.AGC*AVTSLLASELTK.D	0	0.89	0
IPI00220158.1	ADD1 Isoform 3 of Alpha-adducin ENSG00000087274 IP	ADD1	K.TAGPQSQVLC*GVVMDR.S	0.935	0.89	1.035
IPI00011107.2	IDH2 Isocitrate dehydrogenase [NADP], mitochondria	IDH2	K.SSGGFVWAC*K.N	0.94	0.89	0.975
IPI00073602.1	EXOSC6 Exosome complex exonuclease MTR3 ENSG000001	EXOSC6	R.RAPPGGC*EER.E	0	0.89	0.81
IPI00018140.3	SYNCRIP Isoform 1 of Heterogeneous nuclear ribonuc	SYNCRIP	K.SAFLC*GVMK.T	0.975	0.895	0.995
IPI00550746.4	NUDC Nuclear migration protein nudC ENSG0000009027	NUDC	R.WTQTLSELDLAVPFC*VNFR.L	0.97	0.895	0.96
IPI00292753.7	GAPVD1 GTPase activating protein and VPS9 domains	GAPVD1	R.FSLC*SDNLEGISEGPSNR.S	1.05	0.895	1.29
IPI00169383.3	PGK1 Phosphoglycerate kinase 1 ENSG00000102144 IPI	PGK1	R.GCITIIGGGDTATC*C*AK.W	0.985	0.895	1.055
IPI00009949.2	PSMF1 Proteasome inhibitor PI31 subunit ENSG000001	PSMF1	R.QPPWC*DPLGPFVVGGEDLDPFGPR.R	1.14	0.895	1.005
IPI00018946.3	PANK4 Pantothenate kinase 4 ENSG00000157881 IPI000	PANK4	R.C*FPGVVR.S	0.86	0.895	1.195
IPI00643920.2	TKT Transketolase ENSG00000163931 IPI00643920 IPI0	TKT	R.MAAISESNINLC*GSHCGVSIGEDGPSQMALEDLAMFR.S	1.095	0.895	0.98
IPI00013789.5	SMYD5 SET and MYND domain-containing protein 5 ENS	SMYD5	R.LFSQFC*NK.T	0.745	0.9	0.77
IPI00059242.3	SYAP1 Synapse-associated protein 1 ENSG00000169895	SYAP1	K.TQEDEEEISTSPGVSEFVSDAFDAC*NLNQEDLRK.E	0.92	0.9	1.005
IPI00006181.1	EIF3D Eukaryotic translation initiation factor 3 s	EIF3D	K.FMTPVIQDNPSGWGPC*AVPEQFR.D	0.86	0.9	1.11
IPI00103554.1	GATAD2B Transcriptional repressor p66 beta ENSG000	GATAD2B	K.SC*ASLLR.V	0.98	0.9	1.03
IPI00059687.1	C18orf25 Isoform 1 of Uncharacterized protein C18o	C18orf25	K.DGVADSTVISSMPC*LLMELR.R	0.92	0.9	0.995
IPI00106573.6	C20orf7 hypothetical protein LOC79133 isoform 1 EN	C20orf7	R.NFPLALDLGC*GR.G	1.06	0.9	1.075
IPI00016610.2	PCBP1 Poly(rC)-binding protein 1	PCBP1	R.INISEGNC*PER.I	0.995	0.905	1

	ENSG00000169564 I					
IPI00031680.3	ACBD6 Acyl-CoA-binding domain-containing protein 6	ACBD6	R.DQDGCLPEEVTGC*K.T	1.1	0.905	1.02
IPI00174442.2	FAM98A Protein FAM98A ENSG00000119812 IPI00174442	FAM98A	R.EKTAC*AINK.V	0.94	0.905	1.045
IPI00012750.3	RPS25 40S ribosomal protein S25 ENSG00000118181 IP	RPS25	K.ATYDKLC*K.E	0.935	0.905	0.985
IPI00556451.2	ETFB Isoform 2 of Electron transfer flavoprotein s	ETFB	K.EVIAVSCGPAQC*QETIR.T	1.03	0.905	0.985
IPI00024993.4	ECHS1 Enoyl-CoA hydratase, mitochondrial precursor	ECHS1	K.AFAAGADIKEMQNLSFQDC*YSSK.F	1.01	0.905	1
IPI00828021.1	HSPA4L Heat shock protein apg-1 ENSG00000164070 IP	HSPA4L	K.SIDLPIQSSLC*R.Q	1.61	0.905	1.075
IPI00024661.4	SEC24C Protein transport protein Sec24C ENSG000001	SEC24C	R.APPSSGAPPASTAQAPC*GQAAYGQFGQGDVQNGPSSTVQMQR.L	0	0.905	1.015
IPI00472675.2	NUP205 228 kDa protein ENSG00000155561 IPI00783781	NUP205	R.C*QDVSAGSLQELALLTGIISK.A	0.91	0.91	1.125
IPI00796199.1	HNRNPL Uncharacterized protein HNRPL ENSG000001048	HNRNPL	K.QPAIMPGQSYGLEDGSC*SYKDFSESR.N	0.865	0.91	1.005
IPI00642816.2	SRP9 hCG_1781062 Signal recognition particle 9 kDa	SRP9	K.VTDDLVC*LVYK.T	1.055	0.91	1.06
IPI00010720.1	CCT5 T-complex protein 1 subunit epsilon ENSG00000	CCT5	K.VVNSC*HR.Q	1	0.91	1.035
IPI00009010.3	HSPC152 TRM112-like protein ENSG00000173113 IPI000	HSPC152	R.IC*PVEFNPNFVAR.M	0.915	0.91	0.97
IPI00472102.3	HSPD1 61 kDa protein ENSG00000144381 IPI00472102 I	HSPD1	R.AAVEEGIVLGGGC*ALLR.C	0.95	0.91	1.02
IPI00021926.2	PSMC6 26S protease regulatory subunit S10B ENSG000	PSMC6	R.AVASQLDC*NFLK.V	0.89	0.91	1.095
IPI00166123.3	TTC5 Tetratricopeptide repeat protein 5 ENSG000001	TTC5	R.VETPLLLVVNGKPQGSSSQAVATVASRPQC*E.-	0	0.91	0
IPI00302927.6	CCT4 T-complex protein 1 subunit delta ENSG0000011	CCT4	K.ITGC*ASPGK.T	1.02	0.915	1.055
IPI00745518.1	MAP4 Microtubule-associated protein 4 isoform 1 va	MAP4	K.NVC*LPPEMEVALTEDQVPALK.T	1.12	0.915	1.045
IPI00797537.1	NUDCD1 NudC domain-containing protein 1 ENSG000001	NUDCD1	R.DSAQC*AAIAER.L	1.18	0.915	1.03
IPI00219103.6	HPCA Neuron-specific calcium-binding protein hippo	HPCA	R.LLQC*DPSSASQF.-	0.89	0.915	0.87
IPI00790739.1	ACO2 Aconitase 2, mitochondrial ENSG00000100412 IP	ACO2	R.DLGGIVLANAC*GPCIGQWDR.K	0.845	0.915	1
IPI00002966.1	HSPA4 Heat shock 70 kDa protein 4 ENSG00000170606	HSPA4	K.LMSANASDLPLSIEC*FMNDVDVSGTMNR.G	0.98	0.92	1.12
IPI00103087.2	GEMIN6 Gem-associated protein 6 ENSG00000152147 IP	GEMIN6	K.LMHLFTSGDC*K.A	0.88	0.92	1.02
IPI00216682.5	CNN3 Calponin-3 ENSG00000117519 IPI00216682 IPI006	CNN3	K.C*ASQAGMTAYGTR.R	0.96	0.92	0.97
IPI00298111.7	SNX6 sorting nexin 6 isoform b ENSG00000129515 IPI	SNX6	R.IGSSLYALGTQDSTDIC*K.F	1.97	0.92	1.05
IPI00171856.1	DOHH Deoxyhypusine hydroxylase ENSG00000129932 IPI	DOHH	R.PAC*LAALQAHADDPER.V	0.93	0.92	1.29
IPI00032995.1	LANCL2 LanC-like protein 2 ENSG00000132434 IPI0003	LANCL2	R.AFVNPFPDYEAAAGALLASGAAEETGC*VRPPATTDEPGLPFHQDGK.I	0	0.92	0
IPI00018146.1	YWHAQ 14-3-3 protein theta ENSG00000134308 IPI0001	YWHAQ	R.DNLTLWTSDSAGEEC*DAAEGAEN.-	1.05	0.925	0.91
IPI00021305.1	CCNH Cyclin-H ENSG00000134480 IPI00021305 IPI00556	CCNH	R.TC*LSQLLDIMK.S	1.13	0.925	1.035

IPI00441867.1	PEX19 Isoform 1 of Peroxisomal biogenesis factor 1	PEX19	R.VGSDMTSQQEFTSC*LK.E	0.975	0.925	0.99
IPI00002496.2	GMPPB AMIGO3 GDP-mannose pyrophosphorylase B isofo	GMPPB	R.LC*SGPGIVGNVLVDPSAR.I	1.025	0.925	1.09
IPI00456919.2	HUWE1 Isoform 1 of E3 ubiquitin-protein ligase HUW	HUWE1	R.DQSAQC*TASK.S	0.85	0.925	1.12
IPI00397904.6	NUP93 Nuclear pore complex protein Nup93 ENSG00000	NUP93	K.SSGQSAQLLSHEPGDPPC*LR.R	1.015	0.925	0.935
IPI00025491.1	EIF4A1 Eukaryotic initiation factor 4A-I ENSG00000	EIF4A1	K.VVMALGDYMGASC*HACIGGTNVR.A	0.91	0.93	1.065
IPI00008248.3	ANAPC7 Anaphase-promoting complex subunit 7 ENSG00	ANAPC7	R.LEDVENLGC*R.L	0.945	0.93	1.17
IPI00015736.3	UBE1DC1 Ubiquitin-activating enzyme E1 domain-cont	UBE1DC1	R.EGVC*AASLPTTMGVVAGILVQNVLK.F	1.04	0.93	0.975
IPI00719622.1	RPS28 LOC646195 LOC645899 40S ribosomal protein S2	RPS28	R.TGSQGQC*TQVR.V	1.195	0.93	1.07
IPI00643920.2	TKT Transketolase ENSG00000163931 IPI00643920 IPI0	TKT	K.QAFTDVATGSLGQGLGAAC*GMAYTGK.Y	1.24	0.93	0.985
IPI00101645.3	KIAA0828 Putative adenosylhomocysteinase 3 ENSG000	KIAA0828	K.FDNLYC*CR.E	1.2	0.93	1.035
IPI00216746.1	HNRPK Isoform 2 of Heterogeneous nuclear ribonucle	HNRPK	K.IIPTLEEGLQLPSPTATSQLPLESDAVEC*LNYQHYK.G	0.97	0.93	0.99
IPI00183626.8	PTBP1 polypyrimidine tract-binding protein 1 isofo	PTBP1	K.RGSDELFSTC*VTNGPFIMSSNSASAANGNDSK.K	1.085	0.93	0.94
IPI00022977.1	CKB Creatine kinase B-type ENSG00000166165 IPI0002	CKB	R.FC*TGLTQIETLFK.S	0.5	0.93	0
IPI00549467.3	NIT2 Nitrilase family member 2 ENSG00000114021 IPI	NIT2	R.VGLGIC*YDMR.F	1.025	0.935	1.005
IPI00333541.6	FLNA Filamin-A ENSG00000196924 IPI00553169 IPI0030	FLNA	K.AHVVPC*FDASK.V	0.98	0.935	1.02
IPI00646361.2	NUP214 Uncharacterized protein NUP214 ENSG00000126	NUP214	K.VC*ATLPSTVAVTSVCWSPK.G	0	0.935	1.015
IPI00021812.2	AHNAK AHNAK nucleoprotein isoform 1 ENSG0000012494	AHNAK	K.LEGDLTGPSVGVEVPDVELEC*PDAK.L	0.84	0.935	1.12
IPI00008943.3	DDX19B Isoform 1 of ATP-dependent RNA helicase DDX	DDX19B	K.VLVTTNVC*AR.G	0.995	0.935	1.01
IPI00749250.1	ACTR2 45 kDa protein ENSG00000138071 IPI00005159 I	ACTR2	K.LC*YVGYNIEQEQK.L	1.215	0.935	0.98
IPI00747447.1	EIF3B 99 kDa protein ENSG00000106263 IPI00396370 I	EIF3B	R.FSHQGVQLIDFSPC*ER.Y	0	0.935	0.93
IPI00027626.3	CCT6A T-complex protein 1 subunit zeta ENSG0000014	CCT6A	K.NAIDDGC*VVPGAGAVEVAMAEALIK.H	0.92	0.935	0.975
IPI00306369.3	NSUN2 tRNA ENSG00000037474 IPI00306369	NSUN2	K.DGVC*GPPPSKK.M	1.07	0.94	1.08
IPI00041325.1	NOLA2 H/ACA ribonucleoprotein complex subunit 2 EN	NOLA2	K.ADPDGPEAQAEAC*SGER.T	1.08	0.94	1.1
IPI00470779.2	TXLNA Alpha-taxilin ENSG00000084652 IPI00816089 IP	TXLNA	R.VTEAPC*YPGAPSTEASGQTGPQEPTSAR.A	1.04	0.94	1.04
IPI00004839.1	CRKL Crk-like protein ENSG00000099942 IPI00004839	CRKL	K.RVPC*AYDK.T	1.065	0.94	1.02
IPI00298961.3	XPO1 Exportin-1 ENSG00000082898 IPI00784388 IPI002	XPO1	R.QMSVPGIFNPHEIPEEMC*D.-	0.95	0.94	0.935
IPI00020454.1	DCK Deoxycytidine kinase ENSG00000156136 IPI000204	DCK	R.SC*PSFSASSEGTR.I	0.95	0.94	1.055
IPI00007682.2	ATP6V1A Vacuolar ATP	ATP6	R.VLDALFPCVQGG	0.995	0.94	1.04

	synthase catalytic subunit A	V1A	TTAIPGAFGC*GK.T			
IPI00103467.4	ALDH1B1 Aldehyde dehydrogenase X, mitochondrial pr	ALDH1B1	K.LLC*GGER.F	0.88	0.94	1.065
IPI00033030.2	ADRM1 Protein ADRM1 ENSG00000130706 IPI00033030 IP	ADRM1	R.VPQC*PSGR.V	0.875	0.945	0.96
IPI00026138.4	_ Uncharacterized protein ENSP00000371610 ENSG0000	–	K.NC*LTNFHGMDLTR.D	1.03	0.945	0.985
IPI00018522.4	PRMT1 HMT1 hnRNP methyltransferase-like 2 isoform	PRMT1	K.VIGIEC*SSISDYAVK.I	1.06	0.945	1.08
IPI00024993.4	ECHS1 Enoyl-CoA hydratase, mitochondrial precursor	ECHS1	K.ALNALC*DGLIDELNQALK.T	1.01	0.945	1.01
IPI00745345.1	PPP4R2 Protein phosphatase 4 regulatory subunit 2	PPP4R2	K.EVC*PVLDQFLCHVAK.T	0.97	0.945	0.98
IPI00450071.5	C1orf19 tRNA-splicing endonuclease subunit Sen15 E	C1orf19	R.GDSEPTPGC*SGLGPGGVR.G	0.96	0.945	1.015
IPI00644079.2	HNRNPU heterogeneous nuclear ribonucleoprotein U i	HNRNPU	K.MC*LFAGFQR.K	0	0.945	1.85
IPI00549569.4	ISYNA1 Myo-inositol 1-phosphate synthase A1 ENSG00	ISYNA1	R.FC*EVIPGLNDTAENLLR.T	1.075	0.95	1.13
IPI00294739.1	SAMHD1 SAM domain and HD domain-containing protein	SAMHD1	R.VC*EVDNELR.I	1.22	0.95	0
IPI00384708.2	PDSS2 Isoform 1 of Decaprenyl-diphosphate synthase	PDSS2	R.C*LLSDELSNIAMQVR.K	0	0.95	0
IPI00006863.5	SPAG7 Single-stranded nucleic acid binding R3H dom	SPAG7	K.TYGC*VPVANKR.D	0.975	0.95	0.98
IPI00398048.1	_ Uncharacterized protein ENSP00000310225 ENSG0000	–	K.C*GFLPGNEK.V	0.925	0.95	0.885
IPI00000875.6	EEF1G Elongation factor 1-gamma ENSG00000186676 IP	EEF1G	K.AAAPAPEEEMDEC*EQALAAEPK.A	1	0.95	0.99
IPI00004534.3	PFAS Phosphoribosylformylglycinamidine synthase EN	PFAS	K.LMWLFGC*PLLLDDVAR.E	0	0.95	0.93
IPI00007812.1	ATP6V1B2 Vacuolar ATP synthase subunit B, brain is	ATP6V1B2	R.GPVVLAEDFLDIMGQPINPQC*R.I	0.975	0.95	0.97
IPI00376199.2	IRF2BP2 interferon regulatory factor 2 binding pro	IRF2BP2	R.AHGC*FPEGR.S	1.055	0.95	1.035
IPI00037599.3	TFCP2 Isoform 1 of Alpha-globin transcription fact	TFCP2	K.IAQLFSISPC*QISQIYK.Q	0	0.95	0
IPI00012535.1	DNAJA1 DnaJ homolog subfamily A member 1 ENSG00000	DNAJA1	K.GAVEC*CPNCR.G	1	0.955	0.96
IPI00018783.1	ITPA Inosine triphosphate pyrophosphatase ENSG0000	ITPA	R.GC*QDFGWDPCFQPDGYEQTYAEMPK.A	0.97	0.955	0.965
IPI00785096.2	BZW1 similar to basic leucine zipper and W2 domain	BZW1	K.ERFDPTQFQDC*IIQGLTETGTDLEAVAK.F	0.995	0.955	0.97
IPI00217223.1	PAICS Multifunctional protein ADE2 ENSG00000128050	PAICS	K.C*GETAFIAPQCEMIPIEWVCR.R	0.955	0.955	0.965
IPI00018331.3	SNAPAP SNARE-associated protein Snapin ENSG0000014	SNAPAP	R.EQIDNLATELC*R.I	0	0.955	1.105
IPI00786942.1	ALDH7A1 similar to antiquitin ENSG00000164904 IPI0	ALDH7A1	K.GSDC*GIVNVNIPTSGAEIGGAFGGEK.H	1.085	0.955	0.945
IPI00054042.1	GTF2I Isoform 1 of General transcription factor II	GTF2I	R.SILSPGGSC*GPIK.V	0.94	0.955	0.955
IPI00023087.1	UBE2T Ubiquitin-conjugating enzyme E2 T ENSG000000	UBE2T	R.IC*LDVLK.L	1.3	0.955	1.1
IPI00004534.3	PFAS Phosphoribosylformylglycinamidine synthase EN	PFAS	K.FC*DNSSAIQGK.E	1.06	0.96	1.08
IPI00219757.13	GSTP1 Glutathione S-transferase P ENSG00000084207	GSTP1	K.ASC*LYGQLPK.F	1.145	0.96	1.02
IPI00465152.2	SP1 Transcription factor Sp1 ENSG00000185591 IPI00	SP1	R.SSSTGSSSSTGGGGQESQPSPLALLAATC*SR.I	0.985	0.96	1

IPI00465044.2	RCC2 Protein RCC2 ENSG00000179051 IPI00465044	RCC2	K.AVQDLC*GWR.I	0.945	0.96	0.995
IPI00549993.3	C10orf97 chromosome 10 open reading frame 97 ENSG0	C10orf97	K.SSPGLSDTIFC*R.W	1.01	0.96	1.055
IPI00024673.2	MAPK9 Isoform Alpha-2 of Mitogen-activated protein	MAPK9	R.TAC*TNFMMTPYVVTR.Y	1.085	0.96	1.005
IPI00002520.1	SHMT2 Serine hydroxymethyltransferase, mitochondri	SHMT2	R.AALEALGSC*LNNK.Y	1.02	0.96	1.04
IPI00302925.3	CCT8 Uncharacterized protein CCT8 ENSG00000156261	CCT8	K.AHEILPNLVC*CSAK.N	1.15	0.96	0.95
IPI00748223.1	RABGGTB Uncharacterized protein RABGGTB ENSG000001	RABGGTB	K.KDDYEYC*MSEYLR.M	1.07	0.96	0
IPI00217157.5	DDX59 Isoform 1 of Probable ATP-dependent RNA heli	DDX59	K.NLPC*ANVR.Q	1.105	0.965	1.155
IPI00334775.6	HSP90AB1 85 kDa protein ENSG00000096384 IPI0041467	HSP90AB1	R.VFIMDSC*DELIPEYLNFIR.G	0.96	0.97	1
IPI00335449.3	PPP2R1B beta isoform of regulatory subunit A, prot	PPP2R1B	R.LNIISNLDC*VNEVIGIR.Q	1.01	0.97	1.005
IPI00029079.5	GMPS GMP synthase ENSG00000163655 IPI00029079	GMPS	R.VICAEEPYIC*K.D	0.975	0.97	0.99
IPI00177965.5	NT5DC1 5-nucleotidase domain-containing protein 1	NT5DC1	K.HFLSDTGMAC*R.S	1.125	0.97	1.035
IPI00419237.3	LAP3 Isoform 1 of Cytosol aminopeptidase ENSG00000	LAP3	R.QVVDC*QLADVNNIGK.Y	1.03	0.97	1.055
IPI00019169.3	SH3GL1 SH3-containing GRB2-like protein 1 ENSG0000	SH3GL1	R.EPFDLGEPEQSNGGFPC*TTAPK.I	0.96	0.97	0.985
IPI00334159.6	VBP1 Prefoldin subunit 3 ENSG00000155959 IPI003341	VBP1	R.FLLADNLYC*K.A	0.94	0.97	0.975
IPI00025176.1	SMNDC1 Survival of motor neuron-related-splicing f	SMNDC1	K.VGVGTC*GIADKPMTQYQDTSK.Y	1.045	0.97	1.06
IPI00020602.1	CSNK2A2 Casein kinase II subunit alpha ENSG000000	CSNK2A2	K.EQSQPC*ADNAVLSSGLTAAR.-	0.98	0.97	0.97
IPI00414408.2	LOC646799 similar to zygote arrest 1 ENSG000001891	LOC646799	R.RPNFQFLEPKYGYFHCKDC*K.T	1.385	0.97	1.09
IPI00020898.1	RPS6KA3 Ribosomal protein S6 kinase alpha-3 ENSG00	RPS6KA3	R.AENGLLMTPC*YTANFVAPEVLK.R	0.895	0.975	1.035
IPI00165230.1	DAZAP1 Isoform 1 of DAZ-associated protein 1 ENSG0	DAZAP1	R.NIDPKPC*TPR.G	0	0.975	0.995
IPI00008524.1	PABPC1 Isoform 1 of Polyadenylate-binding protein	PABPC1	K.VVC*DENGSK.G	1.02	0.975	0.98
IPI00641743.2	HCFC1 Uncharacterized protein HCFC1 ENSG0000017253	HCFC1	K.LVIYGGMSGC*R.L	1.245	0.975	1.17
IPI00479946.3	STIP1 STIP1 protein ENSG00000168439 IPI00013894 IP	STIP1	K.ALDLDSSC*K.E	1.025	0.975	1.045
IPI00335251.3	DUS1L tRNA-dihydrouridine synthase 1-like ENSG0000	DUS1L	K.AVAIPVFANGNIQC*LQDVER.C	1.085	0.98	1.07
IPI00017617.1	DDX5 Probable ATP-dependent RNA helicase DDX5 ENSG	DDX5	R.LIDFLEC*GK.T	0.99	0.98	1.05
IPI00010240.1	MIF4GD MIF4G domain-containing protein ENSG0000012	MIF4GD	K.VANVIVDHSLQDC*VFSK.E	0.91	0.98	1.145
IPI00549389.3	C9orf32 Protein of unknown function DUF858, methyl	C9orf32	R.IIC*SAGLSLLAEER.Q	1.01	0.98	1
IPI00021329.3	WDR45L WD repeat domain phosphoinositide-interacti	WDR45L	R.C*NYLALVGGGK.K	1.045	0.98	1.08
IPI00792352.1	RAN 26 kDa protein ENSG00000132341 IPI00643041 IPI	RAN	R.VC*ENIPIVLCGNK.V	1.11	0.98	1.025
IPI00329679.3	ZWILCH Zwilch ENSG00000174442 IPI00329679	ZWILCH	R.LNC*AAEDFYSR.L	0.82	0.98	0.9
IPI00550852.4	DCTN4 Dynactin subunit 4 ENSG00000132912 IPI005508	DCTN4	R.LLQPDFQPVC*ASQLYPR.H	1.31	0.98	1.25
IPI00004461.2	DGUOK Isoform 1 of Deoxyguanosine kinase, mitochon	DGUOK	K.AC*TAQSLGNLLDMMYR.E	0.97	0.985	1.08
IPI00008794.1	DFFB Isoform Alpha of DNA fragmentation factor sub	DFFB	R.VLGSMC*QR.L	1.145	0.985	1.05

IPI00746806.1	CTTN CTTN protein ENSG00000085733 IPI00029601 IPI0	CTTN	K.HC*SQVDSVR.G	1.34	0.985	1.53
IPI00464979.4	SUCLA2 Isoform 1 of Succinyl-CoA ligase [ADP-formi	SUCLA2	R.IC*NQVLVCER.K	0.955	0.985	1.025
IPI00216694.3	PLS3 plastin 3 ENSG00000102024 IPI00848312 IPI0021	PLS3	K.EGIC*ALGGTSELSSEGTQHSYSEEEK.Y	1.025	0.99	1.015
IPI00007811.1	CDK4 Cell division protein kinase 4 ENSG0000013544	CDK4	R.LMDVC*ATSR.T	0.81	0.99	0.965
IPI00013949.1	SGTA Small glutamine-rich tetratricopeptide repeat	SGTA	R.AIC*IDPAYSK.A	0.945	0.99	0.975
IPI00334159.6	VBP1 Prefoldin subunit 3 ENSG00000155959 IPI003341	VBP1	K.DSC*GKGEMATGNGR.R	1.005	0.99	0.975
IPI00093057.6	CPOX Coproporphyrinogen III oxidase, mitochondrial	CPOX	K.EGGGGISCVLQDGC*VFEK.A	0.98	0.99	1.045
IPI00473014.5	DSTN Destrin ENSG00000125868 IPI00473014 IPI006432	DSTN	K.LGGSLIVAFEGC*PV.-	1.02	0.99	1.035
IPI00010219.1	SPC25 Kinetochore protein Spc25 ENSG00000152253 IP	SPC25	K.STDTSC*QMAGLR.D	1.045	0.99	0.945
IPI00031647.2	PDCD2L Programmed cell death protein 2-like ENSG00	PDCD2L	R.YSWSGEPLFLTC*PTSEVTELPACSQCGGQR.I	0.97	0.99	0.995
IPI00018465.1	CCT7 T-complex protein 1 subunit eta ENSG000001356	CCT7	K.EGTDSSQGIPQLVSNISAC*QVIAEAVR.T	0.965	0.99	0.995
IPI00470502.2	PPA2 Isoform 2 of Inorganic pyrophosphatase 2, mit	PPA2	R.GQPC*SQNYR.L	1.09	0.99	1.125
IPI00007024.1	FAM96B Protein FAM96B ENSG00000166595 IPI00007024	FAM96B	R.VAAALENTHLLEVVNQC*LSAR.S	1.04	0.99	0.76
IPI00643722.1	ARID1A Isoform 1 of AT-rich interactive domain-con	ARID1A	K.GPADMASQC*WGAAAAAAAAAAASGGAQQR.S	0	0.99	1.23
IPI00003814.1	MAP2K6 Isoform 1 of Dual specificity mitogen-activ	MAP2K6	K.MC*DFGISGYLVDSVAK.T	0.955	0.99	0.88
IPI00005651.3	IPO13 Importin-13 ENSG00000117408 IPI00513961 IPI0	IPO13	R.TSLAVECGAVFPLLEQLLQQPSSPSC*VR.Q	0	0.99	0
IPI00013723.3	PIN1 Peptidyl-prolyl cis-trans isomerase NIMA-inte	PIN1	K.IKSGEEDFESLASQFSDC*SSAK.A	1	0.995	0.965
IPI00298961.3	XPO1 Exportin-1 ENSG00000082898 IPI00784388 IPI002	XPO1	K.DLLGLC*EQK.R	0.985	0.995	0.975
IPI00102856.3	SMAP1L Isoform 1 of Stromal membrane-associated pr	SMAP1L	K.STAPVMDLLGLDAPVAC*SIANSK.T	1.105	0.995	0.98
IPI00016610.2	PCBP1 Poly(rC)-binding protein 1 ENSG00000169564 I	PCBP1	R.LVVPATQC*GSLIGK.G	1.01	0.995	1.005
IPI00002214.1	KPNA2 Importin subunit alpha-2 ENSG00000182481 IPI	KPNA2	K.YGAVDPLLALLAVPDMSSLAC*GYLR.N	0.9	0.995	0.95
IPI00449197.1	GMPR2 GMPR2 protein ENSG00000100938 IPI00385158 IP	GMPR2	R.VTQQVNPIFSEAC*.-	0.98	0.995	0.795
IPI00377005.2	_ Uncharacterized protein ENSP00000340627 ENSG0000	–	K.C*LSAAEEK.Y	1.06	1	0.94
IPI00007927.3	SMC2 Isoform 1 of Structural maintenance of chromo	SMC2	R.FTQC*QNGK.I	1.155	1	0.96
IPI00293975.4	GPX1 glutathione peroxidase 1 isoform 1 ENSG000001	GPX1	R.FQTIDIEPDIEALLSQGPSC*A.-	0.92	1	1.04
IPI00386122.4	MOBKL3 Isoform 1 of Preimplantation protein 3 ENSG	MOBKL3	R.HTLDGAAC*LLNSNK.Y	1.02	1	1.02
IPI00027223.2	IDH1 Isocitrate dehydrogenase [NADP] cytoplasmic E	IDH1	K.SEGGFIWAC*K.N	1.02	1	0.995
IPI00013184.1	ARD1A N-terminal acetyltransferase complex ARD1 su	ARD1A	K.GNSPPSSGEAC*R.E	1.005	1	1.06
IPI00056505.5	NT5C3L Cytosolic 5-nucleotidase	NT5C3	K.NSSAC*ENSGYFQ	0.88	1	0

	III-like protein	L	QLEGK.T			
IPI00302925.3	CCT8 Uncharacterized protein CCT8 ENSG00000156261	CCT8	R.NIQAC*KELAQTTR.T	0.985	1	0.89
IPI00180704.3	WDR73 WD repeat protein 73 (Fragment) ENSG00000177	WDR73	R.LLVTSGLPGC*YLQVWQVAEDSDVIK.A	1.01	1	0.925
IPI00386189.2	NARG1 Isoform 1 of NMDA receptor-regulated protein	NARG1	K.GC*PPVFNTLR.S	0	1	1.08
IPI00027014.1	DCTN3 Isoform 1 of Dynactin subunit 3 ENSG00000137	DCTN3	K.QFVQWDELLC*QLEAATQVKPAEE.-	0	1	1.14
Reverse_IPI00216694.3	PLS3 plastin 3 ENSG00000102024 IPI00848312 IPI0021	PLS3	K.FLEHLEYDC*IFGNSNLDVK.A	1.03	1	1.24
IPI00012835.1	CTBP1 C-terminal-binding protein 1 ENSG00000159692	CTBP1	K.SAGDLGIAVCNVPAASVEETADSTLC*HILNLYR.R	0	1	0
IPI00304071.4	FLJ20920 hypothetical protein LOC80221 ENSG0000016	FLJ20920	R.MVSTPIGGLSYVQGC*TK.K	1.005	1.005	1.045
IPI00291510.3	IMPDH2 Inosine-5-monophosphate dehydrogenase 2 EN	IMPDH2	R.HGFC*GIPITDTGR.M	0	1.005	0
IPI00002519.1	SHMT1 Isoform 1 of Serine hydroxymethyltransferase	SHMT1	R.AVLEALGSC*LNNK.Y	1.61	1.005	1.095
IPI00257882.7	PEPD Xaa-Pro dipeptidase ENSG00000124299 IPI002578	PEPD	R.TVEEIEACMAGC*DK.A	1.185	1.005	1.03
IPI00009790.1	PFKP 6-phosphofructokinase type C ENSG00000067057	PFKP	R.LPLMEC*VQMTQDVQK.A	1.085	1.005	1.055
IPI00029534.1	PPAT Amidophosphoribosyltransferase precursor ENSG	PPAT	K.C*ELENCQPFVVETLHGK.I	1.005	1.005	1.06
IPI00177509.4	TRAPPC5 Trafficking protein particle complex subun	TRAPPC5	K.ENSTLNC*ASFTAGIVEAVLTHSGFPAK.V	1.23	1.01	1
IPI00473014.5	DSTN Destrin ENSG00000125868 IPI00473014 IPI006432	DSTN	K.C*STPEEIKK.R	1.01	1.01	1.065
IPI00789101.1	PTGES3 19 kDa protein ENSG00000110958 IPI00015029	PTGES3	K.HLNEIDLFHC*IDPNDSK.H	0.995	1.01	1.025
IPI00030177.2	RBPJ Isoform APCR-2 of Recombining binding protein	RBPJ	R.IIQFQATPC*PK.E	1.3	1.01	1.135
IPI00456981.2	RP11-11C5.2 Similar to RIKEN cDNA 2410129H14 ENSG0	RP11-11C5.2	R.LC*EQGINPEALSSVIK.E	0.73	1.01	1.025
IPI00024623.3	ACADSB Short/branched chain specific acyl-CoA dehy	ACADSB	K.VGSFC*LSEAGAGSDSFALK.T	0.12	1.01	1.03
IPI00008433.4	RPS5 40S ribosomal protein S5 ENSG00000083845 IPI0	RPS5	K.TIAEC*LADELINAAK.G	1	1.01	0.995
IPI00021327.3	GRB2 Isoform 1 of Growth factor receptor-bound pro	GRB2	K.VLNEEC*DQNWYK.A	1.06	1.01	0
IPI00006113.1	POLR2I DNA-directed RNA polymerase II subunit RPB9	POLR2I	R.NCDYQQEADNSC*IYVNK.I	0.895	1.01	0.97
IPI00430812.4	CNBP Zinc finger protein 9 ENSG00000169714 IPI0043	CNBP	R.DC*DHADEQK.C	0	1.01	0
IPI00177008.1	LOC283871 hypothetical protein LOC283871 ENSG00000	LOC283871	K.NNQESDC*VSK.K	1.04	1.015	0.965
IPI00382470.3	HSP90AA1 heat shock protein 90kDa alpha (cytosolic	HSP90AA1	R.VFIMDNC*EELIPEYLNFIR.G	0.98	1.015	1.06
IPI00853598.1	SEC13 41 kDa protein ENSG00000157020 IPI00845335 I	SEC13	R.FASGGC*DNLIK.L	1.025	1.015	0.99
IPI00005648.1	SAFB2 Scaffold attachment factor B2 ENSG0000013025	SAFB2	K.ILDILGETC*K.S	0.97	1.015	0.99
IPI00554737.3	PPP2R1A Serine/threonine-protein phosphatase 2A 65	PPP2R1A	K.DC*EAEVR.A	1.08	1.015	1.03
IPI00011698.3	SAP18 Histone deacetylase complex subunit SAP18 EN	SAP18	K.TC*PLLLR.V	1.09	1.015	0.925
IPI00019903.1	CCDC44 Coiled-coil domain-containing protein 44 EN	CCDC44	K.KLDSLGLCSVSC*ALEFIPNSK.V	1.17	1.015	1.16

IPI00006167.1	PPM1G Protein phosphatase 1G ENSG00000115241 IPI00	PPM1G	K.C*SGDGVGAPR.L	1.12	1.015	1.085
IPI00553185.2	CCT3 T-complex protein 1 subunit gamma ENSG0000016	CCT3	R.TLIQNC*GASTIR.L	0.945	1.015	0.945
IPI00023647.4	UBE1L2 Isoform 1 of Ubiquitin-activating enzyme E1	UBE1L2	R.KPNVGC*QQDSEELLK.L	1.11	1.02	1.045
IPI00418471.6	VIM Vimentin ENSG00000026025 IPI00418471 IPI008276	VIM	R.QVQSLTC*EVDALK.G	0.975	1.02	0.99
IPI00216951.2	DARS Aspartyl-tRNA synthetase, cytoplasmic ENSG000	DARS	R.LEYC*EALAMLR.E	1.02	1.02	1.13
IPI00218733.5	SOD1 Uncharacterized protein SOD1 ENSG00000142168	SOD1	R.LAC*GVIGIAQ.-	0.955	1.02	1.1
IPI00020451.2	IMPACT IMPACT protein ENSG00000154059 IPI00020451	IMPACT	R.STFQAHLAPVVC*PK.Q	0	1.02	1.065
IPI00000875.6	EEF1G Elongation factor 1-gamma ENSG00000186676 IP	EEF1G	R.FPEELTQTFMSC*NLITGMFQR.L	0.87	1.02	1.06
IPI00100748.3	HSPBP1 Isoform 1 of Hsp70-binding protein 1 ENSG00	HSPBP1	R.LLDRDAC*DTVR.V	1.02	1.02	1.03
IPI00015865.6	ADPRHL2 Poly(ADP-ribose) glycohydrolase ARH3 ENSG0	ADPRHL2	K.C*RDVFEPAR.A	0.84	1.02	0.95
IPI00784614.1	SEPT9 Isoform 1 of Septin-9 ENSG00000184640 IPI007	41526	R.SQEATEAAPSC*VGDMADTPR.D	1.01	1.025	1.04
IPI00033132.3	RNF7 Isoform 1 of RING-box protein 2 ENSG000001141	RNF7	R.VQVMDAC*LR.C	1.275	1.025	1.16
IPI00013452.8	EPRS glutamyl-prolyl tRNA synthetase ENSG000001366	EPRS	K.LSSC*DSFTSTINELNHCLSLR.T	1.135	1.025	0.97
IPI00744127.1	CSTF2 Uncharacterized protein CSTF2 ENSG0000010181	CSTF2	K.LC*VQNSPQEAR.N	1.045	1.025	0.885
IPI00293564.5	HMGCL Hydroxymethylglutaryl-CoA lyase, mitochondri	HMGCL	K.VAQATC*KL.-	1.035	1.025	0.97
IPI00477231.2	MGEA5 Isoform 1 of Bifunctional protein NCOAT ENSG	MGEA5	R.ANSSVVSVNC*K.G	1.085	1.025	1.09
IPI00023138.1	RAC3 Ras-related C3 botulinum toxin substrate 3 pr	RAC3	R.AVLC*PPPVK.K	1.74	1.025	0.96
IPI00845436.1	ARF4 similar to ADP-ribosylation factor 4 ENSG0000	ARF4	K.NIC*FTVWDVGGQDR.I	1.045	1.025	1.05
IPI00554737.3	PPP2R1A Serine/threonine-protein phosphatase 2A 65	PPP2R1A	K.DNTIEHLLPLFLAQLKDEC*PEVR.L	0	1.025	0.94
IPI00019329.1	DYNLL1 Dynein light chain 1, cytoplasmic ENSG00000	DYNLL1	K.NADMSEEMQQDSVEC*ATQALEK.Y	1.14	1.025	0.99
IPI00169383.3	PGK1 Phosphoglycerate kinase 1 ENSG00000102144 IPI	PGK1	R.GCITIIGGGDTATC*CAK.W	0.96	1.025	0.925
IPI00788925.1	BCAT2 Branched chain aminotransferase 2, mitochond	BCAT2	R.EVFGSGTAC*QVCPVHR.I	0	1.03	1.02
IPI00216008.4	G6PD Isoform Long of Glucose-6-phosphate 1-dehydro	G6PD	R.TQVC*GILR.E	1.025	1.03	1.01
IPI00003766.4	ETHE1 ETHE1 protein, mitochondrial precursor ENSG0	ETHE1	R.TDFQQGC*AK.T	0.965	1.03	0.945
IPI00419194.2	IAH1 Isoamyl acetate-hydrolyzing esterase 1 homolo	IAH1	R.VILITPTPLC*ETAWEEQCIIQGCK.L	1.045	1.03	1.045
IPI00304935.5	SAAL1 Uncharacterized protein SAAL1 ENSG0000016678	SAAL1	R.VLQNMEQC*QK.K	1.115	1.03	0.97
IPI00298961.3	XPO1 Exportin-1 ENSG00000082898 IPI00784388 IPI002	XPO1	K.LDINLLDNVVNC*LYHGEGAQQR.M	1.07	1.03	1.01
IPI00033130.3	SAE1 SUMO-activating enzyme subunit 1 ENSG00000142	SAE1	R.YCFSEMAPVC*AVVGGILAQEIVK.A	1.15	1.03	0.82
IPI00025815.2	TARDBP TDP43 ENSG00000120948 IPI00025815 IPI006398	TARDBP	R.NPVSQC*MR.G	0.92	1.03	1.13
IPI00019376.6	SEPT11 Septin-11 ENSG00000138758 IPI00019376	41528	R.QYPWGVVQVENENHC*DFVK.L	0.78	1.03	0.955
IPI00216694.3	PLS3 plastin 3 ENSG00000102024 IPI00848312 IPI0021	PLS3	K.VDLNSNGFIC*DYELHELFK.E	1.06	1.035	0.995
IPI00007675.6	DYNC1LI1 Cytoplasmic dynein 1 light intermediate c	DYNC1LI1	R.VGSFGSSPPGLSSTYTGGPLGNEIASG	0.98	1.035	1.015

			NGGAAAGDDEDGQNLWSC*ILSEVSTR.S			
IPI00219358.7	MPI Isoform 1 of Mannose-6-phosphate isomerase ENS	MPI	K.GDCVECMAC*SDNTVR.A	0.62	1.035	0.945
IPI00442165.1	ZNF346 Isoform 2 of Zinc finger protein 346 ENSG00	ZNF346	K.NQC*LFTNTQCK.V	1.31	1.04	0.885
IPI00003565.1	PSMD10 26S proteasome non-ATPase regulatory subuni	PSMD10	K.GAQVNAVNQNGC*TPLHYAASK.N	1.02	1.04	1.12
IPI00001960.4	CLIC4 Chloride intracellular channel protein 4 ENS	CLIC4	K.AGSDGESIGNC*PFSQR.L	1.065	1.04	1.05
IPI00289807.3	TRNT1 Isoform 1 of tRNA-nucleotidyltransferase 1,	TRNT1	K.YQGEHC*LLK.E	0.955	1.04	1.095
IPI00011951.2	KIAA0427 Isoform 2 of Uncharacterized protein KIAA	KIAA0427	R.VLVC*PIYTCLR.E	0.94	1.04	0.845
IPI00004795.1	CLNS1A Methylosome subunit pICln ENSG00000074201 I	CLNS1A	R.DRSDC*LGEHLYVMVNAK.F	1.67	1.04	1.1
IPI00216805.3	ALDH1A2 Isoform 1 of Retinal dehydrogenase 2 ENSG0	ALDH1A2	K.SPNIIFADADLDYAVEQAHQGVFFNQGQC*CTAGSR.I	0.97	1.04	1.11
IPI00032955.1	ZNF313 Zinc finger protein 313 ENSG00000124226 IPI	ZNF313	R.DC*GGAAQLAGPAAEADPLGR.F	1.05	1.045	0.92
IPI00007682.2	ATP6V1A Vacuolar ATP synthase catalytic subunit A	ATP6V1A	K.WDFTPC*K.N	1.11	1.045	1.075
IPI00004534.3	PFAS Phosphoribosylformylglycinamidine synthase EN	PFAS	R.IVLVDDREC*PVRR.N	0.98	1.045	1.015
IPI00302925.3	CCT8 Uncharacterized protein CCT8 ENSG00000156261	CCT8	K.IAVYSC*PFDGMITETK.G	0.99	1.045	0.99
IPI00186290.6	EEF2 Elongation factor 2 ENSG00000167658 IPI001862	EEF2	K.STLTDSLVC*K.A	0.965	1.045	0.96
IPI00297779.7	CCT2 T-complex protein 1 subunit beta ENSG00000166	CCT2	R.SLHDALC*VLAQTVK.D	0	1.045	1.055
IPI00045939.4	C10orf22 Uncharacterized protein C10orf22 ENSG0000	C10orf22	K.EASSSAC*DLPR.E	0.835	1.045	1.72
IPI00456803.2	_ Uncharacterized protein ENSP00000368765 ENSG0000	–	R.AYCHILLGNYC*VAVADAK.K	0.99	1.05	0.985
IPI00395627.3	CACYBP Isoform 1 of Calcyclin-binding protein ENSG	CACYBP	R.WDYLTQVEKEC*K.E	1.045	1.05	1.015
IPI00002824.7	CSRP2 Cysteine and glycine-rich protein 2 ENSG0000	CSRP2	R.C*CFLCMVCR.K	1.075	1.05	1.005
IPI00010896.3	DDAH2 CLIC1 Chloride intracellular channel protein	DDAH2	K.IGNC*PFSQR.L	1.07	1.05	1.02
IPI00005777.1	MAPKAPK3 MAP kinase-activated protein kinase 3 ENS	MAPKAPK3	K.QAGSSSASQGC*NNQ.-	0.94	1.05	1.125
IPI00060521.1	FLYWCH2 Putative uncharacterized protein LOC114984	FLYWCH2	R.TEDSGLAAGPPEAAGENFAPC*SVAPGK.S	1.065	1.05	1.27
IPI00166873.3	C9orf23 Alba-like protein C9orf23 ENSG00000164967	C9orf23	R.DPLDPNEC*GYQPPGAPPGLGSMPSSSCGPR.S	1.17	1.05	0.935
IPI00029266.1	SNRPE Small nuclear ribonucleoprotein E ENSG000001	SNRPE	R.IEGC*IIGFDEYMNLVLDDAEEIHSK.T	0	1.05	0
IPI00853009.1	CUGBP1 Isoform 4 of CUG-BP- and ETR-3-like factor	CUGBP1	R.GC*AFVTFTTR.A	1.055	1.055	1.18
IPI00026167.3	NHP2L1 NHP2-like protein 1 ENSG00000100138 IPI0002	NHP2L1	K.KLLDLVQQSC*NYK.Q	0.985	1.055	1.05
IPI00647082.1	TBC1D13 TBC1 domain family, member 13 ENSG00000107	TBC1D13	R.LLQDYPITDVC*QILQK.A	1.11	1.055	0.975
IPI00384180.4	YRDC ischemia/reperfusion inducible protein ENSG00	YRDC	R.AGAVVAVPTDTLYGLAC*AASCSAALR.A	0.9	1.055	1.005
IPI00010157.1	MAT2A S-adenosylmethionine synthetase isoform type	MAT2A	K.TC*NVLVALEQQSPDIAQGVHLDR.N	1.105	1.055	1.055
IPI00419575.6	C7orf20 Protein of unknown function DUF410 family	C7orf20	K.EQNYC*ESR.Y	0.98	1.06	1
IPI00100213.2	RRM2B Isoform 1 of Ribonucleoside-diphosphate redu	RRM2B	K.IEQEFLTEALPVGLIGMNC*ILMK.Q	1.005	1.06	0.995

IPI00745613.1	EXOSC4 Uncharacterized protein EXOSC4 ENSG00000178	EXOSC4	K.SC*EMGLQLR.Q	0	1.06	0
IPI00007765.5	HSPA9 Stress-70 protein, mitochondrial precursor E	HSPA9	K.AKC*ELSSSVQTDINLPYLTMDSSGPK.H	1.27	1.06	0
IPI00009315.6	ACBD3 Golgi resident protein GCP60 ENSG00000182827	ACBD3	K.QVLMGPYNPDTC*PEVGFFDVLGNDR.R	0.945	1.065	1.065
IPI00007691.1	TRAPPC4 Trafficking protein particle complex subun	TRAPPC4	K.NPFYSLEMPIRC*ELFDQNLK.L	1.02	1.065	0.935
IPI00031681.1	CDK2 Cell division protein kinase 2 ENSG0000012337	CDK2	R.APEILLGC*K.Y	0.985	1.065	1.04
IPI00003783.1	MAP2K2 Dual specificity mitogen-activated protein	MAP2K2	K.LC*DFGVSGQLIDSMANSFVGTR.S	0.985	1.065	0.89
IPI00010720.1	CCT5 T-complex protein 1 subunit epsilon ENSG00000	CCT5	R.VVYGGGAAEISCALAVSQEADKC*PTLEQYAMR.A	0.995	1.065	1.025
IPI00647082.1	TBC1D13 TBC1 domain family, member 13 ENSG00000107	TBC1D13	K.SLDDSQC*GITYK.M	1.065	1.07	0.98
IPI00029997.1	PGLS 6-phosphogluconolactonase ENSG00000130313 IPI	PGLS	R.AAC*CLAGAR.A	1.1	1.07	1.11
IPI00290416.3	OLA1 Isoform 1 of Putative GTP-binding protein 9 E	OLA1	K.STFFNVLTNSQASAENFPFC*TIDPNESR.V	0.985	1.07	1.025
IPI00025156.4	STUB1 Isoform 1 of STIP1 homology and U box-contai	STUB1	R.AQQAC*IEAK.H	1.035	1.07	1
IPI00646500.1	RPA2 Isoform 3 of Replication protein A 32 kDa sub	RPA2	K.AC*PRPEGLNFQDLK.N	0	1.07	0.955
IPI00022442.2	NDUFAB1 Acyl carrier protein, mitochondrial precur	NDUFAB1	K.LMC*PQEIVDYIADKK.D	0.89	1.07	1.095
IPI00008436.4	POLE4 DNA polymerase epsilon subunit 4 ENSG0000011	POLE4	K.DAYC*CAQQGK.R	1	1.07	0
IPI00783852.1	ACTR10 46 kDa protein ENSG00000131966 IPI00783852	ACTR10	R.IPDWC*SLNNPPLEMMFDVGK.T	1.05	1.075	0.975
IPI00021290.5	ACLY ATP-citrate synthase ENSG00000131473 IPI00021	ACLY	K.FIC*TTSAIQNR.F	1.045	1.075	1.04
IPI00030363.1	ACAT1 Acetyl-CoA acetyltransferase, mitochondrial	ACAT1	K.VC*ASGMK.A	0.85	1.075	1.035
IPI00828189.1	PCMT1 Isoform 2 of Protein-L-isoaspartate(D-aspart	PCMT1	R.MVGC*TGK.V	1.04	1.075	1.02
IPI00012773.1	MTA1 Isoform Long of Metastasis-associated protein	MTA1	R.ALDC*SSSVR.Q	0.985	1.075	1.12
IPI00299155.5	PSMA4 Proteasome subunit alpha type-4 ENSG00000041	PSMA4	R.YLLQYQEPIPCEQLVTALC*DIK.Q	1.045	1.08	1.04
IPI00155601.1	MACROD1 MACRO domain-containing protein 1 ENSG0000	MACROD1	K.LEVDAIVNAANSSLLGGGGVDGC*IHR.A	0.95	1.08	0.88
IPI00658023.1	PTPN11 Isoform 1 of Tyrosine-protein phosphatase n	PTPN11	K.QGFWEEFETLQQQEC*K.L	0.99	1.08	0.99
IPI00007402.2	IPO7 Uncharacterized protein IPO7 ENSG00000205339	IPO7	R.GIDQC*IPLFVEAALER.L	1.09	1.08	1.095
IPI00289862.3	SCRN1 Secernin-1 ENSG00000136193 IPI00289862	SCRN1	K.TQSPC*FGDDDPAKKEPR.F	0.98	1.08	1.055
IPI00797230.1	RPL8 32 kDa protein ENSG00000161016 IPI00012772 IP	RPL8	K.AQLNIGNVLPVGTMPEGTIVC*CLEEKPGDR.G	1.035	1.08	1.005
IPI00016443.1	C11orf79 Protein EMI5 homolog, mitochondrial precu	C11orf79	R.GMLENC*ILLSLFAK.E	0	1.08	0
IPI00334775.6	HSP90AB1 85 kDa protein ENSG00000096384 IPI0041467	HSP90AB1	R.LVSSPC*CIVTSTYGWTANMER.I	1.295	1.085	0.925
IPI00010141.4	POLE3 DNA polymerase epsilon subunit 3 ENSG0000014	POLE3	R.AASVFVLYATSC*ANNFAMK.G	0	1.085	0.99
IPI00029665.8	MMAB Cob ENSG00000139428 IPI00029665 IPI00795427 I	MMAB	K.IQCTLQDVGSALATPC*SSAR.E	1.105	1.09	1.1
IPI00220152.2	BCCIP Isoform 2 of BRCA2 and CDKN1A-interacting pr	BCCIP	R.TNKPC*GK.C	1.055	1.09	1.08
IPI00221172.2	C14orf130 Uncharacterized protein C14orf130 ENSG00	C14orf130	K.VEQNSEPC*AGSSSESDLQTVFK.N	1.12	1.09	0.865

IPI00006980.1	C14orf166 Protein C14orf166 ENSG00000087302 IPI000	C14orf166	K.LTALDYHNPAGFNC*KDETEFR.N	1.05	1.09	1.06
IPI00411706.1	ESD S-formylglutathione hydrolase ENSG00000139684	ESD	K.AETGKCPALYWLSGLTC*TEQNFISK.S	1.045	1.095	0.985
IPI00022745.1	MVD Diphosphomevalonate decarboxylase ENSG00000167	MVD	R.DGDPLPSSLSC*K.V	1.015	1.095	0.855
IPI00006907.1	C12orf5 Uncharacterized protein C12orf5 ENSG000000	C12orf5	K.AAREEC*PVFTPPGGETLDQVK.M	1.025	1.095	0.97
IPI00031519.3	DNMT1 Isoform 1 of DNA (cytosine-5)-methyltransfer	DNMT1	K.NQLC*DLETK.L	1.215	1.095	0.995
IPI00100796.4	CHMP5 Charged multivesicular body protein 5 ENSG00	CHMP5	K.APPPSLTDC*IGTVDSR.A	1.03	1.1	1.055
IPI00647082.1	TBC1D13 TBC1 domain family, member 13 ENSG00000107	TBC1D13	R.ELSFSGIPC*EGGLR.C	1.05	1.1	1.055
IPI00029079.5	GMPS GMP synthase ENSG00000163655 IPI00029079	GMPS	K.TVGVQGDC*R.S	1.07	1.1	0.97
IPI00410666.1	SCRIB Isoform 3 of Protein LAP4 ENSG00000180900 IP	SCRIB	R.SLEPSPSPGPQEEDGEVALVLLGRPSPGAVGPEDVALC*SSR.R	0	1.1	1.105
IPI00306159.7	MECR Trans-2-enoyl-CoA reductase, mitochondrial pr	MECR	R.LALNC*VGGK.S	1.045	1.105	0.99
IPI00382452.1	CHMP1A Isoform 1 of Charged multivesicular body pr	CHMP1A	K.NVEC*AR.V	1.03	1.105	1.07
IPI00220528.6	SNRPF Small nuclear ribonucleoprotein F ENSG000001	SNRPF	R.C*NNVLYIR.G	1.055	1.105	0.945
IPI00742681.1	LSM7 R30783_1 ENSG00000130332 IPI00007163 IPI00742	LSM7	R.GTSVVLIC*PQDGMEAIPNPFIQQQDA.-	0.97	1.105	0.875
IPI00029557.3	GRPEL1 GrpE protein homolog 1, mitochondrial precu	GRPEL1	K.ATQC*VPKEEIKDDNPHLK.N	1.155	1.105	1.11
IPI00177856.8	C14orf172 Uncharacterized protein C14orf172 ENSG00	C14orf172	R.FCSFSPC*IEQVQR.T	1.02	1.11	1.035
IPI00333541.6	FLNA Filamin-A ENSG00000196924 IPI00553169 IPI0030	FLNA	K.VGTEC*GNQK.V	1.06	1.11	1.05
IPI00018146.1	YWHAQ 14-3-3 protein theta ENSG00000134308 IPI0001	YWHAQ	R.YLAEVAC*GDDR.K	1.005	1.11	1.02
IPI00004534.3	PFAS Phosphoribosylformylglycinamidine synthase EN	PFAS	R.GLAPLHWADDDGNPTEQYPLNPNGSPGGVAGIC*SCDGR.H	0.945	1.11	1.025
IPI00303318.2	FAM49B Protein FAM49B ENSG00000153310 IPI00651701	FAM49B	K.VLTC*TDLEQGPNFFLDFENAQPTESEK.E	0.91	1.11	0
IPI00301364.3	SKP1A Isoform 1 of S-phase kinase-associated prote	SKP1A	R.KENQWC*EEK.-	1.05	1.11	1.045
IPI00025285.3	FLJ25715 ATP6V1G1 Vacuolar ATP synthase subunit G	FLJ25715	R.GSC*STEVEKETQEK.M	1.255	1.11	0
IPI00030116.1	PGM3 Isoform 1 of Phosphoacetylglucosamine mutase	PGM3	K.QASC*SGDEYR.S	1.32	1.11	0
IPI00010158.3	CHRAC1 Chromatin accessibility complex protein 1 E	CHRAC1	K.ATELFVQC*LATYSYR.H	1.11	1.115	0.975
IPI00221035.3	BTF3 Uncharacterized protein BTF3 ENSG00000145741	BTF3	R.ARGGC*PGGEATLSQPPPR.G	1.1	1.115	1.055
IPI00006907.1	C12orf5 Uncharacterized protein C12orf5 ENSG000000	C12orf5	K.EADQKEQFSQGSPSNC*LETSLAEIFPLGK.N	0.975	1.115	0.995
IPI00641181.5	MARCKSL1 MARCKS-related protein ENSG00000175130 IP	MARCKSL1	K.EGGGDSSASSPTEEEQEQGEIGAC*SDEGTAQEGK.A	1.52	1.12	1.23
IPI00290566.1	TCP1 T-complex protein 1 subunit alpha ENSG0000012	TCP1	R.IC*DDELILIK.N	0.965	1.12	0.995
IPI00301364.3	SKP1A Isoform 1 of S-phase kinase-associated prote	SKP1A	K.GLLDVTC*K.T	1.045	1.12	1.08
IPI00028412.1	SSSCA1 Sjoegren syndrome/scleroderma autoantigen 1	SSSCA1	R.MLGETC*ADCGTILLQDK.Q	0.935	1.12	1.105

IPI00007682.2	ATP6V1A Vacuolar ATP synthase catalytic subunit A	ATP6V1A	K.YSNSDVIIYVGC*GER.G	1.395	1.12	1.185
IPI00654865.1	DIP2A Isoform 1 of Disco-interacting protein 2 hom	DIP2A	R.GC*PLEAAPLPAEVR.E	0	1.12	0
IPI00022239.7	METAP1 Methionine aminopeptidase 1 ENSG00000164024	METAP1	R.VCETDGC*SSEAK.L	1.125	1.125	0.95
IPI00844329.1	HPRT1 Uncharacterized protein HPRT1 ENSG0000016570	HPRT1	K.SYC*NDQSTGDIK.V	1.065	1.125	1.1
IPI00015809.1	OSGEP Probable O-sialoglycoprotein endopeptidase E	OSGEP	R.AMAHCGSQEALIVGGVGC*NVR.L	0	1.125	1.18
IPI00218782.2	CAPZB Capping protein ENSG00000077549 IPI00026185	CAPZB	R.QMEKDETVSDC*SPHIANIGR.L	1.185	1.13	1.105
IPI00784459.1	CFL1 Uncharacterized protein CFL1 ENSG00000172757	CFL1	K.HELQANC*YEEVKDR.C	1.025	1.13	1.1
IPI00292894.4	TSR1 TSR1, 20S rRNA accumulation ENSG00000167721 I	TSR1	R.DTGTVHLNELGNTQNFMLLC*PR.L	0.89	1.13	1.32
IPI00013212.1	CSK Tyrosine-protein kinase CSK ENSG00000103653 IP	CSK	R.SVLGGDC*LLK.F	0.94	1.13	1.01
IPI00032050.4	WBP2 WW domain-binding protein 2 ENSG00000132471 I	WBP2	K.DC*EIKQPVFGANYIK.G	1.1	1.13	1.02
IPI00290566.1	TCP1 T-complex protein 1 subunit alpha ENSG0000012	TCP1	R.GANDFMC*DEMER.S	1.09	1.13	0.99
IPI00456664.1	NIT1 Isoform 4 of Nitrilase homolog 1 ENSG00000158	NIT1	K.THLC*DVEIPGQGPMCESNSTMPGPSLESPVSTPAGK.I	1.165	1.13	1.02
IPI00056314.1	TSR2 Pre-rRNA-processing protein TSR2 homolog ENSG	TSR2	R.AGVC*AALEAWPALQIAVENGFGGVHSQEK.A	0	1.13	0
IPI00010244.4	MRPS11 Isoform 1 of 28S ribosomal protein S11, mit	MRPS11	K.ASHNNTQIQVVSASNEPLAFASC*GTEGFR.N	1.005	1.135	1.1
IPI00396174.4	CCDC25 Coiled-coil domain-containing protein 25 EN	CCDC25	K.ANSIQGC*K.M	1.19	1.135	1.095
IPI00386189.2	NARG1 Isoform 1 of NMDA receptor-regulated protein	NARG1	R.LFNTAVC*ESK.D	0.965	1.135	1.03
IPI00024670.5	REEP5 Receptor expression-enhancing protein 5 ENSG	REEP5	K.NC*MTDLLAK.L	1.06	1.14	0
IPI00018402.1	TBCE Tubulin-specific chaperone E ENSG00000116957	TBCE	R.NCAVSC*AGEK.G	1.11	1.14	1.03
IPI00152089.3	CXorf38 Isoform 1 of Uncharacterized protein CXorf	CXorf38	R.LNC*AEYK.N	1.15	1.145	1.175
IPI00026328.3	TXNDC12 Thioredoxin domain-containing protein 12 p	TXNDC12	K.SWC*GACK.A	1.155	1.15	1.08
IPI00760837.2	FAM98B family with sequence similarity 98, member	FAM98B	R.INDALSC*EYECR.R	1.16	1.15	1.165
IPI00033770.5	ALKBH4 Isoform 1 of Alkylated DNA repair protein a	ALKBH4	R.MGLYPGLEGFRPVEQCNLDYC*PER.G	0	1.15	1.08
Reverse_IPI00473118.2	MATN2 Isoform 1 of Matrilin-2 precursor ENSG000001	MATN2	K.C*QDHKEELPSGSPK.T	1.54	1.15	0
IPI00024013.1	_ Putative ubiquitin-conjugating enzyme E2 D3-like	_	K.VLLSIC*SLLCDPNPDDPLVPEIAR.I	0.995	1.155	1.065
IPI00024990.6	ALDH6A1 Methylmalonate-semialdehyde dehydrogenase	ALDH6A1	R.C*MALSTAVLVGEAK.K	1.045	1.155	0.9
IPI00397721.1	BLOC1S3 Biogenesis of lysosome-related organelles	BLOC1S3	R.GDLC*ALAER.L	0.975	1.16	0
IPI00216190.1	GSK3B Isoform 2 of Glycogen synthase kinase-3 beta	GSK3B	K.LC*DFGSAK.Q	1.105	1.16	1.18
IPI00514587.1	SARS Uncharacterized protein SARS ENSG00000031698	SARS	K.YAGLSTC*FR.Q	1.02	1.165	1.04
IPI00290279.1	ADK Isoform Long of Adenosine kinase ENSG000001561	ADK	R.TGC*TFPEKPDFH.-	1.16	1.165	1.16
IPI00026216.4	NPEPPS Puromycin-sensitive aminopeptidase ENSG0000	NPEPPS	R.SKDGVC*VR.V	1.1	1.175	1.09
IPI00465054.2	THUMPD1 Putative uncharacterized protein	THUMPD1	R.C*DAGGPR.Q	1.065	1.18	1.09

	DKFZp686C					
IPI00742743.1	TP53BP1 Isoform 2 of Tumor suppressor p53-binding	TP53BP1	K.VADPVDSSNLDTC*GSISQVIEQLPQPNR.T	1.065	1.185	1.115
IPI00643591.5	AP1G1 Adaptor-related protein complex 1, gamma 1 s	AP1G1	R.FTC*TVNR.I	1.06	1.185	1.09
IPI00008433.4	RPS5 40S ribosomal protein S5 ENSG00000083845 IPI0	RPS5	R.VNQAIWLLC*TGAR.E	1.09	1.185	0.975
IPI00306301.2	PDHA1 Mitochondrial PDHA1 ENSG00000131828 IPI00642	PDHA1	K.LPCIFIC*ENNR.Y	0	1.185	0.93
IPI00033494.3	MRLC2 Myosin regulatory light chain ENSG0000011868	MRLC2	R.NAFAC*FDEEATGTIQEDYLR.E	1.045	1.19	1.06
IPI00015866.2	ARL2BP Isoform 1 of ADP-ribosylation factor-like p	ARL2BP	R.GLDLSSGLVVTSLC*K.S	0.995	1.19	1.045
IPI00028296.1	CAMK1 Calcium/calmodulin-dependent protein kinase	CAMK1	K.MEDPGSVLSTAC*GTPGYVAPEVLAQKPYSK.A	0	1.19	1.08
IPI00397904.6	NUP93 Nuclear pore complex protein Nup93 ENSG00000	NUP93	K.LNQVC*FDDDGTSSPQDR.L	0.94	1.19	0.87
IPI00045917.3	CRBN Isoform 1 of Protein cereblon ENSG00000113851	CRBN	K.VQILPEC*VLPSTMSAVQLESLNK.C	0.945	1.195	1.035
IPI00003394.1	SMN2 SMN1 Isoform SMN of Survival motor neuron pro	SMN2	K.NGDIC*ETSGKPK.T	1.04	1.2	1.235
IPI00093057.6	CPOX Coproporphyrinogen III oxidase, mitochondrial	CPOX	R.C*SSFMAPPVTDLGELR.R	1.21	1.21	0.945
IPI00218342.10	MTHFD1 C-1-tetrahydrofolate synthase, cytoplasmic	MTHFD1	K.QGFGNLPIC*MAK.T	1.055	1.215	0.99
IPI00641950.3	GNB2L1 Lung cancer oncogene 7 ENSG00000204628 IPI0	GNB2L1	R.YWLC*AATGPSIK.I	0.72	1.22	0
IPI00329331.6	UGP2 Isoform 1 of UTP--glucose-1-phosphate uridyly	UGP2	K.LNGGLGTSMGC*K.G	1.135	1.225	1.105
IPI00019812.1	PPP5C Serine/threonine-protein phosphatase 5 ENSG0	PPP5C	R.TEC*AEPPRDEPPADGALKR.A	0.94	1.23	0
IPI00645078.1	UBE1 Ubiquitin-activating enzyme E1 ENSG0000013098	UBE1	K.SIPIC*TLK.N	1.175	1.23	1.05
IPI00024067.4	CLTC Isoform 1 of Clathrin heavy chain 1 ENSG00000	CLTC	R.IHEGC*EEPATHNALAK.I	0	1.23	0
IPI00086909.6	LOC440917 similar to 14-3-3 protein epsilon ENSG00	LOC440917	K.LIC*CDILDVLDK.H	0.965	1.24	1.045
IPI00550069.3	RNH1 Ribonuclease inhibitor ENSG00000023191 IPI005	RNH1	R.ELDLSNNC*LGDAGILQLVESVR.Q	0.97	1.24	0.925
IPI00290142.5	CTPS CTP synthase 1 ENSG00000171793 IPI00290142	CTPS	K.SC*GLHVTSIK.I	0.82	1.24	1.09
IPI00022796.2	HMG1L1 High-mobility group protein 1-like 1 ENSG00	HMG1L1	K.MSSYAFFVQTC*R.E	0.985	1.245	0.9
IPI00293276.10	MIF Macrophage migration inhibitory factor ENSG000	MIF	K.LLC*GLLAER.L	1.39	1.25	1
IPI00328868.3	HS1BP3 HCLS1 binding protein 3 ENSG00000118960 IPI	HS1BP3	K.LFDDPDLGGAIPLGDSLLLPAAC*ESGGPTPSLSHR.D	0	1.25	1.14
IPI00013219.1	ILK Integrin-linked protein kinase ENSG00000166333	ILK	K.FSFQC*PGR.M	0.975	1.26	1.02
IPI00414858.3	COG3 Isoform 1 of Conserved oligomeric Golgi compl	COG3	R.ELLLGPSIAC*TVAELTSQNNR.D	0	1.26	1.72
IPI00291419.5	ACAT2 Acetyl-CoA acetyltransferase, cytosolic ENSG	ACAT2	R.ATVAPEDVSEVIFGHVLAAGC*GQNPVR.Q	1.145	1.27	0.975
IPI00004363.1	STK39 STE20/SPS1-related proline-alanine-rich prot	STK39	K.TFVGTPC*WMAPEVMEQVR.G	0	1.27	0
IPI00784131.1	AARS Uncharacterized protein AARS ENSG00000090861	AARS	K.NVGC*LQEALQLATSFAQLR.L	1.08	1.28	1.02
IPI00743454.1	ACN9 Uncharacterized protein ACN9 ENSG00000196636	ACN9	K.AC*FGTFLPEEK.L	1.1	1.285	0.96
IPI00216319.3	YWHAH 14-3-3 protein eta ENSG00000128245 IPI008275	YWHAH	K.NC*NDFQYESK.V	1.145	1.33	1
IPI00827583.1	BSCL2 72 kDa protein ENSG00000168000 IPI00045906 I	BSCL2	K.EGC*TEVSLLR.V	0	1.34	0.96

IPI00220365.5	EIF4G1 EIF4G1 variant protein (Fragment) ENSG00000	EIF4G1	R.LQGINC*GPDFTPSFANLGR.T	0.985	1.345	1.055
IPI00148061.3	LDHAL6A L-lactate dehydrogenase A-like 6A ENSG0000	LDHAL6A	K.NRVIGSGC*NLDSAR.F	1.015	1.35	1.015
IPI00290272.2	POLA2 DNA polymerase subunit alpha B ENSG000000141	POLA2	K.VLGC*PEALTGSYK.S	1.15	1.35	0.97
IPI00844329.1	HPRT1 Uncharacterized protein HPRT1 ENSG0000016570	HPRT1	R.SPGVVISDDEPGYDLDLFC*IPNHYAEDLER.V	0.87	1.35	0
IPI00072534.2	UNC45A Isoform 1 of UNC45 homolog A ENSG0000014055	UNC45A	R.AIQTVSCLLQGPC*DAGNR.A	1.22	1.36	1.375
IPI00646167.2	C14orf142 hypothetical protein LOC84520 ENSG000001	C14orf142	R.VSC*EAPGDGDPFQGLLSGVAQMK.D	1.085	1.37	0.98
IPI00011118.2	RRM2 Ribonucleoside-diphosphate reductase M2 subun	RRM2	K.LIGMNC*TLMK.Q	1.075	1.37	1.625
IPI00001636.1	ATXN10 Ataxin-10 ENSG00000130638 IPI00385153 IPI00	ATXN10	K.ETTNIFSNC*GCVR.A	1.13	1.38	0.995
IPI00797537.1	NUDCD1 NudC domain-containing protein 1 ENSG000001	NUDCD1	K.FFACAPNYSYAALC*ECLR.R	1.18	1.395	0
IPI00045207.2	BTBD14B BTB/POZ domain-containing protein 14B ENSG	BTBD14B	R.NTLANSC*GTGIR.S	0	1.41	0
IPI00456758.4	RPL27A 60S ribosomal protein L27a ENSG00000166441	RPL27A	R.NQSFC*PTVNLDK.L	0	1.415	1.01
IPI00002520.1	SHMT2 Serine hydroxymethyltransferase, mitochondri	SHMT2	K.NTC*PGDR.S	1.085	1.415	1.02
IPI00000875.6	EEF1G Elongation factor 1-gamma ENSG00000186676 IP	EEF1G	K.VPAFEGDDGFC*VFESNAIAYYVSNEELR.G	0.76	1.42	0
IPI00218342.10	MTHFD1 C-1-tetrahydrofolate synthase, cytoplasmic	MTHFD1	R.GDLNDC*FIPCTPK.G	1.155	1.435	1.04
IPI00100460.2	DARS2 Aspartyl-tRNA synthetase, mitochondrial prec	DARS2	R.LIC*LVTGSPSIR.D	0	1.44	1.1
IPI00216587.9	RPS8 40S ribosomal protein S8 ENSG00000142937 IPI0	RPS8	K.NC*IVLIDSTPYR.Q	1.4	1.47	0.945
IPI00018352.1	UCHL1 Ubiquitin carboxyl-terminal hydrolase isozym	UCHL1	K.NEAIQAAHDAVAQEGQC*R.V	1.015	1.475	1.035
IPI00023234.3	SAE2 SUMO-activating enzyme subunit 2 ENSG00000126	SAE2	R.VLVVGAGGIGC*ELLK.N	1.26	1.5	0.99
IPI00216247.2	PSMD4 Proteasome ENSG00000159352 IPI00853415 IPI00	PSMD4	R.SNPENNVGLITLANDC*EVLTTLTPDTGR.I	0.98	1.51	0
IPI00001636.1	ATXN10 Ataxin-10 ENSG00000130638 IPI00385153 IPI00	ATXN10	R.HAELIASTFVDQC*K.T	1.2	1.525	1.03
IPI00465260.4	GARS Glycyl-tRNA synthetase ENSG00000106105 IPI004	GARS	R.QHFIQEEQILEIDC*TMLTPEPVLK.T	0	1.58	1
IPI00217362.2	TPRKB Isoform 3 of TP53RK-binding protein ENSG0000	TPRKB	K.LSSQEESIGTLLDAIIC*R.M	1.53	1.7	1.54
IPI00015141.4	CKMT2 Creatine kinase, sarcomeric mitochondrial pr	CKMT2	R.GLSLPPAC*TR.A	0	1.71	1.01
IPI00024915.2	PRDX5 Isoform Mitochondrial of Peroxiredoxin-5, mi	PRDX5	K.ALNVEPDGTGLTC*SLAPNIISQL.-	1.29	1.78	1.015
IPI00456898.1	LOC440055 Uncharacterized protein ENSP00000302331	LOC440055	R.QAHLC*VLASNCDEPMYVK.L	2.025	1.805	1.065
IPI00290566.1	TCP1 T-complex protein 1 subunit alpha ENSG0000012	TCP1	R.SQMESMLISGYALNC*VVGSQGMPK.R	0.99	1.825	0.99
IPI00145260.3	C1orf69 Putative transferase C1orf69, mitochondria	C1orf69	K.GC*YIGQELTAR.T	1.025	1.83	1.045
IPI00295386.7	CBR1 Carbonyl reductase [NADPH] 1 ENSG00000159228	CBR1	R.DVC*TELLPLIKPQGR.V	0	1.86	1.11
IPI00216587.9	RPS8 40S ribosomal protein S8 ENSG00000142937 IPI0	RPS8	R.LDVGNFSWGSEC*CTR.K	1.35	1.9	0
IPI00024993.4	ECHS1 Enoyl-CoA hydratase, mitochondrial precursor	ECHS1	K.IC*PVETLVEEAIQCAEK.I	1.09	1.99	0.925
IPI00479877.4	ALDH9A1 aldehyde	ALDH	K.TVC*VEMGDVES	1.235	2.035	1.26

	dehydrogenase 9A1 ENSG00000143149	9A1	AF.-			
IPI00022239.7	METAP1 Methionine aminopeptidase 1 ENSG00000164024	METAP1	K.LGIQGSYFCSQEC*FK.G	1.425	2.075	0.69
IPI00306369.3	NSUN2 tRNA ENSG00000037474 IPI00306369	NSUN2	R.MVYSTC*SLNPIEDEAVIASLLEK.S	1.92	2.245	1.125
IPI00847579.1	RPS12 ribosomal protein S12 ENSG00000112306 IPI008	RPS12	R.KVVGCSC*VVVK.D	1.95	2.265	1.035
IPI00033130.3	SAE1 SUMO-activating enzyme subunit 1 ENSG00000142	SAE1	K.GNGIVEC*LGPK.-	0	2.42	0.87
IPI00011118.2	RRM2 Ribonucleoside-diphosphate reductase M2 subun	RRM2	R.EFLFNAIETMPC*VK.K	1.78	2.76	1.055
IPI00550069.3	RNH1 Ribonuclease inhibitor ENSG00000023191 IPI005	RNH1	R.WAELLPLLQQC*QVVR.L	0	3.01	0
IPI00306301.2	PDHA1 Mitochondrial PDHA1 ENSG00000131828 IPI00642	PDHA1	K.NFYGGNGIVGAQVPLGAGIALAC*K.Y	0	3.05	0
IPI00550069.3	RNH1 Ribonuclease inhibitor ENSG00000023191 IPI005	RNH1	R.C*KDISSALR.V	1	3.135	0.61
IPI00002520.1	SHMT2 Serine hydroxymethyltransferase, mitochondri	SHMT2	R.GLELIASENFC*SR.A	0.93	3.575	0
IPI00550069.3	RNH1 Ribonuclease inhibitor ENSG00000023191 IPI005	RNH1	R.SNELGDVGVHC*VLQGLQTPSCK.I	1.41	4.5	1.07
IPI00550069.3	RNH1 Ribonuclease inhibitor ENSG00000023191 IPI005	RNH1	K.LSLQNCC*LTGAGCGVLSSTLR.T	1.36	5.17	1.13
IPI00015018.1	PPA1 Inorganic pyrophosphatase ENSG00000180817 IPI	PPA1	K.C*DPDAAR.A	2.35	7.49	1.02
IPI00015018.1	PPA1 Inorganic pyrophosphatase ENSG00000180817 IPI	PPA1	K.GISC*MNTTLSESPFK.C	1.76	9.72	0
IPI00011200.5	PHGDH D-3-phosphoglycerate dehydrogenase ENSG00000	PHGDH	K.GILVMNTPNGNSLSAAELTC*GMIMCLAR.Q	0	10.535	0
IPI00395939.3	PITPNB Isoform 2 of Phosphatidylinositol transfer	PITPNB	K.ELANSPDC*PQMCAYK.L	1.05	16.655	1.215

Table 3A-4. Mass-spectrometry results of global competitive zinc-binding treatment of HeLa cell lysates with EDTA and IA-alkyne utilizing the quantitative isotopic Azo-tags. Three replicates were performed with the average taken for peptides found in multiple runs. A '0' indicates that the peptide was not found in that particular run. Data were sorted to present those with the highest R ratio within the EDTA runs (highest increase in IA-labeling upon EDTA-treatment). Peptides with an R > 1.50 (1.5-fold increase in IA-labeling upon EDTA-treatment) are highlighted in grey and represent those cysteines most sensitive to EDTA-treatment.

ipi	description	symbol	sequence	EDTA-1	EDTA-2	EDTA-3	EDTA-Avg
IPI00386119.4	SF1 Isoform 5 of Splicing factor 1 ENSG00000168066	SF1	R.SITNTTVC*TK.C	33.2	0	50.9	42.05

IPI00015018.1	PPA1 Inorganic pyrophosphatase ENSG00000180817 IPI	PPA1	K.GISC*MNTTL SESPFK.C	34.52	0	48.16	41.34
IPI00845348.1	ZRANB2 Putative uncharacterized protein DKFZp686N0	ZRAN B2	K.C*GNVNFAR. R	34.75	0	0	34.75
IPI00009841.4	EWSR1 CDNA FLJ31747 fis, clone NT2RI2007377, highl	EWSR 1	R.AGDWQC*PN PGCGNQNFAW R.T	35.44	0	27.93	31.685
IPI00845348.1	ZRANB2 Putative uncharacterized protein DKFZp686N0	ZRAN B2	R.GLFSANDWQ C*K.T	24.36	0	0	24.36
IPI00015018.1	PPA1 Inorganic pyrophosphatase ENSG00000180817 IPI	PPA1	K.C*DPDAAR.A	24.07	0	0	24.07
IPI00000279.2	ZC3H15 erythropoietin 4 immediate early response E	ZC3H1 5	K.SVVC*AFFK. Q	18.59	0	23.38	20.985
IPI00302112.1	MAP2K7 Isoform 2 of Dual specificity mitogen-activ	MAP2 K7	R.YQAEINDLEN LGEMGSGTC*G QVWK.M	37.66	0	1.04	19.35
IPI00430812.4	CNBP Zinc finger protein 9 ENSG00000169714 IPI0043	CNBP	K.TSEVNC*YR. C	15.72	0	0	15.72
IPI00514501.1	C1orf57 Chromosome 1 open reading frame 57 ENSG000	C1orf5 7	R.VC*VIDEIGK. M	15.56	0	13.86	14.71
IPI00027107.5	TUFM Tu translation elongation factor, mitochondri	TUFM	K.GEETPVIVGS ALC*ALEGR.D	12.15	0	14.11	13.13
IPI00845348.1	ZRANB2 Putative uncharacterized protein DKFZp686N0	ZRAN B2	K.TC*SNVNWA R.R	0	0	13.12	13.12
IPI00023234.3	SAE2 SUMO-activating enzyme subunit 2 ENSG00000126	SAE2	R.VLVVGAGGIG C*ELLK.N	0	0	12.02	12.02
IPI00027107.5	TUFM Tu translation elongation factor, mitochondri	TUFM	K.NMITGTAPLD GC*ILVVAAND GPMPQTR.E	0	0	11.48	11.48
IPI00848058.1	ACTB Actin, cytoplasmic 2 ENSG00000075624 IPI00021	ACTB	K.C*DVDIRK.D	0	10.52	0	10.52
IPI00011253.3	RPS3 40S ribosomal protein S3 ENSG00000149273 IPI0	RPS3	K.GC*EVVVSGK .L	8.84	0	8.82	8.83
IPI00007765.5	HSPA9 Stress-70 protein, mitochondrial precursor E	HSPA9	K.AKC*ELSSSV QTDINLPYLTM DSSGPK.H	0	0	8.75	8.75
IPI00432836.2	RPL37 Uncharacterized protein RPL37 ENSG0000014559	RPL37	K.THTLC*R.R	0	7.59	0	7.59
IPI00008433.4	RPS5 40S ribosomal protein S5 ENSG00000083845 IPI0	RPS5	K.TIAEC*LADE LINAAK.G	6.46	7.68	6.57	7.0975
IPI00022239.7	METAP1 Methionine aminopeptidase 1 ENSG00000164024	META P1	K.LQC*PTCIK.L	6.95	0	0	6.95
IPI00004506.3	KCTD5 BTB/POZ domain-containing protein KCTD5 ENSG	KCTD5	R.C*SAGLGALA QRPGSVSK.W	0	6.73	0	6.73
IPI00027107.5	TUFM Tu translation elongation factor, mitochondri	TUFM	R.HYAHTDC*PG HADYVK.N	0	6.62	0	6.62
IPI00021840.1	RPS6 40S ribosomal protein S6 ENSG00000137154 IPI0	RPS6	K.LNISFPATGC* QK.L	0	7.23	4.74	6.6075
IPI00479743.3	POTE2 protein expressed in prostate, ovary, testis	POTE2	K.EKLC*YVALD FEQEMATAASS SSLEK.S	3	7.46	8.42	6.585

IPI00011253.3	RPS3 40S ribosomal protein S3 ENSG00000149273 IPI0	RPS3	R.AC*YGVLR.F	0	0	6.57	6.57
IPI00217030.10	RPS4X 40S ribosomal protein S4, X isoform ENSG0000	RPS4X	R.EC*LPLIIFLR.N	0	6.09	0	6.09
IPI00022240.3	ISCU Isoform 1 of Iron-sulfur cluster assembly enz	ISCU	K.TFGC*GSAIASSSLATEWVK.G	6	0	0	6
IPI00025091.3	RPS11 40S ribosomal protein S11 ENSG00000142534 IP	RPS11	K.NMSVHLSPC*FR.D	0	5.12	0	5.12
IPI00218606.7	RPS23 40S ribosomal protein S23 ENSG00000186468 IP	RPS23	K.ITAFVPNDGC*LNFIEENDEVLVAGFGR.K	4.07	5.62	4.73	5.01
IPI00025091.3	RPS11 40S ribosomal protein S11 ENSG00000142534 IP	RPS11	R.DVQIGDIVTVGEC*RPLSK.T	4.47	0	5.49	4.98
IPI00176655.5	_ Uncharacterized protein ENSP00000348430 ENSG0000	_	K.TPC*GEGSK.T	4.58	0	4.86	4.72
IPI00008433.4	RPS5 40S ribosomal protein S5 ENSG00000083845 IPI0	RPS5	K.AQC*PIVER.L	4.41	4.86	4.62	4.6875
IPI00031820.3	FARSA Phenylalanyl-tRNA synthetase alpha chain ENS	FARSA	K.VNLQMVYDSPLC*R.L	4.61	0	4.63	4.62
IPI00176574.1	LOC284230 Uncharacterized protein ENSP00000351550	LOC284230	R.LECVEPNC*R.S	4.55	0	4.6	4.575
IPI00003814.1	MAP2K6 Isoform 1 of Dual specificity mitogen-activ	MAP2K6	K.TIDAGC*KPYMAPER.I	4.63	0	4.49	4.56
IPI00003783.1	MAP2K2 Dual specificity mitogen-activated protein	MAP2K2	K.LC*DFGVSGQLIDSMANSFVGTR.S	4.35	4.9	4.08	4.5575
IPI00397963.3	_ Uncharacterized protein ENSP00000301828 ENSG0000	_	R.LTEGC*SFR.R	3.66	5.23	4.09	4.5525
IPI00514501.1	C1orf57 Chromosome 1 open reading frame 57 ENSG000	C1orf57	R.NADC*SSGPGQR.V	3.38	6.09	2.48	4.51
IPI00023073.1	XRCC3 DNA-repair protein XRCC3 ENSG00000126215 IPI	XRCC3	R.LSLGC*PVLDALLR.G	0	4.41	3.25	4.12
IPI00025091.3	RPS11 40S ribosomal protein S11 ENSG00000142534 IP	RPS11	K.C*PFTGNVSIR.G	0	4.08	3.95	4.0475
IPI00008433.4	RPS5 40S ribosomal protein S5 ENSG00000083845 IPI0	RPS5	R.VNQAIWLLC*TGAR.E	0.86	0	7.14	4
IPI00396086.1	RPS21 8.2 kDa differentiation factor ENSG000001718	RPS21	R.KC*SASNR.I	0	4.01	3.7	3.9325
IPI00218342.10	MTHFD1 C-1-tetrahydrofolate synthase, cytoplasmic	MTHFD1	K.QGFGNLPIC*MAK.T	0	0	3.92	3.92
IPI00746777.3	ADH5 Alcohol dehydrogenase class-3 ENSG00000197894	ADH5	K.IDPLAPLDKVCLLGC*GISTGYGAAVNTAK.L	0	0	3.92	3.92
IPI00376429.3	LOC391370 Uncharacterized protein ENSP00000352557	LOC391370	K.LGEWVGLC*K.T	3.77	0	4.04	3.905
IPI00719622.1	RPS28 LOC646195 LOC645899 40S ribosomal protein S2	RPS28	R.TGSQGQC*TQVR.V	3.65	0	4.06	3.855
IPI00216587.9	RPS8 40S ribosomal protein S8 ENSG00000142937 IPI0	RPS8	K.NC*IVLIDSTPYR.Q	0	0	3.8	3.8

IPI00479877.4	ALDH9A1 aldehyde dehydrogenase 9A1 ENSG00000143149	ALDH 9A1	K.TVC*VEMGD VESAF.-	3.71	0	0	3.71
IPI00290142.5	CTPS CTP synthase 1 ENSG00000171793 IPI00290142	CTPS	K.SC*GLHVTSI K.I	0	0	3.63	3.63
IPI00790530.1	NUP85 nucleoporin 85 ENSG00000125450 IPI00790530 I	NUP85	R.GC*FSDLDLID NLGPAMMLSD R.L	5.96	0	1.15	3.555
Reverse_IPI00376 429.3	LOC391370 Uncharacterized protein ENSP00000352557	LOC39 1370	K.C*LGVWEGL K.K	3.58	0	3.49	3.535
IPI00028050.2	EEFSEC Selenocysteine-specific elongation factor E	EEFSE C	K.GMQTQSAEC *LVIGQIACQK.L	3.42	0	3.37	3.395
IPI00303207.3	ABCE1 ATP-binding cassette sub-family E member 1 E	ABCE1	R.YC*ANAFK.L	3.51	0	3.17	3.34
IPI00219160.3	RPL34 60S ribosomal protein L34 ENSG00000109475 IP	RPL34	R.AYGGSMC*A K.C	3.32	0	3.32	3.32
IPI00012750.3	RPS25 40S ribosomal protein S25 ENSG00000118181 IP	RPS25	K.ATYDKLC*K. E	3.21	0	0	3.21
IPI00000875.6	EEF1G Elongation factor 1-gamma ENSG00000186676 IP	EEF1G	R.FPEELTQTFM SC*NLITGMFQR .L	8.93	1.26	0	3.1775
IPI00055606.2	FHL1 Isoform 2 of Four and a half LIM domains prot	FHL1	K.C*LHPLANET FVAK.D	0	3.04	0	3.04
IPI00022240.3	ISCU Isoform 1 of Iron-sulfur cluster assembly enz	ISCU	K.NVGTGLVGA PAC*GDVMK.L	2.85	0	3.17	3.01
IPI00297779.7	CCT2 T-complex protein 1 subunit beta ENSG00000166	CCT2	R.SLHDALC*VL AQTVK.D	0	2.97	0	2.97
IPI00006164.4	ILKAP Integrin-linked kinase-associated serine/thr	ILKAP	R.FILLAC*DGLF K.V	0	2.96	2.9	2.945
IPI00013219.1	ILK Integrin-linked protein kinase ENSG00000166333	ILK	K.FSFQC*PGR.M	2.46	3.37	2.39	2.8975
IPI00644079.2	HNRNPU heterogeneous nuclear ribonucleoprotein U i	HNRN PU	R.KAVVVC*PK. D	0	2.89	0	2.89
IPI00788737.1	GAPDH 39 kDa protein ENSG00000111640 IPI00789134 I	GAPD H	R.VPTANVSVV DLTC*R.L	0	0	2.81	2.81
IPI00299214.6	TK1 thymidine kinase 1, soluble ENSG00000167900 IP	TK1	R.NTMEALPAC* LLR.D	2.59	0	2.9	2.745
IPI00059764.4	ZNF428 zinc finger protein 428 ENSG00000131116 IPI	ZNF42 8	R.LCC*PATAPQ EAPAPEGR.A	2.71	0	0	2.71
IPI00140201.3	PDF COG8 Conserved oligomeric Golgi complex compon	PDF	R.LEPAGPAC*P EGGR.A	0	0	2.66	2.66
IPI00470502.2	PPA2 Isoform 2 of Inorganic pyrophosphatase 2, mit	PPA2	R.GQPC*SQNYR .L	2.78	0	2.48	2.63
IPI00419880.6	RPS3A 40S ribosomal protein S3a ENSG00000145425 IP	RPS3A	R.DKMC*SMVK. K	2.46	0	2.67	2.565
IPI00011253.3	RPS3 40S ribosomal protein S3 ENSG00000149273 IPI0	RPS3	R.GLC*AIAQAE SLR.Y	2.22	2.85	2.32	2.56
IPI00147874.1	NANS Sialic acid synthase ENSG00000095380 IPI00147	NANS	K.QLLPCEMAC* NEK.L	0	0	2.56	2.56
IPI00013485.3	RPS2 40S ribosomal protein S2 ENSG00000140988 IPI0	RPS2	R.GC*TATLGNF AK.A	2.19	2.88	2.27	2.555

IPI00290279.1	ADK Isoform Long of Adenosine kinase ENSG000001561	ADK	R.TGC*TFPEKP DFH.-	0	0	2.48	2.48
IPI00788737.1	GAPDH 39 kDa protein ENSG00000111640 IPI00789134 I	GAPD H	K.IISNASC*TTN CLAPLAK.V	2.25	2.46	2.35	2.38
IPI00041127.6	ASF1B Histone chaperone ASF1B ENSG00000105011 IPI0	ASF1B	K.GLGLPGC*IP GLLPENSMDCI.-	3.56	0	1.19	2.375
IPI00215719.6	RPL18 60S ribosomal protein L18 ENSG00000063177 IP	RPL18	K.GC*GTVLLSG PR.K	0	0	2.36	2.36
IPI00749250.1	ACTR2 45 kDa protein ENSG00000138071 IPI00005159 I	ACTR2	K.LC*YVGYNIE QEQK.L	0	0	2.32	2.32
IPI00291939.1	SMC1A Structural maintenance of chromosomes protei	SMC1 A	K.AESLIGVYPE QGDC*VISK.V	2.41	0	2.18	2.295
IPI00219160.3	RPL34 60S ribosomal protein L34 ENSG00000109475 IP	RPL34	K.SACGVC*PGR .L	2.1	0	2.29	2.195
IPI00797038.1	PCK2 mitochondrial phosphoenolpyruvate carboxykina	PCK2	R.YVAAAFPSAC *GK.T	2.08	0	2.19	2.135
IPI00413641.7	AKR1B1 Aldose reductase ENSG00000085662 IPI0041364	AKR1 B1	R.VC*ALLSCTS HK.D	0	2.11	0	2.11
IPI00026138.4	_ Uncharacterized protein ENSP00000371610 ENSG0000	–	K.NC*LTNFHG MDLTR.D	0	2.03	2.21	2.075
IPI00783910.1	KIAA1524 102 kDa protein ENSG00000163507 IPI007839	KIAA1 524	K.DQIC*DVR.I	2.06	0	0	2.06
IPI00028296.1	CAMK1 Calcium/calmodulin-dependent protein kinase	CAMK 1	R.DC*CVEPGTE LSPTLPHQL.-	1.7	0	2.39	2.045
IPI00430622.1	SPG20 Spartin ENSG00000133104 IPI00480185 IPI00430	SPG20	K.VSQFLVDGV CTVANC*VGK.E	2.02	0	0	2.02
IPI00456758.4	RPL27A 60S ribosomal protein L27a ENSG00000166441	RPL27 A	R.NQSFC*PTVN LDK.L	2.01	0	0	2.01
IPI00215919.5	ARF5 ADP-ribosylation factor 5 ENSG00000004059 IPI	ARF5	K.NIC*FTVWDV GGQDK.I	1.9	0	2.07	1.985
IPI00007752.1	TUBB2C Tubulin beta-2C chain ENSG00000188229 IPI00	TUBB2 C	K.NMMAAC*DP R.H	1.86	2.1	1.86	1.98
IPI00641950.3	GNB2L1 Lung cancer oncogene 7 ENSG00000204628 IPI0	GNB2L 1	K.VWNLANC*K. L	1.77	0	2.19	1.98
IPI00007752.1	TUBB2C Tubulin beta-2C chain ENSG00000188229 IPI00	TUBB2 C	K.VSDTVVEPYN ATLSVHQLVEN TDETYC*IDNEA LYDICFR.T	2.1	2.04	1.7	1.97
IPI00007750.1	TUBA4A Tubulin alpha-4A chain ENSG00000127824 IPI0	TUBA4 A	K.AYHEQLSVA EITNAC*FEPAN QMVK.C	1.73	2.21	1.69	1.96
IPI00007752.1	TUBB2C Tubulin beta-2C chain ENSG00000188229 IPI00	TUBB2 C	K.TAVC*DIPPR. G	1.79	2.06	1.85	1.94
IPI00747722.1	GALK1 Uncharacterized protein GALK1 ENSG0000010847	GALK 1	R.AQVCQQAEH SFAGMPC*GIM DQFISLMGQK.G	0	1.93	0	1.93
IPI00016580.6	DSN1 Isoform 1 of Kinetochore-associated protein D	DSN1	K.VFDC*MELV MDELQGSVK.Q	1.66	0	2.18	1.92
IPI00655631.1	POLD1 DNA polymerase ENSG00000062822	POLD1	R.DNC*PLVANL VTASLR.R	0	0	1.9	1.9

	IPI00002894 I						
Reverse_IPI00184021.2	CRIPAK cysteine-rich PAK1 inhibitor ENSG0000017997	CRIPAK	R.C*THAPSCEVHARTILR.A	1.89	0	0	1.89
IPI00002966.1	HSPA4 Heat shock 70 kDa protein 4 ENSG00000170606	HSPA4	R.C*TPACISFGPK.N	0	1.93	1.76	1.8875
IPI00022442.2	NDUFAB1 Acyl carrier protein, mitochondrial precur	NDUFAB1	K.LMC*PQEIVDYIADKK.D	0	1.88	0	1.88
IPI00337307.3	HTF9C Isoform 1 of HpaII tiny fragments locus 9c p	HTF9C	R.VIGVELC*PEAVEDAR.V	1.88	0	0	1.88
IPI00022334.1	OAT Ornithine aminotransferase, mitochondrial prec	OAT	K.VLPMNTGVEAGETAC*K.L	0	0	1.86	1.86
IPI00027251.1	STK38 Serine/threonine-protein kinase 38 ENSG00000	STK38	K.LSDFGLC*TGLK.K	0	0	1.86	1.86
IPI00746351.1	DIS3 Uncharacterized protein DIS3 ENSG00000083520	DIS3	R.LAC*LSEEGNEIESGK.I	2.04	0	1.62	1.83
IPI00848058.1	ACTB Actin, cytoplasmic 2 ENSG00000075624 IPI00021	ACTB	R.C*PEALFQPSFLGMESCGIHETTFNSIMK.C	0	1.83	0	1.83
IPI00305589.3	PFKFB2 Isoform 1 of 6-phosphofructo-2-kinase/fruct	PFKFB2	K.QC*ALVALEDVK.A	1.83	0	0	1.83
IPI00398057.1	LOC389342 Uncharacterized protein ENSP00000353659	LOC389342	K.VDEFPLC*GHMVSDEYEQLSSEALEAAR.I	1.83	0	0	1.83
IPI00217223.1	PAICS Multifunctional protein ADE2 ENSG00000128050	PAICS	K.C*GETAFIAPQCEMIPIEWVCR.R	0	0	1.82	1.82
IPI00180675.4	TUBA1A Tubulin alpha-1A chain ENSG00000167552 IPI0	TUBA1A	K.LADQC*TGLQGFLVFHSFGGGTGSGFTSLLMER.L	0	1.81	0	1.81
IPI00218343.4	TUBA1C Tubulin alpha-1C chain ENSG00000167553 IPI0	TUBA1C	R.AVC*MLSNTTAVAEAWAR.L	1.59	1.92	1.79	1.805
IPI00220766.5	GLO1 Lactoylglutathione lyase ENSG00000124767 IPI0	GLO1	K.C*DFPIMK.F	1.67	0	1.94	1.805
IPI00169383.3	PGK1 Phosphoglycerate kinase 1 ENSG00000102144 IPI	PGK1	R.GCITIIGGGDTATC*C*AK.W	0	0	1.8	1.8
IPI00302925.3	CCT8 Uncharacterized protein CCT8 ENSG00000156261	CCT8	K.AHEILPNLVC*CSAK.N	0	1.75	0	1.75
IPI00182533.5	RPL28 60S ribosomal protein L28 ENSG00000108107 IP	RPL28	R.NC*SSFLIK.R	1.72	0	1.77	1.745
IPI00387130.1	CIAPIN1 Isoform 1 of Anamorsin ENSG00000005194 IPI	CIAPIN1	R.CASC*PYLGMPAFKPGEK.V	0	1.74	0	1.74
IPI00396627.1	ELAC2 Isoform 1 of Zinc phosphodiesterase ELAC pro	ELAC2	K.VVYSGDTMPC*EALVR.M	1.74	0	0	1.74
IPI00007750.1	TUBA4A Tubulin alpha-4A chain ENSG00000127824 IPI0	TUBA4A	R.AVC*MLSNTTAIAEAWAR.L	1.57	1.9	1.56	1.7325
IPI00010153.5	RPL23 60S ribosomal protein L23 ENSG00000125691 IP	RPL23	R.ISLGLPVGAVINC*ADNTGAK.N	0	1.77	1.6	1.7275
IPI00218343.4	TUBA1C Tubulin alpha-1C chain ENSG00000167553 IPI0	TUBA1C	K.AYHEQLTVAEITNAC*FEPANQMVK.C	1.71	0	1.74	1.725

IPI00453476.2	_ Uncharacterized protein ENSP00000348237 ENSG0000	–	R.YADLTEDQLPSC*ESLK.D	0	0	1.71	1.71
IPI00180675.4	TUBA1A Tubulin alpha-1A chain ENSG00000167552 IPI0	TUBA1A	R.TIQFVDWC*PTGFK.V	1.53	1.88	1.54	1.7075
IPI00514587.1	SARS Uncharacterized protein SARS ENSG00000031698	SARS	R.TIC*AILENYQTEK.G	1.77	0	1.6	1.685
IPI00301609.8	NEK9 Serine/threonine-protein kinase Nek9 ENSG0000	NEK9	R.LNPAVTC*AGK.G	0	0	1.68	1.68
IPI00010720.1	CCT5 T-complex protein 1 subunit epsilon ENSG00000	CCT5	K.IAILTC*PFEPPKPK.T	0	1.68	0	1.68
IPI00552897.2	MDC1 Isoform 1 of Mediator of DNA damage checkpoin	MDC1	R.C*NVEPVGR.L	1.67	0	0	1.67
IPI00641635.1	FTO 64 kDa protein ENSG00000140718 IPI00028277 IPI	FTO	K.ANEDAVPLC*MSADFPR.V	0.98	0	2.33	1.655
IPI00514587.1	SARS Uncharacterized protein SARS ENSG00000031698	SARS	K.YAGLSTC*FR.Q	1.57	1.72	1.6	1.6525
IPI00163085.2	AMOT Isoform 1 of Angiomotin ENSG00000126016 IPI00	AMOT	R.QGNC*QPTNVSEYNAAALMELLR.E	1.69	0	1.61	1.65
IPI00219103.6	HPCA Neuron-specific calcium-binding protein hippo	HPCA	R.LLQC*DPSSASQF.-	1.5	0	1.77	1.635
IPI00220158.1	ADD1 Isoform 3 of Alpha-adducin ENSG00000087274 IP	ADD1	K.YSDVEVPASVTGYSFASDGDSGTC*SPLR.H	1.99	0	1.26	1.625
IPI00789740.1	GEMIN4 Gem (Nuclear organelle) associated protein	GEMIN4	R.SDPDAC*PTMPLLAMLLR.G	0	0	1.62	1.62
IPI00552569.1	ERCC6L excision repair protein ERCC6-like ENSG0000	ERCC6L	K.GFGSVEELC*TNSSLGMEK.S	0	0	1.61	1.61
Reverse_IPI00479998.1	ZNF267 Zinc finger protein 267 ENSG00000185947 IPI	ZNF267	R.HQTLC*SSRSFVKGCEK.C	1.61	0	0	1.61
IPI00152089.3	CXorf38 Isoform 1 of Uncharacterized protein CXorf	CXorf38	R.LNC*AEYK.N	0	1.72	1.27	1.6075
IPI00788737.1	GAPDH 39 kDa protein ENSG00000111640 IPI00789134 I	GAPDH	K.IISNASC*TTNC*LAPLAK.V	0	1.6	0	1.6
IPI00031517.1	MCM6 DNA replication licensing factor MCM6 ENSG000	MCM6	R.LGFSEYC*R.I	1.6	0	0	1.6
IPI00297455.4	AKAP8L A-kinase anchor protein 8-like ENSG00000011	AKAP8L	R.GQC*MSGASR.L	1.79	0	1.37	1.58
IPI00790739.1	ACO2 Aconitase 2, mitochondrial ENSG00000100412 IP	ACO2	R.VGLIGSC*TNSSYEDMGR.S	0	0	1.58	1.58
IPI00641950.3	GNB2L1 Lung cancer oncogene 7 ENSG00000204628 IPI0	GNB2L1	R.FSPNSSNPIIVSC*GWDK.L	1.42	0	1.73	1.575
IPI00216085.3	COX6B1 Cytochrome c oxidase subunit VIb isoform 1	COX6B1	R.VYQSLC*PTSWVTDWDEQR.A	1.57	0	0	1.57
IPI00387130.1	CIAPIN1 Isoform 1 of Anamorsin ENSG00000005194 IPI	CIAPIN1	K.NC*TCGLAEELEK.E	1.55	0	0	1.55
IPI00007750.1	TUBA4A Tubulin alpha-4A chain ENSG00000127824 IPI0	TUBA4A	K.YMAC*CLLYR.G	1.35	1.7	1.45	1.55

IPI00028296.1	CAMK1 Calcium/calmodulin-dependent protein kinase	CAMK1	K.MEDPGSVLSTAC*GTPGYVAPEVLAQKPYSK.A	1.36	0	1.71	1.535
IPI00018931.6	VPS35 Vacuolar protein sorting-associated protein	VPS35	R.TQC*ALAASK.L	1.53	0	0	1.53
IPI00742682.1	TPR nuclear pore complex-associated protein TPR EN	TPR	R.RDC*QEQAK.I	1.53	0	0	1.53
IPI00007750.1	TUBA4A Tubulin alpha-4A chain ENSG00000127824 IPI0	TUBA4A	K.RSIQFVDWC*PTGFK.V	1.41	1.64	1.42	1.5275
IPI00787961.1	ZNF703 similar to zinc finger protein 703 ENSG0000	ZNF703	K.SPLALLAQTC*SQIGKPDPPPSSK.L	0	1.52	0	1.52
IPI00852960.1	USP22 Ubiquitin carboxyl-terminal hydrolase 22 ENS	USP22	K.C*DDAIITK.A	1.52	0	0	1.52
IPI00396485.3	EEF1A1 Elongation factor 1-alpha 1 ENSG00000156508	EEF1A1	K.PMC*VESFSDYPPLGR.F	1.4	1.61	1.45	1.5175
IPI00024381.1	CLP1 Pre-mRNA cleavage complex II protein Clp1 ENS	CLP1	K.VGAPTIPDSC*LPLGMSQEDNQLK.L	1.4	0	1.63	1.515
IPI00387130.1	CIAPIN1 Isoform 1 of Anamorsin ENSG00000005194 IPI	CIAPIN1	K.SAC*GNCYLGDAFR.C	1.4	0	1.61	1.505
IPI00641950.3	GNB2L1 Lung cancer oncogene 7 ENSG00000204628 IPI0	GNB2L1	K.LWNTLGVC*K.Y	1.57	0	1.43	1.5
IPI00011951.2	KIAA0427 Isoform 2 of Uncharacterized protein KIAA	KIAA0427	R.VLVC*PIYTCLR.E	0	0	1.5	1.5
IPI00005692.1	MRPS12 28S ribosomal protein S12, mitochondrial pr	MRPS12	K.GVVLC*TFTR.K	0	0	1.5	1.5
IPI00011118.2	RRM2 Ribonucleoside-diphosphate reductase M2 subun	RRM2	R.EFLFNAIETMPC*VK.K	0	0	1.49	1.49
IPI00220150.4	IDH3G Isocitrate dehydrogenase [NAD] subunit gamma	IDH3G	R.TSLDLYANVIHC*K.S	0	0	1.49	1.49
IPI00792352.1	RAN 26 kDa protein ENSG00000132341 IPI00643041 IPI	RAN	R.VC*ENIPIVLCGNK.V	1.45	0	1.53	1.49
IPI00103142.1	NUDCD2 NudC domain-containing protein 2 ENSG000001	NUDCD2	R.DAANC*WTSLLESEYAADPWVQDQMQR.K	1.48	0	0	1.48
IPI00015736.3	UBE1DC1 Ubiquitin-activating enzyme E1 domain-cont	UBE1DC1	R.EGVC*AASLPTTMGVVAGILVQNVLK.F	0	1.48	1.46	1.475
IPI00093057.6	CPOX Coproporphyrinogen III oxidase, mitochondrial	CPOX	R.C*SSFMAPPVTDLGELR.R	1.79	0	1.15	1.47
IPI00021277.1	NUBP1 Nucleotide-binding protein 1 ENSG00000103274	NUBP1	K.NC*DKGQSFFIDAPDSPATLAYR.S	0	0	1.47	1.47
IPI00012433.2	F8A1 F8A2 F8A3 Factor VIII intron 22 protein ENSG0	F8A1	R.LVC*PAAYGEPLQAAASALGAAVR.L	1.47	0	0	1.47
IPI00216190.1	GSK3B Isoform 2 of Glycogen synthase kinase-3 beta	GSK3B	K.LC*DFGSAK.Q	1.18	1.68	1.32	1.465
IPI00021435.3	PSMC2 26S protease regulatory subunit 7 ENSG000001	PSMC2	R.LC*PNSTGAEIR.S	1.41	0	1.52	1.465
IPI00387130.1	CIAPIN1 Isoform 1 of Anamorsin ENSG00000005194 IPI	CIAPIN1	R.AASC*GEGK.K	1.47	0	1.41	1.44
IPI00645078.1	UBE1 Ubiquitin-activating enzyme E1 ENSG0000013098	UBE1	K.SIPIC*TLK.N	1.36	1.42	1.54	1.435

IPI00333541.6	FLNA Filamin-A ENSG00000196924 IPI00553169 IPI0030	FLNA	K.VGTEC*GNQK.V	1.93	0	0.93	1.43
IPI00029629.3	TRIM25 Tripartite motif-containing protein 25 ENSG	TRIM25	K.NTVLC*NVVEQFLQADLAR.E	0	0	1.43	1.43
IPI00007611.1	ATP5O ATP synthase subunit O, mitochondrial precur	ATP5O	R.GEVPC*TVTSASPLEEATLSELK.T	1.43	0	0	1.43
IPI00477231.2	MGEA5 Isoform 1 of Bifunctional protein NCOAT ENSG	MGEA5	R.ANSSVVSVNC*K.G	1.23	1.62	1.24	1.4275
IPI00166130.1	D15Wsu75e DJ347H13.4 protein ENSG00000100418 IPI00	D15Wsu75e	R.GEAYNLFEHNC*NTFSNEVAQFLTGR.K	0	1.53	1.09	1.42
IPI00299214.6	TK1 thymidine kinase 1, soluble ENSG00000167900 IP	TK1	K.LFAPQQILQC*SPAN.-	0	1.52	1.12	1.42
IPI00784131.1	AARS Uncharacterized protein AARS ENSG00000090861	AARS	K.AVYTQDC*PLAAAK.A	0	0	1.42	1.42
IPI00216230.3	TMPO Lamina-associated polypeptide 2 isoform alpha	TMPO	K.SGIQPLC*PER.S	1.34	0	1.5	1.42
IPI00306708.3	PBK Lymphokine-activated killer T-cell-originated	PBK	K.SVLC*STPTINIPASPFMQK.L	0	1.42	0	1.42
IPI00103925.2	IRGQ Immunity-related GTPase family Q protein ENSG	IRGQ	R.EKC*SAGSQK.A	1.42	0	0	1.42
IPI00024623.3	ACADSB Short/branched chain specific acyl-CoA dehy	ACADSB	K.VGSFC*LSEAGAGSDSFALK.T	1.25	0	1.57	1.41
IPI00301609.8	NEK9 Serine/threonine-protein kinase Nek9 ENSG0000	NEK9	R.TFDATNPLNLC*VK.I	1.4	0	1.42	1.41
IPI00216047.3	SMARCC2 Isoform 1 of SWI/SNF-related matrix-associ	SMARCC2	K.SLVQNNCLSRPNIFLC*PEIEPK.L	0	1.41	0	1.41
IPI00024623.3	ACADSB Short/branched chain specific acyl-CoA dehy	ACADSB	R.ASSTC*PLTFENVK.V	1.41	0	0	1.41
IPI00024403.1	CPNE3 Copine-3 ENSG00000085719 IPI00024403 IPI0074	CPNE3	K.NC*LNPQFSK.T	2.16	1.18	1.08	1.4
IPI00398057.1	LOC389342 Uncharacterized protein ENSP00000353659	LOC389342	R.LIPDGC*GVK.Y	0	1.43	1.31	1.4
IPI00007102.3	GLOD4 Uncharacterized protein C17orf25 ENSG0000016	GLOD4	K.AAC*NGPYDGK.W	0	0	1.4	1.4
IPI00644079.2	HNRNPU heterogeneous nuclear ribonucleoprotein U i	HNRNPU	K.MC*LFAGFQR.K	0	1.4	0	1.4
IPI00472102.3	HSPD1 61 kDa protein ENSG00000144381 IPI00472102 I	HSPD1	R.AAVEEGIVLGGGC*ALLR.C	1.27	1.53	1.25	1.395
IPI00163085.2	AMOT Isoform 1 of Angiomotin ENSG00000126016 IPI00	AMOT	R.C*LDMEGR.I	0	0	1.39	1.39
IPI00641743.2	HCFC1 Uncharacterized protein HCFC1 ENSG0000017253	HCFC1	K.TC*LPGFPGAPCAIK.I	0	1.39	0	1.39
IPI00217952.6	GFPT1 Isoform 1 of Glucosamine--fructose-6-phospha	GFPT1	R.VDSTTC*LFPVEEK.A	0	0	1.38	1.38
IPI00760837.2	FAM98B family with sequence similarity 98, member	FAM98B	R.INDALSC*EYECR.R	1.38	0	0	1.38
IPI00398048.1	_ Uncharacterized protein ENSP00000310225	–	K.C*GFLPGNEK.V	1.25	1.59	1.08	1.3775

	ENSG0000						
IPI00020729.1	IRS4 insulin receptor substrate 4 ENSG00000133124	IRS4	R.GSGGGQGSNGQGSSSHSSGGNQC*SGEGQGSR.G	1.7	0	1.04	1.37
IPI00444329.1	BCKDHA CDNA FLJ45695 fis, clone FEBRA2013570, high	BCKDHA	R.DYPLELFMAQC*YGNISDLGK.G	1.34	0	1.4	1.37
IPI00107693.4	MED15 Isoform 1 of Mediator of RNA polymerase II t	MED15	K.QQYLC*QPLLDAVLANIR.S	0	1.46	1.08	1.365
IPI00008248.3	ANAPC7 Anaphase-promoting complex subunit 7 ENSG00	ANAPC7	R.LEDVENLGC*R.L	1.47	0	1.26	1.365
IPI00020578.2	ARAF ARAF protein ENSG00000078061 IPI00020578 IPI0	ARAF	R.TQADELPAC*LLSAAR.L	0	0	1.36	1.36
IPI00790937.1	NMD3 Protein NMD3 homolog ENSG00000169251 IPI00790	NMD3	K.MVEFLQCTVPC*R.Y	0	0	1.36	1.36
IPI00298935.4	JMJD1B Isoform 1 of JmjC domain-containing histone	JMJD1B	K.NLFFQC*MSQTLPTSNYFTTVSESLADDSSSR.D	0	0	1.36	1.36
IPI00026781.2	FASN Fatty acid synthase ENSG00000169710 IPI000267	FASN	R.LGMLSPEGTC*K.A	1.36	0	1.35	1.355
IPI00554737.3	PPP2R1A Serine/threonine-protein phosphatase 2A 65	PPP2R1A	K.DC*EAEVR.A	1.54	0	1.16	1.35
IPI00017726.1	HSD17B10 Isoform 1 of 3-hydroxyacyl-CoA dehydrogen	HSD17B10	K.LGNNC*VFAPADVTSEKDVQTALALAK.G	0	0	1.35	1.35
IPI00790757.1	DUSP3 23 kDa protein ENSG00000108861 IPI00018671 I	DUSP3	R.EIGPNDGFLAQLC*QLNDR.L	0	0	1.35	1.35
IPI00477802.1	TCEAL1 Isoform 2 of Transcription elongation facto	TCEAL1	K.DLFEGRPPMEQPPC*GVGK.H	0	0	1.35	1.35
IPI00414858.3	COG3 Isoform 1 of Conserved oligomeric Golgi compl	COG3	R.ELLLGPSIAC*TVAELTSQNNR.D	1.17	1.4	0	1.3425
IPI00018465.1	CCT7 T-complex protein 1 subunit eta ENSG0000001356	CCT7	R.QLC*DNAGFDATNILNK.L	1.36	0	1.32	1.34
IPI00026492.3	GCAT 2-amino-3-ketobutyrate coenzyme A ligase, mit	GCAT	R.LVATDGAFSMDGDIAPLQEIC*CLASR.Y	1.34	0	0	1.34
IPI00023530.6	CDK5 Cell division protein kinase 5 ENSG0000016488	CDK5	R.ISAEEALQHPYFSDFC*PP.-	1.45	0	1.23	1.34
IPI00423156.1	CHEK2 Isoform 9 of Serine/threonine-protein kinase	CHEK2	K.TLGSGAC*GEVK.L	1.8	1.05	1.44	1.335
IPI00031370.3	TUBB2B Tubulin beta-2B chain ENSG00000137285 IPI00	TUBB2B	K.ESESC*DCLQGFQLTHSLGGGTGSGMGTLLISK.I	0	0	1.33	1.33
IPI00006167.1	PPM1G Protein phosphatase 1G ENSG00000115241 IPI00	PPM1G	K.C*SGDGVGAPR.L	0	0	1.33	1.33
IPI00296337.2	PRKDC Isoform 1 of DNA-dependent protein kinase ca	PRKDC	R.VEQLFQVMNGILAQDSAC*SQR.A	1.33	0	0	1.33
IPI00145260.3	C1orf69 Putative transferase C1orf69, mitochondria	C1orf69	R.VWAVLPSSPEAC*GAASLQER.A	1.32	0	1.33	1.325
IPI00103467.4	ALDH1B1 Aldehyde dehydrogenase X, mitochondrial pr	ALDH1B1	K.LLC*GGER.F	1.16	0	1.49	1.325

IPI00021320.2	MEPCE 7SK snRNA methylphosphate capping enzyme ENS	MEPCE	R.SC*FPASLTASR.G	1.15	0	1.5	1.325
IPI00335449.3	PPP2R1B beta isoform of regulatory subunit A, prot	PPP2R1B	R.LNIISNLDC*VNEVIGIR.Q	1.17	1.52	1.08	1.3225
IPI00025273.1	GART Isoform Long of Trifunctional purine biosynth	GART	R.SGC*KVDLGGFAGLFDLK.A	1.32	0	0	1.32
IPI00456919.2	HUWE1 Isoform 1 of E3 ubiquitin-protein ligase HUW	HUWE1	R.DQSAQC*TASK.S	1.24	0	1.4	1.32
IPI00845436.1	ARF4 similar to ADP-ribosylation factor 4 ENSG0000	ARF4	K.NIC*FTVWDVGGQDR.I	1.34	0	1.29	1.315
IPI00011631.6	ZW10 Centromere/kinetochore protein zw10 homolog E	ZW10	R.LAPILC*DGTATFVDLVPGFR.R	0	1.35	1.19	1.31
IPI00008943.3	DDX19B Isoform 1 of ATP-dependent RNA helicase DDX	DDX19B	K.VLVTTNVC*AR.G	1.33	0	1.29	1.31
IPI00307755.3	PRKAA2 5-AMP-activated protein kinase catalytic s	PRKAA2	R.TSC*GSPNYAAPEVISGR.L	0	0	1.31	1.31
IPI00306017.2	C15orf44 Isoform 1 of UPF0464 protein C15orf44 ENS	C15orf44	R.LIDLNNGEGQIFTIDGPLC*LK.N	1.04	0	1.58	1.31
IPI00646500.1	RPA2 Isoform 3 of Replication protein A 32 kDa sub	RPA2	K.AC*PRPEGLNFQDLK.N	0	1.31	0	1.31
IPI00170877.2	MRPL10 mitochondrial ribosomal protein L10 isoform	MRPL10	R.TVPFLPLLGGC*IDDTILSR.Q	0	1.31	0	1.31
IPI00397721.1	BLOC1S3 Biogenesis of lysosome-related organelles	BLOC1S3	R.GDLC*ALAER.L	1.31	0	0	1.31
IPI00465260.4	GARS Glycyl-tRNA synthetase ENSG00000106105 IPI004	GARS	R.SCYDLSC*HAR.A	1.33	0	1.28	1.305
IPI00021277.1	NUBP1 Nucleotide-binding protein 1 ENSG00000103274	NUBP1	R.LC*ASGAGATPDTAIEEIKEK.M	1.26	0	1.35	1.305
IPI00016610.2	PCBP1 Poly(rC)-binding protein 1 ENSG00000169564 I	PCBP1	R.LVVPATQC*GSLIGK.G	0	1.34	1.19	1.3025
IPI00100748.3	HSPBP1 Isoform 1 of Hsp70-binding protein 1 ENSG00	HSPBP1	R.LLDRDAC*DTVR.V	0	1.3	0	1.3
IPI00719725.1	SAPS3 Isoform 5 of SAPS domain family member 3 ENS	SAPS3	K.C*AAPRPPSSSPEQR.T	0	1.3	0	1.3
IPI00021435.3	PSMC2 26S protease regulatory subunit 7 ENSG000001	PSMC2	R.SVC*TEAGMFAIR.A	1.3	0	0	1.3
IPI00647655.1	POLA1 Uncharacterized protein POLA1 ENSG0000010186	POLA1	R.YIFDAEC*ALEK.L	1.3	0	0	1.3
IPI00064765.3	RPL10L 60S ribosomal protein L10-like ENSG00000165	RPL10L	K.MLSC*AGADR.L	1.16	1.46	1.11	1.2975
IPI00007402.2	IPO7 Uncharacterized protein IPO7 ENSG00000205339	IPO7	R.GIDQC*IPLFVEAALER.L	1.25	1.39	1.16	1.2975
IPI00785096.2	BZW1 similar to basic leucine zipper and W2 domain	BZW1	K.ERFDPTQFQDC*IIQGLTETGTDLEAVAK.F	1.14	1.42	1.21	1.2975
IPI00024670.5	REEP5 Receptor expression-enhancing protein 5 ENSG	REEP5	K.NC*MTDLLAK.L	1.08	0	1.51	1.295
Reverse_IPI00102425.1	P15RS Cyclin-dependent kinase inhibitor-related pr	P15RS	K.KC*SEDTESSVHK.F	1.42	0	1.16	1.29

IPI00019903.1	CCDC44 Coiled-coil domain-containing protein 44 EN	CCDC44	K.KLDSLGLCSVSC*ALEFIPNSK.V	1.27	0	1.31	1.29
IPI00021347.1	UBE2L3 Ubiquitin-conjugating enzyme E2 L3 ENSG0000	UBE2L3	K.GQVC*LPVISAENWKPATK.T	0	1.29	0	1.29
IPI00174962.2	MICALL1 MICAL-like protein 1 ENSG00000100139 IPI00	MICALL1	R.GSSGPQPAKPC*SGATPTPLLLVGDR.S	0	1.29	0	1.29
IPI00397904.6	NUP93 Nuclear pore complex protein Nup93 ENSG00000	NUP93	K.LNQVC*FDDDGTSSPQDR.L	1.29	0	0	1.29
IPI00641743.2	HCFC1 Uncharacterized protein HCFC1 ENSG0000017253	HCFC1	R.VAGINAC*GR.G	1.27	1.35	1.17	1.285
IPI00028412.1	SSSCA1 Sjoegren syndrome/scleroderma autoantigen 1	SSSCA1	R.MLGETC*ADCGTILLQDK.Q	1.23	0	1.34	1.285
IPI00793696.1	RPL24 19 kDa protein ENSG00000114391 IPI00306332 I	RPL24	K.C*ESAFLSK.R	1.21	1.37	1.18	1.2825
IPI00011118.2	RRM2 Ribonucleoside-diphosphate reductase M2 subun	RRM2	K.LIGMNC*TLMK.Q	0	0	1.28	1.28
IPI00146935.4	DNM1L Isoform 1 of Dynamin-1-like protein ENSG0000	DNM1L	K.YIETSELC*GGAR.I	1.28	0	0	1.28
IPI00012197.1	XTP3TPA XTP3-transactivated gene A protein ENSG000	XTP3TPA	K.YTELPHGAISEDQAVGPADIPC*DSTGQTST.-	1.36	0	1.19	1.275
IPI00018465.1	CCT7 T-complex protein 1 subunit eta ENSG000001356	CCT7	K.EGTDSSQGIPQLVSNISAC*QVIAEAVR.T	1.28	0	1.27	1.275
IPI00030363.1	ACAT1 Acetyl-CoA acetyltransferase, mitochondrial	ACAT1	K.DGLTDVYNKIHMGSC*AENTAK.K	1.06	1.4	1.23	1.2725
IPI00023138.1	RAC3 Ras-related C3 botulinum toxin substrate 3 pr	RAC3	R.AVLC*PPPVK.K	0	0	1.27	1.27
IPI00024097.3	TES Isoform 1 of Testin ENSG00000135269 IPI0002409	TES	K.SEALGVGDVKLPC*EMDAQGPK.Q	0	0	1.27	1.27
IPI00745518.1	MAP4 Microtubule-associated protein 4 isoform 1 va	MAP4	K.KKPC*SETSQIEDTPSSKPTLLANGGHGVEGSDTTGSPTEFLEEK.M	0	1.27	0	1.27
IPI00025815.2	TARDBP TDP43 ENSG00000120948 IPI00025815 IPI006398	TARDBP	R.NPVSQC*MR.G	1.27	0	0	1.27
IPI00549189.4	THOP1 Thimet oligopeptidase ENSG00000172009 IPI005	THOP1	K.GLQVGGC*EPEPQVC.-	1.27	0	0	1.27
IPI00550191.2	C9orf78 Uncharacterized protein C9orf78 ENSG000001	C9orf78	K.NAEDC*LYELPENIR.V	1.27	0	0	1.27
IPI00011107.2	IDH2 Isocitrate dehydrogenase [NADP], mitochondria	IDH2	K.SSGGFVWAC*K.N	1.14	1.34	1.23	1.2625
IPI00290566.1	TCP1 T-complex protein 1 subunit alpha ENSG0000012	TCP1	R.DC*LINAAK.T	1.33	0	1.19	1.26
IPI00096066.2	SUCLG2 Succinyl-CoA ligase [GDP-forming] beta-chai	SUCLG2	R.SC*NGPVLVGSPQGGVDIEEVAASNPELIFK.E	1.31	0	1.21	1.26
IPI00550365.2	PCBP3 Poly(RC) binding protein 3 ENSG00000183570 I	PCBP3	R.LVVPASQC*GSLIGK.G	0	1.27	1.23	1.26

IPI00555957.1	_ Heat shock protein 90Ad ENSG00000205100 IPI00555	–	R.DLIMDNC*EELIPEYLNFIR.G	0	0	1.26	1.26
IPI00030363.1	ACAT1 Acetyl-CoA acetyltransferase, mitochondrial	ACAT1	R.QAVLGAGLPISTPC*TTINK.V	0	1.25	1.29	1.26
IPI00411570.2	RANGAP1 KIAA1835 protein (Fragment) ENSG0000010040	RANGAP1	K.ALAPLLLAFVTKPNSALESC*SFAR.H	0	1.26	0	1.26
IPI00302925.3	CCT8 Uncharacterized protein CCT8 ENSG00000156261	CCT8	K.IAVYSC*PFDGMITETK.G	1.19	1.35	1.14	1.2575
IPI00478758.1	C10orf119 Uncharacterized protein C10orf119 ENSG00	C10orf119	R.DASALLDPMEC*TDTAEEQR.V	1.29	0	1.21	1.25
IPI00003918.6	RPL4 60S ribosomal protein L4 ENSG00000174444 IPI0	RPL4	R.SGQGAFGNMC*R.G	1.27	0	1.23	1.25
IPI00033030.2	ADRM1 Protein ADRM1 ENSG00000130706 IPI00033030 IP	ADRM1	R.VPQC*PSGR.V	0	0	1.25	1.25
IPI00301364.3	SKP1A Isoform 1 of S-phase kinase-associated prote	SKP1A	R.KENQWC*EEK.-	1.16	0	1.34	1.25
IPI00418794.1	ENOSF1 Enolase superfamily member 1 ENSG0000013219	ENOSF1	K.ALQFLQIDSC*R.L	1.13	0	1.37	1.25
IPI00513791.2	DOCK7 Isoform 1 of Dedicator of cytokinesis protei	DOCK7	K.AVLPVTC*HR.D	0	1.25	0	1.25
IPI00000874.1	PRDX1 Peroxiredoxin-1 ENSG00000117450 IPI00000874	PRDX1	K.HGEVC*PAGWKPGSDTIKPDVQK.S	0	1.25	0	1.25
IPI00296589.3	ITPK1 ITPK1 protein (Fragment) ENSG00000100605 IPI	ITPK1	R.LGC*NAGVSPSFQQHCVASLATK.A	0	1.25	0	1.25
IPI00154451.6	MMS19 Isoform 1 of MMS19-like protein ENSG00000155	MMS19	R.YHPLSSC*LTAR.L	0	1.25	0	1.25
IPI00027228.1	PET112L Probable glutamyl-tRNA(Gln) amidotransfera	PET112L	R.AGVGLLEVVLEPDMSC*GEEAATAVR.E	1.25	0	0	1.25
IPI00025273.1	GART Isoform Long of Trifunctional purine biosynth	GART	K.SSLQYSSPAPDGC*GDQTLGDLLLTPTR.I	1.25	0	0	1.25
IPI00441867.1	PEX19 Isoform 1 of Peroxisomal biogenesis factor 1	PEX19	R.VGSDMTSQQEFTSC*LK.E	1.34	0	1.15	1.245
IPI00002520.1	SHMT2 Serine hydroxymethyltransferase, mitochondri	SHMT2	R.AALEALGSC*LNNK.Y	0	0	1.24	1.24
IPI00026940.2	NUP50 Nucleoporin 50 kDa ENSG00000093000 IPI000269	NUP50	K.AC*VGNAYHK.Q	0	1.24	0	1.24
IPI00152151.4	FAM122B Isoform 3 of Protein FAM122B ENSG000001565	FAM122B	K.GSATAESPVAC*SNSCSSFILMDDLSPK.-	1.24	0	0	1.24
IPI00332499.1	NASP nuclear autoantigenic sperm protein isoform 1	NASP	R.KPTDGASSSNC*VTDISHLVR.K	0	1.31	1.02	1.2375
IPI00186290.6	EEF2 Elongation factor 2 ENSG00000167658 IPI001862	EEF2	K.STLTDSLVC*K.A	1.25	1.26	1.18	1.2375
IPI00025491.1	EIF4A1 Eukaryotic initiation factor 4A-I ENSG00000	EIF4A1	K.VVMALGDYMGASC*HACIGGTNVR.A	0	1.35	0.89	1.235
IPI00015262.10	CNN2 Calponin-2 ENSG00000064666 IPI00015262 IPI003	CNN2	K.AGQC*VIGLQMGTNK.C	1.4	1.05	1.44	1.235

IPI00643591.5	AP1G1 Adaptor-related protein complex 1, gamma 1 s	AP1G1	R.FTC*TVNR.I	1.19	0	1.28	1.235
IPI00377005.2	_ Uncharacterized protein ENSP00000340627 ENSG0000	_	K.C*LSAAEEK.Y	1.2	1.39	0.95	1.2325
IPI00102425.1	P15RS Cyclin-dependent kinase inhibitor-related pr	P15RS	K.HVSSETDESC*KK.H	1.29	0	1.17	1.23
IPI00293564.5	HMGCL Hydroxymethylglutaryl-CoA lyase, mitochondri	HMGCL	K.VAQATC*KL.-	1.25	0	1.21	1.23
IPI00005511.1	PHF5A PHD finger-like domain-containing protein 5A	PHF5A	R.ICDEC*NYGSYQGR.C	0	0	1.23	1.23
IPI00657888.1	GMPPA Uncharacterized protein GMPPA ENSG0000014459	GMPPA	K.LLPAITILGC*R.V	0	1.23	0	1.23
IPI00376351.2	METTL2B METTL2A Isoform 1 of Methyltransferase-lik	METTL2B	K.ISDLEIC*ADEFPGSSATYR.I	1.23	0	0	1.23
IPI00013214.1	MCM3 DNA replication licensing factor MCM3 ENSG000	MCM3	R.SVHYC*PATK.K	0	1.19	1.34	1.2275
IPI00550746.4	NUDC Nuclear migration protein nudC ENSG0000009027	NUDC	R.WTQTLSELDLAVPFC*VNFR.L	0	1.28	1.06	1.225
IPI00745613.1	EXOSC4 Uncharacterized protein EXOSC4 ENSG00000178	EXOSC4	K.SC*EMGLQLR.Q	1.39	0	1.06	1.225
IPI00742743.1	TP53BP1 Isoform 2 of Tumor suppressor p53-binding	TP53BP1	K.VADPVDSSNLDTC*GSISQVIEQLPQPNR.T	1.19	0	1.26	1.225
IPI00009668.3	CENPH Centromere protein H ENSG00000153044 IPI0000	CENPH	R.AGGPPQVAGAQAAC*SEDR.M	1.12	1.35	1.06	1.22
IPI00016912.1	TTC1 Tetratricopeptide repeat protein 1 ENSG000001	TTC1	K.VTDTQEAEC*AGPPVPDPK.N	1.25	0	1.19	1.22
IPI00641384.2	SEC16A SEC16 homolog A ENSG00000148396 IPI00641384	SEC16A	R.ANNNAAVAPTTC*PLQPVTDPFAFSR.Q	0	0	1.22	1.22
IPI00003814.1	MAP2K6 Isoform 1 of Dual specificity mitogen-activ	MAP2K6	K.AC*ISIGNQNFEVK.A	0	0	1.22	1.22
IPI00456981.2	RP11-11C5.2 Similar to RIKEN cDNA 2410129H14 ENSG0	RP11-11C5.2	R.LC*EQGINPEALSSVIK.E	0	0	1.22	1.22
IPI00796337.1	PCBP2 poly(rC)-binding protein 2 isoform a ENSG000	PCBP2	R.AITIAGIPQSIIEC*VK.Q	0	0	1.22	1.22
IPI00556594.2	ZCCHC8 Isoform 1 of Zinc finger CCHC domain-contai	ZCCHC8	R.IFGSIPMQAC*QQK.D	0	0	1.22	1.22
IPI00827583.1	BSCL2 72 kDa protein ENSG00000168000 IPI00045906 I	BSCL2	K.EGC*TEVSLLR.V	1.22	0	0	1.22
IPI00641582.1	BAG3 BAG family molecular chaperone regulator 3 EN	BAG3	R.SQSPAASDC*SSSSSSASLPSSGR.S	1.22	0	0	1.22
IPI00030116.1	PGM3 Isoform 1 of Phosphoacetylglucosamine mutase	PGM3	K.QASC*SGDEYR.S	1.22	0	0	1.22
IPI00029665.8	MMAB Cob ENSG00000139428 IPI00029665 IPI00795427 I	MMAB	K.IQCTLQDVGSALATPC*SSAR.E	1.23	1.26	1.11	1.215
IPI00333541.6	FLNA Filamin-A ENSG00000196924	FLNA	K.AHVVPC*FDASK.V	0	1.28	1.02	1.215

	IPI00553169 IPI0030						
IPI00012773.1	MTA1 Isoform Long of Metastasis-associated protein	MTA1	R.ALDC*SSSVR.Q	1.19	0	1.24	1.215
IPI00844329.1	HPRT1 Uncharacterized protein HPRT1 ENSG0000016570	HPRT1	K.SYC*NDQSTGDIK.V	1.05	1.44	0.91	1.21
IPI00216975.1	TPM4 Isoform 2 of Tropomyosin alpha-4 chain ENSG00	TPM4	K.EENVGLHQTLDQTLNELNC*I.-	1.23	0	1.19	1.21
IPI00297579.4	CBX3 LOC653972 Chromobox protein homolog 3 ENSG000	CBX3	R.LTWHSC*PEDEAQ.-	1.22	0	1.2	1.21
IPI00607557.1	ELF2 Isoform 5 of ETS-related transcription factor	ELF2	K.IITIPATQLAQC*QLQTK.S	0	0	1.21	1.21
IPI00292753.7	GAPVD1 GTPase activating protein and VPS9 domains	GAPVD1	R.LQELESC*SGLGSTSDDTDVR.E	0	0	1.21	1.21
IPI00003027.1	GEMIN7 Gem-associated protein 7 ENSG00000142252 IP	GEMIN7	R.RAPLRPEVPEIQEC*PIAQESLESQEQR.A	0	1.21	0	1.21
IPI00643920.2	TKT Transketolase ENSG00000163931 IPI00643920 IPI0	TKT	K.QAFTDVATGSLGQGLGAAC*GMAYTGK.Y	1.21	0	0	1.21
IPI00021786.1	RAF1 RAF proto-oncogene serine/threonine-protein k	RAF1	K.DAVFDGSSC*ISPTIVQQFGYQR.R	1.21	0	0	1.21
IPI00033132.3	RNF7 Isoform 1 of RING-box protein 2 ENSG000001141	RNF7	R.VQVMDAC*LR.C	1.1	1.37	0.98	1.205
IPI00018768.1	TSN Translin ENSG00000211460 IPI00018768	TSN	K.ETAAAC*VEK.-	1.23	0	1.18	1.205
IPI00470610.3	PYCR2 Pyrroline-5-carboxylate reductase 2 ENSG0000	PYCR2	R.SLLINAVEASC*IR.T	1.16	0	1.25	1.205
IPI00029079.5	GMPS GMP synthase ENSG00000163655 IPI00029079	GMPS	K.TVGVQGDC*R.S	1.09	0	1.32	1.205
IPI00217442.2	MASK-BP3 EIF4EBP3 MASK-4E-BP3 protein ENSG00000131	MASK-BP3	R.LTSSVSC*ALDEAAAALTR.M	1.26	0	1.14	1.2
IPI00292753.7	GAPVD1 GTPase activating protein and VPS9 domains	GAPVD1	R.FSLC*SDNLEGISEGPSNR.S	1.25	0	1.15	1.2
IPI00290566.1	TCP1 T-complex protein 1 subunit alpha ENSG0000012	TCP1	R.SLHDALC*VVK.R	0	0	1.2	1.2
IPI00290571.3	FBXO30 F-box only protein 30 ENSG00000118496 IPI00	FBXO30	R.SFGVQPC*VSTVLVEPAR.N	0	0	1.2	1.2
IPI00000104.1	RNGTT Isoform 1 of mRNA-capping enzyme ENSG0000011	RNGTT	R.NKPFFDIC*TSR.K	0	1.2	0	1.2
IPI00012828.3	ACAA1 3-ketoacyl-CoA thiolase, peroxisomal precurs	ACAA1	R.DC*LIPMGITSENVAER.F	1.2	0	0	1.2
IPI00020454.1	DCK Deoxycytidine kinase ENSG00000156136 IPI000204	DCK	K.QLC*EDWEVVPEPVAR.W	1.2	0	0	1.2
IPI00008422.5	SMARCAD1 Isoform 2 of SWI/SNF-related matrix-assoc	SMARCAD1	R.VLGC*ILSELK.Q	1.2	0	0	1.2
IPI00022744.5	CSE1L Isoform 1 of Exportin-2 ENSG00000124207 IPI0	CSE1L	K.IC*AVGITK.L	1.2	0	1.19	1.195
IPI00374316.4	C6orf115 similar to Protein C6orf115 ENSG000001463	C6orf115	K.C*ANLFEALVGTLK.A	0	1.22	1.1	1.19

IPI00294536.1	STRAP Serine-threonine kinase receptor-associated	STRAP	K.IGFPETTEEELEEIASENSDC*IFPSAPDVK.A	1.12	1.25	1.14	1.19
IPI00015262.10	CNN2 Calponin-2 ENSG00000064666 IPI00015262 IPI003	CNN2	K.YCPQGTVADGAPSGTGDC*PDPGEVPEYPPYYQEEAGY.-	1.22	0	1.16	1.19
IPI00013871.1	RRM1 Ribonucleoside-diphosphate reductase large su	RRM1	K.IIDINYYPVPEAC*LSNKR.H	0	0	1.19	1.19
IPI00219445.1	PSME3 Isoform 2 of Proteasome activator complex su	PSME3	R.LDEC*EEAFQGTK.V	1.17	0	1.21	1.19
IPI00013452.8	EPRS glutamyl-prolyl tRNA synthetase ENSG000001366	EPRS	K.LGVENC*YFPMFVSQSALEK.E	1.04	0	1.34	1.19
IPI00004534.3	PFAS Phosphoribosylformylglycinamidine synthase EN	PFAS	K.LMWLFGC*PLLLDDVAR.E	0	1.19	0	1.19
IPI00333541.6	FLNA Filamin-A ENSG00000196924 IPI00553169 IPI0030	FLNA	K.ATC*APQHGAPGPGPADASK.V	0	1.19	0	1.19
IPI00013830.1	SNW1 SNW domain-containing protein 1 ENSG000001006	SNW1	K.IPPC*ISNWK.N	0	1.19	0	1.19
IPI00003766.4	ETHE1 ETHE1 protein, mitochondrial precursor ENSG0	ETHE1	R.QMFEPVSC*TFTYLLGDR.E	0	1.19	0	1.19
IPI00005104.1	CHUK ERLIN1 Inhibitor of nuclear factor kappa-B ki	CHUK	R.SLSDC*VNYIVQDSK.I	1.19	0	0	1.19
IPI00019400.1	TPMT Thiopurine S-methyltransferase ENSG0000013736	TPMT	K.C*YADTMFSLLGK.K	1.19	0	0	1.19
IPI00473014.5	DSTN Destrin ENSG00000125868 IPI00473014 IPI006432	DSTN	K.C*STPEEIKK.R	1.18	1.3	0.97	1.1875
IPI00411706.1	ESD S-formylglutathione hydrolase ENSG00000139684	ESD	K.AETGKCPALYWLSGLTC*TEQNFISK.S	0	1.19	1.18	1.1875
IPI00220301.5	PRDX6 Peroxiredoxin-6 ENSG00000117592 IPI00220301	PRDX6	R.DFTPVC*TTELGR.A	1.19	0	1.18	1.185
IPI00641743.2	HCFC1 Uncharacterized protein HCFC1 ENSG0000017253	HCFC1	R.AC*AAGTPAVIR.I	1.05	0	1.32	1.185
IPI00410067.1	ZC3HAV1 Isoform 1 of Zinc finger CCCH type antivir	ZC3HAV1	K.NSNVDSSYLESLYQSC*PR.G	1.11	0	1.25	1.18
IPI00019755.3	GSTO1 Glutathione transferase omega-1 ENSG00000148	GSTO1	R.FC*PFAER.T	1.4	1.17	0.98	1.18
IPI00024719.1	HAT1 Histone acetyltransferase type B catalytic su	HAT1	K.VDENFDC*VEADDVEGK.I	1.21	0	1.15	1.18
IPI00184523.1	ARNT Putative uncharacterized protein DKFZp547B061	ARNT	K.MTAYITELSDMVPTC*SALAR.K	0	0	1.18	1.18
IPI00011698.3	SAP18 Histone deacetylase complex subunit SAP18 EN	SAP18	K.TC*PLLLR.V	0	0	1.18	1.18
IPI00141561.3	COG1 Conserved oligomeric Golgi complex component	COG1	K.AQAISPC*VQNFCSALDSK.L	0	0	1.18	1.18
IPI00009010.3	HSPC152 TRM112-like protein ENSG00000173113 IPI000	HSPC152	R.IC*PVEFNPNFVAR.M	0	0	1.18	1.18
IPI00291006.1	MDH2 Malate dehydrogenase,	MDH2	K.TIIPLISQC*TPK.V	0	0	1.18	1.18

	mitochondrial precursor						
IPI00739117.3	BAT2D1 HBxAg transactivated protein 2 ENSG00000117	BAT2D1	R.IAC*GPPQAK.L	0	0	1.18	1.18
IPI00220152.2	BCCIP Isoform 2 of BRCA2 and CDKN1A-interacting pr	BCCIP	R.TNKPC*GK.C	0	0	1.18	1.18
IPI00010219.1	SPC25 Kinetochore protein Spc25 ENSG00000152253 IP	SPC25	K.STDTSC*QMAGLR.D	1.17	0	1.19	1.18
IPI00018350.3	MCM5 DNA replication licensing factor MCM5 ENSG000	MCM5	K.C*SPIGVYTSGK.G	1.18	0	0	1.18
IPI00005777.1	MAPKAPK3 MAP kinase-activated protein kinase 3 ENS	MAPKAPK3	K.ETTQNALQTPC*YTPYYVAPEVLGPEK.Y	1.18	0	0	1.18
IPI00030774.2	TBCD Isoform 4 of Tubulin-specific chaperone D ENS	TBCD	K.AGAPDEAVCGENVSQIYC*ALLGCMDDYTTDSR.G	1.18	0	0	1.18
IPI00419237.3	LAP3 Isoform 1 of Cytosol aminopeptidase ENSG00000	LAP3	R.SAGAC*TAAAFLK.E	1.06	1.3	1.05	1.1775
IPI00008524.1	PABPC1 Isoform 1 of Polyadenylate-binding protein	PABPC1	K.VVC*DENGSK.G	1.35	0	1	1.175
IPI00644674.1	NUBP2 Nucleotide-binding protein 2 ENSG00000095906	NUBP2	K.ILDATPAC*LP.-	1.25	0	1.1	1.175
IPI00030363.1	ACAT1 Acetyl-CoA acetyltransferase, mitochondrial	ACAT1	K.QGEYGLASIC*NGGGGASAMLIQK.L	1.06	1.26	1.12	1.175
IPI00007682.2	ATP6V1A Vacuolar ATP synthase catalytic subunit A	ATP6V1A	K.WDFTPC*K.N	1.4	0	0.95	1.175
IPI00020898.1	RPS6KA3 Ribosomal protein S6 kinase alpha-3 ENSG00	RPS6KA3	R.AENGLLMTPC*YTANFVAPEVLK.R	1.21	0	1.14	1.175
IPI00024993.4	ECHS1 Enoyl-CoA hydratase, mitochondrial precursor	ECHS1	K.ALNALC*DGLIDELNQALK.T	1.11	1.25	1.08	1.1725
IPI00013184.1	ARD1A N-terminal acetyltransferase complex ARD1 su	ARD1A	K.GNSPPSSGEAC*R.E	0	1.17	1.17	1.17
IPI00796337.1	PCBP2 poly(rC)-binding protein 2 isoform a ENSG000	PCBP2	R.YSTGSDSASFPHTTPSMC*LNPDLEGPPLEAYTIQGQYAIPQPDLTK.L	0	0	1.17	1.17
IPI00024673.2	MAPK9 Isoform Alpha-2 of Mitogen-activated protein	MAPK9	R.TAC*TNFMMTPYVVTR.Y	0	0	1.17	1.17
IPI00216951.2	DARS Aspartyl-tRNA synthetase, cytoplasmic ENSG000	DARS	R.LEYC*EALAMLR.E	0	0	1.17	1.17
IPI00479946.3	STIP1 STIP1 protein ENSG00000168439 IPI00013894 IP	STIP1	K.ALDLDSSC*K.E	1.12	0	1.22	1.17
IPI00550917.3	TWF2 Twinfilin-2 ENSG00000212130 IPI00550917	TWF2	K.HLSSC*AAPAPLTSAER.E	0	1.17	0	1.17
IPI00017726.1	HSD17B10 Isoform 1 of 3-hydroxyacyl-CoA dehydrogen	HSD17B10	K.VC*NFLASQVPFPSR.L	0	1.17	0	1.17
IPI00419237.3	LAP3 Isoform 1 of Cytosol aminopeptidase ENSG00000	LAP3	R.QVVDC*QLADVNNIGK.Y	1.23	0	1.1	1.165
IPI00658023.1	PTPN11 Isoform 1 of Tyrosine-protein	PTPN11	K.QGFWEEFETLQQQEC*K.L	1.23	0	1.1	1.165

	phosphatase n						
IPI00639841.2	PECI Peroxisomal 3,2-trans-enoyl-CoA isomerase ENS	PECI	R.WLSDEC*TNAVVNFLSR.K	1.15	1.2	1.11	1.165
IPI00093057.6	CPOX Coproporphyrinogen III oxidase, mitochondrial	CPOX	K.EGGGGISCVLQDGC*VFEK.A	1.21	0	1.12	1.165
IPI00008530.1	RPLP0 60S acidic ribosomal protein P0 ENSG00000089	RPLP0	R.AGAIAPC*EVTVPAQNTGLGPEK.T	1.16	0	1.17	1.165
IPI00218733.5	SOD1 Uncharacterized protein SOD1 ENSG00000142168	SOD1	R.LAC*GVIGIAQ.-	1.1	0	1.23	1.165
IPI00026216.4	NPEPPS Puromycin-sensitive aminopeptidase ENSG0000	NPEPPS	R.SKDGVC*VR.V	1.16	1.24	1.01	1.1625
IPI00007811.1	CDK4 Cell division protein kinase 4 ENSG0000013544	CDK4	R.LMDVC*ATSR.T	1.11	1.26	1.02	1.1625
IPI00008453.3	CORO1C Coronin-1C ENSG00000110880 IPI00008453 IPI0	CORO1C	K.C*DLISIPK.K	0	1.2	1.04	1.16
IPI00006907.1	C12orf5 Uncharacterized protein C12orf5 ENSG000000	C12orf5	K.EADQKEQFSQGSPSNC*LETSLAEIFPLGK.N	1.06	1.25	1.08	1.16
IPI00099996.2	RG9MTD1 RNA (guanine-9-) methyltransferase domain-	RG9MTD1	K.SSVQEEC*VSTISSSKDEDPLAATR.E	1.11	0	1.21	1.16
IPI00025176.1	SMNDC1 Survival of motor neuron-related-splicing f	SMNDC1	K.VGVGTC*GIADKPMTQYQDTSK.Y	1.17	0	1.15	1.16
IPI00395939.3	PITPNB Isoform 2 of Phosphatidylinositol transfer	PITPNB	K.ELANSPDC*PQMCAYK.L	1.17	0	1.15	1.16
IPI00010720.1	CCT5 T-complex protein 1 subunit epsilon ENSG00000	CCT5	K.VVNSC*HR.Q	0	0	1.16	1.16
IPI00006754.1	WDR68 WD repeat-containing protein 68 ENSG00000136	WDR68	R.VPC*TPVAR.L	0	0	1.16	1.16
IPI00100160.3	CAND1 Isoform 1 of Cullin-associated NEDD8-dissoci	CAND1	K.NC*IGDFLK.T	0	0	1.16	1.16
IPI00301609.8	NEK9 Serine/threonine-protein kinase Nek9 ENSG0000	NEK9	R.LLTFGC*NK.C	0	0	1.16	1.16
IPI00009949.2	PSMF1 Proteasome inhibitor PI31 subunit ENSG000001	PSMF1	R.QPPWC*DPLGPFVVGGEDLDPFGPR.R	0	1.16	0	1.16
IPI00377005.2	_ Uncharacterized protein ENSP00000340627 ENSG0000	_	K.EEHLC*TQR.M	1.16	0	0	1.16
IPI00045939.4	C10orf22 Uncharacterized protein C10orf22 ENSG0000	C10orf22	K.EASSSAC*DLPR.E	1.16	0	0	1.16
IPI00007927.3	SMC2 Isoform 1 of Structural maintenance of chromo	SMC2	R.FTQC*QNGK.I	1.32	0	0.99	1.155
IPI00647082.1	TBC1D13 TBC1 domain family, member 13 ENSG00000107	TBC1D13	R.LLQDYPITDVC*QILQK.A	1.06	1.23	1.1	1.155
IPI00018146.1	YWHAQ 14-3-3 protein theta ENSG00000134308 IPI0001	YWHAQ	R.YLAEVAC*GDDR.K	1.17	0	1.14	1.155
IPI00016610.2	PCBP1 Poly(rC)-binding protein 1 ENSG00000169564 I	PCBP1	R.INISEGNC*PER.I	1.09	1.2	1.12	1.1525
IPI00293975.4	GPX1 glutathione peroxidase 1 isoform 1	GPX1	R.FQTIDIEPDIEALLSQGPSC*A.-	1.18	1.2	1.02	1.15

	ENSG000001						
IPI00301364.3	SKP1A Isoform 1 of S-phase kinase-associated prote	SKP1A	K.GLLDVTC*K.T	1.19	0	1.11	1.15
IPI00472675.2	NUP205 228 kDa protein ENSG00000155561 IPI00783781	NUP205	R.C*QDVSAGSLQELALLTGIISK.A	1.16	0	1.14	1.15
IPI00021766.4	RTN4 Isoform 1 of Reticulon-4 ENSG00000115310 IPI0	RTN4	K.YSNSALGHVNC*TIK.E	0	0	1.15	1.15
IPI00295851.4	COPB1 Coatomer subunit beta ENSG00000129083 IPI002	COPB1	K.ALSGYC*GFMAANLYAR.S	0	0	1.15	1.15
IPI00002496.2	GMPPB AMIGO3 GDP-mannose pyrophosphorylase B isofo	GMPPB	R.LC*SGPGIVGNVLVDPSAR.I	0	0	1.15	1.15
IPI00005791.1	NDC80 Kinetochore protein Hec1 ENSG00000080986 IPI	NDC80	K.FNPEAGANC*LVK.Y	0	0	1.15	1.15
IPI00021812.2	AHNAK AHNAK nucleoprotein isoform 1 ENSG0000012494	AHNAK	K.LEGDLTGPSVGVEVPDVELEC*PDAK.L	0	0	1.15	1.15
IPI00746806.1	CTTN CTTN protein ENSG00000085733 IPI00029601 IPI0	CTTN	K.HC*SQVDSVR.G	0	0	1.15	1.15
IPI00473014.5	DSTN Destrin ENSG00000125868 IPI00473014 IPI006432	DSTN	K.LGGSLIVAFEGC*PV.-	1.14	0	1.16	1.15
IPI00072534.2	UNC45A Isoform 1 of UNC45 homolog A ENSG0000014055	UNC45A	K.LLAAGVVSAMVC*MVK.T	0	1.15	0	1.15
IPI00554824.1	SGOL1 Isoform 1 of Shugoshin-like 1 ENSG0000012981	SGOL1	R.SFIAAPC*QIITNTSTLLK.N	0	1.15	0	1.15
IPI00018009.2	EDC3 Enhancer of mRNA-decapping protein 3 ENSG0000	EDC3	K.SQDVAVSPQQQQC*SK.S	1.15	0	0	1.15
IPI00456919.2	HUWE1 Isoform 1 of E3 ubiquitin-protein ligase HUW	HUWE1	R.AQC*ETLSPDGLPEEQPQTTK.L	1.15	0	0	1.15
IPI00018352.1	UCHL1 Ubiquitin carboxyl-terminal hydrolase isozym	UCHL1	K.NEAIQAAHDAVAQEGQC*R.V	1.06	1.24	1.05	1.1475
IPI00257508.4	DPYSL2 Dihydropyrimidinase-related protein 2 ENSG0	DPYSL2	R.GLYDGPVC*EVSVTPK.T	1.18	0	1.11	1.145
IPI00298111.7	SNX6 sorting nexin 6 isoform b ENSG00000129515 IPI	SNX6	R.IGSSLYALGTQDSTDIC*K.F	1.17	0	1.12	1.145
IPI00299214.6	TK1 thymidine kinase 1, soluble ENSG00000167900 IP	TK1	R.YSSSFC*THDR.N	1.14	0	1.15	1.145
IPI00022796.2	HMG1L1 High-mobility group protein 1-like 1 ENSG00	HMG1L1	K.MSSYAFFVQTC*R.E	1.12	0	1.17	1.145
IPI00013871.1	RRM1 Ribonucleoside-diphosphate reductase large su	RRM1	R.NTAAMVC*SLENRDECLMCGS.-	1.02	0	1.27	1.145
IPI00007682.2	ATP6V1A Vacuolar ATP synthase catalytic subunit A	ATP6V1A	R.VLDALFPCVQGGTTAIPGAFGC*GK.T	0	1.09	1.31	1.145
IPI00030328.1	SRR Serine racemase ENSG00000167720 IPI00030328	SRR	K.LEGIPAYIVVPQTAPDC*K.K	1.06	0	1.22	1.14
IPI00304417.6	IDH3B Isocitrate dehydrogenase [NAD] subunit beta,	IDH3B	K.LGDGLFLQC*CEEVAELYPK.I	0.96	0	1.32	1.14

IPI00103925.2	IRGQ Immunity-related GTPase family Q protein ENSG	IRGQ	R.TDGEGEDPEC*LGEGK.M	0	0	1.14	1.14
IPI00478208.2	hCG_2004593 hypothetical protein LOC645296 ENSG000	hCG_2004593	R.INPYMSSPC*HIEMILTEK.E	0	0	1.14	1.14
IPI00031680.3	ACBD6 Acyl-CoA-binding domain-containing protein 6	ACBD6	R.DQDGCLPEEVTGC*K.T	0	0	1.14	1.14
IPI00555734.3	ASRGL1 asparaginase-like 1 protein ENSG00000162174	ASRGL1	K.GAQKTDC*QK.N	0	0	1.14	1.14
IPI00450071.5	C1orf19 tRNA-splicing endonuclease subunit Sen15 E	C1orf19	R.GDSEPTPGC*SGLGPGGVR.G	0	0	1.14	1.14
IPI00027443.5	CARS cysteinyl-tRNA synthetase isoform c ENSG00000	CARS	R.VQPQWSPPAGTQPC*R.L	0	0	1.14	1.14
IPI00152998.3	LRRC40 Leucine-rich repeat-containing protein 40 E	LRRC40	R.FLPEFPSC*SLLK.E	0	0	1.14	1.14
IPI00334683.1	GAMT guanidinoacetate N-methyltransferase isoform	GAMT	K.VQEAPIDEHWIIEC*NDGVFQR.L	0	0	1.14	1.14
IPI00003881.5	HNRPF Heterogeneous nuclear ribonucleoprotein F EN	HNRPF	R.DLSYC*LSGMYDHR.Y	1.13	0	1.15	1.14
IPI00830108.1	ZRF1 Isoform 1 of DnaJ homolog subfamily C member	ZRF1	R.LELASLQC*LNETLTSCTK.E	1.13	0	1.15	1.14
IPI00480131.1	FLNB Uncharacterized protein FLNB ENSG00000136068	FLNB	R.SSTETC*YSAIPK.A	1.14	0	0	1.14
IPI00290416.3	OLA1 Isoform 1 of Putative GTP-binding protein 9 E	OLA1	K.STFFNVLTNSQASAENFPFC*TIDPNESR.V	1.12	1.21	1.01	1.1375
IPI00216298.6	TXN Thioredoxin ENSG00000136810 IPI00552768 IPI002	TXN	K.C*MPTFQFFK.K	0	1.15	1.1	1.1375
IPI00029079.5	GMPS GMP synthase ENSG00000163655 IPI00029079	GMPS	R.VICAEEPYIC*K.D	1.18	0	1.09	1.135
IPI00020602.1	CSNK2A2 Casein kinase II subunit alpha ENSG000000	CSNK2A2	K.EQSQPC*ADNAVLSSGLTAAR.-	1.1	0	1.17	1.135
IPI00031647.2	PDCD2L Programmed cell death protein 2-like ENSG00	PDCD2L	R.YSWSGEPLFLTC*PTSEVTELPACSQCGGQR.I	1.01	0	1.26	1.135
IPI00018402.1	TBCE Tubulin-specific chaperone E ENSG00000116957	TBCE	R.NCAVSC*AGEK.G	1.3	1.12	0.99	1.1325
IPI00006863.5	SPAG7 Single-stranded nucleic acid binding R3H dom	SPAG7	K.TYGC*VPVANKR.D	0	1.17	1.02	1.1325
IPI00303318.2	FAM49B Protein FAM49B ENSG00000153310 IPI00651701	FAM49B	K.VLTC*TDLEQGPNFFLDFENAQPTESEK.E	1.25	0	1.01	1.13
IPI00022228.1	HDLBP Vigilin ENSG00000115677 IPI00022228 IPI00443	HDLBP	K.AAC*LESAQEPAGAWGNK.I	1.16	0	1.1	1.13
IPI00008982.1	ALDH18A1 Isoform Long of Delta-1-pyrroline-5-carbo	ALDH18A1	K.LGSAVVTRGDEC*GLALGR.L	1.13	0	1.13	1.13
IPI00294008.4	ZWINT ZW10 interactor ENSG00000122952 IPI00646553	ZWINT	K.LLC*SQLQVADFLQNILAQEDTAK.G	0	0	1.13	1.13
IPI00004534.3	PFAS Phosphoribosylformylglycinamidine synthase EN	PFAS	R.IVLVDDREC*PVRR.N	0	0	1.13	1.13

IPI00023087.1	UBE2T Ubiquitin-conjugating enzyme E2 T ENSG000000	UBE2T	R.IC*LDVLK.L	0	0	1.13	1.13
IPI00291646.2	MTHFD1L methylenetetrahydrofolate dehydrogenase (N	MTHFD1L	R.SSC*SPGGR.T	1.11	0	1.15	1.13
IPI00022827.1	SLK Isoform 1 of STE20-like serine/threonine-prote	SLK	K.MTGESEC*LNPSTQSR.I	1.09	0	1.17	1.13
IPI00174390.3	2-PDE 2-phosphodiesterase ENSG00000174840 IPI001	2-PDE	K.SRPNASGGAAC*SGPGPEPAVFCEPVVK.L	0	1.13	0	1.13
IPI00056505.5	NT5C3L Cytosolic 5-nucleotidase III-like protein	NT5C3L	K.NSSAC*ENSGYFQQLEGK.T	1.13	0	0	1.13
IPI00025273.1	GART Isoform Long of Trifunctional purine biosynth	GART	K.QVLVAPGNAGTAC*SEK.I	1.13	1.08	1.22	1.1275
IPI00298961.3	XPO1 Exportin-1 ENSG00000082898 IPI00784388 IPI002	XPO1	K.DLLGLC*EQK.R	1.23	0	1.02	1.125
IPI00334775.6	HSP90AB1 85 kDa protein ENSG00000096384 IPI0041467	HSP90AB1	R.LVSSPC*CIVTSTYGWTANMER.I	1.16	0	1.09	1.125
IPI00215610.2	MPP1 55 kDa erythrocyte membrane protein ENSG00000	MPP1	R.VASMAQSAPSEAPSC*SPFGK.K	1.15	0	1.1	1.125
IPI00418471.6	VIM Vimentin ENSG00000026025 IPI00418471 IPI008276	VIM	R.QVQSLTC*EVDALK.G	1.15	0	1.1	1.125
IPI00828189.1	PCMT1 Isoform 2 of Protein-L-isoaspartate(D-aspart	PCMT1	R.MVGC*TGK.V	1.15	0	1.1	1.125
IPI00647082.1	TBC1D13 TBC1 domain family, member 13 ENSG00000107	TBC1D13	K.SLDDSQC*GITYK.M	1.14	0	1.11	1.125
IPI00014177.3	SEPT2 Septin-2 ENSG00000168385 IPI00014177	41519	R.LTVVDTPGYGDAINC*R.D	1.14	0	1.11	1.125
IPI00334159.6	VBP1 Prefoldin subunit 3 ENSG00000155959 IPI003341	VBP1	R.FLLADNLYC*K.A	1.12	0	1.13	1.125
IPI00045207.2	BTBD14B BTB/POZ domain-containing protein 14B ENSG	BTBD14B	R.NTLANSC*GTGIR.S	1.11	0	1.14	1.125
IPI00060521.1	FLYWCH2 Putative uncharacterized protein LOC114984	FLYWCH2	R.TEDSGLAAGPPEAAGENFAPC*SVAPGK.S	1.06	0	1.19	1.125
IPI00021290.5	ACLY ATP-citrate synthase ENSG00000131473 IPI00021	ACLY	K.FIC*TTSAIQNR.F	1.1	1.16	1.07	1.1225
IPI00220528.6	SNRPF Small nuclear ribonucleoprotein F ENSG000001	SNRPF	R.C*NNVLYIR.G	1.08	1.19	1.02	1.12
IPI00020454.1	DCK Deoxycytidine kinase ENSG00000156136 IPI000204	DCK	R.SC*PSFSASSEGTR.I	1.17	0	1.07	1.12
IPI00005777.1	MAPKAPK3 MAP kinase-activated protein kinase 3 ENS	MAPKAPK3	K.QAGSSSASQGC*NNQ.-	1.16	0	1.08	1.12
IPI00844388.1	HELLS 103 kDa protein ENSG00000119969 IPI00012073	HELLS	K.ILENSEDSSPEC*LF.-	1.14	0	1.1	1.12
IPI00384180.4	YRDC ischemia/reperfusion inducible protein ENSG00	YRDC	R.AGAVVAVPTDTLYGLAC*AASCSAALR.A	1.14	0	1.1	1.12
IPI00221172.2	C14orf130 Uncharacterized protein C14orf130 ENSG00	C14orf130	K.VEQNSEPC*AGSSSESDLQTVFK.N	0	0	1.12	1.12

IPI00008422.5	SMARCAD1 Isoform 2 of SWI/SNF-related matrix-assoc	SMARCAD1	K.NTEMC*NVMMQLR.K	0	0	1.12	1.12
IPI00061623.1	SGTB Small glutamine-rich tetratricopeptide repeat	SGTB	K.ISPEDTHLAVSQPLTEMFTSSFC*K.N	0	0	1.12	1.12
IPI00025087.1	TP53 Isoform 1 of Cellular tumor antigen p53 ENSG0	TP53	R.C*SDSDGLAPPQHLIR.V	0	0	1.12	1.12
IPI00024403.1	CPNE3 Copine-3 ENSG00000085719 IPI00024403 IPI0074	CPNE3	K.EALAQC*VLAEIPQQVVGYFNTYK.L	0	0	1.12	1.12
IPI00022977.1	CKB Creatine kinase B-type ENSG00000166165 IPI0002	CKB	K.DYEFMWNPHLGYILTC*PSNLGTGLR.A	0	1.12	0	1.12
IPI00456803.2	_ Uncharacterized protein ENSP00000368765 ENSG0000	_	R.AYCHILLGNYC*VAVADAK.K	0	1.17	0.97	1.12
IPI00549389.3	C9orf32 Protein of unknown function DUF858, methyl	C9orf32	R.IIC*SAGLSLLAEER.Q	1.05	1.17	1.08	1.1175
IPI00018783.1	ITPA Inosine triphosphate pyrophosphatase ENSG0000	ITPA	R.GC*QDFGWDPCFQPDGYEQTYAEMPK.A	1.11	0	1.12	1.115
IPI00148061.3	LDHAL6A L-lactate dehydrogenase A-like 6A ENSG0000	LDHAL6A	K.NRVIGSGC*NLDSAR.F	1.17	0	1.06	1.115
IPI00021329.3	WDR45L WD repeat domain phosphoinositide-interacti	WDR45L	R.C*NYLALVGGGK.K	1.14	0	1.09	1.115
IPI00549993.3	C10orf97 chromosome 10 open reading frame 97 ENSG0	C10orf97	K.SSPGLSDTIFC*R.W	1.13	0	1.1	1.115
IPI00059687.1	C18orf25 Isoform 1 of Uncharacterized protein C18o	C18orf25	K.DGVADSTVISSMPC*LLMELR.R	1.13	0	1.1	1.115
IPI00011200.5	PHGDH D-3-phosphoglycerate dehydrogenase ENSG00000	PHGDH	K.VLISDSLDPC*CR.K	1.13	0	1.1	1.115
IPI00054042.1	GTF2I Isoform 1 of General transcription factor II	GTF2I	R.SILSPGGSC*GPIK.V	1.1	0	1.13	1.115
IPI00797537.1	NUDCD1 NudC domain-containing protein 1 ENSG000001	NUDCD1	R.DSAQC*AAIAER.L	1.09	0	1.14	1.115
IPI00220158.1	ADD1 Isoform 3 of Alpha-adducin ENSG00000087274 IP	ADD1	K.TAGPQSQVLC*GVVMDR.S	1.08	0	1.15	1.115
IPI00010141.4	POLE3 DNA polymerase epsilon subunit 3 ENSG0000014	POLE3	R.AASVFVLYATSC*ANNFAMK.G	0	0	1.11	1.11
IPI00748935.1	ELP4 59 kDa protein ENSG000000109911 IPI00847770 IP	ELP4	K.VEPC*SLTPGYTK.L	0	0	1.11	1.11
IPI00030876.6	DIAPH1 Diaphanous 1 ENSG00000131504 IPI00030876 IP	DIAPH1	K.AGC*AVTSLLASELTK.D	0	0	1.11	1.11
IPI00291510.3	IMPDH2 Inosine-5-monophosphate dehydrogenase 2 EN	IMPDH2	R.HGFC*GIPITDTGR.M	0	1.11	0	1.11
IPI00004928.1	EGLN1 Isoform 1 of Egl nine homolog 1 ENSG00000135	EGLN1	K.AKPPADPAAAASPC*R.A	0	1.11	0	1.11
IPI00296441.5	ADA Adenosine deaminase ENSG00000196839 IPI0029644	ADA	K.FDYYMPAIAGC*R.E	1.11	0	0	1.11
IPI00032995.1	LANCL2 LanC-like protein 2 ENSG00000132434 IPI0003	LANCL2	R.SVVC*QESDLPDELLYGR.A	1.11	0	0	1.11

IPI00382470.3	HSP90AA1 heat shock protein 90kDa alpha (cytosolic	HSP90AA1	R.VFIMDNC*EELIPEYLNFIR.G	0.98	1.23	1	1.11
IPI00550069.3	RNH1 Ribonuclease inhibitor ENSG00000023191 IPI005	RNH1	R.ELDLSNNC*LGDAGILQLVESVR.Q	1.14	0	1.08	1.11
IPI00021808.3	HARS Histidyl-tRNA synthetase, cytoplasmic ENSG000	HARS	R.TGQPLC*IC.-	1.14	0	1.08	1.11
IPI00015141.4	CKMT2 Creatine kinase, sarcomeric mitochondrial pr	CKMT2	R.LGYILTC*PSNLGTGLR.A	0	1.17	0.92	1.1075
IPI00010896.3	DDAH2 CLIC1 Chloride intracellular channel protein	DDAH2	K.IGNC*PFSQR.L	1.38	1.04	0.97	1.1075
IPI00647337.1	_ OTTHUMP00000016411 ENSG00000181524 IPI00647337	_	K.VELC*SFSGYK.I	1.16	0	1.05	1.105
IPI00026781.2	FASN Fatty acid synthase ENSG00000169710 IPI000267	FASN	K.ADEASELAC*PTPK.E	1.09	0	1.12	1.105
IPI00301421.5	ZC3HC1 Isoform 1 of Nuclear-interacting partner of	ZC3HC1	R.LC*SSSSSDTSSR.S	1.02	0	1.19	1.105
IPI00334775.6	HSP90AB1 85 kDa protein ENSG00000096384 IPI0041467	HSP90AB1	R.VFIMDSC*DELIPEYLNFIR.G	1.09	1.14	1.04	1.1025
IPI00008531.1	RCOR1 REST corepressor 1 ENSG00000089902 IPI000085	RCOR1	R.GRNNAAASASAAAASAAASAAC*ASPAATAASGAAASSASAAAASAAAPNNGQNK.S	1.1	1.23	0.84	1.1
IPI00257882.7	PEPD Xaa-Pro dipeptidase ENSG00000124299 IPI002578	PEPD	R.TVEEIEACMAGC*DK.A	1.21	0	0.99	1.1
IPI00449197.1	GMPR2 GMPR2 protein ENSG00000100938 IPI00385158 IP	GMPR2	R.VTQQVNPIFSEAC*.-	1.13	0	1.07	1.1
IPI00220158.1	ADD1 Isoform 3 of Alpha-adducin ENSG00000087274 IP	ADD1	R.VSMILQSPAFC*EELESMIQEQFKK.G	0	0	1.1	1.1
IPI00550882.2	PYCR1 Pyrroline-5-carboxylate reductase 1 ENSG0000	PYCR1	R.C*MTNTPVVVR.E	0	0	1.1	1.1
IPI00852816.1	SMARCD1 SWI/SNF-related matrix-associated actin-de	SMARCD1	R.AEFYFQPWAQEAVC*R.Y	0	0	1.1	1.1
IPI00787501.1	LOC727737 similar to APG4 autophagy 4 homolog B is	LOC727737	K.NFPAIGGTGPTSDTGWGC*MLR.C	0	0	1.1	1.1
IPI00641743.2	HCFC1 Uncharacterized protein HCFC1 ENSG0000017253	HCFC1	K.LVIYGGMSGC*R.L	0	0	1.1	1.1
IPI00020898.1	RPS6KA3 Ribosomal protein S6 kinase alpha-3 ENSG00	RPS6KA3	K.AYSFC*GTVEYMAPEVVNR.R	0	0	1.1	1.1
IPI00154645.7	TBC1D15 Isoform 1 of TBC1 domain family member 15	TBC1D15	R.NDSPTQIPVSSDVC*R.L	1.1	0	0	1.1
IPI00514510.1	ANXA7 annexin VII isoform 2 ENSG00000138279 IPI005	ANXA7	R.LGTDESC*FNMILATR.S	1.11	0	1.08	1.095
IPI00019169.3	SH3GL1 SH3-containing GRB2-like protein 1 ENSG0000	SH3GL1	R.EPFDLGEPEQSNGGFPC*TTAPK.I	1.08	0	1.11	1.095
IPI00329321.3	LYRM7 LYR motif-containing protein 7 ENSG000001866	LYRM7	R.KDLLVENVPYC*DAPTQK.Q	1.05	0	1.14	1.095

IPI00216682.5	CNN3 Calponin-3 ENSG00000117519 IPI00216682 IPI006	CNN3	K.C*ASQAGMT AYGTR.R	1.04	0	1.15	1.095
IPI00086909.6	LOC440917 similar to 14-3-3 protein epsilon ENSG00	LOC44 0917	K.LIC*CDILDVL DK.H	1.11	0	1.07	1.09
IPI00219217.3	LDHB L-lactate dehydrogenase B chain ENSG000001117	LDHB	K.GMYGIENEVF LSLPC*ILNAR.G	0	0	1.09	1.09
IPI00301051.3	NHLRC2 NHL repeat-containing protein 2 ENSG0000019	NHLR C2	K.AILFSQPLQIT DTQQGC*IAPVE LR.Y	0	0	1.09	1.09
IPI00177965.5	NT5DC1 5-nucleotidase domain-containing protein 1	NT5DC 1	K.HFLSDTGMA C*R.S	0	0	1.09	1.09
IPI00015866.2	ARL2BP Isoform 1 of ADP-ribosylation factor-like p	ARL2B P	R.GLDLSSGLVV TSLC*K.S	0	0	1.09	1.09
IPI00030177.2	RBPJ Isoform APCR-2 of Recombining binding protein	RBPJ	R.IIQFQATPC*P K.E	0	0	1.09	1.09
IPI00010157.1	MAT2A S-adenosylmethionine synthetase isoform type	MAT2 A	K.VAC*ETVAK. T	1.07	0	1.11	1.09
IPI00145260.3	C1orf69 Putative transferase C1orf69, mitochondria	C1orf6 9	K.GC*YIGQELT AR.T	1.06	0	1.12	1.09
IPI00554737.3	PPP2R1A Serine/threonine-protein phosphatase 2A 65	PPP2R 1A	K.DNTIEHLLPLF LAQLKDEC*PE VR.L	0	1.09	0	1.09
IPI00020729.1	IRS4 insulin receptor substrate 4 ENSG00000133124	IRS4	R.GGQGSNGQG SGGNQC*SR.D	1.09	0	0	1.09
IPI00303962.3	PPCDC Isoform 1 of Phosphopantothenoylcysteine dec	PPCDC	K.LVC*GDEGLG AMAEVGTIVDK .V	1.09	0	0	1.09
IPI00025156.4	STUB1 Isoform 1 of STIP1 homology and U box-contai	STUB1	R.AQQAC*IEAK. H	1.14	0	1.04	1.09
IPI00465044.2	RCC2 Protein RCC2 ENSG00000179051 IPI00465044	RCC2	K.AVQDLC*GW R.I	1.13	0	1.05	1.09
IPI00182757.9	KIAA1967 Uncharacterized protein KIAA1967 ENSG0000	KIAA1 967	R.GEASEDLC*E MALDPELLLLR. D	1.13	0	1.05	1.09
IPI00025746.5	ANKRD54 Isoform 1 of Ankyrin repeat domain-contain	ANKR D54	R.LDDLC*TR.L	1.02	0	1.16	1.09
IPI00640364.2	OTUD5 Isoform 1 of OTU domain-containing protein 5	OTUD 5	R.ATSPLVSLYP ALEC*R.A	1.02	0	1.16	1.09
IPI00479385.3	ASMTL Uncharacterized protein ASMTL ENSG00000016909	ASMT L	K.VDASAC*GM ER.L	0	1.12	0.99	1.0875
IPI00465152.2	SP1 Transcription factor Sp1 ENSG00000185591 IPI00	SP1	R.SSSTGSSSSTG GGGQESQPSPL ALLAATC*SR.I	1.14	0	1.03	1.085
IPI00853598.1	SEC13 41 kDa protein ENSG00000157020 IPI00845335 I	SEC13	R.FASGGC*DNL IK.L	1.02	1.14	1.04	1.085
IPI00012866.2	AKT1 RAC-alpha serine/threonine-protein kinase ENS	AKT1	K.TFC*GTPEYL APEVLEDNDYG R.A	1.1	0	1.07	1.085
IPI00298961.3	XPO1 Exportin-1 ENSG00000082898 IPI00784388 IPI002	XPO1	K.LDINLLDNVV NC*LYHGEGAQ QR.M	1.08	1.09	1.08	1.085
IPI00030363.1	ACAT1 Acetyl-CoA acetyltransferase, mitochondrial	ACAT1	K.VC*ASGMK.A	1.09	1.08	1.09	1.085

IPI00748696.1	AP3S2 44 kDa protein ENSG00000157823 IPI00025115 I	AP3S2	K.C*NFTGDGK.T	1.07	0	1.1	1.085
IPI00103554.1	GATAD2B Transcriptional repressor p66 beta ENSG000	GATAD2B	K.SC*ASLLR.V	1.07	0	1.1	1.085
IPI00102856.3	SMAP1L Isoform 1 of Stromal membrane-associated pr	SMAP1L	K.STAPVMDLLGLDAPVAC*SIANSK.T	1.12	1.09	1.03	1.0825
IPI00748256.1	PSME1 Uncharacterized protein PSME1 ENSG0000009201	PSME1	K.VDVFREDLC*TK.T	0	0	1.08	1.08
IPI00745345.1	PPP4R2 Protein phosphatase 4 regulatory subunit 2	PPP4R2	K.EVC*PVLDQFLCHVAK.T	0	0	1.08	1.08
IPI00025366.4	CS Citrate synthase, mitochondrial precursor ENSG0	CS	K.LPC*VAAK.I	0	0	1.08	1.08
IPI00002824.7	CSRP2 Cysteine and glycine-rich protein 2 ENSG0000	CSRP2	R.C*GDSVYAAEK.I	0	0	1.08	1.08
IPI00101652.4	SCLY Selenocysteine lyase ENSG00000132330 IPI00101	SCLY	R.DAPAPAASQPSGC*GK.H	0	0	1.08	1.08
IPI00789101.1	PTGES3 19 kDa protein ENSG00000110958 IPI00015029	PTGES3	K.HLNEIDLFHC*IDPNDSK.H	0	0	1.08	1.08
IPI00018955.1	ZNF174 Isoform 1 of Zinc finger protein 174 ENSG00	ZNF174	R.LQHLGHQPTRSAKKPYKC*DDCGK.S	0	1.08	0	1.08
IPI00021327.3	GRB2 Isoform 1 of Growth factor receptor-bound pro	GRB2	K.VLNEEC*DQNWYK.A	1.08	0	0	1.08
IPI00026781.2	FASN Fatty acid synthase ENSG00000169710 IPI000267	FASN	K.AINC*ATSGVVGLVNCLR.R	0	1.1	1.01	1.0775
IPI00386189.2	NARG1 Isoform 1 of NMDA receptor-regulated protein	NARG1	R.LFNTAVC*ESK.D	1.18	1.03	1.07	1.0775
IPI00005011.1	CNOT2 Isoform 1 of CCR4-NOT transcription complex	CNOT2	R.SSPSIIC*MPK.Q	1.04	0	1.11	1.075
IPI00018146.1	YWHAQ 14-3-3 protein theta ENSG00000134308 IPI0001	YWHAQ	R.DNLTLWTSDSAGEEC*DAAEGAEN.-	1.15	0	1	1.075
IPI00658023.1	PTPN11 Isoform 1 of Tyrosine-protein phosphatase n	PTPN11	K.YSLADQTSGDQSPLPPCTPTPPC*AEMR.E	1.08	0	1.06	1.07
IPI00298308.6	ALDH1L2 Aldehyde dehydrogenase family 1 member L2	ALDH1L2	K.SPLIIFNDC*ELDK.T	0	0	1.07	1.07
IPI00448751.2	KIAA1598 Isoform 3 of Shootin-1 ENSG00000187164 IP	KIAA1598	K.VTFQPPSSIGC*R.K	0	0	1.07	1.07
IPI00033130.3	SAE1 SUMO-activating enzyme subunit 1 ENSG00000142	SAE1	R.YCFSEMAPVC*AVVGGILAQEIVK.A	1.02	0	1.12	1.07
IPI00025178.3	BCAS2 Breast carcinoma amplified sequence 2 ENSG00	BCAS2	K.NDITAWQEC*VNNSMAQLEHQAVR.I	1.07	0	0	1.07
IPI00162563.5	RNF40 Isoform 1 of E3 ubiquitin-protein ligase BRE	RNF40	R.LTCPC*CNTR.K	1.07	0	0	1.07
IPI00177509.4	TRAPPC5 Trafficking protein particle complex subun	TRAPPC5	K.ENSTLNC*ASFTAGIVEAVLTHSGFPAK.V	0	1.13	0.88	1.0675
IPI00786942.1	ALDH7A1 similar to antiquitin ENSG00000164904 IPI0	ALDH7A1	K.GSDC*GIVNVNIPTSGAEIGGAFGGEK.H	1.16	0	0.97	1.065

IPI00007694.4	PPME1 Isoform 1 of Protein phosphatase methylester	PPME1	R.FAEPIGGFQC*VFPGC.-	1.16	0	0.97	1.065
IPI00013949.1	SGTA Small glutamine-rich tetratricopeptide repeat	SGTA	R.AIC*IDPAYSK.A	1.09	0	1.04	1.065
IPI00032050.4	WBP2 WW domain-binding protein 2 ENSG00000132471 I	WBP2	K.DC*EIKQPVFGANYIK.G	1.09	0	1.04	1.065
IPI00090720.4	QRSL1 Glutaminyl-tRNA synthase-like protein 1 ENSG	QRSL1	K.QVQFPVIQLQELMDDC*SAVLENEK.L	1.04	0	1.09	1.065
IPI00152998.3	LRRC40 Leucine-rich repeat-containing protein 40 E	LRRC40	R.DC*GTSVPQGLLK.A	1.03	0	1.1	1.065
IPI00549189.4	THOP1 Thimet oligopeptidase ENSG00000172009 IPI005	THOP1	-.MKPPAAC*AGDMADAASPCSVVNDLR.W	0	0	1.06	1.06
IPI00386122.4	MOBKL3 Isoform 1 of Preimplantation protein 3 ENSG	MOBKL3	R.HTLDGAAC*LLNSNK.Y	0	0	1.06	1.06
IPI00742743.1	TP53BP1 Isoform 2 of Tumor suppressor p53-binding	TP53BP1	K.TMSVLSCIC*EAR.Q	0	0	1.06	1.06
IPI00216319.3	YWHAH 14-3-3 protein eta ENSG00000128245 IPI008275	YWHAH	K.NC*NDFQYESK.V	0	0	1.06	1.06
IPI00784131.1	AARS Uncharacterized protein AARS ENSG00000090861	AARS	K.NVGC*LQEALQLATSFAQLR.L	0	1.06	0	1.06
IPI00030781.1	STAT1 Isoform Alpha of Signal transducer and activ	STAT1	R.NLSFFLTPPC*AR.W	0	1.06	0	1.06
IPI00337397.1	NUP98 Isoform 5 of Nuclear pore complex protein Nu	NUP98	K.FTSGAFLSPSVSVQEC*R.T	1.06	0	0	1.06
IPI00008794.1	DFFB Isoform Alpha of DNA fragmentation factor sub	DFFB	R.VLGSMC*QR.L	0	1.06	1.05	1.0575
IPI00290566.1	TCP1 T-complex protein 1 subunit alpha ENSG0000012	TCP1	R.IC*DDELILIK.N	1.08	0	1.03	1.055
IPI00219757.13	GSTP1 Glutathione S-transferase P ENSG00000084207	GSTP1	K.ASC*LYGQLPK.F	1.08	0	1.03	1.055
IPI00646512.1	RBBP7 Retinoblastoma binding protein 7 ENSG0000010	RBBP7	R.VHIPNDDAQFDASHC*DSDKGEFGGFGSVTGK.I	1.04	0	1.07	1.055
IPI00027223.2	IDH1 Isocitrate dehydrogenase [NADP] cytoplasmic E	IDH1	K.SEGGFIWAC*K.N	1.04	0	1.07	1.055
IPI00000875.6	EEF1G Elongation factor 1-gamma ENSG00000186676 IP	EEF1G	K.AAAPAPEEEMDEC*EQALAAEPK.A	1.12	0.99	1.12	1.055
IPI00019812.1	PPP5C Serine/threonine-protein phosphatase 5 ENSG0	PPP5C	R.TEC*AEPPRDEPPADGALKR.A	1.13	0	0.98	1.055
IPI00004839.1	CRKL Crk-like protein ENSG00000099942 IPI00004839	CRKL	K.RVPC*AYDK.T	0.91	1.16	0.99	1.055
IPI00011200.5	PHGDH D-3-phosphoglycerate dehydrogenase ENSG00000	PHGDH	K.NAGNC*LSPAVIVGLLK.E	0	1.1	0.91	1.0525
IPI00784614.1	SEPT9 Isoform 1 of Septin-9 ENSG00000184640 IPI007	41526	R.SQEATEAAPSC*VGDMADTPR.D	1.18	0	0.92	1.05
IPI00301263.2	CAD CAD protein ENSG00000084774	CAD	K.AQILVLTYPLIGNYGIPPDEMD	0	1.07	0.99	1.05

	IPI00301263		EFGLC*K.W				
IPI00646361.2	NUP214 Uncharacterized protein NUP214 ENSG00000126	NUP214	K.VC*ATLPSTVAVTSVCWSPK.G	1.07	0	1.03	1.05
IPI00183626.8	PTBP1 polypyrimidine tract-binding protein 1 isofo	PTBP1	K.RGSDELFSTC*VTNGPFIMSSNSASAANGNDSK.K	1.06	0	1.04	1.05
IPI00550069.3	RNH1 Ribonuclease inhibitor ENSG00000023191 IPI005	RNH1	R.SNELGDVGVHC*VLQGLQTPSCK.I	0	0	1.05	1.05
IPI00304935.5	SAAL1 Uncharacterized protein SAAL1 ENSG0000016678	SAAL1	R.VLQNMEQC*QK.K	0	0	1.05	1.05
IPI00154451.6	MMS19 Isoform 1 of MMS19-like protein ENSG00000155	MMS19	R.LMGLLSDPELGPAAADGFSLLMSDC*TDVLTR.A	0	0	1.05	1.05
IPI00291570.9	CASP2 Isoform ICH-1L of Caspase-2 precursor ENSG00	CASP2	R.SDMICGYAC*LK.G	0.98	0	1.12	1.05
IPI00304596.3	NONO Non-POU domain-containing octamer-binding pro	NONO	R.FAC*HSASLTVR.N	0	1.05	0	1.05
IPI00022745.1	MVD Diphosphomevalonate decarboxylase ENSG00000167	MVD	R.DGDPLPSSLSC*K.V	1.05	0	0	1.05
IPI00010860.1	PSMD9 Isoform p27-L of 26S proteasome non-ATPase r	PSMD9	K.GIGMNEPLVDC*EGYPR.S	1.05	0	0	1.05
IPI00157304.1	SSBP3 Isoform 1 of Single-stranded DNA-binding pro	SSBP3	R.DTC*EHSSEAK.A	1.05	0	0	1.05
IPI00103247.1	HNRPLL Isoform 1 of Heterogeneous nuclear ribonucl	HNRPLL	R.GLC*ESVVEADLVEALEK.F	1.05	0	0	1.05
IPI00744127.1	CSTF2 Uncharacterized protein CSTF2 ENSG00000010181	CSTF2	K.LC*VQNSPQEAR.N	0.97	1.03	1.16	1.0475
IPI00745518.1	MAP4 Microtubule-associated protein 4 isoform 1 va	MAP4	K.NVC*LPPEMEVALTEDQVPALK.T	1.17	0	0.92	1.045
IPI00642816.2	SRP9 hCG_1781062 Signal recognition particle 9 kDa	SRP9	K.VTDDLVC*LVYK.T	1.1	0	0.99	1.045
IPI00100796.4	CHMP5 Charged multivesicular body protein 5 ENSG00	CHMP5	K.APPPSLTDC*IGTVDSR.A	1.06	0	1.03	1.045
IPI00742681.1	LSM7 R30783_1 ENSG00000130332 IPI00007163 IPI00742	LSM7	R.GTSVVLIC*PQDGMEAIPNPFIQQQDA.-	1.01	0	1.08	1.045
IPI00302112.1	MAP2K7 Isoform 2 of Dual specificity mitogen-activ	MAP2K7	K.LC*DFGISGR.L	1.01	0	1.08	1.045
IPI00290272.2	POLA2 DNA polymerase subunit alpha B ENSG000000141	POLA2	K.VLGC*PEALTGSYK.S	1	0	1.09	1.045
IPI00009790.1	PFKP 6-phosphofructokinase type C ENSG00000067057	PFKP	R.LPLMEC*VQMTQDVQK.A	1.07	0	1.01	1.04
IPI00024990.6	ALDH6A1 Methylmalonate-semialdehyde dehydrogenase	ALDH6A1	R.C*MALSTAVLVGEAK.K	1.06	0	1.02	1.04
IPI00018235.3	PEF1 Peflin ENSG00000162517 IPI00018235	PEF1	K.QALVNC*NWSSFNDETCLMMINMFDK.T	0	0	1.04	1.04
IPI00005648.1	SAFB2 Scaffold attachment factor B2	SAFB2	K.ILDILGETC*K.S	0	0	1.04	1.04

	ENSG0000013025						
IPI00072534.2	UNC45A Isoform 1 of UNC45 homolog A ENSG0000014055	UNC45A	R.AIQTVSCLLQGPC*DAGNR.A	0	0	1.04	1.04
IPI00026230.1	HNRPH2 Heterogeneous nuclear ribonucleoprotein H	HNRPH2	R.DLNYC*FSGMSDHR.Y	1.02	0	1.06	1.04
IPI00011916.1	JTV1 Multisynthetase complex auxiliary component p	JTV1	R.VELPTC*MYR.L	1.01	0	1.07	1.04
IPI00020451.2	IMPACT IMPACT protein ENSG00000154059 IPI00020451	IMPACT	R.STFQAHLAPVVC*PK.Q	0	1.04	0	1.04
Reverse_IPI00376572.2	LOC391722 similar to myosin regulatory light chain	LOC391722	K.CCC*NQSPPSSASSVPAMNRNKNVNRQER.F	0	1.04	0	1.04
IPI00302112.1	MAP2K7 Isoform 2 of Dual specificity mitogen-activ	MAP2K7	R.SAGC*AAYMAPER.I	1.04	0	0	1.04
IPI00025285.3	FLJ25715 ATP6V1G1 Vacuolar ATP synthase subunit G	FLJ25715	R.GSC*STEVEKETQEK.M	1.04	0	0	1.04
IPI00221035.3	BTF3 Uncharacterized protein BTF3 ENSG00000145741	BTF3	R.ARGGC*PGGEATLSQPPPR.G	0	1.03	1.06	1.0375
IPI00334159.6	VBP1 Prefoldin subunit 3 ENSG00000155959 IPI003341	VBP1	K.DSC*GKGEMATGNGR.R	1.02	0	1.05	1.035
IPI00220301.5	PRDX6 Peroxiredoxin-6 ENSG00000117592 IPI00220301	PRDX6	K.DINAYNC*EEPTEK.L	1	0	1.07	1.035
IPI00018009.2	EDC3 Enhancer of mRNA-decapping protein 3 ENSG0000	EDC3	K.DLPTSPVDLVINC*LDCPENVFLR.D	1	1.09	0.95	1.0325
IPI00001287.1	C20orf72 Uncharacterized protein C20orf72 ENSG0000	C20orf72	R.GVAQTPGSVEEDALLC*GPVSK.H	1.04	0	1.02	1.03
IPI00012535.1	DNAJA1 DnaJ homolog subfamily A member 1 ENSG00000	DNAJA1	K.GAVEC*CPNCR.G	0	0	1.03	1.03
IPI00298961.3	XPO1 Exportin-1 ENSG00000082898 IPI00784388 IPI002	XPO1	R.QMSVPGIFNPHEIPEEMC*D.-	0	0	1.03	1.03
IPI00103087.2	GEMIN6 Gem-associated protein 6 ENSG00000152147 IP	GEMIN6	K.LMHLFTSGDC*K.A	0	0	1.03	1.03
IPI00008982.1	ALDH18A1 Isoform Long of Delta-1-pyrroline-5-carbo	ALDH18A1	K.CEYPAAC*NALETLLIHR.D	0	0	1.03	1.03
IPI00023547.1	MAPK10 Isoform Alpha-2 of Mitogen-activated protei	MAPK10	K.VIEQLGTPC*PEFMK.K	1.03	0	0	1.03
IPI00305383.1	UQCRC2 Ubiquinol-cytochrome-c reductase complex co	UQCRC2	R.NALANPLYC*PDYR.I	1.03	0	0	1.03
IPI00549467.3	NIT2 Nitrilase family member 2 ENSG00000114021 IPI	NIT2	R.VGLGIC*YDMR.F	0.92	1.14	0.91	1.0275
IPI00026167.3	NHP2L1 NHP2-like protein 1 ENSG00000100138 IPI0002	NHP2L1	K.KLLDLVQQSC*NYK.Q	0.93	1.11	0.95	1.025
IPI00013789.5	SMYD5 SET and MYND domain-containing protein 5 ENS	SMYD5	R.LFSQFC*NK.T	1.1	0	0.95	1.025
IPI00299155.5	PSMA4 Proteasome subunit alpha type-4 ENSG00000041	PSMA4	R.YLLQYQEPIPCEQLVTALC*DIK.Q	1.08	0	0.97	1.025

IPI00001960.4	CLIC4 Chloride intracellular channel protein 4 ENS	CLIC4	K.AGSDGESIGN C*PFSQR.L	0.98	1.07	0.98	1.025
IPI00329331.6	UGP2 Isoform 1 of UTP--glucose-1-phosphate uridyly	UGP2	K.LNGGLGTSM GC*K.G	1.03	0	1.02	1.025
IPI00002214.1	KPNA2 Importin subunit alpha-2 ENSG00000182481 IPI	KPNA2	R.TDC*SPIQFES AWALTNIASGT SEQTK.A	1.03	0	1.02	1.025
IPI00013212.1	CSK Tyrosine-protein kinase CSK ENSG00000103653 IP	CSK	R.SVLGGDC*LL K.F	1.02	0	1.03	1.025
IPI00396174.4	CCDC25 Coiled-coil domain-containing protein 25 EN	CCDC2 5	K.ANSIQGC*K. M	1.11	1.01	0.96	1.0225
IPI00292771.4	NUMA1 Isoform 1 of Nuclear mitotic apparatus prote	NUMA 1	R.QFC*STQAAL QAMER.E	1.11	0	0.93	1.02
IPI00006167.1	PPM1G Protein phosphatase 1G ENSG00000115241 IPI00	PPM1G	R.GTEAGQVGEP GIPTGEAGPSC* SSASDKLPR.V	1.06	0	0.98	1.02
IPI00017799.5	TXN2 Thioredoxin, mitochondrial precursor ENSG0000	TXN2	R.VVNSETPVVV DFHAQWC*GPC K.I	0	0	1.02	1.02
IPI00015956.3	EXOSC3 Exosome complex exonuclease RRP40 ENSG00000	EXOS C3	K.LLAPDC*EIIQ EVGK.L	1.01	0	1.03	1.02
IPI00010240.1	MIF4GD MIF4G domain-containing protein ENSG0000012	MIF4G D	K.VANVIVDHSL QDC*VFSK.E	1	0	1.04	1.02
IPI00745568.1	TIPRL Uncharacterized protein TIPRL ENSG0000014315	TIPRL	K.VAC*AEEWQ ESR.T	0.98	0	1.06	1.02
IPI00170916.1	NECAP1 Isoform 1 of Adaptin ear-binding coat-assoc	NECA P1	K.LC*IGNITNK. K	1.02	0	0	1.02
IPI00655704.1	PDK1 Mitochondrial pyruvate dehydrogenase kinase i	PDK1	K.QFLDFGSVNA C*EK.T	1.02	0	0	1.02
IPI00302673.3	ATPAF1 ATP synthase mitochondrial F1 complex assem	ATPAF 1	K.C*AQNQNKT. -	0.91	1	1.16	1.0175
IPI00470779.2	TXLNA Alpha-taxilin ENSG00000084652 IPI00816089 IP	TXLN A	R.VTEAPC*YPG APSTEASGQTG PQEPTSAR.A	1.05	0	0.98	1.015
IPI00031681.1	CDK2 Cell division protein kinase 2 ENSG0000012337	CDK2	R.APEILLGC*K. Y	0.98	0	1.05	1.015
IPI00009542.1	MAGED2 Isoform 1 of Melanoma-associated antigen D2	MAGE D2	R.MGIGLGSENA AGPC*NWDEAD IGPWAK.A	0.9	0	1.13	1.015
IPI00216746.1	HNRPK Isoform 2 of Heterogeneous nuclear ribonucle	HNRP K	K.IIPTLEEGLQL PSPTATSQLPLE SDAVEC*LNYQ HYK.G	0	1.01	1.02	1.0125
IPI00023785.6	DDX17 DEAD box polypeptide 17 isoform 1 ENSG000001	DDX17	R.TTSSANNPNL MYQDEC*DR.R	1.13	0	0.89	1.01
IPI00479877.4	ALDH9A1 aldehyde dehydrogenase 9A1 ENSG00000143149	ALDH 9A1	K.GALMANFLT QGQVC*CNGTR .V	0	1.03	0.95	1.01
IPI00021305.1	CCNH Cyclin-H ENSG00000134480 IPI00021305 IPI00556	CCNH	R.TC*LSQLLDI MK.S	1.01	0	1.01	1.01
IPI00015911.1	DLD Dihydrolipoyl dehydrogenase, mitochondrial pre	DLD	K.NETLGGTC*L NVGCIPSK.A	0	0	1.01	1.01
IPI00025746.5	ANKRD54 Isoform 1 of Ankyrin repeat domain-contain	ANKR D54	K.LNILQEGHAQ C*LEAVR.L	0	0	1.01	1.01

IPI00008994.2	NDRG2 Isoform 1 of Protein NDRG2 ENSG00000165795 I	NDRG2	K.YFLQGMGYMASSC*MTR.L	0	0	1.01	1.01
IPI00220373.4	IDE Insulin-degrading enzyme ENSG00000119912 IPI00	IDE	R.EMDSC*PVVGEFPCQNDINLSQAPALPQPEVIQNMTEFKR.G	0	0	1.01	1.01
IPI00024317.1	GCDH Isoform Long of Glutaryl-CoA dehydrogenase, m	GCDH	K.GYGC*AGVSSVAYGLLAR.E	0	0	1.01	1.01
IPI00292894.4	TSR1 TSR1, 20S rRNA accumulation ENSG00000167721 I	TSR1	R.DTGTVHLNELGNTQNFMLLC*PR.L	0	0	1.01	1.01
IPI00001636.1	ATXN10 Ataxin-10 ENSG00000130638 IPI00385153 IPI00	ATXN10	R.HAELIASTFVDQC*K.T	1	0	1.02	1.01
IPI00029534.1	PPAT Amidophosphoribosyltransferase precursor ENSG	PPAT	K.C*ELENCQPFVVETLHGK.I	0.98	0	1.04	1.01
IPI00844375.1	PSMB2 Proteasome beta 2 subunit variant (Fragment)	PSMB2	R.NLADC*LR.S	0.96	0	1.06	1.01
IPI00007935.4	PDLIM5 PDZ and LIM domain protein 5 ENSG0000016311	PDLIM5	R.QPTVTSVC*SETSQELAEGQR.R	1.01	0	0	1.01
IPI00220991.2	AP2B1 Putative uncharacterized protein DKFZp781K07	AP2B1	K.DC*EDPNPLIR.A	1.01	0	0	1.01
IPI00004461.2	DGUOK Isoform 1 of Deoxyguanosine kinase, mitochon	DGUOK	K.AC*TAQSLGNLLDMMYR.E	0	1.03	0.93	1.005
IPI00514983.3	HSPH1 Isoform Alpha of Heat shock protein 105 kDa	HSPH1	R.C*TPSVISFGSK.N	0.97	0	1.04	1.005
IPI00301139.5	MED17 Isoform 1 of Mediator of RNA polymerase II t	MED17	K.MELLMSALSPC*LL.-	0.94	0	1.07	1.005
IPI00009315.6	ACBD3 Golgi resident protein GCP60 ENSG00000182827	ACBD3	K.QVLMGPYNPDTC*PEVGFFDVLGNDR.R	1.08	0	0.92	1
IPI00646167.2	C14orf142 hypothetical protein LOC84520 ENSG000001	C14orf142	R.VSC*EAPGDGDPFQGLLSGVAQMK.D	1.07	0	0.93	1
IPI00013871.1	RRM1 Ribonucleoside-diphosphate reductase large su	RRM1	R.DECLMC*GS.-	1.03	0	0.97	1
IPI00556494.3	MED4 Mediator of RNA polymerase II transcription s	MED4	R.ISASNAVC*APLTWVPGDPR.R	0	0	1	1
IPI00007818.3	CPSF3 Cleavage and polyadenylation specificity fac	CPSF3	R.NFNYHILSPC*DLSNYTDLAMSTVK.Q	0	0	1	1
IPI00007074.5	YARS Tyrosyl-tRNA synthetase, cytoplasmic ENSG0000	YARS	K.AFC*EPGNVENNGVLSFIK.H	0	0	1	1
IPI00217157.5	DDX59 Isoform 1 of Probable ATP-dependent RNA heli	DDX59	K.NLPC*ANVR.Q	0	0	1	1
IPI00001539.8	ACAA2 3-ketoacyl-CoA thiolase, mitochondrial ENSG0	ACAA2	R.LC*GSGFQSIVNGCQEICVK.E	0.97	0	1.03	1
IPI00647082.1	TBC1D13 TBC1 domain family, member 13 ENSG00000107	TBC1D13	R.ELSFSGIPC*EGGLR.C	0.96	0	1.04	1
IPI00219025.3	GLRX Glutaredoxin-1 ENSG00000173221 IPI00219025	GLRX	K.VVVFIKPTC*PYCR.R	0	1	0	1
IPI00294739.1	SAMHD1 SAM domain and HD domain-containing protein	SAMHD1	R.C*DDSPR.T	1	0	0	1

IPI00018206.3	GOT2 Aspartate aminotransferase, mitochondrial pre	GOT2	R.VGAFTMVC*K.D	1.23	0	0.76	0.995
IPI00101600.5	CWF19L1 CWF19-like 1, cell cycle control ENSG00000	CWF19L1	K.QILAPVEESAC*QFFFDLNEK.Q	1.04	0	0.95	0.995
IPI00216298.6	TXN Thioredoxin ENSG00000136810 IPI00552768 IPI002	TXN	K.LVVVDFSATWC*GPCK.M	0	1.01	0.94	0.9925
IPI00029997.1	PGLS 6-phosphogluconolactonase ENSG00000130313 IPI	PGLS	R.AAC*CLAGAR.A	0.98	1.04	0.9	0.99
IPI00419194.2	IAH1 Isoamyl acetate-hydrolyzing esterase 1 homolo	IAH1	R.VILITPTPLC*ETAWEEQCIIQGCK.L	0	1	0.96	0.99
IPI00004534.3	PFAS Phosphoribosylformylglycinamidine synthase EN	PFAS	R.GLAPLHWADDDGNPTEQYPLNPNGSPGGVAGIC*SCDGR.H	0	0	0.99	0.99
IPI00024317.1	GCDH Isoform Long of Glutaryl-CoA dehydrogenase, m	GCDH	R.ASATGMIIMDGVEVPEENVLPGASSLGGPFGC*LNNAR.Y	0	0	0.99	0.99
IPI00045917.3	CRBN Isoform 1 of Protein cereblon ENSG00000113851	CRBN	K.VQILPEC*VLPSTMSAVQLESLNK.C	0	0	0.99	0.99
IPI00329638.10	ZAK Isoform 1 of Mitogen-activated protein kinase	ZAK	K.FDDLQFFENC*GGGSFGSVYR.A	0	0	0.99	0.99
IPI00743454.1	ACN9 Uncharacterized protein ACN9 ENSG00000196636	ACN9	K.AC*FGTFLPEEK.L	0.9	0	1.08	0.99
IPI00008436.4	POLE4 DNA polymerase epsilon subunit 4 ENSG0000011	POLE4	K.DAYC*CAQQGK.R	0.99	0	0	0.99
IPI00456919.2	HUWE1 Isoform 1 of E3 ubiquitin-protein ligase HUW	HUWE1	K.ACSPCSSQSSSSGIC*TDFWDLLVK.L	0.99	0	0	0.99
IPI00010438.2	SNAP23 Isoform SNAP-23a of Synaptosomal-associated	SNAP23	K.TTWGDGGENSPC*NVVSK.Q	0.99	0	0	0.99
IPI00003766.4	ETHE1 ETHE1 protein, mitochondrial precursor ENSG0	ETHE1	R.TDFQQGC*AK.T	0.89	1.07	0.92	0.9875
IPI00018522.4	PRMT1 HMT1 hnRNP methyltransferase-like 2 isoform	PRMT1	K.VIGIEC*SSISDYAVK.I	0.98	1	0.97	0.9875
IPI00026337.1	RANBP3 Isoform 1 of Ran-binding protein 3 ENSG0000	RANBP3	K.ALSQTVPSSGTNGVSLPADC*TGAVPAASPDTAAWR.S	1.11	0	0.86	0.985
IPI00024579.1	RAD18 E3 ubiquitin-protein ligase RAD18 ENSG000000	RAD18	K.TQCPTCC*VTVTEPDLK.N	1.06	0	0.91	0.985
IPI00016862.1	GSR Isoform Mitochondrial of Glutathione reductase	GSR	K.LGGTC*VNVGCVPK.K	1.16	0	0.81	0.985
IPI00019376.6	SEPT11 Septin-11 ENSG00000138758 IPI00019376	41528	K.STSQGFC*FNILCVGETGIGK.S	1	0	0.97	0.985
IPI00155601.1	MACROD1 MACRO domain-containing protein 1 ENSG0000	MACROD1	K.LEVDAIVNAANSSLLGGGGVDGC*IHR.A	0	0	0.98	0.98
IPI00023647.4	UBE1L2 Isoform 1 of Ubiquitin-activating enzyme E1	UBE1L2	R.KPNVGC*QQDSEELLK.L	0	0	0.98	0.98
IPI00796199.1	HNRNPL Uncharacterized protein HNRPL ENSG000001048	HNRNPL	K.QPAIMPGQSYGLEDGSC*SYKDFSESR.N	0	0	0.98	0.98

IPI00017617.1	DDX5 Probable ATP-dependent RNA helicase DDX5 ENSG	DDX5	R.LIDFLEC*GK.T	0	0	0.98	0.98
IPI00748490.1	AARSD1 Alanyl-tRNA synthetase, class IIc family pr	AARSD1	R.VVNIEGVDSNMC*CGTHVSNLSDLQVIK.I	0	0	0.98	0.98
IPI00007675.6	DYNC1LI1 Cytoplasmic dynein 1 light intermediate c	DYNC1LI1	R.VGSFGSSPPGLSSTYTGGPLGNEIASGNGGAAAGDDEDGQNLWSC*ILSEVSTR.S	0.93	0	1.03	0.98
IPI00396627.1	ELAC2 Isoform 1 of Zinc phosphodiesterase ELAC pro	ELAC2	K.VC*FGDFPTMPK.L	0.98	0	0	0.98
IPI00783852.1	ACTR10 46 kDa protein ENSG00000131966 IPI00783852	ACTR10	R.IPDWC*SLNNPPLEMMFDVGK.T	1.04	0	0.91	0.975
IPI00374272.3	LOC285636 hypothetical protein LOC285636 ENSG00000	LOC285636	R.C*PIQLNEGVSFQDLDTAK.L	0.97	0	0.98	0.975
IPI00177008.1	LOC283871 hypothetical protein LOC283871 ENSG00000	LOC283871	K.NNQESDC*VSK.K	0.93	0.99	0.98	0.9725
IPI00100213.2	RRM2B Isoform 1 of Ribonucleoside-diphosphate redu	RRM2B	K.IEQEFLTEALPVGLIGMNC*ILMK.Q	0	0	0.97	0.97
IPI00019640.1	VRK1 Serine/threonine-protein kinase VRK1 ENSG0000	VRK1	K.VGLPIGQGGFGC*IYLADMNSSESVGSDAPCVVK.V	0	0	0.97	0.97
IPI00291510.3	IMPDH2 Inosine-5-monophosphate dehydrogenase 2 EN	IMPDH2	R.VGMGSGSIC*ITQEVLACGRPQATAVYK.V	0	0.97	0	0.97
IPI00006907.1	C12orf5 Uncharacterized protein C12orf5 ENSG000000	C12orf5	K.AAREEC*PVFTPPGGETLDQVK.M	0.96	0	0.97	0.965
IPI00026781.2	FASN Fatty acid synthase ENSG00000169710 IPI000267	FASN	K.LTPGC*EAEAETEAICFFVQQFTDMEHNR.V	0	0.94	1.04	0.965
IPI00646689.1	TXNDC17 Thioredoxin domain-containing protein 17 E	TXNDC17	K.DAGGKSWC*PDCVQAEPVVR.E	0.97	0	0.95	0.96
IPI00455153.2	NFU1 HIRA interacting protein 5 isoform 2 ENSG0000	NFU1	K.LQGSCTSC*PSSIITLK.N	0.97	0	0.95	0.96
IPI00032900.1	BOLA1 BolA-like protein 1 ENSG00000178096 IPI00032	BOLA1	R.VCLC*QGSAGSGAIGPVEAAIR.T	0	0	0.96	0.96
IPI00045051.3	PURB Transcriptional activator protein Pur-beta EN	PURB	R.GGGGGPC*GFQPASR.G	0	0	0.96	0.96
IPI00003768.1	PES1 Isoform 1 of Pescadillo homolog 1 ENSG0000010	PES1	K.AGEGTYALDSESC*MEK.L	0	0	0.96	0.96
IPI00336008.1	ALDH5A1 aldehyde dehydrogenase 5A1 precursor, isof	ALDH5A1	R.NTGQTC*VCSNQFLVQR.G	0.95	0	0.97	0.96
IPI00298547.3	PARK7 Protein DJ-1 ENSG00000116288 IPI00298547	PARK7	K.GLIAAIC*AGPTALLAHEIGFGSK.V	0	0.96	0	0.96
IPI00007752.1	TUBB2C Tubulin beta-2C chain ENSG00000188229 IPI00	TUBB2C	K.LTTPTYGDLNHLVSATMSGVTTC*LR.F	0	0.97	0.92	0.9575
IPI00031563.4	C19orf58 Uncharacterized protein C19orf58 ENSG0000	C19orf58	R.FHADSVC*K.A	0.91	1	0.92	0.9575
IPI00026328.3	TXNDC12 Thioredoxin domain-containing protein	TXNDC12	K.SWC*GACK.A	0.99	0	0.92	0.955

	12 p						
IPI00013452.8	EPRS glutamyl-prolyl tRNA synthetase ENSG000001366	EPRS	K.LSSC*DSFTSTINELNHCLSLR.T	0.91	0	1	0.955
IPI00041325.1	NOLA2 H/ACA ribonucleoprotein complex subunit 2 EN	NOLA2	K.ADPDGPEAQAEAC*SGER.T	0.97	0	0.94	0.955
IPI00220503.9	DCTN2 dynactin 2 ENSG00000175203 IPI00220503 IPI00	DCTN2	R.C*DQDAQNPLSAGLQGACLMETVELLQAK.V	0.82	0.96	1.08	0.955
IPI00218782.2	CAPZB Capping protein ENSG00000077549 IPI00026185	CAPZB	R.QMEKDETVSDC*SPHIANIGR.L	1.12	0	0.78	0.95
IPI00304071.4	FLJ20920 hypothetical protein LOC80221 ENSG0000016	FLJ20920	R.MVSTPIGGLSYVQGC*TK.K	0.99	0	0.91	0.95
IPI00301058.5	VASP Vasodilator-stimulated phosphoprotein ENSG000	VASP	K.SSSSVTTSETQPC*TPSSSDYSDLQR.V	0.99	0	0.91	0.95
IPI00299263.5	ARFGAP3 ADP-ribosylation factor GTPase-activating	ARFGAP3	R.LGMGFGNC*R.S	0	0	0.95	0.95
IPI00797537.1	NUDCD1 NudC domain-containing protein 1 ENSG000001	NUDCD1	K.FFACAPNYSYAALC*ECLR.R	0	0	0.95	0.95
IPI00019380.1	NCBP1 Nuclear cap-binding protein subunit 1 ENSG00	NCBP1	K.SAC*SLESNLEGLAGVLEADLPNYK.S	0	0.95	0	0.95
IPI00439415.6	EIF4B eukaryotic translation initiation factor 4B	EIF4B	K.SLENETLNKEEDC*HSPTSKPPKPDQPLK.V	0	0.95	0	0.95
IPI00746806.1	CTTN CTTN protein ENSG00000085733 IPI00029601 IPI0	CTTN	K.C*ALGWDHQEK.L	0.95	0	0	0.95
IPI00031519.3	DNMT1 Isoform 1 of DNA (cytosine-5)-methyltransfer	DNMT1	K.NQLC*DLETK.L	0.95	0	0	0.95
IPI00386755.2	ERO1L ERO1-like protein alpha precursor ENSG000001	ERO1L	K.HDDSSDNFC*EADDIQSPEAEYVDLLLNPER.Y	0.96	0	0.93	0.945
IPI00479385.3	ASMTL Uncharacterized protein ASMTL ENSG0000016909	ASMTL	K.LTAC*QVATAFNLSR.F	0	0	0.94	0.94
IPI00796038.1	ARL6IP4 OGFOD2 SRp25 nuclear protein isoform 1 ENS	ARL6IP4	R.GDC*LAFQMR.A	0	0	0.94	0.94
IPI00216230.3	TMPO Lamina-associated polypeptide 2 isoform alpha	TMPO	K.VDDEILGFISEATPLGGIQAASTESC*NQQLDLALCR.A	0	0	0.94	0.94
IPI00016458.2	L2HGDH Isoform 1 of L-2-hydroxyglutarate dehydroge	L2HGDH	K.AC*FLGATVK.Y	0.94	0	0	0.94
IPI00029091.1	_ Putative nucleoside diphosphate kinase ENSG00000	_	R.GDFC*IQVGR.N	0	0	0.93	0.93
IPI00302688.7	ECHDC1 Isoform 1 of Enoyl-CoA hydratase domain-con	ECHDC1	K.SLGTPEDGMAVC*MFMQNTLTR.F	0	0	0.93	0.93
Reverse_IPI00418790.3	EML5 echinoderm microtubule associated protein lik	EML5	K.VGC*SVLKNPQYLDWSIDFIR.D	0	0	0.93	0.93
IPI00398009.2	IPO4 Isoform 2 of Importin-4 ENSG00000196497 IPI00	IPO4	K.LC*PQLMPMLEEALR.S	0.93	0	0	0.93
IPI00032955.1	ZNF313 Zinc finger protein 313 ENSG00000124226 IPI	ZNF313	R.DC*GGAAQLAGPAAEADPLGR.F	1.03	0	0.83	0.93

IPI00556451.2	ETFB Isoform 2 of Electron transfer flavoprotein s	ETFB	K.HSMNPFC*EIAVEEAVR.L	0.94	0	0.92	0.93
IPI00299524.1	NCAPD2 Condensin complex subunit 1 ENSG00000010292	NCAPD2	K.VACC*PLER.C	0.94	0	0.92	0.93
IPI00018331.3	SNAPAP SNARE-associated protein Snapin ENSG0000014	SNAPAP	R.EQIDNLATELC*R.I	0.94	0	0.92	0.93
IPI00333763.7	GLRX5 Glutaredoxin-related protein 5 ENSG000001825	GLRX5	K.GTPEQPQC*GFSNAVVQILR.L	0.94	0	0.92	0.93
IPI00784459.1	CFL1 Uncharacterized protein CFL1 ENSG00000172757	CFL1	K.HELQANC*YEEVKDR.C	0.91	0.94	0.9	0.9225
IPI00101645.3	KIAA0828 Putative adenosylhomocysteinase 3 ENSG000	KIAA0828	K.FDNLYC*CR.E	0	0	0.92	0.92
IPI00748353.1	WDHD1 126 kDa protein ENSG00000198554 IPI00748353	WDHD1	K.NVLSETPAIC*PPQNTENQRPK.T	0	0	0.92	0.92
IPI00382452.1	CHMP1A Isoform 1 of Charged multivesicular body pr	CHMP1A	K.NVEC*AR.V	0	0	0.92	0.92
IPI00384708.2	PDSS2 Isoform 1 of Decaprenyl-diphosphate synthase	PDSS2	R.C*LLSDELSNIAMQVR.K	0	0	0.92	0.92
IPI00073602.1	EXOSC6 Exosome complex exonuclease MTR3 ENSG000001	EXOSC6	R.RAPPGGC*EER.E	0	0.92	0	0.92
IPI00797038.1	PCK2 mitochondrial phosphoenolpyruvate carboxykina	PCK2	R.QC*PIMDPAWEAPEGVPIDAIIFGGR.R	0.92	0	0	0.92
IPI00024915.2	PRDX5 Isoform Mitochondrial of Peroxiredoxin-5, mi	PRDX5	K.ALNVEPDGTGLTC*SLAPNIISQL.-	0.78	1.02	0.85	0.9175
IPI00099986.5	FN3KRP Ketosamine-3-kinase ENSG00000141560 IPI0009	FN3KRP	R.ATGHSGGGC*ISQGR.S	0	0.93	0.86	0.9125
IPI00291419.5	ACAT2 Acetyl-CoA acetyltransferase, cytosolic ENSG	ACAT2	R.QASVGAGIPYSVPAWSC*QMICGSGLK.A	0	0	0.91	0.91
IPI00788879.2	TBC1D23 Isoform 1 of TBC1 domain family member 23	TBC1D23	K.FLENTPSSLNIEDIEDLFSLAQYYC*SK.T	0	0	0.91	0.91
IPI00828021.1	HSPA4L Heat shock protein apg-1 ENSG00000164070 IP	HSPA4L	K.LMSANASDLPLNIEC*FMNDLDVSSK.M	0.99	0	0.83	0.91
IPI00014589.1	CLTB Isoform Brain of Clathrin light chain B ENSG0	CLTB	K.VAQLC*DFNPK.S	0	0	0.9	0.9
IPI00306369.3	NSUN2 tRNA ENSG00000037474 IPI00306369	NSUN2	K.DGVC*GPPPSKK.M	0	0	0.9	0.9
IPI00028091.3	ACTR3 Actin-like protein 3 ENSG00000115091 IPI0002	ACTR3	R.YSYVC*PDLVK.E	0	0	0.9	0.9
IPI00335251.3	DUS1L tRNA-dihydrouridine synthase 1-like ENSG0000	DUS1L	K.AVAIPVFANGNIQC*LQDVER.C	0	0	0.9	0.9
IPI00412771.1	CD2AP CD2-associated protein ENSG00000198087 IPI00	CD2AP	K.DTC*YSPKPSVYLSTPSSASK.A	0.76	0	1.04	0.9
IPI00386755.2	ERO1L ERO1-like protein alpha precursor ENSG000001	ERO1L	K.RPLNPLASGQGTSEENTFYSWLEGLC*VEK.R	0	0.9	0	0.9
IPI00174442.2	FAM98A Protein FAM98A ENSG00000119812 IPI00174442	FAM98A	R.EKTAC*AINK.V	0.9	0	0	0.9

IPI00303439.1	SMARCB1 CDNA FLJ13963 fis, clone Y79AA1001299, hig	SMARCB1	R.NTGDADQWC*PLLETLTDAEMEK.K	0.9	0	0	0.9
IPI00013871.1	RRM1 Ribonucleoside-diphosphate reductase large su	RRM1	R.VETNQDWSLMC*PNECPGLDEVWGEEFEK.L	0.9	0	0	0.9
IPI00026216.4	NPEPPS Puromycin-sensitive aminopeptidase ENSG0000	NPEPPS	K.NSC*SSSR.Q	0.96	0	0.84	0.9
IPI00065671.1	UCK2 Isoform 1 of Uridine-cytidine kinase 2 ENSG00	UCK2	R.QTNGC*LNGYTPSR.K	0.9	0	0.89	0.895
IPI00007691.1	TRAPPC4 Trafficking protein particle complex subun	TRAPPC4	K.NPFYSLEMPIRC*ELFDQNLK.L	0.8	0	0.99	0.895
IPI00299263.5	ARFGAP3 ADP-ribosylation factor GTPase-activating	ARFGAP3	K.LANTC*FNEIEK.Q	0	0	0.89	0.89
IPI00383460.7	GRSF1 G-rich RNA sequence binding factor 1 isoform	GRSF1	R.YIELFLNSC*PK.G	0	0	0.88	0.88
IPI00013774.1	HDAC1 Histone deacetylase 1 ENSG00000116478 IPI005	HDAC1	K.VMEMFQPSAVVLQC*GSDSLSGDR.L	0	0	0.88	0.88
IPI00456898.1	LOC440055 Uncharacterized protein ENSP00000302331	LOC440055	R.QAHLC*VLASNCDEPMYVK.L	0.88	0	0	0.88
IPI00743416.1	IKBKAP inhibitor of kappa light polypeptide gene e	IKBKAP	R.GDGQFFAVSVVC*PETGAR.K	0.9	0	0.85	0.875
IPI00002966.1	HSPA4 Heat shock 70 kDa protein 4 ENSG00000170606	HSPA4	K.LMSANASDLPLSIEC*FMNDVDVSGTMNR.G	0.89	0	0.86	0.875
IPI00219156.7	RPL30 60S ribosomal protein L30 ENSG00000156482 IP	RPL30	R.VC*TLAIIDPGDSDIIR.S	0.75	0	1	0.875
IPI00028091.3	ACTR3 Actin-like protein 3 ENSG00000115091 IPI0002	ACTR3	K.LGYAGNTEPQFIIPSC*IAIK.E	0	0	0.87	0.87
IPI00646105.3	PYCRL Pyrroline-5-carboxylate reductase ENSG000001	PYCRL	R.AATMSAVEAATC*R.A	0	0	0.87	0.87
IPI00296053.3	FH Isoform Mitochondrial of Fumarate hydratase, mi	FH	K.FEALAAHDALVELSGAMNTTAC*SLMK.I	0	0	0.87	0.87
IPI00022239.7	METAP1 Methionine aminopeptidase 1 ENSG00000164024	METAP1	K.LGIQGSYFCSQEC*FK.G	0.86	0	0.88	0.87
IPI00009146.4	TRAFD1 TRAF-type zinc finger domain-containing pro	TRAFD1	R.STSGPRPGCQPSSPC*VPK.L	0	0.87	0	0.87
IPI00168009.1	NUDT16L1 Isoform 2 of Protein syndesmos ENSG000001	NUDT16L1	R.VLGLGLGC*LR.L	0	0.87	0	0.87
IPI00216694.3	PLS3 plastin 3 ENSG00000102024 IPI00848312 IPI0021	PLS3	K.EGIC*ALGGTSELSSEGTQHSYSEEEK.Y	0.91	0	0.82	0.865
IPI00001636.1	ATXN10 Ataxin-10 ENSG00000130638 IPI00385153 IPI00	ATXN10	K.ETTNIFSNC*GCVR.A	0.79	0	0.94	0.865
IPI00289807.3	TRNT1 Isoform 1 of tRNA-nucleotidyltransferase 1,	TRNT1	K.YQGEHC*LLK.E	0	0.7	1.35	0.8625
IPI00069693.4	_ Uncharacterized protein ENSP00000350479 ENSG0000	_	R.ALVDGPC*TQVR.R	0.91	0	0.81	0.86
IPI00549569.4	ISYNA1 Myo-inositol 1-phosphate synthase A1 ENSG00	ISYNA1	R.FC*EVIPGLNDTAENLLR.T	0	0	0.86	0.86

IPI00294739.1	SAMHD1 SAM domain and HD domain-containing protein	SAMHD1	R.VC*EVDNELR.I	0	0	0.86	0.86
IPI00004534.3	PFAS Phosphoribosylformylglycinamidine synthase EN	PFAS	K.FC*DNSSAIQGK.E	0.89	0	0.79	0.84
IPI00002966.1	HSPA4 Heat shock 70 kDa protein 4 ENSG00000170606	HSPA4	R.GC*ALQCAILSPAFK.V	0	0	0.84	0.84
IPI00018272.3	PNPO Pyridoxine-5-phosphate oxidase ENSG000001084	PNPO	K.KLPEEEAEC*YFHSRPK.S	0	0.84	0	0.84
IPI00240909.1	hCG_15200 Uncharacterized protein ENSP00000343276	hCG_15200	K.TC*FSPNR.V	0	0.84	0	0.84
IPI00465054.2	THUMPD1 Putative uncharacterized protein DKFZp686C	THUMPD1	R.C*DAGGPR.Q	0.93	0.76	0.9	0.8375
IPI00008454.1	DNAJB11 DnaJ homolog subfamily B member 11 precurs	DNAJB11	R.FQMTQEVVCDEC*PNVK.L	0.94	0	0.71	0.825
IPI00644290.1	NDRG3 NDRG family member 3 ENSG00000101079 IPI0021	NDRG3	R.FALNHPELVEGLVLINVDPC*AK.G	0	0.81	0	0.81
IPI00029485.2	DCTN1 Isoform p150 of Dynactin subunit 1 ENSG00000	DCTN1	K.VTFSC*AAGFGQR.H	1	0	0.61	0.805
IPI00456664.1	NIT1 Isoform 4 of Nitrilase homolog 1 ENSG00000158	NIT1	K.IGLAVC*YDMR.F	1.02	0.67	0.86	0.805
IPI00003565.1	PSMD10 26S proteasome non-ATPase regulatory subuni	PSMD10	K.GAQVNAVNQNGC*TPLHYAASK.N	0	0	0.8	0.8
IPI00026781.2	FASN Fatty acid synthase ENSG00000169710 IPI000267	FASN	K.AFDTAGNGYC*R.S	0	0	0.79	0.79
IPI00183626.8	PTBP1 polypyrimidine tract-binding protein 1 isofo	PTBP1	K.LSLDGQNIYNAC*CTLR.I	0	0	0.78	0.78
IPI00010244.4	MRPS11 Isoform 1 of 28S ribosomal protein S11, mit	MRPS11	K.ASHNNTQIQVVSASNEPLAFASC*GTEGFR.N	0	0	0.77	0.77
IPI00002214.1	KPNA2 Importin subunit alpha-2 ENSG00000182481 IPI	KPNA2	K.YGAVDPLLALLAVPDMSSLAC*GYLR.N	0	0.77	0	0.77
IPI00216008.4	G6PD Isoform Long of Glucose-6-phosphate 1-dehydro	G6PD	R.TQVC*GILR.E	0.75	0	0.75	0.75
IPI00514983.3	HSPH1 Isoform Alpha of Heat shock protein 105 kDa	HSPH1	K.LMSSNSTDLPLNIEC*FMNDKDVSGK.M	0	0	0.75	0.75
IPI00002824.7	CSRP2 Cysteine and glycine-rich protein 2 ENSG0000	CSRP2	R.C*CFLCMVCR.K	0	0.77	0.68	0.7475
IPI00853009.1	CUGBP1 Isoform 4 of CUG-BP- and ETR-3-like factor	CUGBP1	R.GC*AFVTFTTR.A	0	0	0.74	0.74
IPI00641181.5	MARCKSL1 MARCKS-related protein ENSG00000175130 IP	MARCKSL1	K.EGGGDSSASSPTEEEQEQGEIGAC*SDEGTAQEGK.A	0	0	0.74	0.74
IPI00852960.1	USP22 Ubiquitin carboxyl-terminal hydrolase 22 ENS	USP22	K.ITSNC*TIGLR.G	0.68	0	0.78	0.73
IPI00006504.3	EIF2B3 Isoform 1 of Translation initiation factor	EIF2B3	K.EANTLNLAPYDAC*WNACR.G	0.73	0	0	0.73
IPI00018140.3	SYNCRIP Isoform 1 of Heterogeneous nuclear ribonuc	SYNCRIP	K.SAFLC*GVMK.T	0.72	0	0.73	0.725
IPI00010158.3	CHRAC1 Chromatin accessibility complex	CHRAC1	K.ATELFVQC*LATYSYR.H	0	0	0.72	0.72

	protein 1 E						
IPI00018206.3	GOT2 Aspartate aminotransferase, mitochondrial pre	GOT2	K.EYLPIGGLAEFC*K.A	0	0	0.71	0.71
IPI00419575.6	C7orf20 Protein of unknown function DUF410 family	C7orf20	K.EQNYC*ESR.Y	0	0	0.7	0.7
IPI00033494.3	MRLC2 Myosin regulatory light chain ENSG0000011868	MRLC2	R.NAFAC*FDEEATGTIQEDYLR.E	0.62	0	0.78	0.7
IPI00013723.3	PIN1 Peptidyl-prolyl cis-trans isomerase NIMA-inte	PIN1	K.IKSGEEDFESLASQFSDC*SSAK.A	0.9	0.47	0.95	0.6975
IPI00306159.7	MECR Trans-2-enoyl-CoA reductase, mitochondrial pr	MECR	R.LALNC*VGGK.S	0.69	0	0.7	0.695
IPI00442165.1	ZNF346 Isoform 2 of Zinc finger protein 346 ENSG00	ZNF346	K.NQC*LFTNTQCK.V	0.94	0	0.44	0.69
IPI00419237.3	LAP3 Isoform 1 of Cytosol aminopeptidase ENSG00000	LAP3	R.LILADALC*YAHTFNPK.V	0.69	0	0	0.69
IPI00152432.2	GPT2 Isoform 1 of Alanine aminotransferase 2 ENSG0	GPT2	K.LLEETGIC*VVPGSGFGQR.E	0.71	0	0.66	0.685
IPI00788925.1	BCAT2 Branched chain aminotransferase 2, mitochond	BCAT2	R.EVFGSGTAC*QVCPVHR.I	0	0	0.68	0.68
IPI00011107.2	IDH2 Isocitrate dehydrogenase [NADP], mitochondria	IDH2	K.DLAGC*IHGLSNVK.L	0.67	0	0	0.67
IPI00005780.3	OGT Isoform 3 of UDP-N-acetylglucosamine--peptide	OGT	K.VMAEANHFIDLSQIPC*NGK.A	0	0	0.62	0.62
IPI00177856.8	C14orf172 Uncharacterized protein C14orf172 ENSG00	C14orf172	R.FCSFSPC*IEQVQR.T	0.65	0	0.54	0.595
IPI00302927.6	CCT4 T-complex protein 1 subunit delta ENSG0000011	CCT4	K.ITGC*ASPGK.T	0.57	0	0	0.57
IPI00022239.7	METAP1 Methionine aminopeptidase 1 ENSG00000164024	METAP1	R.VCETDGC*SSEAK.L	0.54	0	0.58	0.56
IPI00448095.3	DCXR L-xylulose reductase ENSG00000169738 IPI00448	DCXR	R.GVPGAIVNVSSQC*SQR.A	0.46	0.51	0.47	0.4875
IPI00029557.3	GRPEL1 GrpE protein homolog 1, mitochondrial precu	GRPEL1	K.ATQC*VPKEEIKDDNPHLK.N	0	0.34	0	0.34
IPI00024013.1	_ Putative ubiquitin-conjugating enzyme E2 D3-like	_	K.VLLSIC*SLLCDPNPDDPLVPEIAR.I	0	0.17	0.23	0.185
IPI00216694.3	PLS3 plastin 3 ENSG00000102024 IPI00848312 IPI0021	PLS3	K.VDLNSNGFIC*DYELHELFK.E	0.12	0	0.09	0.105

Appendix III

Protein gels

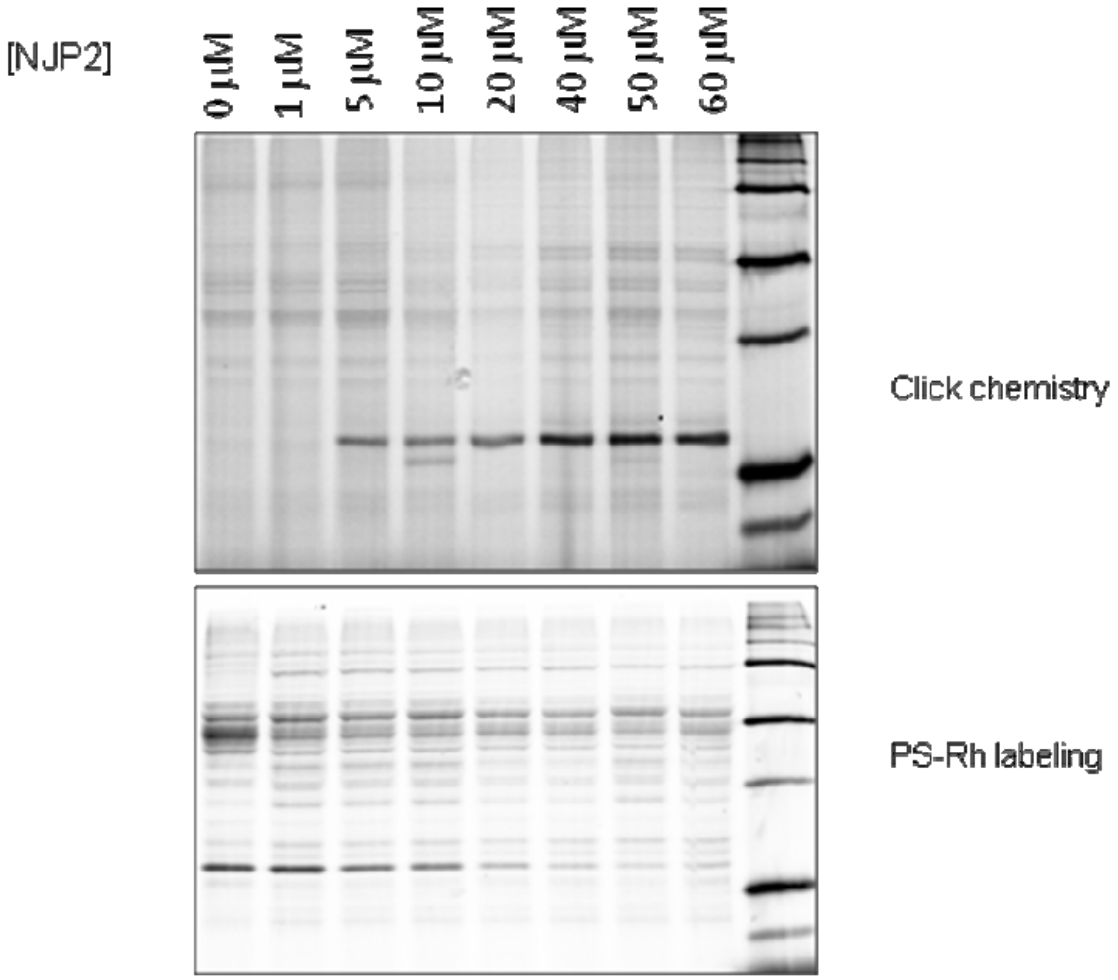

Figure 2A-1. Apoptotic, NJP2-treated, HeLa lysates were subjected to either click chemistry or PS-Rh labeling, followed by in-gel fluorescence analysis.

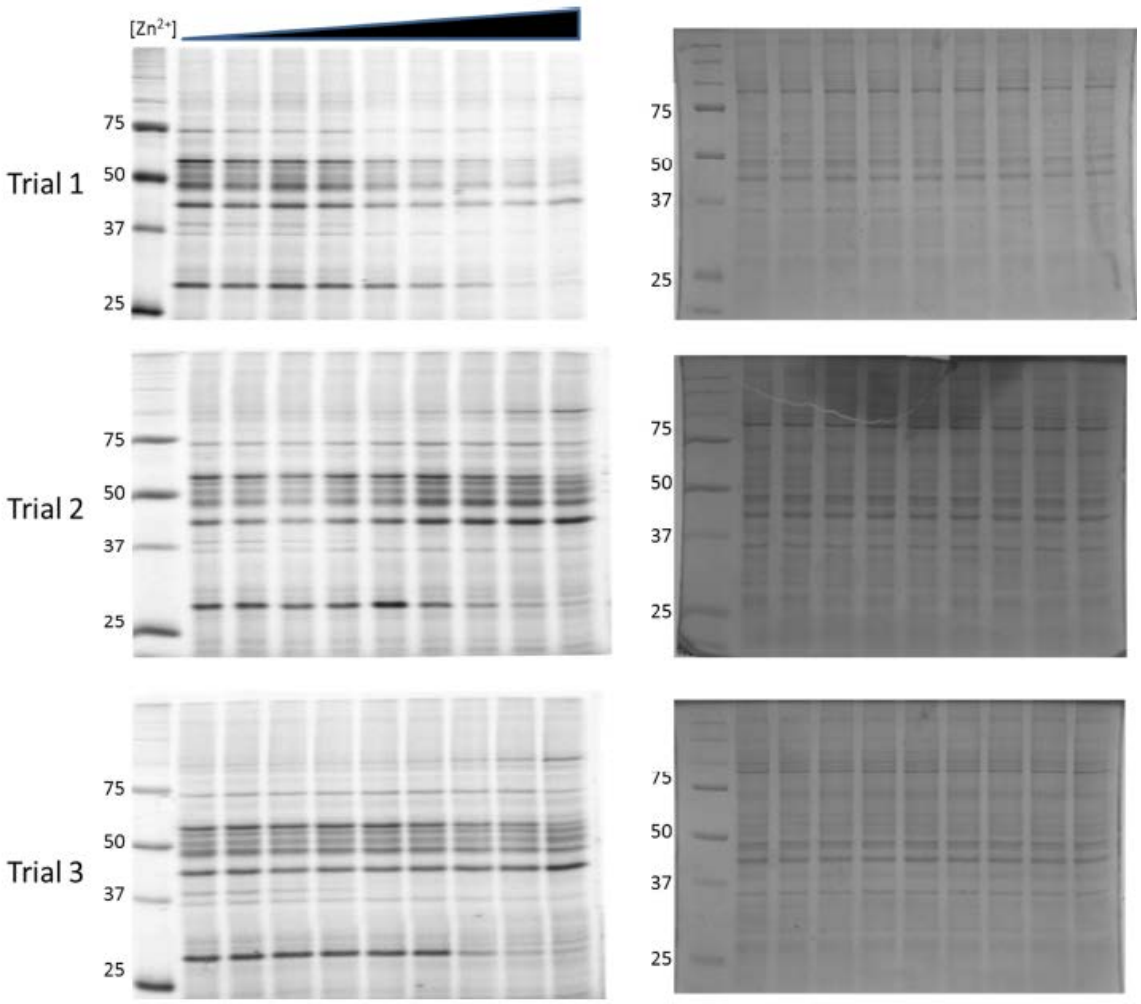

Figure 3A-1. Zn^{2+}-affinity gels. HeLa lysates were treated with increasing concentrations of Zn^{2+}, followed by NJP14 and underwent in-gel fluorescence analysis.

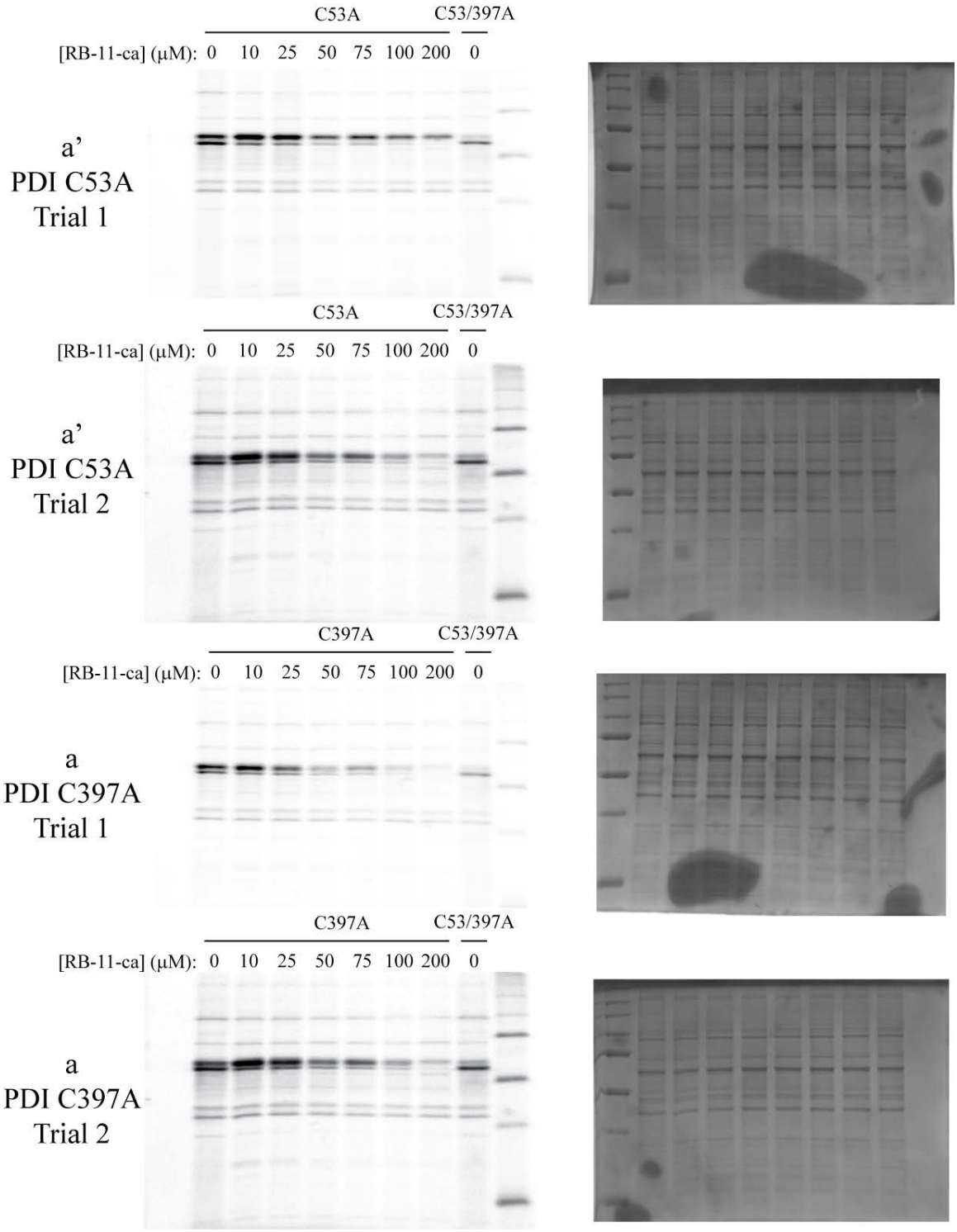

Figure 4A-1. Competitive in-gel fluorescence platform of PDI C53A and C397A administered RB-11-ca.

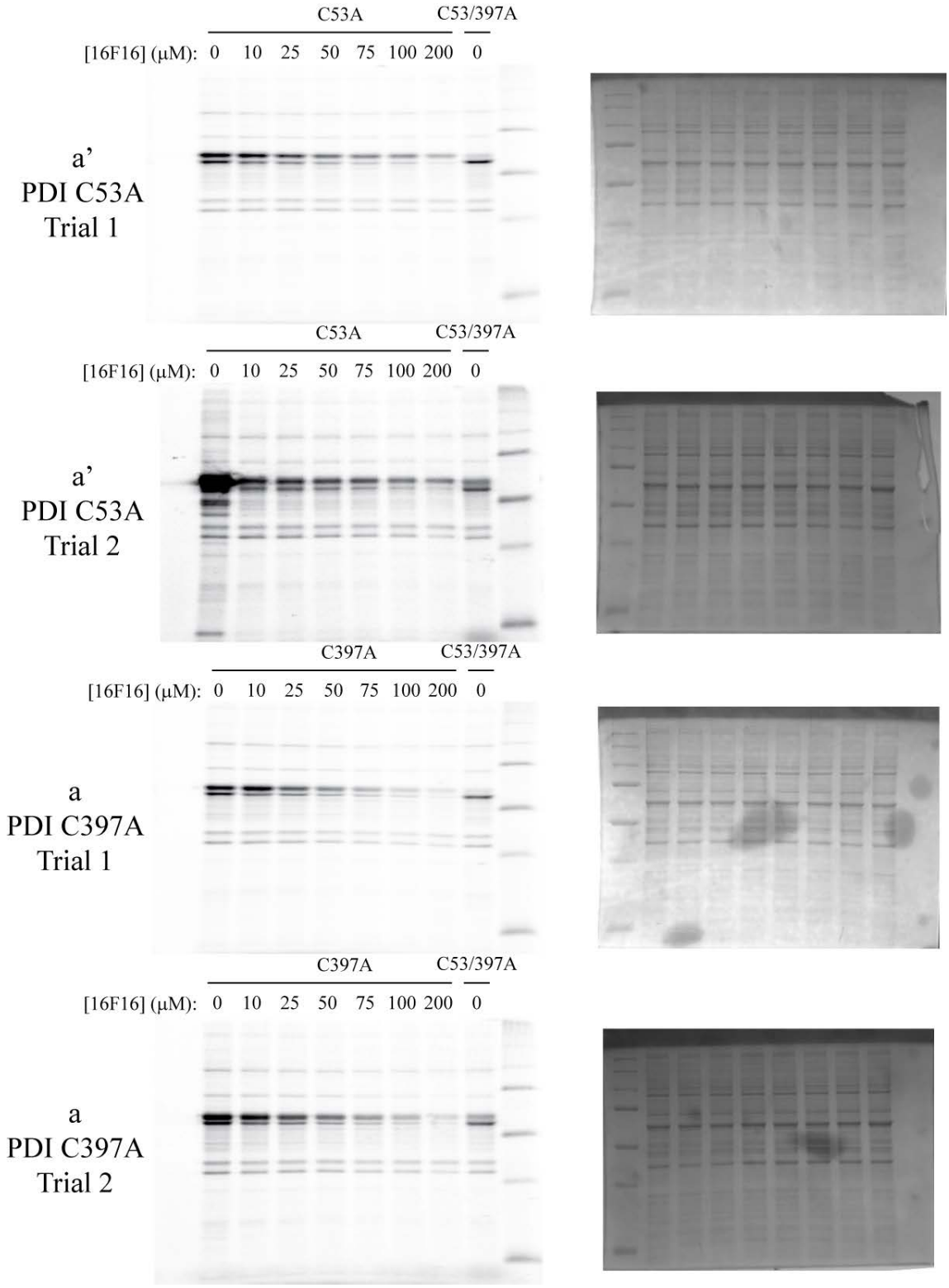

Figure 4A-2. Competitive in-gel fluorescence platform of PDI C53A and C397A administered 16F16.

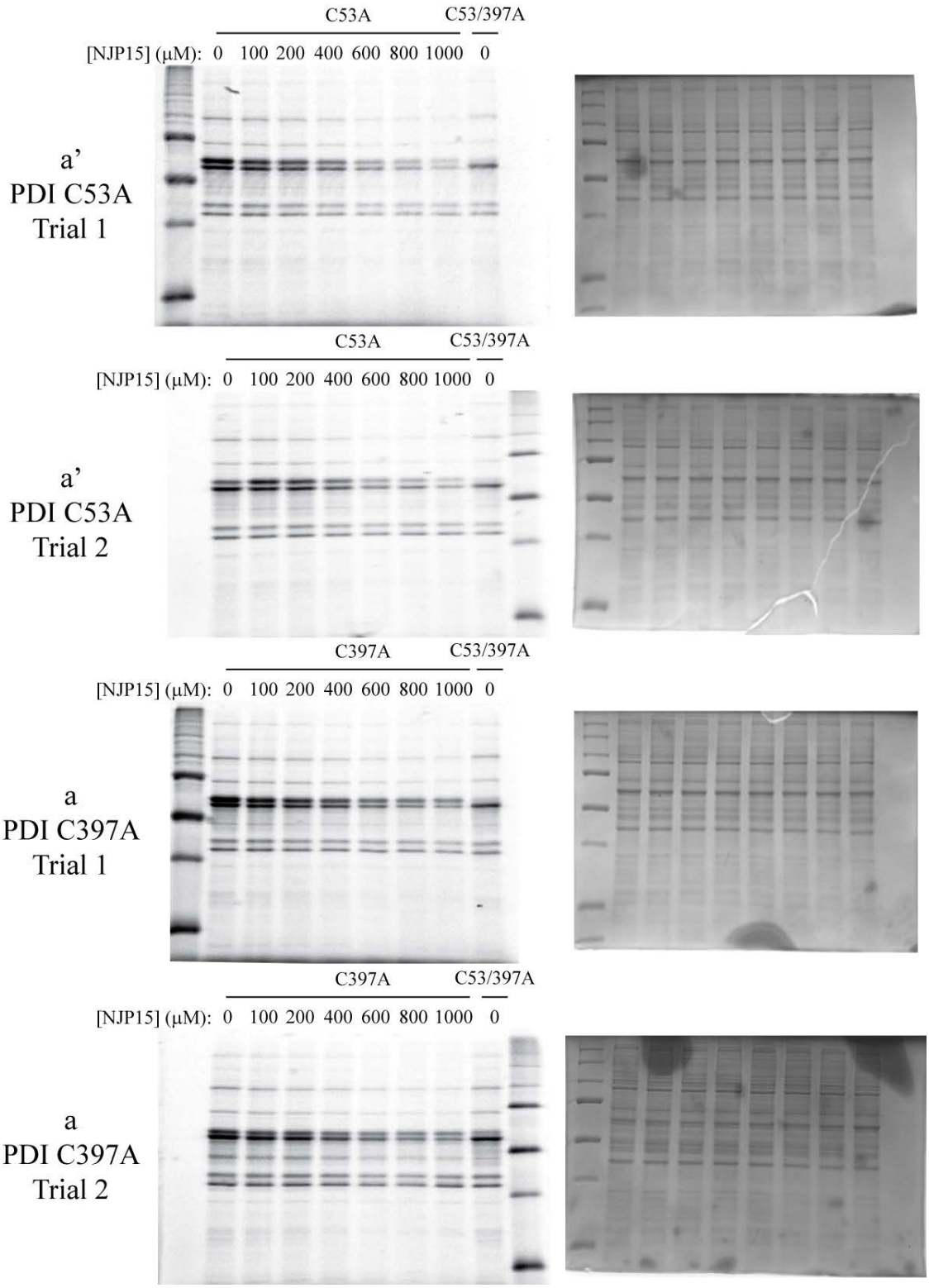

Figure 4A-3. Competitive in-gel fluorescence platform of PDI C53A and C397A administered NJP15.

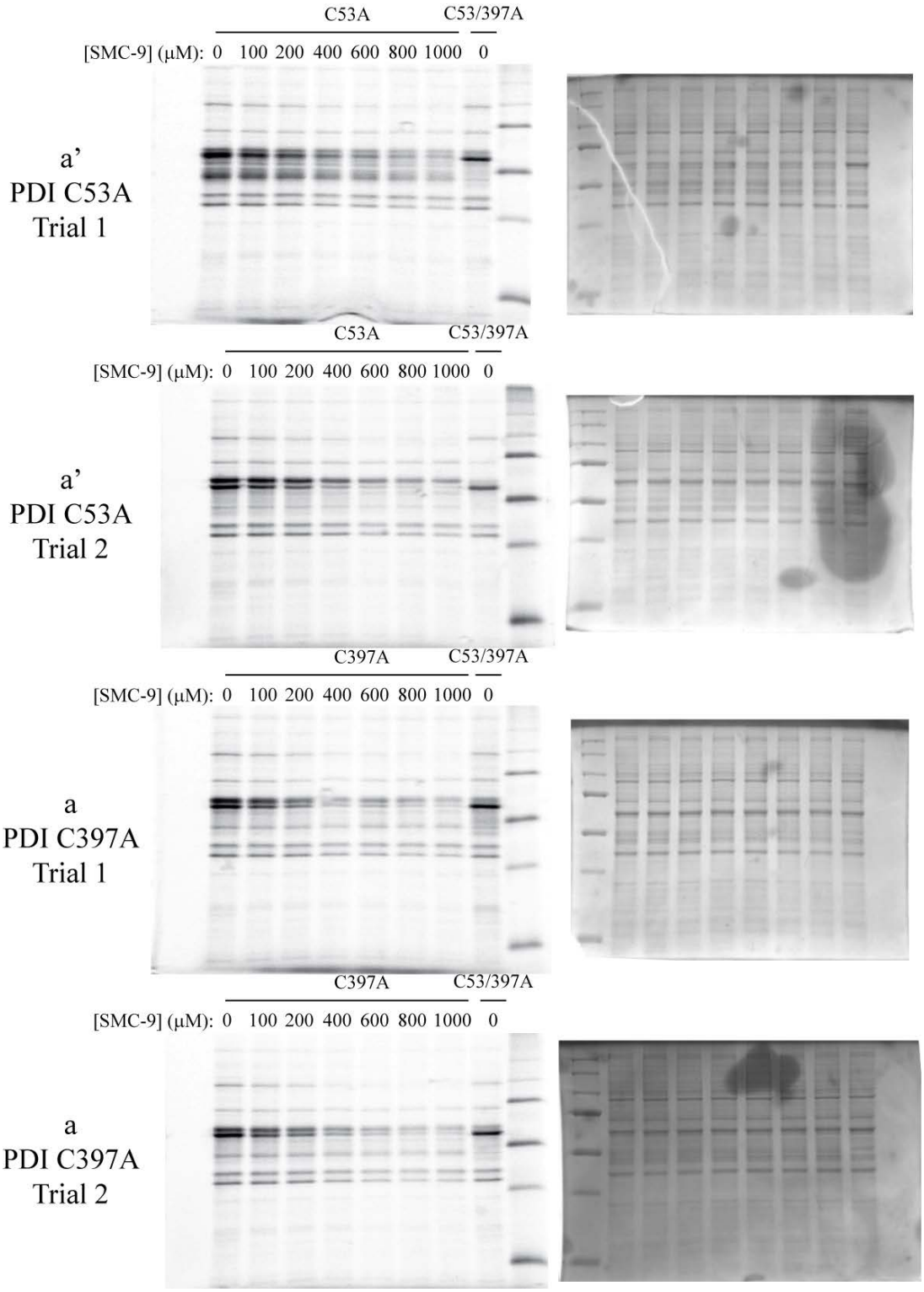

Figure 4A-4. Competitive in-gel fluorescence platform of PDI C53A and C397A administered SMC-9.